Talanta

The International Journal of Pure and Applied Analytical Chemistry

Publication information: *Talanta* (ISSN 0039-9140). For 2007, volumes 71–73 are scheduled for publication. Subscription prices are available upon request from the Publisher or from the Regional Sales Office nearest you or from this journal's website (http://www.elsevier.com/locate/talanta). Further information is available on this journal and other Elsevier products through Elsevier's website: (http://www.elsevier.com). Subscriptions are accepted on a prepaid basis only and are entered on a calendar year basis. Issues are sent by standard mail (surface within Europe, air delivery outside Europe). Priority rates are available upon request. Claims for missing issues should be made within six months of the date of dispatch.

Orders, claims, and journal enquiries: please contact the Customer Service Department at the Regional Sales Office nearest you:
Orlando: Elsevier, Customer Service Department, 6277 Sea Harbor Drive, Orlando, FL 32887-4800, USA; phone: (+1) (877) 8397126 [toll free number for US customers], or (+1) (407) 3454020 [customers outside US]; fax: (+1) (407) 3631354; e-mail: usjcs@elsevier.com
Amsterdam: Elsevier, Customer Service Department, PO Box 211, 1000 AE Amsterdam, The Netherlands; phone: (+31) (20) 4853757; fax: (+31) (20) 4853432; e-mail: nlinfo-f@elsevier.com
Tokyo: Elsevier, Customer Service Department, 4F Higashi-Azabu, 1-Chome Bldg, 1-9-15 Higashi-Azabu, Minato-ku, Tokyo 106-0044, Japan; phone: (+81) (3) 5561 5037; fax: (+81) (3) 5561 5047; e-mail: jp.info@elsevier.com
Singapore: Elsevier, Customer Service Department, 3 Killiney Road, #08-01 Winsland House I, Singapore 239519; phone: (+65) 63490222; fax: (+65) 67331510; e-mail: asiainfo@elsevier.com

USA mailing notice: *Talanta* (ISSN 0039-9140) is published monthly by Elsevier B.V. (P.O. Box 211, 1000 AE Amsterdam, The Netherlands). Annual subscription price in the USA US$ 3,818 (valid in North, Central and South America), including air speed delivery. Application to mail at periodical postage rate is paid at Rathway, NJ and additional mailing offices.
USA POSTMASTER: Send address changes to *Talanta*, Publications Expediting Inc., 200 Meacham Avenue, Elmont, NY 11003.
AIRFREIGHT AND MAILING in the USA by Publications Expediting Inc., 200 Meacham Avenue, Elmont, NY 11003.

Available online at www.sciencedirect.com
ScienceDirect
Talanta 73 (2007) 346–351
Talanta
www.elsevier.com/locate/talanta

Precise coulometric titration of sodium thiosulfate and development of potassium iodate as a redox standard

Toshiaki Asakai [a,*], Mariko Murayama [a], Tatsuhiko Tanaka [b]

[a] *National Institute of Technology and Evaluation, 2-49-10, Nishihara, Shibuya-ku, Tokyo 151-0066, Japan*
[b] *Faculty of Engineering, Tokyo University of Science, 1–3, Kagurazaka, Shinjuku-ku, Tokyo 162-8601, Japan*

Received 14 February 2007; received in revised form 23 March 2007; accepted 23 March 2007
Available online 1 April 2007

Abstract

In this paper, we determine the effective purity of potassium iodate as a redox standard with a certified value linked to the international system of units (SI units). Concentration measurement of sodium thiosulfate solution was performed by precise coulometric titration with electrogenerated iodine, and an assay of potassium iodate was carried out by gravimetric titration based on the reductometric factor of sodium thiosulfate assigned by coulometry. The accuracy of the coulometric titration method was evaluated by examining the current efficiency of iodine electrogeneration, stability of sodium thiosulfate solutions and dependence on the amount of sodium thiosulfate solution used. The measurement procedure for gravimetric titration of potassium iodate with sodium thiosulfate was validated based on determination of a reference material of known purity (potassium dichromate determined by coulometry with electrogenerated ferrous ions) using the same gravimetric method. Solutions of 0.2 and 0.5 mol/L sodium thiosulfate were stable over 17 days without stabilizer. Investigation of the dependency of titration results on the amount of sodium thiosulfate solution used showed no significant effects, no evidence of diffusion of the sample, and no effect of contamination appearing during the experiment. Precise coulometric titration of sodium thiosulfate achieved a relative standard deviation of less than 0.005% under repeating conditions (six measurements). For gravimetric titration, the results obtained for the effective purity of potassium dichromate were sufficiently close to its certified value to allow confirmation of the validity of the gravimetric titration was confirmed. The relative standard deviation of gravimetric titration for potassium iodate was less than 0.011% (nine measurements), and a redox standard with a certified value linked to SI units was developed.

Keywords: Constant-current coulometry; Stoichiometric standards; Sodium thiosulfate; Potassium dichromate; Potassium iodate; Certified reference material

1. Introduction

High reliability in reference materials has been rapidly increasing in importance owing to recent advances in R&D and industrial activities requiring highly reliable analytical data. Furthermore, it is essential that there is access to accurate and global reference materials that have traceability to the international system of units (SI units) or are in compliance with ISO guides, because mutual recognition and laboratory accreditation based on the International Organization for Standardization/International Electrotechnical Commission (ISO/IEC) 17025 quality system are becoming increasingly common, with the aim of eliminating technical barriers to international trade.

Titrimetric analysis is one of the most fundamental and precise methods for determination of a constituent based on the effective purity of reference materials for stoichiometric analysis. It is used in neutralization, redox, chelatometric, and precipitation titration processes. In Japan, eleven materials are listed as standard materials for volumetric or other analysis in the Japanese Industrial Standard (JIS K 8005) [1], and are referred to in more than 300 Japanese industrial standards, and other standards such as the Japanese Pharmacopoeia. Of these, potassium dichromate ($K_2Cr_2O_7$) and potassium iodate (KIO_3) are particularly important in stoichiometric analysis by redox reaction. $K_2Cr_2O_7$ is extremely stable and easily purified, can be used for direct titration of ions such as $S_2O_3^{2-}$ or Fe^{2+}, and is recommended as a primary standard in various countries [2–4]. Reports

* Corresponding author. Tel.: +81 3 3481 1921; fax: +81 3 3481 2900.
E-mail address: asakai-toshiaki@nite.go.jp (T. Asakai).

0039-9140/$ – see front matter © 2007 Elsevier B.V. All rights reserved.
doi:10.1016/j.talanta.2007.03.052

on coulometric titration of $K_2Cr_2O_7$ [5–10] and an investigation of drying conditions [10,11] are available, and a comparison of the certified values of reference materials obtained from different laboratories in different countries has been carried out in order to validate reliability [12].

Another useful material is KIO_3, which is used for direct titration with $S_2O_3^{2-}$, Fe^{2+}, I^-, etc. It is also recommended as a primary standard [2–4]. Iodimetry and coulometric iodimetry with electrogenerated iodine are sensitive and useful methods for standardization of redox standards [2,4,13]. Determination of arsenious oxide and antimony were studied by coulometric iodimetry, and electrical end-point determination for iodimetry was investigated [14–18]; however, there are few reports of accurate determination of purity of KIO_3. Tuthill et al. reported an assay of KIO_3 by comparison with arsenic trioxide, and achieved a precision of ±0.04% at a 95% confidence level [19].

The discussion of uncertainty, SI unit traceability and method validation, which has been gaining importance in recent years, is interesting. Ma [20] reported the determination of KIO_3 using sodium thiosulfate ($Na_2S_2O_3$) assigned by coulometry with electrogenerated iodine. Excess $Na_2S_2O_3$ including KIO_3 was back-titrated in the coulometric cell with a buffer solution (pH = 4.5); however, in terms of method validation, in such areas as dependency on sample mass, solution stability, current density and comparison among materials, this investigation was insufficient.

This paper describes an accurate measurement procedure for KIO_3 using a $Na_2S_2O_3$ solution whose effective concentration is determined by coulometry. For validation of the coulometric method, we determined the fluctuation in pH value in the coulometric cell during the experiment, the current efficiency of iodine electrogeneration, the stability of $Na_2S_2O_3$ solutions, and dependence on the amount of the sample solution used. In addition, the gravimetric titration procedure between $Na_2S_2O_3$ and KIO_3 was validated by conducting measurements using $K_2Cr_2O_7$ of known purity, determined by coulometry.

2. Experimental

2.1. Apparatus (coulometric titration)

The automated coulometric system comprised a coulometric titration cell, electrolysis unit, indicating unit, and PC/AT-based controlling system (written in LabVIEW®), which is illustrated in Fig. 1. The electrolysis unit comprised a 6181C Model-2400 constant current source (Keithley Instruments Inc., OH, USA), a custom-built timer and switching circuit (Taiyo Corp., Tokyo, Japan), Type-1794 standard resistors (10 and 100 Ω: Yokogawa Electric Corporation, Tokyo, Japan), and a Type-1281 voltmeter (Wavetek Ltd., CA, USA). The resistors used were chosen to be appropriate for different applied currents. The value of the applied current was calculated using a voltmeter and standard resistors connected in series based on Ohm's law. The working electrode was platinum foil (25 mm × 40 mm) and the cathode was a coiled platinum wire (1.2φ × 120 mm). The indicating unit, which was used as an end-point detector, comprised a Type-7651 voltage source (Yokogawa), a Type-7562 ampere meter (Yokogawa), and a Type-512 Pt–Pt indicating electrode (two plates 5 mm × 5 mm: Kyoto Electronics Manufacturing Co., Ltd., Kyoto, Japan). The end-point was detected by a dead-stop method with an applied voltage of 150 mV between two Pt plates. The same end-point determination method was used for gravimetric titration of $K_2Cr_2O_7/Na_2S_2O_3$ and $KIO_3/Na_2S_2O_3$.

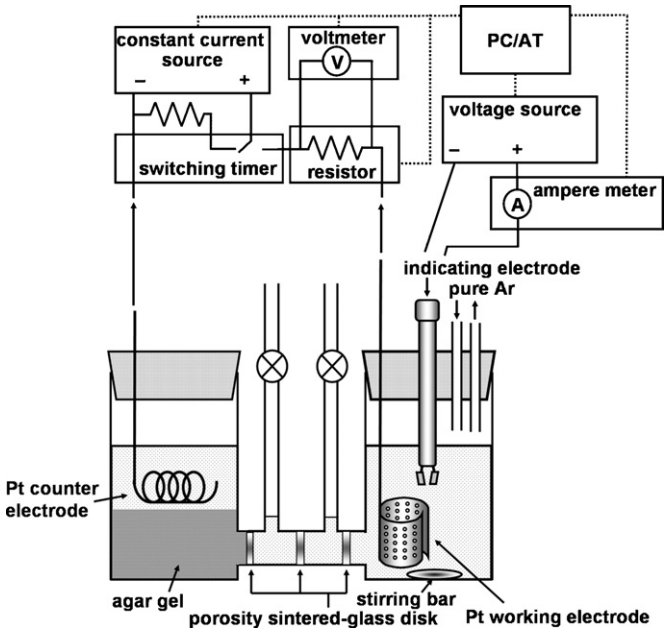

Fig. 1. Schematic diagram of the automated coulometric system.

2.2. Chemicals

Analytical reagent-grade chemicals were used unless otherwise stated. The salt bridge in the coulometric cell consisted of 100 mL of 33 g/L sodium sulfate containing 3% agar gel, and was prepared in advance. The composition of the catholyte was 0.05 mol/L potassium dihydrogen phosphate and 0.05 mol/L disodium hydrogen phosphate. The anolyte consisted of 0.05 mol/L potassium dihydrogen phosphate, 0.05 mol/L disodium hydrogen phosphate and 0.1 mol/L potassium iodide (pH about 6.8). $K_2Cr_2O_7$ (used for gravimetric method validation) and KIO_3 (for determination) were obtained from Yanagishima Pharmaceutical Co., Ltd. (Tokyo, Japan), and were compliant with JIS K 8005 (Table 1); the former was the same material used in previous research [12]. The drying conditions used were in accordance with the instructions in JIS K 8005; $K_2Cr_2O_7$ was crushed, dried at 150 °C for 1 h, and cooled in a desiccator with anhydrous magnesium perchlorate for 1 h. KIO_3 was crushed, dried at 130 °C for 2 h, and cooled in a desiccator with anhydrous magnesium perchlorate for 1 h. The molar mass and density of $K_2Cr_2O_7$ were 294.1846 g/mol (K: 39.0983(1), Cr: 51.9961(6), O: 15.9994(3)) and 2.676 g/cm^3; those of KIO_3 were 214.00097 g/mol (K: 39.0983(1), I: 126.90447(3), O: 15.9994(3)) and 3.89 g/cm^3 [21]. The density of the $Na_2S_2O_3$ solution was measured, and buoyancy corrections were applied for each sample and solution.

Table 1
Specifications of $K_2Cr_2O_7$ and KIO_3 in JIS K 8005

	K_2,Cr_2O_7	KIO_3
Assay	≥99.98% $K_2Cr_2O_7$	≥99.95% KIO3
Insoluble matter	2.0 g in 30 ml of water	1.0 g in 20 ml of water
Chloride (Cl)	≤5 ppm	–
Sulfate (SO_4)	≤0.003%	≤0.001%
Sodium (Na)	≤0.01%	≤0.005%
Calcium (Ca)	≤0.002%	–
Iron (Fe)	≤2 ppm	≤1 ppm
pH (50 g/L at 25 °C)	–	5.0–8.0
Chloride and bromide (as Cl)	–	≤0.001%
Iodide (I)	–	≤2 ppm
Nitrate (NO_3)	–	≤5 ppm
Cupper (Cu)	–	≤1 ppm
Lead (Pb)	–	≤1 ppm
Ammonium (NH_4)	–	≤5 ppm

2.3. Procedure (pH conditions and current efficiency)

$Na_2S_2O_3$ is smoothly oxidized by I_2 between pH 5 and pH 9 (reaction (1)) [2,4,22]:

$$2Na_2S_2O_3 + I_2 \rightarrow 2NaI + Na_2S_4O_6 \quad (1)$$

Rowley et al. examined coulometric titration of $Na_2S_2O_3$ with electrolytically generated iodine at various pH values [22]. Conditions at pH values higher than 9 and lower than 5 lead to prominently large titration biases. I_2 is easily hydrolyzed above pH 9, and air oxidation of I^- and production of sulfurous acid are observed below pH 5. To determine the changes in pH level in the coulometric titration cell under all experimental conditions, pH was measured after addition of 0–25 mL of ca. 0.1, 0.2 and 0.5 mol/L $Na_2S_2O_3$, and 0–16 g of KI to 100 mL of the catholyte in advance of the coulometric titration.

Marinenko et al. reported that the current efficiency for electrogeneration of I_2 from a Pt anode was approximately 100% [15]. However, it was important to investigate the current efficiency of the coulometric titration using our own Pt electrode and coulometric cell. The curve of generating current versus potential was drawn using a Type HABF-5001 potentiostat/galvanostat (Hokuto Denko Corporation, Tokyo, Japan) for 100 mL of the catholyte containing 0–3.2 g of KI. The potential was measured for the Pt generating electrode versus an Ag/AgCl reference electrode, linked with a Luggin capillary, and saturated KCl solution.

2.4. Procedure (coulometric titration)

Approximately 150 mL of the anolyte and 100 mL of the catholyte were placed in the coulometric titration cell, and dissolved air was removed by bubbling Ar gas (>99.999% purity) through for 30 min in advance. During the experiment, the anode compartment was purged with Ar gas. The end-point was detected by a dead-stop method with an applied voltage of 150 mV between two Pt plates. Pre-titration was carried out using small constant-current pulses (2 mA × 6 s) to about 40 mC after the end-point in order to eliminate impurities in the supporting electrolyte. In the main titration, 3–9 g of ∼0.2 mol/L $Na_2S_2O_3$ solution, which was weighed with a resolution of 10 μg using a Gastight™ syringe with a needle made of peak and to which a buoyancy correction was applied, was titrated using a large constant current (100 mA) to about 30 mC before the end-point. The redox assay was calculated from experimental electric charge, the sample mass, and the Faraday constant (96485.3383(83) C/mol) [23].

The determination of the effective purity of KIO_3 has two steps: determination of the reductometric factor of $Na_2S_2O_3$ by coulometry, and gravimetric titration of $Na_2S_2O_3$ and KIO_3. Therefore, it was necessary to carry out short-term stability testing of the $Na_2S_2O_3$ solution. Samples (500 mL) of ∼0.1, 0.2 and 0.5 mol/L $Na_2S_2O_3$ were stored without any stabilizer in a high-density polyethylene bottle purged with Ar gas at room temperature (approximately 22 °C) for 17 days, and the reductometric factors of solutions, 5 g of 0.1 mol/L, 2.5 g of 0.2 mol/L and 1 g of 0.5 mol/L, were measured by coulometry.

2.5. Procedure (gravimetric titration)

The titrations of $K_2Cr_2O_7$ with $Na_2S_2O_3$ and KIO_3 with $Na_2S_2O_3$ are based on the following reactions (reactions (2), (3), and (4)):

$$K_2Cr_2O_7 + 6KI + 7H_2SO_4 \rightarrow Cr_2(SO_4)_3 + 4K_2SO_4 + 7H_2O + 3I_2 \quad (2)$$

$$KIO_3 + 5KI + 3H_2SO_4 \rightarrow 3K_2SO_4 + 3H_2O + 3I_2 \quad (3)$$

$$2Na_2S_2O_3 + I_2 \rightarrow 2NaI + Na_2S_4O_6 \quad (4)$$

Prior to the titration, the time dependence of the I_2 generation after addition of H_2SO_4 to $K_2Cr_2O_7$ in reaction (2) and KIO_3 in reaction (3) with KI was investigated. Approximately 0.2 g of $K_2Cr_2O_7$, dried in accordance with JIS K 8005, was placed in a 300 mL beaker, to which 150 mL of deaerated water was added. KI (1–4 g) and 3.2 mol/L H_2SO_4 (5 mL, *conc.* H_2SO_4:water = 1:5) were added, and the indicating current was monitored, using the same end-point determination system as that of the coulometric titration. For KIO_3, approximately 0.15 g of KIO_3 and KI (0.5–3 g) were used.

In the determination of $K_2Cr_2O_7$ using $Na_2S_2O_3$, about 0.2 g of dried $K_2Cr_2O_7$ was dissolved in 150 mL water, and 3 g KI and 5 mL of 3.2 mol/L H_2SO_4 were added. The titration beaker was covered and placed in a cool dark space for 10 min, after which $K_2Cr_2O_7$ was gravimetrically titrated with ca. 0.2 mol/L $Na_2S_2O_3$ using a 25 mL Gastight™ syringe with a needle made of peak. The end-point was determined in a similar manner to that of coulometric titration, using a dead-stop method with an applied voltage of 150 mV between two Pt plates, but the titration curve was reversed. Blanks were estimated using the same indicator.

The assay of KIO_3 using $Na_2S_2O_3$ was carried out in a similar manner to the determination of $K_2Cr_2O_7$, except for the amounts used: approximately 0.15 g of KIO_3 and 2 g of KI.

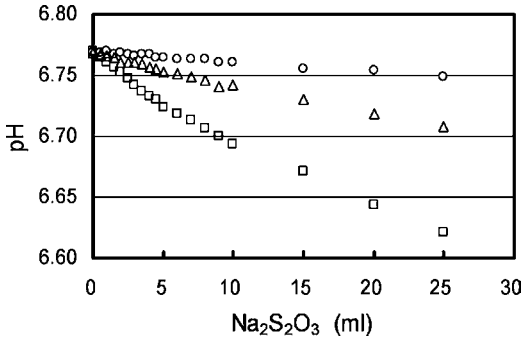

Fig. 2. Changes in pH value obtained by adding 0–25 mL of ca. 0.1 mol/L (◯), 0.2 mol/L (△) and 0.5 mol/L (□) $Na_2S_2O_3$.

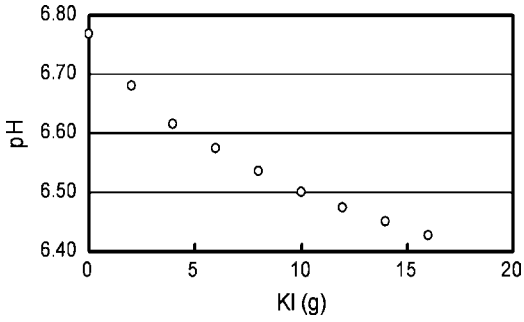

Fig. 3. Changes in pH value obtained by adding 0–16 g of KI.

3. Results and discussion

3.1. pH conditions and current efficiency

Changes in pH due to addition of 0–25 mL of ca. 0.1, 0.2 and 0.5 mol/L $Na_2S_2O_3$, and 0–16 g of KI to 100 mL of the catholyte are shown in Figs. 2 and 3, respectively. The pH values remained between 6 and 7 under all experimental conditions. In addition, after addition of 25 mL of ca. 0.1, 0.2 and 0.5 mol/L $Na_2S_2O_3$, the pH values of the solutions containing $Na_2S_2O_3$ completely oxidized by I_2 were 6.686, 6.640, and 6.550, respectively; hence, reaction (1) proceeds smoothly using this electrolyte in the coulometric titration cell.

Fig. 4 shows the relationship between current and electrode potential for catholyte solutions containing 0, 0.4, 0.8, 1.2, 1.6, 2.4 and 3.2 g of KI. The dependence of the Pt anode (25 mm × 40 mm) potential on the electrolysis current was measured with respect to an Ag/AgCl reference electrode linked to the generating electrode via a Luggin capillary and saturated KCl solution. The current efficiency for coulometric titration with electrogenerated I_2 can be calculated from the ratio of the electric currents in the electrolyte with and without KI [15,16,24]. The estimated current efficiency was approximately 100% using a phosphate buffer containing 1.2–3.2 g of KI; therefore, in the experiment, we used phosphate buffer with about 1.6 g of KI as a supporting electrolyte in order to take into account electrolyte dilution due to sample addition.

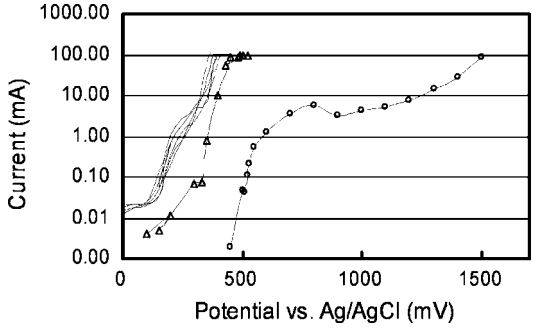

Fig. 4. Relationship between current and electrode potential. Catholyte containing 0 g KI (◯), 0.2 g KI (△) and 0.4 g–3.2 g KI (thin line).

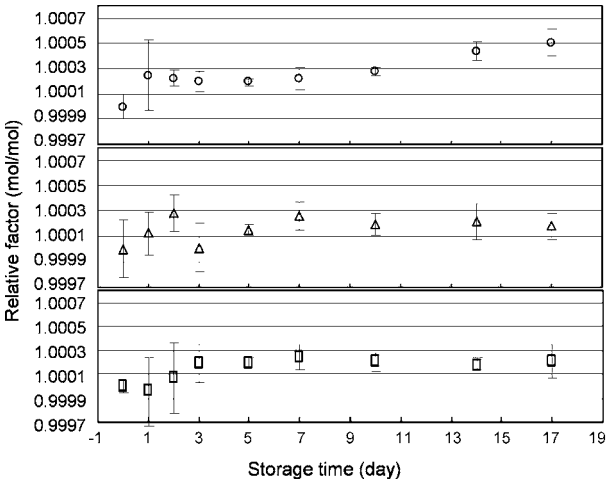

Fig. 5. Dependence of coulometric titration results on short-term storage time: ca. 0.1 mol/L (◯), 0.2 mol/L (△) and 0.5 mol/L (□) $Na_2S_2O_3$ solutions.

3.2. Determination of $Na_2S_2O_3$ by coulometry

The end-point using a dead-stop detection method was estimated by extrapolation of the plot of linear indicator current versus amount of electrolysis to the intercept (0.00 μA) after the end-point.

The results of short-term stability testing are shown in Fig. 5. $Na_2S_2O_3$ solutions of 0.2 and 0.5 mol/L were stable for 17 days except for an initial couple of days. In comparison with these, the 0.1 mol/L $Na_2S_2O_3$ solution was relatively unstable. $Na_2S_2O_3$ slowly decomposes in solution with O_2 and CO_2 according to the following reactions:

$$Na_2S_2O_3 + H_2CO_3 \rightarrow H_2S_2O_3 + Na_2CO_3 \quad (5)$$

$$H_2S_2O_3 \rightarrow H_2SO_3 + S \quad (6)$$

or

$$Na_2S_2O_3 \rightarrow Na_2SO_3 + S \quad (7)$$

$$2Na_2SO_3 + O_2 \rightarrow 2Na_2S_2O_4 \quad (8)$$

The reductometric factor of the solution containing decomposed $Na_2S_2O_3$ rises because 1 mol SO_3^{2-} reacts with 1 mol I_2 in a redox reaction. To prevent decomposition of $Na_2S_2O_3$, Cu, which acts as a catalyst for air oxidation, is precipitated as $CuCO_3$ by adding Na_2CO_3 as a stabilizer. Some manufacturers in Japan produce a $Na_2S_2O_3$ solution for titrimetry containing 0.5–0.8% of 3-methyl-1-butanol as a stabilizer instead of

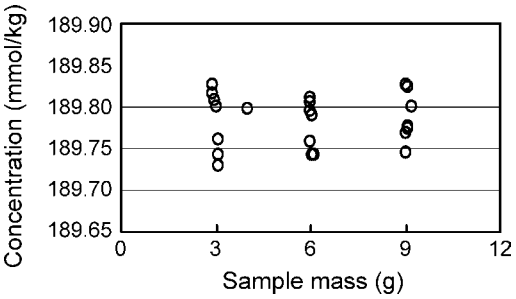

Fig. 6. Dependence of titration results on amount of $Na_2S_2O_3$ solution used.

Na_2CO_3. Small rises in the reductometric factors of the $Na_2S_2O_3$ solutions within 2–3 days after preparation are expected as a result of the initial decomposition of $Na_2S_2O_3$ caused by dissolved air. The relative instability of the 0.1 mol/L $Na_2S_2O_3$ solution may be due to the presence of a larger amount of air in the upper space of the bottle, because the amount of the solution removed for sampling was greater than for the other solutions. It was concluded that for 0.2 and 0.5 mol/L solutions, coulometric titration and gravimetric titration must be carried out within 17 days at the least estimate, but not within the first 2 days.

The dependence of the coulometric results on the amount of $Na_2S_2O_3$ used is shown in Fig. 6. This investigation confirmed that there was no loss of $Na_2S_2O_3$ as a result of diffusion into the counter-electrode chamber and no other external causes due to an increase in electrolysis time. Changes in the titration parameter did not have any significant effect on the titration results; therefore, we adopted 9 g as the most suitable amount of $Na_2S_2O_3$ in order to minimize the uncertainties due to sample weighing and end-point determination.

Finally, 0.2 mol/L $Na_2S_2O_3$ was assayed by coulometric titration for certification of KIO_3 and determination of $K_2Cr_2O_7$ for method validation. We used a 0.2 mol/L solution of $Na_2S_2O_3$ because the gravimetric titration volume was sufficiently large to minimize the uncertainties of titrant weighing and end-point determination. The uncertainties of the measurements for $Na_2S_2O_3$ are shown in Table 2 [25]. The combined expanded uncertainty for determination of $Na_2S_2O_3$ was 0.0077%, calculated based on the uncertainties of the equipment (resistor, timer, voltmeter and linearity of balance), fundamental constants (Faraday constant) and other chemical determinations (repeatability, end-point determination and dependence on the amount of the samples).

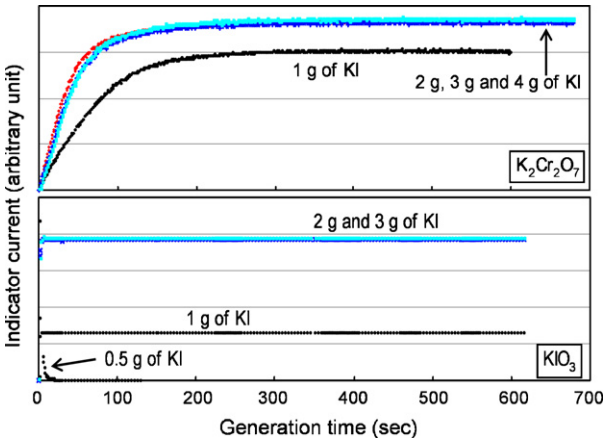

Fig. 7. Time dependence of I_2 generation on I^- concentration.

3.3. Certification of KIO_3 and determination of $K_2Cr_2O_7$ by gravimetric titration

Fig. 7 shows the time dependence of the I_2 generation in solutions containing 1–4 g of KI after the starting reaction (2) and 0.5–3 g of KI after the starting reaction (3), obtained by monitoring the indicator current based on a dead-stop method. The indicator current is not directly proportional to the concentration of I_2, and it has an upper limit; however, it is relative data regarding the rate and amount of I_2 generation. For $K_2Cr_2O_7$, it was concluded that a time of 7 min was not enough for complete generation of I_2, and while there were no differences among the 2–4 g of KI, the results for 1 g of KI were lacking. For determination of $K_2Cr_2O_7$ with $Na_2S_2O_3$, 3 g of KI and 10 min generation time were adopted as experimental conditions. In reaction (3), there were no differences among the 2–3 g of KI, however, 0.5–1 g of KI were not enough for generation of I_2 because lacking of I^- in the solution led to the deposition of solid I_2. For determination of KIO_3 with $Na_2S_2O_3$, 2 g of KI and 10 min generation time were adopted to maintain consistency with JIS K 8005 [1] and previous research [12].

The results of titration between $K_2Cr_2O_7$ and coulometrically determined $Na_2S_2O_3$ are shown in Fig. 8, and uncertainty esti-

Table 2
Uncertainty of coulometric analysis of $Na_2S_2O_3$

Uncertainty source	Relative expanded uncertainty (%, $k=2$), n = number of measurements	Note
Repeatability	0.00400, $n=6$	198.293 mmol/kg
End-point (1)	0.00144	Regarding collinear approximation
End-point (2)	0.00239	Incomplete rinsing
Faraday constant	0.0000172	96485.3383(83) C/mol
Resistor	0.00035	10 and 100-Ω
Timer	0.00121	±10 ppm + 3 ms
Voltmeter	0.0013	25 mV–10 V
Mass of $Na_2S_2O_3$	0.00534	Linearity, sample 9 g
Dependence on the amount of $Na_2S_2O_3$	0.00203	
Combined expanded uncertainty	0.00772	

Table 3
Sources of uncertainty in the determination of $K_2Cr_2O_7$ and KIO_3 with $Na_2S_2O_3$ by gravimetric titration

Uncertainty source	Relative expanded uncertainty (%, $k=2$), n = number of measurements	
	$K_2Cr_2O_7$	KIO_3
Value of $Na_2S_2O_3$	0.0111, $n=5$	0.0077, $n=6$
Repeatability	0.0106, $n=9$	0.0072, $n=9$
End-point	0.0112	0.00857
Weighing $K_2Cr_2O_7$ or KIO_3	0.00707	0.00943
Weighing $Na_2S_2O_3$	0.00229	0.00229
Molar mass of $K_2Cr_2O_7$ or KIO_3	0.000953	0.000489
Blank	0.00163	0.000674
Combined expanded uncertainty	0.0205	0.0167

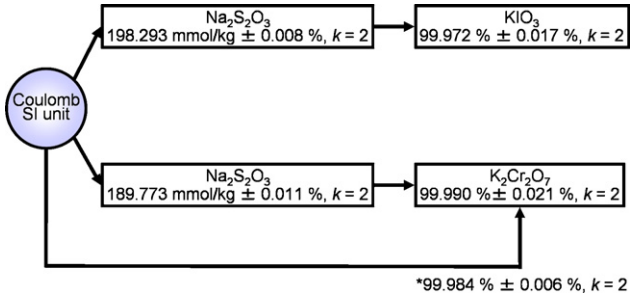

Fig. 8. Results of determination for $K_2Cr_2O_7$ and KIO_3. (*) See reference [12].

mates are shown in Table 3. The titration trial was carried out one day after the coulometric determination. The uncertainties were derived from the following: repeatability of titration, end-point determination (fluctuation of collinear approximation), sample weighing (linearity of balance), molar mass of $K_2Cr_2O_7$, and blank (correction, fluctuation in blank); the combined expanded uncertainty was 0.021% ($k=2$).

The effective purity of $K_2Cr_2O_7$ was $99.984\% \pm 0.006\%$ ($k=2$), which was directly determined by coulometry with electrogenerated ferrous ions [12]. The assay of $K_2Cr_2O_7$ by gravimetric titration based on the reductometric factor of $Na_2S_2O_3$ determined by coulometry was $99.990\% \pm 0.021\%$ ($k=2$); these results were sufficiently close to the certified value to confirm the validity of gravimetric titration between $K_2Cr_2O_7$ and $Na_2S_2O_3$ and the coulometric titration of $Na_2S_2O_3$. The results and uncertainty estimations on KIO_3 are shown in Fig. 8 and Table 3, respectively. The assay of KIO_3 was $99.972\% \pm 0.017\%$ ($k=2$) determined in a similar manner to $K_2Cr_2O_7$, and KIO_3 was developed as a redox standard with a certified value linked to SI units.

4. Conclusions

Redox reference materials were studied by coulometric and gravimetric titration. The accuracy of the coulometric method was investigated by examining the areas of dependency on sample mass, current efficiency of I_2 electrogeneration and stability of $Na_2S_2O_3$ solutions. For the gravimetric titration method, validity was ascertained using $K_2Cr_2O_7$ of known purity. The results presented for $Na_2S_2O_3$, $K_2Cr_2O_7$ and KIO_3 were established with high accuracy, SI unit traceability, and uncertainty.

References

[1] Japanese Industrial Standard (JIS), K 8005, Reference Materials for Volumetric Analysis, Japanese Standards Association, 2006.
[2] I.M. Kolthoff, R. Belcher, Volumetric Analysis, vol. 3, Titration Methods: Oxidation-reduction Reactions, Interscience Publishers, Inc., New York, 1957, pp. 169–243 and 449–473.
[3] V.A. Stenger, Anal. Chem. 23 (1951) 1540.
[4] I.M. Kolthoff, E.B. Sandell, E.J. Meehan, S. Bruckenstein, Quantitative Chemical Analysis, The Macmillan Company Collier-Macmillan Limited, London, 1969 (Chapter 44).
[5] J. Knoeck, H. Diehl, Talanta 16 (1969) 181.
[6] G. Marinenko, J.K. Taylor, J. Res. NBS (Phys. Chem.) 67A (1963) 453.
[7] K.W. Pratt, Anal. Chim. Acta 289 (1994) 125.
[8] M. Mariassy, L. Vyskocil, A. Mathiasova, Accredit. Qual. Assur. 5 (2000) 437.
[9] C.E. Champion, G. Marinenko, J.K. Taylor, W.E. Schmidt, Anal. Chem. 42 (1970) 1210.
[10] T. Yoshimori, Talanta 22 (1975) 827.
[11] T. Yoshimori, N. Sakaguchi, Talanta 22 (1975) 233.
[12] T. Asakai, Y. Kakihara, Y. Kozuka, S. Hossaka, M. Murayama, T. Tanaka, Anal. Chim. Acta 567 (2006) 269.
[13] S. Popoff, J.L. Whitman, J. Am. Chem. Soc. 47 (1925) 2259.
[14] J.J. Lingane, A.J. Bard, Anal. Chim. Acta 16 (1957) 271.
[15] G. Marinenko, J.K. Taylor, Anal. Chem. 39 (1967) 1568.
[16] A. Hioki, M. Kubota, A. Kawase, Analyst 117 (1992) 997.
[17] W.J. Ramsey, P.S. Farrington, E.H. Swift, Anal. Chem. 22 (1950) 332.
[18] C.W. Foulk, A.T. Bawden, J. Am. Chem. Soc. 48 (1926) 2045.
[19] S.M. Tuthill, R.S. Sprague, W.C. Stoecker, Anal. Chem. 36 (1964) 1994.
[20] L. Ma, Accredit. Qual. Assur. 7 (2002) 163.
[21] Atomic Weights of the Elements 2001 (IUPAC technical report), Pure Appl. Chem. 75 (2003) 1107.
[22] K. Rowley, E.H. Swift, Anal. Chem. 26 (1954) 373.
[23] P.J. Mohr, B.N. Taylor, Rev. Mod. Phys. 77 (2005) 1.
[24] G. Marinenko, J.K. Taylor, J. Res. NBS (Phys. Chem.) 67A (1963) 402.
[25] BIPM, IEC, IFCC, ISO, IUPAC, IUPAP and OIML, Guide to the expression of uncertainty in measurement, first ed., Geneva, 1995.

Available online at www.sciencedirect.com
ScienceDirect
Talanta 73 (2007) 394–399
Talanta
www.elsevier.com/locate/talanta

Short communication

Improvement of analytical performances of a disposable electrochemical immunosensor by using magnetic beads

S. Centi *, S. Laschi, M. Mascini

Università degli Studi di Firenze, Dipartimento di Chimica, Via della Lastruccia 3, 50019 Sesto Fiorentino, FI, Italy

Received 11 January 2007; received in revised form 9 March 2007; accepted 15 March 2007
Available online 24 March 2007

Abstract

A comparison of two electrochemical immunosensing strategies for PCBs detection, based on the use of two different solid phases, is here discussed. In both cases, carbon-based screen-printed electrodes (SPEs) are used as transducers in a direct competitive immunoassay scheme, where PCBs in solution compete with the tracer PCB28-alkaline phosphatase (AP) labeled for antibodies immobilized onto the solid-phase.

In the standard format (called EI strategy), SPEs are both the solid-phase for immunoassay and electrochemical transducers: in this case the immunochemical reaction occurs onto the working electrode. Finally, the enzymatic substrate is added and an electroactive product is generated and detected by electrochemical measurement. In order to improve the performances of the system, a new approach (called EMI strategy) is developed by using functionalized magnetic beads as solid phase for the competitive assay; only after the immunosensing step they are captured by a magnet onto the working surface of the SPE for the electrochemical detection.

Experimental results evidenced that the configuration based on the use of separate surfaces for immunoassay and for electrochemical detection gave the best results in terms of sensitivity and speed of the analysis. The improvement of analytical performances of the immunosensor based on EMI strategy was also demonstrated by the analysis of some spiked samples.

Keywords: Screen-printed electrodes; Magnetic beads; PCB; Competitive assay; Electrochemical detection

1. Introduction

The development of rapid, inexpensive, sensitive, high sample throughput and on-site analytical strategies, which can be used as screening system to rapidly detect polychlorinated biphenyls (PCBs) in food and environmental samples, is an important issue [1,2]. Immunoassays provide sensitive and reliable screening techniques for detecting trace amount of chemicals as PCBs for both laboratory and field analysis. Among the high number of immunoassay techniques, the Enzyme-Linked ImmunoSorbent Assays (ELISAs) combined with a colorimetric end point measurement are the most widely used [3,4].

An alternative but interesting approach is the use of electrochemical immunosensor technology. Electrochemical sensors have revolutionized modern analysis because of their technical simplicity and speed in response by the direct transduction to an electronic equipment [5]. Mass-fabrication, low cost and decentralized in field analysis are other important features of electrochemical sensors. Electrochemical immunosensors based on screen-printed electrodes have recently been applied to the detection of environmental pollutants such as PCBs, PAHs, pesticides [6–9] and of important molecules in clinical and food field [10–12]. Electrochemical immunosensors are based on the use of screen-printed electrodes as solid-phase for the immunoassay and as electrochemical transducers: antibody or antigen molecules are directly immobilized at the sensor surface (transducer) and one of these species is enzyme-labeled in order to generate an electroactive product which can be detected at the screen-printed electrodes surface. Therefore, this approach is very interesting because a single surface is used for both immunochemical reaction and electrochemical revelation, by simplifying all the procedure.

A different approach can involve the use of screen-printed electrodes for the transduction step and the use of another physical support for the affinity reaction [13]. Actually the use of

* Corresponding author. Tel.: +39 0554573311.
E-mail address: sonia.centi@unifi.it (S. Centi).

0039-9140/$ – see front matter © 2007 Elsevier B.V. All rights reserved.
doi:10.1016/j.talanta.2007.03.025

the electrode surface as solid phase as well as electrochemical transducer can give some problems: a shielding of the surface by biospecifically bound antibody molecules can cause hindrance of the electron transfer, resulting in a reduced electrochemical signal. The use of micro-particles (micro-beads) as solid phase is a relatively new possibility, widely documented in literature [13–18]. Various kinds of beads can be used in electrochemical biosystems. The beads range from non-conducting (glass, etc.), conducting (graphite particles) to magnetic materials. Particles are available with a wide variety of surface functional groups and size and have the possibility of reaction kinetics similar to those found in free solution. Graphite and magnetic particles represent the most commonly used beads in bioelectroanalytical systems. Magnetic particles respond to an applied magnetic field and re-disperse upon removal of the magnet. They consist of 36–40% magnetite dispersed within a copolymer matrix consisting of styrene and divinyl-benzene. Their binding capacity varies with the bead size, composition and the size of the binding ligand. There is a general consensus that the use of magnetic beads greatly improves the performance of the immunological reaction, due to an increase in the surface area, as well as the faster assay kinetics achieved because the beads are in suspension and the analytical target does not have to migrate very far [19].

This approach separates the steps related to the immunoreaction from the electrochemical detection step; for this reason, the working electrode surface is easily accessible by the enzymatic product, which diffuses onto the bare electrode surface [20]. Using this strategy, finding the optimum conditions for both the immunoassay on the magnetic beads and the electrochemical detection on the transducer (carbon screen-printed electrodes) is much easier than in the usual one (electrode) surface systems, because optimum conditions for immunoassay do not conform with those for electrochemical detection and vice versa.

In our knowledge, a comparison of analytical performances of immunosensors developed using those two different strategies is not yet reported. In this work, an electrochemical immunosensor (EI) and an electrochemical magneto-immunosensor (EMI) for detection of PCBs are compared in terms of sensitivity, reproducibility and analysis times. Both strategies are based on the development of a direct competitive assay using alkaline phosphatase (AP) as enzymatic label. Carbon-based screen-printed electrodes (SPEs) are used as transducers for the evaluation of the extent of the immunochemical reaction and the electrochemical detection is thus achieved through the addition of the AP substrate (α-naphthyl-phosphate) and by the use of differential pulse voltammetry (DPV) as electrochemical technique.

The configuration based on the use of two surfaces, magnetic beads for immunoassay and screen-printed electrodes for electrochemical detection, gave the best analytical performances in terms of sensitivity and speed of the analysis. However, the EI strategy remains very attractive because a single surface is used for both immunochemical reaction and electrochemical revelation, by simplifying all the procedure. Both strategies were also applied to the analysis of some spiked samples, by demonstrating their suitability for real samples analysis, but evidencing also their difference in the sensitivity.

2. Experimental

2.1. Chemicals and immunochemicals

Bovine IgG (bIgG), serum albumine bovine (BSA), IgG anti-sheep, α-naphthyl-phosphate (NP), diethanolamine (DEA) and polyoxyethylene-sorbitanmonolaurate (Tween 20) were purchased from Sigma (Milan, Italy). Methanol, KCl, $MgCl_2$, NaH_2PO_4, Na_2HPO_4, $NaHCO_3$, and other reagents were purchased from Merck (Milan, Italy). Aroclor 1016, 1242 and 1248 mixtures were purchased from AccuStandard Inc. (New Haven, USA).

Sheep polyclonal antibodies against PCB28 (sIgG anti-PCB28) and the tracer solution containing PCB28-alkaline phosphatase conjugate (PCB28-AP) were provided by Prof. M. Fránek, Veterinary Research Institute, Brno, Czech Republic.

2.2. Materials and equipment

Magnetic beads coupled with protein G were obtained from Dynal Biotech (Milan, Italy). These are uniform, superparamagnetic polymer particles with protein G covalently coupled to the surface and have got a diameter of 2.8 μm (CV < 3%). The main advantage of using this kind of particles is, together with the potential wide applicability of this immunosensing approach, the proper orientation of the antibody binding sites. The coupling of antibodies to magnetic beads protein G-coated was achieved through the specific affinity to protein G for the Fc part of the sheep antibody molecules.

All solutions were prepared using water from a Milli-Q Water Purification System (Millipore, UK). The electrochemical cells were planar three electrode strips formed by a carbon working electrode, a carbon counter electrode and a silver pseudo-reference electrode. The electrodes were screen-printed in-house using a DEK 248 screen-printing machine (DEK, Weymouth, UK). Silver based (Electrodag PF-410) and graphite-based (Electrodag 423 SS) polymeric inks were obtained from Acheson (Milan, Italy); the insulating ink (Vinylfast 36-100) was from Argon (Lodi, Italy). A polyester flexible film (Autostat CT5), obtained from Autotype (Milan, Italy), was used as printing substrate.

Electrochemical measurements were performed using a μAutolab type II PGSTAT with a GPES 4.9 software package (Metrohm, Rome, Italy). All the measurements were carried out at room temperature by using differential pulse voltammetry (DPV) with the following parameters: range potential 0/+600 mV, step potential 7 mV, modulation amplitude 70 mV, standby potential 200 mV, interval time 0.1 s.

The sample mixer with 12-tube mixing wheels and the magnets were purchased from Dynal Biotech (Milan, Italy).

PCBs-free marine sediment extracts were obtained by the Fisheries Research Service of Marine Laboratory (FRS-ML), Aberdeen, Scotland (UK). They were collected, extracted by Soxhlet and certified as PCB-free by GC-ECD in provenance laboratory.

2.3. Buffer

The buffers used for EI strategy were the following:

(a) 0.1 M carbonate buffer (CB) pH 9.6 for antibody dilutions.
(b) 10 mM phosphate buffer (PBS) pH 7.4 containing 1% methanol and 4% BSA for affinity reaction.
(c) 10 mM phosphate buffer pH 7.4 containing 0.1% of Tween 20 (PBS-T) for washing steps.
(d) 0.1 M diethanolamine buffer (DEA) pH 9.6 with 0.1 M KCl and 1 mM $MgCl_2$.

Buffers and solutions used for EMI approach were:

(e) 0.1 M sodium-phosphate solution pH 5 for washing and immobilization steps.
(f) 0.3 mM sodium-phosphate buffer pH 7.2 containing NaCl 5 mM and methanol 1% (v/v) (PBS buffer) for affinity reaction.
(g) DEA buffer as reported above.

2.4. Immunoassay scheme

EI and EMI strategies were developed on the basis of a competitive assay scheme (Fig. 1) and carbon screen-printed electrodes and magnetic beads were, respectively, the solid support for the immunoassay. Both the solid phases were modified by immobilization of antibodies against PCB28. A competition was then performed by incubating the optimized tracer dilution and the sample.

After molecular recognition, the extent of the affinity reaction was evaluated by addition of the enzymatic substrate (NP), which was transformed in an electroactive product and oxidized at the electrode surface.

The competitive curves were analyzed with four-parameter logistic equation using a proper software (Graph Pad, Prism 4 for Windows, Graph Pad Software Inc.) according to the formula $Y = A + ((B - A)/(1 + 10^{[\log EC_{50} - X]^{\text{Hill slope}}}))$, where A is the Y-value at the bottom plateau of the curve, B the Y-value at the top plateau of the curve, EC_{50} the antigen concentration necessary to halve the current signal and Hill slope is the slope of the linear part of the curve.

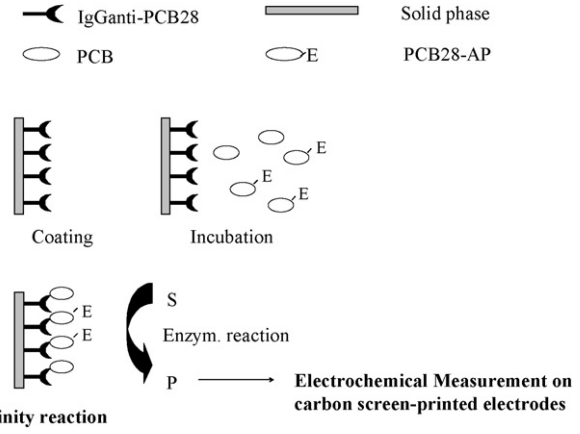

Fig. 1. Competitive immunoassay scheme used in both analytical strategies.

2.4.1. Electrochemical immunosensor (EI) strategy

Carbon SPEs were coated with 10 μL of CB buffer containing 5 μg/mL of sIgG anti-PCB28. After 1 h at room temperature, each electrode was rinsed with 150 μL of PBS-T and dried carefully. Once prepared, these modified electrodes can be stored at +4 °C in a dried chamber for several days without a decrease in the sensitivity. A competition solution was prepared by mixing a PCBs standard solution with a suitable volume of the tracer solution. Ten microliters of this solution were then deposited onto the working electrode and incubated for 1 h at room temperature and then the electrode was rinsed again with 150 μL of PBS-T buffer and covered with 60 μL of enzymatic substrate solution (NP 1 mg/mL in DEA buffer). After 5 min, the DPV measurement was performed.

2.4.2. Electrochemical magneto-immunoassay (EMI) strategy

After each incubation or washing step, the magnetic beads were separated from the supernatant by placing the tubes in a magnet separator until the beads migrated to the tube sides and the liquid was clear.

Magnetic beads coupled with protein G were washed with 500 μL solution (e) to remove the NaN_3 preservative, as advised by the manufacturer. A suspension of 10 μL of the beads was introduced in a tube containing 500 μL of antibody solution (IgG anti-PCB28) 100 μg/mL prepared in solution (e). *After 20 min of incubation time under stirring in the sample mixer*, each tube was positioned on a magnet holding block. Once the beads were deposited on the bottom of the test tube, the supernatant was removed and the beads were then washed twice with 500 μL of solution (e). Each washing step consisted of a re-suspension of the beads in the washing solution for 2 min, followed by the separation with the magnet holding block to remove the supernatant. In this way, antibody-coated beads were obtained.

The competition was performed by mixing 50 μL of suspension containing antibody-coated beads with 940 μL of sample solution and 10 μL of tracer solution (PCB28-AP). The competitive reaction was left to proceed with gentle shaking for 20 min at room temperature. The beads were washed two times and finally the beads were re-suspended in 100 μL of working assay buffer. Ten microliters of the suspension were transferred onto the surface of the working electrode. To better localize the beads onto the electrode, the magnet holding block was placed on the bottom part of the electrode. Then 60 μL of a solution containing the enzymatic substrate (NP) 1 mg/mL in DEA buffer were deposited on the screen-printed strip, making attention to close the electrochemical cell. After 5 min, the enzymatic product was finally detected by DPV.

2.5. Samples treatment

Marine sediment extracts were spiked to obtain contaminated samples. At this purpose, 1 mL of each sample was evaporated in order to remove the organic solvent and then reconstituted in the same volume of PBS buffer. Subsequently, 10 μL of the standard solution (Aroclor mixture) were added in order to obtain final

concentrations in the range: 0.5–1000 ng/mL. Afterwards, the competition reaction was performed.

3. Results and discussion

3.1. Assay optimization

3.1.1. EI strategy

Solid-phase modification is a critical point in the development of an electrochemical immunosensor. Two factors have to be considered: the sensitivity of the immunosensor against the target analyte and the non-specific adsorption onto the working surface.

The first point depends on the quantity of antibodies present in the solid-phase and on the ratio between antibody and tracer, whereas the second effect can be minimized by the use of a blocking agent. However, it is important that the blocking agent does not isolate the electrode surface for electrochemical measurement. Thus, some experiments were performed to evaluate the non-specific adsorption using IgG anti-sheep, bovine serum albumine (BSA) and bovine IgG (bIgG) as different blocking agents.

Immunoglobulins G anti-sheep have got affinity for the Fc fraction of sheep antibodies. Two effects could be obtained using this blocking agent: the blocking of the electrode surface and the orientation of the antigenic sites of antibodies towards the solution. The use of BSA as blocking agent is very common in ELISA: such blocking agent can be directly added to the buffer containing the sample. The use of non-specific IgG (bovine IgG) is a method called *pre-coating method*, that provides for the deposition of these onto the solid-phase followed by the co-adsorption of antibodies against the target molecule.

Ten microliters of blocking agent (IgG anti-sheep or bIgG) solution 1 μg/mL in buffer (a) were deposited onto graphite surface. After 1 h at +4 °C, the working electrode surface was washed with 10 μL of PBS-T buffer. Then, 10 μL of sheep IgG anti-PCB28 (sIgG anti-PCB28) 5 μg/mL in buffer (a) were deposited on the working electrode and incubated 1 h at room temperature. Then, 10 μL of buffer (b) (without BSA) containing the enzyme tracer diluted 1:15,000 respect to the stock solution were deposited on the working electrode surface and allowed to incubate 1 h at room temperature. After washing, the electrochemical measurement was performed depositing 200 μL of NP 1 mg/mL in buffer (d) onto the strip in order to cover all the electrochemical cell. After 5 min of incubation time, the DPV measurement was carried out.

A slightly different procedure was adopted by using BSA as blocking agent. In this case BSA is not deposited onto the working surface but added by using the buffer (b) containing 5% BSA. All the others steps were the same. Moreover, the experiments were repeated without the immobilization of sIgG.

The results obtained are shown in Fig. 2, where the comparison between the signal obtained in presence and in absence of sIgG is shown for the three different blocking agents. Using BSA, a significant difference of signal was measured in both cases, whereas using IgG anti-sheep and bIgG the signals were similar. Thus, further experiments were performed adding directly 5% of BSA in buffer (b).

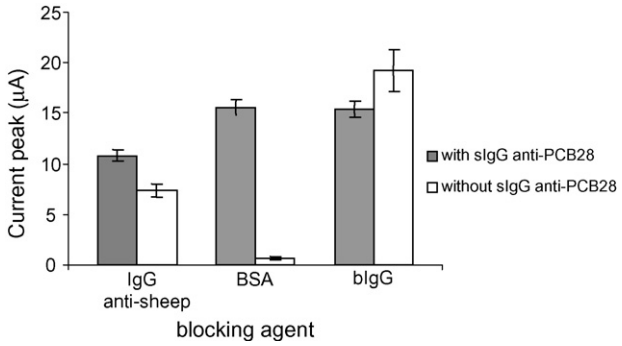

Fig. 2. Optimization of the blocking agent using EI strategy. Such choice was carried out comparing the specific signals and those non-specific measured using different blocking agents.

The tracer concentration was another important parameter to optimize: this has to be in limiting amount, that means in a quantity such to saturate the antibodies immobilized on the solid phase. This concentration was optimized by incubation different dilutions of PCB28-AP on electrodes modified by adsorption of sIgG anti-PCB. In Fig. 3 the binding curve is shown: for dilutions 1:10,000 and 1:5000 the current reaches a steady-state and it means that all antibodies sites are saturated. Thus, 1:15,000 was chosen as dilution to perform the competition.

3.1.2. EMI strategy

The best conditions for the development of the competitive assay on the magnetic beads were optimized as reported in [13]. Experiments were performed using 20 min for the antibody immobilization on the particles and for carrying out the competition and choosing 1:1000 as the best dilution of PCB28-AP for competition. *The ratio between the beads stock solution and the re-suspension volumes was chosen by evaluating the best results in terms of sensitivity and reproducibility of the assay (data not shown). At these conditions, no diffusion effect due to the beads amount was observed in the electrochemical measurement.*

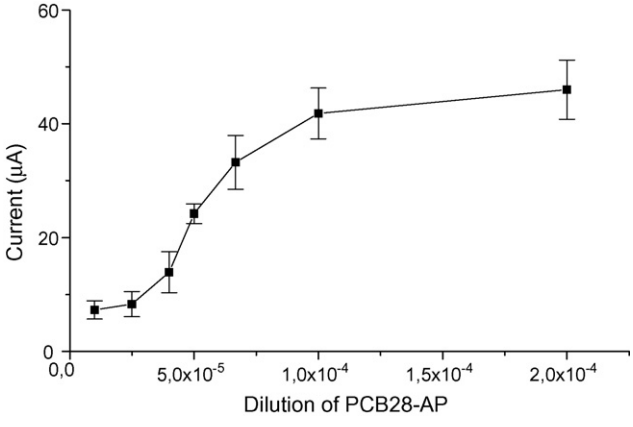

Fig. 3. Optimization of the tracer dilution using EI strategy.

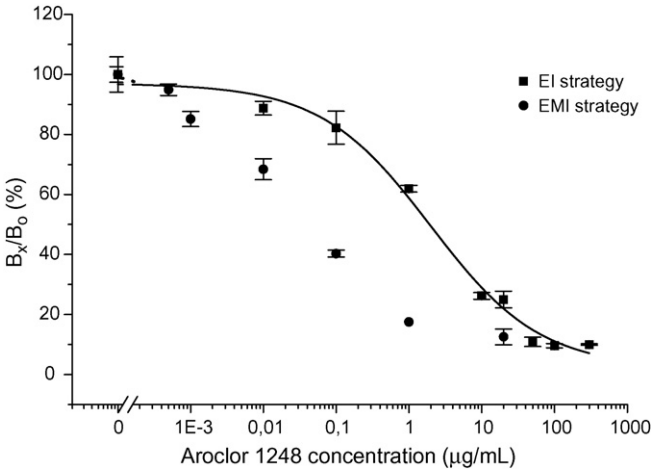

Fig. 4. Comparison between the calibration curves of Aroclor 1248 performed using EI and EMI strategies.

3.2. Comparison between EI and EMI strategies

3.2.1. Calibration curves

A comparison between the two strategies was carried out by detecting some Aroclor mixtures. Calibration curves for Aroclor 1248, 1242 and 1016 were performed with both methods. In Fig. 4 the two curves for Aroclor 1248 mixture, reported as binding percentage B_x/B_o (%), are compared. As it can be seen, the sensitivity obtained by EMI strategy was of two order degrees higher than that obtained with the EI approach; a DL of 0.4 ng/mL for Aroclor 1248 mixture was found using the EMI approach, while a DL of 40 ng/mL was measured using the EI approach. A similar behavior was observed for other Aroclor mixtures and the results are reported in Table 1.

The average CVs were calculated for all cases, and the obtained values were very similar and around 9%. For both methods, the non-specific binding was evaluated by performing the immunoassay in absence of antibodies against PCB. The signal without antibodies was very low and independent on the mixture concentration (data not shown).

From the data comparison it emerges that, using the EMI strategy, detection limits for all PCB mixtures were lower than approximately two orders of magnitude. The use of magnetic beads greatly improves the yield of the affinity reaction, because the surface area of the solid phase is greater and the assay kinetics are faster. Moreover, during the electrochemical measurement the working electrode surface is easily accessible by the enzymatic product, which diffuses onto a bare electrode surface.

The measurement time was another important point: for the EMI strategy, the time necessary to perform the analysis was faster (45 min, including the antibody immobilization onto the beads) respect to 125 min for the EI strategy. Thus, the EMI strategy allowed to obtain a faster and a more sensitive immunochemical detection respect to the strategy which employs a single surface as a screen-printed electrode. For this reason, this approach can be advised in the development of different electrochemical immunosensors for various analytical purposes.

Table 1
Analytical results for some Aroclor mixtures obtained by using both EI and EMI strategies

Mixture	Methods	Concentration range (µg/mL)	DL (ng/mL)	IC_{50} (ng/mL)	CV (%)	Measure time (min)
Aroclor 1248	EI	$0.1–1.0 \times 10^2$	40	2×10^{-3}	7	125
	EMI	1.0×10^{-4}–20	0.4	24	6	45
Aroclor 1242	EI	$0.1–1.0 \times 10^2$	50	6×10^{-3}	6	125
	EMI	1.0×10^{-4}–20	0.5	8	10	45
Aroclor 1016	EI	$0.1–1.0 \times 10^2$	200	5×10^{-3}	9	125
	EMI	1.0×10^{-4}–20	0.8	94	7	45

The detection limit of the method (DL) was calculated by evaluation of the mean of the blank solution (not containing PCBs) response minus two times the standard deviations.

Table 2
Results obtained from the analysis of marine sediment extracts

Sample code	Spiked aroclor mixture	Spiked concentration (ng/mL)	EI response (B_x/B_o (%))	EMI response (B_x/B_o (%))
1	Aroclor 1242	1000	70 ± 6	11 ± 4
2	Aroclor 1242	10	91 ± 4	51 ± 2
3	Aroclor 1242	1	100 ± 5	86 ± 3
4	Aroclor 1242	0.5	100 ± 7	92 ± 3
5	Aroclor 1248	1000	59 ± 6	17 ± 3
6	Aroclor 1248	10	84 ± 5	68 ± 3
7	Aroclor 1248	1	100 ± 6	83 ± 3
8	Aroclor 1248	0.5	100 ± 6	95 ± 3
9	Aroclor 1016	1000	75 ± 9	16 ± 2
10	Aroclor 1016	10	87 ± 6	73 ± 6
11	Aroclor 1016	1	100 ± 4	89 ± 5
12	Aroclor 1016	0.5	100 ± 6	94 ± 4

A comparison between the signals obtained using EI and EMI strategies is reported. The points correspond to the B_x/B_o percentage ±S.D. calculated for $n = 3$ repetitions.

3.2.2. Samples analysis

Marine sediment extracts were spiked with different concentrations and mixtures of PCBs and analyzed using both strategies. The obtained results are shown in Table 2. The measured signals are expressed as residual percentage respect to the blank signal, which is assumed as 100%. Non-spiked samples were also analyzed in order to evaluate the potential matrix effect. This one was experimentally demonstrated that it does not affect the measure (data not shown).

For both systems the signal measured for each sample was in accordance with the spiked concentrations: precisely, the percentage signal measured for Aroclor 1242 formulation in sample 1 was lower than the value obtained for samples 2–4, containing the same mixture at a lower concentration (10, 1 and 0.5 ng/mL versus 1000 μg/mL).

All spiked samples gave a signal decrease when analyzed by EMI strategy, whereas the samples 3, 4, 7, 8, 11 and 12, e.g., the samples containing the lowest concentration of the Aroclor mixture (0.5 or 1 ng/mL), resulted as not contaminated using EI strategy. Thus, these results demonstrate that both systems are suitable for PCB detection in samples, but that the performances of the EMI assay allow to detect lower PCB quantities with a high reproducibility.

4. Conclusions

The aim of this paper is the comparison between the analytical performances of two immunosensing strategies applied to PCBs detection. These are based on the use of different solid phases for the immunoassay development. The first strategy involves the use of disposable carbon screen-printed electrodes as solid support for the immunoassay development and as transducers; whereas the second strategy involves the coupling of magnetic beads which are used as solid phase for the molecular recognition to disposable carbon screen-printed electrodes. All the parameters which can influence the immunoassay development have been optimized. This optimization was of paramount importance, since the performances of the immunoassay performed onto different solid supports (screen-printed electrodes or magnetic beads) can vary considerably.

From the comparison of experimental data it emerges that, both strategies were suitable for PCB detection, even if the use of the EMI strategy gave the best results: the detection limits for all analyzed mixtures were lower than approximately two orders of magnitude respect with those obtained using EI strategy. Actually, the EMI strategy allowed to obtain a faster and a more sensitive immunochemical detection respect to the strategy which employs a single surface as a screen-printed electrode. For this reason, this approach is advised in the development of different electrochemical immunosensors for analytical purposes.

The good performances of the EMI strategy in the detection of PCBs in marine sediment extracts suggests the possibility of using the proposed approach for environmental investigations.

References

[1] R. Angulo, P. Martínez, M.L. Jodral, Food Chem. Toxicol. 37 (1999) 1081–1088.
[2] J.G. Vos, E. Dybing, H.A. Greim, O. Ladefoged, C. Lambré, J.V. Tarazona, I. Brandt, A.D. Vethaak, Crit. Rev. Toxicol. 30 (2000) 71–133.
[3] G. Fillmann, T.S. Galloway, R.C. Sanger, M.H. Depledge, J.W. Readman, Anal. Chim. Acta 461 (2002) 75.
[4] J.C. Johnson, J.M. Van Emon, A.N. Clarke, B.N. Wamsley, Anal. Chim. Acta 428 (2001) 191.
[5] D.R. Thévenot, K. Toth, R.A. Durst, F.S. Wilson, Biosensor Bioelectron. 16 (2001) 121–131.
[6] S. Laschi, M. Mascini, G. Scortichini, M. Fránek, M. Mascini, J. Agric. Food Chem. 51 (2003) 1816–1822.
[7] K.A. Fähnrich, M. Pravda, G.G. Guilbault, Biosensor Bioelectron. 18 (2003) 73–82.
[8] S. Laschi, M. Mascini, Ann. Chim. 92 (2002) 425–433.
[9] S. Hleli, C. Martelet, A. Abdelghani, N. Burais, N. Jaffrezic-Renault, Sensor Actuator B: Chem. 113 (2) (2006) 711–717.
[10] C. Valat, B. Limoges, D. Huet, J.L. Romette, Anal. Chim. Acta (2000) 187–194.
[11] L. Micheli, R. Grecco, M. Badea, D. Moscone, G. Palleschi, Biosensor Bioelectron. 21 (4) (2005) 588–596.
[12] L. Micheli, R. Rodoi, R. Guarrina, R. Massaud, C. Bala, D. Moscone, G. Palleschi, Biosensor Bioelectron. 20 (2) (2004) 190–196.
[13] S. Centi, S. Laschi, M. Fránek, M. Mascini, Anal. Chim. Acta 538 (2005) 205–212.
[14] S. Solé, A. Merkoçi, S. Alegret, Trends Anal. Chem. 20 (2) (2001).
[15] E. Paleček, R. Kizek, L. Havran, S. Billova, M. Fojta, Anal. Chim. Acta 469 (2002) 73–83.
[16] Alefantis, P. Grewal, J. Ashton, A.S. Khan, J.J. Valdes, V.G. Del Vecchio, Molecul. Cell. Probes (2004) 1–4.
[17] M. Dequaire, C. Degrand, B. Limoges, Anal. Chem. 71 (1999) 2571–2577.
[18] D. Yu, B. Blankert, E. Bodoki, S. Bollo, J.C. Viré, R. Sandulescu, A. Nomura, J.M. Kauffmann, Sensor Actuator B 113 (2006) 749–754.
[19] E. Zacco, M.I. Pividori, S. Alegret, R. Galve, M.P. Marco, Anal. Chem. 78 (2006) 1780–1788.
[20] V. Kourilov, M. Steinitz, Anal. Biochem. 311 (2002) 166–170.

Available online at www.sciencedirect.com
ScienceDirect
Talanta 73 (2007) 358–365
Talanta
www.elsevier.com/locate/talanta

Organic vapour sensing using localized surface plasmon resonance spectrum of metallic nanoparticles self assemble monolayer

Chia-Sheng Cheng, Yu-Quan Chen, Chia-Jung Lu *

Department of Chemistry, Fu-Jen Catholic University, 510 Chung Cheng Road, Hsingchuang, Taiwan, ROC

Received 12 December 2006; received in revised form 28 March 2007; accepted 28 March 2007
Available online 7 April 2007

Abstract

The response of localized surface plasmon resonance (LSPR) spectra of gold and silver nanoparticles, and gold nanoshells to organic vapors was investigated. The surface area of nanomaterials was sufficiently high for quantitative adsorption of volatile organic compounds (VOCs). Surface adsorption and condensation of VOCs caused the environmental refractive index to increase from $n = 1.00$ in pure air to as high as $n = 1.29$ in near saturated toluene vapor. The extinction and wavelength shift of the LSPR spectra were very sensitive to changes in the surface refractive index of the nanoparticles. Responses of the LSPR band were measured with a real-time UV–vis spectrometer equipped with a CCD array detector. The response of silver nanoparticles to organic vapors was most sensitive in changes in extinction, while gold nanoshells exhibited red-shifts in wavelength (∼250 nm/RIU) when exposed to organic vapors. The LSPR spectral shifts primarily were determined by the volatility and refractive indices of the organic species. The T_{90} response time of the VOC–LSPR spectrum was less than 3 s and the response was completely reversible and reproducible.

Keywords: Surface plasmon resonance; VOCs; Optical sensor

1. Introduction

A collective oscillation of free electrons at the surface boundary of metal film, known as surface plasmon resonance (SPR), has attracted broad research interest in the past few decades [1]. Traditionally, this phenomenon is measured using a prism coated with a thin metal film (i.e. the Kretschmann configuration). The changes in SPR are measured by either the shift of the incident angle or attenuation at a fixed reflection angle. SPR is sensitive to changes in the refractive index of the liquid medium adjacent to a metal film. Therefore, SPR can be used for detection of selective adsorption of large biochemical molecules to the modified metal surface in the liquid phase. In the past few years, a significant amount of research on the application of SPR biosensors, has been published and reviewed [1]. For example, a protein-modified SPR immunosensor recently was used to detect an environmentally hazardous precursor of dioxin in solution [2].

Although the majority of SPR sensor research has focused on the application of SPR in liquid phase bio-chemical detection, one of the earliest SPR sensors was a gas/vapor sensor invented by Nylander et al. [3] and Liedberg et al. [4]. In order to facilitate vapor detection, an absorptive polymer layer (e.g. OV-225) was used to coat the metal film, enhancing vapor sorption. The SPR signal responds to the changes in the thickness and refractive index of the polymer film that result from sorption of the vapor molecule. Langmuir–Blodgett films of phthalocyanine derivatives also have been used as adsorbent on prism-type SPR sensors for the detection of toluene [5] and NO_x [6]. Shenoy and co-workers coated SPR sensors with cavitands and were able to selectively detect aromatic vapors [7]. Rella and co-workers demonstrated alcohol sensing by using the SPR changes in TiO_2 nanocrystal film layered on metal film [8]. Each of these SPR gas sensors requires an organic or inorganic absorbent film on a metal surface to enhance sensitivity and to serve as a refractive index transducer for incoming gas/vapors.

Other than the Kretschmann configuration, surface plasmon sensors using fiber optical couplers also have been reported. Niggemann et al. [9] and Abdelghani et al. [10] used this metal film-fiber configuration coated with sorptive polymer to detect

* Corresponding author. Tel.: +8 862 2905 3573; fax: +8 862 2902 3209.
E-mail address: 056470@mail.fju.edu.tw (C.-J. Lu).

0039-9140/$ – see front matter © 2007 Elsevier B.V. All rights reserved.
doi:10.1016/j.talanta.2007.03.058

chemical vapors. Booksh and co-workers created an SPR sensor for organic vapor using a specific tapered angle between a reflective mirror and the sensing surface, which was glass coated with thin Au film at the tip of the optical fiber [11].

SPR phenomenon also is found in noble metal nanoparticles, namely, the localized surface plasmon resonance (LSPR). It occurs when the incident light frequency matches the collective oscillation frequency of the conducting electrons within a nanoparticle; the light energy absorbed and scattered results in an absorbance band in the UV–vis spectrum. The absorbance and wavelength of the LSPR band are highly dependent on the size, shape, and local environment of the nanoparticles (i.e. refractive index or surface binding molecules) [12,13]. The LSPR of nanoparticles can be readily measured by UV–vis spectrometry and does not require a delicate optical coupler (e.g. a controlled thickness metal thin film deposited on prism or optical fiber). Nanoparticles can be used as the SPR sensing medium by measuring the UV–vis spectrum of either a colloidal suspension or a nanoparticle film that has been chemically immobilized to a glass substrate [14]. Either method is much cheaper and easier for fabrication of sensors in conventional chemical laboratories. Many novel sensors based on the LSPR spectrum of nanoparticles have been developed. The applications span from glucose detection to biotin-streptavidin sensing to DNA detection [15–17]. Sun and Xia recently reported that an Au nanoshell was more sensitive than are Au nanoparticles to environmental refractive index changes in the liquid phase [18]. In terms of gas detection using the LSPR of nanoparticles, Ando et al. investigated a series of gas-sensing film composites of metal-oxides (e.g. WO_3, CuO, NiO, etc.) doped with noble metal colloid (e.g. Au, Pd and Pt), and tested their response characteristics to inorganic gases such as CO, H_2, etc. [19–21]. Yanase and Komiyama found that the LSPR of nano-Ag film shifted as the atmosphere changed from 5% H_2 to 1% O_2 in helium background [22]. They attributed the changes of SPR to the surface adsorption of O_2 on the silver nanoparticles.

In this paper, an organic vapor sensor using the LSPR spectra of metallic nanoparticles was developed. Nanoparticles were immobilized on a glass substrate via a self-assemble monolayer (SAM) reaction and the LSPR spectra were measured using a real-time CCD array UV–vis spectrometer. In contrast to the traditional SPR vapor sensor that required an absorbent layer on a smooth metal film to enhance the vapor sorption, the large surface area of SAM nanoparticles facilitated quantitative adsorption of organic vapors. Three different metallic nanoparticles: silver nanoparticles, gold nanoparticles and gold nanoshells were synthesized and tested for their vapor-sensing properties. Factors and mechanisms that influence the sensitivity of the LSPR sensor to organic vapors were investigated.

2. Experimental section

2.1. Metallic nanoparticles synthesis [17,18]

Gold nanoparticles were prepared by sodium citrate reduction of hydrogen tetrachlororaurate ($HAuCl_4$, Alfa Aesar). 100-mL of an aqueous solution of 1 mM $HAuCl_4$ was boiled with vigorous stirring in a round-bottom flask. 10 mL of 38.8 mM $NaBH_4$ were added rapidly to the solution. The solution was boiled for 10 min and the color of the solution changed from yellow to purple-red. The solution was cooled to room temperature with continual stirring. The solution was filtered and stored in a refrigerator at 4 °C for further experiments. Silver nanoparticles were synthesized by reduction of $AgNO_3$ in an ethylene glycol solution containing polyvinylpyrolidone (PVP). PVP (2 g) was dissolved in 10 mL ethylene glycol, followed by addition of 130 mg of $AgNO_3$ with continuous stirring. The solution was slowly heated at approximately 1 °C/min until the temperature reached 120 °C, and was then refluxed for 22 h. The solution gradually turned dark yellow and was cooled at room temperature.

Gold nanoshells were synthesized using silver nanoparticles as a template. The surface atoms of silver nanoparticles were gradually replaced by the addition of $HAuCl_4$ solution. 1 mL of silver nanoparticles solution was diluted to 20 mL with deionized water and heated to boiling. 3.2 mM $HAuCl_4$ solution was slowly dripped into the solution until the color turned blue. The solution was then cooled to room temperature; white precipitate (AgCl) was formed by centrifuge.

2.2. Nanoparticle self-assemble monolayer on glass substrate [17,18]

Glass substrates were prepared by cutting cover glass to 9 mm by 18 mm, followed by immersion in cleaning solution (70% H_2SO_4 and 30% H_2O_2), sonication for 30 min and rinsing with deionized water. The substrates were then dried under N_2, heated in a 100 °C oven for 10 min, and placed in a 10% solution of 3-aminopropyl-trimethoxysilane (APTMS) in methanol for 1 h. These surface modified glass substrates were rinsed thoroughly with methanol and deionized water to remove any unreacted APTMS. Glass substrates were then immersed in the solution containing metal nanoparticles. The reaction between gold nanoparticles and surface amino groups is much faster than with silver nanoparticles and gold nanoshells. Gold nanoparticles are bound to the surface of the glass substrates after 40 min compared with the 24 h required for silver nanoparticles and gold nanoshells. The formation of a nanoparticle layer can be visually confirmed by the color of the glass surface: purple-red for Au nanoparticles, yellow for Ag nanoparticles and blue for Au nanoshells. The UV–vis spectra of the nanoparticle SAM on glass slides also were recorded. The glass slides were rinsed with ethanol and water, repeatedly, until the UV–vis spectra remained constant. Images of the nanoparticles SAM on glass were captured using a field emission scanning electron microscope (FESEM, JSM-6500F).

2.3. Vapor generation and detection system

A dynamic flow system was constructed in order to generate variable organic vapor concentrations for testing the LSPR sensors. Compressed air was passed through a two-stage trap consisting of a molecular sieve and charcoal to remove background moisture and organics. A high efficiency particle filter

was placed in the line to remove any particles that were produced by the traps. The temperature and humidity of this background air stream were monitored by a humidity meter (DO9861T-R1, Delta Ohm, Padua, Italy). The humidity was less than the detection limit (<1%) for all experiments. A saturated vapor concentration at room temperature was produced by passing the background air through a bubbler. The organic vapor concentration was then varied by diluting the saturated vapor with background air using different flow rates. Mass flow-controllers (5850i, Brooks Instrument, PA) were calibrated with a bubble burette before being installed in the vapor generation system. A three-way solenoid valve was connected in front of the test cell, which allowed computer-controlled switching between the background air and the test vapor. The vapor concentrations were calibrated with GC-FID (HP-5890, Agilent) to the mass-response of calibration curves obtained by CS_2 solution injection of the same compound.

LSPR spectra were measured using a CCD array UV–vis spectrometer (USB-2000, Ocean Optics). In order to enhance the signal-to-noise ratio, a customized 10-slide stainless steel holder that fits into a conventional optical cube was made. Ten glass substrates, with nanoparticle SAM on both sides, were placed in the holder and exposed to organic vapor inside the flow cell cube (Fig. 1). The absorbance signal of the nanoparticle LSPR was enhanced 10-fold, according to Beer's law.

3. Result and discussion

3.1. Self assemble monolayer of nanoparticles on glass

Fig. 2 shows the FESEM images and UV–vis spectra of the three types of nanoparticles as SAM on glass substrate. As shown in Fig. 2a, gold nanoparticles form a uniform and well-scattered monolayer. The wavelength for the maximum absorption band of gold nanoparticle film LSPR is 532 nm, which is slightly more red-shifted than the LSPR band obtained from Au nanoparticles in solution (524 nm). The reason for the red-shift is the short distances between nanoparticles. The Au nanoparticle diameter is about 25 ± 4.5 nm. The distance between most particles is less than 30 nm (Fig. 2a). When incubation time for the Au colloid solution was increased to 4 h, the Au nanoparticles started to aggregate and there was a dramatic red-shift of the LSPR band. To prevent aggregation of Au nanoparticles, the assembling time for Au SAM was kept under 40 min in all experiments.

The size distribution of Ag nanoparticles (i.e. 51.2 ± 16 nm) was wider than that of gold nanoparticles. In addition, the SAM of Ag nanoparticles was less uniform than that of Au nanoparticles (Fig. 2c). Also, the assembling process of the Ag nanoparticles monolayer was much slower than that of Au nanoparticles. A very faint yellow color was evident on the glass substrate after a minimum of 12 h. The polymer (PVP) used to protect the Ag nanoparticles may also reduce the effectiveness of the surface binding between Ag nanoparticles and APTMS. Most of the Ag nanoparticle monolayer was formed by small clusters of 2–3 Ag nanoparticles. The affinity between APTMS and Ag was weakened by PVP, which enables the mobilization and clotting of Ag nanoparticles on the glass surface. The partial aggregation of Ag nanoparticles causes the broadening and tailing of the LSPR band toward the long wavelength (Fig. 2d). A similar phenomenon was found in Au SAM nanoshells (Fig. 2e and f). The Au nanoshells were synthesized using Ag nanoparticles as template that already had PVP protection. The mean size of gold nanoshell is 59.3 nm, which is slightly larger than Ag nanoparticles. The LSPR band of Au nanoshells also red-shifted compared to those suspended in solution. The broad size distribution and random clotting of nanoshells resulted in a broad LSPR band.

Initially, the LSPR spectrum was tested with a single glass slide. The absorbance was very low (i.e. <0.1 a.u.), because it contained only two monolayers of nanoparticles (i.e. one monolayer on each side). This absorbance value was similar to previously reported values [17,18]. The single-slide configuration resulted in significant spectrum to spectrum variation during exposure to the test vapor concentrations. Therefore, a 10-slide holder was made to increase by 10-fold the number of nanoparticle monolayers in the light path. As shown in Fig. 2b, d and f, all LSPR absorbances were greater than 1.0, significantly enhancing the signal-to-noise ratio. Increasing the

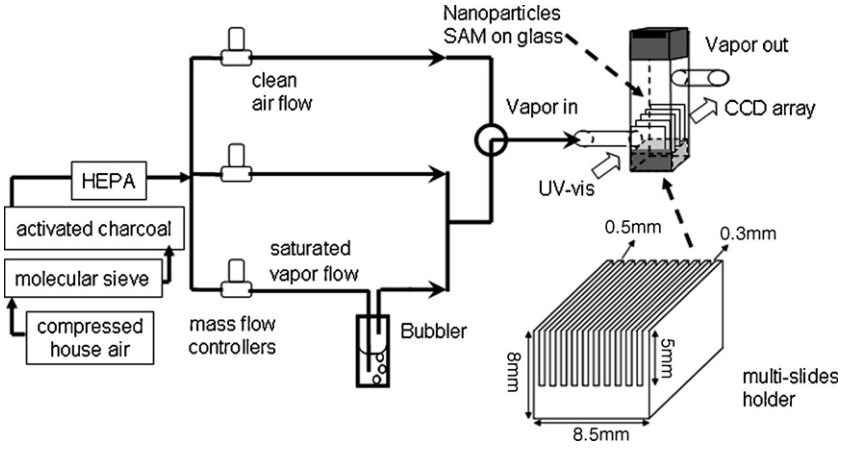

Fig. 1. Diagram of LSPR–VOC sensor testing system.

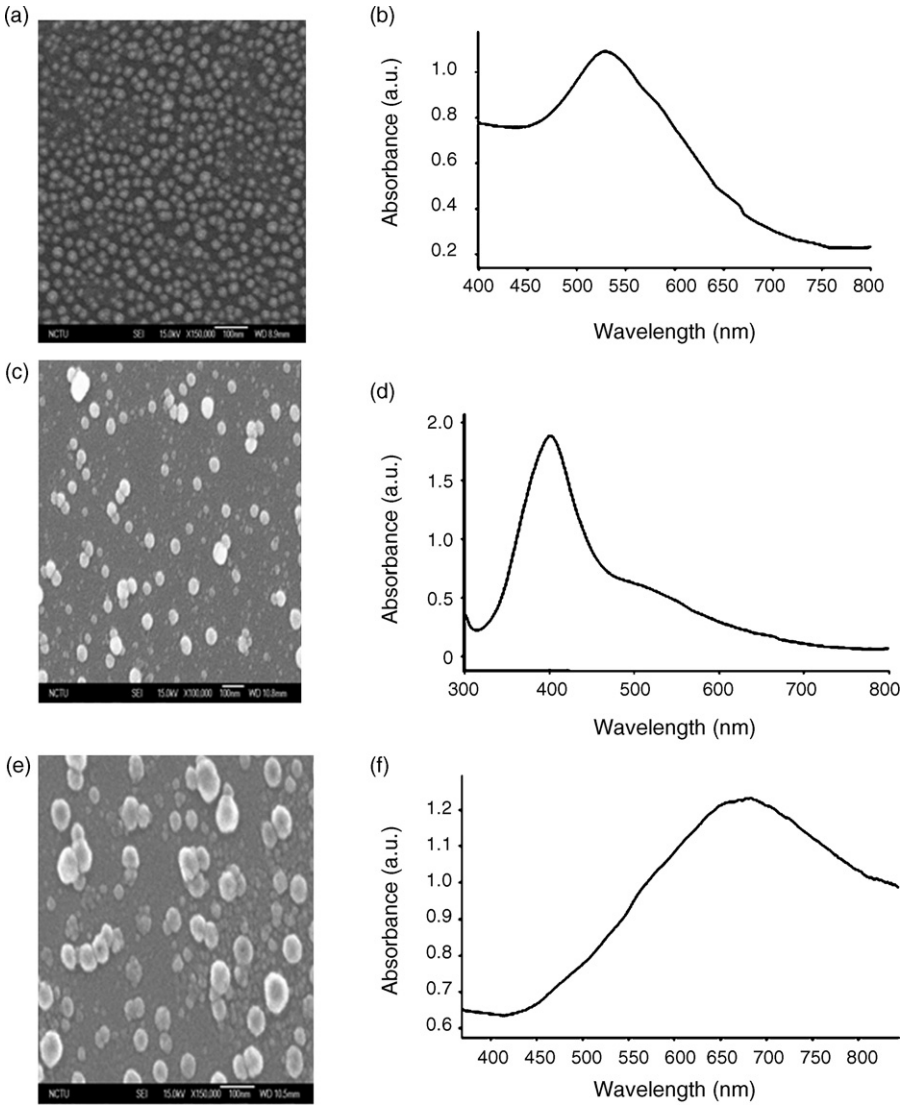

Fig. 2. FESEM picture and LSPR spectrum for SAM on glass of (a, b) Au nanoparticles, (c, d) Ag nanoparticles, and (e, f) Au nanoshells.

number of glass slides only influences the absorbance signals; the LSPR wavelength shift, due to changes in vapor concentration, yields the same results with a single slide. An alternative way to increase the absorbance signal would be growing multilayers of nanoparticles on a single glass slide using dithiol cross-linker, with repeated immersion into the nanoparticle solution. However, this approach created a multilayer structure with all nanoparticles closely linked to organic species, such that the environmental refractive index was very similar to that of the absorbed organic molecules. Thus, the LSPR spectrum of organically linked multilayers is already shifted to the extent that it can no longer respond to changes in vapor concentration.

3.2. LSPR spectrum response to vapor concentrations

Fig. 3 shows the LSPR spectrum changes of three types of nanoparticles when exposed to different relative saturation toluene concentrations ($P/P_{sat} \times 100\%$). Au nanoparticles showed significant absorbance changes, but relatively small shifts in the wavelength of the LSPR band. Both absorbance increases and wavelength shift of Ag nanoparticles were more sensitive than with Au nanoparticles. The responses of Au nanoshells were unique: the maximum absorbance increases were minimal, but the wavelength shift of the full LSPR band was very sensitive to changes in toluene concentration. (Fig. 3c)

The Ag LSPR responses to altered vapor concentrations of organic compounds with various functional groups and volatilities are shown in Fig. 4. Both absorbance (Fig. 4a) and wavelength shift (Fig. 4b) of the LSPR band increased as concentration of the VOC increases. The wavelength used for determining the absorbance changes was 402 nm. Among the five vapors tested, chlorobenzene, *m*-xylene, and pentanol showed a fairly good linear response, but octane and toluene showed curvi-linear calibration lines. The shape of the octane and toluene curves fits the type IV BET adsorption isotherm, which describes multi-layer adsorption and limited physical

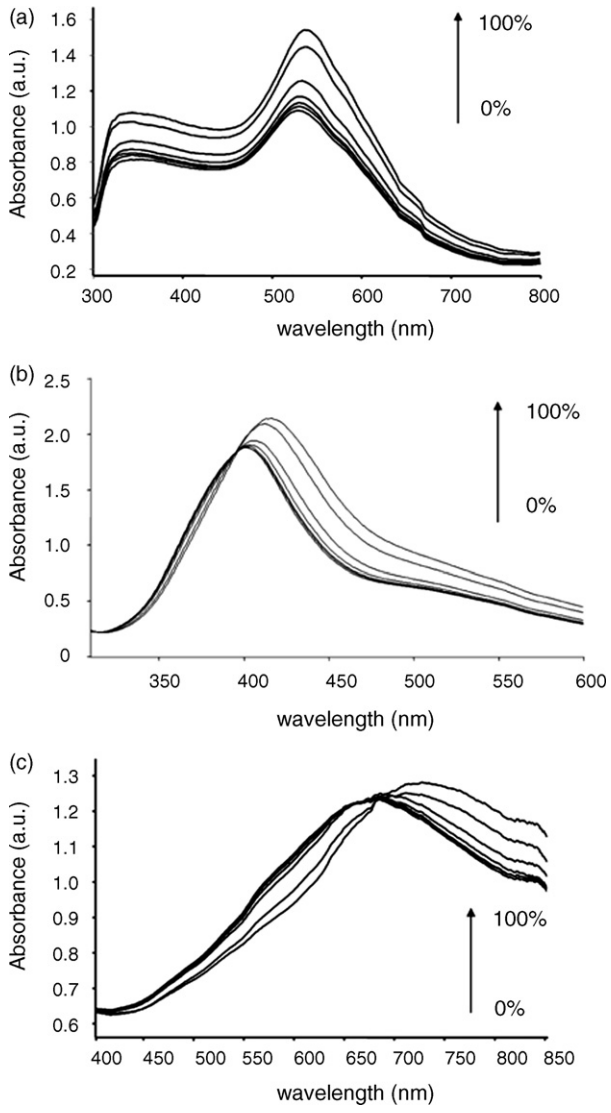

Fig. 3. LSPR spectrums responding to 0∼100% relative saturated toluene vapor concentrations. (a) Au nanoparticles, (b) Ag nanoparticles, and (c) Au nanoshells.

surface adsorption. For those compounds with relatively good linear responses, the boundary between adsorption and condensation was blurred due to early condensation. This phenomenon was caused by either low volatility or strong inter-molecular attraction.

The detailed response mechanism of the LSPR sensor to changes in vapor concentration is illustrated in Fig. 5. When the nanoparticle monolayer was exposed to low vapor concentration, the organic vapor physically adsorbed onto the surface of the nanoparticles as the first monolayer. In this region, the sensitivity of the LSPR sensor was relatively low. Once the concentration of the organic vapor was sufficiently high, surface condensation took place and multi-layers of organic adsorbate formed thin liquid phases that partly covered the surface of the nanoparticles. Up to this point, the sensitivity increased as the thickness of the surface condensation layer increased. The condensed organic layers caused the surface refractive index to change from air to a portion of the organic liquid refractive index.

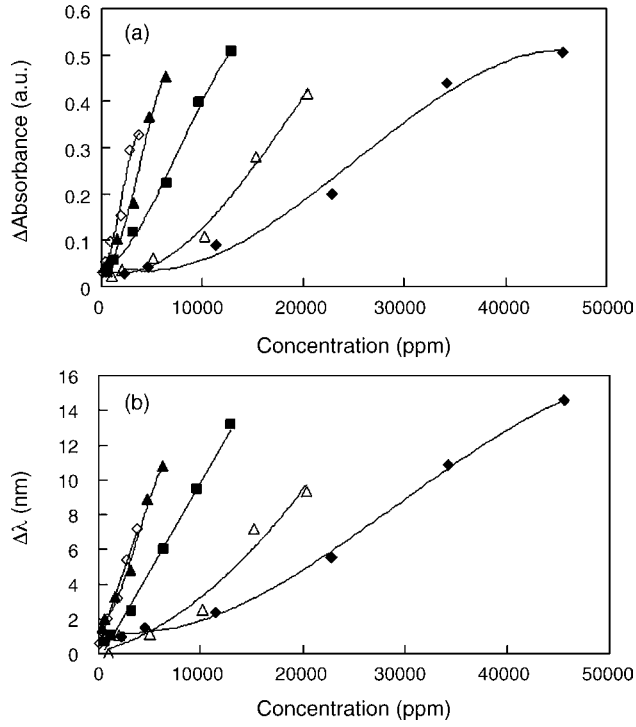

Fig. 4. Ag nanoparticles LSPR vapor response calibration curves of (a) absorbance at 402 nm and (b) wavelength shift (♦: toluene, △: *n*-octane, ■: chlororbenzene, ▲: *m*-xylene, ◇: petanol).

To estimate the surface refractive index changes during vapor detection, the LSPR wavelength shift of Ag nanoparticle SAM was measured in air ($n = 1$) and in liquid octane ($n = 1.39$), in pentanol ($n = 1.41$), in toluene ($n = 1.49$), and in chlorobenzene ($n = 1.52$). The results are plotted in Fig. 6. The wavelength shifts were used instead of absorbance here because light scattering by the liquid interfered with the magnitude of absorbance, but not the wavelength shift. The wavelength shift was proportional to the environmental refractive index, with a sensitivity of 71.7 nm/RIU for the Ag nanoparticles. The maximum wavelength shifts due to vapor adsorption at near saturated vapor concentration were 14.6 nm for toluene and 9.4 for octane (Fig. 4b). The equivalent surface refractive indices for toluene and octane were calculated to be 1.21 and 1.14, respectively. This is equivalent to changes of only 43% (toluene) and 36% (octane) in refractive index changes compared to the liquid state. Table 1 summarizes the surface refractive index calculations for all three nano-materials and the five tested vapors at the highest tested concentration that was generated by the system employed in this study. The surface refractive indices ranged from 1.11 to 1.29, which are all less than the liquid refractive index. These data indicate that the condensed organic layer either partly covered the nanoparticle or is very thin (i.e. few molecules in thickness), such that the electromagnetic field of LSPR can reach beyond the thickness of this adsorbed layer. Van Duyne and co-workers [13] estimated that the electromagnetic field of a nanoparticle LSPR probes into the surrounding media as far as 50 nm in nano Ag core-shell experiments. Thus, the LSPR senses the combined refractive index of the condensed organic liquid and the nearby air region.

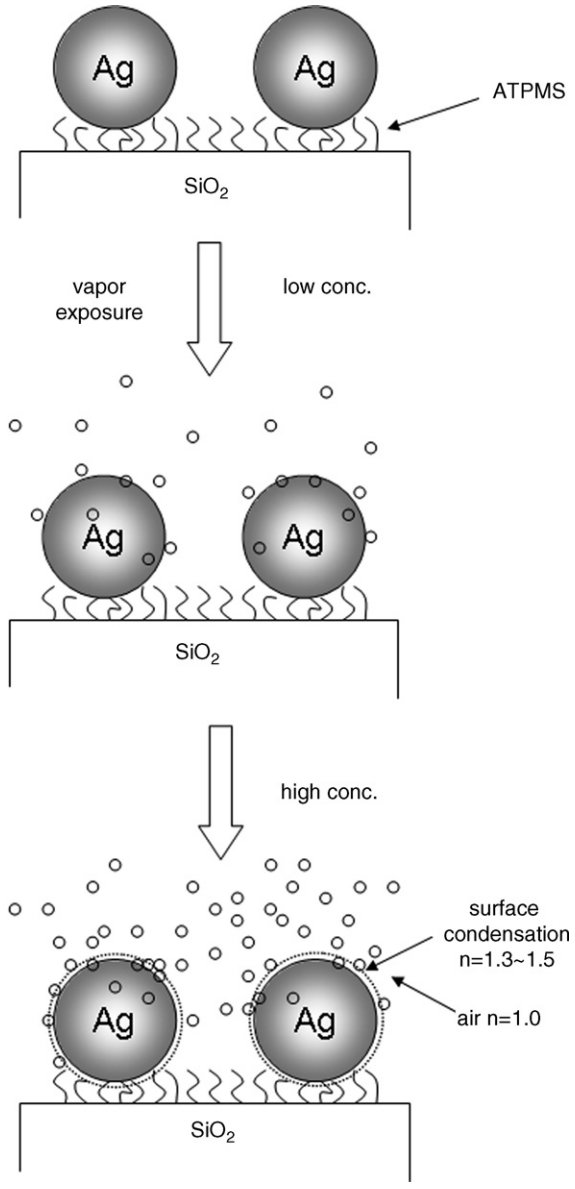

Fig. 5. Illustrations for LSPR–VOC sensor response mechanism.

3.3. Factors influencing sensitivities

The absorbance calibration data of six vapors testing all three nano-materials are shown in Fig. 7. The calibration curves of Au nanoparticles and Au nanoshells are not shown here, to reduce the redundancy of similar figures. The best-fit straight lines were

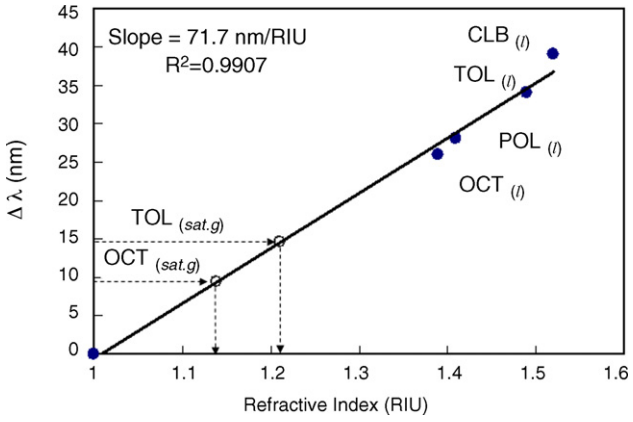

Fig. 6. Calibration for LSPR wave length shift of Ag nanoparticles SAM versus environmental refractive index.

determined and the slopes (i.e. the absorbance sensitivities) versus the reciprocal of vapor pressure ($1/P_v$) were plotted for each organic compound. As shown in Fig. 7, the vapor sensitivities of all three nano-materials increased almost linearly with decreasing vapor volatility (i.e. lower volatility = higher $1/P_v$) regardless of the chemical structure of the organic compounds. Thus, the interaction between metallic nanoparticles and organic vapors was limited to physical adsorption. Chemical differences in the functional groups did not contribute to the sensor response. The regression lines in Fig. 7 represent the relationship between sensitivity and volatility. Besides the common trend of a linear increase in sensitivity versus $1/P_v$, there were variations among compounds. *m*-xylene ($n = 1.49$) and chlorobenzene ($n = 1.52$)

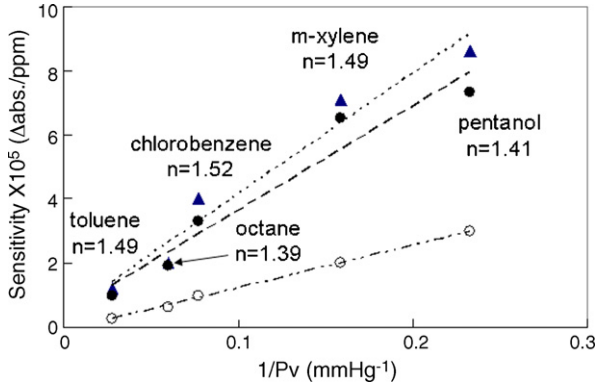

Fig. 7. LSPR–VOC sensor absorbance sensitivity vs. the volatility of tested organic vapor (▲: Ag nanoparticles, ●: Au nanoparticles, ◯: Au nanoshell).

Table 1
Equivalent surface refractive index at high vapor concentrations

Liquid R.I. calib.		Vapor concentrations (ppm) and calculated surface R.I.				
Slope (nm/RIU)	R^2	Toluene 45639	Octane 20382	Chlorobenzene 12921	*n*-Xylene 6348	Pentanol 3759
Au Np						
32.7	0.992	1.29	1.26	1.26	1.25	1.18
Ag Np						
71.7	0.990	1.21	1.14	1.19	1.12	1.11
Au Ns						
249.8	0.997	1.18	1.11	1.18	1.18	1.18

exhibited small positive deviations, while pentanol ($n = 1.41$) and octane ($n = 1.39$) demonstrated small negative deviations from the regression lines in Fig. 7. Compounds with a higher refractive index were slightly more sensitive (i.e. the positive deviation) than the volatility trend would predict, while the lower refractive index compounds fell below the regression lines.

Despite the relatively low absorbance sensitivity for Au nanoshells, the wavelength shift sensitivity to refractive changes of the Au nanoshells outperformed that of the Au and Ag nanoparticles: Au nanoshells (249.8 nm/RIU) > Ag nanoparticles (71.7 nm/RIU) > Au nanoparticles (32.7 nm/RIU) as shown in Table 1. The original response spectra (Fig. 3) provide a better visual comparison of the differences between the three nano-materials tested in this study.

3.4. Response time of VOC–LSPR sensor

The dynamic vapor response signals of the Ag nanoparticle LSPR are shown in Fig. 8. The *m*-xylene concentration of 4766 ppm was switched on for 20 s then switched off for 40 s during the five test cycles. The LSPR spectra were collected at 1 s intervals. The responses of the LSPR sensors to changes in vapor concentration were rapid, reversible, and reproducible. Fig. 8a shows the response signal of single point absorbance at $\lambda = 405$ nm. The single wavelength absorbance response appeared to be noisy due to the small background vibrations of the instrument and optic fiber. Longer averaging time for UV–vis spectrum improved the signal to noise ratio, but the data acquisition rate was slower. Fig. 8b shows the response signal of the integrated LSPR band area to be between $\lambda = 350\sim550$ nm of the spectrum. As can be seen in Fig. 8, with the spectrum area, there was less variation than with a single point absorbance. The integration of the absorbance over a given wavelength range averaged the noise along the spectrum and, therefore, greatly improved signal-to-noise ratio. The same approach previously was used by de Julian Fernandez et al. [23] in a study of polyimide/Au ion composite SPR gas sensors. The limit of detection (3σ) was calculated to be 87.8 ppm for *m*-xylene based on the results in Fig. 8b without any smoothing of the data. The 90% full-scale response time (i.e. T_{90}) was about 3 s, including the time required for vapor concentration to reach equilibrium in the test chamber.

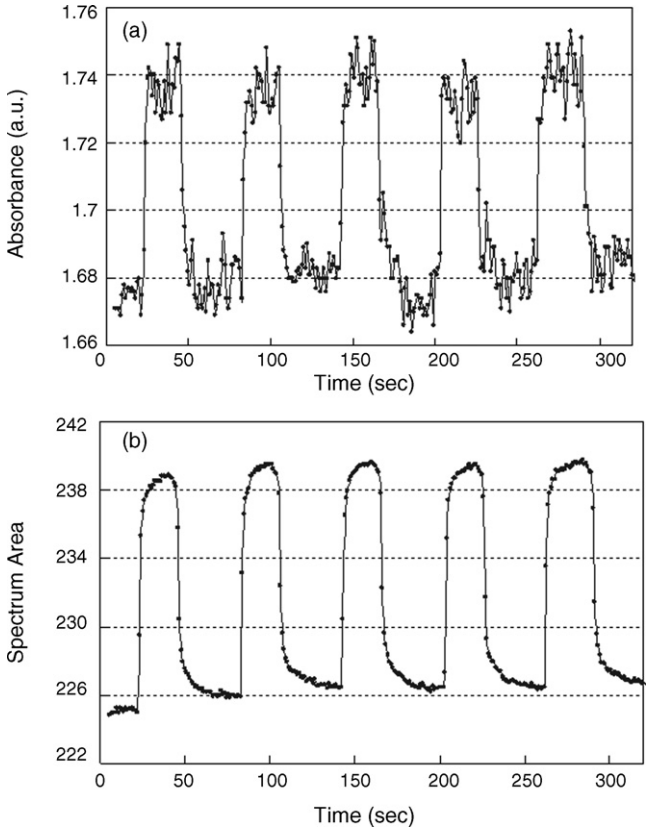

Fig. 8. Real-time response signal of Ag nanoparticles LSPR–VOC sensor (a) absorbance at $\lambda = 405$ nm (b) spectrum integration area between $\lambda = 350\sim550$ nm.

3.5. Comparison with conventional VOC sensors

There are several types of well-known sensors that are also capable of detecting VOCs in air, such as metal oxide (particularly, SnO_2), surface acoustic wave (SAW), and monolayer protected nanocluster (MPC) coated chemiresistor [24–28]. There are certain advantages and disadvantages associated with each type of sensor. For example, the SnO_2 sensor is sensitive to low concentrations of alcohol and ketones, i.e. on the order of ppm. However, the dynamic range of the SnO_2 sensor is fairly limited. The sensor presented in this study has a limit of detection near several tenths of a ppm, which is about one order higher than a SnO_2 sensor. However, the LSPR sensor responds linearly to increases in VOC until near saturated concentrations. In addition, the SnO_2 sensor is limited by the toxic effect of halogen compounds. In this study, cholorobenzene was used to test the LSPR sensor and no toxic effect was observed.

Both SAW and MPC chemiresistor sensors are known for their wide dynamic ranges and low sensitivities [25–28]. Both of these sensors performed better than the LSPR sensor at low concentrations. However, the detection limits of the LSPR sensor are improved if a spectrometer with greater stability and sensitivity is used (i.e. photomultiplier instead of CCD detector). SAW and MPC sensors also require a finite time for vapor molecules to diffuse the sensing film during the response process. The typical T_{90} for these two sensors are around >10 s. In the current study, the typical T_{90} of the LSPR sensor was 3 s, limited by the speed of gas mixing in the test chamber. Thus, LSPR responds to surface adsorption almost instantly.

4. Conclusion

In this study, we developed and tested the concept of using the LSPR spectra of metal nanoparticle, self-assembled monolayers as VOC sensors. The high surface area of nanoparticles provided a sufficient route for vapor adsorption and condensation. Upon the adsorption and condensation of VOC molecules, the surface refractive index changed from air ($n = 1.0$) to an average of $n = 1.2$, depending on the vapor volatility, concentrations, and the refractive index of the organic species. The interaction between the organic vapor and the nanoparticles was limited to

physical adsorption, regardless of the functional groups present on the organic molecule. The metal properties (i.e. gold or silver) or nanostructure (i.e. particle or shell) determined whether the sensor exhibited changes in absorbance or wavelength. The contribution of the organic liquid refractive index toward vapor sensitivity was detectable, but minor. This effect is small because most of the sensor signal comes from the surface refractive index deviation from air instead of from the small differences between organic compounds. Studies to improve sensitivity of sensors using fiber optical fiber designs and modification of the nanoparticle surfaces are underway.

Acknowledgement

The authors would like to thank Miss Rui-Xuan Huang for her assistance in carrying out these experiments. The funding for this project was provided by National Science Council (NSC) of Taiwan, ROC, and is gratefully acknowledged.

References

[1] J. Homola, S.S. Yee, G. Gauglitz, Sens. Actuat. B 54 (1999) 3.
[2] N. Soh, T. Tokuda, T. Watanabe, K. Mishima, T. Imato, T. Masadome, Y. Asano, S. Okutani, O. Niwa, S. Brown, Talanta 60 (2003) 733.
[3] C. Nylander, B. Liedberg, T. Lind, Sens. Actuat. 3 (1982/1983) 79.
[4] B. Liedberg, C. Nylander, I. Lundstrom, Sens. Actuat. 4 (1983) 299.
[5] C. Granito, J.N. Wilde, M.C. Petty, S. Houghton, P.J. Iredale, Thin Solid Film 284 (1996) 98.
[6] T. Basova, E. Kol'tsov, A.K. Ray, A.K. Hassan, A.G. Gurek, V. Ahsen, Sens. Actuat. B 113 (2006) 127.
[7] E.B. Feresenbet, E. Dalcanale, C. Dulcey, D.K. Shenoy, Sens. Actuat. B 97 (2004) 211.
[8] M.G. Manera, G. Leo, M.L. Curri, P.D. Cozzoli, R. Rella, P. Siciliano, A. Agostiano, L. Vasanelli, Sens. Actuat. B 100 (2004) 75.
[9] M. Niggemann, A. Katerkamp, M. Pellmann, P. Bolsmann, J. Reinbold, K. Cammann, Sens. Actuat. B 34 (1996) 328.
[10] A. Abdelghani, J.M. Chovelon, N. Jaffrezic-Renault, C. Veilla, H. Gagnaire, Anal. Chim. Acta 337 (1997) 225.
[11] Y.-C. Kim, S. Banerji, J.-F. Masson, W. Peng, K.S. Booksh, Analyst 130 (2005) 838.
[12] S. Underwood, P. Mulvaney, Langmuir 10 (1994) 3427.
[13] M.D. Malinsky, K.L. Kelly, G.C. Schatz, R.P. Van Duyne, J. Am. Chem. Soc. 123 (2001) 1471.
[14] K.C. Grabar, K.R. Brown, C.D. Keating, S.J. Stranick, S.-L. Tang, M.J. Natan, Anal. Chem. 69 (1997) 471.
[15] J. Shi, Y. Zhu, X. Zhang, W.R.G. Baeyens, A.M. Garcia-Campana, Trends Anal. Chem. 23 (2004) 351.
[16] A.J. Haes, D.A. Stuart, S. Nie, R.P. Van Duyne, J. Fluoresc. 14 (2004) 355.
[17] S.-F. Cheng, L.-K. Chau, Anal. Chem. 75 (2003) 16.
[18] Y. Sun, Y. Xia, Anal. Chem. 74 (2002) 5297.
[19] M. Ando, T. Kobayashi, M. Haruta, Sens. Actuat. B 24–25 (1995) 851.
[20] M. Ando, T. Kobayashi, S. Iijima, M. Haruta, J. Mater. Chem. 7 (1997) 1779.
[21] M. Ando, R. Chabicovsky, M. Haruta, Sens. Actuat. B 76 (2001) 13.
[22] A. Yanase, H. Komiyama, Surf. Sci. 264 (1992) 147.
[23] C. de Julian Fernandez, M.G. Manera, J. Spadavecchia, G. Maggioni, A. Quaranta, G. Mattei, M. Bazzan, E. Cattaruzza, M. Bonafini, E. Negro, A. Vomiero, S. Carturan, C. Scian, G. Della Mea, R. Rella, L. Vasanelli, P. Mazzoldi, Sens. Actuat. B 111–112 (2005) 225.
[24] N. Barsan, D. Koziej, U. Weimar, Sens. Actuat. B 121 (2007) 18.
[25] H. Wohltjen, Sens. Actuat. 5 (1984) 307.
[26] S.J. Patrash, E.T. Zellers, Anal. Chem. 65 (1993) 2055.
[27] H. Wohltjen, A.W. Snow, Anal. Chem. 70 (1998) 2856.
[28] C.-Y. Yang, C.-L. Lin, C.-J. Lu, Anal. Chim. Acta 565 (2006) 17.

Available online at www.sciencedirect.com
ScienceDirect
Talanta 73 (2007) 332–339
Talanta
www.elsevier.com/locate/talanta

NMR relaxation data for quality characterization of Balsamic vinegar of Modena

R. Consonni *, L.R. Cagliani

Istituto per lo Studio delle Macromolecole, Lab. NMR, CNR, v. Bassini 15, 20133 Milan, Italy

Received 12 January 2007; received in revised form 22 March 2007; accepted 23 March 2007
Available online 30 March 2007

Abstract

In this paper, 22 samples consisting of Balsamic vinegar of Modena and two Traditional Balsamic vinegar of Modena samples have been analyzed by means of ^{1}H NMR spectroscopy. Some selected resonances have been used for quantification and for $T1$ (spin–lattice relaxation time) measurements. Statistical protocols applied to NMR data for quantification of selected resonances revealed the possibility to differentiate the samples according to their ageing process. Additionally, $T1$ measurements revealed a strong correlation with the ageing process and these new data were added for improving the statistical model, which was used to predict $T1$ relaxation time of selected compounds for Balsamic vinegar samples. Our results indicate that the use of NMR data and statistical methods is a valid approach that can be successfully used for ageing characterization of Balsamic vinegar of Modena samples.

Keywords: Balsamic vinegar of Modena; PCA; PLS; ^{1}H NMR; Spin–lattice relaxation times; Vinegar ageing process

1. Introduction

Balsamic vinegar of Modena (BVM) is an original and typical product whose consumption undergoes to a large increase of production; in the last 8 years (1995–2003) a 300% of increase has been observed. Almost 21 millions of concentrated must were produced in 2005 with a corresponding amount of 60 millions of litres of vinegar. BVM is exported in more than 60 nations, and in 2003 the invoice was more than €200 million. The producers, joining the "Modena Balsamic Vinegar Consortium" can obtain the red or the white seal for matured or aged BVM samples, carrying the mention "refined" or "aged" if they experienced up to 3 or more than 3 years of ageing process respectively.

The set of rules (D.M., December 3, 1965) describes the preparation procedure for BVM, which consists of a mixture of wine vinegar, caramel and eventually a small addition of aged (10 years) wine vinegar. BVM samples can then experience the ageing process, which confers additional quality parameters to the final product. The producers of BVM, by means of the certified production consortium (Cpcabm), applied for Protected Geographical Indication (P.G.I.) status to UE Commission, but up to now no official answers are reported. In the meantime, a D.M. of August 3, 2006, temporarily permits the use of P.G.I. for this product.

Traditional Balsamic vinegar of both Modena (TBVM) and Reggio Emilia (TBVRE), are completely different products; they are obtained from cooked must which has been aged in wood barrels of decreasing size for at least 12 years before to be sold, and no additional products can be added. Also in this case, set of rules (D.M., February 9, 1987 and D.M., March 3, 1987 no. 191 for TBVM and TBVRE, respectively) have to be observed for correct production procedures and again the consortiums supervised the complete process up to the product commercialization. In addition, P.D.O. stamp was recently obtained (Reg. CEE n. 813/2000 of April 17, 2000) for both these traditional products.

Different analytical studies focused their attention on TBVM [1–5]; some were also applied in identification of isotopic ratio for authentication of natural vinegar [6,7] and a quite old study inferred the comparison of quality specifications for the two vinegar products [8]. Moreover, no objective analytical techniques have been officially defined for ageing determination, which is actually the most required information for quality assessment.

* Corresponding author. Tel.: +39 02 23699578; fax: +39 02 23699620.
E-mail address: roberto.consonni@ismac.cnr.it (R. Consonni).

0039-9140/$ – see front matter © 2007 Elsevier B.V. All rights reserved.
doi:10.1016/j.talanta.2007.03.045

BVM and TBVM quality certifications are nowadays obtained by means of sensory analysis (D.M., February 9, 1987 and D.M., March 3, 1987 no. 191) and by very simple chemical physical property determinations, like total acidity, density and dry residual. These analyses are performed by private certification corporations with their own protocols; as a matter of fact, direct ageing determination is not available. Balsamic vinegar consortium could evaluate and certify the quality of BVM samples with the use of two different stamps for lower or upper 3 years of ageing (red and white stamp, respectively). These certified BVM samples will be sold at higher price because they report this certification on the bottle seal; besides the producers are not obliged to ask for the consortium certification. On the other hand, Italian market admits also the presence of BVM without any stamp; this does not indicate necessarily a lower quality for these samples. In fact, good quality and aged BVM could characterize both BVM samples with white stamp or without stamp. Furthermore, within certified red stamp BVM, as well as in no certified ones, poor quality samples (called "first price") can be present and they are sold at very low price because essentially obtained by mixing wine vinegar and caramel. In this contest, NMR analysis is here proposed as a rapid and feasible tool that could answer this commercial requirement, by means of ageing determination and quality characterization. For exhaustive data evaluation, chemometric techniques, known to handle large data matrices and to compare the metabolite content through a series of analyzed samples, can helpfully be used in combination with NMR data.

NMR has achieved during last years general acceptance as a powerful method for food quality investigations [9–13]; its non-invasive characteristic, the high reproducibility and the sensitivity has demonstrated its powerfulness in a large range of applications. Food displays an enormous range of structural and compositional complexity and heterogeneity, which explains its sensory and safety properties. For these reasons, investigation of such products requires the use of non-invasive techniques providing quantitative information on the spatial organization. Some NMR parameters such as proton density and chemical shift measurements, may give information and quantification of different food characteristics. These include determination of chemical composition, quantification of the structure over distance scales ranging from molecular to macroscopic level while estimation of relaxation times (spin–lattice $T1$ and spin-spin $T2$) can provide additional information of the molecular structure. Several results were obtained in the oil/water mixtures content determination in different foods [14–17]. Correlation between the measured relaxation times and increasing soluble sugar concentration was found in the analysis of wine grapes [18]. Relaxation times reflect molecular motion and can provide information on physiological changes during vinegar ageing process, induced by the water loss, like polymer formation, oxidation and degradation processes, etc. In our previous work, we proposed ^{1}H NMR spectroscopy for quantification of selected compounds applied in combination with statistical methods as a possible tool for ageing determination in TBVM [5]. In this paper, we characterized commercial BVM samples by the use of high-resolution ^{1}H NMR technique and $T1$ spin–lattice relaxation measurements, combined with multivariate statistical analysis. The combination of these NMR data offers the possibility to create a training set with good predictability which enables to determine the age of BVM sample of unknown ageing process, by predicting the $T1$ value.

2. Experimental

NMR. 22 BVM commercial samples of different producers have been used for quantitative metabolite determination with the declared ageing process (<3 or >3 years) directly indicated on the bottle labels only for 20 samples. Two samples were over 5 years (>8 and >12) of ageing process while one TBVM of 20 years and a "young" TBVM sample (4 year) were also included for comparison in the calculations. Among all analyzed samples, 24 in total, most were purchased in commercial stores while the two TBVM were gifted by "Consorteria di Spilamberto". ^{1}H NMR spectra for quantitative analysis have been recorded on a Bruker DMX 500 spectrometer operating at 11.7 T and equipped with a 5-mm reverse probe with z-gradient. Samples for quantitative determination were prepared by dissolving 50 μL of vinegar in 450 μL of DMSO-$^2H_6$. An external calibrated TSP reference (trimethylsylyl [2,23,3-2H4] propionate) has been used to obtain quantitative measurements. All spectra have been acquired with low power water signal irradiation, phase and baseline corrected before FT transformation and standard integration routine from TOPSPIN program (1.3 Bruker version) have been used for signal quantification. Selected resonances (hydroxyl–methyl–furfural, hereafter denoted HMF, β-glucose, malic acid, acetic acid and ethanol) being the most significant compounds for monitoring the ageing process in agreement with literature [5], were evaluated. In case of HMF, a medium value was selected for resonances at 9.67, 7.63 and 6.74 ppm, as indicated in Fig. 1C.

Samples for $T1$ measurements were used directly, without any solvent addition; an external capillary filled with deuterated solvent (DMSO-$^2H_6$) was added only for locking the signal. $T1$ measurements were performed on a Bruker DRX 400 spectrometer equipped with a 5-mm reverse probe with z-gradient. Standard $T1$ Bruker library sequence was used without modifications; the sequence is based on the classical "inversion recovery" sequence built with inversion recovery time spanning from 5 μs up to 20 s, repetition time 20 s, 128 scans and 30 experiments were acquired for each sample over 64 K points. The heights of peaks were used to calculate the longitudinal relaxation values. The experimental data were fitted following the Levenberg–Marquardt algorithm implemented in the TOPSPIN Bruker software.

2.1. Statistical methods

NMR integrated resonances were included in Excel worksheet (Microsoft) and imported into SIMCA-P 11 (Umetrics, Umea Sweden). Principal Component Analysis (PCA) and Partial Least Square (PLS) performed with NMR integrated resonances and $T1$ measurements were scaled with "Pareto" and "Unit Variance" (UV) as data pre-treatment [19,20] respectively.

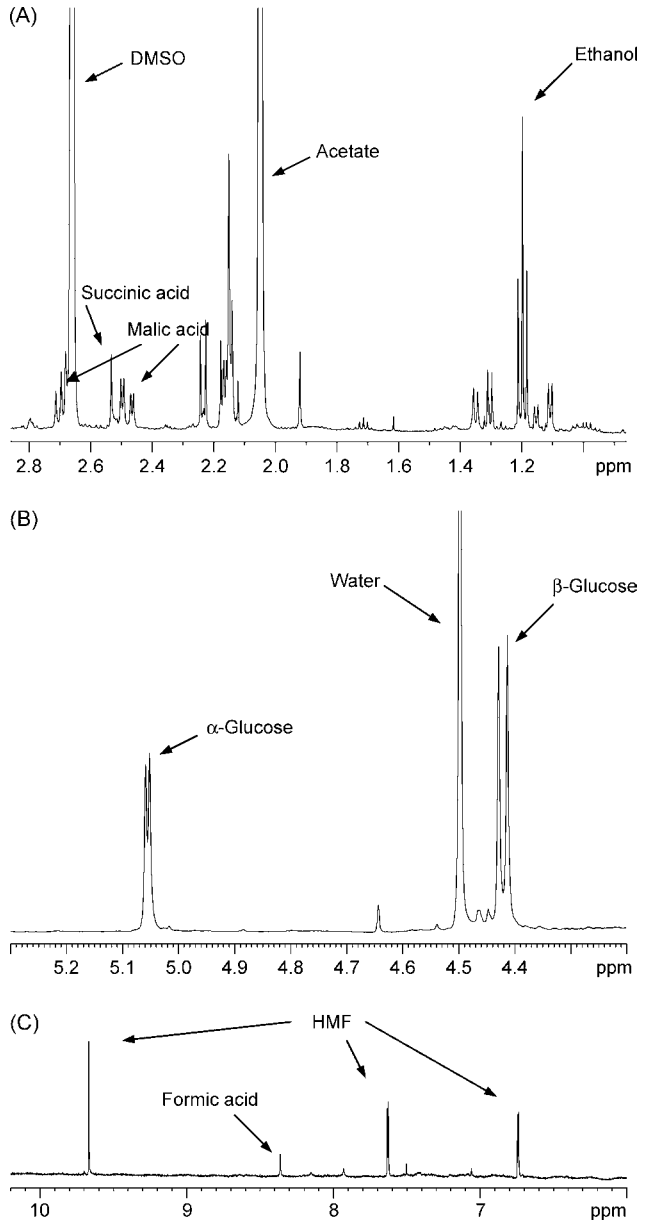

Fig. 1. ^{1}H spectrum of a BVM sample, with different expansions: (A) aliphatic, (B) anomeric and (C) aromatic region. The assignment of resonances used for selective quantification and other signals is reported.

3. Results and discussion

Quantitative measurements of five selected compounds, being HMF, β-glucose, malic acid, acetic acid and ethanol were obtained from ^{1}H NMR spectra, as previously described [5] and indicated in Fig. 1 together with other assigned resonances not useful for ageing determination. In particular, the selected resonances were integrated and evaluated with respect to the TSP as reference for quantitative determination. Only the β-anomeric proton signal for glucose was used because the anomeric protons of α- and β-glucose revealed the mutarotational equilibrium naturally present in water solution [21]. All analyzed samples with the declared ageing process were summarized in Table 1.

Significant concentration distribution of the selected compounds among all samples is denoted and preliminary remarks can be easily deduced; for example, sample nos. 8, 21, 22, 23 and 24 showed large malic acid and β-glucose content. Concerning sample no 8 this is due to a special procedure used for its preparation, obtained with a large addition of cooked must, as stated by the producer. Sample no. 24 is a TBVM sample while samples nos. 22 and 23 are aged BVM samples. Finally sample no. 21 is a on the way to be a real TBVM, obtained from cooked must and this explains the difference in both malic acid and β-glucose content with respect to all the other samples being BVM that were subjected to a completely different production procedure.

Principal Component Analysis (PCA) was initially explored, by using these resonances for all samples, to reduce dimensionality of multivariate data and to preserve most of the variance present [22]. This unsupervised technique, is a useful tool for visualization of grouping within multivariate dataset, with the usual bi-dimensional graphical representation.

The resulted two components model performed with 21 samples (BVM with declared ageing process >8, >12 and the TBVM sample with 20 years of ageing were omitted because resulting as strong outliers) explained 95.9% of the total variance, and as can be observed in the score plot of Fig. 2A; the first two pc's, accounting for pc1 = 82.1% and pc2 = 13.8%, gave a good sample separation. Samples with declared ageing process lower than 3 years were clustered on the negative values of pc1 in the score plot, while samples >3 years were in the opposite direction. As the samples separation is concerned, pc1 axes can be considered as the ageing axe. In this respect, is noteworthy that all these samples were far away from the TBVM sample (4 years), which was not yet a real TBVM sample due to insufficient ageing process, but nevertheless, it went through a completely different production procedure, even though at a very young stage, thus explaining its position within the score plot. Circled sample (<3 years, number 8 in Table 1) needs particular considerations; it resulted as a strong outlier in score plot of Fig. 2A due to additional charges in concentrated must and large addition of wine vinegar, thus conferring high sugar and acetic acid content. The loading plot for both pc1 and pc2 (Fig. 2B) accounted for the samples separation observed in the previous score plot. In particular, the circled sample (<3 years) reflected its particular preparation showing large sugar and acetic acid content; samples with <3 years of ageing process, showed positive contribution to the second component, being positively affected by larger acetic acid content. Samples with ageing >3 years were positively correlated with pc1 and negatively correlated with pc2, being characterized by larger sugar content. The other compounds (i.e. HMF and ethanol) showed minor variance, thus not affecting the sample separation, thus confirming the initial considerations made by the inspection of metabolic content quantification of vinegar samples.

The measurement of the spin–lattice relaxation times for acetic acid and β-glucose anomeric signal for all samples are summarized in Table 1, showing a clear sample differentiation. Shorter relaxation times were associated with increasing solid soluble concentration, typically observed for older vinegar samples. This is consistent with previous results [23,24] where

Table 1
Selected signals quantification (g/L) and $T1$ values (ms) for BVM and TBVM samples with declared ageing process

Sample	Age (years)	EtOH	AcOH	Malic acid	β-Glu	HMF	$T1$-βGlu anomeric	$T1$-AcOH	$T1$-βGlu predicted
1	<3	0.730	77,980	6,168	52,116	0,639	677,29	1321	695,943
2	<3	1.621	63,453	6,584	39,150	1,150	703,981	1435	652,809
3	<3	1.546	77,077	6,327	49,213	1,608	710,065	1309	693,947
4	<3	0.958	76,797	6,150	60,779	0,603	725,36	1585	665,371
5	<3	0.979	108,855	8,120	70,951	0,884	873,377	1450	732,244
6	<3	1.201	108,330	5,844	77,970	0,244	829,322	1870	730,187
7	<3	0.821	80,786	5,684	55,020	1,126	631,564	1295	688,698
8	<3	5.209	166,637	18,809	231,054	0,580	365,39	518,03	459,453
9	<3	1.035	87,910	4,906	65,844	0,635	822,65	1778	689,996
10	<3	2.090	114,131	7,661	62,109	0,264	784,396	1447	777,224
11	<3	1.130	91,071	5,266	57,901	0,861	671,19	1533	719,309
12	<3	2.875	88,764	8,211	76,744	0,934	685,25	1507	662,174
13	<3	1.008	99,151	1,873	69,385	0,040	783,321	1584	745,647
14	<3	1.308	92,789	7,628	78,949	0,093	712,252	1751	651,078
15	>3	2.291	88,999	17,605	130,595	2,448	537,855	1150	470,969
16	>3	2.660	79,649	12,506	122,940	2,017	500,488	1156	470,078
17	>3	1.734	99,463	9,778	117,564	1,485	515,2	962,356	571,020
18	>3	2.301	58,209	10,546	91,092	1,190	473,148	916,801	502,643
19	>3	2.157	67,565	10,344	99,070	1,247	516,455	914,646	499,803
20	>3	1.868	65,800	10,112	100,972	1,148	386,725	607,652	498,811
21	4	1.181	122,450	33,592	136,302	2,389	290,023	385,327	555,823
22	>8	3.091	163,654	32,719	285,316	7,764	342,44	499,48	222,498
23	>12	1.656	40,613	30,305	169,656	4,011	196,781	204,007	293,543
24	20	1.067	69,526	45,069	276,390	13,012	48,727	96,675	11,396

Underlined samples were omitted in the training set of the PLS model (see text for more details).

measuring spin–lattice relaxation times in aqueous solution of glucose and sucrose, $T1$ decrease for higher concentrations of sugar was found, reflecting the molecular interaction between sugar and water molecules. Sample no 8 showed shorter $T1$ values than what was expected for its real ageing process, typical of an older sample. This result is in agreement with previous data concerning selected compound quantification, thus confirming the particular preparation for this sample. New PCA analysis could be performed with the introduction of $T1$ measurements for the analyzed samples as additional variables.

The PCA score plot (Fig. 3A) obtained by the addition of $T1$ values, improved sample separation increasing the explanation up to 97.5% of the total variance; pc1 accounted for 74.8% and pc2 for 17.8%. The model diagnostics are summarized by the fit goodness (R^2_{cum}) and more important, by the prediction goodness parameter (Q^2_{cum}); the cross validation (CV) is used to estimate the predictive ability of the model [25]. The squared differences between predicted and observed values are summed to form the predictive residual sum of squares (PRESS) which is a measure of the predictive power of the tested model. In SIMCA-P, CV (internal validation) is conducted for each consecutive model dimension starting from the beginning, giving a PRESS which is compared with the residual sum of squares (RSS) of the previous dimension. When PRESS is not significantly smaller than RSS, the tested dimension is considered insignificant and the model building is stopped. In our case, Q^2_{cum} improved up to 0.74 (while $Q^2_{cum} = 0.46$ for the previous determination) thus conferring higher predictability. The corresponding loading plot (Fig. 3B) reflected the higher $T1$ values for younger BVM samples, which affected positively pc2 component.

Partial least square projections to latent structures (PLS) is a regression extension of PCA and is a method for relating two data matrices, namely X and Y to each other by linear multivariate model [26]. When a PLS model has been created and judged reliablly through the interpretation of model parameters like cross-validation tests, it can be used for predicting the Y data for new observations that have not influenced the model. Therefore, this methodology can predict the responses in the observations, by extracting latent variables T (X scores) and U (Y scores) from sampled factors and responses, respectively. This is resembled in the t_1/u_1 plot; in this representation, the observations in the projected X (T) and Y (U) space are displayed and show how well the Y space correlates to the X space; the better the correlation, the better the points which are normally distributed, following close to a straight line. We created a reliable model and we tried to predict the $T1$ values for new BVM samples for which only quantification of the selected resonances were known.

In this respect, we performed PLS on 16 samples by using six variables (the quantification of five selected compounds and $T1$ values for β-glucose used as Y) as training set. Then we included as prediction set 8 samples, with their corresponding selected compounds quantified values as variables, to perform predictions on β-glucose $T1$ values for all samples. The samples used for prediction were selected casually; in particular, nos. 1, 2, 4, 6, 13, 14, 17, 20 (compare Table 1). This procedure was repeated different times by using different samples to create the training set, and we obtained the same trend in the predicted $T1$ values. Last column in Table 1 indicates the predicted $T1$ values for β-glucose whose magnitude order is indicative of ageing differentiation among samples; younger than 3 years were clus-

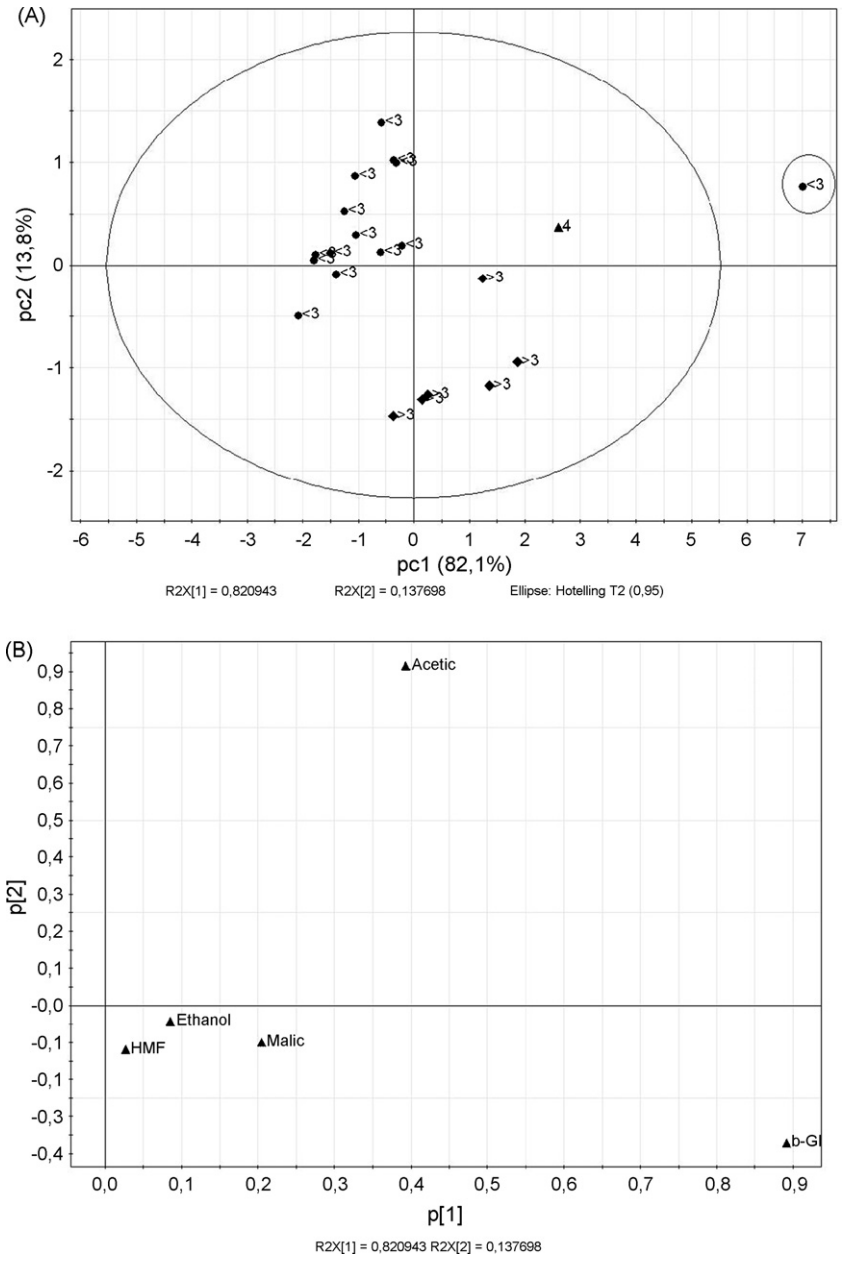

Fig. 2. (A and B) Score and loading PCA plots for 21 samples (BVM and TBVM) by using five selected compounds; the model diagnostics are $R^2_{cum} = 0.959$, $Q^2_{cum} = 0.461$. Samples with declared different ageing process are represented with different filled symbols: circle for <3 years, diamond for >3 years and triangle for TBVM of 4 years ageing. Integrated resonances were pre-treated with Pareto scaling.

tered among 780 and 650 ms, older than 3 years among 570 and 470 ms, while the oldest samples showed values lower than 300 ms. Very good agreement is observed for sample no. 21, being 4 years old TBVM, showed a predicted $T1$ value typical for >3 years BVM. Sample no. 8 again showed a predicted $T1$ value for β-glucose typical of older than 3 years samples, thus confirming its anomaly.

We tried to repeat the prediction procedure using $T1$ values for acetic acid, and we obtained the same trend for $T1$ predicted values. These data are not shown. Validation of the PLS model can be evaluated by performing different tests; one over all the CV (cross validation) test, in other words looking, as previously described, at the Q^2 values change as function of increasing model complexity; by inspection of the linearity correlation between X and Y scores (t_1/u_1 plot) and finally performing the response permutation test [27]. In our case, two components for PLS model appeared to be appropriate because looking at the R^2Y and Q^2 statistics change as a function of increasing model (data not shown) it revealed a marginal decrease of Q^2 by introducing the third component ($Q^2 = 0.66$ and $Q^2 = 0.62$, for two and three model components respectively). Another graphical representation indicative of the model goodness is the linearity of the u/t plot, which explains the correlation between X and Y. Fig. 4A showed the t_1/u_1 plot for the PLS model, indi-

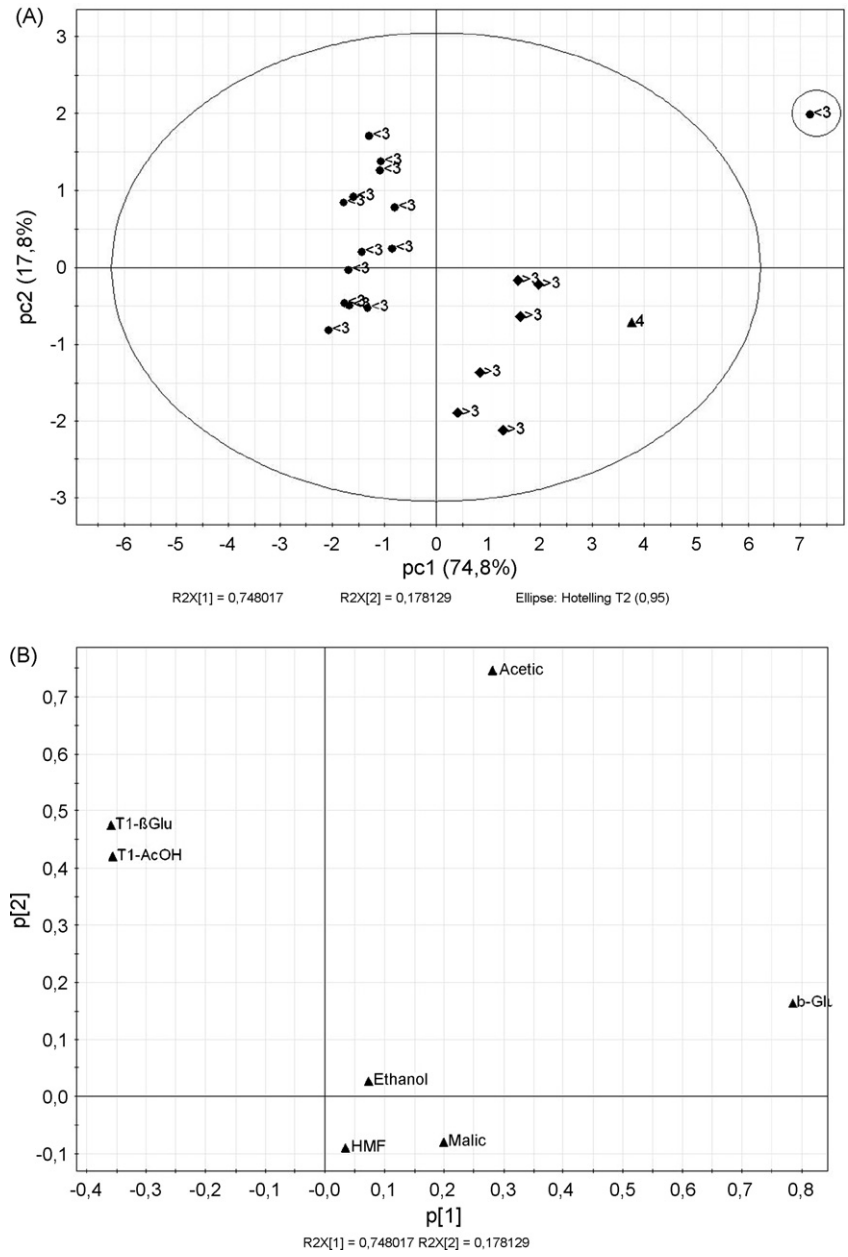

Fig. 3. (A and B) Score and loading PCA plots for the 21 samples (BVM and TBVM) by using five selected compounds and $T1$ values for acetic acid and β-glucose; the model diagnostics are $R^2_{cum} = 0.975$, $Q^2_{cum} = 0.742$. Samples with declared different ageing process are represented with different filled symbols: circle for <3 years, diamond for >3 years and triangle for TBVM of 4 years ageing. Integrated resonances were pre-treated with Pareto while for $T1$ values UV scaling (Unit Variance) was used.

cating a good linear correlation (0.63) with no outliers. Finally, Fig. 4B represented the validate model plot of "$T1$ of β-glucose" response, which was well modelled; R^2Y and Q^2 values were in good agreement with the reference limits for intercepts, thus conferring statistical significance of the estimated predictive power of the PLS model.

Inspection of the normal probability plot (data not shown), resulted in a strong linear pattern (correlation coefficient $R^2 = 0.988$), thus demonstrating that the normal distribution provided a very good model for the data.

In conclusion, our results indicated that our previously determined protocol [5] consisting of ^{1}H NMR selected compounds quantification and multivariate statistical protocols applied to TBVM, can be successfully used for assessing the ageing process also for BVM. The $T1$ spin–lattice relaxation time of the most abundant vinegar compounds, such as β-glucose and acetic acid, have been shown to be strongly correlated with ageing process and quality. The additional use of $T1$ values for the analyzed samples improved the statistical model, raising a better ageing differentiation for BVM. The proposed model can finally predict $T1$ values of some selected compounds, such as acetic acid or β-glucose on the basis of previous NMR quantification, thus giving rise to a rapid ageing identification for BVM samples of unknown ageing process.

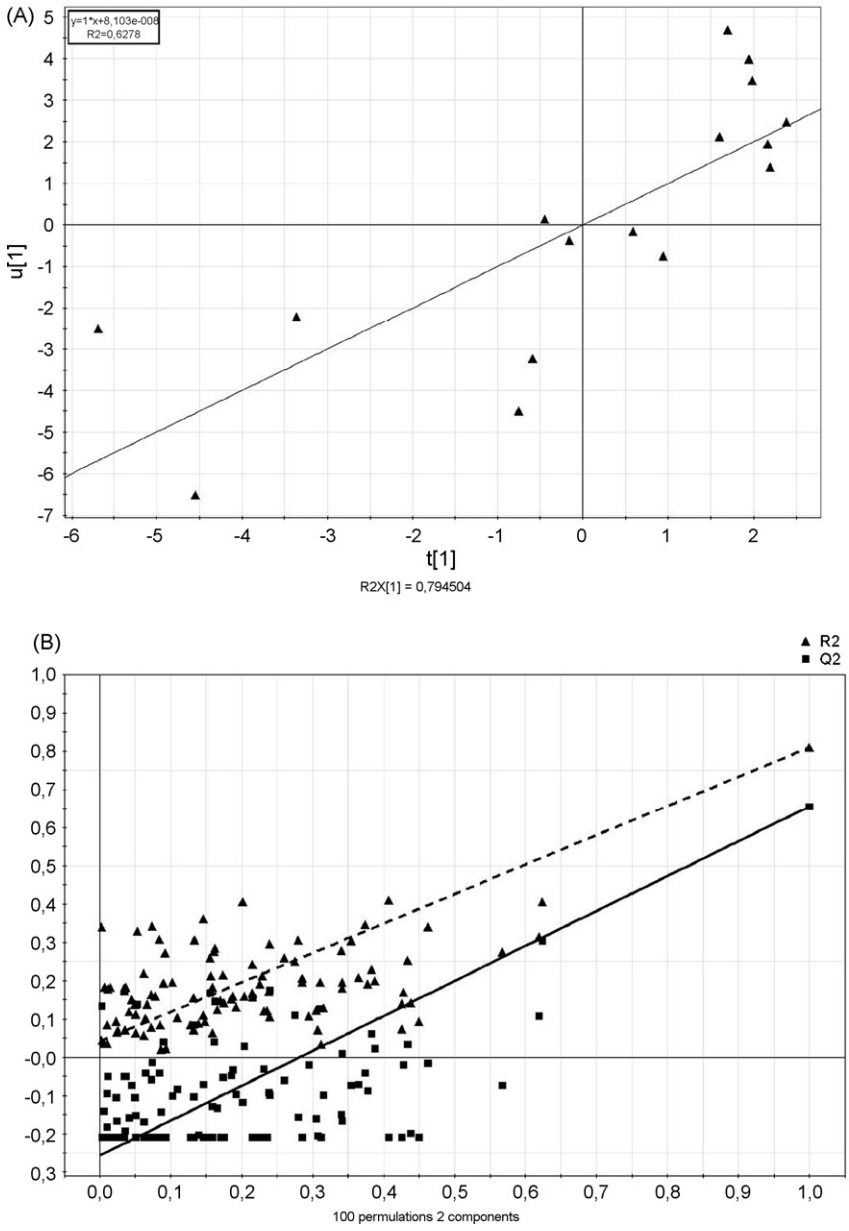

Fig. 4. (A) t_1/u_1 score plot for PLS model indicating strong correlation between factors and responses; no outliers were detected. (B) Validate model plot of response "*T*1 of β-glucose"; the *Y* axis represents R^2Y (triangles) and Q^2 (squares) for every model, while *X* axis indicates the correlation coefficient between original (triangles) and permutated (squares) data. The 100 permutations have been performed for this plot. Conventional regression analysis performed in the two set of points, dash line for triangles and solid line for squares, designates the intercepts which are meaningful of the measure of the background of R^2Y and Q^2 obtained by fitting the random data. Usually, R^2Y should not exceed 0.3–0.4 and Q^2 0.05.

Acknowledgments

Prof. Vincenzo Ferrari Amorotti and Prof. Francesco Saccani of Consorteria di Spilamberto of Modena are acknowledged for their kind availability and scientific supporting.

References

[1] M. Plessi, D. Bertelli, F. Miglietta, J. Food Compos. Anal. 19 (2006) 49.
[2] M. Cocchi, C. Durante, M. Grandi, P. Lambertini, D. Manzini, A. Marchetti, Talanta 69 (2006) 1166.
[3] M. Gullo, C. Caggia, L. De Vero, P. Giudici, Int. J. Food Microbiol. 106 (2006) 209.
[4] D. Sanarico, S. Motta, L. Bertolini, A. Antonelli, J. Liq. Chromatogr. R.T. 26 (2003) 2177.
[5] R. Consonni, A. Gatti, J. Agric. Food Chem. 52 (2004) 3446.
[6] A. Hermann, Eur. Food Res. Technol. 212 (2001) 683.
[7] G. Remaud, C. Guillou, C. Vallet, G.J. Martin, Fres. J. Anal. Chem. 342 (1992) 457.
[8] A. Del Signore, B. Campisi, F. Di Giacomo, J. AOAC Int. 81 (1998) 1087.
[9] D.W. Lachenmeier, W. Frank, E. Humpfer, H. Schäfer, S. Keller, M. Mörtter, M. Spraul, Eur. Food Res. Technol. 220 (2005) 215.
[10] P.M. Falcone, A. Baiano, A. Conte, L. Mancini, G. Tromba, F. Zanini, M.A. Del Nobile, Adv. Food Nutr. Res. 51 (2006) 205.
[11] L. Laghi, M.A. Cremonini, G. Placucci, S. Sykora, K. Wright, B. Hills, Magn. Reson. Imag. 23 (2005) 501.
[12] A.J. Charlton, W.H. Farrington, P. Brereton, J. Agric. Food Chem. 50 (2002) 3098.

[13] I.S. Arvanitoyannis, C. Chalhoub, P. Gotsiou, N. Lydakis-Simantiris, P. Kefalas, Crit. Rev. Food Sci. Nutr. 45 (2005) 193.
[14] H. Hickey, B. MacMillan, B. Newling, M. Ramesh, P. Van Eijck, B. Balcom, Food Res. Int. 39 (2006) 612.
[15] H. Todt, G. Guthausen, W. Burk, D. Schmalbein, A. Kamlowski, Food Chem. 96 (2006) 436.
[16] F. Mariette, Comp. Rendus Chim. 7 (2004) 221.
[17] R. Lakshmanan, J.A. Parkinson, J.R. Piggott, LWT-Food Sci. Technol. 40 (2007) 544.
[18] J.E. Andaur, A.R. Guesalaga, E.E. Agosin, M.W. Guarini, P. Irrarazaval, J. Agric. Food Chem. 52 (2004) 165.
[19] S. Wold, E. Johansson, M. Sjöström, M. Sandberg, S. Rännar, Anal. Chim. Acta 277 (1993) 239.
[20] S. Wold, E. Johansson, M. Cocchi, 3D-QSAR in Drug Design, Theory, Methods and Applications, ESCOM Science, Leiden, 1993, pp. 523–550.
[21] D. Horton, Z. Waleszek, Carbohydr. Res. 105 (1982) 145.
[22] L. Erikson, E. Johansson, N. Kettaneh-Wold, S. Wold, Multi and Megavariate Data Analysis, Umetrix Academy, Umeå, Sweden, 2001.
[23] V. Arulmozhi, A. Srinivasa, Phys. Chem. 26 (1993) 201.
[24] S. Sattiacoumar, V. Arulmozhi, Bull. Soc. Chim. Belg. 10 (1993).
[25] H. Wold, Technometrics 20 (1978) 397.
[26] S. Wold, M. Sjöström, L. Eriksson, PLS in Chemistry, The Encyclopaedia of Computational Chemistry, in: Schleyer, P., v., R., Allinger, N.L., Clark, T., Gasteiger, J., Kollman, P.A., Schaefer, III, H.F., Schreiner, P.R., (Eds.), Wiley, Chichester (1999), 2006.
[27] H. Van der Voet, Chemometr. Intell. Lab. 25 (1994) 313.

Available online at www.sciencedirect.com
ScienceDirect
Talanta 73 (2007) 321–325
Talanta
www.elsevier.com/locate/talanta

The effect of various drying techniques on apricot volatiles analysed using direct thermal desorption-GC–TOF/MS

Fahrettin Göğüş [a,*], Mustafa Z. Özel [b,1], Alastair C. Lewis [c]

[a] *The University of Gaziantep, Engineering Faculty, Food Engineering Department, 27310 Gaziantep, Turkey*
[b] *The University of Pamukkale, Faculty of Science & Arts, Chemistry Department, P.O. 286, 20017 Denizli, Turkey*
[c] *The University of York, Department of Chemistry, Heslington, YO10 5DD York, UK*

Received 20 December 2006; received in revised form 15 March 2007; accepted 23 March 2007
Available online 31 March 2007

Abstract

The volatile constituents obtained from dried Şekerpare-type apricots by direct thermal desorption were examined using gas chromatography (GC) coupled with time of flight mass spectrometry (TOF/MS). Various commercially used drying techniques (sun, hot air and microwaves) were employed to dry the apricot samples before desorption. Some apricots were dried using only a desiccator and the volatile desorbed from these was used as a standard. Limonene (16.33%); (*E*)-2-hexenal (9.32%); γ-decalactone (7.89%); butyl acetate (6.94%); β-ionone (5.96%); acetic acid (4.83%) and isobutanal were found to be the major components in the desiccator-dried samples. This is the first study to report the detection of isobutanal, tridecanol and 1-pentadecanol as dried apricot constituents. The profiles of the volatiles desorbed changed when other drying techniques (sun, hot air, and microwaves) were used. The major components found in samples dried by these three methods were 5-hydroxymethylfurfural (5-HMF), 2,3-dihydro-4-*H*-pyran-4-one and furfural.

Keywords: Apricot; Direct thermal desorption; Volatiles; Drying

1. Introduction

Volatiles are known to affect the sensorial quality of both fresh and processed fruits. The concentration of fruit volatiles can be affected by processing conditions as well as agronomic factors [1]. There have been some studies done on the volatile components of various fruits [1,2]. There are also a few studies on the volatile components of various varieties of apricot [3–6] and apricot juice [7]. However, all of these studies concentrated on fresh apricots, and there is scarcely any data found in the literature on the volatiles of dried apricots. Komes et al. [8] studied the effect of trehalose on the flavor retention of freeze-dried and foam-mat dried apricot puree.

Drying is the most important process in the successful storage of apricots. Though sun drying is the most common method employed, it is time consuming and prone to contamination with dust and insects, aside from being weather-dependent. Microwave drying and hot-air drying methods are also used. When a wet solid is exposed to microwave heating, its temperature may reach the boiling point of the liquid it contains. The accompanying generation of vapour due to the internal evaporation of moisture brings about a gas pressure gradient that can rapidly expel the moisture from the interior of the solid. Microwave heating has the specific advantage of rapid and uniform heating due to penetration of microwaves into the body of the product [9]. This process leads to very rapid drying without overheating the atmosphere or the surface in comparison to hot air drying. Apricots at the time of harvest have a moisture content of 80–85% (wet basis). When dried for consumption as a dried fruit product, the desired moisture content is around 25–30% (wet basis).

The analysis of volatiles is generally accomplished by an extraction step, followed by concentration, chromatographic separation, and subsequent detection. Well-established methods of analysis of volatiles of apricot include steam distillation, vacuum steam distillation, solvent extraction and dynamic headspace techniques [4,6]. An overview of sample preparation

* Corresponding author: Tel.: +90 342 360 1200; fax: +90 342 360 1105.
E-mail address: fahret@gantep.edu.tr (F. Göğüş).
[1] The University of York, School of Chemistry, Heslington, YO10 5DD York, UK.

0039-9140/$ – see front matter © 2007 Elsevier B.V. All rights reserved.
doi:10.1016/j.talanta.2007.03.048

methods is provided by Pillonel et al. [10] for food volatiles and by Wilkes et al. [11] for food flavors and off-flavors. The chromatographic profile will vary depending upon the method of sample preparation employed, and it is not uncommon to produce artifacts during this step.

The dynamic headspace technique is a very popular method for analyzing volatile compounds in plant materials [12,13], and in cheese [14]. Direct thermal desorption (DTD) is one version of a dynamic headspace technique with cryogenic trapping post desorption used to enrich the analytes prior to separation. DTD has important advantages over the other methods such as the ability to be directly coupled to gas chromatography–mass spectrometry [15], the requirement of only a small amount of sample and of course the fact that it is a rapid method. DTD also has disadvantages, e.g. the thermal decomposition of thermo labile compounds and the adverse affects that water in the sample. According to previous literature, the DTD method has been applied to various systems such as beef [16], plant material [13], sugar [17], and cheese [18].

A great future strength of the technique, however, is that it may allow the elimination of the traditional sample preparation stages in a number of areas. The analytical technique of DTD coupled with GC is a very viable one. It is suitable especially for rapid qualitative compound analysis.

The direct thermal desorption technique used here has been applied in only a limited fashion previously [15–19], and we believe that there is significant scope for DTD coupled with GC separation online. In the present investigation efforts have been made to examine the effect of different drying techniques on the volatile components of apricot using DTD coupled with GC–TOF/MS.

2. Materials and methods

2.1. Materials

Fresh Şekerpare-type apricots (*Prunus armeniaca*) were purchased from a local producer in Malatya, Turkey. They were dried on the day of purchase, using either the sun or hot air, microwaves or a desiccator. The initial moisture content of the apricots was 81.23% (wet basis). Prior to drying; each apricot was halved and the pit removed.

2.2. Drying methods

Sun drying was achieved by spreading the apricot samples on cloth for 3 days under the effect of the sun's rays. The samples dried to a moisture content of 25% wet basis which is the level of drying normally used in commercial production.

Hot air drying was performed in a pilot plant tray dryer (UOP 8 tray dryer, Armfield Ltd., UK), which was operated at an air velocity of 1.5 m s^{-1} at a temperature of 60 °C. The drying process took 18 h to reach a moisture content of 25% wet basis.

For microwave drying, a programmable domestic microwave oven (Arçelik ARMD 580, Turkey), with a maximum output of 700 W at 2450 MHz was used. A power level of 70 W was used after a few trials. The product dried at these conditions was used in this study. The drying process was ended after 140 min when the material had reached a moisture content of 25% wet basis.

Some apricots were dried using only a desiccator. This was done so that the resulting desorbed volatile could be used as a control since with the low temperature applied and less severe conditions, the desiccator-only dried samples were thought to be most alike fresh ones. The samples to be dried in the desiccator were cut into very small pieces. The cut pieces were placed in a glass desiccator which contained PCl_5 at the bottom. The glass desiccator was flushed with nitrogen gas and stored in the dark at 5 °C until the apricot samples were dry. The final moisture content of the apricot samples was less than 5%. Maximum drying time in the desiccator was 72 h.

For direct thermal desorption, samples of very low water content are necessary. The samples dried by the commercial methods of sun, hot air and microwaves would be too high in water content at 25% wet basis. Further drying was therefore needed and to avoid any deleterious effects of further drying by these three methods, these samples were further dried in the desiccator to below 5% wet basis, undergoing the same process in the desiccator as described above. All apricot samples were kept in polyethylene bags at 5 °C until being used.

2.3. Direct thermal desorption

DTD was carried out in an ATD 400 unit (Perkin-Elmer, Norwalk, CT, USA). Dry samples (2–5 mg) were introduced into a stainless steel tube (desorption cartridge, 89 mm × 4.5 mm i.d. × 6.5 mm o.d.), and desorbed under a helium flow at 150 °C for 5 min. Volatile compounds were cryofocused using a dual graphitized carbon black and carbon molecular sieve trap (Perkin Elmer) at −30 °C, which after 4 min was rapidly heated at a rate of 40 °C/s to 325 °C and held for 30 min. The desorbed volatiles were transferred to the GC column through a heated fused-silica line at 225 °C.

2.4. Chromatographic analysis

The GC–time of flight mass spectrometry (TOF/MS) system consisted of an HP 6890 (Agilent Technologies, Palo Alto, CA, USA) gas chromatograph and a Pegasus III TOF-MS (LECO, St. Joseph, MI, USA). The column was a non-polar DB5 (60 m × 0.32 mm i.d. × 1 μm film thickness) purchased from J&W Scientific (Folsom, CA, USA).

Helium was used as a carrier gas. The initial temperature of the column was 35 °C for 7 min and the subsequent temperature programme was a heating rate of 15 °C min^{-1} until 240 °C was reached and held for 10 min. Peak identification was made using TOF/MS with electron impact ionisation (70 eV). The mass spectrometer used a push plate frequency of 5 kHz, with transient spectra averaging to give unit resolved mass spectra between 35 and 350 amu at a rate of 50 spectra s^{-1}. Mass spectra were compared against the NIST ĭ98 (National Institute of Standards and Technology, Gaithersburg, MD) mass spectral library.

3. Results and discussion

The volatile constituents of dried apricot samples were isolated by thermal desorption with a cryo-focusing trap and analyzed using GC–TOF/MS. The optimization of the DTD temperature has been studied previously and 150 °C was found to be the best from the 100–250 °C range studied [20]. The DTD temperature used, therefore, was 150 °C. The time of thermal desorption was 5 min at this temperature. The volatile constituents of the apricot samples obtained from this were immediately analysed using in-line GC–TOF/MS. As has been discussed by Grimm et al. [21], sample preparation is the crucial step for the further analysis of compounds. Pillonel et al. [10] described some of the advantages of the thermal desorption techniques as follows: (i) analysis of 100% of the trap content (instead of an aliquot part), (ii) no solvent peak, (iii) no waste and (iv) no contamination.

The samples dried only in the desiccator at 5 °C were prepared as a standard to represent the volatile constituents of the fresh apricot. Results are the mean of four experiments and the standard deviation of each compound is given. A range of hydrocarbons, esters, lactones, aldehydes, ketones and acids are present in the volatiles of apricot. The major components identified in the desiccator-dried apricot were limonene (16.33%); (*E*)-2-hexenal (9.32%); γ-decalactone (7.89%); butyl acetate (6.94%); β-ionone (5.96%); acetic acid (4.83%) and isobutanal (4.78%). It has been reported by Guillot et al. [3] who studied six varieties of fresh apricot that limonene, and (*E*)-2-hexenal are among the major components. Takeoka et al. [4] also reported for fresh apricots of the Blenheim variety that (*E*)-2-hexenal, γ-decalactone, and β-ionone were among the major contributors to apricot aroma. However, they found that esters (>85%) were the dominant constituents using headspace analysis. Ethyl acetate, butyl acetate and hexyl acetate with a total percentage of 10.52% were the only esters found in the desiccator-dried apricots of the Şekerpare variety. Isobutanal, tridecanol and 1-pentadecanol were reported as apricot constituents for the first time in this study.

Table 1 lists the compounds identified in the volatiles of dried apricot samples using DTD together with their Kovats indices, corresponding percentage compositions and their standard deviations. It should be noted that the peak identification of components is based on both library mass spectra and Kovats indices. Identification was based on a mass spectral library search using similarity and reverse factors above 750 and 800, respectively. Lower values than these were counted as unknown and components having these low values were not compared for their Kovats indices. Dalluge et al. [22] and Özel et al. [20] also used similarity and reverse factors above 750 and 800, respectively.

It was seen that the method of drying the apricot samples resulted in a change in compositions of their volatiles. The number of components of volatile fractions obtained for the desiccator, sun, hot air and microwave dried samples was 32, 28, 32 and 30, respectively. Components having a percentage of less than 0.05%, even if identified by GC–TOF/MS, are not shown in this paper. The number of identified components common to all apricot samples was 21. Ethyl acetate, hydroxyacetone and 2-decen-1-ol were found only in the desiccator-dried apricot samples.

The major volatile components of apricot changed drastically when dried by commercial techniques (sun, hot air and microwaves). The main components identified using these drying techniques were 5-hydroxymethylfurfural (5-HMF), 2,3-dihydro-4-*H*-pyran-4-one and furfural. These compounds together with other minor ones (5-methyl furfural, pentyl furan, furaneol) are known to be the result of browning reactions. It is known that the heat treatment of fruits and vegetables often reduces the number of original volatile flavor compounds, whilst at the same time, introducing additional ones through the autoxidation of unsaturated fatty acids and thermal decomposition and/or initiation of caramelisation and/or Maillard reactions. Maillard reaction products may negatively affect the flavor of the dried product, whereas it is desirable to preserve some naturally present compounds such as β-ionone, β-decalactone and butyl acetate which positively enhance the flavor. Apricot with its very low fat and high sugar content particularly tends to produce browning reaction products. Sugars are very important in the quality of dried apricots. There are four major sugars, namely sucrose, glucose, fructose and maltose in apricot. The browning reaction products were only 5% in the desiccator-dried apricot samples. However, they were 53.20, 62.24 and 64.83% for the sun, microwave and hot air dried samples of apricot, respectively (Fig. 1). There is no quantitative data given in this study to compare the percentage retention of the volatiles between fresh and dried samples. Komes et al. [8] found that the retention of apricot aroma after foam-mat drying (7.3% moisture content) and freeze drying (2% moisture content) was only 17.81 and 43.23% of the original, respectively.

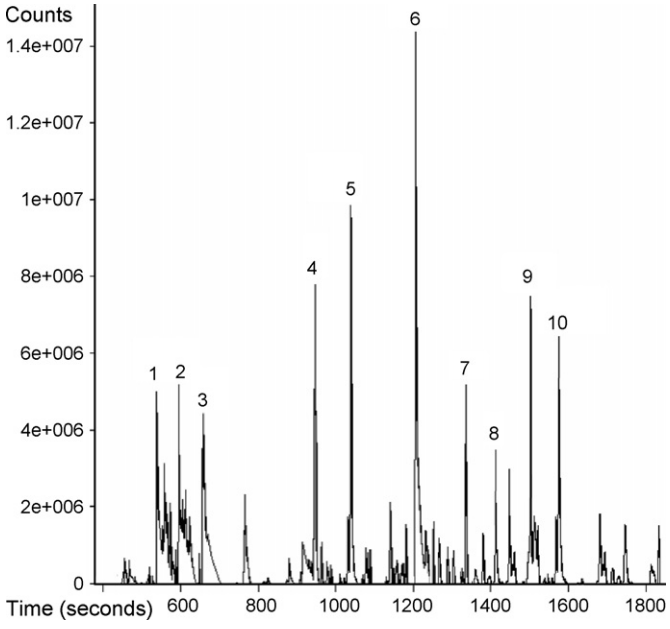

Fig. 1. GC-TOF/MS chromatogram of Sekerpare apricot volatile components at 150 °C using the DTD technique (1: Isobutanal; 2: Acetic acid; 3: Ethyl acetate; 4: Butyl acetate; 5: (E)-2-Hexenal; 6: Limonene; 7: Decanol; 8: Butyrolactone; 9: γ-decalactone; 10: β-ionone).

Table 1
Compounds, retention indices, percentage compositions of Şekerpare-type apricot volatile constituents for various drying techniques

Compound[a]	RI[b]	Sun (%)[c]	Microwave (%)[c]	Hot air (%)[c]	Desiccator (%)[c]
Isobutanal	540	0.37 ± 0.03[d]	–[e]	–	4.78 ± 0.36
Acetic acid	600	2.68 ± 0.22	2.87 ± 0.19	1.77 ± 0.22	4.83 ± 0.51
Ethyl acetate	628	–	–	–	3.37 ± 0.30
Methylbutanal	641	0.61 ± 0.05	1.32 ± 0.12	–	–
Pentanal	732	0.09 ± 0.02	0.14 ± 0.02	0.65 ± 0.09	–
Hexanal	801	0.70 ± 0.06	0.17 ± 0.03	1.02 ± 0.08	1.27 ± 0.23
Hydroxyacetone	803	–	–	–	0.47 ± 0.09
2,3-Butanediol	806	–	–	0.65 ± 0.08	
Butyl acetate	816	1.71 ± 0.15	–	0.13 ± 0.03	6.94 ± 0.77
Furfural	829	3.05 ± 0.22	4.27 ± 0.25	4.15 ± 0.51	1.11 ± 0.12
(*E*)-2-Hexenal	854	3.43 ± 0.31	3.18 ± 0.31	3.78 ± 0.44	9.32 ± 0.67
1-Nonene	891	–	0.13 ± 0.02	0.15 ± 0.03	0.17 ± 0.03
α-Pinene	939	0.05 ± 0.01	0.05 ± 0.01	–	–
Benzaldehyde	960	0.68 ± 0.08	0.54 ± 0.04	0.45 ± 0.06	0.82 ± 0.09
5-Methylfurfural	978	–	0.96 ± 0.07	1.38 ± 0.11	
1-Octen-3-ol	982	–	–	0.22 ± 0.04	0.28 ± 0.04
6-Methyl-5-heptenone	985	1.65 ± 0.12	1.57 ± 0.11	1.12 ± 0.15	0.87 ± 0.06
Pentylfuran	993	0.32 ± 0.04	0.23 ± 0.04	0.47 ± 0.08	–
Decane	1000	0.32 ± 0.05	0.18 ± 0.03	0.47 ± 0.06	2.71 ± 0.21
Hexyl acetate	1014	0.82 ± 0.07	0.52 ± 0.06	0.36 ± 0.04	0.21 ± 0.03
2-Ethylhexanol	1032	1.83 ± 0.09	1.56 ± 0.21	0.27 ± 0.05	1.37 ± 0.15
Limonene	1033	7.71 ± 0.69	5.41 ± 0.49	4.34 ± 0.52	16.33 ± 2.03
Phenylacetaldehyde	1048	–	0.52 ± 0.05	1.72 ± 0.24	–
Furaneol	1064	–	0.85 ± 0.09	1.41 ± 0.15	–
2-Decen-1-ol	1110	–	–	–	0.71 ± 0.09
2,3-Dihydro-3,5-dihydroxy-6-methyl-4*H*-pyran-4-one	1140	13.15 ± 1.28	12.18 ± 1.13	17.54 ± 1.54	2.11 ± 0.30
Nonanol	1169	1.97 ± 0.22	–	–	2.78 ± 0.23
α-Terpineol	1195	0.87 ± 0.06	1.12 ± 0.20	2.18 ± 0.23	1.51 ± 0.20
(*E*,*Z*)-2,4-Nonadienal	1196	–	–		1.06 ± 0.12
Dodecane	1200	0.84 ± 0.07	0.37 ± 0.04	0.45 ± 0.09	0.40 ± 0.08
Decanal	1209	1.63 ± 0.11	0.96 ± 0.07	0.49 ± 0.06	2.34 ± 0.22
5-HMF	1241	38.68 ± 2.59	43.75 ± 4.11	39.88 ± 3.81	1.78 ± 0.20
Decanol	1263	–	–	1.43 ± 0.11	3.83 ± 0.45
Butyrolactone	1299	1.31 ± 0.14	1.64 ± 0.15	1.43 ± 0.24	3.27 ± 0.29
Tetradecane	1400	1.23 ± 0.09	1.76 ± 0.23	1.15 ± 0.26	1.12 ± 0.15
Geranyl acetone	1448	–	–	0.61 ± 0.09	–
γ-Decalactone	1472	3.79 ± 0.32	3.52 ± 0.21	3.64 ± 0.44	7.89 ± 0.92
β-Ionone	1493	2.67 ± 0.36	2.11 ± 0.25	1.18 ± 0.20	5.96 ± 0.59
Tridecanol	1593	1.49 ± 0.11	0.53 ± 0.08	0.38 ± 0.09	2.22 ± 0.29
Hexadecane	1600	0.38 ± 0.05	1.06 ± 0.09	0.59 ± 0.09	1.46 ± 0.12
1-Pentadecanol	1787	0.59 ± 0.06	0.55 ± 0.07	–	1.38 ± 0.14
Unknown		5.38 ± 0.45	6.01 ± 0.64	4.54 ± 0.71	5.33 ± 0.68

RI: retention index.
[a] As identified by GC–TOF/MS software; names according to NIST mass spectral library, and by comparing their Kovats retention indices.
[b] Kovats retention indices of each component was collected from the literature for column DB5.
[c] Percentage of each component is calculated as peak area of analyte divided by peak area of total ion chromatogram times 100 (in the case of multiple identification, the areas of the peaks that belong to one analyte were combined to find the total area for this particular analyte).
[d] The standard deviations for four ($n = 4$) experiments.
[e] Not detected or percentage of the component is lower than 0.05%.

Over 87% of the volatiles defined were the same whether sun, hot air or microwave-drying had been used. However, hot air and microwave drying made a difference to the volatile profiles. For example 5-methyl furfural, phenylacetaldehyde and furaneol only appeared in the hot air and microwave dried samples. These degradation products were found at 2.33% and 4.51% in microwave dried and hot air dried samples, respectively. Phenylacetaldehyde has previously been found to be one of the major degradation products of the oxidation of phenylalanine [23]. Furaneol and 5-methyl furfural have also been found as Maillard reaction products in dried prunes [24]. Among the three commercial techniques studied, sun-drying was found to be best in that fewer degradation products were produced and the components of its resulting volatile were more alike that of the desiccator-only dried sample.

4. Conclusions

It was found that the number of components extracted at a desorption temperature of 150 °C were 32, 28, 32 and 30 for the

desiccator, sun, hot air and microwave dried samples, respectively. The major components of the volatiles changed with the various drying techniques. Among the three commercial techniques studied, sun-drying was found to be best in that fewer degradation products were produced and the components of its resulting volatile were more alike that of the dessicator-only dried sample.

It has been shown that direct thermal desorption is an extremely useful technique. Its main advantage is that it does not require a sample preparation stage unlike other methods. This means it is more rapid, easily carried out and compounds are not lost or contamination produced during sample preparation. Isobutanal, tridecanol and 1-pentadecanol were reported as apricot constituents for the first time in this study which demonstrates that using this technique is advantageous in detecting compounds which may have previously been lost in sample preparation stages.

A useful application of DTD coupled with GC–TOF/MS could be its use in industry to monitor the quality of the drying process of apricots. Samples could be rapidly and easily analyzed without the need for costly and time consuming sample preparation stages. However, the drying process in the desiccator should be considered as a time factor. Batches of dried apricots could be analyzed to check their levels of degradation products. This technique could even be used during the drying process itself to determine the end-point of drying. Drying could be halted, therefore, when the level of degradation products (or loss of the desirable flavor compounds) became unacceptably high. Further study would, of course, be needed to determine these levels.

Acknowledgements

The financial support of the UK Engineering and Physical Sciences Research Council, UK EPSRC and the UK Natural Environment Research Council are gratefully acknowledged. The authors would also like to thank Karen Özel for her comments and help in correcting our written English.

References

[1] C. Visai, M. Vanoli, Sci. Horticul. 70 (1997) 15.
[2] A. Koulibaly, M. Sakho, J. Crouzet, Lebensm-Wis. u-Technol. 25 (1992) 374.
[3] S. Guillot, L. Peytavi, S. Bureau, R. Boulanger, J.P. Lepoutre, J. Crouzet, S. Schorr-Galindo, Food Chem. 96 (2006) 147.
[4] G.R. Takeoka, R.A. Flath, T.R. Mon, R. Teranishi, M. Guentert, J. Agric. Food Chem. 38 (1990) 471.
[5] G. Chairote, F. Rodriguez, J. Crouzet, J. Food Sci. 46 (1981) 1898.
[6] C.S. Tang, W.G. Jennings, J. Agric. Food Chem. 15 (1967) 24.
[7] M. Riu-Aumatell, M. Castellari, E. Lopez-Tamames, S. Galassi, S. Buxaderas, Food Chem. 87 (2004) 627.
[8] D. Komes, T. Lovric, K.K. Ganic, J.G. Klujusuric, M. Banovic, Int. J. Food Sci. Technol. 40 (2005) 425.
[9] V. Velu, A. Nagender, P.G.P. Rao, D.G. Rao, J. Food Eng. 74 (2006) 30.
[10] L. Pillonel, J.O. Bosset, R. Tabacchi, Lebensm-Wis. u-Technol. 35 (2002) 1.
[11] J.G. Wilkes, E.D. Conte, Y. Kim, M. Holcomb, J.B. Sutherland, D.W. Miller, J. Chromatogr. A 880 (2000) 3.
[12] J.L. Esteban, I. Martinez-Castro, J. Sanz, J. Chromatogr. A 657 (1993) 155.
[13] M.Z. Özel, F. Göğüş, A.C. Lewis, J. Chromatogr. A 1114 (2006) 164.
[14] G. Arora, F. Cormier, B. Lee, J. Agric. Food Chem. 43 (1995) 748.
[15] J.L. Esteban, I. Martinez-Castro, R. Morales, B. Fabrellas, J. Sanz, Chromatographia 43 (1996) 63.
[16] A.M. Spanier, C.C. Grimm, J.A. Miller, ACS Symposium Series 564, Washington, DC, 1994, pp. 49–62.
[17] R.T. Marsili, N. Miller, G.J. Kilmer, R.E. Simmons, J. Chromatogr. Sci. 32 (1994) 165.
[18] F. Göğüş, M.Z. Özel, A.C. Lewis, J. Sep. Sci. 29 (2006) 1217.
[19] R. Shellie, P. Marriott, Flavour Frag. J. 18 (2003) 179.
[20] M.Z. Özel, F. Göğüş, J. Hamilton, A.C. Lewis, Chromatographia 60 (2004) 79.
[21] C.C. Grimm, S.W. Lloyd, J.A. Miller, A.M. Spanier, in: R. Marsili (Ed.), Flavor, Fragrance, and Odor Analysis, Marcel Dekker, New York, 2002, pp. 55–74.
[22] J. Dalluge, L.L.P. Van Stee, X. Xu, J. Williams, J. Beens, R.J.J. Vreuls, U.A. Th Brinkman, J. Chromatogr. A 974 (2002) 169.
[23] J. Adamiec, J. Rössner, J. Velisek, K. Cejpek, J. Savel, Eur. Food Res. Technol. 212 (2001) 135.
[24] J. Crouzet, P. Etievant, C. Bayonove, Food flavors. Part C, in: I.D. Morton, A.J. McLeod (Eds.), The Flavor of Fruit, Elsevier Science Publishers, Amsterdam, Netherlands, 1990, pp. 43–92.

Available online at www.sciencedirect.com
ScienceDirect
Talanta 73 (2007) 314–320
Talanta
www.elsevier.com/locate/talanta

Simultaneous analysis of neutral and acidic pharmaceuticals as well as related compounds by gas chromatography–tandem mass spectrometry in wastewater

M.J. Gómez [a], A. Agüera [a,*], M. Mezcua [a,b], J. Hurtado [a], F. Mocholí [a], A.R. Fernández-Alba [a]

[a] *Pesticide Residue Research Group, University of Almería, 04120 Almería, Spain*
[b] *Department of Chemical Engineering and Analytical Chemistry, University of Alcalá de Henares, Spain*

Received 5 December 2006; received in revised form 20 March 2007; accepted 23 March 2007
Available online 1 April 2007

Abstract

This work presents a new multi-residue analytical method based on solid phase extraction (SPE) with Oasis HLB sorbent, followed by gas chromatography tandem mass spectrometry (GC–MS/MS) for the simultaneous determination of a group of 10 acidic and neutral pharmaceuticals and related compounds in wastewaters. The typical derivation step was avoided, allowing the determination of acidic and neutral pollutants in a single analysis as well as providing a fast and easy method suitable for routine monitoring. Target pollutants include: anti-inflammatory drugs (ibuprofen, acetaminophen and diclofenac); an antiepileptic agent (carbamazepine); stimulants (caffeine and nicotine); an antiseptic (triclosan); a plasticizer (bisphenol A) and two of their more relevant metabolites (2,8-dichlorodibenzo-*p*-dioxin and 1,7-dimethylxanthine). Recoveries between 66 and 112% were achieved for all the target compounds (except for 2,8-dichlorodibenzo-*p*-dioxin). Good linearity was observed within the studied ranges ($R^2 > 0.993$). Acceptable intra and inter-day precision was obtained, with relative standard deviation between 2 and 18%. The application of the optimized MS/MS mode allowed method detection limits in the range of 0.2–16 ng/L, with the exception of ibuprofen (120 ng/L). Finally, the methodology was successfully applied to the analysis of hospital effluent samples. All target analytes were detected at concentrations between 1 ng/L and 83215 μg/L. Even in the absence of derivatization, all the analytes showed good peak shape, except acetaminophen, which exhibited peak tailing. However, the method proved to be repetitive and reproducible, and the peak shape did not represent a problem for the reliable quantification of this compound. For most of the analytes studied, the detection limits achieved compare well against values reported in previously published methods.

Keywords: Gas chromatography–tandem mass spectrometry; Wastewater; Hospital effluents; Pharmaceuticals; caffeine; Nicotine; Bisphenol A

1. Introduction

Nowadays, one of the most relevant topics in environmental analytical chemistry is water quality. Ever since the presence of non-regulated contaminants was pointed out as a possible cause of the quality reduction of natural water, many studies have been performed to evaluate the source, occurrence, fate and environmental effects of these pollutants [1–8]. Active pharmaceutical ingredients, surfactants, personal care products or substances with endocrine disrupting activities are among the compounds which have provoked greatest interest over the last decade. These compounds and their active metabolites are continually introduced into the aquatic environment in the form of complex mixtures via a number of routes, but primarily by both untreated and treated municipal wastewater. Contrasting with the wide-ranging information concerning the occurrence of pharmaceuticals and other emergent contaminants in effluents from conventional sewage treatment plants (STPs) [1,5], data is still lacking relating to the contribution of other different sources, such as hospitals. Hospital effluents generally reach the municipal sewer network without preliminary treatment and may represent a significant source of chemicals released into the aquatic environment. Research has also shown that conventional treatments employed in STPs are not specifically designed to remove many of these compounds efficiently [1–9] and they have been identified in the receiving water in the ng/L to μg/L range [3,4,10].

* Corresponding author. Tel.: +34 950015531; fax: +34 950015483.
E-mail address: aaguera@ual.es (A. Agüera).

0039-9140/$ – see front matter © 2007 Elsevier B.V. All rights reserved.
doi:10.1016/j.talanta.2007.03.053

Due to the biological activity of these emergent contaminants [11,12,13] their concentration, fate and behaviour in the environment must be understood and quantified. With this purpose in mind, accurate and sensitive analytical methods have to be developed capable of monitoring these residues at the ng/L level. To date, numerous analytical methodologies for the determination of pollutants and their metabolites in water are available in the literature. However, most of them encompass only groups of compounds containing similar polarities, similar structures or similar activities [14,15,16]. The development of multi-residue methods useful for the determination of a broad group of compounds is required in order to obtain a correct chemical evaluation of the effluents [5,17]. Nevertheless, the majority of these methods require separate and time-consuming sample pre-treatment and/or different analysis for each group of compounds. A simultaneous extraction and analysis for various compound classes generally require a compromise in the selection of experimental conditions, but result in shortened overall analysis time, cost reduction and is more suitable for routine analysis [1,18]. Öllers et al. [19] have reported a GC–MS method for the simultaneous analysis of neutral and acidic pharmaceuticals and pesticides in surface and wastewater, but two separated analyses were required, since the acidic compounds were derivatized and simultaneous derivatization of both neutral and acidic analytes, was not advisable. Verenitch et al. [3], found that caffeine was completely destroyed during methylation processes and for this reason it could not be determined along with other acidic drugs.

Solid phase extraction (SPE) is the most common sample isolation and pre-concentration technique for the target analytes and Oasis HLB® the preferred sorbent, used for this purpose [1,3,4]. Gas chromatography coupled to mass spectrometry (GC–MS or GG–MS/MS) or liquid chromatography coupled to mass spectrometry (LC–MS) or tandem mass spectrometry (LC–MS/MS) are the most widely used techniques [1,3,11,20]. Recently, the authors have applied a LC–TOF/MS technique to determine polar pharmaceuticals in hospital effluents [18], demonstrating that it can be a useful approach. LC–MS/MS has progressed over the last decades, and nowadays it is the main choice in determining ultratrace concentrations of polar pharmaceuticals in environmental samples [20,21]. However, when highly complex samples are analysed, such as wastewater, suppression of the electrospray ionization is likely to occur, especially with electrospray ionization (ESI). The published papers have reported GC–MS in selective ion monitoring (SIM) and GC–MS/MS as very suitable methods for the environmental analysis of the majority of the studied compounds, which are neutral or medium acidic [1,3,19,22]. Although, due to the poor volatility of some compounds and the presence of various polar groups in the molecule, derivatization steps aimed to produce more volatile products and improve the sensitivity of subsequent GC analysis, are applied [3,19]. Thus, the advantages of better sensitivity are sometimes largely offset by loss of sample during the additional manipulation. Most of the analytical methods proposed in the literature apply derivatization procedures before GC–MS analysis.

The group of organic compounds which are the object of this study includes the anti-inflammatory drugs ibuprofen, acetaminophen and diclofenac, the antiepileptic agent carbamazepine, the plasticizer bisphenol A, the antiseptic triclosan and its toxic metabolite 2,8-dichlorodibenzo-*p*-dioxin (2,8-DCDD) and the stimulants nicotine, caffeine and its metabolite 1,7-dimethylxanthine. This group of compounds was selected based on preliminary studies performed in a municipal STP where the selected hospital discharges the effluent. The authors have documented in a previous work [1] the presence of this group of compounds in the influent and effluent of the STP.

A single method based on SPE and direct analysis of the extract by GC–MS/MS is proposed, avoiding the tedious and critical step of derivatization. A comparison of MDLs achieved with other different published methods, for the analysis of these compounds in wastewater is discussed in this paper.

The aim of this study was to develop a sensitive analytical method for the rapid and quantitative determination of neutral and acidic organic contaminants in wastewaters. The described method was then used to analyze hospital effluent samples collected from a hospital in Almería (Spain).

2. Experimental

2.1. Chemicals and reagents

Pure standards (>98%) of acetaminophen, ibuprofen, caffeine, 1,7-dimethylxanthine, carbamazepine, diclofenac, (−)-nicotine, triclosan and bisphenol A were purchased by Sigma–Aldrich (Steinheim, Germany). 2,8-dichlorodibenzo-*p*-dioxin (DCDD) was obtained from LGC Promochem (USA). Individual stock standard solutions were prepared in ethyl acetate, or methanol in the case of carbamazepine, 1,7-dimethylxanthine, diclofenac and acetaminophen, and stored at −20 °C. Standard mixtures, at different concentrations, were prepared by appropriate dilution of the stock solutions.

Pesticide-grade ethyl acetate was obtained from Panreac (Barcelona, Spain) and HPLC-grade methanol from Merck (Darmstadt, Germany).

2.2. Sampling and sample preparation

Discrete samples were collected from the main sewer of a health-care centre with a 75 bed capacity. Amber glass bottles rinsed with ultra-pure water were used for this purpose. Once in the laboratory, the samples were vacuum filtered through a 0.7 μm glass fibre filter (Teknokroma, Barcelona, Spain) and stored at 4 °C until solid phase extraction (SPE), which was performed within 24 h in order to avoid any degradation.

A SPE procedure was applied to the samples using commercial Oasis HLB® (divinylbenzene/*N*-vinylpyrrolidone copolymer) cartridges (200 mg, 6 cm^3) from Waters (Mildford, MA, USA). An automated sample processor ASPEC XL fitted with an 817 switching valve and an external 306 LC pump from Gilson (Villiers-le-Bel, France) was used for this purpose. A conditioning step was performed with 5 ml of ethyl acetate, 5 ml of methanol and 5 ml of LC-grade water at a flow rate of 1 ml/min. After the conditioning step, sample aliquots of 100 ml (pH adjusted to 7 with H_2SO_4) were passed through the car-

tridges at a flow rate of 10 ml/min and then rinsed with 5 ml of deionized water prior to elution. After that, the cartridges were dried by nitrogen stream for approximately 10 min and finally eluted with 2× 4 ml of ethyl acetate at 1 ml/min. The extracts were evaporated until almost dry using a Turbo-Vap from Zymark (Hopkinton, Massachusetts), with the water bath at 40 °C. The samples were then reconstituted with 1 ml of ethyl acetate and transferred to an auto-sampler vial for direct analysis by GC–MS.

2.3. GC-IT-(EI) MS/MS analysis

Determination was performed using a Varian 4000-GC–MS/MS system with a 1079 PTV injector and a CP-8400 autosampler (Varian, Walnut Creek, CA, USA). Data acquisition and processing were performed using the Varian Star Workstation software 6.42 version. The system worked in internal ionization mode. A fused silica untreated capillary column (1 m × 0.25 mm i.d.) from Varian (Middelburg, The Netherlands) was used as a guard column, connected to a Varian FactorFour VF-5ms capillary column (5% diphenyl 95% dimethylsiloxane), 30 m × 0.25 mm i.d., 0.25 μm film thickness. The helium carrier gas flow was constant and set at 1 ml/min. Automatic injections (1 μL) were performed in splitless mode at 280 °C and with the split vet opening set at 1.5 min. Transfer line temperature was 290 °C and ion trap temperature was 200 °C.

The GC temperature program was 70 °C for 2.00 min, programmed to 200 °C at 30 °C/min, then programmed to 220 °C at 2 °C/min (held for 6 min) and finally programmed to 300 °C at 10 °C/min and held at this temperature for 5 min. Total run time was 31.33 min.

3. Results and discussions

This work presents an easy multi-residue analytical method, useful for the rapid and simultaneous determination of acidic and neutral pharmaceutical residues in wastewater samples. Most of the GC-based analytical methods described in the literature for the analysis of acidic pharmaceuticals apply a derivatization technique prior to injection in order to transform polar analytes into their less polar and more volatile forms. The reduction in polarity improves the chromatographic properties and/or the sensitivity of the detection.

Nevertheless, derivatization procedures are laborious and time-consuming, and present other disadvantages such as the reduction in the analytical columns lifetimes or side effects that can occur during the derivatization reactions. In addition, some derivatization processes are susceptible to reaction inversion, while preparation and use of the most commonly used derivatization reagents carries some risk because of their toxicity, carcinogenicity or danger of explosions. Besides these difficulties, the derivatization can destroy non-acidic compounds, as in the case of caffeine [3], or reduce the analysis efficiency of the neutral analytes [19], and therefore, these pharmaceuticals have to be processed separately from acid drugs. To overcome these difficulties, a rapid and simple GC–MS/MS based method, without previous derivatization of acidic drugs, is proposed. Tandem mass spectrometry is a highly selective and sensitive technique that provides very good results in the analysis of trace compounds in complex matrices, so representing a very good choice in the analysis of wastewater samples. The advantages and suitability of the method for each compound is discussed and compared with previous works.

3.1. GC-IT-(EI) MS/MS method

Fig. 1 shows the selected ion GC–MS/MS chromatogram obtained from a hospital effluent extract spiked at the 500 ng/L level. As it can be seen, a complete separation of the compounds is achieved in a total time of 31 min. The last analyte eluted at 20 min, but the analysis was maintained until reaching a final temperature of 300 °C to ensure complete elimination of the matrix components from the analytical column. Even in the absence of derivatization, all the peaks showed a good peak shape, with the exception of acetaminophen, which suffered from peak tailing. Although this is an undesirable effect in chromatographic analysis, it did not represent an obstacle for the reliable determination of this compound, as will be discussed later on. Furthermore, the sensitivity obtained was enough to achieve a detection limit according to the concentration levels present in the samples.

MS–MS parameters were individually optimized for each analyte. Spiked hospital effluent extracts, at a concentration level of 10 μg/L, were used for this purpose because the presence of a matrix had an effect upon the intensity ration that needed to be evaluated. The different optimized parameters and the precursor ion isolated, together with the main product ions obtained, and their relative intensities, are presented in Table 1. Since the molecular ion is considered as the most characteristic ion for each compound, it was selected as the precursor ion in the case of nicotine, caffeine, 1,7-dimethylxanthine, 2,8-DCDD, and triclosan. For these compounds, the molecular ion also coincided with the base peak – with the exception of nicotine, which presented a base peak at m/z 84. This low-mass ion, which resulted from the loss of the pyridyl group, was not selective enough, thus increasing the probability of matrix interference. In addition, further fragmentation of this ion did not provide structural information of interest, so the molecular ion at m/z 161, was selected. The precursor ion chosen for diclofenac was the fragment ion at m/z 277, corresponding to the loss of water $[M - H_2O]^+$. The molecular ion is not present in the *full scan* spectrum. The base peak in this case corresponded to $[M - H_2OClCO]^+$ ($m/z = 214$), but the ion at $m/z = 277$ provided more structural information, with a characteristic product ion at $m/z = 242$, corresponding with the loss of one chlorine atom. For ibuprofen, acetaminophen, carbamazepine and bisphenol A, the base peak of the EI spectrum was selected as the precursor ion in order to get higher sensitivity. For ibuprofen, this peak corresponded with the loss of carbon dioxide $[M - H - CO_2]^+$ ($m/z = 161$), typical of carboxylic acids. The ion $[M - COCH_3]^+$ ($m/z = 109$), was the base peak in the case of acetaminophen. For the neutral drug carbamazepine, the base peak was observed at $m/z = 193$ due to the loss of the $CONH_2$ group. It must be pointed out

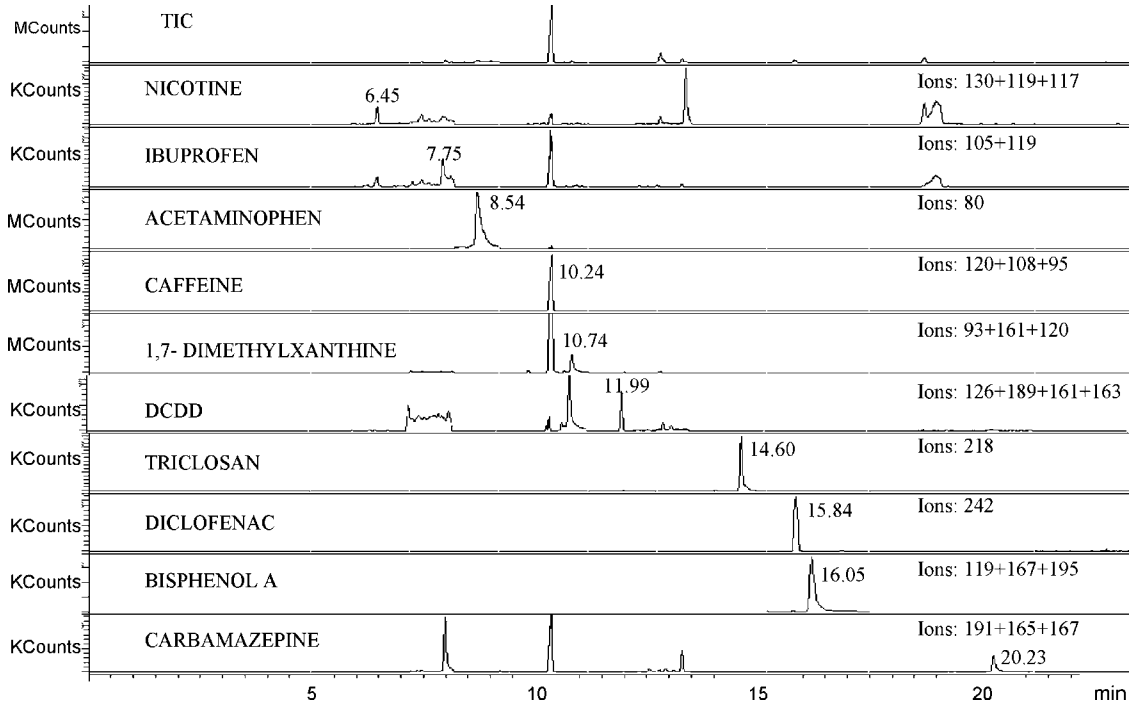

Fig. 1. Total ion (TIC) and selected ion GC–MS/MS chromatograms corresponding to a spiked wastewater sample at 0.5 (g/l level.

that typical degradation of carbamazepine to iminostilbene as a consequence of thermal degradation in the injection port of the gas-chromatograph, was observed. However, as will be discuss later on, precision studies showed an acceptable repeatability and reproducibility for the carbamazepine peak (around 10%), and the MDL (0.2 ng L^{-1}) obtained. Despite degradation, it was low enough to reach the concentration levels present in the samples. For this reason, the contribution of iminostilbene was not considered for quantification. The most intense fragment for bisphenol A was the ion at $m/z = 213$, which corresponded to the loss of a methyl group $[M - 15]^+$. In all these cases, selected precursor ions delivered daughter ions which were indicative of the structure of the analyte, considered adequate for an accurate identification.

At least three fragments were selected as qualifier ions, which are shown in Table 1. The most intense fragment ion/s in the MS/MS spectrum of each pharmaceutical, were selected for quantification purposes.

3.2. Performance of the analytical method

The analytical method was evaluated to prove its applicability to the analysis of neutral and acidic chemicals in wastewater. Recoveries, linearity range, precision and sensitivity were calculated. Validation results, determined in hospital effluent extracts, are presented in Table 2. Concentrations of the pharmaceuticals under investigation in the original hospital effluent samples have been taken into account.

Table 1
Diagnostic ions and quantification masses (in bold) used for the GC–MS/MS analysis of the studied compounds in wastewater

Compound	Rt window (min)	Rt (min)	Molecular ion (*m/z*)	Precursor ion (*m/z*)	Product ions (*m/z*) (relative abundance, %)	Storage level (*m/z*)	Excitation voltage (V)
Nicotine	5.0–7.2	6.45	162.23	161	**130** (100), **119** (90), **117** (56)	60	58
Ibuprofen	7.2–8.2	7.75	206.28	161	**105** (100), **119** (68), 91 (35)	40	40
Acetaminophen	8.2–9.2	8.54	151.17	109	**80** (100), 81 (43), 53 (10)	60	46
Caffeine	9.2–10.6	10.24	194.19	194	**120** (100), **108** (78), **95** (62)	60	53
1,7-Dimethylxanthine	10.6–11.2	10.74	180.17	180	**93** (100), **161** (68), **120** (28)	70	66
DCDD	11.2–12.25	11.99	252.88	252	**126** (100), **189** (92), **161** (79), **163** (31)	90	85
Triclosan	13.2–15.2	14.60	287.95	288	**218** (100), 146 (35), 220 (27)	100	75
Diclofenac	15.2–17.5	15.84	295.13	277	**242** (87), 243 (26), 207 (16), 214(8)	100	66
Bisphenol A	15.2–17.5	16.05	228.29	213	**119** (100), **167** (49), **195** (39)	80	69
Carbamazepine	17.5–24.0	20.23	236.27	193	**191** (100), **165** (97), **167** (35)	80	81

Retention times obtained for each compound and fragmentation conditions are also included.
Isolation window: 3.0; excitation time: 20 ms.

Table 2
Analytical parameters obtained with the GC–MS/MS method for the analysis of selected compounds in wastewater

Compound	Recovery (R.S.D., %), $n=3$	Linearity			MDL (ng/L)	MQL (ng/L)	Repeatability (R.S.D., %), $n=10$	Reproducibility (R.S.D, %), $n=10$
		Range (ng/L)	Cal. equation	R^2				
Nicotine	66 (10)	50–1000	$Y=1231x+1.8e+5$	0.9969	6	21	2	8
Ibuprofen	80 (8)	500–1000	$Y=2774x-4.7e+4$	0.9939	120	401	8	18
Acetaminophen	71 (5)	100–1000	$Y=4152x+3.2e+6$	0.9974	16	55	13	11
Caffeine	92 (5)	10–1000	$Y=6295x-3.1e+4$	0.9995	0.7[a]	2.3[a]	3	4
1,7-Dimethylxanthine	92 (7)	50–1000	$Y=1776x+9.8e+5$	0.9966	10	34	8	13
DCDD	25 (9)	10–1000	$Y=4718x+2.2e+4$	0.9998	1.5	5	2	3
Triclosan	112 (10)	10–1000	$Y=2168x+1.4e+4$	0.9998	2	8	12	12
Diclofenac	79 (3)	10–1000	$Y=873x+4014$	0.9997	1.1	4	6	7
Bisphenol A	72 (4)	10–1000	$Y=1e+4x+2.6e+5$	0.9999	0.5	2	11	14
Carbamazepine	81 (5)	1–1000	$Y=6807x+9.4e+4$	0.9993	0.2	0.7	9	10

R.S.D.: relative standard deviation; MDL: method detection limit; MQL: method quantification limit.
[a] Calculated from a pure solvent standard solution.

3.2.1. Recovery

Recovery studies were performed in triplicate by spiking wastewater samples at a concentration level of 1 μg/l, before and after extraction. Quantitative recoveries obtained for the target compounds ranged from 66 to 112%, except for 2,8-DCDD, which showed a lower recovery (25%). Most of the methods described in the literature for the extraction of polychlorinated dibenzo-*p*-dioxins in environmental samples are focused on solid samples. For the analysis of water samples, SPE with C_{18} sorbent yields better recoveries [23]. However, this hydrophobic stationary phase does not efficiently extract acidic compounds [24]. Simultaneous extraction of acidic and neutral pharmaceutical residues is better obtained by HLB cartridges at pH = 7 [1,18,20,24]. Ethyl acetate was selected as the elution solvent because it desorbs analytes efficiently over a wide range of polarities. Despite the variety of chemical classes of compounds analyzed, which makes it difficult to obtain the best extraction conditions for all of them, HLB-SPE cartridges represented a very good choice with good results in most of the cases. Although the recovery obtained for 2,8-DCDD was not enough for reliable quantitative analysis, other validation parameters such as sensitivity (MDL, 1.5 ng/L) or repeatability (R.S.D., 1.7%) were quite good, and therefore an acceptable quantitative estimation of the concentration of 2,8-DCDD in the samples could be obtained.

3.2.2. Linear dynamic range

The linearity in the response was studied using matrix-matched calibration solutions prepared by spiking hospital effluent extracts at seven concentration levels, ranging from 10 to 1000 ng/L in the samples. The linear dynamic ranges, calibration equations and correlation coefficients (r^2) obtained are shown in Table 2. Good linearity was observed in the studied range with r^2 values higher than 0.99 in all of the cases.

3.2.3. Sensitivity

Method detection limits (MDLs) and method quantification limits (MQLs) were determined from spiked wastewater samples, taking into account the concentration of the target pharmaceuticals in the original samples. Only in the case of caffeine, were MDL and MQL determined from a standard solution in ethyl acetate, due to the fact that caffeine was found at very high concentration in all the analyzed samples. Values obtained ranged from 0.2 to 16 ng/L and 0.7 to 55 ng/L, respectively, except for ibuprofen, which exhibited higher detection and quantification limits, 120 and 401 ng/L, respectively. These levels were low enough however to quantify this compound in the samples. Better detection limits, of 61 and 0.8 ng/L, have been reported [3,7] for ibuprofen after derivatization by GC–MS and GC–MS/MS, respectively, and a MDL of 31 ng/L was achieved by LC–MS/MS [20].

For acetaminophen, even though this compound did not show a very good peak shape, an acceptable MDL (16 ng/L) was reached. Higher levels have been previously reported by GC–MS (129 ng/L) [1] or LC–MS/MS (47 ng/L) [20].

The neutral drug carbamazepine, present in the samples at the lower concentration levels, achieved a MDL of 0.2 ng/L, which was lower than others previously reported by GC–MS, with and without derivatization (100 and 159 ng/L, respectively) [1,5] or. by LC–MS/MS (7 ng/L) [20], which has also been frequently used.

A detection limit of 0.5 ng/L was obtained for bisphenol A. MDLs of 0.5, 2, 27, 396 and 1 ng/L were previously reported for the analysis of bisphenol A by GC–MS/MS with and without derivatization, GC–MS with and without derivatization and LC–MS/MS, respectively [25,26,1,27,21].

Triclosan yielded a MDL of 2.5 ng/L derivatization however, considerably, improves the response of this acidic compound. MDLs of 200, 31 and 10 ng/L have been reported in previous works by GC–MS with and without derivatization and by LC–MS/MS, respectively [1,7,28].

The diclofenac detection limit was 1 ng/L. The same value was reported by GC–MS/MS analysis with derivatization [3], and MDLs of 144, 62 and 30 ng/L were achieved by GC–MS without and with derivatization and LC–MS/MS, respectively [1,7,20].

The neutral drugs caffeine and nicotine could be detected at very low concentrations (0.7 and 6 ng/L), which were, in all cases, one or two orders of magnitude lower than the MDLs reported by other authors (from 14 to 397 ng/l) [3,1,10].

It must be considered that detection limits depend on the sample nature and the preconcentration factor reached during the sample treatment. Most of the papers previously cited analyzed wastewater effluent samples, but the preconcentration factors applied were different.

Although lower MDLs could be obtained by increasing the preconcentration factor, this is not recommendable since it leads to more complex extracts, making the use of additional clean-up steps necessary.

3.2.4. Precision

In order to evaluate the precision of the proposed method, within-laboratory repeatability and reproducibility were estimated. To ensure correct quantification of the underivatized analytes, a spiked extract at 1 μg/L was analyzed 10 times in the same day and 10 times in different days. The repeatability, expressed as percent relative standard deviation (R.S.D.), varied between 2 and 13%, a little bit higher variability was achieved for the reproducibility, from 3 to 18%.

3.2.5. Identification capability of the GC–MS/MS method

Under the conditions described, the MS/MS method provided high sensitivity and selectivity. The isolation of only one ion from the rest of the matrix to obtain the product ion spectra, reduces background interferences and increases the signal-to-noise (S/N) ratio, thus improving confidence in the identification.

The confirmation criteria applied to the target analytes in the samples was based on the peak retention times and the product ion spectra. A peak retention time window within 2% and the presence of three of the most intensive and characteristic ions of the MS/MS spectrum were used to verify a correct identification. The ratio of each parent/product peak combination has to fall within 30% of the established references.

These results indicated a good performance for the developed method.

Table 3
Concentration of selected compounds in hospital effluent samples

Compounds	Sample 1 (ng/L)	Sample 2 (ng/L)	Sample 3 (ng/L)
Nicotine	428	3786	1573
Ibuprofen	3573	4572	921
Acetaminophen	1090	3130	1080
Caffeine	11266	68404	83215
1,7-Dimethylxanthine	1028	1243	638
DCDD	522	714	28
Triclosan	115	212	268
Diclofenac	96	37	510
Bisphenol A	25	82	146
Carbamazepine	3	1	8

3.3. Application of the method to real samples

To demonstrate the applicability of the optimized method, three discrete hospital effluent samples were analyzed. Results obtained are summarized in Table 3. All the target compounds were present in the three samples. Variations in concentrations between samples are explained by the use of discrete samples [20]. Maximum concentrations were detected for caffeine, with concentrations between 11266 and 83215 ng/L. Nicotine, 1,7-dimethylxanthine and the antiinflammatories

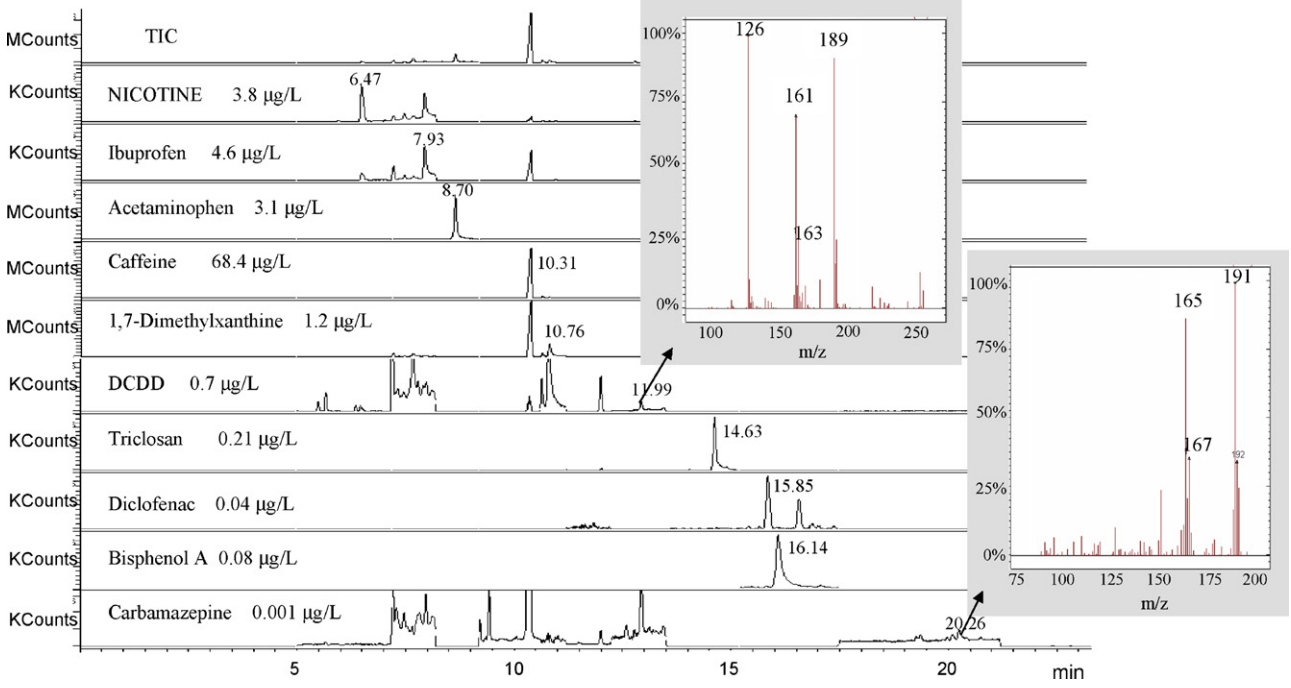

Fig. 2. Selected ion GC–MS/MS chromatogram corresponding to an hospital effluent sample where the target compounds have been identified. Spectra of two of the analytes found at lower concentration are also included.

ibuprofen and acetaminophen were found in the samples at concentrations higher than 1000 ng/L. Carbamazepine was the compound present in the samples at lower concentrations, from 1 to 8 ng/L. The rest of the compounds were detected at concentrations between 25 and 700 ng/L. Fig. 2 shows an extracted ion GC–MS/MS chromatogram of a hospital effluent extract in which all the compounds have been identified. As can be observed in the figure, the high selectivity and structural information provided by the product ions mass spectra allows a reliable identification of the target compounds in wastewater, even with the analytes found at lower concentrations. These results demonstrate the usefulness of the proposed method for this application. The LODs achieved are also low enough to determinate these analytes in urban wastewater, at the levels currently reported in the literature.

4. Conclusions

In the present work, a simple and fast multi-residue method based on SPE followed by GC–MS/MS has been developed for the simultaneous extraction and analysis of neutral and underivatized acid pharmaceuticals and related compounds in wastewater samples. It has been shown that this method represents an easy and fast analytical approach, viable for routine analysis, avoiding the inconvenience associated with the application of derivatization processes. Quantitative recoveries were obtained for all the target compounds, ranging from 66 to 112% (except for 2,8-DCDD: 25%). Linearity with $R^2 > 0.994$ and precision of the method with relative standard deviation between 2 and 18% were also acceptable. With the application of the optimized MS/MS parameters, MDLs of 0.2–16 ng/L can be achieved, except for ibuprofen (120%). For this acid pharmaceutical, derivatization prior to the analysis has been reported to give better MDLs, but this detection limit was low enough to analyze ibuprofen in hospital effluent samples. Most of detection limits achieved were lower than those obtained with previously published methods.

The higher selectivity and structural information provided by the product ions mass spectra allows reliable confirmation of the target compounds in these complex matrices.

This method was successfully applied to the analysis of the studied compounds in hospital effluents. All the compounds were detected, except the carbazepine metabolite. Even in the absence of derivatization, the proposed method showed a high sensitivity for the target compounds and all the analytes showed a good peak shape, with the exception of acetaminophen, which suffered from peak tailing, although this did not represent an impediment to the reliable quantification of this compound. The proposed method is therefore, a useful alternative to previous methods, for simultaneously analyzing neutral and acidic compounds in wastewaters.

Acknowledgements

The authors acknowledge The Spanish Ministry of Education and Science (Project No. CTM2004-06265-C03-03 and Programa Consolider Ingenio 2010 CE-CSD2006-004). M. Mezcua acknowledges the "Juan de la Cierva" research contract from The Spanish Ministry of Science and Technology and M.J. Gómez acknowledges the fellowship from The Spanish Ministry of Science and Technology.

References

[1] M.J. Gómez, M.J. Martinez, S. Lacorte, A.R. Fernández-Alba, A. Agüera, Chemosphere 66 (2007) 993.
[2] P.H. Roberts, K.V. Thomas, Sci. Total Environ. 356 (2006) 143.
[3] S.S. Verenitch, C.J. Lowe, A. Mazumder, J. Chromatogr. A 1116 (2006) 193.
[4] Z. Moldovan, Chemosphere 64 (2006) 1808.
[5] T.A. Ternes, Trends Anal. Chem. 20 (2001) 419.
[6] M.D. Hernando, M. Mezcua, A.R. Fernández-Alba, D. Barceló, Talanta 69 (2006) 334.
[7] L. Lishman, S.A. Smyth, K. Sarafin, S. Kleywegt, J. Toito, T. Peart, B. Lee, M. Servos, M. Beland, P. Seto, Sci. Total Environ. 367 (2006) 544.
[8] A. Agüera, A.R. Fernández-Alba, L. Piedra, M. Mézcua, M.J. Gómez, Anal. Chem. Acta 480 (2003) 193.
[9] N. Paxeus, Water Sci. Technol. 50 (2004) 253.
[10] J.D. Cahill, E.T. Furlong, M.R. Burkhardt, D. Kolpin, L.G. Anderson, J. Chromatogr. A (2004) 171.
[11] E. Emmanuel, G. Keck, J.-M. Blanchard, P. Vermande, Y. Perrodin, Environ. Int. 30 (2004) 891.
[12] T. Schwartz, W. Kohnen, B. Jansen, U. Obs, FEMS Microbiol. Ecol. 1470 (2002) 1.
[13] A.K. Gautam, S. Kumar, P.C. Sabumon, J. Environ. Manage., in press.
[14] T. Kosjek, E. Heath, A. Krbavcic, Environ. Int. 31 (2005) 679.
[15] K.D. Brown, J. Kulis, B. Thomson, T.H. Chapman, D.B. Mawhinney, Sci. Total Environ., in press.
[16] R. Lindberg, P. Jarnheimer, B. Olsen, M. Johansson, M. Tysklind, Chemosphere 57 (2004) 1479.
[17] F. Sacher, F. Thomas Lange, H.J. Brauch, I. Blankenhorn, J. Chromatogr. A 938 (2001) 199.
[18] M.J. Gómez, O. Malato, I. Ferrer, A. Agüera, A.R. Fernández-Alba, J. Environ. Monit. 9 (2007) 718.
[19] S. Öllers, H. Singer, P. Fassler, S.R. Müller, J. Chromatogr. A 911 (2001) 225.
[20] M.J. Gómez, M. Petrovic, A.R. Fernández-Alba, D. Barceló, J. Chromatogr. A 1114 (2006) 224.
[21] B.J. Vanderford, R.A. Pearson, D.J. Rexing, S.A. Snyder, Anal. Chem. 75 (2003) 6265.
[22] S. Morales-Muñoz, J.L. Luque-García, M.J. Ramos, A. Fernández-Alba, M.D. Luque de Castro, Anal. Chem. Acta 552 (2005) 50.
[23] J.-F. Focant, C. Pirard, E. Pauw, Talanta 63 (2004) 1101.
[24] W.-C. Lin, H.-C. Chen, W.-H. Ding, J. Chromatogr. A 1065 (2005) 279.
[25] M.J. Gómez, M. Mezcua, M.J. Martinez, A.R. Fernández-Alba, A. Agüera, Intern. J. Environ. Anal. Chem. 86 (2006) 3.
[26] R. Jeannot, H. Sabik, E. Sauvard, T. Dagnac, K. Dohrendorf, J. Chromatogr. A 974 (2002) 143.
[27] M.D. Hernando, M. Mezcua, M.J. Gómez, O. Malato, A. Agüera, A.R. Fernández-Alba, J. Chromatogr. A 1047 (2004) 129.
[28] W. Hua, E.R. Bennett, R.J. Letcher, Environ. Int. 31 (2005) 621.

Available online at www.sciencedirect.com
ScienceDirect
Talanta 73 (2007) 227–231
Talanta
www.elsevier.com/locate/talanta

Study on the co-luminescence effect of Tb–Gd–epinephrine system and its application to the sensitive determination of epinephrine at nanomol level

Yumei Guo, Jinghe Yang *, Xia Wu, Hongzhi Mao

Key Laboratory of Colloid and Interface Chemistry (Shandong University), Ministry of Education, School of Chemistry and Chemical Engineering, Shandong University, Jinan 250100, People's Republic of China

Received 14 November 2006; received in revised form 14 March 2007; accepted 14 March 2007
Available online 20 March 2007

Abstract

A new fluorimetric method for the determination of epinephrine is established by rare earth co-luminescence effect of Tb–Gd–E–Tris system. Under optimum conditions, a linear relationship has been obtained between the fluorescence intensity and the concentration of epinephrine in the range of 1.8×10^{-8} to 2.5×10^{-6} mol/l, and the detection limit is 4.5×10^{-9} mol/l (S/N = 3). The method is applied for the determination of epinephrine in injection and the recovery test in urine by standard addition method, and the results obtained are satisfactory. The mechanism of the co-luminescence in the system was also discussed.

Keywords: Epinephrine (E); Rare earth co-luminescence effect; Fluorimetric analysis

1. Introduction

Epinephrine (E) plays important roles as a neurotransmitter and a hormone. It exists as an organic cation in the nervous tissue and biological body fluid and many diseases are related to the changes of its concentration in body fluid. Thus, the determination of epinephrine has attracted much attention. Fluorimetric method and high-performance liquid chromatography method [1] are often used for the determination of epinephrine. Other analytical methods have been reported, for example, electrochemiluminescence [2], flow injection chemiluminescence method [3–5], flow injection capillary electrophoresis method [6,7], molecular imprinting probe [8,9], etc. Several fluorimetric methods such as the trihydroxyindole (THI) method [10], terbium (Tb)(III) fluorescence probe method [11] and condensation method [12,13] have been proposed, but their detection limits are not low enough or a lot of time are need in the processes. Rare earth co-luminescence is a fluorescence enhancement effect which was first found and studied by our research group in 1986 [14]. This effect has become an important way to improve the sensitivity of rare earth ions [15], pharmaceutical and biological molecules [16,17] by fluorimetry.

It is found that Gd^{3+} can enhance the fluorescence intensity of the Tb^{3+}–E–Tris system, this is a new co-luminescence system. This system has been used for the determination of epinephrine, its detection limit is 4.5×10^{-9} mol/l (S/N = 3). Compared with other fluorimetric methods, this method is a simple, reliable and fast method with a larger linear range. The mechanism of luminescence enhancement of the Tb^{3+}–Gd^{3+}–E–Tris system is also discussed.

2. Experimental

2.1. Apparatus

All fluorescence measurements were made on a FL-4500 spectrofluorimeter (Hitachi, Japan). All pH measurements were made on a Delta 320-S pH meter (Mettler Toledo).

2.2. Regents and solutions

(1) An epinephrine standard stock solution (1.36×10^{-3} mol/l) was prepared by dissolving 0.025 g epinephrine (Fluka,

* Corresponding author.
E-mail address: yjh@sdu.edu.cn (J. Yang).

0039-9140/$ – see front matter © 2007 Published by Elsevier B.V.
doi:10.1016/j.talanta.2007.03.022

HPLC) in 100 ml, 0.01 mol/l hydrochloric acid and stored at 4 °C. Working solutions were prepared by diluting with doubly deionized water.

(2) Stock standard solutions (1.00×10^{-2} mol/l) of rare-earth ions were prepared by dissolving the corresponding oxides (Yuelong Chemical Co., Shanghai, 99.9%) in hydrochloric acid and diluting with deionized water.

(3) A 0.20 mol/l Tris–HCl buffer solution was prepared by dissolving 12.5 g of Tris in 500 ml deionized water, and adjusting the pH to 10.0 with HCl (6.0 mol/l). All the chemicals used were of analytical grade and doubly deionized water was used throughout.

2.3. Procedure

To a 25 ml test tube, solutions were added in the following order: E, Gd^{3+}, Tb^{3+} and Tris–HCl buffer. The mixture was diluted to 10 ml with doubly deionized water. The fluorescence intensity was measured in a 1 cm quartz cell. The excitation and emission slits were both 10 nm.

3. Result and discussion

3.1. Fluorescence spectra

Excitation and emission spectra of Tb^{3+}–Tris (1), Tb^{3+}–Gd^{3+}–Tris (2), Tb^{3+}–E–Tris (3) and Tb^{3+}–Gd^{3+}–E–Tris (4) systems at emission and excitation wavelength of 493 and 300 nm are shown in Fig. 1. From this figure, it can be seen that the systems of (1)–(4) have the same emission peaks at 493 and 548 nm of Tb^{3+}, corresponding to the $^5D_4$–$^7F_6$ and $^5D_4$–$^7F_5$ transitions of Tb^{3+}, respectively. The fluorescence intensity at 548 nm is the strongest. From Fig. 1, it is also seen that the fluorescence intensity of the E–Tb^{3+}–Tris system is weak. However, the fluorescence intensity of the system is much enhanced by Gd^{3+} and the excitation peak moves from 325 to 300 nm. This is a newly found co-luminescence system. So, we choose 548 nm as the emission peak in this research.

3.2. Optimization of the general procedure

According to the recommended procedure, the experiments indicate that the addition of Gd^{3+}, La^{3+} and Y^{3+} all can enhance the fluorescence of the system, among which Gd^{3+} has the greatest enhancement. So Gd^{3+} is chosen as the enhancing ion. It is found that the fluorescence intensity remains maximum when pH is in range of 9.8–10.2. So pH 10.0 is fixed in the research. In addition, different buffers are in detail studied, including HMTA, Tris–HCl, $Na_2B_4O_7$–NaOH, NH_4Cl–NH_3, $NaHCO_3$–Na_2CO_3 and NH_2CH_2·COOH–NaOH. Experimental results indicated that the Tris–HCl is the most suitable buffer among them. Thus, the strongest fluorescence signal as the criterion to determine the optimum conditions for the determination of E as follows: 1.0×10^{-5} mol/l Tb^{3+}, 5.0×10^{-5} mol/l Gd^{3+}, and 4.0×10^{-2} mol/l Tris–HCl buffer (pH 10.0).

3.3. The addition order and stability of this system

In this system, we also investigate the effect of the adding order. The result indicates that the order of E, Gd^{3+}, Tb^{3+} and Tris–HCl is the best.

Under the optimum condition, the effect of time on the fluorescence intensity is studied. The result shows that the fluorescence intensity immediately reaches a maximum after all the reagents had been added and remained stable for over 20 minute under the permission of ±5% relative error. Therefore, this method fits for the determinating of E rapidly.

3.4. Effect of foreign substances

The interference of foreign substances is tested for 1.0×10^{-5} mol/l E and the results are shown in Table 1. It is indicated that noepinephrine, dopamine, and proteins have considerable interference, whereas other substances tested have little effect on the determination of E under the permission of ±5% relative error.

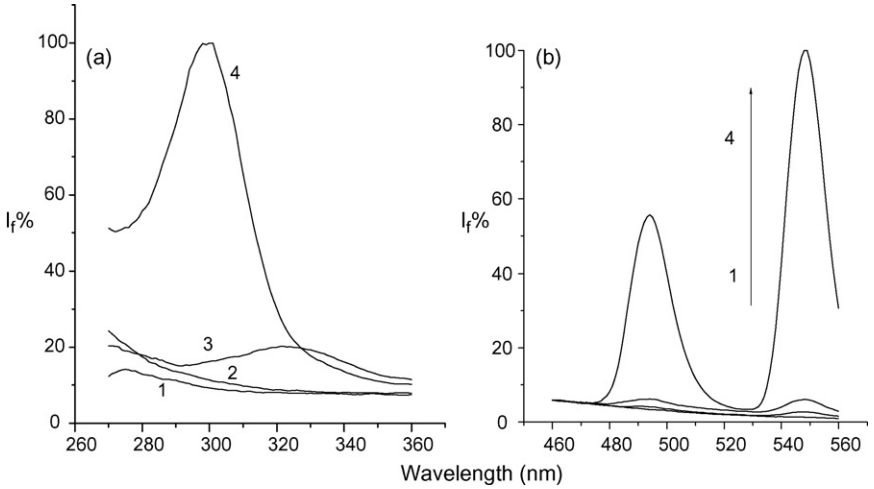

Fig. 1. Fluorescence spectra. (a) Excitation spectra (λ_{em} = 493 nm). (b) Emission spectra (λ_{ex} = 300 nm). 1: Tb^{3+}–Tris; 2: Tb^{3+}–Gd^{3+}–Tris; 3: Tb^{3+}–E–Tris; 4: Tb^{3+}–Gd^{3+}–E–Tris. Conditions: E, 1.0×10^{-5} mol/l; Gd^{3+}, 5.0×10^{-5} mol/l; Tb^{3+}, 1.0×10^{-5} mol/l; Tris–HCl, 0.020 mol/l, pH 10.0.

Table 1
Interference from foreign substances

Foreign substances	Coexiting concentration ($\times 10^{-4}$ mol/l)	Change of ΔI_f (%)
$AlCl_3$	2.5	−4.8
$CaCl_2$	1.3	−5.0
KCl	2.5	−5.0
$MgSO_4$	2.5	−5.0
NaCl	1.5	−4.6
NH_4Cl	1.5	−4.6
$ZnCl_2$	0.5	−4.1
Dopamine	0.047	+5.0
NE	0.013	+4.0
HSA	0.032	+9.3
RNA	1.0×10^{-6} g/ml	−5.2

Table 3
The test of recovery in urine

Standard value, 2×10^6 (mol/l)	0.450
Determination value, 2×10^6 (mol/l)	0.492, 0.434, 0.461 0.468, 0.441
Average, 2×10^6 (mol/l)	0.463
Recovery (%)	103
R.S.D. (%)	2.6

Table 4
The determination of epinephrine in the injection

Trihydroxyindole (THI) method, 2×10^6 (mol/l)	0.545
This method, 2×10^6 (mol/l)	0.569, 0.520, 0.531 0.554, 0.559
Average, 2×10^6 (mol/l)	0.547
R.S.D. (%)	2.0

4. Analytical applications

4.1. The calibration curve and detection limit

Under the optimum conditions defined here, a linear relationship is obtained between the fluorescence intensity and the concentration of epinephrine in the range of 1.8×10^{-8} to 2.5×10^{-6} mol/l, with a detection limit of 4.5×10^{-9} mol/l (S/N = 3). The regression equation is as follows: $y = 0.49415 + 12.8185 \times 10^7 C$, with a correlation coefficient of 0.9991. From Table 2, it can be seen that the proposed method has a lower detection limit, compared with most of other luminescence methods.

4.2. Recovery test and sample determination

Considering the effects of foreign substances on the fluorescence intensity of the system, the standard addition method is used for the recovery test and sample determination. The test of the recovery efficiency for known amounts of epinephrine in human urine is made. This urine sample is obtained from a healthy donor. The urine sample is collected during 3 h in a bottle container, and adjusted the pH to 2.0 with HCl (6.0 mol/l) in order to prevent E degradation and stored at 4 °C. The urine is diluted 100-fold in the final assay solutions. The results of the recovery test are shown in Table 3 and indicate that the recovery efficiency of E in human urine is about 103%.

The proposed method is used for the determination of epinephrine in the epinephrine hydrochloride injection (Shanghai Harvest Pharmaceutical Co., Ltd.), and compared with the original trihydroxyindole (THI) method. The results are shown in Table 4. From these results, we can see that the proposed method can be efficiently used for the determination of E in injection.

5. Interaction mechanism of the system

5.1. Resonance light scattering (RLS) spectra

Resonance light scattering (RLS) spectra of Tb^{3+}–Tris (1), Tb^{3+}–E–Tris (2), Tb^{3+}–Gd^{3+}–Tris (3) and Tb^{3+}–Gd^{3+}–E–Tris (4) systems are shown in Fig. 2. It can be seen that when E, Gd^{3+} and E–Gd^{3+} are added to Tb^{3+}–Tris system, respectively, the resonance light scattering intensities of the systems are enhanced. However, the RLS intensity of Tb^{3+}–Gd^{3+}–E–Tris system is higher than those of other three systems, which indicates that there is the interaction among them, and forms a large complex in this system.

It is known that Tb^{3+} can combine with E and form Tb^{3+}–E complex [11]. On the basis of similar chemical properties of all lanthanide elements, it is considered that both Tb^{3+}–E and Gd^{3+}–E complexes are formed in Tb^{3+}–Gd^{3+}–E–Tris system. Because the test condition is alkalescent in this system, so Tb^{3+} and Gd^{3+} not only combine with E, but also combine with hydroxy of solution [16]. Then, Tb^{3+} and Gd^{3+} complexes can

Table 2
Comparison of luminescence methods for determination of E

Method	Linear relationship (mol/l)	Detection limit (mol/l)	References
The proposed method	1.8×10^{-8} to 2.5×10^{-6}	4.5×10^{-9}	
Electrochemiluminescence	4.0×10^{-8} to 2.0×10^{-7}	2.4×10^{-8}	[2]
Flow injection chemiluminescence	5.0×10^{-9} to 2.5×10^{-7}	3.0×10^{-9}	[4]
Flow-injection electrogenerated chemiluminescence	7.0×10^{-8} to 6.0×10^{-6}	2.8×10^{-8}	[5]
Trihydroxyindole (THI) method	4.1×10^{-7} to 4.8×10^{-5}	2.7×10^{-8}	[11]
Terbium fluorescence probe method	8.2×10^{-8} to 9.8×10^{-5}	2.3×10^{-8}	[12]
2,3-Diaminonaphthalene	6.0×10^{-8} to 1.0×10^{-5}	5.0×10^{-8}	[13]
O-Phenylenediamine	2.0×10^{-8} to 6.0×10^{-6}	9.3×10^{-9}	[14]

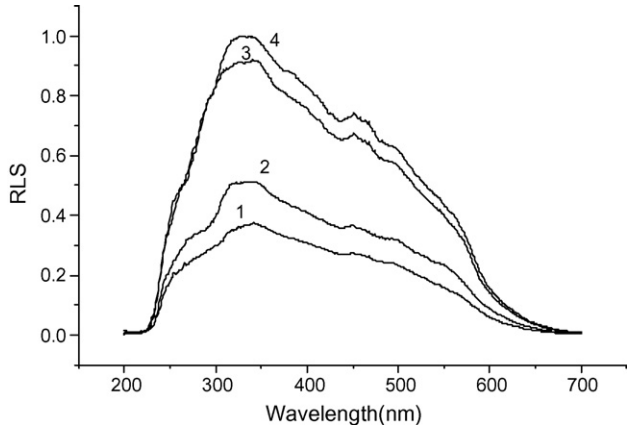

Fig. 2. Resonance light scattering (RLS). 1: Tb^{3+}–Tris; 2: Tb^{3+}–E–Tris; 3: Tb^{3+}–Gd^{3+}–Tris; 4: Tb^{3+}–Gd^{3+}–E–Tris. Conditions: E, 1.0×10^{-5} mol/l; Gd^{3+}, 5.0×10^{-5} mol/l; Tb^{3+}, 1.0×10^{-5} mol/l; Tris–HCl: 0.020 mol/l, pH 10.0.

be connected by oxygenic bridge and form a larger congeries. Therefore, the RLS intensity of Tb^{3+}–Gd^{3+}–E–Tris is larger than those of others.

5.2. Fluorescence enhancement mechanism

From Fig. 1, it can be seen that the fluorescence intensity of the Tb^{3+}–Gd^{3+}–E–Tris system is much larger than that of Tb^{3+}–E–Tris system which comes from the intramolecular energy transfer. From Fig. 3, it can be seen that the fluorescence peak of 324 nm in this system is attributed to the emission of E. After continuously adding Gd^{3+} to Tb^{3+}–E–Tris system, the fluorescence of E is gradually weaken and that of Tb^{3+} is gradually enhanced. This indicates that there has the intermolecular energy transfer between Tb^{3+} and Gd^{3+} complexes. When this system is excited, Tb^{3+} complex absorbs the energy and then consumes it by emitting the characteristic luminescence of Tb^{3+}. For Gd^{3+} complex, the luminescent level of Gd^{3+} is higher than the triplet state of E, the energy absorbed by E can not be transferred to

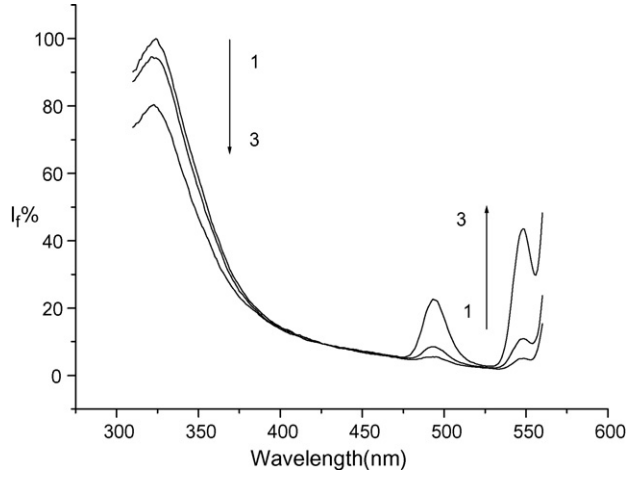

Fig. 3. Energy transfer of between Gd^{3+} and Tb^{3+} (λ_{ex} = 290 nm). 1: Gd^{3+}, 0; 2: Gd^{3+}, 1.0×10^{-5} mol/l; 3: Gd^{3+}, 5.0×10^{-5} mol/l. Conditions: E, 1.0×10^{-5} mol/l; Tb^{3+}, 1.0×10^{-5} mol/l; Tris–HCl; 0.020 mol/l, pH 10.0.

Table 5
Fluorescence lifetime of Tb^{3+} in the systems

System	Lifetime (ns)
Tb^{3+}–Tris	6.86
Tb^{3+}–Gd^{3+}–Tris	7.43
Tb^{3+}–E–Tris	32.35
Tb^{3+}–Gd^{3+}–E–Tris	1807

Gd^{3+}, but can be transferred to Tb^{3+} complex through oxygen bridge, which results in the fluorescence enhancement of this system.

Fluorescence enhancement also originates from the energy-insulating sheath as well as intramolecular and intermolecular energy transfer in this system. Because the concentration of Gd^{3+} complex is much greater than that of the Tb^{3+} complex, each Tb^{3+} complex is surrounded by many Gd^{3+} complexes. This surrounding complex can act as an energy-insulating sheath, which can prevent collision with water molecules and decrease the energy loss of Tb^{3+} complex. Therefore, the luminescence intensity of Tb^{3+}–E–Tris system is considerably enhanced in the presence of Gd^{3+}.

The above mechanism can be proved by fluorescence lifetime of Tb^{3+} in different systems, which shown in Table 5. When E is added to the Tb^{3+}–Tris system, the fluorescence lifetime of Tb^{3+} can be delayed from 6.86 to 32.35 ns. This shown that E replace water molecule coordinated in Tb^{3+}, resulting in both the decrease of energy loss on Tb^{3+} and the increase of the fluorescence lifetime of Tb^{3+}. While Gd^{3+} is added to the Tb^{3+}–E–Tris system, the fluorescence lifetime of Tb^{3+} is greatly prolonged from 32.35 to 1807 ns. This is due to both intermolecular energy transfer between Tb^{3+} and Gd^{3+} complexes, and the energy-insulating sheath. Therefore, the fluorescence lifetime of Tb^{3+} is greatly increased.

6. Conclusion

This paper studied the fluorescence enhancement effect of Tb^{3+}–Gd^{3+}–E–Tris system. Experiment shows that the fluorescence intensity of Tb^{3+}–E–Tris system can be greatly enhanced by Gd^{3+}. Under the optimum conditions, the enhanced intensity is in proportion to the concentration of E in the range of 1.8×10^{-8} to 2.5×10^{-6} mol/l, the detection limit is 4.5×10^{-9} mol/l, which is lower than those of most fluorimetric methods in Table 2. The study of interaction mechanism indicates that both Tb^{3+} and Gd^{3+} complexes can form a large complex by the link of the oxygen bridge. Thus, intermolecular energy transfer is possible to enhance the fluorescence of Tb^{3+} through accepting energy from the Gd^{3+} complex. In addition, many Gd^{3+} complexes surround Tb^{3+} complex to form an energy-insulating sheath, resulting in the prevention of the collision with water molecules. Therefore, both the fluorescence lifetime and the fluorescence intensity of Tb^{3+} in this system are significantly enhanced.

Acknowledgements

This work was supported by Natural Science Foundations of China (20575035) and Shandong Province (Y2003B02), and by Visiting Scholar Foundation of Key Lab in the University.

References

[1] A.M. Fotopou Lou, C.P. Loannou, Anal. Chim. Acta 462 (2002) 179.
[2] Y.Y. Su, J. Wang, G.N. Chen, Talanta 65 (2005) 531.
[3] J.V.G. Mateo, A. Kojlo, J. Pharm. Biomed. Anal. 15 (1997) (1821).
[4] J.X. Du, L.H. Shen, J.R. Lu, Anal. Chim. Acta 489 (2003) 183.
[5] X.W. Zheng, Z.H. Guo, Z.J. Zhang, Anal. Chim. Acta 441 (2001) 81.
[6] P.B. Mckibbin, J. Wong, D.D.Y. Chen, J. Chromatogr., A 853 (1999) 535.
[7] X.H. Sun, X.R. Yang, E.K. Wang, J. Chromatogr., A 991 (2003) 109.
[8] C.D. Liang, H. Peng, A.H. Zhou, L.H. Nie, S.Z. Yao, Anal. Chim. Acta 415 (2000) 135.
[9] P. Hernández, I. Sánchez, F. Patón, L. Hernández, Talanta 46 (1998) 985.
[10] C.L. Tong, G.C. Lu, Z.L. Xu, J. Zhejiang Univ. (Science Ed.) 27 (2000) 530.
[11] X. Wu, C.L. Tong, B.Y. Su, F. Huang, J.H. Yang, J. Shandong Univ. China 34 (1998) 352.
[12] J.H. Yang, G.L. Zhang, X. Wu, F. Huang, C.G. Lin, X.H. Cao, L.M. Sun, Y.J. Ding, Anal. Chim. Acta 363 (1998) 105.
[13] J.H. Yang, G.L. Zhang, X.H. Cao, L.M. Sun, Y.J. Ding, Anal. Chim. Acta, Spectrochim. Acta, Part A 53 (1997) 1671.
[14] J.H. Yang, G.Y. Zhu, J. Shandong Univ. 21 (1986) 133.
[15] W. Jiang, Y.D. Ma, W.Y. Zhao, Y. Feng, N.X. Wang, Z.K. Si, Microchim. Acta (2003).
[16] L. Li, J.H. Yang, X. Wu, C.X. Sun, G.J. Zhou, Talanta 59 (2003) 81.
[17] C.X. Sun, J.H. Yang, X. Wu, Biochimie 86 (2004) 569.

Available online at www.sciencedirect.com
ScienceDirect
Talanta 73 (2007) 220–226
Talanta
www.elsevier.com/locate/talanta

Chemical analysis of acidic silicon etch solutions I. Titrimetric determination of HNO_3, HF, and H_2SiF_6

Antje Henßge [a,c], Jörg Acker [b,c,*]

[a] Department of Chemical Engineering, Hochschule für Technik und Wirtschaft Dresden-University of Applied Science, Friedrich-List-Platz 1, Dresden 01069, Germany
[b] Department of Biotechnology, Chemical Engineering, and Process Technology, Fachhochschule Lausitz - University of Applied Sciences, Großenhainer Straße 57, D-01968 Senftenberg, Germany
[c] Leibniz-Institute for Solid State and Materials Research Dresden (IFW Dresden), P.O. Box 270016, D-01171 Dresden, Germany

Received 24 July 2006; received in revised form 30 January 2007; accepted 5 February 2007
Available online 15 February 2007

Abstract

The chemical etching of silicon using HF–HNO_3 mixtures is a widely used process in the processing of silicon wafers for microelectronic or photovoltaic applications. The control of the etch bath composition is the necessary condition for an effective bath utilization, for the replenishment of the consumed acids, and to maintain a certain etch rate. The present paper describes two methods for the total analysis of the individual etch bath constituents HF, HNO_3, and H_2SiF_6. Both methods start with an aqueous acid–base titration determining the total acid concentration and the concentration of H_2SiF_6. The first method is an acid–base titration using a 0.1 mol L^{-1} methanolic solution of cyclohexylamine (CHA) as non-aqueous titrant to determine the content of nitric acid. Then, the amount of hydrofluoric acid is calculated from the difference between the total acid and nitric acid content. The second method is based on the determination of the total fluoride concentration using a fluoride ion-selective electrode (F-ISE). The content of hydrofluoric acid is obtained from the difference between the total fluoride content and the amount of fluoride bound as H_2SiF_6. The amount of nitric acid results finally calculated as difference to the total acid content.

Keywords: HF–HNO_3 Etch solution; Potentiometric titration; Non-aqueous titrant; Ion-selective electrode; Silicon; H_2SiF_6

1. Introduction

The isotropic wet chemical etching of silicon by HF–HNO_3 acid mixtures is an essential step in the processing of semiconductor and solar grade silicon. Main applications are the removal of surface roughness of wafers after slicing from silicon ingots (saw damage) and the chemical polishing of the wafer surfaces well as the texturing of silicon wafer surfaces for the application as solar cells.

For sake of simplicity, the dissolution of silicon is described by the following net equation [1]:

$$3Si + 18HF + 4HNO_3 \rightarrow 3H_2SiF_6 + 4NO + 8H_2O \quad (1)$$

During the etch process HF and HNO_3 concentrations decrease gradually, whereas H_2SiF_6 becomes enriched in the etch solution. As consequence of the formation of water and H_2SiF_6, the etch behavior changes significantly [2]. In order to maintain a certain etch rate or surface quality such as texturing or polishing either the utilized etch solution has to be replaced by a new one or the already used etching solution has to be replenished by the addition of concentrated acids [3–5]. However, the number of replenishment cycles is restricted, since an increasing concentration of H_2SiF_6 affects the morphology of the etched surface [6] and may lead to the deposition of SiO_2 (stains) on the silicon. The precondition for an effective etch bath control is the exact knowledge of the amount of the etch solution constituents HNO_3, HF, and H_2SiF_6 as reaction product.

Recently, a potentiometric acid–base titration method for the determination of the silicon content in HF–HNO_3 etch solutions independent of the composition, density and of the state of aging [4] was published. A typical titration curve shows two equivalence points. The first one consists of the total amount of

* Corresponding author at: Department of Biotechnology, Chemical Engineering, and Process Technology, Fachhochschule Lausitz - University of Applied Sciences, Großenhainer Straße 57, D-01968 Senftenberg, Germany.
Tel.: +49 35 73 85 839; fax: +49 35 73 85 809.
E-mail address: jacker@hf-lausitz.de (J. Acker).

0039-9140/$ – see front matter © 2007 Elsevier B.V. All rights reserved.
doi:10.1016/j.talanta.2007.02.004

Table 1
Parameters of the sample series 1 obtained by dissolution of SiO_2 in HF–HNO_3 mixtures

Sample	m(HF) (g)	c(HF) (mol L^{-1})	m(HNO_3) (g)	c(HNO_3) (mol L^{-1})	m(SiO_2) (g)	m(total) (g)	w(Si) (mg g^{-1})
S1-A	41.2924	22.87	20.8163	14.34	1.3955	63.6131	10.2
S1-B	39.9472	22.87	20.7147	14.44	2.3786	63.2255	17.6
S1-C	40.1436	22.87	20.6319	14.44	3.2767	64.3083	23.8
S1-D	40.1652	22.87	20.7388	14.34	4.1872	65.4180	29.9
S1-E	40.1046	22.87	20.6483	14.44	5.1473	66.3023	36.3
S1-F	39.9411	22.87	20.6350	14.44	6.0224	67.0686	42.0
S1-G	40.0898	22.87	20.7407	14.34	6.9951	68.3716	47.8

protons in the sample because of the close pKs values of HF, HNO_3, and H_2SiF_6 which are indistinguishable by titration in aqueous solution:

$$H_2SiF_6 + 2NaOH \rightarrow Na_2SiF_6 + 2H_2O \quad (2)$$

$$HNO_3 + NaOH \rightarrow NaNO_3 + H_2O \quad (3)$$

$$HF + NaOH \rightarrow NaF + H_2O \quad (4)$$

Further titration using NaOH yields into the cleavage of the SiF_6^{2-} ion giving the second equivalence point:

$$Na_2SiF_6 + 4NaOH \rightarrow Si(OH)_4 + 6NaF \quad (5)$$

The described method points to the major problem to analyse such mixtures, the quantification of the amounts of the individual acids HF, HNO_3, and H_2SiF_6. Two different approaches had been developed for this purpose that meet the required precision necessary for an industrial etch bath process control. The first one, designated as method 1, is a solution for the general problem of indistinguishable equivalent points in such acid mixtures by an acid–base titration using a non-aqueous titrant. As alternative to circumvent this problem, a method based on the determination of the total fluoride content was developed, designated as method 2. The development of both methods was performed using the same sample series that were prepared by dissolution of either SiO_2 or Si in HF–HNO_3 mixtures to model the complex matrix behavior. Both methods are compared with respect to their analytical performance.

2. Experimental

2.1. Sample preparation

The present study bases on two series of synthetic etch solutions. Series 1 (Table 1) was obtained by dissolution of SiO_2 (99.8% (w/w) p.a., Alfa Aesar, Karlsruhe, Germany) in HF–HNO_3 mixtures. A weighed amount of fumed, carefully dried SiO_2 was dispersed in 15 mL HNO_3 (65% (w/w), p.a., Merck, Darmstadt, Germany). Then, 35 mL HF (40% (w/w), p.a., Merck, Darmstadt, Germany) were added in small portions in order to minimize the losses of SiF_4. Series 2 (Table 2) was prepared by slow dissolution of 50 mg pieces of Si-wafer (4 in. diameter, polished, 675 μm thickness; Silchem GmbH, Freiberg, Germany) in an acid mixture of 35 mL 40% (w/w) HF and 15 mL 65% (w/w) HNO_3. The dissolution processes were carried out by the addition of small portions of Si to the acid mixtures cooled to 1 °C in order to reduce the reaction rate and to minimize the evaporation of water and the loss of SiF_4. The concentrations of the used acids given in Tables 1 and 2 were determined by titration. All masses given throughout this paper were obtained by weighing (AT 200, Mettler-Toledo AG, Schwerzenbach, Switzerland). Only HDPE (high density polyethylene) vessels were used for sample preparation and storage.

The uncertainty of all given experimental values is given as 1σ.

2.2. Titration using an aqueous titrant

For titration 0.5 mL aliquots of the sample were weighed and diluted with deionized water (18 MΩ, Seral, Ransbach-Baumbach, Germany) to a total volume of 60 mL in a PE (polyethylene)-beaker. Titrant is 0.5 mol L^{-1} NaOH (diluted from 1 mol L^{-1} NaOH; Titrisol, Merck, Darmstadt, Germany). The titer of this solution was determined by titration of 1 mol L^{-1} HCl (Titrisol, Merck, Darmstadt, Germany). The equivalence point is obtained from the first derivative of the titration curve. For the calculation of the Si resp. H_2SiF_6 content a calibration corresponding to [7] was used. Titrations were performed by computerized titrator of the type DL 70 using a HF resistant

Table 2
Parameters of the sample series 2 obtained by dissolution of Si in HF–HNO_3 mixtures

Sample	m(HF) (g)	c(HF) (mol L^{-1})	m(HNO_3) (g)	c(HNO_3) (mol L^{-1})	m(Si) (g)	m(total) (g)	w(Si) (mg g^{-1})
S2-A	40.4769	23.18	21.0890	14.41	0.7054	62.3208	11.3
S2-B	40.9007	22.87	20.9368	14.34	1.4040	62.8647	22.3
S2-C	40.4247	23.18	21.1297	14.41	2.1110	63.4408	33.3
S2-D	40.9859	22.87	20.8916	14.34	2.8082	63.7983	44.0
S2-E	39.3316	23.18	21.1692	14.41	3.5022	63.2000	55.4
S2-F	40.8715	22.87	20.9031	14.34	3.7733	65.2275	57.8
S2-G	40.8051	22.87	20.794	14.34	4.0285	65.2582	61.7

glass electrode InLab 429 (Mettler-Toledo AG, Schwerzenbach, Switzerland).

2.3. Titration using a non-aqueous titrant

Titrant is 0.1 mol L^{-1} solution of cyclohexylamine (CHA) (Merck, Darmstadt, Germany) in methanol (p.a., Merck, Darmstadt, Germany). The titer of the solution was frequently measured by titration with 0.1 mol L^{-1} HCl (Titrisol, Merck, Darmstadt, Germany). The developed titration method is designed for a total silicon concentration in the etch solution of 0.56 mg mL^{-1}. Therefore, a weighed aliquot of the etch solution has to be diluted. The required amount of water is calculated from the preceding titration of the total silicon content as written above.

For the acid–CHA titration 2 mL diluted sample solution, 4 mL deionized water and 40 mL ethanol (absolute p.a., Merck, Darmstadt, Germany) were mixed in the titration beaker and 0.5 g KCl (p.a., Merck, Darmstadt, Germany) were added. The beaker was covered with parafilm "M" (laboratory film, Pechiney plastic packaging, Chicago, USA) and cooled at 4–8 °C for at least 2 h. The cold sample solution was then titrated in the cold with 0.1 mol L^{-1} CHA solution using the automated titrator DL 70 and a HF resistant glass electrode.

2.4. Determination of the total fluoride content using a fluoride ion-selective electrode

The total fluoride content in etch solutions is measured with a fluoride ion-selective electrode (F-ISE) (Mettler Toledo GmbH) and accompanying reference electrode. The F-ISE requires a regular calibration. Calibration is made by at least four fluoride calibration solutions between 2 and 2×10^{-4} g L^{-1} prepared from NaF standard solution (Certipur 1000 mg/L Fluorid, Merck, Darmstadt, Germany). An aliquot of 50 mL from the calibration solution and 5 mL TISAB solution (TISAB III solution, Mettler Toledo GmbH, Urdorf, Schweiz) were mixed.

One hundred microliters of the concentrated etch solutions are weighed, diluted by 50 mL water, and titrated with 0.1 mol L^{-1} NaOH to a final pH of 5 by means of an automated titrator DL 70. This solution is transferred into a 200 mL flask and filled up with water. For the analysis 50 mL were transferred in a titration beaker and 5 mL TISAB added corresponding to the calibration conditions.

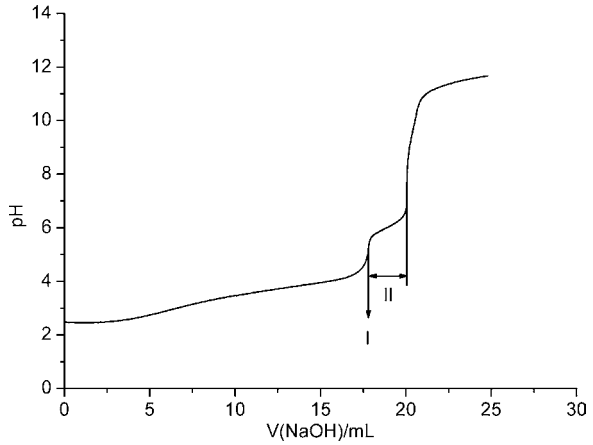

Fig. 1. Curve of the potentiometric titration of a 0.5 mL sample (0.7073 g Si dissolved in 35 mL HF and 15 mL HNO_3) with 0.5 mol L^{-1} NaOH in water.

3. Development of analytic methods for the characterization of etch solutions

3.1. Survey about the developed methods

Table 3 gives a survey about the developed methods for the determination of the acid contents in etch solutions.

3.2. Determination of the Si content by aqueous acid–base titration

Fig. 1 shows a typical acid–base titration curve from which the amount of dissolved silicon is calculated. The first equivalence point (denoted as I in Fig. 1) results from the neutralization of the protons of the three present acids according to Eqs. (2)–(4), i.e. the total acid concentration. The titrated amount of NaOH between the first and second equivalence point (denoted as II in Fig. 1) represents the amount of silicon, formally described as reaction of Na_2SiF_6 to $Si(OH)_4$ according to Eq. (5).

It had been shown in [7], that the linear relationship of Eq. (6) has to be used to calculate the molar amount of silicon, n_{Si} (equivalent to the molar amount of H_2SiF_6, $n_{H_2SiF_6}$) from the consumed amount of NaOH between the second and first equivalence point:

$$n_{Si} = n_{H_2SiF_6} = \frac{n_{NaOH} - 0.06}{4.06} \quad (6)$$

It has to kept in mind that Eq. (6) is only valid for at least 1% (w/w) Si and as long as free HF is present [7]. This relation-

Table 3
Survey about the developed titrimetric procedures for the determination of the individual acids constituents in concentrated etch solutions

	Method 1	Method 2
Step 1	Acid–NaOH titration to determine the amount of total acid and H_2SiF_6	
Step 2	Acid–CHA titration to determine the amount of HNO_3	Determination of total fluoride content by F-ISE; the HF amount is calculated as the difference between total fluoride content and the fluoride content bound in H_2SiF_6
Step 3	Calculation of the amount of HF as difference between total acid concentration, H_2SiF_6, and HNO_3	Calculation of the amount of HNO_3 as difference between the total acid concentration, H_2SiF_6, and HF

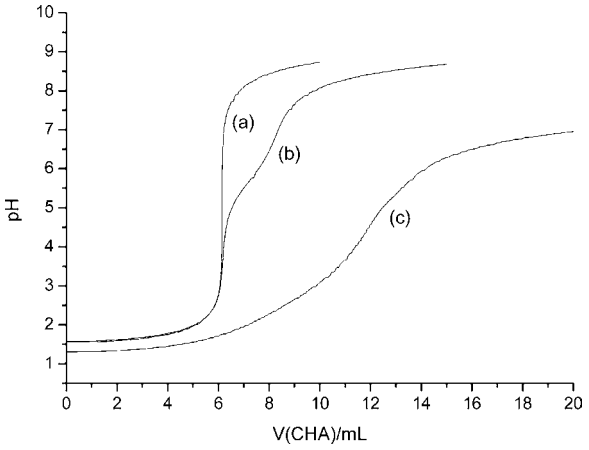

Fig. 2. Potentiometric titration curve of different acid mixtures with 0. 1 mol L^{-1} CHA as titrant. Each sample solution contains 40 mL acetone, each acid has a concentration of 0.1 mol L^{-1}: (a) 6 mL HNO_3 and 6 mL water; (b) 6 mL HNO_3, 2 mL HF and 4 mL water; (c) 6 mL HNO_3, 2 mL HF, 2 mL H_2SiF_6 and 2 mL water.

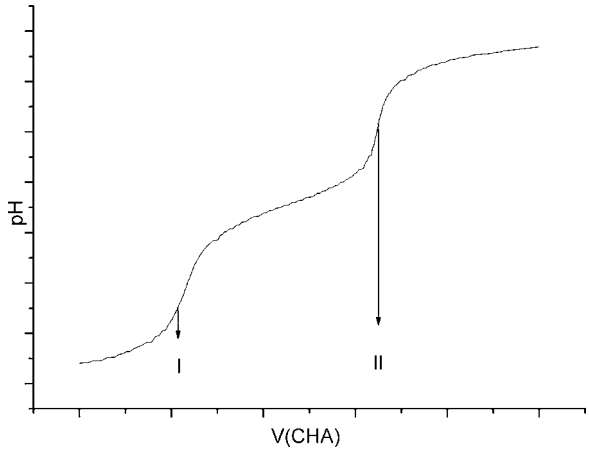

Fig. 3. Schematic drawing of a potentiometric titration curve of an ethanolic HF–HNO_3–H_2SiF_6 acid mixture using a methanolic CHA solution as titrant. H_2SiF_6 was precipitated before the titration by the addition of KCl to the ethanolic acid mixture. For detailed explanation see text.

ship holds not for supersaturated H_2SiF_6 solutions such for the samples S2-F and S2-G.

3.3. Description of method 1

3.3.1. Determination of the HNO_3 content using a non-aqueous titrant

Common procedures to separate overlapping equivalence points are titrations in a non-aqueous media or the use of non-aqueous titrants with a proper solvent having a dielectric constant different from that of water [8]. For the present system, solvents like methanol, ethanol, isopropanol, or acetone were found to be useful. Exemplarily for the mentioned organic solvents, Fig. 2 shows the separation of the equivalence points of HNO_3 and HF by titration in an acetone–water media using methanolic CHA solution as titrant. Curve a in Fig. 2 shows the titration curve of a only HNO_3 sample as reference. Curve b represents the titration curve of a HF–HNO_3 mixture. The stronger acid HNO_3 is fully titrated at the first equivalence point, the amount of the weaker acid HF is given by the difference between the second and the first equivalence point. However, this procedure fails if the acid mixture contains H_2SiF_6 (curve c).

As a consequence, H_2SiF_6 has to be eliminated from the acid mixtures which is achieved by the precipitation of K_2SiF_6 in ethanolic solution and in the cold after addition of a defined amount of KCl in excess with respect to H_2SiF_6:

$$H_2SiF_6 + 2KCl \rightarrow K_2SiF_6 + 2HCl \quad (7)$$

This yields to an ethanolic solution of HNO_3, HF, and an amount of HCl equivalent to the amount of H_2SiF_6 according to Eq. (7) in presence of the K_2SiF_6 precipitate. The titration of this solution with methanolic CHA solution results in two equivalence points (Fig. 3).

The first equivalence point (designed as I in Fig. 3) consists of the sum of HNO_3 and HCl, the strongest acids in this mixture, as well as of a further contribution. The additional contribution arises from a shift of the first equivalence point to a higher CHA volume (Fig. 2) that is observed by the addition of 0.5 g KCl to a mixture of H_2SiF_6/H_2O/ethanol. For this constant molar ratio between Si and KCl of 5.95×10^{-3} the shift leads to a constant recovery of HCl of 102% for the given Si concentration of 0.56 g L^{-1}. It might be assumed that the precipitation of K_2SiF_6 is incomplete and a small amount of H_2SiF_6 is titrated with CHA that contributes to the first equivalence point.

Due to the sensitivity to small changes in the concentration of H_2SiF_6 the described method was optimized with respect to the ratio between the aqueous and ethanolic phase as well as to the amount of KCl for a fixed silicon concentration of 0.56 mg mL^{-1} in the sample solution. It turned out, that an amount of 0.5 g KCl in ethanolic solution is of advantage for the crystallization and sedimentation of the formed K_2SiF_6 since the excessive amount of KCl precipitates as well.

Applying the method to synthetic sample solutions consisting of HCl, HNO_3, HF and 0.5 g KCl recoveries of $(100.6 \pm 1.2)\%$ ($m = 14$) and $(100.5 \pm 1.4)\%$ ($m = 14$) were obtained for HNO_3 and HF, respectively. In such synthetic samples the amount of HF is represented by the difference between the second (designed as II in Fig. 3) and the first equivalence point. However, the determination of the HF content fails for synthetic etch solutions containing HNO_3, HF, and H_2SiF_6 because the precipitated K_2SiF_6 which is present throughout the titration starts to react with the CHA titrant at a pH above 5.

The amount of HNO_3 can be calculated using Eq. (8). Variable c denotes the concentration in mol L^{-1}, v is the titrated volume of CHA (in L) at the first equivalence point (1.EP). The expression $1.02(cv)_{CHA,\,HCl}$ describes the molar amount of CHA necessary to titrate the fraction of formed HCl including the recovery of 102%. The mass fraction of an individual component is calculated using the initial weight and its molar mass:

$$n_{CHA,HNO_3} = (cv)_{CHA,1.EP} - 1.02(cv)_{CHA,HCl} \quad (8)$$

with

$$1.02(cv)_{\mathrm{CHA,HCl}} = 2n_{\mathrm{H_2SiF_6}} \quad (9)$$

The result of the aqueous acid–base titration according to Eq. (6) is $n_{\mathrm{H_2SiF_6}}$.

3.3.2. Calculation of the HF content

The HF content is calculated from the contents of the total acid and of H_2SiF_6 derived from the acid–base titration (Section 3.2) and from the HNO_3 content obtained from the CHA titration (Section 3.3.1):

$$n_{\mathrm{HF}} = (cv)_{\mathrm{NaOH,1.EP}} - (cv)_{\mathrm{CHA,HNO_3}} - n_{\mathrm{H_2SiF_6}} \quad (10)$$

The expression $(cv)_{\mathrm{NaOH,1.EP}}$ denotes the molar amount of consumed NaOH at the first equivalence point in the aqueous acid–base titration, i.e. the total acid concentration. The amount of HNO_3 from the CHA titration is expressed by $(cv)_{\mathrm{CHA,HNO_3}}$. The amount of H_2SiF_6, $n_{\mathrm{H_2SiF_6}}$, is obtained from Eq. (6).

3.4. Method 2

3.4.1. Determination of HF content

According to the survey in Table 3, the HF content can be calculated if the H_2SiF_6 and the total fluoride contents are known. The procedure for the determination of the total fluoride content by F-ISE was described in Section 2.4. Essential is the addition of TISAB solution to adjust a certain ionic strength and a constant pH of 5 to convert all known complex HF species into free fluoride ions. Furthermore, Si^{4+} is re-complexed under cleavage of the SiF_6^{2-} ion and liberating the fluoride ions.

The molar amount of fluoride bound in HF, $n_{\mathrm{F,HF}}$, is obtained by the difference between the molar amount of total fluoride measured by F-ISE, $n_{\mathrm{F,tot\text{-}ISE}}$, and the fraction of fluoride bound as H_2SiF_6, $n_{\mathrm{F,H_2SiF_6}}$:

$$n_{\mathrm{F,HF}} = n_{\mathrm{F,tot\text{-}ISE}} - n_{\mathrm{F,H_2SiF_6}} \quad (11)$$

Subsequently, $n_{\mathrm{F,HF}}$ is converted by the initial weight and the molar mass into the amount of HF, n_{HF}.

3.4.2. Determination of HNO_3 content

The HNO_3 content is calculated from the first equivalence point of the aqueous acid–base titration curve in analogy to the determination of HF with method 1:

$$n_{\mathrm{HNO_3}} = (cv)_{\mathrm{NaOH,1.EP}} - n_{\mathrm{HF}} - n_{\mathrm{H_2SiF_6}} \quad (12)$$

4. Discussion

4.1. Determination of the silicon content by aqueous acid–base titration

Table 4 displays the contents of H_2SiF_6 in the sample series 1 and 2 obtained by titration with NaOH in aqueous solution. The recoveries are calculated with respect to the initially weighed amounts of silicon and SiO_2 before dissolution. Series 1 (Table 4) is characterized by a quite poor recovery. It was observed that white vapor left the reaction vessel during the addition of HF to the HNO_3/SiO_2 mixture which can be attributed to a loss of SiF_4. In case of series 2 (Table 4) the recoveries are much more satisfying and within the range of uncertainty of the applied titrimetric procedure [6]. However, a loss of volatile SiF_4 can never be excluded, even if the dissolution is carried out at 1 °C.

Table 4
Determination of the H_2SiF_6 contents in series 1 and 2 by titration with NaOH in aqueous solution (m denotes the number of analyses)

Sample	m	Recovery (%)	$w(H_2SiF_6)$ (mg g^{-1})
S1-A	4	97.3	51.2 ± 1.2
S1-B	3	96.8	87.3 ± 0.5
S1-C	4	96.7	118.1 ± 0.6
S1-D	4	99.0	148.8 ± 1.1
S1-E	4	97.2	181.0 ± 0.5
S1-F	3	97.3	209.5 ± 1.6
S1-G	4	97.3	238.6 ± 0.3
S2-A	5	99.3	57.7 ± 0.3
S2-B	4	99.6	114.1 ± 0.5
S2-C	5	99.6	170.1 ± 0.9
S2-D	4	99.7	225.1 ± 0.7
S2-E	4	100.5	285.8 ± 0.9
S2-F	5	99.4	294.9 ± 2.7
S2-G	4	93.4	295.8 ± 2.1

4.2. Determination of HNO_3 content by both methods

4.2.1. Series 1

The determination of the HNO_3 content in sample series 1 can be used to validate the developed method since the dissolution of SiO_2 in a HNO_3–HF mixture gives no change in the amount of HNO_3. As shown in Table 5, the results of the HNO_3 titration using methanolic CHA solution as titrant (method 1) are close to the initial values. A poor recovery was found for sample S1-D. The highest uncertainty exhibits sample S1-C with 2.2% (1σ). Apart from these values, the CHA titration gives a relative uncertainty of about 1% (1σ) and recoveries of about (100 ± 1)%. Less satisfying are the results from the calculation in method 2 which are significantly below the expected values. Since the used electrode gives reliable values for fluoride standard solutions, the method appears less reliable for the studied acid mixtures. The remarkable high uncertainties of the obtained HNO_3 contents result from the propagation of uncertainty according to Eq. (12). The major contributions stem from the content of obtained by titration and the total fluoride content by F-ISE.

4.2.2. Series 2

A calculation of the expected amount of HNO_3 is not possible since unknown amounts of undefined nitric oxides evolve during the dissolution of silicon in the HF/HNO_3 mixtures. The results of the CHA titration with the values obtained from the combination of aqueous acid–base titration and F-ISE of method 2 are in reliable agreement (Table 6).

Table 5
Determination of the HNO_3 contents in samples of series 1 by method 1 and method 2 (m denotes the number of analyses)

Sample	$w(HNO_3)$ initial (mg g^{-1})	CHA titration (method 1)			Calculated (method 2)		
		$w(HNO_3)$ analyzed (mg g^{-1})	m	Recovery (%)	$w(HNO_3)$ analyzed (mg g^{-1})	m	Recovery (%)
S1-A	212.7	214.1 ± 1.4	3	100.6	200.9 ± 8.7	3	94.4
S1-B	214.5	212.5 ± 2.2	11	99.1	208.8 ± 7.2	3	97.3
S1-C	210.1	215.9 ± 4.7	4	102.8	197.3 ± 6.9	3	93.9
S1-D	206.1	214.7 ± 3.5	9	104.2	197.4 ± 8.8	3	95.8
S1-E	203.9	202.8 ± 1.6	4	99.5	193.8 ± 6.7	4	95.0
S1-F	201.4	200.1 ± 0.6	4	99.3	193.2 ± 7.0	3	95.9
S1-G	197.2	197.1 ± 2.5	4	99.9	193.5 ± 5.5	3	98.1

Table 6
Determination of the HNO_3 contents in samples of series 2 by method 1 and method 2 (m denotes the number of analyses)

Sample	CHA titration (method 1)		Calculated (method 2)	
	$w(HNO_3)$ analyzed (mg g^{-1})	m	$w(HNO_3)$ analyzed (mg g^{-1})	m
S2-A	203.5 ± 1.2	2	197.4 ± 1.4	4
S2-B	184.6 ± 1.5	3	181.1 ± 3.2	3
S2-C	175.1 ± 5.3	3	168.7 ± 2.3	3
S2-D	143.4 ± 0.6	3	150.6 ± 1.6	4
S2-E	130.5 ± 3.0	4	136.5 ± 2.6	4
S2-F	116.3 ± 2.2	4	121.1 ± 0.7	3
S2-G	121.2 ± 0.2	3	100.7 ± 1.2	3

4.3. Determination of HF content by both methods

4.3.1. Series 1

Table 7 summarizes the analytical results of the fluoride content analysis by both methods. The deviation between the two methods amounts to 3.4%.

The relative uncertainties for method 1, calculated from the propagation of the individual uncertainties, range between 1.5 and 2.5%. The major contribution of the uncertainty comes from the total acid content titration followed by the CHA titration to determine the HNO_3 content. Although the mean relative uncertainty of the total acid titration is about 0.8%, the absolute values exceed that of the contribution from the CHA titration up to a factor of 8. According to Table 4, the titrimetric determination of H_2SiF_6 gives the highest values of relative uncertainty. This results mainly from the determination of the first equivalence point of the titration curve which is less pronounced than the second equivalence point. However, the absolute uncertainties of the H_2SiF_6 contents are so small that their impact on the uncertainty of the HF content is negligible.

Table 7
HF contents in samples of series 1 calculated via method 1 and method 2

Sample	w(HF) (mg g^{-1})	
	Calculated via method 1	Calculated via method 2
S1-A	212.6 ± 2.4	217.8 ± 2.4
S1-B	178.3 ± 2.2	179.9 ± 0.9
S1-C	146.9 ± 2.4	153.4 ± 0.7
S1-D	115.6 ± 2.1	123.5 ± 2.0
S1-E	91.0 ± 1.7	93.9 ± 1.3
S1-F	61.2 ± 1.5	63.5 ± 1.5
S1-G	37.7 ± 1.5	38.8 ± 1.0

Table 8
HF contents in samples of series 2 calculated via method 1 and method 2

Sample	w(HF) (mg g^{-1})	
	Calculated via method 1	Calculated via method 2
S2-A	208.60 ± 2.3	210.26 ± 0.9
S2-B	161.63 ± 2.0	162.05 ± 1.6
S2-C	109.77 ± 2.3	108.7 ± 4.6
S2-D	69.11 ± 1.4	66.74 ± 0.9
S2-E	0.36 ± 1.3	10.87 ± 2.8
S2-F	−2.54 ± 1.3	7.43 ± 2.7
S2-G	3.04 ± 1.1	9.83 ± 2.1

The calculated uncertainties of the HF content obtained by method 2 result from the ISE determination. Although their relative uncertainties are below the ones from the H_2SiF_6 titration, the absolute uncertainties exceed them by factors up to 4.

4.3.2. Series 2

Both methods give results of acceptable agreement (Table 8) if only the samples S2-A to S2-D are considered. Regarding the calculated uncertainties the same statements are valid as in the section above.

The limitations of the developed methods are shown by the samples S2-E to S2-G. S2-F and S2-G are over-saturated in their silicon content with respect to Eq. (1). Sample S2-E has a very low HF content. The involvement of three experimental values to calculate the content of HF in Eq. (10) explains the very low or even negative value for sample S2-F. At this point it is not possible to decide if the results obtained by method 2 are reliable.

5. Conclusion

This paper presents the first description of two independent analytical methods for the robust determination of the contents of H_2SiF_6, HNO_3, and HF in synthetic etch solutions. Both methods are based on the titrimetric determination of the total acid content and the content of H_2SiF_6. In order to circumvent the problem of overlapping equivalence points in such complex acid mixtures, a method using a non-aqueous titrant had been developed. This procedure allows a clear separation of the equivalence points of HF and HNO_3. However, this method fails if H_2SiF_6 is present. After removing H_2SiF_6 by precipitation, the content

of HNO_3 can be extracted from the obtained titration curve. The finally calculated HF content is mainly affected by the uncertainty of the H_2SiF_6 titration. The second method is based on the measurement of the total fluoride content.

These methods were developed for the needs of technical application and with the option to be incorporated in an automated process control. The results of both methods agree within a limit of 3–5%. It becomes obvious that a value, which is calculated from two or more experimental results, has a poorer recovery due to error propagation than a directly measured value. The methods are not applicable to etch solution over-saturated with respect to silicon and a very low or no concentration of free HF. A final discussion of the results here is given in the second part of this publication.

Acknowledgements

The authors gratefully acknowledge the European Regional Development Fund 2000–2006 and the Free State of Saxony for funding within the project "SILCYCLE" under contract number 8323/1293 at the Sächsische Aufbaubank (SAB). The authors thank Ms. Anja Rietig and Ms. Romy Keller for technical assistance.

References

[1] H. Robbins, B. Schwartz, J. Electrochem. Soc. 106 (1959) 505–508.
[2] M. Steinert, J. Acker, A. Henßge, K. Wetzig, J. Electrochem. Soc. 152 (2005) C843–C850.
[3] S. DeWolf, P. Choulat, E. Vazsonyi, R. Einhaus, E. van Kerschaver, K. DeClercq, J. Szlufcik, Proceedings of the 16th EC PVSEC, Glasgow, 2000, pp. 1521–1523.
[4] W. Weinreich, Diploma Thesis, Freiberg University of Mining and Technology, Freiberg, Germany, 2005.
[5] I. Röver, K. Wambach, W. Weinreich, G. Roewer, K. Bohmhammel, Proceedings of the 20th EU-PVSEC, Barcelona, 2005, pp. 899–902.
[6] W. Weinreich, J. Acker, I. Gräber, submitted for publication.
[7] A. Henßge, J. Acker, C. Müller, Talanta 68 (2006) 581–585.
[8] I. Gyenes, Titration in Non-aqueous Media, Akademiai Kiado, Budapest, 1967.

Available online at www.sciencedirect.com
ScienceDirect
Talanta 73 (2007) 326–331
Talanta
www.elsevier.com/locate/talanta

Determination of amino acids in tea leaves and beverages using capillary electrophoresis with light-emitting diode-induced fluorescence detection

Ming-Mu Hsieh *, Sheng-Min Chen

Department of Applied Chemistry, Fooyin University, Kaohsiung, 151 Chin-Hsueh Road, Ta-Liao Hsiang, Kaohsiung Hsien 831, Taiwan

Received 5 January 2007; received in revised form 23 March 2007; accepted 23 March 2007
Available online 31 March 2007

Abstract

The combination of capillary electrophoresis (CE) and light-emitting diode-induced fluorescence (LED-IF) detection has been demonstrated in the analysis of major amino acids in tea leaves and beverages. The separation efficiency of amino acids, which were derivatized with naphthalene-2,3-dicarboxaldehyde (NDA), depended on the capillary length and PEO concentration. We suggested that the interactions between the NDA derivatives and poly(ethylene oxide) (PEO) molecules are based on hydrogen bonding, hydrophobic patches, and Van der Waals forces. The magnitude of EOF and the interactions between them can be further controlled by the capillary length. The separation of 17 NDA-amino acids derivatives was completed within 16 min using 0.5% PEO and 60 cm capillary length. The relative standard deviations (R.S.D.) of their migration times ($n = 5$) were less than 2.7%. Additionally, the limits of detection at signal-to-noise ratio 3 for the tested amino acids ranged from 3.6 to 28.3 nM. Quantitative determination of amino acids in tea leaves and beverages was accomplished by our proposed method. This study showed that amino acid present in highest concentration in tea leaves and beverages is γ-aminobutyric acid and theanine, respectively. The experimental results suggest that our proposed methods have great potential in the investigation of the biofunction of different tea samples.

Keywords: Amino acids; Capillary electrophoresis; Light-emitting diode; Naphthalene-2,3-dicarboxaldehyde; Tea

1. Introduction

Tea is one of the most widely consumed beverages in the word, second only to water and can be grouped into six categories which are black tea, green tea, Oolong tea, yellow tea, white tea, and dark compressed tea [1–6]. Compared with them, green tea has recently received much scientific attention because of its medical and/or psychological effectiveness. Interestingly, the amino acids contained in tea not only play an important role in determining its taste and quality [7,8], but also have been shown to influence the levels of norepinephrine and serotonin in brain [9] and blood pressure [10]. For example, γ-aminobutyric acid (GABA), which is the main inhibitory amino acid neurotransmitter in the mammalian central nervous system [11,12], has been found to be associated with a decline in blood pressure with continuous drinking of anaerobically treated tea [13].

Due to biological and clinical significance of amino acids contained in tea, a variety of approaches have been developed to determine their concentrations in different kinds of tea [14–16]. Since the most common amino acids do not contain a chromophoric group, many of fluorescent dyes, such as *o*-phthalaldehyde, phenylthiocarbamoyl chloride, fluorescein isothiocyanate, 4-fluoro-7-nitro-2,1,3-benzoxadiazole, and naphthalene-2,3-dicarboxaldehyde (NDA) have been developed for derivatization of amino acids. The high performance liquid chromatography (HPLC) with laser-induced fluorescence (LIF) is a common approach for the analysis of tea samples; the amino acid can be studied at subfemtomole levels [17–21]. However, until now, HPLC analysis has been limited to long analysis times and often required large sample volumes [22]. By contrast, capillary electrophoresis in conjunction with LIF has become increasingly attractive for the determination of amino acids in

* Corresponding author. Tel.: +886 7 781 1151 604; fax: +886 7 782 6732.
E-mail address: sc126@mail.fy.edu.tw (M.-M. Hsieh).

0039-9140/$ – see front matter © 2007 Elsevier B.V. All rights reserved.
doi:10.1016/j.talanta.2007.03.049

tea samples because they provide many advantages, including rapidity, high resolution, sensitivity, flexibility, and small sample volume required [23]. Unfortunately, LIF detection depends on the use of bulky and expensive laser sources for sufficient excitation of analyte fluorescence, especially in UV-absorbing analytes. Light-emitting diodes (LEDs) are attractive as alternative light sources for CE due to small size, low cost, low power consumption, and available in a wide spectral range [24,25]; but, the light from LEDs is divergent and non-monochromatic. It is difficult to focus light to small capillary column and a relatively high fluorescence background usually occurs. To overcome such limitations, a representative focusing system consisting of a plastic lens and an objective was constructed to allow light to be focused effectively onto small capillaries [20,25–29]. Without requiring a focusing system, the determination of FITC-labeled amino acids has been successful using a liquid-core waveguide technique with an LED source.

In this report, we introduced a sensitive and cost-effective CE method for the analysis of major amino acids in different kinds of tea using a violet-LED as source. By using poly(ethylene oxide) (PEO) as buffer additive and NDA as derivatizing reagent, the limits of detection (LODs) at signal-to-noise (S/N) of three for most amino acids are down to nanomolar range. The improvement of separation efficiency was achieved by increasing the capillary length, but at the expense of analysis time. The practicality of the proposed method was further validated by the determination of amino acids in Taiwanese and Japanese tea infusions and tea beverages.

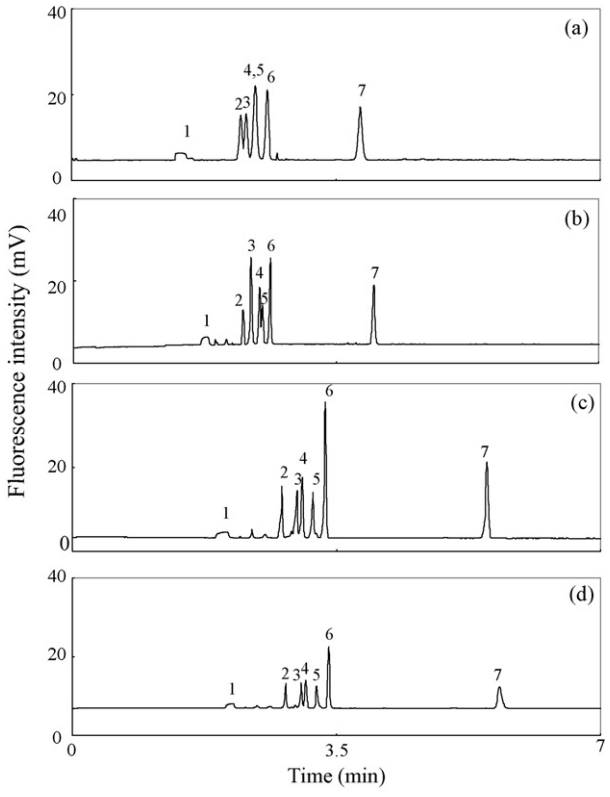

Fig. 1. Determination of NDA-amino acids derivatives (1 μM) by CE–LED-IF in the presence of: (a) 0%, (b) 0.2%, (c) 0.5%, and (d) 1.0% PEO solutions. The capillary was filled with 10 mM $Na_2B_4O_7$ (pH 9.3) prior to separation. Electrophoresis conditions: 40 cm capillary (30 cm to detector); applied voltage, 15 kV; hydrodynamic injection at 30 cm height for 10 s. A UV LED with emission maximum at 410 nm was used as an excitation source for NDA-derivatized analytes. Peak identities: 1, Arg; 2, Phe; 3, Thea; 4, GABA; 5, Ser; 6, Gly; 7, Glu. The analyte concentrations are all 1 μM.

2. Material and methods

2.1. Chemicals

Arginine (Arg), tryptophan (Trp), tyrosine (Tyr), phenylalanine (Phe), leucine (Leu), isoleucine (Ile), histidine (His), asparagine (Asn), threonine (Thr), theanine (Thea), valine (Val), methionine (Met), glutamine (Gln), GABA, serine (Ser), alanine (Ala), glycine (Gly), aspartic acid (Asp), proline (Pro), cysteine (Cys), lysine (Lys), NaCN, and $Na_2B_4O_7$ were obtained from Sigma (St. Louis, MO, USA). PEO (M_w 8,000,000 g/mol), HCl, methanol, and acetonitrile (ACN) were obtained from Aldrich (Milwaukee, WI, USA). NDA was purchased from Tokyo Chemical Industry (Tokyo, Japan) and was prepared in methanol prior to use for derivatization of amino acid. Buffer solutions are 10 mM $Na_2B_4O_7$ at pH 9.3. All the prepared solutions were stored at 4 °C and used within a week.

2.2. CE–LED-IF system

The CE–LED-induced fluorescence (CE–LED-IF) system (CE/LED-IF, Model: 2100) was purchased from Pebio Scientific Company (Taipei, Taiwan). A violet LED (InGaN; type No. M053UVC; Monarchal Electronics; price: <US$ 2.0) with a luminous intensity of 300 mcd (operating current: 20 mA; viewing angle: $2\theta_{1/2} = 30°$; peak emission wavelength: 410 nm; spectral half width: 15 nm) was purchased on the Taipei electronic market. Fused-silica capillaries (Polymicro Technologies, Phoenix, AZ, USA) with 75 μm i.d. and 365 μm o.d. were

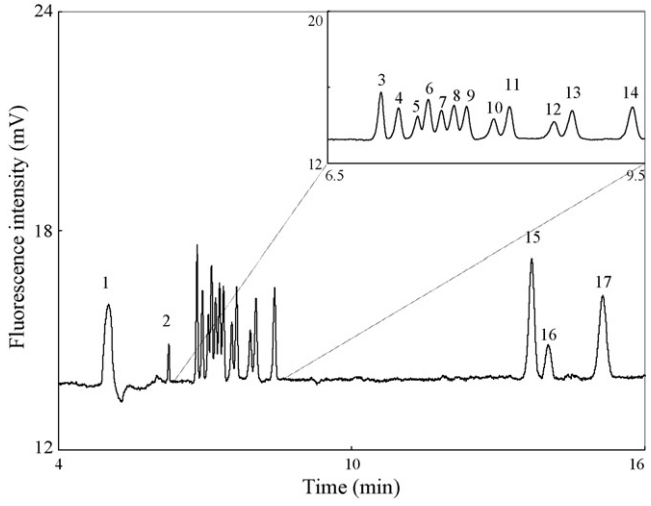

Fig. 2. Separation of NDA-amino acids derivatives using 60 cm capillary (50 cm to detector) in the presence of 0.5% PEO solution. Peak identities: 1, Arg; 2, Trp; 3, Tyr; 4, Phe; 5, Leu; 6, Ile; 7, His; 8, Thea; 9, Met; 10, Gln; 11, GABA; 12, Ser; 13, Ala; 14, Gly; 15, Glu; 16, Lys; 17, Asp. The analyte concentrations are all 1 μM (except for Lys 10 μM). Other conditions are the same as in Fig. 1.

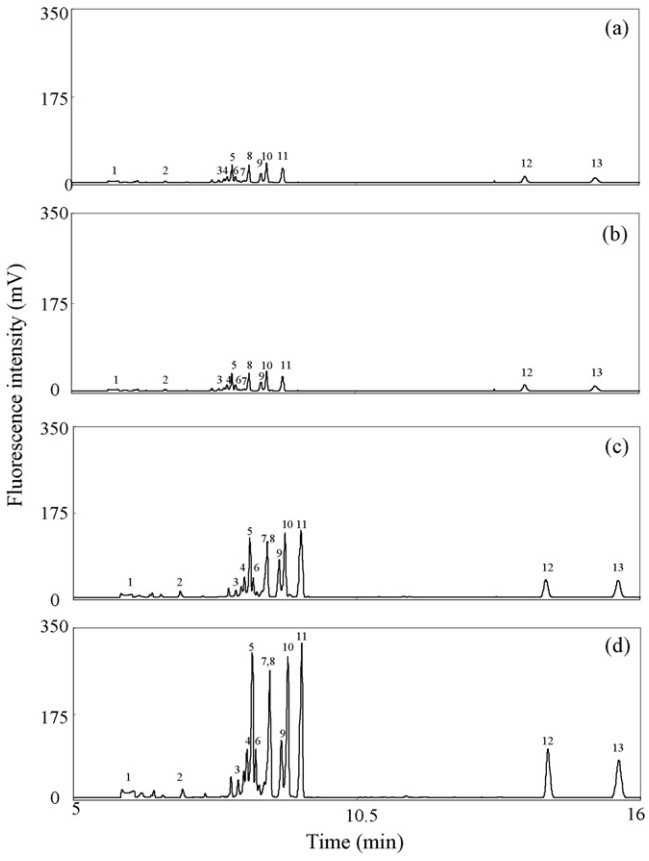

Fig. 3. Analysis of amino acids in tea leaves by CE–LED-IF in the presence of 0.5% PEO solution. The tea leaves were treated with: (a) 25, (b) 50, (c) 75, and (d) 100 °C for 1 min. Peak identities: 1, Arg; 2, Trp; 3, Phe; 4, Leu; 5, Thea; 6, Met; 7, Gln; 8, GABA; 9, Ser; 10, Ala; 11, Gly; 12, Glu; 13, Asp. Other conditions are the same as in Fig. 2.

used for amino acid separations without any further coating process.

2.3. Precolumn derivatization

Derivatization of amino acids with NDA was conducted in 1.5 mL centrifuge tubes using a procedure modified from a previous report [27]. Equal volumes (50 μL) of 10 mM $Na_2B_4O_7$, 10 mM NaCN (prepared in deionized water), and 10 mM NDA solutions were mixed with 50 μL of desirable concentration of amino acids; the resulting mixture (200 μL) was diluted by the addition of 300 μL deionized water. After gentle shaking, the solution was reacted at room temperature for 30 min. The derivative solution was injected for separation without additional purification.

2.4. Preparation of tea samples

The amino acids were released by immersing 4 g tea leaves (GABA tea, Chiayi, Taiwan) in 100 mL water at different temperatures (25, 50, 75, and 100 °C) and infusion time (1, 5, and 15 Times). Subsequently, the mixture was centrifuged at 2500 rpm for 5 min at room temperature. The resulting supernatant (50 μL) was directly mixed with the derivatized solutions, which consists of 10.0 mM $Na_2B_4O_7$ (50 μL), 10 mM NaCN (50 μL), 10 mM NDA (50 μL), and 99.8% ACN (200 μL). The resulting mixtures were diluted with 100 μL deionized water and subsequently incubated at room temperature for 30 min. The large biomolecules can be precipitated from the solution with ACN [30]. The same procedures were used for derivatization of amino acids in tea beverages, including Taiwanese green tea, Taiwanese red tea, and Japanese green tea.

2.5. Electrophoresis procedure

Prior to analysis, the capillaries were treated overnight with 0.5 M NaOH solution [20]. The derivatized standard samples were injected by hydrodynamic injection (30 cm height between the injection and exit ends of the capillary) when the capillaries filled with 10 mM $Na_2B_4O_7$. After sample injection from the anode end, the two ends of the capillary were immersed in PEO solutions (prepared in 10 mM $Na_2B_4O_7$ at pH 9.3) and subsequently the separation was conducted at 15 kV. It is not required to fill the outlet vial with PEO solution. We note that the injection of sample and the filling of PEO solution into the capillary are not easily performed by pressure since the PEO solution is very high viscosity polymer. Since the electro-osmotic flow (EOF) was greater than the electrophoretic mobilities of the amino acid-NDA derivatives, the detection window was located at 10 cm from the cathode end. After each run, the capillary was equilibrated with 0.5 M NaOH at 1 kV for 10 min – to remove

Table 1
Effect of PEO concentrations on the migration time, peak width, and resolution

Analytes	PEO concentration											
	Migration time (min); R.S.D.% ($n=5$)				Resolution				Width (min)			
	0%	0.2%	0.5%	1.0%	0%	0.2%	0.5%	1.0%	0%	0.2%	0.5%	1.0%
Arg	1.46 (1.7)	1.77 (1.7)	2.04 (1.8)	2.11 (1.9)	4.5	3.2	4.4	6.0	0.19	0.18	0.17	0.11
Phe	2.28 (1.7)	2.27 (1.8)	2.78 (1.8)	2.83 (2.0)	1.2	2.0	3.93	4.6	0.05	0.03	0.03	0.03
Thea	2.35 (1.8)	2.37 (1.8)	2.98 (1.9)	3.03 (2.0)	0.9	2.0	1.2	1.2	0.05	0.03	0.03	0.03
GABA	2.47 (1.9)	2.48 (2.0)	3.05 (2.1)	3.09 (2.2)	0	0.8	2.5	2.4	0.07	0.03	0.03	0.03
Ser	2.47 (1.9)	2.52 (2.1)	3.19 (2.1)	3.24 (2.3)	1.8	2.4	2.9	2.4	0.07	0.03	0.03	0.04
Gly	2.63 (2.2)	2.63 (2.3)	3.35 (2.3)	3.40 (2.4)	12.8	19.1	32.0	25.0	0.05	0.03	0.03	0.04
Glu	3.86 (2.3)	3.70 (2.4)	5.50 (2.5)	5.67 (2.7)					0.07	0.04	0.05	0.07

Experimental conditions are the same as in Fig. 1.

Table 2
Quantitative determination of amino acids in tea leaves in different heating temperatures and infusion times

Amino acid	Regression[a]	Correlation coefficient (R^2)	Concentration (μM) (R.S.D.%, $n=5$)					
			Temperature (°C)			Infusion times[b]		
			25	50	100	1	10	15
Trp	$y=0.3841x+0.7786$	0.9942	4.71 (1.8)	13.50 (1.7)	36.36 (1.9)	86.11 (2.3)	6.28 (2.3)	2.17 (2.3)
Phe	$y=1.4786x+0.3748$	0.9912	0.88 (1.8)	2.49 (1.8)	7.10 (1.9)	15.94 (2.5)	0.73 (2.4)	0.75 (2.3)
GABA	$y=1.1782x+4.1462$	0.9956	27.16 (2.3)	77.67 (2.0)	204.87 (2.2)	52.83 (2.7)	7.61 (2.8)	3.12 (2.6)
Ser	$y=0.8623x+2.4816$	0.9914	15.65 (2.3)	46.20 (2.1)	121.61 (2.3)	147.66 (2.7)	5.59 (2.8)	3.60 (2.7)
Ala	$y=0.8655x+4.4301$	0.9965	29.07 (2.5)	117.19 (2.4)	325.80 (2.3)	119.21 (2.9)	8.88 (2.9)	7.50 (2.6)
Gly	$y=1.1968x+3.6934$	0.9986	23.45 (2.6)	71.99 (2.3)	175.62 (2.5)	364.20 (2.9)	13.23 (3.0)	4.36 (2.7)
Glu	$y=1.3465x+4.1506$	0.9953	9.92 (2.7)	30.76 (2.6)	67.05 (2.8)	107.26 (3.0)	2.98 (3.3)	1.31 (2.9)
Asp	$y=1.2444x+2.6724$	0.9927	4.55 (2.8)	17.95 (2.9)	43.66 (3.0)	61.98 (3.1)	1.92 (3.4)	1.06 (3.2)

[a] y represents peak height (v) and x represents the concentrations of spiked analytes.
[b] The heating temperature was set at 100 °C.

PEO molecules and to generate the bulk EOF – and then filled with 10 mM $Na_2B_4O_7$ buffer. This treatment process was quite successful at generating constant bulk EOF mobility; the relative standard deviation (R.S.D.) from five consecutive runs was below 1.5% [31]. For the analysis of tea leaves and tea beverages, a standard addition method was conducted to determine the concentration of amino acids.

3. Results and discussion

3.1. Effect of PEO

When using PEO solution as buffer additive, we have found that the separation efficiency can be improved significantly by the optimization of PEO concentration, ionic strength of PEO solution, and the electrolytes used to fill a capillary. The adsorption of PEO molecules on the capillary wall can be reduced by filling a capillary with a solution at high pH and high ionic strength [32]. Based on our previous results [33], we have learned that 1.5 M Tris–borate (pH 10) is proper to fill a capillary. To prevent serious PEO adsorption that leads to slow EOF and thus a long separation time, PEO solutions at concentrations above 1.0% were not tested in this study. The separations of NDA derivatives of seven amino acids – Arg, Phe, Thea, GABA, Ser, Gly, and Asp – were evaluated in the presence of 0–1.0% PEO (10 mM $Na_2B_4O_7$ at pH 9.3) at 15 kV using a 40 cm capillary. In the absence of PEO, the electropherograms depicted in Fig. 1a indicate that GABA- and Ser-NDA derivatives were not resolved. Oppositely, all of the seven amino acid-NDA derivatives were successfully separated in the presence of 0.5% PEO solution (Fig. 1c). The resolution values for the pairs of GABA/Ser NDA-derivatives were 0, 0.8, 2.5, and 2.4 in the presence of 0, 0.2, 0.5, and 1.0% PEO, respectively. The separation efficiency, enhanced by PEO molecules, is mainly due to the interactions of the NDA derivatives with PEO molecules through hydrogen bonding, hydrophobic patches, and Van der Waals forces. The increases in resolution observed with the increasing PEO concentration in the separation buffer could be also related to the decreases in EOF caused by the presence of PEO in the separation buffer. Another reason is that band broadening and analyte adsorption could be reduced by the use of viscous PEO solution. However, once PEO concentrations reached above 0.5% PEO, we did not see further improvements in peak efficiency, but at the expense of separation times [27]. In

Table 3
Comparison of the concentration of amino acids in three different tea beverages

Tea beverage	Amino acids	Regression[a]	Correlation coefficient (R^2)	Concentration (μM) (R.S.D.%) ($n=5$)
Taiwanese	Trp	$y=0.3582x+1.4286$	0.9942	4.0 (2.4)
Green tea	GABA	$y=0.4508x+1.0638$	0.9934	2.4 (2.6)
	Gly	$y=0.153x+7.4994$	0.9965	49.0 (3.1)
	Asp	$y=1.0945x+3.4116$	0.9924	3.1 (3.2)
Japanese	Trp	$y=0.9865x+4.6826$	0.9916	4.7 (2.9)
Green tea	GABA	$y=0.448x+0.2212$	0.9968	0.5 (2.7)
	Gly	$y=2.8178x+1.6628$	0.9912	0.6 (3.0)
	Asp	$y=1.4483x+4.7544$	0.9964	3.2 (3.3)
Taiwanese	Trp	$y=0.7807x+0.9041$	0.9963	1.2 (2.4)
Red tea	GABA	$y=0.7558x+3.9422$	0.9957	5.2 (2.6)
	Gly	$y=0.5004x+8.5030$	0.9912	17.0 (2.7)
	Asp	$y=1.0659x+3.9036$	0.9975	3.7 (3.2)

[a] y represents peak height (v) and x represents the concentrations of spiked analytes.

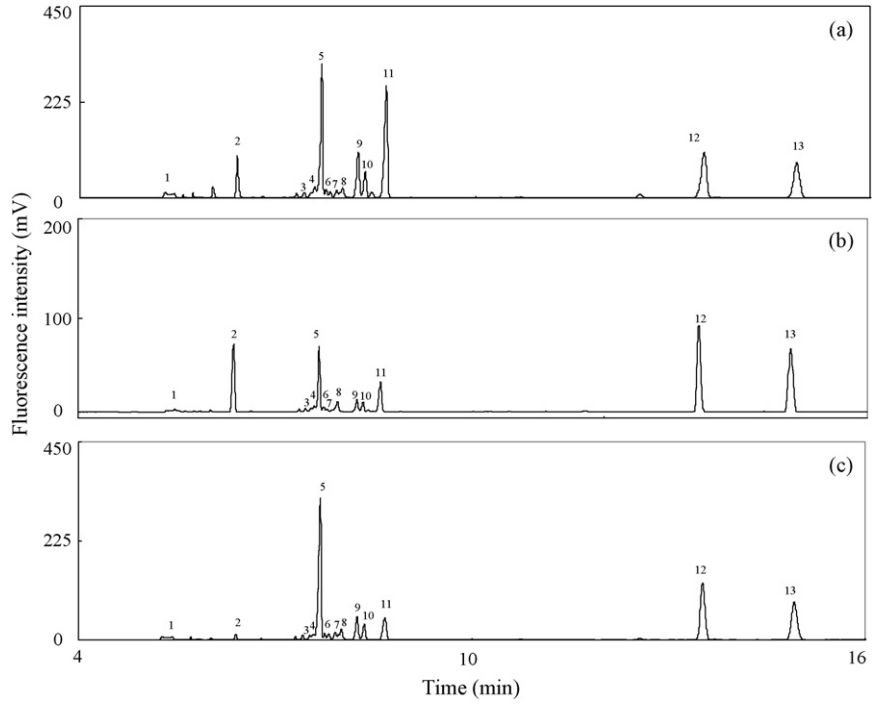

Fig. 4. Analysis of amino acids in three different tea beverages by CE–LED-IF in the presence of 0.5% PEO. The tea beverages include: (a) Taiwanese green tea, (b) Japanese green tea, and (c) Taiwanese red tea, respectively. Peak identities: 1, Arg; 2, Trp; 3, Phe; 4, Leu; 5, Thea; 6, Met; 7, Gln; 8, GABA; 9, Ser; 10, Ala; 11, Gly; 12, Glu; 13, Asp. Other conditions are the same as in Fig. 2.

contrast to their sensitivity, a decrease in fluorescence signal was observed when 1.0% PEO was used as buffer additive. This is because that high background signal resulted from the high concentration of PEO solutions. Thus, we chose to use 0.5% PEO for this study. On the other hand, the broad peak for Arg was observed in all the electropherograms. The band broadening is caused by the multiple labeling of Arg with NDA derivatization. Another reason is that the secondary amine found in Arg does not react with NDA, resulting in the interaction between the Arg and capillary wall. The R.S.D. values of the migration times for the analytes are <2.7% ($n = 5$) as listed in Table 1 when using 0.5% PEO solution as buffer additives.

3.2. Effect of capillary length

To achieve better separation efficiency, the capillary length was extended to 60 cm. It is well known that the resolution is proportional to the square root of capillary length [34]. It is implied that a 1.5-fold increase capillary length would increase resolution by a factor of only 1.2. Interestingly, we obtained improved resolution between GABA and Ser from 0.1 to 0.7 by changing the capillary length from 40 to 60 cm. We point out that, unlike standard CE methods, the capillary length dependence of resolution is due to dynamic bulk EOF and the interactions between the analytes and PEO molecules. Thus, we suggested that the resolution can be enhanced by varying the capillary length. Except of Pro, Val, Asn, Tyr, and Lys, Fig. 2 shows that separation of 17 amino acids was achieved within 16 min using 0.5% PEO solution. It is well known that the secondary amine of Pro does not react with NDA. Additionally, the maximum excitation wavelength of NDA-Lys is 460 nm, which is not appropriate to use violent LED as detection source [35]. Although the peak overlaps among Asn, Thea, and Thr, as well as between Val and Met were observed, the concentration of Val, Tyr, and Asn in tea sample is relatively low as compared to Thea. Thea consists of one half of all amino acids that are found in tea [15]. Under this separation condition, the LODs at a S/N ratio of 3 were estimated by the detection of 0.1 μM amino acids. The LODs for Arg, Trp, Phe, Ser, Ala, Gly, Glu, and Asp were 22.1, 28.3, 4.5, 18.2, 6.7, 5.7, 3.6, and 3.6 nM, in sequence. However, the baseline resolution cannot be achieved in the analysis of the other amino acids. The R.S.D. values of their migration time are less than 2.7%. The results suggest that the combination of CE–LED-IF system and appropriate derivatizing reagents hold great potential for the analysis of biological samples that contain trace amounts of amino acids.

3.3. Analysis of major amino acid in tea leaves and beverages

With high separation efficiency and sensitivity, our proposed methods have been further considered to test a complex sample. To demonstrate this potential, we determined the concentrations of major amino acids in tea leaves and beverages. When compared with the other CE separation methods corresponding to capillary zone electrophoresis and micellar electrokinetic chromatography, a small matrix effect was observed in the analysis of amino acids in tea samples (data not shown). The amino acids were obtained by immersing tea leaves in water at 25, 50, 75, and 100 °C) for 1 min, respectively. After derivatization of amino

acids with NDA, the samples were injected at 30 cm height for 10 s and separated at 15 kV under the optimal conditions. As expected, the electropherograms displayed in Fig. 3 demonstrated that greater amounts of the amino acids were infused to water with increasing temperature. By applying the standard addition method, Table 2 shows that good linearity for each analyte was obtained in the concentration range over 3×10^{-7} to 1.2×10^{-6} M, with correlation coefficients (R^2) > 0.9910. The concentrations of eight amino acids (Trp, Phe, GABA, Ser, Ala, Gly, Glu, and Asp) in tea leaves prepared at different temperatures are also listed in Table 2. In comparison, the relatively high concentrations of GABA (204.8 μM) and Ala (325.8 μM) were observed in tea leaves. The concentration of Thea in tea samples has been not obtained due to the peak overlap between Ile and Thea. We also observed that the concentrations of the amino acids decreased with increasing the infusion time. The results listed in Table 2 display that the concentrations of the amino acids after 15 times infusion are at least 40-fold dilution in comparison of the first infusion.

Next, we compared the species and concentrations of amino acids in three different tea beverages, including Taiwanese green tea, Japanese green tea, and Taiwanese red tea (Fig. 4). Interesting, the relatively high concentration of Thea corresponding to peak 5 was observed. By applying a standard addition method, we determine the concentrations of Trp, GABA, Gly, Asp, and the results are listed in Table 3. The within-run precision (repeatability) of the methods was satisfactory as indicated by the fact that the R.S.D. values for the quantitative results are less than 3.5% from five replicated analyses.

4. Conclusions

A simple, rapid, and sensitive method was developed for the analysis of amino acids in tea leaves and beverages. By using 0.5% PEO and 60 cm capillary length, 16 NDA-amino acids derivatives were completely resolved within 16 min. We suggest that PEO molecules not only affect the magnitude of EOF but also interact with the analytes. As a result, the separation efficiency can be enhanced. We also found that the highest concentration of amino acid in tea leaves and beverages is GABA and Thea, respectively. In comparison of the use of laser source, the LODs for amino acids, which were obtained using LED source, are good enough for determination of their concentration in biological samples. Thus, the use of CE–LED-IF should be commonly accepted because of the consideration of cost. We suggested this proposed method provides the following advantages: (a) the resolution and speed can be optimized by varying the capillary length; (b) the use of CE–LED-IF is relatively cheap as compared to laser source; (c) a small matrix effect was observed using PEO as separation media; (d) this method should be performed under stacking conditions.

Acknowledgment

This work was supported by the National Science Council of Taiwan under contracts NSC 94-2113-M-242-004.

References

[1] M.E. Harbowy, D.A. Balentine, Tea Chem., Crit. Rev. Plant Sci. 16 (1997) 415.
[2] S. Gupta, B. Saha, A.K. Giri, Mutat. Res. 512 (2002) 37.
[3] N. Ahmad, S.K. Katiyar, H. Mukhtar, Cancer chemoprevention by tea polyphenols, in: C. Ionnides (Ed.), Nutrition and Chemical Toxicity, Wiley, West Sussex, UK, 1998, p. 301.
[4] Y. Liang, J. Lu, L. Zhang, S. Wu, Y. Wu, Food Chem. 80 (2003) 283.
[5] P.R. Haddad, W. Buchberger, C.W. Klampfl, J. Chromatogr. A 881 (2000) 357.
[6] S. Oguri, J. Chromatogr. B 747 (2000) 1.
[7] Y. Ding, H. Yu, S. Mou, J. Chromatogr. A 982 (2002) 237.
[8] M.T. Veledo, M. de Frutos, J.C. Diez-Masa, J. Chromatogr. A 1079 (2005) 335.
[9] D.C. Chu, K. Kobayashi, L.R. Juneja, T. Yamamoto, in: T. Yamamoto, L.R. Juneja, D.C. Chu, M. Kim (Eds.), Chemistry and Application of Green Tea, CRC Press, Boca Raton, FL, 1997, p. 129.
[10] H. Yokogoshi, Y. Kato, Y.M. Sagesaka, T. Takihara-Matsuura, T. Kakuda, N. Takeuchi, Biosci. Biotech. Biochem. 59 (1995) 615.
[11] D.F. Owens, A.R. Kriegstein, Nat. Rev. Neurosci. 3 (2002) 715.
[12] A.J. Smith, P.B. Simpson, Anal. Bioanal. Chem. 377 (2003) 843.
[13] K. Hakamata, JARQ 24 (1990) 105.
[14] K. Ohta, A. Yoshida, K. Harada, J. Agric. Chem. Soc. Jpn. 69 (1995) 1331.
[15] M. Kato, Y. Gyoten, K. Sakai-Kato, T. Toyo'oka, J. Chromatogr. A 1013 (2003) 183.
[16] H. Horie, T. Mukai, K. Kohata, J. Chromatogr. A 758 (1997) 332.
[17] S. Hu, N.J. Dovichi, Anal. Chem. 74 (2002) 2833.
[18] T. Fukushima, N. Usui, T. Santa, K. Imai, J. Pharm. Biomed. Anal. 30 (2003) 1655.
[19] C. Aoyama, T. Santa, M. Tsunoda, T. Fukushima, C. Kitada, K. Imai, Biomed. Chromatogr. 18 (2004) 630.
[20] M.J. Lu, T.C. Chiu, P.L. Chang, H.T. Ho, H.T. Chang, Anal. Chim. Acta 538 (2005) 143.
[21] T. Kawasaki, T. Higuchi, K. Imai, O.S. Wong, Anal. Biochem. 180 (1989) 279.
[22] R. Gatti, M.G. Gioia, P. Andreatta, G. Pentassuglia, J. Pharm. Biomed. Anal. 35 (2004) 339.
[23] Y. Ma, G. Liu, M. Du, I. Stayton, Electrophoresis 25 (2004) 1473.
[24] W.J.M. Underberg, J.C.M. Waterval, Electrophoresis 23 (2002) 3922.
[25] A.K. Su, C.H. Lin, J. Chromatogr. B 785 (2003) 39.
[26] S. Hillebrand, J.R. Schoffen, M. Mandaji, C. Termignoni, H.P.H. Grieneisen, T.B.L. Kist, Electrophoresis 23 (2002) 2445.
[27] S.J. Chen, M.J. Chen, H.T. Chang, J. Chromatogr. A 1017 (2003) 215.
[28] S.C. Wang, M.D. Morris, Anal. Chem. 72 (2000) 1448.
[29] S.L. Wang, X.J. Huang, Z.L. Fang, Anal. Chem. 73 (2001) 4545.
[30] Q. Li, C.W. Huie, Electrophoresis 22 (2001) 763.
[31] W.L. Tseng, H.T. Chang, Electrophoresis 22 (2001) 763.
[32] W.L. Tseng, H.T. Chang, Anal. Chem. 72 (2000) 4805.
[33] M.M. Hsieh, C.E. Hsu, W.L. Tseng, H.T. Chang, Electrophoresis 23 (2002) 1633.
[34] M.G. Khaledi, High-Performance Capillary Electrophoresis: Theory, Techniques and Applications, vol. 146, John Wiley, New York, 1998, p. 54.
[35] N. Siri, M. Lacroix, J.-C. Garrigues, V. Poinsot, F. Couderc, Electrophoresis 27 (2006) 4446.

Available online at www.sciencedirect.com
ScienceDirect
Talanta 73 (2007) 274–281
Talanta
www.elsevier.com/locate/talanta

Mesoporous titanium dioxide as a novel solid-phase extraction material for flow injection micro-column preconcentration on-line coupled with ICP-OES determination of trace metals in environmental samples

Chaozhang Huang, Zucheng Jiang, Bin Hu *

Department of Chemistry, Wuhan University, Wuhan 430072, PR China

Received 17 November 2006; received in revised form 17 March 2007; accepted 20 March 2007
Available online 30 March 2007

Abstract

Mesoporous titanium dioxide as a novel solid-phase extraction material for flow injection micro-column preconcentration on-line coupled with ICP-OES determination of trace metals (Co, Cd, Cr, Cu, Mn, Ni, V, Ce, Dy, Eu, La and Yb) in environmental samples was described. Possessing a high adsorption capacity towards the metal ions, mesoporous titanium dioxide has found to be of great potential as an adsorbent for the preconcentration of trace metal ions in samples with complicated matrix. The experimental parameters including pH, sample flow rate, volume, elution and interfering ions on the recovery of the target analytes were investigated, and the optimal experimental conditions were established. Under the optimized operating conditions, a preconcentration time of 90 s and elution time of 18 s with enrichment factor of 10 and sampling frequency of 20 h^{-1} were obtained. The detection limits of this method for the target elements were between 0.03 and 0.36 $\mu g\,L^{-1}$, and the relative standard deviations (R.S.D.s) were found to be less than 6.0% (n =7, c =5 ng mL^{-1}). The proposed method was validated using a certified reference material, and has been successfully applied for the determination of the afore mentioned trace metals in natural water samples and coal fly ash with satisfactory results.

Keywords: Mesoporous titanium dioxide; Flow injection; ICP-OES; On-line micro-column preconcentration; Trace elements; Environmental samples

1. Introduction

Heavy metal pollution has become a worldwide problem for environmental protector. Based on the contributing factors, heavy metal pollution caused by the city can be separated into two types. One is formed with air and another is with water as a carrier of heavy metals [1]. And heavy metals can easily enter the food chain through a number of pathways and cause progressive toxic effects due to gradual accumulation in living organisms during their life span and long-term exposure to the contaminated environment. Whilst, since rare earth elements (REEs) were valuable indicators of many geochemical processes, including the evolution of earth's mantle and crust, magma genesis, sedimentary petrology and ore genesis, geologists and geochemists have investigated REEs in natural samples such as natural water, ore (coal), marine particulate and rock reference materials, etc. [2]. In view of that, there is need to develop a monitoring technique for heavy metal and REEs in nature water and some geological samples to gaining more information for environmental protector and geologists.

However, direct determination of trace elements at low concentrations by modern inductively coupled plasma optical emission spectrometry (ICP-OES) is often difficult, not only because of the insufficient sensitivity of the methods, but also because of matrix effects. Recently, the coupling of flow injection (FI) on-line micro-column separation and preconcentration techniques to ICP-OES has been proved to be a good idea [3,4]. This combination not only provides an improvement in detection limits and reduces the interference from matrix, but also significantly enhances the analytical performance of the methods [5–7]. In comparison with their off-line batch counterparts, these systems have a number of significant advantages for trace determination—greater efficiency, lower consumption of sample and reagent, improved precision, possibility of working in a closed system with a significant reduction of airborne contamination, and increased sampling frequency.

* Corresponding author. Tel.: +86 27 87218764; fax: +86 27 68754067.
E-mail address: binhu@whu.edu.cn (B. Hu).

0039-9140/$ – see front matter © 2007 Elsevier B.V. All rights reserved.
doi:10.1016/j.talanta.2007.03.046

On-line column preconcentration systems coupled with ICP-OES are based on retention of the analytes in micro-column packed with adsorbent that determines the sensitivity and the selectivity of the analytical method. Therefore, new adsorbent is explored and searched actively in SPE technique. Many adsorption materials, such as organic chelate resin, C18-bonded silica gel [8–10], activated carbon [11], activated alumina [12,13] and microcrystalline material [14] are used in this technology. More recently, nanometer-sized materials [15–19], C60–C70 fullerene and its derivative [20–22], multiwalled carbon nanotubes [23,24] were also explored for this purpose.

Since its discovery in 1992, mesoporous materials have gained interest throughout the scientific community [25,26]. These kinds of materials possess large surface area, mesoporous structure, very tight pore size distributions and hence regarded as attractive candidates for a wide range of applications including shape-selective catalysis [27], sorption of large organic molecules [28] and chromatographic separations [29]. The potential of mesoporous material as adsorbent could be viewed in three perspectives: (1) As a new nanometer material with unsaturated surface atoms that can bind with other atoms, it possess highly chemical activity, very high adsorption capacity and selective adsorption of metal ions. (2) Due to its large surface area, mesoporous material provides more active sites, this would result in achieving quantitative adsorption in short time. (3) By virtue of mesoporous structure, fast adsorption and desorption could be obtained. Recently, Feng et al. [30] reported a new material of functionalized monolayerson mesoporous (FMMS) supports which could remove heavy metals from natural water by modifying mesoporous material with γ-mercapto-propytrimethoxysilane. Xu et al. [31] synthesized an organofunctional silane monolayer which has been prepared on the surface of Ti MCM 41 and found that it was an effective adsorbent for Pb^{2+}, Cd^{2+}, Zn^{2+}, Cu^{2+}, Mg^{2+} and Na^{+}. Recently, some modified mesoporous silicas are synthesized and used for adsorbing Hg, Cd or Pb ions [32–36]. All these facts mentioned above clearly indicate that mesoporous material may have great analytical potential as a solid-phase extraction adsorbent for metal ions.

Owing to its high-surface-area, nontoxic and highly catalysis and steady, mesoporous titanium dioxide has been used widely for gas sensing [37], photocatalysts [38], photoelectrodes [39] and solar energy conversion [40]. However, to the best of our knowledge, no research works on the use of mesoporous titanium dioxide as a sorbent material for adsorption of trace metals and its application in trace analysis have been reported. In this work, mesoporous titanium dioxide was synthesized and was used as the packing materials for flow injection on-line micro-column separation/preconcentration ICP-OES simultaneous determination of trace metals in environmental samples.

2. Experimental

2.1. Synthesis of mesoporous titanium dioxide

2.1.1. Apparatus and reagents

Ultrasonic oscillator (Shengyuan Instrument Factory, Shanghai, China) and a 7312-I electric agitator (Master Pattern Factory, Shanghai, China) were used in the synthesis procedure.

X2-6-13 muffle furnace (Yingshan Yahua Instrument Factory, Hubei, China) was used to achieve the desired temperature.

All reagents used, including tetrabutyl titanate, H_3PO_4 and ethanol, were of analytical reagent grade. Doubly deionized water (DDW) was prepared by an apparatus purchased from the Park-Rich International Co. Ltd. (Hong Kong, China), and was used throughout the all experiments.

2.1.2. Synthesis procedure

The method used for synthesis of mesoporous titanium dioxide was based on the procedure reported in Ref. [41]. Briefly, 3.6 g of tetrabutyl titanate was dissolved in 32 mL of absolute ethanol by stirring. The rapid hydrolysis of tetrabutyl titanate could be controlled effectively by using ethanol as the solvent. After 15 min, 0.48 mL of 2.0 mol L^{-1} H_3PO_4 was added. The resulting suspension was stirred for 3 h at room temperature, followed by the addition of 5 mL DDW under vigorous stirring. The solution was stirred for an additional 2 h to obtain the sol solution, it is then followed by the vaporization of water and ethanol at about 78 °C. The resulting solid product was exhaustively washed with DDW and ethanol, dried in vacuum drying box at 80 °C overnight, and then calcined at 500 °C for 3 h.

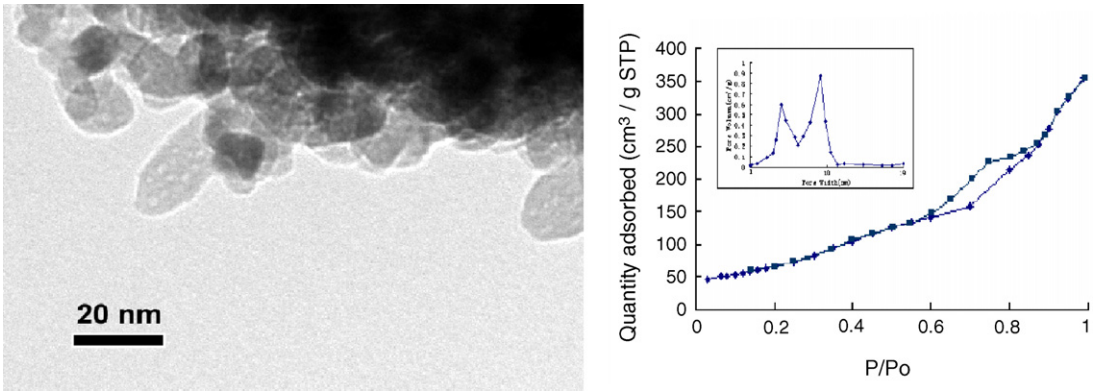

Fig. 1. Characterization of mesoporous TiO_2 powders by TEM and nitrogen adsorption.

2.1.3. Characterization of mesoporous titanium dioxide

A TEM pattern of mesoporous titanium dioxide, which was shown in Fig. 1, was obtained using a Transmission Electron Microscope (JEM-100CX, Japan). It can be seen that there are particles possessing pore structure with particle size of 20–30 nm. The nitrogen adsorption and desorption isotherms at 77 K were measured on an auto N_2 adsorption instrument (ASAP 2010, Micrometrics, USA) after samples were degassed at 120 °C. The result shows the BET surface area of mesoporous TiO_2 is 206 m^2/g and the average pore width is 7.5 nm, which is closed to results of the Ref. [41] whose BET surface area is 227 m^2/g and the average pre width is 8.9 nm.

2.2. Preconcentration and determination

2.2.1. Apparatus

Intrepid XSP Rasial ICP-OES (Thermo. USA) with a concentric model nebulizer and a cinnabar model spray chamber was used for the determination. The optimum operation conditions were summarized in Table 1. The pH values were controlled with a Mettler Toledo 320-S pH meter (Mettler Toledo Instruments Co. Ltd., Shanghai, China) supplied with a combined electrode. A WX-3000 microwave accelerated digestion system (EU Chemical Instruments Co. Ltd., Shanghai, China) was used for sample digestion. An IFIS-C flow injection system (Ruimai Tech. Co. Ltd., Xi'an, China) and a self-made PTFE micro-column (20 mm × 4.0 mm i.d.) packed with mesoporous titanium dioxide were used in the on-line separation/preconcentration process.

2.2.2. Standard solution and reagents

The stock standard solutions (1 g L^{-1}) of metal ions (V, Cr, Co, Mn, Ni, Cu and Cd) were prepared by dissolving appropriate amounts of NH_4VO_3, $Cr(NO_3)_3{\cdot}9H_2O$, $Co(NO_3)_2{\cdot}6H_2O$, $MnSO_4$, $NiSO_4{\cdot}(NH_4)_2SO_4{\cdot}6H_2O$, $CuSO_4{\cdot}5H_2O$ and $Cd(NO_3)_2$ (The First Reagent Factory, Shanghai, China) in DDW, respectively; the stock standard solutions (1 g L^{-1}) of other metal ions (La, Y, Yb, Eu and Dy) were prepared by dissolving their Specpure oxides (Shanghai Reagent Factory, Shanghai, China) in dilute HCl, and diluting to a certain volume with DDW. Working solutions were prepared daily by appropriate dilutions of stock solutions. All reagents used were analytical-reagent grade. DDW was used throughout.

Table 1
Operation parameters of Intrepid XSP Rasial ICP-OES

RF generator power	1150 W
Frequency of RF generator	27.12 MHz
Coolant gas flow rate	14 L min^{-1}
Carrier gas flow rate	0.6 L min^{-1}
Auxiliary gas	0.5 L min^{-1}
Observation height	15 mm
Solution uptake rate	1.0 mL min^{-1}
Max integration times (s)	15
Analytical wavelength (nm)	
Cd	326.106
Ce	413.380
Co	238.892
Cr	283.563
Cu	324.754
Dy	353.170
Eu	381.967
La	408.672
Mn	257.610
Ni	341.476
V	309.311
Yb	328.937

2.3. Micro-column preparation

A total of 50 mg of mesoporous titanium dioxide was filled into a PTFE (Shanghai Jinyou-Tech Co. Ltd., Shanghai, China) micro-column (20 mm × 2.0 mm i.d.) plugged with a small portion of glass-wool (Yichang Yafeng Co. Ltd., Yichang, China) at both ends. Before use, methanol and DDW were passed through the column in sequence in order to clean it. Then, the column was conditioned to the desired pH with 0.1 mol L^{-1} NH_4NO_3 buffer solution.

2.4. General procedure

The operation sequence of the FI on-line column preconcentration and determination is shown in Fig. 2. In preconcentration step, pump P1 was activated, so that the sample was drawn through the column; the effluent from the column was flowing to waste. And in elution step, pump P2 was activated while the injection valve turned to the elution position to propel eluent through the column reversedly for eluting the analyte retained on the column. In this instance, the continuous impact on the sor-

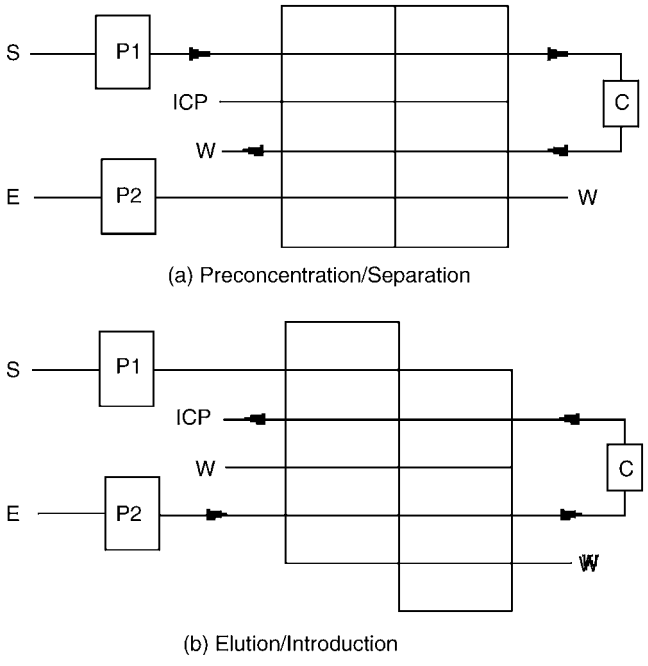

Fig. 2. FI manifold and operation for on-line preconcentration/separation and ICP-OES determination. (a) Preconcentration/separation step and (b) elution/introduction step. For details see text. S, sample; E, elution; W, waste; C, micro-column packed with mesoporous TiO_2; P1, P2, peristaltic pumps; ICP, ICP-OES.

bent could be avoided. Then, the eluting solution was introduced into the ICP-OES for determination.

2.5. Sample preparation

(i) *Soil*. The certified reference material of GBW07401 (GSS-1) soil was provided by the Institute of Geophysical and Geochemical prospecting, Langfang, China. 0.0500 g of GBW07401 (GSS-1) was weighed and placed into PTFE digestion vessel. After adding 4 mL of HNO_3, 1 mL of $HClO_4$ and 1 mL of HF (The First Reagent Factory, Shanghai, China), the vessel was capped and shaken for 3 min to allow thorough mixing of the sample and acids. The vessel was then place on the turntable. The operation parameters for the microwave digestion was as follows: 2 min at 8 atm and 600 W; 3 min at 12 atm and 800 W; 8 min at 16 atm and 800 W [42]. The blank solution was prepared under the same mixed acids and microwave program. After digestion, the vessel was cooled in air to room temperature. And then, the digest was filtered and transferred into 100 mL of flask, adjusted to pH 8.5 and diluted to calibration with DDW for analysis.

(ii) *Water*. Water samples, including river water, lake water, pond water and well water were obtained from Wuhan, China. After collecting, they were filtered through a 0.45 μm membrane filter (Tianjing Jinteng Instrument Factory, Tianjin, China), acidified to pH of about 1 with concentrated HCl prior to storage for use. Before use, the pH value was adjusted to 8.5 with 0.1 mol L^{-1} HCl and 0.1 mol L^{-1} $NH_3{\cdot}H_2O$.

(iii) *Coal fly ash*. 0.0500 g of coal fly ash (provided by coal-fired power plant, Whuhan, China) were weighed and put into PTFE digestion vessel. After adding 4 mL of HNO_3, 1 mL of $HClO_4$ and 1 mL of HF, the vessel was capped and shaken for 3 min to allow thorough mixing of the sample and acids. The vessel was then place on the turntable. The operation parameters for the microwave digestion was as follows: 2 min at 8 atm and 600 W; 3 min at 12 atm and 800 W; 8 min at 16 atm and 800 W [42]. The blank solution was prepared under the same mixed acids and microwave program. After digestion, the vessel was cooled in air to room temperature. And then, the digest was filtered and transferred into 100 mL of flask, adjusted to pH 8.5 and diluted to calibration with DDW for analysis.

3. Results and discussion

3.1. Selectivity and probably adsorptive mechanism of mesoporous titanium dioxide to metal ions

pH value play a great role in the SPE procedure. An appropriate pH value can not only improve the adsorption efficiency, but also depress the interference of the matrix. The adsorption behavior of various metal ions on mesoporous titanium dioxide was studied according to the general procedure by using an analytical mixture of 100 μg L^{-1} each metal. Fig. 3 is the dependence of adsorption percentage of tested metal ions on the pH. It can be seen that the adsorption percentage of the analytes increased with an increase in pH. The experimental results also show the possibility of concentrating these metal cations simultaneously at a constant pH value. Thus, the pH 8.5 was used throughout.

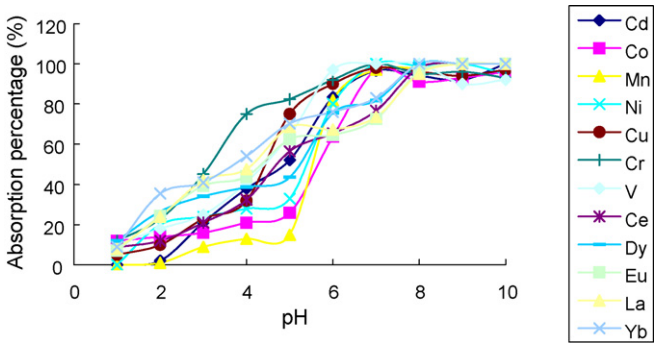

Fig. 3. The dependence of adsorption percentage of tested metal ions on pH.

Two types of hydroxyl groups are suggested to exist on the surface of titanium dioxide [43]. One kind of hydroxyl group is assumed to be bound to one Ti^{4+} site (terminal OH) and the other is bound to two Ti^{4+} sites (bridged OH). Since the bridged (OH) should be strongly polarized by the cations, it is expected to be acidic in character, whereas the terminal (OH) could be predominantly basic. Both of them participate in the adsorptive process of metal cations (see Fig. 4). In acidic condition, parts of metal ions may be adsorbed on the surface of titanium dioxide by exchange with bridged (OH) (reaction 1). It is a reversible reaction. It indicates that the adsorption percentage of titanium dioxide to metal ions could enhance with the increase of pH, namely, with decrease of the concentration of $[H^+]$, the reversible reaction would shift to the right. While the pH values higher than the IEP of titania (6.2), the oxide surface is covered with OH groups and is negatively charged [44]. As a result, the terminal OH also becomes active towards cation adsorption (reaction 2). The adsorption mechanism of mesoporous titanium dioxide towards metal ions (Fig. 4) may be proposed on the basis of our results: where L is ligand and M^{n+} is a metal cation.

3.2. The optimization of elution conditions

With respect to the stripping of target analytes from the mesoporous titanium dioxide packed microcolumn, HCl/HNO_3 was employed. We found that 1–2.5 mol L^{-1} HCl/HNO_3 was sufficient for quantitative recovery of all the metals. In this work, 2 mol L^{-1} HCl was chosen.

The elution volume and the elution flow rate could affect the efficiency of the elution heavily. The influence of the elution volume on recovery for triplicate determination of the target analytes at concentration of 100 μg L^{-1} was investigated. The result shows that 0.3 mL HCl (2 mol mL^{-1}) was sufficient for complete elution. And we also found that quantitative recoveries could be obtained with elution flow rate varying among 0.2–1.2 mL min^{-1}. Thus, the elution volume of 0.3 mL and the elution flow rate of 1.0 mL min^{-1} were used in the following experiments.

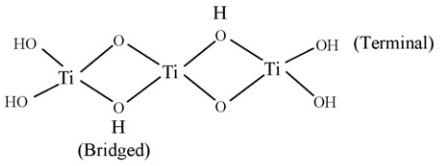

Two types of hydroxyl groups on the surface of titanium dioxide

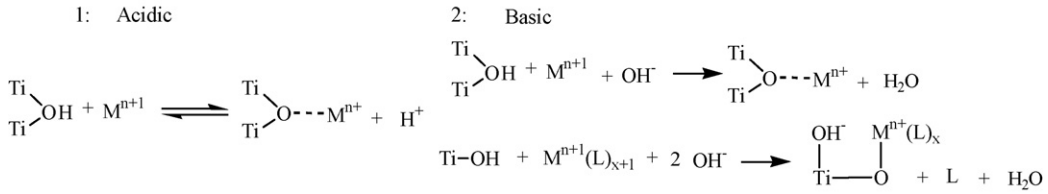

Fig. 4. The adsorptive mechanism of mesoporous titanium dioxide to metal ions.

Table 2
Comparison of sorption capacities (mg g^{-1})

Element	Mesoporous TiO_2	Multiwalled carbon nanotubes [23,24]	Nano-sized TiO_2 [15,16]	Amberlite XAD-2 (Pyrogallol) [8]	High surface area ZrO_2 [6]	Silica gel (ATDAT) [9]
Cu	8.1	–	6.89	4.5	<5	0.96
Mn	22.3	4.86	2.12	4.5	<5	–
Cd	8.1	6.89	–	5.2	<5	3.92
Co	13.9	–	–	4.1	<5	0.59
Ni	8.6	7.42	1.98	4.1	<5	0.94
Cr	14.8	–	7.58	–	<5	–
V	13.1	–	–	–	<5	–
La	21.3	8.30	10.4	–	–	–
Eu	19.5	9.43	12.1	–	–	–
Ce	13.8	–	–	–	–	–
Dy	16.7	–	8.8	–	–	–
Yb	26.5	8.57	12.8	–	–	–

3.3. The effect of sample flow rate and sample volume

The sample flow rate should be optimized to ensure quantivative retention along with minimization of the time required for sample processing. It was found that the flow rate in the range of 0.5–2.5 mL min^{-1} had no significant effect on the recoveries of the studied ions. It means that the adsorption kinetics of the mesoporous titanium dioxide is very excellent to the studied ions. For further experiments, a sample flow rate of 2.0 mL min^{-1} was applied. Since the sample volume was 3 mL, a sample loading time of 90 s was employed.

In order to obtain higher enrichment factor, a large volume of sample solution was required. It was found that quantitative recoveries for all analytes were obtained when sample volumes were less than 30 mL. So an enrichment factor of 100 could be achieved by this method. It should be pointed out that 30 mL sample loading would take a longer time and thus resulting in a low sampling frequency. To trade off the enrichment factor and analytical speed, a sample volume of 3 mL and an elution volume of 0.3 mL were used, so that an enrichment factor of 10 and a sampling frequency of 20 h^{-1} were obtained in this work.

3.4. Adsorption capacity and regeneration

Adsorption capacity is an important factor to evaluate, because it determines how much mesoporous titanium dioxide is required to quantitatively concentrate the analytes from a given solution. The method used in capacity study was adapted from that recommended by Maquieira et al. [45]. For comparison, the adsorption capacity data of mesoporous TiO_2 and other methods reported in the literatures [6,8,9,15,16,23,24] were also listed in Table 2. As can be seen, generally, the capacity of

Table 3
Effect of coexisting ions on the adsorption of analytes

Coexisting ions	Tolerance limit of ions (mg L^{-1})
K^+	10,000
Na^+	8 ,000
Ca^{2+}, Mg^{2+}	5 ,000
Al^{3+}	1 ,000
Fe^{3+}	40
Zn^{2+}	20
SO_4^{2-}, H_2PO^-	2 ,000
SiO_3^{2-}	1 ,000

Table 4
The analytical performance data of the on-line FI-ICP-MS system

	Co	Cd	Cr	Cu	Mn	Ni	V	Ce	Dy	Eu	La	Yb
LOD ($\mu g\,L^{-1}$)	0.09	0.36	0.17	0.12	0.06	0.28	0.11	0.35	0.10	0.07	0.16	0.03
R.S.D.s (%) ($n=7$, $c=5\,\mu g\,L^{-1}$)	2.9	5.7	3.5	4.9	2.9	5.4	2.5	6.0	3.8	2.1	3.6	2.7
Sampling frequency (h^{-1})						20						
Enrichment factor						10						

mesoporous titanium dioxide is significantly higher than other reported adsorbents.

It is imperative to investigate the change in the adsorption capacity of mesoporous titanium dioxide after several adsorption/elution steps. Based on the analysis conducted, it was observed that, mesoporous titanium dioxide is highly stable with long column life time, enabling more than one hundred of load and elution cycles to be performed without loss of analytical performance. Our results indicate that mesoporous titanium dioxide is a suitable substance for multi-element-extraction procedures and effective matrix separation.

3.5. Co-existing ions interference

The study of interference by other coexisting ions, such as K^+, Na^+, Ca^{2+}, Mg^{2+}, Al^{3+}, Fe^{3+}, and Zn^{2+}, on the preconcentration and determination of analytes were examined under the optimum conditions described above using the FI-ICP-OES set up shown in Fig. 2. The results summarized in Table 3 show that the method has a good tolerance to interference.

3.6. Analytical performance

Under the optimized operating conditions, a preconcentration time of 90 s and elution time of 18 s with enrichment factor of 10 and sampling frequency of $20\,h^{-1}$ were obtained. The detection limits (evaluated as the concentration corresponding to three times the standard deviation of 11 runs of the blank solution) along with the relative standard deviations (R.S.D.s) ($n=7$, $c=5\,ng\,mL^{-1}$) for the targets analytes by on-line FI-ICP-MS system are summarized in Table 4. As could be seen, the detection limits are from $0.03\,ng\,L^{-1}$ for Yb to $0.36\,ng\,L^{-1}$ for Cd with R.S.D.s ranging from 2.1% for Eu to 6.0% for Ce.

3.7. Sample analysis

The accuracy of the proposed method was tested by determining certain metal ions in a certified reference material. The analytical results were given in Table 5. As can be seen, the determined values were in good agreement with the certified values.

The proposed method was also applied to the determination of analytes in coal fly ash and water samples (river, pond, well and lake). The analytical results and the recoveries for the spiked samples were given in Tables 6 and 7. It can be seen that the recovery for the spiked samples is between 86.7 and 110.2%.

3.8. Conclusion

A simple, rapid and reliable method was developed for the FI on-line preconcentration and ICP-OES determination of trace metal ions in environmental samples by using mesoporous titanium dioxide as micro-column packing material. The adsorption behavior of metal ions on mesoporous titanium dioxide has been studied systematically, and it was found that Mesoporous titanium dioxide possesses a high adsorption capacity towards the metal ions, and the analytes retained on its surface can be easily desorbed. Hence, Mesoporous titanium di oxide has found to be of great potential as an adsorbent for the preconcentration of trace metal ions in samples with complicated matrix.

Table 5
Analysis of certified material of GBW07401 (GSS-1) soil sample (mean ± S.D., $n=3$)

Element	Certified ($\mu g\,g^{-1}$)	Determined ($\mu g\,g^{-1}$)
Co	14.2 ± 1.5	14.0 ± 1.2
Cd	4.3 ± 0.6	3.2 ± 0.4
Cr	62 ± 6	63 ± 2
Cu	21 ± 2	21.6 ± 1.9
Mn	1760 ± 98	1755 ± 40
Ni	20.4 ± 2.7	20.1 ± 1.3
V	86 ± 6	85 ± 2
Ce	70 ± 5	67 ± 6.8
Dy	4.6 ± 0.3	4.4 ± 0.4
Eu	1.0 ± 0.1	0.9 ± 0.1
La	34 ± 3	31 ± 3
Yb	2.7 ± 0.4	2.6 ± 0.3

Table 6
Determination of metal ions in coal fly ash (mean ± S.D., $n=3$)

Sample (coal fly ash)	Contents ($\mu g\,g^{-1}$)	Added	Found ($\mu g\,g^{-1}$)	Recovery (%)
Cu	39.6 ± 2.3	20	56.7 ± 3.8	95.1
Co	7.4 ± 0.6	20	25.6 ± 1.6	93.4
Cr	36.5 ± 2.4	20	57.1 ± 2.2	101.6
Cd	nd	20	18.8 ± 1.4	94.0
V	79.6 ± 4.6	20	97.8 ± 6.6	98.2
Mn	250.2 ± 24.1	20	268.4 ± 20.2	99.2
Ni	38.4 ± 2.6	20	57.2 ± 3.1	97.9
Ce	194.6 ± 7.1	20	200.5 ± 18.2	93.4
La	135.6 ± 6.8	20	147 ± 11.3	94.8
Eu	nd	20	17.9 ± 1.3	89.5
Dy	5.8 ± 0.6	20	23.5 ± 1.8	91.1
Yb	3.8 ± 0.2	20	22.1 ± 1.9	92.9

nd: not detected.

Table 7
Determination of trace metals in water samples (mean ± S.D., $n = 3$, unit = $\mu g\,L^{-1}$)

Elements	River water			Lake water			Pond water			Well water		
	Added	Found	Recovery (%)	Added	Found	Recovery (%)	Added	Found	Recovery (%)	Added	Found	Recovery (%)
Cu	0	4.7 ± 0.4	–	0	4.0 ± 0.3	–	0	3.5 ± 0.2	–	0	3.8 ± 0.5	–
	20	24.7 ± 2.0	100.0	20	23.0 ± 1.4	95.8	20	22.4 ± 1.7	95.3	20	24.5 ± 1.6	102.9
Co	0	3.1 ± 0.3	–	0	2.9 ± 0.2	–	0	1.9 ± 0.2	–	0	3.4 ± 0.3	–
	20	20.8 ± 1.7	90.0	20	21.1 ± 1.3	92.1	20	22.1 ± 1.6	100.9	20	21.3 ± 1.5	91.0
Cr	0	3.5 ± 0.4	–	0	2.0 ± 0.2	–	0	2.2 ± 0.2	–	0	2.7 ± 0.2	–
	20	22.1 ± 1.1	94.0	20	19.7 ± 1.9	89.5	20	20.1 ± 1.6	90.5	20	19.7 ± 1.9	86.7
Cd	0	nd	–	0	nd	–	0	nd	–	0	nd	–
	20	19.1 ± 2.1	95.5	20	18.9 ± 1.2	94.9	20	19.9 ± 1.5	99.9	20	18.8 ± 1.1	92.4
V	0	8.0 ± 0.7	–	0	8.7 ± 0.8	–	0	7.4 ± 0.5	–	0	24.1 ± 2.1	–
	20	27.9 ± 2.7	99.6	20	26.9 ± 2.4	93.7	20	24.7 ± 2.1	90.1	20	45.6 ± 2.6	103.4
Mn	0	8.2 ± 0.7	–	0	7.1 ± 0.5	–	0	3.9 ± 0.3	–	0	4.7 ± 0.5	–
	20	25.4 ± 1.8	90.1	20	26.8 ± 1.7	98.8	20	22.7 ± 1.9	94.9	20	22.5 ± 1.6	91.1
Ni	0	2.3 ± 0.3	–	0	5.4 ± 0.4	–	0	1.7 ± 0.2	–	0	3.4 ± 0.2	–
	20	22.1 ± 2.1	99.1	20	24.8 ± 1.1	97.6	20	20.8 ± 1.7	96.3	20	21.1 ± 1.3	90.2
Ce	0	nd	–	0	nd	–	0	nd	–	0	nd	–
	20	19.8 ± 2.1	99.0	20	18.8 ± 1.4	94.0	20	19.5 ± 1.2	97.5	20	20.7 ± 1.3	103.5
La	0	4.4 ± 0.3	–	0	3.2 ± 0.3	–	0	1.9 ± 0.2	–	0	2.5 ± 0.3	–
	20	22.7 ± 1.3	93.0	20	21.6 ± 1.0	93.1	20	18.9 ± 1.7	86.3	20	22.3 ± 1.3	99.1
Eu	0	nd	–	0	nd	–	0	nd	–	0	nd	–
	20	21.3 ± 2.1	106.5	20	19.7 ± 1.2	98.5	20	18.2 ± 1.3	91.0	20	20.2 ± 1.1	101.0
Dy	0	2.7 ± 0.2	–	0	3.2 ± 0.3	–	0	1.4 ± 0.1	–	0	1.2 ± 0.1	–
	20	21.4 ± 1.9	94.3	20	23.5 ± 1.8	101.3	20	21.2 ± 1.5	99.1	20	21.7 ± 1.9	102.4
Yb	0	4.5 ± 0.2	–	0	3.8 ± 0.2	–	0	3.0 ± 0.3	–	0	4.6 ± 0.4	–
	20	27.0 ± 1.6	110.2	20	24.7 ± 1.3	103.8	20	22.6 ± 2.2	98.3	20	25.6 ± 1.9	104.1

nd: not detected.

Acknowledgments

Financial supports from the Science Fund for Creative Research Groups of NSFC (No. 20621502), and NCET-04-0658, MOE of China are gratefully acknowledged.

References

[1] H. Zhang, D. Ma, Q. Xie, X. Chen, Environ. Geol. 38 (1999) 223.
[2] N. Bahramifar, Y. Yamini, Anal. Chim. Acta 540 (2005) 325.
[3] C. Valerie, Spectrochim. Acta Part B 58 (2003) 1177.
[4] N. Yunes, S. Moyano, S. Cerutti, J.A. Gásquez, L.D. Martinez, Talanta 59 (2003) 943.
[5] C.Z. Hang, B. Hu, Z.C. Jiang, N. Zhang, Talanta 71 (2007) 1239.
[6] F. Barbosa, C.D. Palmer, F.J. Krug, P.J. Parsons, J. Anal. At. Spectrom. 19 (2004) 1000.
[7] R.S. Praveen, S. Daniel, T. Prasada Rao, S. Sampath, K. Sreenivasa Rao, Talanta 70 (2006) 437.
[8] M. Kumar, D.P.S. Rathore, A.K. Singh, Microchim. Acta 137 (2001) 127.
[9] R.L. Dutra, H.F. Maltez, E. Carasek, Talanta 69 (2006) 488.
[10] H.M. Jiang, B. Hu, Z.C. Jiang, Y.C. Qin, Talanta 70 (2006) 7.
[11] R.A. Gil, S. Cerutti, J.A. Gásquez, R.A. Olsina, L.D. Martinez, Talanta 68 (2006) 1065.
[12] M.J. Marques, A. Morales-Rubio, A. Salvador, M. Guardia, Talanta 53 (2001) 1229.
[13] L. Ebdon, A.S. Fisher, P.J. Worsfold, J. Anal. At. Spectrom. 9 (1994) 611.
[14] Z.G. Wei, F.S. Hong, M. Yin, H.X. Li, F. Hu, G.W. Zhao, J.W.C. Wong, Anal. Bioanal. Chem. 380 (2000) 677.
[15] P. Liang, Y.C. Qin, B. Hu, T.Y. Peng, Z.C. Jiang, Anal. Chim. Acta 440 (2001) 207.
[16] P. Liang, B. Hu, Z.C. Jiang, Y.C. Qin, T.Y. Peng, J. Anal. At. Spectrom. 16 (2001) 863.
[17] P. Liang, Y.C. Qin, B. Hu, C.X. Li, T.Y. Peng, Z.C. Jiang, Fresenius' J. Anal. Chem. 368 (2000) 638.
[18] J. Yin, Z.C. Jiang, G. Chang, B. Hu, Anal. Chim. Acta 540 (2005) 333.
[19] X.L. Pu, Z.C. Jiang, B. Hu, H.B. Wang, J. Anal. At. Spectrom. 19 (2004) 984.
[20] J.X. Yu, L. Dong, C.Y. Wu, L. Wu, J. Xing, J. Chromatogr. A 978 (2002) 37.
[21] M.G. Pereira, E.R. Pereira-Filho, H. Berndt, M.A.Z. Arruda, Spectrochim. Acta Part B 59 (2000) 515.
[22] B.A. Lesniewska, I. Godlewska, Z.B. Godlewska, Spectrochim. Acta Part B 60 (2005) 377.
[23] P. Liang, Y. Liu, L. Guo, J. Zeng, H.B. Lu, J. Anal. At. Spectrom. 19 (2004) 1489.
[24] P. Liang, Y. Liu, L. Guo, Spectrochim. Acta Part B 60 (2005) 125.
[25] C.T. Kresge, M.E. Leonowicz, W.J. Roth, J.C. Vartuli, J.S. Beck, Nature 359 (1992) 710.
[26] J.S. Back, J.C. Vartuli, W.J. Roth, M.E. Leonowicz, C.T. Kresge, K.D. Schmitt, J. Am. Chem. Soc. 114 (1992) 10835.
[27] R. Garro, M.T. Navarro, J. Primo, J. Catal. 233 (2005) 342.
[28] Y.I. Aristov, M.M. Tokarev, G. Restuccia, React. Kinet. Catal. Lett. 59 (1996) 335.
[29] J.G. Hou, Q. Ma, X.Z. Du, H.L. Deng, J.Z. Gao, Talanta 62 (2004) 241.
[30] X. Feng, G.E. Fryxell, L.Q. Wang, A.Y. Kim, J. Liu, Science 276 (1997) 923.
[31] Y.M. Xu, R.S. Wang, Chem. J. Chin. Univ. 20 (1999) 1002.
[32] S. Oshima, J.M. Perera, K.A. Northcott, H. Kokusen, G.W. Stevens, Y. Komatsu, Sep. Sci. Technol. 41 (2006) 1635.
[33] D. Perez-Quintanilla, I. del Hierro, M. Fajardo, I. Sierra, J. Hazard. Mater. 134 (2006) 245.
[34] D. Perez-Quintanilla, I. del Hierro, I. Sierra, J. Mater. Chem. 16 (2006) 1757.
[35] L. Li, C.M. Liu, A.F. Geng, Mater. Res. Bull. 41 (2006) 319.
[36] M. Kargol, J. Zajac, D.J. Jones, Thermochim. Acta 434 (2005) 15.

[37] E. Palomares, R. Vilar, A. Green, Adv. Funct. Mater. 14 (2004) 111.
[38] D.W. Jing, Y.J. Zhang, L.J. Guo, Chem. Phys. Lett. 415 (2005) 74.
[39] T.N. Murakami, Y. Kijitori, N. Kawashima, J. Photochem. Photobiol. A: Chem. 164 (2004) 187.
[40] M. Gratzel, Inorg. Chem. 44 (2005) 6841.
[41] D. Huang, G.S. Luo, Y.J. Wang, Micropor. Mesopor. Mater. 84 (2005) 27.
[42] L. Moberg, K. Pettersson, I. Gustavssonb, B. Karlberg, J. Anal. At. Spectrom. 14 (1999) 1055.
[43] J. Ragai, S.T. Selim, J. Colloid Interf. Sci. 115 (1987) 139.
[44] E. Vassileva, I. Proinova, K. Hadjiivanov, Analyst 121 (1996) 607.
[45] A. Maquieira, H.A.M. Elmahadi, R. Puchades, Anal. Chem. 66 (1994) 3632.

Available online at www.sciencedirect.com
ScienceDirect
Talanta 73 (2007) 287–295
Talanta
www.elsevier.com/locate/talanta

Size exclusion chromatography with dual-beam refractive index gradient detection of polystyrene samples

Elizabeth M. Humston [a], Adam D. McBrady [a], Maribel Valero [b], Robert E. Synovec [a,*]

[a] *Department of Chemistry, Box 351700, University of Washington, Seattle, WA 98195, USA*
[b] *Los Andes University, IVAIQUIM, Faculty of Sciences, P.O. Box 542, Merida 5101-A, Venezuela*

Received 9 February 2007; received in revised form 20 March 2007; accepted 20 March 2007
Available online 25 March 2007

Abstract

Non-aqueous size exclusion chromatography (SEC) of polystyrenes (as model analytes) is examined using the microscale molar mass sensor (μ-MMS) for detection. The μ-MMS is combined with SEC to demonstrate this simultaneously universal and molar mass selective detection method for polymer characterization. The μ-MMS is based on measuring the refractive index gradient (RIG) at two positions (upstream and downstream) within a T-shaped microfluidic channel. The RIG is produced from a sample stream (eluting analytes in the mobile phase) merging with a mobile phase stream (mobile phase only). The magnitude of the RIG is measured as a probe beam deflection angle and is related to analyte diffusion coefficient, the time allowed for analyte diffusion from the sample stream toward the mobile phase stream, and the bulk phase analyte refractive index difference relative to the mobile phase. Thus, two deflection angles are measured simultaneously, the upstream angle and the downstream angle. An angle ratio is calculated by dividing the downstream angle by the upstream angle. The μ-MMS was found to extend the useful molar mass calibration range of the SEC system (nominally limited by the total exclusion and total permeation regions from ∼100,000 g/mol to ∼800 g/mol), to a range of 3,114,000–162 g/mol. The injected concentration LOD (based on 3 s statistics) was 2 ppm for the upstream detection position. The point-by-point time-dependent ratio, termed a 'ratiogram', is demonstrated for resolved and overlapped peaks. Within detector band broadening produces some anomalies in the ratiogram shapes, but with highly overlapped distributions of peaks this problem is diminished. Ratiogram plots are converted to molar mass as a function of time, demonstrating the utility of SEC/μ-MMS to examine a complex polymer mixture.

Keywords: Non-aqueous; Molar mass; Diffusion coefficient; Polymer characterization; Size exclusion chromatography; Molar mass sensor

1. Introduction

Informative polymer characterization is important to many applications [1]. Polymer behavior depends on both the physical and the chemical properties of the individual polymer chains. The most commonly studied properties relate to molar mass of the polymer. There are several techniques currently used to determine molar mass averages and distributions for polymer samples. One of the most well-known methods for obtaining molar mass information is size exclusion chromatography (SEC). A recent review contains an excellent overview to many SEC detection techniques including light scattering, viscometry, and mass spectrometry [2]. These detection approaches, while providing considerable information for many applications, face a combination of differing molar mass sensitivities, and/or significant sample preparation, and/or long analysis time, and/or incompatibilities with certain polymer/solvent systems.

Refractive index (RI) detection is an attractive technique for polymer characterization because of its universality, and often, acceptable sensitivity. The universality of RI detection allows nearly all polymer samples to be separated by SEC and detected with little or no sample preparation (albeit in a suitable solvent). RI detection is often employed to provide a signal response that is proportional to the polymer concentration, but typically requires one of the other detection methods stated above to provide molar mass data (i.e., molar mass and polymer distribution information). Recently, we developed a dual-beam refractive index gradient (RIG) detector, referred to here as the microscale-molar mass sensor (μ-MMS), that has been shown to be a molar mass-sensitive universal detector that implements microfluidics [3,4]. The μ-MMS applies a microfabricated device that utilizes microfluidics with laminar flow generated concentration

* Corresponding author.
E-mail address: synovec@chem.washington.edu (R.E. Synovec).

0039-9140/$ – see front matter © 2007 Elsevier B.V. All rights reserved.
doi:10.1016/j.talanta.2007.03.040

gradients that are probed in such a way as to provide diffusion coefficient information of the detected sample. In so much as the analyte diffusion coefficient correlates to analyte molar mass, which is often the case with polymer analyses, the data from the μ-MMS can be readily calibrated to provide molar mass information. Thus, the molar mass information provided by the μ-MMS is not absolute and depends upon calibration, whereas molar masses obtained using an on-line light scattering detector are absolute. Even though the μ-MMS requires a new calibration for different polymer types, solvent or system parameters, it can be precisely tuned to span essentially any desired mass range. Here, we report the examination of the μ-MMS in combination with the non-aqueous SEC separation of polystyrene standards.

Refractive index gradient detection for small volume detection of flowing liquids, as is the situation with the μ-MMS, is based on monitoring the deflection of a laser probe beam by a concentration gradient created by a flowing sample plug, which in turn produces a RIG [5–12]. The μ-MMS signal transduction mechanism is dependent upon the formation of a concentration gradient between a sample stream (coming from the SEC column) and a receiving stream containing the SEC mobile phase using a T-shaped flow channel. The microfluidic channel arrangement utilized by the μ-MMS is essentially the same as that pioneered by Yager and co-workers (i.e., with the fluorescence-based T-sensor) [13,14]. The microfabricated flow channel allows two streams, the sample stream and the receiving stream, to merge at the junction of the T, as illustrated in Fig. 1. The difference between the two merging streams is that the sample stream contains the eluting analyte(s) within a host solvent (mobile phase), while the receiving stream contains only host solvent (mobile phase). Upon reaching the junction of the T, the two streams merge sufficiently under laminar conditions and flow parallel to each other down the central channel of the T. After merging, the analytes begin to diffuse from the sample stream into the receiving stream, producing a concentration gradient across the central channel of the T. The concentration gradient is perpendicular to the flow and creates a RIG. As the analytes travel through the central channel their diffusion gradually reduces the 'sharpness' of the initial RIG across the channel. Thus, the change in the RIG for a given polymer is dependent upon its diffusion coefficient, and thus, dependent on its molar mass.

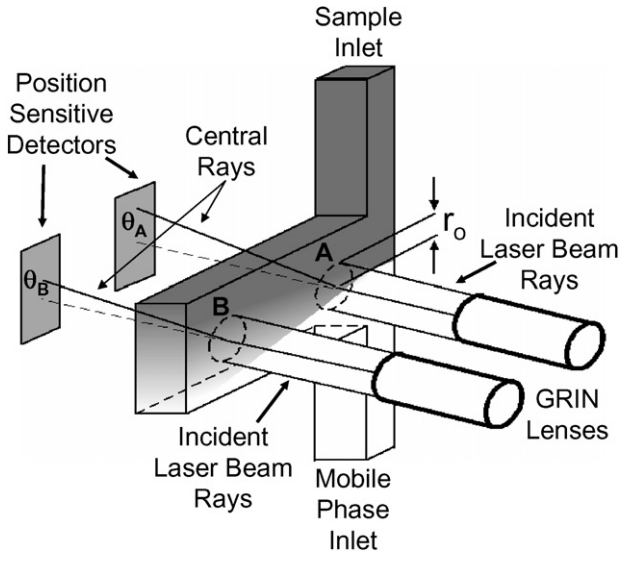

Fig. 1. Schematic representation of the μ-MMS detector is shown. Two diode laser beams with radius, r_0, which are transmitted by fiber optic cables and collimated by GRIN lenses probe the main channel of the T-junction. The sample stream (dark for illustration) merges with the mobile-phase stream (light for illustration) and flow down the main channel. The merging of these two streams produces a concentration gradient (i.e., refractive index gradient) that deflects the probe beams. Each deflection is detected by a PSD. The angles of deflection, θ_A and θ_B, can be related as a ratio to give polymer diffusion coefficient information that is readily correlated to polymer molar mass.

The μ-MMS uses two collimated small-diameter probe beams to optically interrogate the RIG at two positions along the central channel of the T. The two positions are termed the upstream and the downstream position. The upstream position is located a short distance after the merge point, before appreciable diffusion occurs. The downstream position is a user-selected distance farther away from the merge point. Interaction of a given probe beam with the analyte RIG results in the beam being deflected toward the fluidic region of higher RI. The deflection angles at each probe position (upstream and downstream) are recorded on position-sensitive detectors (PSDs), and subsequently reported in microradians (μrad). The ratio of the two probe beam deflection angles, the downstream divided by the upstream, is a measure of the change in the 'sharpness' of the RIG, and thus contains diffusion coefficient information. Analytes that diffuse more rapidly, quickly reduce the sharpness of their RIG, while analytes that do not, remain with a relatively sharp RIG. Therefore, for a homologous series of analytes (e.g., a particular class of polymers), the larger molar mass analytes have more intense downstream signals, and thus higher angle ratios. Smaller molar mass analytes, with large diffusion coefficients, yield small ratio values.

This report focuses on the examination and application of the μ-MMS for non-aqueous SEC. Initial studies are aimed at illustrating the ability of the μ-MMS to extend the traditional calibration range of SEC columns (i.e., log molar mass versus retention time). The angle ratio values provided by the μ-MMS extend the useful molar mass calibration range of the SEC column to include both the total permeation and total exclusion volumes. We further evaluate the detector by examining the angle ratios calculated using maximum peak height. The concept of peak height angle ratios is extended to span the entire width of the chromatogram creating a 'ratiogram', in which the angle ratio is plotted as a function of the elution time axis. The observation and consequences of band broadening that occurs between the upstream and downstream detection positions are discussed in relation to the ratiogram of resolved and overlapped peaks.

2. Experimental

The μ-MMS chip was fabricated using isotropic etching with HF in a procedure that has previously been described in detail [3], with the T channel of the chip illustrated in Fig. 1. The

sample and receiving stream inlets of the T were fabricated to have dimensions 1 cm long × 100 μm wide × 200 μm deep and the main flow channel to have dimensions 5 cm long × 500 μm wide × 200 μm deep. The 200 μm depth of the T channel corresponds to the path length for the collimated probe beams.

The sample and receiving stream were driven by two syringe pumps (Isco, μLC 500, Lincoln, NE, USA). The sample stream passed through an eight-port auto injection valve (Rheodyne, Lab PRO, Rohnert Park, CA, USA) that allowed for the injection of sample, fitted with a 5 μl sample loop. After the injector, the sample stream passed through a 30 cm × 1 mm ID Supelcosil column packed with 5 μm silica particles with 12 nm pores (Supelcosil LC-SI 5 μm, Bellafonte, PA, USA). This column served adequately for SEC separations as is reported herein. PEEK tubing (Upchurch Scientific, Oak Harbor, WA, USA) was used to connect the syringe pumps to and from the injector, column, and μ-MMS. The tubing was interfaced to the μ-MMS via Nanoport Assemblies (N-126S, Upchurch Scientific, Oak Harbor, WA, USA).

Two collimated probe beams were set up to pass through the main flow channel of the T, one at the upstream position prior to significant diffusion and one at the downstream position after diffusion had occurred, as illustrated in Fig. 1 [3]. The upstream beam position was 0.25 cm downstream from the merge point. The downstream position was selected such as to provide an 18 s time difference at the volumetric flow rate used in the SEC separations (7.5 μl/min). The two collimated probe beams originated from a 635 nm single mode diode laser (Thor Labs, S1FC635, Newton, NJ, USA) that is attached to a 1 × 2 single mode fiber optic coupler. The coupler has an FC connector at the input and bare fibers as the outputs (Newport, F-CPL-1x2-OPT-50-10-NN, Irvine, CA, USA). Each bare fiber is connected to a GRIN lens (Newport, LGI630-2, Irvine, CA, USA) before the resulting beam passes through the channel orthogonal to the direction of flow. The beam deflections were recorded by two PSDs (Hamamatsu USA, Bridgewater, NJ, USA). The signals from both the upstream and downstream PSDs were recorded with a National Instruments DAQ board (SCD-68, Austin, TX, USA) connected to a PC. A LabVIEW (National Instruments, SCD-68, Austin, TX, USA) program, written in-house, controlled injection and data acquisition. The microfabricated chip, and PSDs were all mounted on three-dimensional translational stages (Melles Griot, MicroLab Translational Stages, Irvine, CA, USA) that allowed for precise alignment.

Polystyrene (PS) standards (Polymer Laboratories, Amherst, MA, USA) with low polydispersity were dissolved in methylene chloride (EMD Chemicals, Gibbstown, NJ, USA) at ~400 ppm. Methylene chloride was used as the mobile phase for all SEC separations. Single polystyrene samples were used for probe beam optimization and angle ratio calibration. Polystyrene mixtures were made for further analysis. The beam optimization was performed by incrementally adjusting each probe beam position across the detection channel of the T as shown in Fig. 1 in order to achieve maximum overlap between the RIG and the beam radius, and therefore optimal detection sensitivity [15]. The collimated probe beams emanated from the GRIN lenses that were mounted on high precision *x–y–z* translational stages (Newport, 460-x-y-z, Fountain Valley, CA, USA) allowing for precise adjustment. Each PSD provides a real-time measure of the deflection distance of each probe beam (via calibration as previously reported) [4]. Since the distance from the PSDs to the microfluidic channel is known (0.95 m), the deflection angles at the upstream (θ_A) and downstream (θ_B) are readily measured and calculated, as illustrated in Fig. 1.

A MATLAB (Mathworks, Natick, MA, USA) program was written in-house to model the experimental data (chromatographic peaks obtained by the SEC separation). This simulation program output exponentially modified Gaussian (EMG) peak shapes using retention time, peak height, peak width at 10% of the height, and the asymmetry factor as variables. Both real SEC/μ-MMS data and simulated SEC/μ-MMS data were analyzed with ORIGIN 5.0 (Microcal Software, Northampton, MA, USA) and MATLAB software (Mathworks, Natick, MA, USA).

3. Results and discussion

Earlier studies by our group have focused on using the μ-MMS as an independent microfluidic sensor, and constructing a rigorous theoretical model to predict the ratio (downstream signal/upstream signal) using experimental parameters [3]. The angle ratio, R, is defined as the downstream deflection angle, θ_B, divided by the upstream deflection angle, θ_A, as seen in Fig. 1. The theoretical model culminated in the following equation, which described the angle ratio, R, in terms of the interrogating beam radius, r_0, the time between stream merger and upstream detection, t_A, the time between stream merger and downstream detection, t_B, and the diffusion coefficient of the analyte, D.

$$\text{angle ratio } (R) = \left(\frac{r_0^2 + 8Dt_A}{r_0^2 + 8Dt_B}\right)^{1/2} = \frac{\theta_B}{\theta_A} \quad (1)$$

Note that $t_B > t_A$ and as a result the ratio becomes smaller as D becomes larger. A more thorough discussion of the theoretical model has been reported previously [3].

Before discussing the angle ratio versus molar mass calibration, it is useful to provide an example of the typical data obtained via the μ-MMS. Fig. 2A shows the upstream and downstream angle data for SEC chromatograms of PS standards detected with the μ-MMS. The signal from just the upstream or downstream signal alone is very similar to traditional RI detectors. The chromatograms were collected at a flow rate of 7.5 μl/min. The three peaks in Fig. 2A are 170,800 g/mol, 10,680 g/mol, and 1060 g/mol polystyrene standards at 522 ppm, 615 ppm, and 726 ppm, respectively. Each sample injection yields two chromatograms, one upstream and one downstream. In the figure, the downstream chromatograms have been shifted up in time 18 s (the time delay between the two detection positions). Essentially, two chromatograms are obtained simultaneously with a 18 s delay. The high resolution in this chromatogram allows for the analytes' angle ratio per Eq. (1) to be calculated from either peak area or peak height. For the data in Fig. 2A, averages of the area-based and height-based angle ratios for each analyte are, within experimental error, equivalent to each other. Because many of the remaining mixtures analyzed in the current report

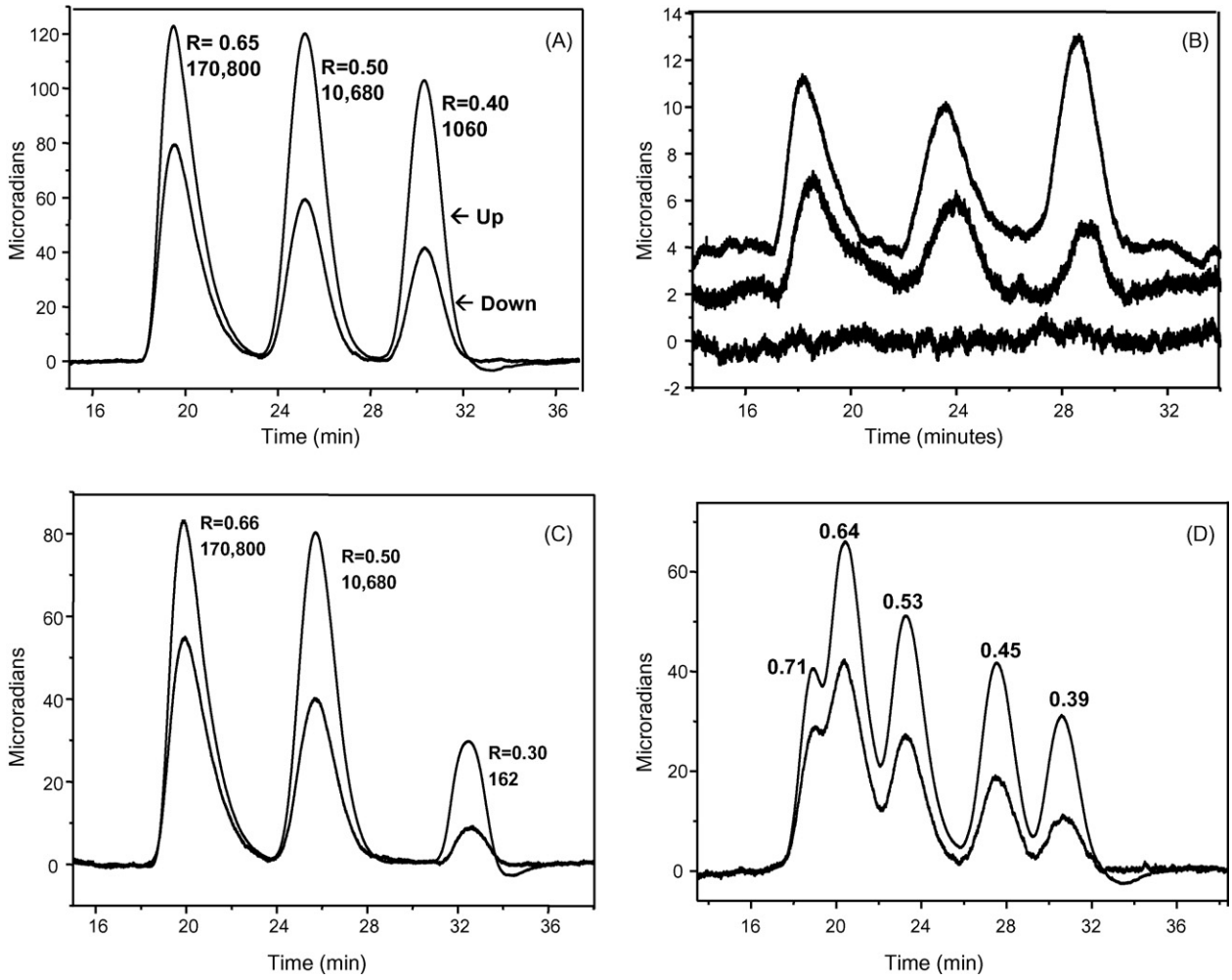

Fig. 2. SEC/μ-MMS chromatograms run at 7.5 μl/min. (A) The detected upstream (Up) and downstream (Down) signals. The three PS standard peaks with molar masses are labeled 170,800 g/mol, 10,680 g/mol, and 1060 g/mol, with injected concentrations of 522 ppm, 615 ppm, 726 ppm, respectively. The downstream signal has been shifted 18 s up in time for alignment. The height-based angle ratios, *R*, are included beside each peak. (B) The same peaks as shown in (A) with lower concentrations for the LOD study. The chromatograms are offset by 2 μrad and 4 μrad, respectively, for clarity. The three peaks are 170,800 g/mol, 10,680 g/mol, and 1060 g/mol PS standards, with injected concentrations 28 ppm, 33 ppm, 64 ppm, respectively. (C) Upstream and downstream signals for SEC separation of 170,800 g/mol, 10,680 g/mol, and 162 g/mol PS standards, with *R* values. (D) SEC/μ-MMS chromatograms of five PS standards: 1,373,000 g/mol, 63,350 g/mol, 19,880 g/mol, 5030 g/mol and 1060 g/mol.

do not have baseline resolution, the height-based ratios are more generally applicable. The ratio values from peak height are listed adjacent to the peaks in Fig. 2A.

We now investigate the limit of detection (LOD) for this SEC/μ-MMS system. Fig. 2B shows the upstream and downstream angle data collected for one 5 μl injection of a sample containing 170,800 g/mol, 10,680 g/mol, and 1060 g/mol polystyrene standards at 28 ppm, 33 ppm, and 64 ppm, respectively. For clarity, the upstream chromatogram is shown offset 4 μrad and the downstream chromatogram is offset 2 μrad from a sample blank chromatogram. The average injected concentration LOD (3 s of the baseline noise) was 2 ppm for the three PS standards shown in Fig. 2B in the upstream chromatogram. Since the baseline noise is generally equivalent for the two detection positions, the downstream LOD is equal to the upstream LOD for a particular analyte scaled by the angle ratio value of that analyte. Thus, the downstream LOD is larger than the upstream LOD.

Fig. 2C and D shows additional examples of the upstream and downstream data for SEC chromatograms of PS standards detected with the μ-MMS. The chromatogram in Fig. 2C used a similar mixture to Fig. 2A and B, but with a different third PS standard, a mixture of 170,800 g/mol, 10,680 g/mol, and 162 g/mol PS standards at respective concentrations of 348 ppm, 414 ppm, and 665 ppm. The height-based angle ratios are listed adjacent to each peak. Fig. 2D contained five PS standards: 1060 g/mol, 5030 g/mol, 19,880 g/mol, 63,350 g/mol, and 1,373,000 g/mol at respective concentrations of 224 ppm, 244 ppm, 218 ppm, 220 ppm, and 175 ppm. The benefit of calculating height-based ratios rather than area-based ratios becomes apparent with this sample. The chromatographic resolution is insufficient to determine the peak areas, however, the peak maxima are more accurately quantified. Inspection of Eq. (1) indicates the angle ratios allow for a qualitative analysis of the relative diffusion coefficient (and therefore an analysis of molar mass) of the PS standards.

At first, the information the angle ratios provide may appear to be redundant with the information given by traditional calibration of the PS standards' SEC elution volume behavior (i.e., at constant flow rate, log molar mass versus retention time plots). However, upon closer inspection of the last PS standards eluting in Fig. 2A and C we notice that the ratio value provides analyte distinguishing selectivity, even though the two standards (1060 g/mol and 162 g/mol) both elute very near each other (in the total permeation limit for the SEC separation). The useful calibration range of an SEC separation is limited by the pore size of the particles within the column. Analytes that are totally excluded or totally permeating cannot be distinguished from one another with SEC alone. The PS 162 and 1060 g/mol standards would be difficult to distinguish due to their similar retention times. However, the difference in the two standards' diffusion coefficients allows the μ-MMS to easily distinguish the two since the angle ratio values are 0.30 versus 0.40.

In order to more clearly demonstrate the utility of the μ-MMS to provide complementary information relative to the traditional SEC retention time calibration, a dual calibration was performed. The calibration was performed using 13 narrowly distributed PS standards that covered the mass range of 162–3,114,000 g/mol. The first calibration is the traditional approach for SEC, with log molar mass plotted versus retention volume, in which the retention time for the upstream angle data was converted to retention volume using the mobile phase flow rate of 7.5 μl/min, and is shown in Fig. 3A. The column used for the SEC separations has a 5 μm particle diameter with nominally a 12 nm average pore diameter. The regions of total exclusion and total permeation create a calibration that does not effectively distinguish PS molar mass greater than ∼100,000 g/mol or less than ∼800 g/mol, which can be seen by the significant change in slope beyond these points. It does not appear that the analytes in the total exclusion region are all eluting at the same retention volume. Although the polymers are likely larger than the biggest pores of the stationary phase, there may be a hydrodynamic chromatography mechanism in the interstitial medium influencing the separation [16]. It is also possible that the analytes in the lower mass region have not quite reached the region of total permeation as their elution volumes are not identical.

If the same upstream angle data is evaluated with the downstream angle data, a log molar mass versus angle ratio calibration is produced, by calculating the angle ratio using Eq. (1). The μ-MMS based calibration is presented in Fig. 3B using the height-based angle ratio for each individually injected PS standard. Note that PS standards eluting within the totally excluded and totally permeating range are more easily distinguished by their angle ratios in Fig. 3B, then they are in the retention time based calibration in A. We acknowledge that other SEC columns may have molar mass calibration ranges greater than that of the column used in this report. However, the μ-MMS could be tuned to extend the range of any of these columns into either the total exclusion or permeation range, and sometimes both [3]. While it may seem this procedure merely replaces one relative calibration method with another, there is the added benefit of exceptional mass resolution with the μ-MMS compared to SEC methods. The μ-MMS parameters can be readily tuned to

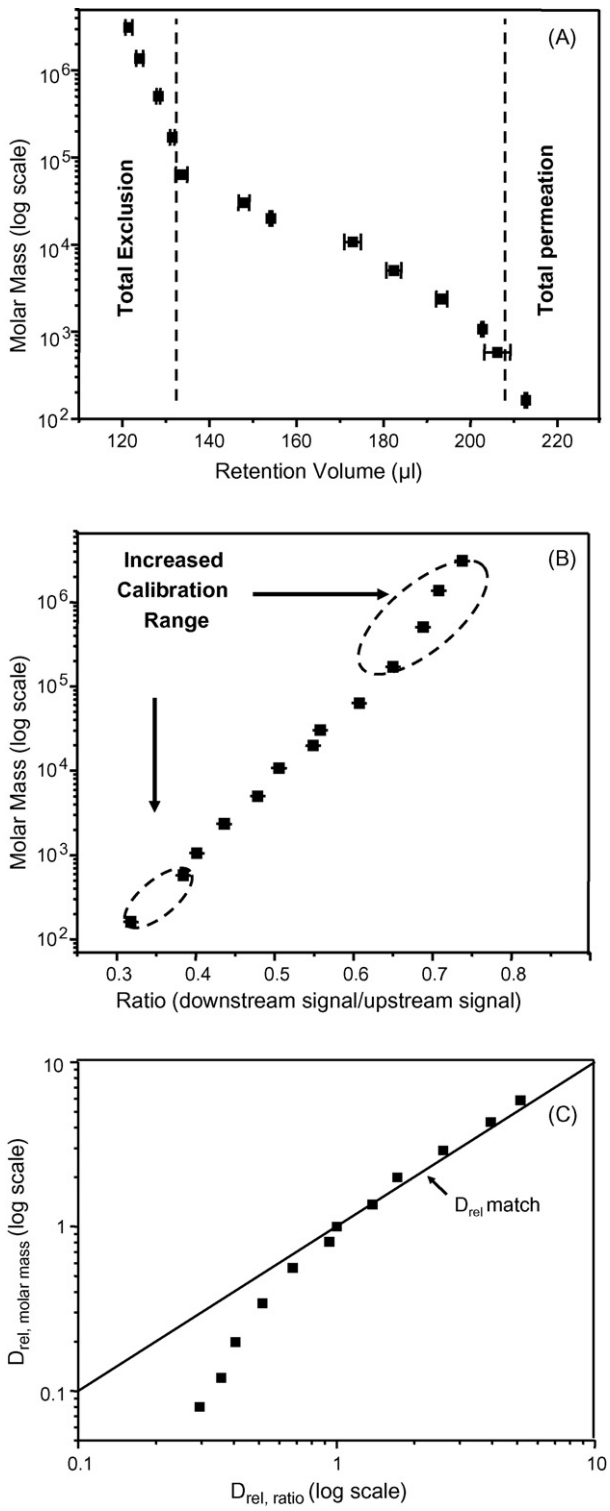

Fig. 3. The calibrations at a flow rate of 7.5 μl/min using 13 PS standards spanning 162–3,114,000 g/mol. Data were collected in triplicate. The error bars represent plus and minus one standard deviation. (A) Traditional SEC calibration of log molar mass vs. retention volume; (B) height-based angle ratio calibration (log molar mass vs. angle ratio) with increased information at the high and low molar mass ranges; (C) comparison of relative diffusion coefficients as determined using $D_{rel,\ ratio}$ (Eq. (2)) using $t_A = 2$ s, $t_B = 20$ s, the angle ratios obtained in the calibration, and PS 19,880 g/mol as the reference polymer, and $D_{rel,\ molar\ mass}$ (Eq. (4)) using $b = 0.5$, and PS 19,880 g/mol as the reference polymer.

distinguish differences between analytes of the same mass with different diffusion coefficients, as we have previously reported [4].

The angle ratio can, in principle, be combined with knowledge of r_0, t_A, and t_B, to calculate the analyte diffusion coefficient using Eq. (1) in a rearranged form, as has been demonstrated in a previous report from our group [3]. By rearranging Eq. (1), we now examine the diffusion coefficients obtained from the measured angle ratios. In practice this is not an easy task as accurately measuring the beam radius r_0 is not trivial [3]. However, relative diffusion coefficients, $D_{\text{rel, ratio}}$, is easily determined as all other parameters are readily obtained. The following equation provides $D_{\text{rel, ratio}}$ for one polymer (i) relative to a reference polymer (ref):

$$D_{\text{rel, ratio}} = \frac{D_i}{D_{\text{ref}}} = \left(\frac{1 - R_i^2}{t_B R_i^2 - t_A}\right)\left(\frac{t_B R_{\text{ref}}^2 - t_A}{1 - R_{\text{ref}}^2}\right) \quad (2)$$

Likewise, diffusion coefficients can be calculated from a general equation relating diffusion coefficient to molar mass:

$$D = a(M)^{-b} \quad (3)$$

The parameters a and b depend on both the polymer and the solvent. Using Eq. (3), a $D_{\text{rel, molar mass}}$ analogous to Eq. (2) can be calculated:

$$D_{\text{rel, molar mass}} = \frac{D_i}{D_{\text{ref}}} = \left(\frac{M_i}{M_{\text{ref}}}\right)^{-b} \quad (4)$$

Note that the parameter a cancels in the $D_{\text{rel, molar mass}}$ equation. Inspection of the polymer handbook indicates the b value varies only slightly for linear polystyrenes in various "good" solvents, averaging about 0.5 [17]. Thus, D_{rel} values from Eqs. (2) and (4) were determined using PS 19,880 g/mol as the reference polymer, resulting in D_{rel} of 1.0. From these calculations, $D_{\text{rel, ratio}}$ and $D_{\text{rel, molar mass}}$ are compared in Fig. 3C. The monomer unit, at 162 g/mol, was not included in the plot because it does not follow typical polymer behavior per Eq. (3). In Fig. 3C, good agreement is obtained for the two methods to determine D_{rel}, however with a deviation observed at the higher masses. The deviation is a result of the angle ratios beginning to reach a constant value as can be seen with close inspection of Fig. 3B, indicating the upper mass limit for the μ-MMS at these parameters is being approached. However, the results in Fig. 3C are encouraging that it is indeed possible to determine the translational diffusion coefficient with the μ-MMS as previously noted as well [3], and thus, one could also relate the diffusion coefficient to the hydrodynamic radius.

The ability to obtain even more information from the SEC/μ-MMS data is enabled by considering the idea of taking the point-by-point angle ratio as a function of elution time, which we refer to as a 'ratiogram'. The ratiogram is the angle ratio of the downstream signal to the upstream signal at every point along the retention time axis, after the downstream retention time is corrected for the 18 s time delay. Hypothetically, the ratiogram should be flat for a truly mono-disperse polymer peak, and have a negative slope for a polydisperse analyte peak. An example of a ratiogram is shown in Fig. 4A. The upstream and downstream

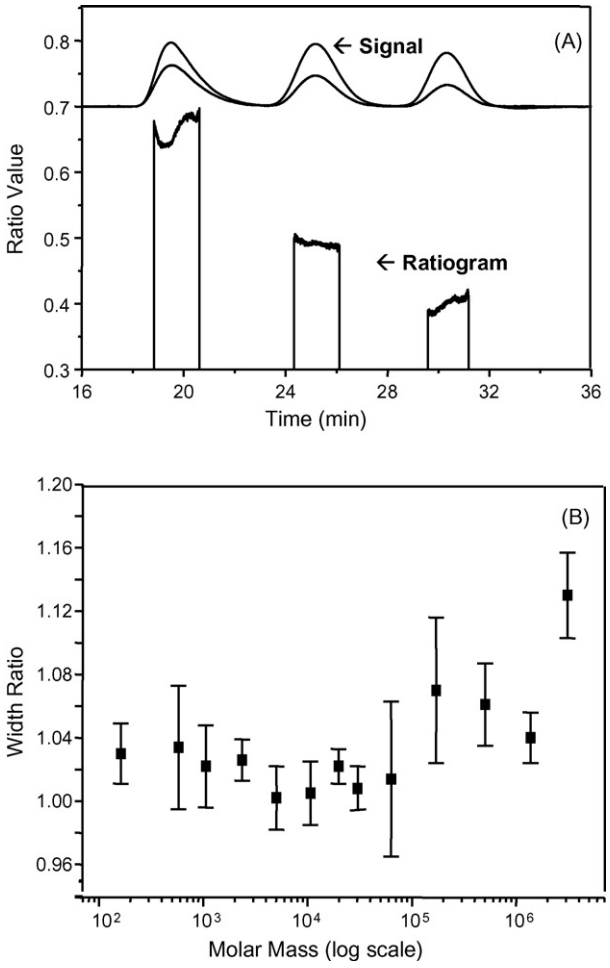

Fig. 4. (A) The time-dependent ratiogram is plotted using the data shown in Fig. 2A, with original SEC/μ-MMS chromatograms shown for clarity. The ratio is calculated when the downstream signal is greater than 50% of the maximum downstream peak height, and is otherwise set to zero. (B) Width ratio data plot (W_R) against molar mass. Width ratios were calculated as the width of the downstream peak at 10% of the peak height divided by width of the upstream peak at 10% of the peak height.

angle data used to obtain the ratiogram is the same as presented in Fig. 2A. As expected, the ratiogram values around the maximum peak height represent well the calibration between molar mass and angle ratio (as presented in Fig. 3B). However, for the complete ratiogram for some of the SEC peaks, some abnormalities are seen, especially away from the peak maxima. On the first peak in Fig. 4A (170,800 g/mol PS), the time-dependent ratiogram has a noticeable dip. Ideally, for the first peak, the ratiogram would be flat with a value of ~0.67. Similar dips were seen with most large analytes (e.g., 170,800 g/mol PS and larger). This was not attributed to the inherent polydispersity of the samples, as polydispersity index values for the PS standards were essentially equal to one. Instead, the divergence from an ideal flat ratio is primarily attributed to within-detector band broadening between the upstream and downstream detection positions. To quantify the band broadening within the detector a width ratio (W_R) was measured, being defined as the downstream peak width at 10% of the peak height divided by the upstream peak width at 10% of the peak height. The W_R plot

against the molar mass is shown in Fig. 4B. If no within-detector band broadening occurred, the W_R would be equal to one. It was found through simulations that chromatographic peaks with a W_R greater that 1.02 began to produce a noticeable abnormality in the ratiogram shape (i.e., the ratiogram would begin to diverge from a constant value). It should be noted that for the peaks shown in Fig. 4A, the peak with the flattest ratiogram has the lowest W_R, and the ratiogram with the largest abnormality corresponds to the PS standard with the highest W_R. The within-detector band broadening likely arises from a complicated interplay between the fluid dynamics in the flow channel and PS standard diffusion. It is possible that both radial (orthogonal to flow) and axial (along the flow) diffusion play important roles. Additional study would be needed to provide more insight into this matter, however, the data in Fig. 4B clearly points to a molar mass dependence (and thus PS diffusion coefficient dependence) on the band broadening occurring in the detector. Algorithms to correct for this within-detector band broadening were considered. After much consideration it was concluded that useful information could still be attained from ratiograms even with accepting the limitation of within-detector band broadening for the higher molar mass PS analytes. Such an example is demonstrated next for a mixture of six unresolved PS standards. Both simulated and actual SEC/μ-MMS data for the real mixture are compared.

In Fig. 5A and B are shown the simulation of SEC/μ-MMS data for the upstream and downstream peaks of six unresolved PS standards. In order to accurately model the peak shapes and relative peak heights, data from the two calibrations (Fig. 3A and B) were compiled for each PS standard in the mixture. The experimentally observed retention time, peak intensity, asymmetry factor, and W_R were input into an in-house written MATLAB program to produce an EMG peak shape for each PS component in the mixture. The asymmetry ratio is defined for EMG peaks as the distance from the peak maximum to the backside of the peak divided by the distance from the peak maximum to the front side of the peak at 10% of the peak height [18–20]. The components of the mixture were 19,880 g/mol, 30,230 g/mol, 63,350 g/mol, 504,500 g/mol, 1,373,000 g/mol, and 3,114,000 g/mol PS standards. Each component was simulated individually and the sum of each individual peak created a concentration trace of the mixture. The downstream peaks are shown in Fig. 5B and were

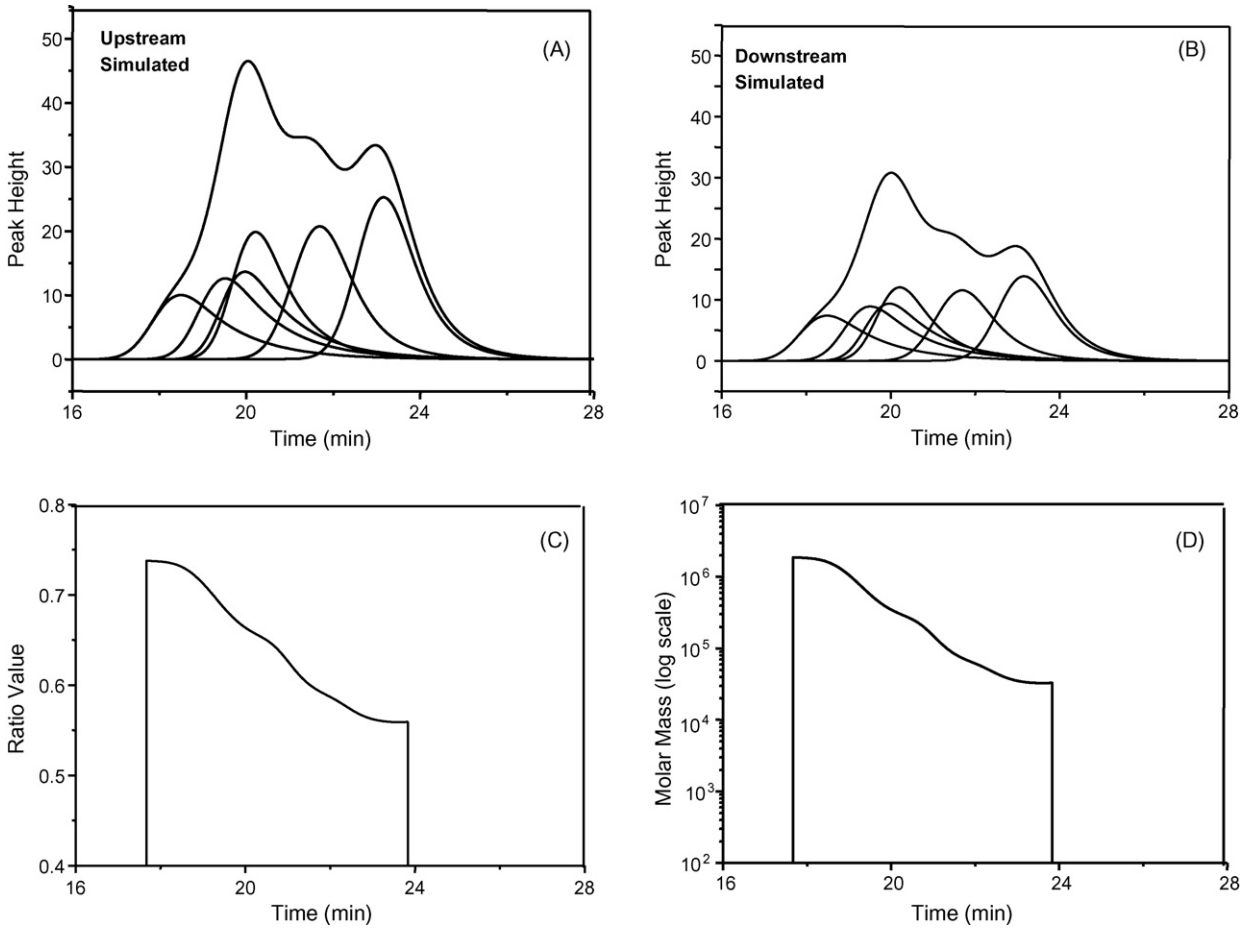

Fig. 5. A simulated mixture of six unresolved polystyrenes (19,880 g/mol, 30,230 g/mol, 63,350 g/mol, 504,500 g/mol, 1,373,000 g/mol, and 3,114,000 g/mol). (A) The upstream peak relative signal was obtained by simulating each component of the mixture individually taking into account the peak width, peak height, asymmetry factor and retention time. These were all based on experimental observations of the data collected for the calibration in Fig. 3. (B) The downstream simulated data used the same method as the upstream. The width ratio was set to 1.00. Each individual downstream peak was multiplied by its ratio value as found in the calibration data prior to the summation of all six peaks to give the mixture. (C) The simulated ratiogram arising for simulated mixtures in (A) and (B) is shown. (D) The simulated molar mass gram. The values of the ratiogram were converted to molar mass using Eq. (5), derived from the calibration in Fig. 3B.

created the same way as the upstream peaks in Fig. 5A, but additionally were scaled by the observed ratio value. The simulated data presented have had each PS standard W_R set to 1.0 for simplicity, and the corresponding ratiogram is shown in Fig. 5C. To convert the ratiogram data into a format that would be more useful, an equation was fit to the calibration data relating molar mass to the observed angle ratio (Fig. 3B data). That experimentally observed function is the following:

$$\text{molar mass} = 0.104 \times 10^{9.83R} \quad (5)$$

Eq. (5) was used to convert every ratiogram point along the time axis in Fig. 5C into a "molar mass gram" as shown in Fig. 5D.

The actual SEC/μ-MMS data for the six-component PS standard mixture is very similar when compared to the simulated data presented previously. The same six PS standard components were combined with the same proportions as in the simulation. The upstream and downstream chromatograms for the mixture are overlaid in Fig. 6A. From the data in Fig. 6A, the ratiogram was obtained and presented in Fig. 6B. Our evaluation of the ratiogram in Fig. 6B concluded that it was relatively void of the anomalies due to W_R increases from a value of 1.0. Indeed, the simulated ratiogram that best approximated this real data and real ratiogram was obtained for PS standard component peaks with W_R all of 1.0. This simulated ratiogram, with all W_R equal to 1.0, best fits the real data because of the highly overlapped nature of the separation. The edges of ratiograms are the area of highest error, yet they represent a small fraction of analyte molecules. The upstream and downstream signals in Fig. 6A are due in large part to the center of the overlapped PS component at a given retention time. Only the edges of the ratiogram in Fig. 6B (near 18 min and 23 min) showed a moderate difference from the simulated ratiogram (Fig. 5C). There is a deviation of less than 3% between the simulated and the real ratiograms. Additionally, Fig. 6C shows the molar mass gram when the ratio to molar mass conversion function in Eq. (5) was applied. This figure illustrates that SEC/μ-MMS is capable of producing informative ratiograms, and therefore molar mass traces, of significantly overlapped or broadly distributed SEC samples with equal to or less than 3% error. This analytical methodology could be used to study polymer distributions of high polydispersity, and is especially useful for low molar mass polymers. Thus, SEC/μ-MMS should be complementary to SEC/light scattering.

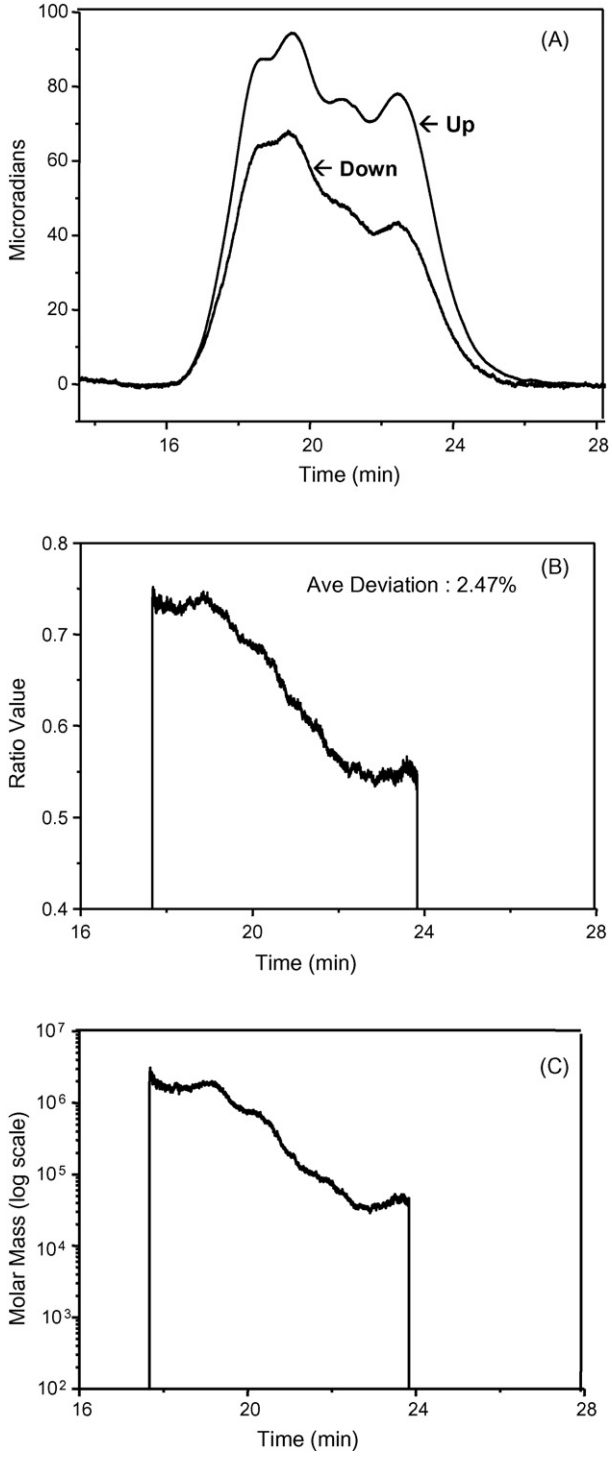

Fig. 6. The real data is studied for the blend of six unresolved polystyrenes that were simulated in Fig. 5A and B. (A) The aligned upstream and downstream data are shown. (B) The ratiogram is shown which has a calculated average percent deviation from the simulated data in Fig. 5C of 2.5%. (C) The actual molar mass gram. The values of the ratiogram were converted to molar mass using the same relationship as in Fig. 5D.

4. Conclusions

The combination of SEC with μ-MMS detection has been demonstrated. The μ-MMS is a sensitive molar mass-sensitive detector based on RI detection. The injected concentration LOD achieved was 2 ppm on average at the upstream detection position. Angle ratio values can be calculated for fully or partially resolved standards to create a molar mass calibration that includes the total exclusion and/or total permeation ranges. The angle ratio is calculated by dividing the peak height at the downstream position by the peak height at the upstream position. Furthermore, time-dependent ratiograms can be calculated to give molar mass information across the width of SEC-eluting polydisperse peaks. Within-detector band broadening was observed and can influence the accuracy of the ratiograms. However, this band broadening effect is found to be advantageously diminished in highly overlapped chromatograms. It

would be of interest in future studies to examine branched polymers with the μ-MMS system and compare the required calibration to that obtained in this study, which was limited to linear polymers.

Acknowledgements

M. Valero thanks the Los Andes University for supporting her research as a visiting scientist at the University of Washington. The authors thank Ashland Chemical for support of the research.

References

[1] A.M. Striegel, Multiple Detection in Size-Exclusion Chromatography, American Chemical Society, Washington, DC, 2005.
[2] A.M. Striegel, Anal. Chem. 77 (2005) 104A.
[3] C.D. Costin, A.D. McBrady, M.E. McDonnell, R.E. Synovec, Anal. Chem. 76 (2004) 2725.
[4] C.D. Costin, R.K. Olund, B.A. Staggemeier, A.K. Torgerson, R.E. Synovec, J. Chromatogr. A 1013 (2003) 77.
[5] J. Pawliszyn, Anal. Chem. 58 (1986) 243.
[6] J. Pawliszyn, Anal. Chem. 58 (1986) 3207.
[7] J. Pawliszyn, Anal. Chem. 60 (1988) 766.
[8] D.O. Hancock, C.N. Renn, R.E. Synovec, Anal. Chem. 62 (1990) 2441.
[9] C.N. Renn, R.E. Synovec, J. Chromatogr. A 536 (1991) 289.
[10] L.R. Lima, R.E. Synovec, Anal. Chem. 65 (1993) 128.
[11] V. Murugaiah, R.E. Synovec, Anal. Chim. Acta 246 (1991) 241.
[12] V. Murugaiah, R.E. Synovec, Anal. Chem. 64 (1992) 2130.
[13] A.E. Kamholz, B.H. Weigl, B.A. Finlayson, P. Yager, Anal. Chem. 71 (1999) 5340.
[14] A. Hatch, A.E. Kamholz, K.R. Hawkins, M.S. Munson, E.A. Schilling, B.H. Weigl, P. Yager, Nat. Biotechnol. 19 (2001) 461.
[15] C.D. Costin, R.E. Synovec, Talanta 58 (2002) 551.
[16] G. Stegeman, J.C. Kraak, H. Poppe, J. Chromatogr. 550 (1991) 721.
[17] J. Brandrup, Immergut, H. Edmund, Grulke, A. Eric, Abe, Akihiro, Bloch, R. Daniel, Polymer Handbook, 4th ed., John Wiley & Sons, 2005, pp. 109–133.
[18] J.P. Foley, J.G. Dorsey, Anal. Chem. 55 (1983) 730.
[19] D. Hanggi, P.W. Carr, Anal. Chem. 57 (1985) 2394.
[20] M.S. Jeansonne, J.P. Foley, J. Chromatogr. 594 (1992) 1.

Available online at www.sciencedirect.com
ScienceDirect
Talanta 73 (2007) 366–371
Talanta
www.elsevier.com/locate/talanta

Fluoroimmunoassay for tumor necrosis factor-α in human serum using $Ru(bpy)_3Cl_2$-doped fluorescent silica nanoparticles as labels

Xu Hun [a,b], Zhujun Zhang [a,*]

[a] Department of Chemistry, School of Chemistry and Materials Science, Shaanxi Normal University, Xi'an 710062, China
[b] School of Materials & Chemical Engineering, Xi'an Technological University, Xi'an 710032, China

Received 5 November 2006; received in revised form 27 March 2007; accepted 29 March 2007
Available online 8 April 2007

Abstract

A novel fluoroimmunoassay (FIA) method was developed for the determination of tumor necrosis factor-α (TNF-α) in this study. The proposed method has the advantage of showing the specificity of immunoassays and sensitivity of fluorescent nanoparticles label technology. With the well-established inverse microemulsion polymerisation process, the tris(2′,2-bipyridyl)dichlororuthenium(II) hexahydrate (Rubpy)-doped fluorescent silica nanoparticles (RuDFSNs) were prepared. Then a RuDFSNs-labeled anti-TNF-α monoclonal antibody was prepared and used for FIA of TNF-α in human serum samples with a sandwich FIA by using the low fluorescent 96-well transparent microtiter plates. The assay response was linear from 1.0 to about 250.0 pg/mL with a detection limit of 0.1 pg/mL for TNF-α. The intra- and inter-assay precision are 4.9%, 4.4%, 4.6%; 6.1%, 5.9%, 5.3% for five parallel measurements of 2.0, 20.0, 200.0 pg/mL TNF-α respectively, and the recoveries are in the range of 96–104% for human serum sample measurements by standard-addition method. We also explored the application of fluorescence microscopy imaging in the study of the FIA for TNF-α with the fluorescent nanoparticle labels. The results demonstrate that the method offers potential advantages of sensitivity, simplicity and good reproducibility for the determination of TNF-α, and is applicable to the determination of TNF-α in serum samples and being capable of fluorescence microscopy imaging for the determination of TNF-α.

Keywords: Tumor necrosis factor-α; Fluorescent nanoparticle; Rubpy; Fluoroimmunoassay; Fluorescence microscopy imaging

1. Introduction

Tumor necrosis factor-α (abbreviated as TNF-α), also known as cachectin, is one of the most important regulatory cytokines and mediates a variety of cell functions, including the stimulation of nitric oxide (NO) production which has been related to oxidative stress and diseases such as arthritis, diabetes, stroke, and chronic inflammation [1–3]. Under normal conditions, human serum concentrations of TNF-α are very low. Elevated TNF-α concentrations in human serum have been associated with a broad series of pathological states, such as neonatal listeriosis, severe meningococcemia, HIV infection, systemic erythema nodosum leprosum, endotoxic shock, graft rejection and rheumatoid arthritis [4]. Therefore, from these and other studies it appeared that determination of TNF-α concentration in human serum might be helpful in the staging and prognosis of diseases. And also it is very important for the understanding of tumor biological processes, inherent mechanisms, and discovering drugs as well as having a therapeutic potential for the treatment of diseases [5].

The published methods for the detection of TNF-α include enzyme-linked immunosorbent assays (ELISA) [6,7–9], radioimmunoassays (RIA) [10], bioassays [11], chemiluminescence and enhanced chemiluminescence imaging [12,13], time-resolved immunofluorometric assay and dissociation-enhanced lanthanide fluorometric assay (DELFLA) [14,15], enzyme-amplified lanthanide luminescence (EALL) [16], matrix-assisted laser desorption/ionization mass spectrometry (MALDI-MS) [17], immuno-PCR and immuno-PCR assay [18,19], fluorescence immunoassay [20–22] and electrochemical immunosensor [5]. However, these methods often suffer from different disadvantages: ELISA offers the advantages of good reproducibility and high specificity. However, active enzymes which require special storage and carcinogenic reagents are often required in colorimetric assay. RIA used in the early 1970s was selective and relatively sensitive but had drawbacks such as

* Corresponding author. Tel.: +86 29 85308748; fax: +86 29 85308748.
E-mail address: zzj18@hotmail.com (Z. Zhang).

0039-9140/$ – see front matter © 2007 Elsevier B.V. All rights reserved.
doi:10.1016/j.talanta.2007.03.059

the use of radioisotopes, health hazard, waste disposal problems, short half-life, conjugate radiolysis and legislative bias. Bioassays have been used for the quantification of TNF-α for several years. However, they have the disadvantage of poor reproducibility, low specificity and high cost, while chemoluminescence assays require careful manipulation and ultrapure water is needed absolutely in the experiment in order to eliminate the interfering factors coming from the experimental surroundings and the solutions. And the traditional FIAs also suffer from the disadvantages like the inefficiency of labeling, lacking of photostability in addition to the problem of relatively low fluorescence intensity of dyes such as fluorescein isothiocyanate (FITC) [23,24]. As an alternative to it, the establishment of simple and sensitive immunoassays analytical methods is necessary. In the past few years, the rapidly evolving field of nanoscience and nanotechnology has opened up a new and promising era and increasing attention have been paid to the rapid development and extensive applications of nanomaterials in analytical and bioanalytical chemistry [25,26]. Due to the unique chemical and physical properties, such as high surface-to-volume area, inertness and stability to chemical and physical agents, silica nanoparticles or gel matrixes offer a promising possibility of improving some analytical performances like e.g. enhancement of the signal response, increase of the sensitivity, and improved reproducibility in various tests and assays [27–35].

The new generation of FIAs using fluorescent nanoparticle labels shows promising applicability in the diagnosis of trace biomolecules because the nanoparticle-based amplification platforms and amplification processes have been reported to dramatically enhance the intensity of the fluorescent signal and lead to ultrasensitive determinations [34,36–38]. To the authors' best knowledge, although the preparation and the conjugation of biomolecules for the fluorescence labeling with the fluorescent dye Rubpy-doped silica nanoparticles have been developed, there are lack of detailed informations about the application of immunoassay by using this kind of fluorescent nanoparticles in the issued papers [28,34]. It was the aim of the study presented here, to develop and validate a novel method for the determination of TNF-α with the sandwich FIA by using the RuDFSNs as the labeling.

2. Materials and methods

2.1. Reagents and solution

All chemicals and reagents used in this study were of analytical grade. The water used for the preparation of solutions was deionized and doubly distilled. Tetraethyl orthosilicate (TEOS), *n*-hexanol, Triton X-100 (4-(1,1,3,3-tetramethylbutyl)phenyl-polyethylene glycol) (TX-100), and cyclohexane were obtained from Shanghai Chemical Plant (Shanghai, China). Tris(2′,2-bipyridyl)dichlororuthenium(II) hexahydrate (Rubpy) and bovine serum albumin (BSA) was obtained from Sigma (St. Louis, USA). Tumor necrosis factor-α (TNF-α), two rHu monoclonal antibodies against TNF-α were kindly donated by Prof. Jin BQ (Department of Immuno, The Fourth Military Medical University, Xi'an, China). Defined newborn calf serum was obtained from LaiBo Technology Development Company (Xi'an, China). Na_2CO_3, $NaHCO_3$, KH_2PO_4, $Na_2HPO_2{\cdot}12H_2O$, NaCl, KCl, Tween-20, and NaH_2PO_2 were also obtained from Shanghai Chemical Plant (Shanghai, China). Unless otherwise stated all chemicals and reagents used in this study were of analytical grade quality. The low fluorescent 96-well transparent microtiter plates used for the assay were obtained from Corning Incorporated (Michigan, USA).

The coating solution was 0.05 mol/L carbonate buffer, pH 9.6. PBS (phosphate buffered saline) buffer was 0.15 mol/L, pH 7.4. Ninety-six well plates were rinsed with PBST washing buffer solution (PBST: 0.15 mol/L PBS solution containing 0.05% (v/v) Tween-20). Standard TNF-α (0.01–312.0 pg/mL) solution was prepared by appropriate dilutions of the TNF-α stock solution in assay buffer (PBST + 0.2% BSA) and 100 mL of defined newborn calf serum was added and stored below 4 °C.

2.2. Instrumentation

Fluorescence emission measurements were carried out with a fluorescence spectrophotometer (Shimadzu RF-540, Shimadzu, Tokyo, Japan) which employs a 100 W xenon lamp excitation source and a bifurcated glass optical fiber bundle with 4.0 mm diameter at the common end (Oriel Co., Stratford, CT, USA). The excitation and emission slits were set both at 5 nm throughout. Fluorescence microscopy imaging was performed on an Olympus inverted microscope system with a 100 W high pressure mercury lamp (Olympus, Model BH2-RFL-T3, Toyko, Japan) used as the light source.

2.3. Preparation of RuDFSNs–antibody conjugates

(a) The preparation of RuDFSNs. Preparation of RuDFSNs was carried out according to method described by previous paper with little change [37]. The procedure is briefly described as follows. At first, 1.77 mL of the surfactant TX-100, 7.5 mL lipophilic cyclohexane, and 1.8 mL of the co-surfactant *n*-hexane were mixed by magnetic force stirring at room temperature (RT) for 30 min. Then, 0.48 mL Rubpy dye solution was added and the resulting mixture was homogenized by magnetic force stirring to form water-in-oil microemulsion. In the presence of 100 μL of TEOS (added to the emulsion), a hydrolyzation reaction was initiated by adding 60 μL $NH_3{\cdot}H_2O$ (28–30 wt.%). The reaction mixture was allowed to stir for 12 h by magnetic force stirring. Then 100 μL of APS and 60 μL of $NH_3{\cdot}H_2O$ were added to the reaction mixtures under stirring. The reaction mixture was allowed to stir for another 12 h, and about 25 mL acetone was added to break the microemulsion. And finally, the particles were recovered by centrifugation at 8000 rpm for 10 min. The particle-containing pellet was washed using centrifugation and ultrasonication with ethanol and water several times to remove surfactant molecules and physically adsorbed Rubpy dye from the particle's surface. The particles were air dried. The synthesized RuDFSNs were characterized by spectrofluorometry for fluorescence inten-

sity and transmission electron microscope (TEM; Hitachi H700) for size and morphology.

(b) Immobilization of the antibody onto RuDFSNs surface. The anti-TNF-α monoclonal antibody was immobilized onto the RuDFSNs according to the well-established glutaraldehyde method: firstly, 2 mg RuDFSNs were dispersed in PBS buffer containing 5% glutaraldehyde for about 2 h at RT by stirring. Secondly, the RuDFSNs were separated by centrifugation and washed with PBS three times. After the RuDFSNs had been re-dispersed in PBS, they were further incubated with 20 mg BSA in 1.0 mL of 0.1 M phosphate buffer pH 7.4 at 4 °C for 12 h with shaking. Then the RuDFSNs were centrifuged and washed with water and were re-dispersed in PBS. Thirdly, the BSA-loaded RuDFSNs were dispersed in PBS buffer containing 5% glutaraldehyde for another 2 h. Fourthly, the RuDFSNs were incubated with monoclonal TNF-α antibody for 12 h at 4 °C with shaking. Finally, the RuDFSNs-labeled antibody was washed with PBS several times to remove excess TNF-α antibody and kept at 4 °C in PBS.

2.4. Procedure of the RuDFSNs-labeled TNF-α sandwich FIA

A typical sandwich FIA was used in this study. After unlabeled monoclonal TNF-α antibody diluted 100-fold in coating solution, had been coated to the wells (100 μL per well) of a 96-well plate by physical absorption overnight at 4 °C, the wells were washed three times with PBST solution. The TNF-α standards or test samples (100 μL per well) were added to each well. After incubation at 37 °C for 1 h, the wells were washed with PBST buffer. The RuDFSNs-labeled antibody (100 μL per well) was added to each well and the plate was incubated at 37 °C for 1 h. Then, the wells were washed three times with PBS buffer, and fluorescence emission (λ_{ex}: 435 nm, λ_{em}: 600 nm) was measured using a spectrofluorophotometer with xenon discharge excitation source and a bifurcated glass optical fiber bundle with 4.0 mm diameter at the common end (Oriel Co., Stratford, CT, USA). A new framework was made to hold one end of the bifurcated fiber optical bundle on the way of the excitation beam and another end on the way of the detect system. And the common end inserted perpendicularly in the well was also fixed with the framework. In the experimentation, the 96-well plate was flatly placed into the pedestal of fluorometer. Then one end of the bifurcated fiber optical bundle fixed with the framework was placed perpendicularly into the well of 96-well plate. Because there are four brackets fixed on the framework which also can be placed reposefully onto the pedestal, the distance between bottom of 96-well plate and end of the fiber remains unchanging while the fiber moves from well to well.

2.5. Sample preparation

Fresh blood was collected in clean plastic tubes; no anticoagulant was added to the blood samples allowing the blood coagulation naturally and then centrifuged at 3000 rpm for 5 min. The supernatant part was extracted as serum with a mini sample collector. Serums were stored at −20 °C until assayed. The serum was properly diluted in assay buffer before using.

2.6. Fluorescence microscopy imaging

The results from a RuDFSNs-labeled TNF-α sandwich FIA were evaluated by fluorescence microscopy imaging using Olympus inverted microscope system. For this purpose, the 96-well plate was mounted on the microscope stage. The excitation light (λ_{ex}: 420–480 nm) which comes from high pressure mercury was introduced through the inverted microscope objective from underneath the chamber. Image was collected by a microscope objective. A CCD camera (1.2 Million Pixel, Pixera, model PVC100C, Los Gatos, USA) and a computer were applied for acquisition of the fluorescence images. Data processing was done by using the dedicated software.

3. Results and discussion

3.1. Preparation and characterization of RuDFSNs

A variety of techniques have been developed to prepare different types of fluorescent nanoparticles. However, the inverse microemulsion polymerization method is most often used by researchers to prepare dye-doped nanoparticles. This technique has the advantage that the RuDFSNs can be prepared under mild conditions using inexpensive reagents and simple procedures. The resulting RuDFSNs have advantages of uniform size, good dispersivity and easily being labeled which makes them popular for various research and clinical applications. In our experiments, TEOS and APS underwent simultaneously hydrolysis to form the monodisperse spherical RuDFSNs with free amino groups presented on the surface of the nanoparticles. The synthesized RuDFSNs were characterized by transmission electron microscope to control size and morphology. The results showed that the particle sizes of RuDFSNs were about 48 ± 5 nm. In addition, spectrofluorometric measurements were used to characterize the RuDFSNs. Unbound Rubpy dye emitted fluorescence light at 595 nm when excited at 435 nm in aqueous solution. However, the emission maximum of the RuDFSNs shifted with 4 nm to the longer wavelength, indicating that the spectral characteristics of the Rubpy dye were changed only insignificantly after encapsulation in the nanoparticles.

3.2. Preparation of covalent RuDFSNs–anti-TNF-α conjugates

The amino groups-activated surface of RuDFSNs could be modified easily for binding biomolecules, e.g., by using the well-established glutaraldehyde method [39,40]. Although nanoparticles and antibodies can be bound by direct conjugation, we found in our experiments that this construct was not suited for the determination of TNF-α because the FIA showed only low sensitivity (Fig. 1). The same problem has been described by other authors [39,40]. We enhanced the sensitivity by a two-step conjugation of the RuDFSNs. They were coupled first to BSA, and secondly with the monoclonal anti-TNF-α antibody. The

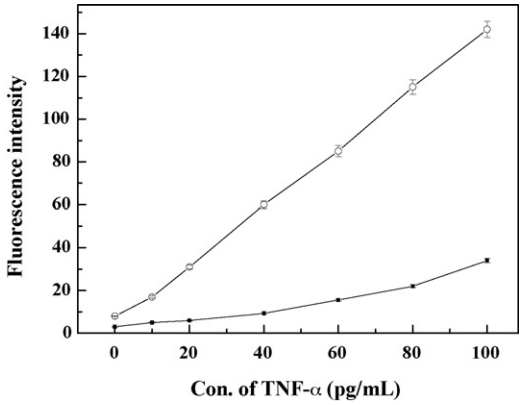

Fig. 1. Comparison of assay responses for RuDFSNs–anti-TNF-α antibody conjugates produced with indirect coupling using BSA-"bridges" (open circles) or direct coupling (closed squares).

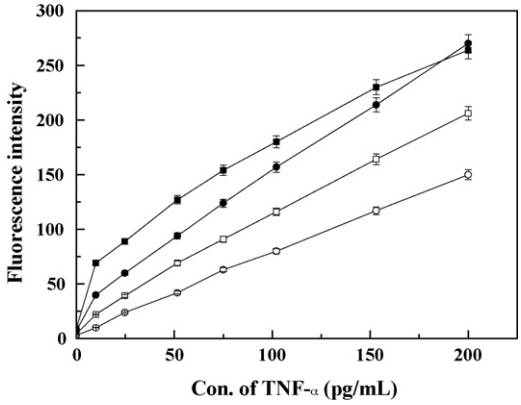

Fig. 2. Effect of fluorescent nanoparticle surface antibody density variations on the assay response. Antibody density was increased by increasing amounts of antibody incubated per milligram of nanoparticles: 5 μg (open circles), 50 μg (open squares), 100 μg (closed circles) and 200 μg (closed squares).

BSA functioned as a flexible "bridge" between nanoparticle and antibody, and thus, the steric hindrance between the nanoparticle and antigen was decreased. Therefore, the immunochemical reaction between the RuDFSNs-labeled antibody and the antigen could occur more easily. With the BSA-mediated conjugation method, the RuDFSNs-labeled TNF-α sandwich FIA gained a lower detection limit (LOD) of only 0.1 pg/mL which is lower than the previously reported detection limits of most sensitive assay for TNF-α [13,15,22,5,17] and equal to the most sensitive assay [6,41], whereas the LOD for a method using the directly conjugated construct was about 5 pg/mL.

3.3. Optimization of the RuDFSNs-labeled TNF-α sandwich FIA

The method developed was a typical "sandwich" FIA. As we all know that it has higher specificity by using monoclonal than that of polyclonal in immunoassay, so we use a pair of monoclonal antibodies of TNF-α in this study. A pair of monoclonal antibodies that recognize different epitopes of same antigen was used to capture and detect a certain antigen. For optimization of the fluorescent nanoparticle surface antibody density, we incubated fluorescent nanoparticles with variable amounts of antibody and examined the effect on the antibody dose–response curve. We observed (Fig. 2) that 5 μg antibody per mg fluorescent nanoparticles there was only about 30% dose response at concentration of 50 pg/mL compared with that when 100 μg antibody was used. As the amount of antibody was increased from 5 to 50 to 100 μg antibody per mg fluorescent nanoparticles, the assay response increased. Because the assay reached saturation with 200 μg/mg RuDFSNs, at this concentration, the assay response was increased slowly. Thus, there existed an optimum of antibody density at about 100 μg/mg RuDFSNs, resulting in the best assay response. Therefore, this ration was chosen for the RuDFSNs-labeled TNF-α sandwich FIA.

For optimization of the fluorescent nanoparticle concentration, the assay response was monitored at different concentrations of RuDFSNs–anti-TNF-α antibody conjugates (Fig. 3). We observed that the fluorescent intensity was enhanced significantly when the fluorescent nanoparticle concentration was increased from 0.1 to 10 μg/mL. However, at concentrations >10 μg/mL the binding curve (graph a) became more flattened, probably because of specific antigen–antibody saturation. The noise (graph b) caused by unspecific binding increased slowly from 0.1 to 10 μg/mL, whereas it became more disturbing at higher nanoparticle concentrations. Thus, the optimal signal/noise ratio was obtained at an intermediate concentration of RuDFSNs–anti-TNF-α antibody conjugates, and 20 μg/mL was chosen for the procedure of the RuDFSNs-labeled TNF-α FIA.

3.4. Performance of the RuDFSNs-labeled TNF-α sandwich FIA

In this study, TNF-α was measured based on interaction between antigen and antibody. This method has the advantage of specificity in immunoassay, because the interaction between antigen and antibody is specific intrinsically. Although there are crossreactivities in immunoassay, in previous experiment done by our group [21] it has been proved that the interaction between

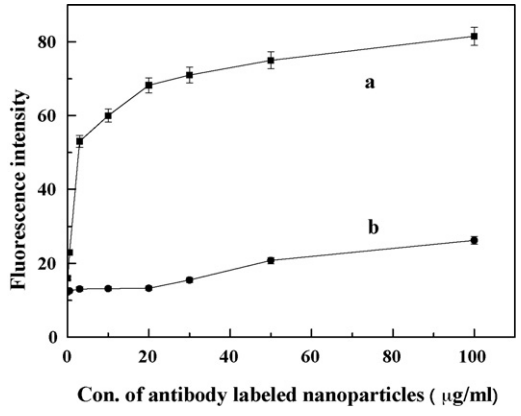

Fig. 3. Effect of different fluorescent nanoparticle concentrations on the assay response (a, signal; b, noise). The fluorescent nanoparticle surface antibody density is constant at 100 μg antibody/mg nanoparticle, the TNF-α concentration is 40 pg/mL.

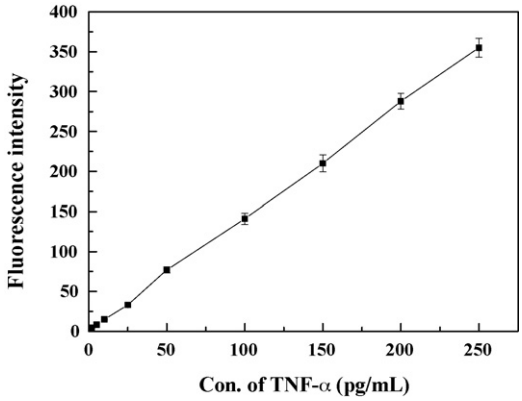

Fig. 4. Standard curve of the RuDFSNs-labeled TNF-α sandwich FIA.

TNF-α antigen and TNF-α monoclonal antibody is also specific. The non-specificity interaction does not exist between TNF-α antigen and immunoglobulin, and the cytokine, such as, IL-2, IL-3, IL-4, IL-5, IL-6, IL-8, IL-9, IL-11, TNF-β and IFN-γ. The calibration curve of sandwich FIA (Fig. 4) with RuDFSNs for TNF-α is $I_F = 1.3 + 1.428$ [TNF-α] (pg/mL) with $R^2 = 0.9979$. The assay response is linear from 1.0 to about 250.0 pg/mL. The detection limit, calculated based on 100 μL of a solution of calibrators is 0.1 pg/mL with 3S.D. This is more than 10-, 60-, 200-, 500-, 10 000-fold lower, respectively, than the previously reported detection limits of most sensitive assay for TNF-α [13,15,22,5,17] and equal to the most sensitive assay [6,41]. We evaluated the intra-assay precision of the method by analyzing the same concentration samples five times with multiple replicates and the inter-assay precision by analyzing the same concentration samples on five consecutive days. Intra- and inter-assay precision tests indicated good repeatability of our method for fluorescent signal intensity (Table 1). As always, leaching of fluorescent components for dye-doped is a critical factor. We found that the speed of leaching is very fast during the first hours in aqueous solution, and then the speed of leaching slows. One possibility is that free Rubpy that was not washed away during the synthesis procedure may have been attached to the outer surface of the silica nanoparticles. In order to improve precision of the FIA, carefully washing is absolutely necessary to eliminate the phenomenon of decreasing of fluorescence intensity during washing in future experiment. The feasibility of applying the proposed sandwich FIA to measure TNF-α in a complex matrix was studied. This was conducted by adding various levels of TNF-α into human serum samples (the samples were diluted appropriately step by step to be in the linear range of the proposed method). The results of recovery test were shown in Table 2. The results indicate that the present method is highly reliable.

Table 1
Intra-assay and inter-assay precision data

Concentration (pg/mL)	Relative S.D. (%)	
	Intra-assay	Inter-assay
2.0	4.9	6.1
20.0	4.4	5.9
200.0	4.6	5.3

Table 2
Accuracy, measured as recovery

Original (pg/mL)	Added(pg/mL)	Detected (mean ± S.D.) (pg/mL)[a]	Recovery ratio (%)[b]
5.0	5.0	10.2 ± 0.13	104.0
5.0	5.0	9.8 ± 0.16	96.0
20.0	20.0	39.3 ± 0.13	96.5
50.0	50.0	100.4 ± 1.9	100.8
50.0	50.0	100.7 ± 2.1	101.4
150.0	50.0	198.2 ± 3.9	96.4

[a] $n = 5$.
[b] Recovery (%) = ((detected concentration − background content)/added concentration) × 100%.

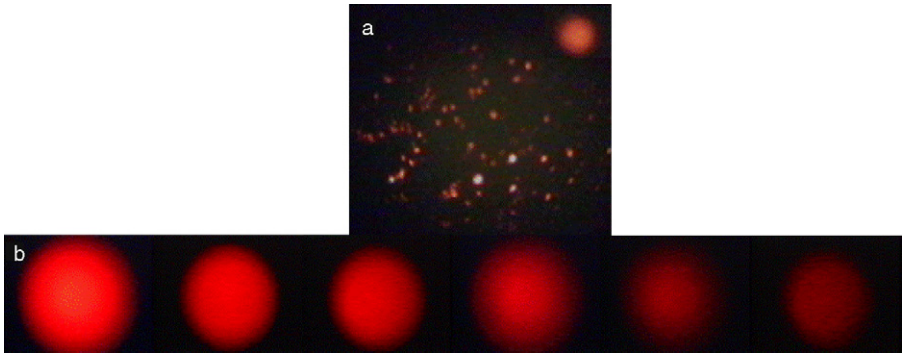

Fig. 5. Fluorescence microscopy image of RuDFSNs–anti-TNF-α antibody conjugates. The solution of RuDFSNs was dropped onto a slide ((a) magnification 1:100, insert 1:400). Image of a microtiter plate after performing the RuDFSNs-labeled TNF-α sandwich FIA with different concentrations of TNF-α: 200, 100, 50, 25, 12.5, 6.25 pg/mL from left to right ((b) magnification 1:4).

3.5. Fluorescence microscopy imaging of TNF-α detected by RuDFSNs-labeled antibodies

The dispersivity of the fluorescent nanoparticles or quantum dots (QDs) often can be investigated with the TEM or SEM (scanning electron microscope). And the fluorescence images of the fluorescent nanoparticles are usually observed onto the fluorescent microscope system for optical imaging and observation of dispersivity [42–44]. In our experiments, the RuDFSNs–anti-TNF-α antibody conjugates were sufficiently dispersed (Fig. 5). To investigate the feasibility of fluorescence microscopy for the imaging of FIA, various concentrations of the TNF-α-standard were analyzed. The fluorescence intensity gradually increased with increasing concentration of the TNF-α. According to the results of fluorescence microscopy for the imaging of FIA, this method could be used in clinical diagnose and the cellular and tissue imaging are also developed in our group.

4. Conclusions

The ability to measure accurately and precisely very low amounts of TNF-α is very important for the elucidation and clinical investigation of many TNF-α dependent pathological condition. In the study presented here, a novel RuDFSNs-labeled TNF-α sandwich FIA was developed and evaluated. The method showed high sensitivity, good precision and accuracy, and was suited for the detection of TNF-α in human serum. The new assay was adapted to the 96-well plate format and does not need elaborate instrumentation which makes it suitable for a wide range of different applications.

Acknowledgement

We gratefully acknowledge the Chinese Natural Science Foundation for financial support (Project no. 30470886).

References

[1] J. Wang, G. Mazza, J. Agric. Food Chem. 50 (2002) 4183.
[2] T. Akaike, S. Fujii, A. Kato, J. Yoshitake, Y. Miyamoto, T. Sawa, S. Okamoto, M. Suga, M. Asakawa, Y. Nagai, H. Maeda, FASEB J. 14 (2000) 1447.
[3] S. Moncada, R.M. Palmer, E.A. Higgs, Pharmacol. Rev. 43 (1991) 109.
[4] S. de Kossodo, V. Houba, G.E. Grau, A. Waage, A. Meager, S.M. Kramer, et al., J. Immunol. Methods 182 (1995) 107.
[5] C. Petrovas, S.M. Daskas, E.S. Lianidou, Clin. Biochem. 32 (1999) 241.
[6] J. Wang, G.D. Liu, M.H. Engelhard, Y.H. Lin, Anal. Chem. 78 (2006) 6974.
[7] A. Ledur, C. Fitting, B. David, C.J.M. Hamberger, J. Immunol. Methods 186 (1995) 171.
[8] M. Weghofer, H. Karlic, A. Haslberger, Ann. Hematol. 80 (2001) 733.
[9] M.W. Linden, T.W.J. Huizinga, D.J. Stoeken, A. Sturk, R.G.J. Westendorp, J. Immunol. Methods 218 (1998) 63.
[10] A.M. Teppo, C.P. Maury, Clin. Chem. 33 (1987) 2024.
[11] L.J. Jones, V.L. Singer, Anal. Biochem. 293 (2001) 8.
[12] F. Berthier, C. Lambert, C. Genin, J. Bienvenu, Clin. Chem. Lab. Med. 37 (1999) 593.
[13] L.R. Luo, Z.J. Zhang, L.F. Ma, Anal. Chim. Acta 539 (2005) 277.
[14] A. Ogata, H. Tagoh, T. Lee, T. Kuritani, Y. Takahara, T. Shimamura, et al., J. Immunol. Methods 148 (1992) 15.
[15] U. Turpeinen, U.H. Stenman, Scand. J. Clin. Lab. Invest. 54 (1994) 475.
[16] R.A. Evangelista, A. Pollak, E.F.G. Templeton, Anal. Biochem. 197 (1991) 213.
[17] G.B. Hurst, M.V. Buchanan, L.J. Foote, S.J. Kennel, Anal. Chem. 71 (1999) 4727.
[18] K. Saito, D. Kobayashi, M. Komatsu, T. Yajima, A. Yagihashi, Y. Ishikawa, R.M.N. Watanabe, Clin. Chem. 46 (2000) 1703.
[19] K. Saito, D. Kobayashi, M. Sasaki, H. Araake, T. Kida, A. Yagihashi, et al., Clin. Chem. 45 (1999) 665.
[20] M. Okubo, M.P. Brown, K. Chiba, R. Kasukawa, T. Nishimaki, Mol. Biol. Rep. 25 (1998) 217.
[21] M. Takahashi, T. Funato, K.K. Ishii, M. Kaku, T. Sasaki, J. Lab. Clin. Med. 137 (2001) 101.
[22] S. Cesaro-Tadic, G. Dernick, D. Juncker, G. Buurman, H. Kropshofer, B. Michel, et al., Lab. Chip. 4 (2004) 563.
[23] M. Dyba, S.W. Hell, Appl. Opt. 42 (2003) 5123.
[24] X.H. Fang, W.H. Tan, Anal. Chem. 71 (1999) 3101.
[25] S.B. Zhang, Z.S. Wu, M.M. Guo, G.L. Shen, R.Q. Yu, Talanta 71 (2007) 1530.
[26] J. Kang, X.Y. Zhang, L.D. Sun, X.X. Zhang, Talanta 71 (2007) 1186.
[27] U. Karst, Anal. Bioanal. Chem. 384 (2006) 559.
[28] S. Santra, P. Zhang, K.M. Wang, R. Tapec, W.H. Tan, Anal. Chem. 73 (2001) 4988.
[29] H. Xu, J.W. Ayloott, R. Kopelman, T.J. Miller, M. Philbert, Anal. Chem. 73 (2001) 4124.
[30] H. Harma, T. Soukka, T. Lovgren, Clin. Chem. 47 (2001) 561.
[31] H. Wang, J.S. Li, Y.J. Ding, C.X. Lei, G.L. Shen, R.Q. Yu, Anal. Chim. Acta 501 (2004) 37.
[32] Z.P. Wang, J.Q. Hu, Y. Jin, X. Yao, J.H. Li, Clin. Chem. 52 (2006) 1958.
[33] B. Panchapakesan, Oncology Issues 22-24 (S/O 2005) 26.
[34] S. Santra, D. Dutta, G.A. Walter, B.M. Moudgil, Technol. Cancer. Res. Treat. 4 (2005) 593.
[35] W. Lian, S.A. Litherland, H. Badrane, W.H. Tan, D.H. Wu, H.V. Baker, et al., Anal. Biochem. 334 (2004) 135.
[36] W. Yang, C.G. Zhang, H.Y. Qu, H.H. Yang, J.G. Xu, Anal. Chim. Acta 503 (2004) 163.
[37] R.P. Bagwe, C.Y. Yang, L.R. Hilliard, W.H. Tan, Langmuir 20 (2004) 8336.
[38] A. Valanne, S. Huopalahti, R. Vainionpaa, T. Lovgren, H. Harma, J. Virol. Methods 129 (2005) 83.
[39] Z.Q. Ye, M.Q. Tan, G. Wang, J.L. Yuan, Anal. Chem. 76 (2004) 513.
[40] Z.Q. Ye, M.Q. Tan, G. Wang, J.L. Yuan, Talanta 65 (2005) 206.
[41] V.A. Polunovsky, C.H. Wendt, D.H. Ingbar, M.S. Peterson, P.B. Bitterman, Exp. Cell. Res. 214 (1994) 584.
[42] K.P. McNamara, Z. Rosenzweig, Anal. Chem. 70 (1998) 4853.
[43] X.H. Gao, W.C. Chan, S.M. Nie, J. Biomed. Opt. 7 (2002) 532.
[44] H.Y. Xie, Z. Chao, Y. Liu, Z.L. Zhang, D.W. Pang, X.L. Li, et al., Small 1 (2005) 506.

Available online at www.sciencedirect.com
ScienceDirect
Talanta 73 (2007) 380–386
Talanta
www.elsevier.com/locate/talanta

Development and validation of a highly sensitive ELISA for the determination of pharmaceutical indomethacin in water samples

Song-Min Huo [a], Hong Yang [b,1], An-Ping Deng [a,*]

[a] College of Chemistry, Sichuan University, Chengdu 610064, China
[b] West China School of Pharmacy, Sichuan University, Chengdu 610041, China

Received 1 February 2007; received in revised form 27 March 2007; accepted 29 March 2007
Available online 6 April 2007

Abstract

The development and validation of a highly sensitive and specific indirect competitive enzyme-linked immunosorbent assay (ELISA) for the detection of pharmaceutical indomethacin in water samples was presented. The immunogen and coating antigen were prepared by covalently linking indomethacin to bovine serum albumin and ovalbumin by anhydride ester method. Two rabbits were immunized by standard immunization processes and the superior antibody was characterized in terms of sensitivity, specificity, precision, accuracy and stability. Under optimal experimental conditions, the standard curve was constructed in the concentration range of 0.01–10 ng/mL. For 10 consecutive standard curves run in 2 weeks, IC_{50} value (the concentration of analyte producing 50% of inhibition) were found within 0.10–0.25 ng/mL, and the detection limit (DL) at a signal-to-noise ratio of 3 (S/N = 3) was about 0.01 ng/mL. The antiserum recognized acemetacin, a precursor of indomethacin with 92.3% cross-reactivity, while the cross-reactivity values of antiserum with other tested compounds were very low. From the spiking experiments, the recoveries were found within 98–123%. The ELISA was applied for the determination of indomethacin in different water samples and the results were confirmed by conventional HPLC. The correlation coefficient of 0.988 was obtained, demonstrating a good correlation of ELISA with HPLC.

Keywords: Enzyme-linked immunosorbent assay (ELISA); Indomethacin; Water sample; Environmental analysis

1. Introduction

Within the last years a number of reports have demonstrated the wide occurrence of pharmaceuticals and their metabolites in natural waters [1–8]. Many drugs are distributed and excreted to the environment and are of increasing public concern. Among them, nonsteroidal anti-inflammatory drug (NSAID) established as a new kind of ubiquitous environmental pollutants. Long-term presence of such xenobiotic compounds in the aquatic environment will increase the potential of menace to the endocrine systems of humans.

Indomethacin [1-(4-chloro-benzoyl)-5-methoxy-2-methyl-1*H*-indole-3-acetic acid, Fig. 1] is an indole derivative, known as a NSAID. Indomethacin gels and ointments are broadly used for calming down acute joint and backbone pain and for the treatment of degenerative diseases of joints and ligaments such as rheumatoid arthritis, osteoarthritis and ankylotic spondylitis. Indomethacin is also used for the treatment of a patent ductus arteriosus (PDA) in neonates. Indomethacin is a powerful NSAID that is believed to act by inhibiting cyclooxygenase and consequently, prostaglandin synthesis, but it also causes severe gastric ulceration, increases blood pressure and decreases kidney function in a certain percentage of the population [9]. Meanwhile, the severity of the gastrointestinal (GI) toxicities of indomethacin is highlighted by the drug's contraindication in dogs due to fatal GI ulceration and hemorrhage [10]. From both human and veterinary usage, a significant proportion of indomethacin may pass through the body unmetabolized. As indomethacin is considered stable in the normal environment, although acute effect of the exposure of indomethacin and other NSAID to aquatic animals may not be appeared immediately, however, long-term presence of such xenobiotic microcontaminant in aquatic systems may increase the chronic toxicity and subtle effects such as endocrine disruption, growth inhibition and cytotoxicity on aquatic animals [11]. Numerous methods, including gas chromatography (GC) [12],

* Corresponding author. Tel.: +86 28 85471302; fax: +86 28 85412907.
E-mail addresses: denganping6119@yahoo.com.cn, denganping6119@126.com (A.-P. Deng).
[1] Current address: College of Pharmacy, University of Kentucky, 725 Rose Street, Lexington, KY 40536-0082, USA.

0039-9140/$ – see front matter © 2007 Elsevier B.V. All rights reserved.
doi:10.1016/j.talanta.2007.03.055

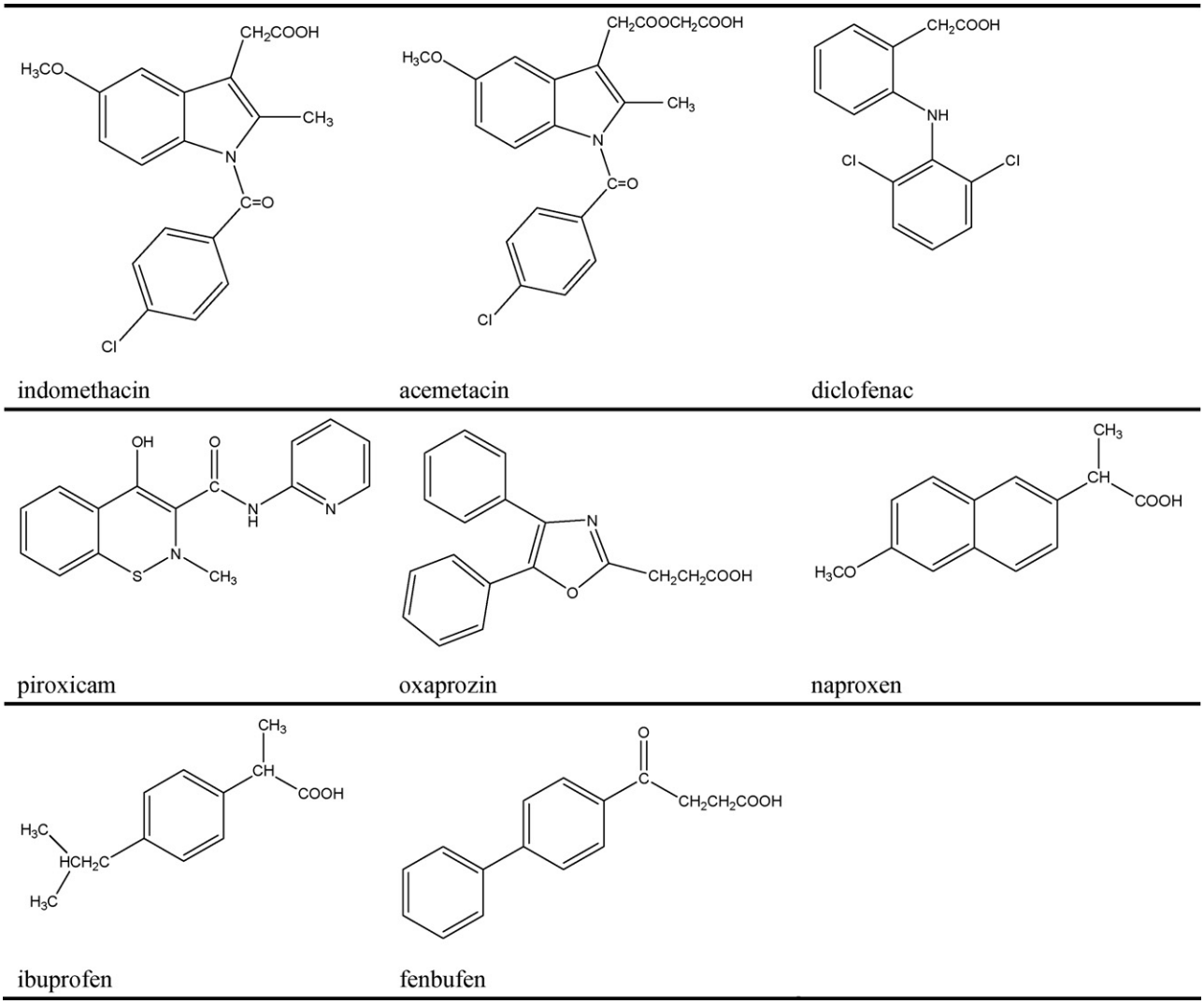

Fig. 1. Molecular structures of indomethacin and other nonsteroidal anti-inflammatory drugs tested of cross-reactivity.

GC–mass spectrometry [13], HPLC method [14], microscale HPLC method [15], HPLC–mass spectrometry [16], capillary electrophoresis (CE) [17], micellar electrokinetic chromatography [18], the USP 26 method [19] and a titration method by the European Pharmacopoeia [20], were reported for the determination of indomethacin in biological and drug samples. The drawbacks of the methods mentioned above are that they cannot reach the trace levels in the waters and most of them have long run times, tedious sample preparation and complex instrument. Few reports were observed for the detection of indomethacin in water samples by HPLC [21], thus concern over indomethacin's possible environmental and health impact leads to the need of rapid, simple, sensitive and selective analytical methods for the determination of indomethacin in water samples.

By taking advantage of highly sensitive and specific combination of the antigen and the antibody, immunochemical techniques, especially enzyme-linked immunosorbent assay (ELISA), with the features of inexpensive instrumentation, simple sample preparation, small sample volumes and rapid analysis have been widely applied for the environmental analysis [22–29]. To our knowledge, the production of antibodies against indomethacin and the establishment of an ELISA for detection of indomethacin in water samples have not been reported. The aim of this study is to develop a fast, simple, sensitive and specific ELISA for detection of indomethacin in water samples. The research is focused on the preparation of anti-indomethacin polyclonal antibodies, development and validation of ELISA method.

2. Experimental

2.1. Materials

Reagents and chemicals: indomethacin (IDM, 99.9%) was purchased from Shanghai No. 10 pharmaceutical factory (China). Bovine serum albumin (BSA), chicken egg ovalbumin (OVA), goat anti-rabbit IgG-horseradish peroxidase conjugate (GaRIgG-POD), Freund's complete and incomplete adjuvants, and casein were the products of Sigma. Dimethyl sulfoxide (DMSO), dimethylformamide (DMF) and tetramethylbenzidine

(TMB) were purchased from Amresco. *N*-Hydroxysuccinimide (NHS), and *N*,*N*′-dicyclohexylcarbodiimide (DCC) were obtained from Fluka. All other chemicals were of analytical grade.

Buffers and solutions—(1) coating buffer: 0.05 mol/L carbonate buffer, pH 9.8; (2) 0.01 mol/L phosphate-buffered saline (PBS) pH 7.4; (3) washing buffer (PBST): PBS with 0.1% (v/v) of Tween-20; (4) blocking buffer: 1% of casein in PBS; (5) acetate buffer: 100 mmol/L sodium acetate acid buffer pH 5.7; (6) substrate solution (TMB + H_2O_2): 200 μL of 10 mg/mL TMB dissolved in DMF, 20 μL of 5% H_2O_2 and 1 mL of acetate buffer were added to 20 mL of pure water; (7) sulfuric acid (5%).

Apparatus: ELISA reader (Tecan, Sunrise Remote/Touch Screen, Columbus plus, Austria), microtiter plate washer (Tecan, M12/2R, Columbus plus, Austria), spectrophotometer (UV-2300, Techcomp., Shanghai, China), microtiter plate shaker (KJ-201C, Oscillator, Jiangsu Kangjian Medical Apparatus, Co., Ltd.), pH meter (PS-10, Sarturius, Germany), electronic balance (BS 124S, Sarturius, Germany). Microtiter plates were from Jiangsu (Haimen, China). Deionized-RO water machine (DZG-303A) was purchased from AK Company (Taiwan).

2.2. Synthesis of immunogen and coating antigen

By anhydride ester method [30], indomethacin was respectively conjugated to carrier proteins, BSA and OVA. Briefly, indomethacin (0.15 mmoL/53.6 mg), NHS (0.15 mmoL/17.3 mg) and DCC (0.15 mmoL/30.9 mg) were dissolved in 300 μL of DMF. The activation reaction was carried out overnight at 25 °C. After the activated derivatives were centrifuged at 12,000 rpm for 10 min, the respective volume of the supernatant was added slowly to 100 mg of BSA or OVA in 0.13 M $NaHCO_3$ (5 mL) under continuous stirring. After reaction for 4 h at 25 °C, the possibly existed precipitate was separated by centrifugation and the supernatant was intensively dialyzed in 0.01 mol/L $(NH_4)_2CO_3$ for 4 days with many changes of the dialyzing buffer solution. The solutions of indomethacin–protein conjugates were lyophilized and stored at refrigerator until use. In this study, indomethacin–BSA conjugate was used as immunogen for antibody production, while indomethacin–OVA conjugate was used as coating antigen for establishment of ELISA.

2.3. Antisera production

Two New Zealand adult rabbits were chosen for polyclonal antibody production. The immunization dose for one rabbit in each immunization was about 1 mg of immunogen which would be injected to rabbit's back. The immunogen dissolved in physiological saline solution was emulsified with the same volume of Freund's complete adjuvant for first immunization. For booster immunizations, the same volume of Freund's incomplete adjuvant was replaced. Injections were made intradermally at multiple sites on the animals' back and the interval of the booster immunization was about 4 weeks. The titers of antisera (e.g. the highest dilution of the antiserum which can be effectively used for establishing an ELISA) were monitored by ELISA using checkerboard titration. Ten days after last injection, the rabbits were bled, and the antisera were collected and stored at −20 °C.

2.4. Indomethacin standard solution

The stock solution was prepared by diluting indomethacin with methanol to a concentration of 500 μg/mL and stored at 4 °C. Indomethacin standard solution was prepared by diluting the stock solution in pure water with concentrations of 0.01, 0.03, 0.1, 0.3, 1, 3, 10 ng/mL.

2.5. Sample collection and preparation

Water samples including tap water, drinking water, surface water, and wastewater were collected between July and November 2006 from different sites in Chengdu area. Tap water was obtained from this lab. The drinking water was from the student's canteen at Sichuan University. Three surface water samples were collected respectively from Jinjiang river, Funan river in Chengdu, and a pool closed to the affiliated hospital of Sichuan University. Three wastewater samples were collected from the drainage of the same hospital, and from the influent and effluent wastewater of Chengdu Wastewater Treatment Plant (WTP). All collected water samples were analyzed by ELISA. Tap water and drinking water were analyzed without dilution. For surface water, before analysis, a simple filtration step with 0.45 μm nylon membrane filter was needed. For wastewater samples, due to the existence of interference compounds, besides filtration, it was necessary to dilute the samples with pure water at an appropriate fold to avoid the matrix effects, and to adjust the samples' pH values about 6.0 to prevent the analyte taking the ionic form.

2.6. Spiking experiment

Tap water, drinking water and two surface water samples (Jinjiang river, Funan river) were spiked with indomethacin at concentrations of 0.05, 0.2, 0.5, 2.0, and 5.0 ng/mL. The spiked water samples were analyzed by the developed ELISA. The measured concentrations of analyte were calculated from the standard curve run in the same plate. Analytical parameters such as precision and the recovery (after subtracting the background concentration) were obtained from the spiking experiment.

2.7. Procedures of ELISA

An indirect competitive ELISA format was adopted for analyzing indomethacin. The ELISA procedures were as follows: 200 μL/well of coating antigen dissolved in carbonate buffer, pH 9.8 was added to a microtiter plate (96 wells). The plate was incubated overnight at 4 °C and then washed with PBST using an automatic plate washer. Some binding sites not occupied by the coating antigen were then blocked by the blocking buffer (280 μL/well) for 1 h at room temperature. After the plate was washed as before, standard solutions or samples (100 μL/well) and diluted antiserum (100 μL/well) were added and incubated

for 1 h at room temperature. After washing plate, GaRIgG-POD was added (200 μL/well) and the plate was incubated for 1 h at room temperature. Washing plate again, the substrate solution (200 μL/well) was added and then the plate was shaken for about 15 min for the color development. Sulfuric acid (5%, 80 μL/well) was added to stop the enzyme reaction and the absorbance was measured at 450 nm with ELISA reader. The calibration curve in the form of absorbance $\sim \log C$ was plotted automatically by the corresponding software embedded in ELISA reader. The calibration curve also could be constructed in the form of $(B/B_0) \times 100\% \sim \log C$, where B and B_0 were the absorbances of the analyte at the standard point and at zero concentration of the analyte, respectively. The concentrations of indomethacin in samples could be calculated from a standard curve.

2.8. Cross-reactivity

Cross-reactivity (CR) was determined to evaluate the specificity of the antiserum. In this study, some NSAIDs (the molecular structures were illustrated in Fig. 1) were chosen for cross-reactivity determination. The preparation of working solutions of all tested chemicals was similar to that of indomethacin standard solution. The concentrations of tested compounds were prepared in the range of 0.01–10,000 ng/mL and applied to the ELISA procedures.

2.9. Pre-treatment of samples for HPLC

The water samples were pre-concentrated by solid phase extraction (SPE) using C18 SPE cartridge. Prior to SPE extraction, the samples were only submitted to filtration with 0.45 μm nylon membrane filter. Water samples were collected in amber glass bottles, stored at 4 °C and tested within 2 days. Before the samples were applied, the cartridge was pre-conditioned with 5 mL of methanol and water (pH 2.0 with HCl), respectively, and then dried in vacuum. One hundred millilitres of the sample was applied to the cartridge and the flow rate was controlled about 4 mL/min. After the sample was loaded, a wash step was carried out with 2 mL methanol (2%). Following the dryness of the cartridge in vacuum, the analytes were then eluted with 10 mL methanol. After the elution, the filtrates were evaporated by a rotary evaporator at 50 °C and then re-dissolved with 1 mL methanol to obtain 100-fold pre-concentration.

2.10. HPLC method

A HPLC system (Alltech, USA) with C18 column (4.6 mm × 250 mm, 5 μm) was applied to analyze the water samples. Detection of water samples was completed with UVIS 201 detector. The detection wavelength was set at 237 nm and 20 μL sample loop was used. HPLC was performed with binary mobile phase composed of acetonitrile and 0.2% phosphoric acid (70:30, v/v) as mobile phases at flow rate of 0.9 mL/min. Calibration standards were constructed in concentrations of 10, 20, 50, 100, 200, 500, 1000, 2000 ng/mL.

3. Results and discussion

3.1. Preparation of immunogen and the production of antisera

As a carboxylic group is existed in indomethacin molecular structure, indomethacin can be directly activated by anhydride ester method. The activated indomethacin is then covalently coupled to carrier proteins. In this study, indomethacin–BSA conjugate was used as an immunogen for polyclonal antibodies production. Before immunization, the molar ratio of indomethacin to BSA in indomethacin–BSA conjugate was estimated by ultraviolet/visible spectrometric method. The characteristic peaks of indomethacin and BSA were located at 322 and 280 nm, respectively, which were separated clearly and no interference between them. The value of indomethacin/BSA was about 8.4. Two rabbits were immunized with indomethacin–BSA conjugate according to standard immunization processes.

3.2. Primary testing of the antisera

The polyclonal antisera from two immunized rabbits were collected and the quality of the antisera was primarily tested based on an indirect ELISA procedure using checkerboard titration. For the antiserum of fifth injection, it was found that the titer of rabbit II was as high as 1:150,000, while the titer of rabbit I was 1:100,000, a little lower compared to that of rabbit II, therefore, the rabbits were bled after fifth injections. Although a high titer for these two antisera was achieved, further characterization steps for the antisera were required.

3.3. Optimization of assay conditions

To develop a highly sensitive and specific ELISA, the assay conditions including the concentrations of coating antigen, dilutions of antiserum and GaRIgG-POD used for immunization reaction, the concentration of blocking reagent, the temperature, the time of incubation and color development, etc. should be carefully optimized.

In this study, the optimal assay conditions were found as follows: the appropriate concentration of coating antigen for coating plate was 30 ng/mL; the best dilutions of antisera were 1:150,000 for antiserum II and 1:100,000 for antiserum I; the suitable dilution of GaRIgG-POD was 1:10,000; the blocking reagent was 1% casein dissolved in PBS; 1 h of incubation was used for immunization reaction and 15 min incubation was employed for color development.

3.4. Sensitivity and stability of the ELISA

Under optimal assay conditions, the calibration curves for indomethacin analysis were constructed in the standard concentration range of 0.01–10 ng/mL using antiserum I and antiserum II. The calibration curves were plotted in the form of $B/B_0 \sim \log C$, as shown in Fig. 2. It was seen from Fig. 2 that IC_{50} value (e.g. at 50% of B/B_0) obtained from the calibration curve of

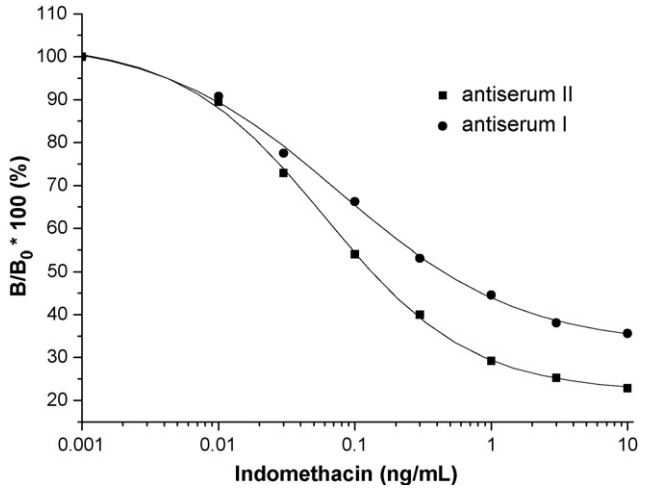

Fig. 2. The standard curves of ELISA for the determination of indomethacin using antiserum I (upper, with the IC_{50} of 0.45 ng/mL) and antiserum II (lower, with the IC_{50} of 0.12 ng/mL). The standard curves were constructed in standard range of 0.01–10 ng/mL.

antiserum I was 0.45 ng/mL; while the IC_{50} value of antiserum II was 0.12 ng/mL. In a competitive ELISA for the analysis of small molecular compound, the lower the IC_{50} value, the higher the sensitivity of the corresponding ELISA. Obviously, compared to antiserum I, antiserum II not only presented a higher titer (1:150,000), but also showed a higher sensitivity. Usually the sensitivity is a very important parameter for the development of an ELISA, thus in this study antiserum II was chosen for the further experiments.

To test the stability of the developed ELISA, the calibration curves from antiserum II were consecutively performed for 10 times within 2 weeks. As shown in Fig. 3, the R.S.D. of the measured absorbance in four replicates at each calibration point on 10 curves was within 10%; the IC_{50} value for 10 standard curves was in the range of 0.10–0.25 ng/mL;

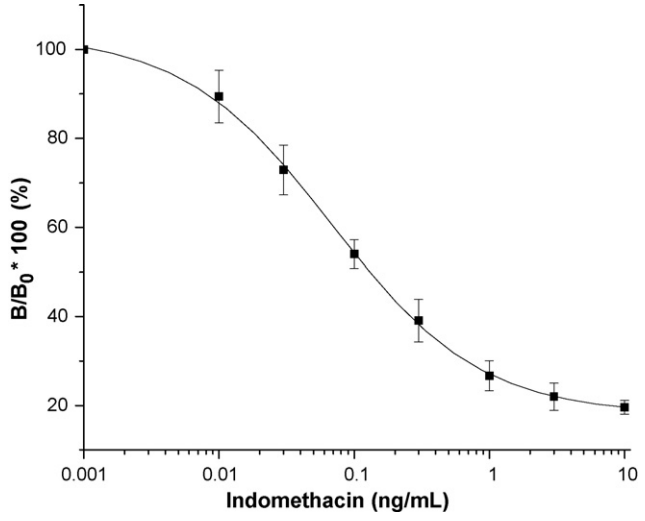

Fig. 3. The stability of the standard curves using antiserum II run in 10 times within 2 weeks. The bars represent the standard derivations of the values of B/B_0 ($n = 10$). The IC_{50} was in the range of 0.10–0.25 ng/mL; and the DL at S/N = 3 was about 0.01 ng/mL.

Table 1
Cross-reactivities among indomethacin and selected NSAIDs for antibody

Compound	IC_{50} (ng/mL)	Cross-reactivity (%)
Indomethacin	0.12	100
Acemetacin	0.13	92.3
Diclofenac	>900	<0.01
Piroxicam	>900	<0.01
Oxaprozin	>900	<0.01
Naproxen	>900	<0.01
Ibuprofen	>900	<0.01
Fenbufen	>900	<0.01

and the DL at a signal-to-noise ratio of 3 (S/N = 3) was about 0.01 ng/mL.

3.5. Specificity of antiserum

Specificity of the antiserum was detected by cross-reactivity experiment. A series of NSAIDs was selected to react with the antiserum in this assay. The value of cross-reactivity (%) was calculated: CR(%) = (IC_{50} of analyte/IC_{50} of tested compound) × 100%. The results of CR are presented in Table 1. The highest CR was found to be acemetacin (92.3%), a precursor of indomethacin, due to its similarity in molecular structure to that of indomethacin. The values of CR for other compounds were very low and could be negligible. The CR values appeared at the optimized ELISA showed a comparatively high specificity for the analysis of the target analyte.

3.6. Precision and accuracy of the ELISA

The values of precision and accuracy of the ELISA were obtained from spiking experiment. Tap water, drinking water, and two surface water samples were spiked with indomethacin at concentrations of 0.05, 0.2, 0.5, 2 and 5 ng/mL and analyzed by the developed ELISA in four replicates. The relative standard deviations ($n = 4$) for all measurements were lower than 9.5%. As shown in Table 2, the mean recovery was found to be 106% for tap water and 98% for drinking water. For the water samples from Jinjiang river, the recoveries were quite acceptable, e.g. 108% in original state and 98% in two-fold dilution. For Funan river, however, the recovery in original state was as high as 123%, indicating the possibility of interference existence. This postulation was confirmed by the fact that, after 10-fold dilution, the recovery in diluted water sample was improved to be 105%.

3.7. Analysis of water samples

Tap water and drinking water were directly analyzed by ELISA without dilution. It could be seen from Table 2 that no detectable indomethacin was found in tap water and drinking water. However, small amount of indomethacin was observed in two surface water samples, with the concentrations of 0.024 ng/mL in Jinjiang river and 0.109 ng/mL in Funan river.

For the analysis of water sample from the pool and other three wastewater samples, besides filtration with 0.45 μm nylon membrane, an appropriate dilution with pure water to reduce existed

Table 2
Indomethacin concentrations and recoveries measured in spiked tap water, drinking water and surface water by ELISA

Added indomethacin (ng/mL)	Tap water (ng/mL)	Drinking water (ng/mL)	Surface water (ng/mL)			
			Jinjiang river		Funan river	
			Original	1:2 dilution	Original	1:10 dilution
0	0	0	0.024	0.013	0.109	0.015
0.05	0.051	0.048	0.071	0.062	0.172	0.068
0.2	0.212	0.202	0.254	0.207	0.361	0.21
0.5	0.549	0.555	0.564	0.523	0.764	0.577
2	2.164	1.881	2.148	1.913	2.289	2.032
5	5.207	4.524	5.974	5.027	6.159	5.362
Recovery (%)						
0.05	102.0	96.0	94.0	98.0	126.0	106.0
0.2	106.0	101.0	115.0	97.0	126.0	97.5
0.5	109.8	111.0	108.0	102.0	131.0	112.4
2.0	108.2	94.1	106.2	95.0	109.0	100.9
5.0	104.1	90.5	119.0	100.3	121.0	106.9
Mean	106.0	98.5	108.4	98.5	122.6	104.7

matrix effect was required before analysis. In this study, the water samples were diluted with pure water at different dilutions and applied to ELISA. As shown in Table 3, the indomethacin concentrations detected at the dilutions of 1:10, 1:20 and 1:50 were in a good agreement, with the values of R.S.D. between 3.5 and 10.6%, demonstrating that the 1:10 dilution would be sufficient to eliminate the matrix effect and the precision of the measurements was acceptable. It was also revealed from Table 3 the mean concentrations of indomethacin found in influent, effluent, hospital, and pool were 1.412, 0.871, 2.548, and 0.857 ng/mL, respectively, obviously indicating the existence of the contamination with indomethacin in these water samples. The lower concentration of indomethacin in effluent compared to that in influent might be resulted from the degradation of the indomethacin in the treatment process performed in the wastewater treatment plant. As the hospital is a big comprehensive one in Southwest of China, where many various patients including arthritis patients are treated, the application of indomethacin might be wide. It was not surprised that the highest indomethacin concentration with the value of 2.548 ng/mL was found in the drainage of the hospital, and as a consequence, leading a presence of indomethacin with the concentration of 0.857 ng/mL in the samples collected in the pool closed to the hospital.

Table 3
Indomethacin concentrations in different water samples detected by ELISA at different dilution

	Influent	Effluent	Hospital	Pool
Original	1.306	0.869	2.177	0.854
1:10	1.512	0.897	2.807	0.813
1:20	1.485	0.902	2.529	0.874
1:50	1.344	0.816	2.678	0.886
Mean	1.412	0.871	2.548	0.857
S.D.	0.10	0.04	0.27	0.03
R.S.D. (%)	7.1	4.6	10.6	3.5

3.8. Comparison of ELISA with HPLC

To validate the developed ELISA, HPLC operation was done and the calibration curve for indomethacin detection were constructed in concentrations range of 10–2000 ng/mL with linear correlation coefficient of 0.9991, detection limit of 5 ng/mL and relative standard deviation for six repeated measurements ranging from 3.3 to 9.4%.

Six water samples collected from Jinjiang river, Funan river, pool, hospital, influent and effluent were also analyzed by HPLC and the comparison of the resultant measurements from HPLC with those obtained from ELISA was listed in Table 4. As the different sensitivities among these two techniques (DL: 0.01 ng/mL for ELISA and 5 ng/mL for HPLC), from Table 4 it was observed that there was no detection of analyte in the samples of Jinjiang river by HPLC, while the same samples measured by ELISA acquired the detection value of 0.024 ng/mL. In contrast, for Funan river analysis, the concentration of indomethacin measured by HPLC (0.142 ng/mL) was a little higher than that obtained from ELISA (0.109 ng/mL). However, for the measurements of other four types of water samples, a general finding was that the concentrations of analyte obtained from ELISA were higher than those from HPLC, which might be resulted from some extent of cross-reactivity and relative to existed matrix effect (less importance after 1:10-fold dilution). The correlation

Table 4
Comparison of ELISA and HPLC for indomethacin determination in different water samples ($n = 4$)

Water types	ELISA (ng/mL)	HPLC (ng/mL)
Jinjiang river	0.024 ± 0.004	No detection
Funan river	0.109 ± 0.07	0.142 ± 0.08
Pool	0.857 ± 0.03	0.663 ± 0.15
Hospital	2.574 ± 0.24	2.091 ± 0.53
Influent	1.412 ± 0.10	1.049 ± 0.40
Effluent	0.871 ± 0.04	0.523 ± 0.21

of ELISA (x) with HPLC (y) was expressed by linear regression equation: $y = 0.802x - 0.037$, with the correlation coefficient of 0.988, demonstrating a very good correlation of ELISA with HPLC. Apparently, the slope obtained from the linear regression equation with the value of 0.802 revealed that the measurement by HPLC was slightly underestimated compared to that by ELISA.

4. Conclusion

As a xenobiotic compound in the aquatic environment, long-term exposure of indomethacin or other NSAID to the ecosystems is suspected to interfere with the endocrine systems of aquatic animals. In this work, a highly sensitive indirect ELISA for the detection of indomethacin in different water samples was developed and validated by conventional HPLC. Indomethacin was covalently linked to carrier proteins by anhydride ester method and the selected polyclonal antibody produced in the normal immunization processes was characterized in terms of sensitivity, specificity, precision and accuracy. High sensitivity of the assay was achieved and, in cross-reactivity experiment, the antiserum did not recognize the tested compounds except a precursor of indomethacin. The proposed ELISA was applied for the determination of indomethacin in different water samples. The matrix effect of water samples was greatly reduced simply by diluting samples at 10-fold. The comparison of the experimental data for analyzing real water samples obtained by ELISA and HPLC demonstrated a good correlation between ELISA with HPLC. The proposed ELISA is also potentially applicable for indomethacin detection in complex matrices such as animal tissues and biological fluids with a suitable clean up process.

Acknowledgement

The authors thank the National Natural Science Foundation of China (NSFC) for financial support of this study (contract No. 20675054).

References

[1] H.R. Buser, T. Poiger, M.D. Müller, Environ. Sci. Technol. 33 (1999) 2529.
[2] P.D. Anderson, V.J. D'aco, P. Shanahan, S.C. Chapra, M.E. Buzby, V.L. Cunningham, B.M. Duplessie, E.P. Hayes, F.J. Mastrocco, N.J. Parke, J.C. Rader, J.H. Samuelian, B.W. Schwab, Environ. Sci. Technol. 38 (2004) 838.
[3] S. Castiglioni, R. Bagnati, R. Fanelli, F. Pomati, D. Calamari, E. Zuccato, Environ. Sci. Technol. 40 (2006) 357.
[4] J. Debska, A. Kot-Wasik, J. Namiesnik, J. Sep. Sci. 28 (2005) 2419.
[5] A.P. Deng, M. Himmelsbach, Q.-Z. Zhu, S. Frey, M. Sengl, W. Buchberger, R. Niessner, D. Knopp, Environ. Sci. Technol. 37 (2003) 3422.
[6] C. Coestsier, L.M. Lin, B. Roig, E. Touraud, Anal. Bioanal. Chem. 387 (2007) 1163.
[7] S. Babić, D. Ašperger, D. Mutavdžić, A.J.M. Horvat, M. Kaštelan-Macan, Talanta 70 (2006) 732.
[8] M.M. Huber, A. Göbel, A. Joss, N. Hermann, D. Löffler, C.S. Mcardell, A. Ried, H. Siegrist, T.A. Ternbs, U. Gunten, Environ. Sci. Technol. 39 (2005) 4290.
[9] C.T. Dillon, T.W. Hambley, B.J. Kennedy, P.A. Lay, Q. Zhou, N.M. Davies, J.R. Biffin, H.L. Regtop, Chem. Res. Toxicol. 16 (2003) 28.
[10] G.O. Ewing, J. Am. Vet. Med. Assoc. 161 (1972) 1665.
[11] K. Fent, A.A. Weston, D. Caminada, Aquat. Toxicol. 76 (2006) 122.
[12] P. Guissou, G. Cuisinaud, J. Sassard, J. Chromatogr. 277 (1983) 368.
[13] A.K. Singh, Y. Jang, U. Mishra, J. Chromatogr. 568 (1991) 351.
[14] L. Nováková, L. Matysová, L. Havlíková, P. Solich, J. Pharm. Biomed. Anal. 37 (2005) 899.
[15] M.A. Al Za' abi, G.H. Dehghanzadeh, R.L.G. Norris, B.G. Charles, J. Chromatogr. B 830 (2006) 364.
[16] P.J. Taylor, C.E. Jones, H.M. Dodds, N.S. Hogan, A.G. Johnson, Ther. Drug Monit. 20 (1998) 691.
[17] C. Mardones, A. Ríos, M. Valcácel, Electrophoresis 22 (2001) 484.
[18] S.-J. Lin, Y.-R. Chen, Y.-H. Su, H.-I. Tseng, S.-H. Chen, J. Chromatogr. B 830 (2006) 306.
[19] USP 26, United States Pharmacopoeial Convention Ino., 2002.
[20] European Pharmacopoeia, 4th ed., Council of Europe, Strasbourg, 2002.
[21] A. Nikolaon, A. Meric, D. Fatta, Anal. Bioanal. Chem. 387 (2007) 1225.
[22] J.C. Chuang, J.M. Van Emon, J. Durnford, K. Thomas, Talanta 67 (2005) 658.
[23] A. Knopp, D. Knopp, R. Niessner, Environ. Sci. Technol. 33 (1999) 358.
[24] R. Céspedes, K. Skryjová, M. Raková, J. Zeravik, M. Fránek, S. Lacorte, D. Barceló, Talanta 70 (2006) 745.
[25] N. Pastor-Navarro, E. Gallego-Iglesias, Á. Maquieira, R. Puchades, Talanta 71 (2006) 923.
[26] A.P. Deng, H. Yang, M. Fránek, Chin. J. Anal. Chem. 27 (1999) 657.
[27] F. Kondo, Y. Ito, H. Oka, S. Yamada, K. Tsuji, M. Imokawa, Y. Niimi, K-i. Harada, Y. Ueno, Y. Miyazaki, Toxicon 40 (2002) 893.
[28] A.P. Deng, V. Kolář, R. Ulrich, M. Fránek, Anal. Bioanal. Chem. 373 (2002) 685.
[29] J. Zeravik, K. Skryjová, Z. Nevoranková, M. Fránek, Anal. Chem. 76 (2004) 1021.
[30] M. Fránek, A.P. Deng, V. Kolář, J. Socha, Anal. Chim. Acta 444 (2001) 131.

Available online at www.sciencedirect.com
ScienceDirect
Talanta 73 (2007) 195–201
Talanta
www.elsevier.com/locate/talanta

Review

A chelating resin with bis[2-(2-benzothiazolylthioethyl)sulfoxide]: Synthesis, characterization and properties for the removal of trace heavy metal ion in water samples

Chunnuan Ji, Rongjun Qu *, Chunhua Wang, Hou Chen, Changmei Sun, Qiang Xu, Yanzhi Sun, Chao Wei

School of Chemistry & Materials Science, Ludong University, Yantai 264025, China

Received 22 October 2006; received in revised form 20 March 2007; accepted 22 March 2007
Available online 27 March 2007

Abstract

A new chelating resin containing bis[2-(2-benzothiazolylthioethyl)sulfoxide] was synthesized using chloromethylated polystyrene as material and characterized by elemental analysis and infrared spectra. The adsorption capacities of the newly formed resin for Hg^{2+}, Ag^{+}, Cu^{2+}, Zn^{2+}, Pb^{2+}, Mn^{2+}, Ni^{2+}, Cd^{2+} and Fe^{3+} were investigated over the pH range 1.0–6.0. The resin exhibited no affinity for alkali or alkaline earth metal ions. The maximum adsorption capacities of the resin for Hg^{2+}, Ag^{+}, Cu^{2+}, Zn^{2+}, Pb^{2+}, Mn^{2+}, Ni^{2+}, Cd^{2+} and Fe^{3+} were 1.49, 0.96, 0.58, 0.11, 0.37, 0, 0.24, 0.36 and 0.25 mmol g^{-1}, respectively. In column operation it had been observed that Hg^{2+} and Ag^{+} in trace quantity could be separated from different binary mixtures and Hg^{2+} could be effectively removed from industrial wastewater and the natural water spiked with Hg^{2+} at usual pH.

Keywords: Chelating resin; Bis[2-(2-benzothiazolylthioethyl)sulfoxide]; Recovery; Metal ions

Contents

* Corresponding author.
E-mail addresses: rongjunqu@sohu.com, qurongjun@eyou.com (R. Qu).

0039-9140/$ – see front matter © 2007 Published by Elsevier B.V.
doi:10.1016/j.talanta.2007.03.043

1. Introduction

Much attention has been drawn to the synthesis of chelating resins and to the investigation of their adsorption behavior for the selective and quantitative separation of specific metal ions from various matrices, because both their adsorption ability and adsorption selectivity are superior to those of ion exchangers in a trace or ultra concentration range [1–3]. In general, the adsorption selectivity of chelating resins has been reported to be dependent mainly on the chelate forming properties of functional groups chemically bonded on the supports such as silica gel, cellulose and macroporous copolymers [4]. Chelating resins containing heterocyclic functional groups receive a great deal of attention since they display high affinity towards heavy and noble metal ions [5]. Many chelating resins obtained by immobilization of heterocyclic functional groups on solid supports have been practically applied in separation of trace metals from a variety of matrices [6,7]. Several heterocycles such as pyridine [8,9], imidazole [10], imidazolylazo [11], benzimidazolylazo [12], quinoline [13] and 2-mercaptobenzothiazole (MBZ) [14–17] have been immobilized on a resin bed for this purpose. Among the above-mentioned chelating resins, the ones containing 2-mercaptobenzothiazole exhibit high affinity for heavy and noble metal ions, especially for mercury [16]. In Ref. [18], the separation properties of the resin containing sulphur and MBZ for Hg^{2+} and Ag^{+} has been studied. The results obtained show that the resin can separate Hg^{2+} and Ag^{+} quantitatively in aqueous solution.

Recently, the synthesis of chelating resins with *N*,*N*′-substituted diamides of malonic acid [19,20] and *N*,*N*′-dialkyl aliphatic amides [21] has been reported. These resins are proved to have good adsorption properties for metal ions owing to the close proximity of donor atoms, which can increase the probability of formation of stronger complexes [22].

Considering the above we have designed a new chelating resin containing bis[2-(2-benzothiazolylthioethyl)sulfoxide] as functional group. The present report describes the synthesis and characterization of the resin. Its adsorption capacity for Hg^{2+}, Ag^{+}, Cu^{2+}, Zn^{2+}, Pb^{2+}, Mn^{2+}, Ni^{2+}, Fe^{3+} and Cd^{2+} was investigated. The recovery of Hg^{2+} and Ag^{+} from several binary mixtures and the recovery of Hg^{2+} from natural waters spiked with Hg^{2+} and industrial wastewater were also studied.

2. Experimental

2.1. Apparatus and reagents

A flame atomic absorption spectrophotometer (Model 932A, made in Australia) was used for metal ion determination. The operating condition was presented in Table 1. The infrared spectra were recorded on a Nicolet MAGNA-IR550 (series II) spectrometer (made in American); test condition: potassium bromide pellets, scanning 32 times, resolution 4 cm^{-1}. The elemental analysis was carried out using an Elementar Analysensysteme Gmbh Varioel (made in Germany). Semi-automatic sequential injection hydride generation double-channel atomic fluorescence spectrometer (Model AFS-920, made in China) was used to determine the content of Hg^{2+} in river water and ground water. The BET surface area was determined by ASAP-2020 Surface Area and Porosity Analyzer (made in American). The adjustment of pH was done with microprocessor pH meter (Model HANNA pH211, made in Portugal).

Chloromethylated polystyrene (PS-Cl, crosslinked with 10% DVB, 5.49 mmol g^{-1} Cl, 30–40 mesh, BET surface area 31.85 m^2 g^{-1}) was purchased from Chemical Factory of Nankai University of China. 2-Mercaptoethanol, 30% hydrogen peroxide solution, urotropine, 2-mercaptobenzothiazole (MBZ), benzenesulfonyl chloride (BsCl), and other reagents, solvents were of analytical reagent grade and were used without further purification.

Stock solutions of the metal ions (1 mg ml^{-1} each) were prepared by dissolving appropriate amounts of analytical grade nitrates in distilled water, and further diluted prior to use. The buffer solutions were prepared by addition of dilute NH_4OH or HNO_3 to 0.1 M ammonium acetate solution.

2.2. Preparation of the resin

The target chelating resin was synthesized as follows (Scheme 1).

Resin **I** was obtained according to the similar procedure described in literature [23]: 30.0 g of PS-Cl was reacted with urotropine (96.0 g) in a mixture of ethanol and water (34:20, v/v) at 90 °C for 36 h. Then 250 ml of hydrochloric acid was added and the mixture was stirred at 90 °C for 9 h. After filtration, the residue was washed with distilled water and ethanol and dried under vacuum at 50 °C. 32.9 g of resin **I** was obtained. Elemental analysis (%): N, 3.58.

Table 1
Operating parameters used for recording AAS for different metal ions[a]

Metal ion	Lamp current (mA)	Slit width (nm)	Wavelength (nm)
Ag^{+}	4.0	0.5	338.1
Cd^{2+}	3.0	0.5	228.8
Cu^{2+}	3.0	0.2	217.9
Hg^{2+}	3.0	0.5	253.7
Mn^{2+}	5.0	0.2	279.8
Pb^{2+}	5.0	0.5	283.3
Ni^{2+}	4.0	0.2	232.0
Fe^{3+}	7.0	0.2	248.3

[a] The flame type of AAS used in this paper was air-acetylene (oxidizing).

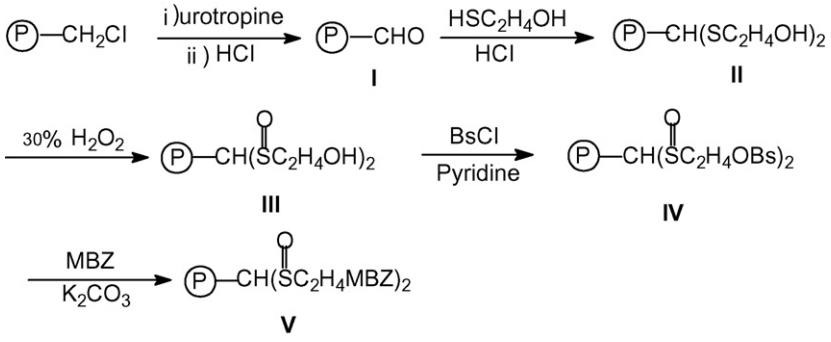

Scheme 1. Synthetic route of the resin.

Resin **I** (32 g) was reacted with 2-mercaptoethanol in a mixture of ethanol and hydrochloric acid (2:1, v/v) at 50 °C for 72 h. Then the product was filtered off and washed with distilled water and ethanol. After drying under vacuum at 50 °C, 37.0 g of resin **II** was obtained. Elemental analysis (%): N, 2.94; S, 15.33.

Resins **III** and **IV** were synthesized according to the same reaction condition described in literature [24]. 5.5 g of resin **II** were swollen in 100 ml of acetone for 30 min, then 11.2 g of hydrogen peroxide was added dropwise within 10 min. The mixture was stirred mechanically for 6 h. Then the reaction was heated to reflux for 2 h. Finally, the product was filtered off and washed with distilled water and ethanol and then was dried under vacuum at 50 °C. 6.1 g of resin **III** was obtained. Elemental analysis (%): N, 2.55; S, 14.12.

A mixture of 6.0 g of resin **III** and 100 ml of pyridine was cooled in an ice-water bath, and 20.6 ml of BsCl was added dropwise. The mixture was stirred at room temperature for 24 h. Then the reaction were filtered and washed with distilled water and ethanol and then was dried under vacuum at 50 °C. 6.7 g of resin **IV** was obtained. Elemental analysis (%): N, 2.52; S, 13.94.

At the last step, resin **IV** (6.5 g), 2-mercaptobenzothiazole (14.7 g) and K_2CO_3 (4.1 g) were suspended in DMF (150 ml), the mixture was stirred at 85 °C for 24 h. Then the reaction was filtered off and washed with distilled water, ethanol and dried under vacuum at 50 °C. 5.7 g of resin **V** was obtained. Elemental analysis (%): N, 3.16; S, 13.47.

2.3. Water regain

Water regain was defined as the amount of water absorbed by 1 g of polymer [20]. It was measured according to the method: approximately 1 g of the resin was stirred in double distilled water for 48 h, then filtered off by suction, weighted, dried at 80 °C for 48 h. After cooling in a desiccator, the resin was reweighed. The water regain was calculated as $(m_w - m_d)/m_d$, where m_w was the weight of water swollen polymer and m_d was the dry weight.

2.4. Resin stability test

Fifty milligrams of the resin was shaken continuously with 25 ml of 1–5 M hydrochloric acid or alkaline solutions, respectively for 7 days, then filtered off and washed with distilled water until neutral. After drying, the adsorption capacity of the resin for Hg^{2+} was measured by batch method.

2.5. Batch experiment

Thirty milligrams of the resin was added to 20 ml of metal ion solution (5×10^{-3} M) adjusted to the desired pH and the mixture was shaken for 24 h at 25 °C. The mixture was filtered off and the concentration of the solution was determined by FAAS. The adsorption capacities were calculated according to the following equation:

$$Q = \frac{(C_0 - C)V}{W}$$

where Q is the adsorption amount (mmol g^{-1}); C_0 and C are the initial concentration and the concentration of metal ion in solution when the adsorbent is separated (mmol ml^{-1}); V is the volume (ml); W is the dry weight of resins (in g).

2.6. Adsorption kinetic

The adsorption kinetics was determined according to the following procedure: 20 ml of metal ion solution (5×10^{-3} M) was shaken with 30 mg of the resin at room temperature. At predetermined intervals, aliquots of 1 ml solution were withdrawn for analysis and the concentration of metal ion was determined by FAAS. The loading half time $t_{1/2}$, i.e. the time required to reach 50% of the resin total loading capacity was estimated from the resulting isotherm.

2.7. Effect of diverse metal ions on adsorption capacities

One hundred milligrams of the resin was shaken with 20 ml of standard solutions of Hg^{2+}, Ag^{+} (10 μg ml^{-1} each) and 25 ml of diverse metal ion solutions containing the alkali and alkaline earth metal ions (80 μg ml^{-1} each). After 24 h, the resin sorbed metal ions was separated and completely eluted, the concentration of metal ion in the eluent was measured by FAAS.

2.8. Separation of Hg^{2+} and Ag^{+} from several binary mixtures

Separation of Hg^{2+} and Ag^{+} from several binary mixtures was performed by batch and column operation. The batch experiment was same as described above except for the amount of the resin was 200 mg instead of 100 mg. In column operation, a column of length 5 cm and 0.4 cm inner diameter was packed with 300 mg of the resin. The resin column was equilibrated by passing 30 ml of 0.1 M acetate buffer solution of an appropriate pH. In batch operation, a 40 ml solution containing 250 μg of Ag^{+} or Hg^{2+} and the interfering ions (500 μg each) was shaken for 24 h with 200 mg resin. In column operation, solutions of same amount of binary mixtures were passed through the resin at a flow rate of 0.25 ml min^{-1}. After eluting the metal ion sorbed on the resin with 10 ml of 5% thiourea in 0.1 M HNO_3, the concentration of metal ion in eluent was determined by FAAS.

2.9. Removal of Hg^{2+} from river and ground water

River and ground water were employed for the removal of Hg^{2+} in this experiment. To river water or ground water Hg^{2+} solution was added to make a solution of the concentration of mercury of 2 μg ml^{-1}. This solution was passed through the glass column having 300 mg of the resin at a flow rate of 0.25 ml min^{-1}. The metal ion sorbed on the resin was eluted with eluting agents, and then the amount of metal ion in eluent was determined by FAAS.

2.10. Removal of Hg^{2+} from industrial wastewater

The industrial wastewater was collected in pre-washed polyethylene bottles from Goldentide Battery Co. Ltd. (Yantai, China). The sample was immediately filtered through a Millipore cellulose nitrate membrane (45 μm), acidified to pH 2.0 with 2.0 mol l^{-1} HNO_3 and neutralized and then buffered to the desired pH. The content of the sample was determined by FAAS. For separation, 100 ml of the sample was passed through the column containing 300 mg of the resin. Hg^{2+} was subsequently eluted with 10 ml of 5% thiourea in 0.1 M HNO_3, the concentration of Hg^{2+} in eluent was determined by FAAS.

3. Results and discussion

3.1. Characterization of the resin

Fig. 1 showed the infrared spectra of PS-Cl and resins **I**–**V**. By comparison with the curve of PS-Cl, the characteristic peak of 1265 and 675 cm^{-1} almost disappeared in the curve of resin **I**, and a new strong band appeared at 1697 cm^{-1}, which was the characteristic absorbance of C=O group [23], indicating that the aldehyde group had been introduced into the polymeric matrix successfully. The data of elemental analysis indicated that the nitrogen contents in resins **I**–**IV** were 3.58, 2.94, 2.55 and 2.52%, respectively. The existence of nitrogen could be ascribed to the incomplete conversion of the intermediate (a) in the formation of resin **I** (shown as Scheme 2). Resin **II** was characterized by the absence of the absorbance of C=O and the presence of a band at 1046 cm^{-1} corresponding to C–OH group. The sulphur content found by elemental analysis in resin **II** (4.79 mmol g^{-1}) indicated that more than 43.6% of the chloromethyl groups were functionalized. In the spectrum of resin **III**, a strong absorption peak at 1039 cm^{-1} belonging to the characteristic absorbance of S=O was observed [25], which indicated that the sulphide had been oxidized into sulfoxide. Resin **IV** was confirmed by the presence of two bands at 1187 and 614 cm^{-1} belonging to the

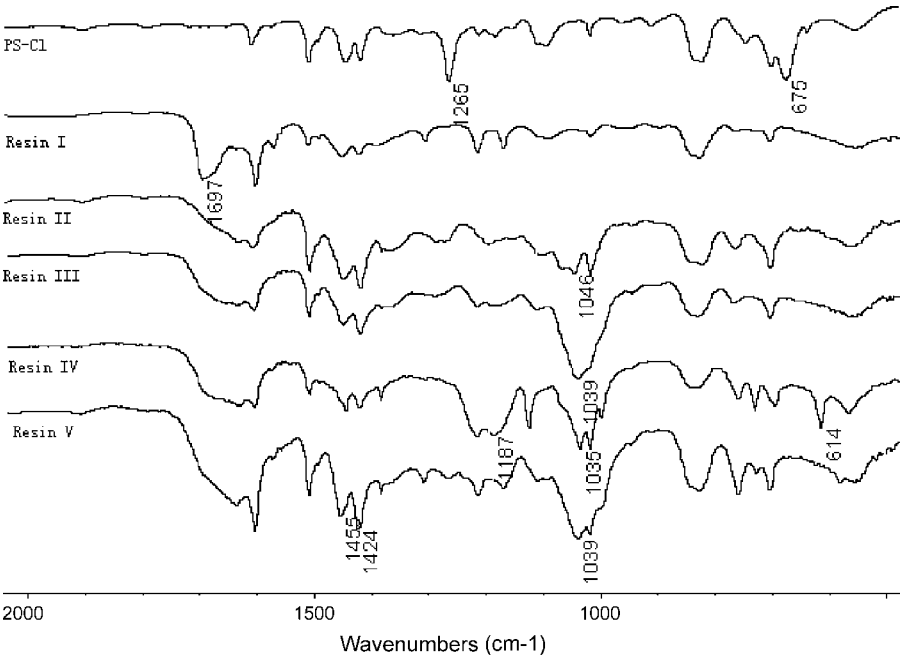

Fig. 1. FTIR spectra of PS-Cl and resins **I**–**V**.

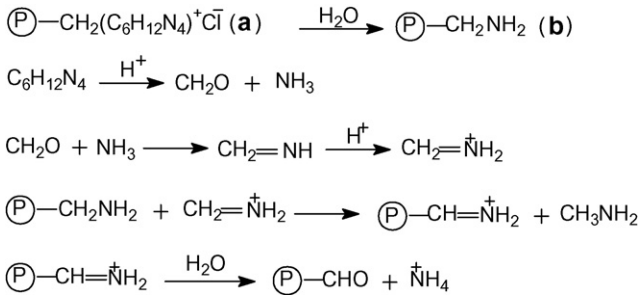

Scheme 2. The formation mechanism of resin **I**.

characteristic absorbance of benzenesulfonate. In the spectrum of resin **V**, the absorption bands at 1455 and 1424 cm^{-1} due to the skeletal vibration of the benzothiazole group were observed [18]. Sulphur content for resin **V** was 13.47%, which meant the functional group of MBZ was 1.40 mmol g^{-1}.

The chemical stability was evaluated by measuring the change of adsorption capacity of the resin for Hg^{2+} after successive contact of the resin with acid or alkali solutions in the various concentration ranges. No obvious decrease in the adsorption capacity of Hg^{2+} was observed. These experimental results indicated that the resin was sufficiently stable in acidic and alkaline solutions.

The adsorption kinetic of the resin for Hg^{2+} and Ag^{+} was determined at the corresponding pH of maximum adsorption. The results were shown in Fig. 2. The $t_{1/2}$ of the resin for Hg^{2+} and Ag^{+} was 30 and 35 min, respectively. The water regain value of the resin was 35.6 mmol g^{-1}. All these data showed that the resin was quite suitable for column operation at a low flow rate.

3.2. Adsorption capacities for metal ions

The adsorption capacities of the resin for different metal ions were determined by batch method at various pH values. The results were tabulated in Table 2. From Table 2, it could be noted that the adsorption capacities of the resin for the metal ions decreased in the following order: $Hg^{2+} > Ag^{+} > Cu^{2+} > Pb^{2+} > Cd^{2+} > Fe^{3+} > Ni^{2+} > Zn^{2+} > Mn^{2+}$.

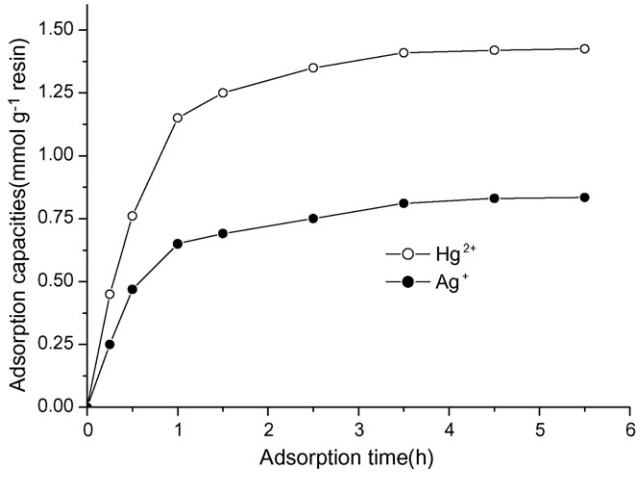

Fig. 2. Adsorption rate curve of the resin for Hg^{2+} and Ag^{+}.

Table 2
Adsorption capacity of the resin for different metal ions vs. pH (mmol g^{-1})

pH	Ag^{+}	Cu^{2+}	Hg^{2+}	Zn^{2+}	Pb^{2+}	Ni^{2+}	Cd^{2+}	Fe^{3+}	Mn^{2+}
1.0	0.71	0.58	1.49	0.09	0.13	0.11	0.15	0.18	0
2.0	0.66	0.54	1.36	0.07	0.31	0.14	0.18	0.13	0
3.0	0.71	0.51	1.23	0.05	0.27	0.07	0.24	0.17	0
4.0	0.77	0.39	1.31	0.07	0.35	0.09	0.16	0.16	0
5.0	0.95	0.47	1.28	0.08	0.25	0.19	0.35	0.21	0
6.0	0.96	0.46	1.35	0.11	0.37	0.24	0.36	0.25	0

The highest adsorption capacities for Hg^{2+} and Ag^{+} were 1.49 and 0.96 mmol g^{-1}, respectively. These results could be interpreted as follows: according to the theory of soft and hard acids and bases (SHAB), ligands with "soft" type donors prefer interactions with "soft", i.e. large and more easily polarizable, acceptors such as noble and heavy metal ions [26]. The functional groups of sulfoxide and MBZ presented in the investigated resin belong to soft bases, thus the resin had higher adsorption capacities for Hg^{2+} and Ag^{+} than that for Cu^{2+}, Pb^{2+}, Cd^{2+}, Fe^{3+}, Ni^{2+}, Zn^{2+} and Mn^{2+}, which were base metal ions. One could observe that, Mn^{2+} was not recognized by the resin. The reason for this could be ascribe to the low accepting ability of Mn^{2+} with chelating group described by Irving-Williams series [27].

As could be seen in Table 2, the pH values had a slight effect on the adsorption capacities of the resin for the metal ions. The maximum adsorption capacities of the metal ions were obtained under the optimal pH 1.0 for Hg^{2+} and Cu^{2+}, 6.0 for Ag^{+}, Pb^{2+}, Cd^{2+}, Ni^{2+}, Zn^{2+} and Fe^{3+} in this paper.

3.3. Separation of Hg^{2+} and Ag^{+} from alkali and alkaline earth metal ions

Separation of Hg^{2+} and Ag^{+} from several binary mixtures with alkali and alkaline earth metal ions at their corresponding maximum pH was carried out. The recovery of Hg^{2+} and Ag^{+} were 100% and 96+%, respectively. As could be expected that, the presence of large excess of alkali and alkaline earth metal ions did not affect the recovery of Hg^{2+} and Ag^{+} from the solution, which meant that the resin could be used for removal of trace mercury and silver from natural samples.

3.4. Separation of Hg^{2+} and Ag^{+} from binary mixtures

The ability to remove particular metal ions selectively from aqueous solution under competitive condition is of utmost importance in designing a resin for environmental remediation applications. The recovery of Hg^{2+} and Ag^{+} by the resin in the presence of diverse metal ions such as Cu^{2+}, Zn^{2+}, Pb^{2+}, Ni^{2+}, Cd^{2+}, Fe^{3+} and Mn^{2+} was determined by batch and column method. The results were shown in Table 3. From Table 3, it could be seen that the recovery of the resin for Hg^{2+} and Ag^{+} was 96.3+%, 94.5+%, respectively. The experimental results showed that the resin could remove Hg^{2+} and Ag^{+} from aqueous solution quantitatively, even in the presence of two-fold excess of competing metal ions.

Table 3
Separation of Hg^{2+} and Ag^{+} from binary mixtures at corresponding pH of maximum adsorption[a]

Metal ion	Recovery (%)			
	Ag(I)		Hg(II)	
	Batch method	Column method	Batch method	Column method
Cu^{2+}	95.7 ± 1.5	97.0 ± 2.3	97.5 ± 1.3	98.6 ± 1.4
Zn^{2+}	98.3 ± 1.4	98.6 ± 2.7	98.8 ± 2.9	99.0 ± 3.4
Pb^{2+}	95.4 ± 1.1	100 ± 2.6	100 ± 1.5	99.6 ± 2.3
Ni^{2+}	98.8 ± 2.3	98.7 ± 3.1	98.7 ± 4.2	99.4 ± 2.7
Cd^{2+}	98.9 ± 3.5	97.6 ± 2.5	98.5 ± 2.3	98.6 ± 3.4
Mn^{2+}	97.1 ± 2.3	98.3 ± 1.4	99.2 ± 1.8	100 ± 5.6
Fe^{3+}	95.3 ± 1.6	94.5 ± 2.0	96.3 ± 3.3	97.8 ± 4.3

[a] The amount of Hg^{2+} and Ag^{+} in binary mixture was 250 μg and the amount of interferences such as Cu^{2+}, Zn^{2+}, Pb^{2+}, Ni^{2+}, Cd^{2+}, Fe^{3+} and Mn^{2+} was 500 μg, respectively.

Table 4
Recovery of Hg^{2+} from natural waters and industrial wastewater

Sample	Measured value (μg l^{-1})	Amount spiked (μg)	Amount recovered (μg)	Recovery (%)
River water	0.1	50.0	49.6 ± 3.9	99.2 ± 7.8
River water	0.1	100.0	98.5 ± 1.5	98.5 ± 1.5
Ground water	0.05	50.0	50.0 ± 1.8	100.0 ± 3.6
Ground water	0.05	100.0	99.1 ± 1.9	99.1 ± 1.9
Wastewater	538.4	–	50.0 ± 2.3	92.9 ± 2.3

3.5. Removal of Hg^{2+} from natural waters and industrial wastewater

Experiments on the recovery of Hg^{2+} were carried out using column method. Before the natural waters and industrial wastewater were used, the contents of Hg^{2+} were determined by using Semi-automatic sequential injection hydride generation double-channel atomic fluorescence spectrometer and FAAS. From Table 4, it could be seen that the recovery of Hg^{2+} was 92.9+%, which meant the trance amount of Hg^{2+} could be recovered quantitatively with the resin from natural waters and industrial wastewater.

4. Conclusions

A new chelating resin containing bis[2-(2-mercaptobenzothiazolylethyl)sulfoxide] was synthesized and characterized. It was stable in acidic and alkaline medium. The resin had high affinity for Hg^{2+} and Ag^{+}. The presence of alkali or alkaline earth metal ions such as Na^{+}, Mg^{2+}, Ca^{2+} and Ba^{2+} had no effect on the recovery of Hg^{2+} and Ag^{+}. This resin could efficiently remove Hg^{2+} and Ag^{+} from binary mixtures in batch and column method. The recovery of the resin for Hg^{2+} and Ag^{+} were 96.3+% and 94.5+%, respectively. The recovery of Hg^{2+} from spiked natural waters and industrial wastewater was 92.9+%.

Acknowledgements

The authors are grateful for the financial support by the Nature Science Foundation of Shandong Province (No. Y2005F11), the Postdoctoral Science Foundation of China (No. 2003034330), the Nature Science Foundation of Ludong University (Nos. 032912, 20052901, 042920).

References

[1] D.E. Leyden, W. Wegscheider, Anal. Chem. 53 (1981) 1059A.
[2] C. Kantipuly, S. Katragadda, A. Chow, H.D. Gesser, Talanta 37 (1990) 491.
[3] G. Schmuckler, Talanta 10 (1963) 745.
[4] G.V. Myasoedova, O.P. Eliseeva, S.B. Savvin, J. Anal. Chem. 26 (1971) 1939.
[5] R.A. Beauvais, S.D. Alexandratos, React. Funct. Polym. 36 (1998) 113.
[6] P. Chattopadhyay, C. Sinha, D.K. Pal, Fresenius J. Anal. Chem. 357 (1997) 368.
[7] D. Das, A.K. Das, C. Sinha, Talanta 48 (1999) 1013.
[8] Y.Y. Chen, B.X. Lu, X.W. Chen, J. Macromol. Sci. Chem. A25 (1988) 1443.
[9] K. Brajter, E.D. Zlotorzynska, Analyst 113 (1988) 1571.
[10] J.P. Collman, R.R. Gagne, J. Kouba, H. Lausberg-Wahren, J. Am. Chem. Soc. 96 (1974) 6800.
[11] S. Pramanik, P.K. Dhara, P. Chattopadhyay, Talanta 63 (2004) 435.
[12] N.L. Filho, Y. Gushikem, W.L. Polito, J.C. Moreira, E.O. Ehirim, Talanta 42 (1995) 1625.
[13] R.S. Praveen, P. Metilda, S. Daniel, T. Prasada Rao, Talanta 67 (2005) 960.
[14] K. Terada, K. Matsumoto, H. Kimura, Anal. Chim. Acta 153 (1983) 237.
[15] Q. Pu, Q. Sun, Z. Hu, Z. Su, Analyst 123 (1998) 239.
[16] N.L. Filho, Y. Gushikem, W.L. Polito, Anal. Chim. Acta 306 (1995) 167.
[17] J. Chwastowska, A. Rogowska, E. Sterlinska, J. Dudek, Talanta 49 (1999) 837.
[18] C.N. Ji, R.J. Qu, C.M. Sun, C.H. Wang, Y.Z. Sun, N. Zhao, H.M. Xie, J. Appl. Polym. Sci. 100 (2006) 5034.
[19] A.W. Trochimczuk, Eur. Polym. J. 34 (1998) 1657.

[20] A.W. Trochimczuk, B.N. Kolarz, Eur. Polym. J. 36 (2000) 2359.
[21] D. Prrabhakaran, M.S. Subramanian, Talanta 65 (2005) 179.
[22] J. Jezierska, A.W. Trochimczuk, J. Kedzierska, J. Polym. 40 (1999) 3611.
[23] M.J. Chen, C.Y. Liu, J. Chin. Chem. Soc. 46 (1999) 833.
[24] R.J. Qu, C.M. Sun, C.H. Wang, C.N. Ji, Y.Z. Sun, L.X. Guan, M.Y. Yu, G.X. Cheng, Eur. Polym. J. 41 (2005) 1525.
[25] Y.Z. Shi, X.Z. Sun, Y.H. Jiang, T.N. Zhao, H.X. Zhu, Spectroscopy and Chemical Identification of Organic Compounds, Jiangsu Science and Technology Press, Jiangsu Province of China, 1988, p. 138.
[26] R.G. Pearson, J. Am. Chem. Soc. 85 (1963) 3533.
[27] R.W. Stanley, G.E. Cheney, Talanta 13 (1966) 1619.

Available online at www.sciencedirect.com
ScienceDirect
Talanta 73 (2007) 352–357
Talanta
www.elsevier.com/locate/talanta

DRC™ ICP-MS coupled with automated flow injection system with anion exchange minicolumns for determination of selenium compounds in water samples

Kritsana Jitmanee [a,b,*,1], Norio Teshima [a], Tadao Sakai [a,**], Kate Grudpan [b]

[a] *Department of Applied Chemistry, Aichi Institute of Technology, 1247 Yachigusa, Yakusa-cho, Toyota 470-0392, Japan*
[b] *Department of Chemistry, Faculty of Science, Chiang Mai University, Chiang Mai 50200, Thailand*

Received 28 December 2006; received in revised form 27 March 2007; accepted 27 March 2007
Available online 3 April 2007

Abstract

A flow injection system with anion exchange resin minicolumns was coupled with dynamic reaction cell (DRC™) ICP-MS for the determination and speciation of selenite and selenate at sub $\mu g\,L^{-1}$ levels. The charged selenate and uncharged selenite were separated on the first resin column in which only selenate was retained. The unretained selenite was then deprotonated with alkaline solution, and the resulting anionic selenite species was collected on the second column serially connected downstream. By setting a sample loop, total selenium can be determined together with selenite and selenate. The selenium species was eluted by nitric acid and carried to DRC™ ICP-MS for their detection. Using ammonia as reaction gas, the detection of ^{78}Se was improved. The enrichment factor was 20 for 10 mL of sample. The standard deviations ($n=5$) of peak heights were 4.9%, 4.1%, and 7.0% for a $5.0 \times 10^{-2}\ \mu g\,L^{-1}$ selenite and selenate, and total Se, respectively. The calibration graphs were linear from 2.0×10^{-2} to $1.0\ \mu g\,L^{-1}$ selenite and selenate. And, the linearity for total selenium was good in the range of 10.0×10^{-2} to $1.0\ \mu g\,L^{-1}$. The proposed method has been demonstrated for the application to natural and bottled drinking water samples.

Keywords: DRC™ ICP-MS; Speciation; Inorganic selenium; Selenite and selenate; Automated flow injection system; Anion exchange resin minicolumn

1. Introduction

Selenium is an essential nutrient which has been concerned with the cancer prevention [1,2] and its metabolic pathway in human body has been reported [3]. The guideline level of selenium in drinking water set by WHO [4] was $10\ \mu g\,L^{-1}$ and recently has been revised to be about $5\ \mu g\,L^{-1}$ by USEPA [5].

Selenium speciation is currently of interest. In natural water, inorganic selenium species, i.e. selenite and selenate, while organic selenium such as selenocystine could be found.

Recently, the speciation of selenium species, especially organic species in biological/clinical samples has been focused [6–10]. Selenite (Se(IV)) and selenate (Se(VI)) present as anions in environmental water and these species may enter in other biological and physiological systems. Therefore, it is interesting in the speciation of inorganic and organic selenium in environmental water samples.

The frequently used techniques for speciation of selenium species are the chromatographic separation, i.e. HPLC, IC, coupled with atomic spectrometric detection such as AAS, AFS, ICP-AES and ICP-MS. Guerin et al. [11] have reviewed the HPLC separation techniques with hyphenation for speciation of arsenic and selenium species. And also, their applications on the selenium determination and speciation with hyphenation have been reviewed [12]. The concentration of selenium in natural water is quite low, i.e. several $\mu g\,L^{-1}$ to sub $\mu g\,L^{-1}$ level. Accordingly, it is difficult to determine selenium directly in such samples. Since selenium, especially inorganic Se(IV), is able to form hydride, hydride generation techniques are usually employed for improvement of sensitivity.

* Corresponding author at: Department of Applied Chemistry, Aichi Institute of Technology, 1247 Yachigusa, Yakusa-cho, Toyota 470-0392, Japan. Tel.: +81 565 48 8121; fax: +81 565 48 0076.
** Corresponding author. Tel.: +81 565 48 8121; fax: +81 565 48 0076.
E-mail addresses: jitmanee@chiangmai.ac.th (K. Jitmanee), tadsakai@aitech.ac.jp (T. Sakai).
[1] On leave from Department of Chemistry, Faculty of Science, Chiang Mai University, Chiang Mai, Thailand.

0039-9140/$ – see front matter © 2007 Elsevier B.V. All rights reserved.
doi:10.1016/j.talanta.2007.03.054

Some interesting preconcentration methods have been proposed for the determination of selenium species in environmental water samples [13] including solid-phase extraction (SPE) which is useful for the collection and high enrichment factor of analytes. Ion exchange, chelating and hydrophobic resins are also of interest.

The on-line simultaneous preconcentration of selenite and selenate using strong anion exchange resin column prior to liquid chromatographic separation and ICP-MS detection was reported [14]. Chelating resin such as Amberlite IRA-743 was used for collection of several selenium species prior to analysis by HPLC-ICP-MS [15]. However, the elution of selenium species is complicated. Coupling the anion exchange resin with C_{18} cartridge has been reported for preconcentration of inorganic and volatile organic selenium species before separation and quantification with GC–MS [16]. However, the derivatization step was required and the 1000 mL sample was used for sensitivity enhancement. 3-Mercaptopropyl-trimethoxylane modified silica gel [17], Fe(III) loaded Chelex-100 resin [18] and activated alumina [19,20] have been reported for the reactive selenite species. However, two different eluents were required for selective elution of selenite and selenate.

The on-line dual solid-phase columns-in-valve has shown its potential for speciation analysis [21–23]. Therefore, it is possible to employ such concept for the pre-concentration and speciation of selenite and selenate by ICP-MS.

We propose a new automated flow injection system using four valves with anion exchange resin minicolumn coupled with DRC^{TM} ICP-MS for speciation of total selenium, selenite, and selenate. The separation is based on the formation of charged selenate ($HSeO_4^-$) and uncharged selenite (H_2SeO_3) at difference pH values.

2. Experimental

2.1. Reagents

A 1000 mg L^{-1} (as Se) stock solution of selenite was prepared by dissolving sodium selenite (99.999%: Sigma–Aldrich) in water. Ultra-purified water obtained by an Elix 3/Milli-Q Element System (Nihon Millipore, Japan) was used. Similarly, a 1000 mg L^{-1} (as Se) stock solution of selenate was prepared by dissolving sodium selenate decahydrate (99.999%: Sigma–Aldrich) in water. Accurately diluted solutions of selenite and selenate were prepared daily. An ammonia solution was prepared from concentrated ammonia (28% extra pure reagent: Nacalai Tesque, Japan). Ammonium acetate solutions were prepared by dissolving ammonium acetate (>97.0% analytical-reagent: Sigma–Aldrich Japan, Tokyo) in water and adjusted to a desired pH with concentrated ammonia or glacial acetic acid (99–100% super special grade: Wako Pure Chemical Industries, Osaka). The eluent was obtained by mixing nitric acid (61% analytical-reagent: Sigma–Aldrich Japan, Tokyo) with methanol (99.0% extra pure reagent: Nacalai Tesque, Kyoto) and diluted with water. An anion exchange resin Muromac® 2 × 8, 100–200 mesh in Cl-form (Muromachi Technos Co., Japan) was used for collection of selenite and selenate.

2.2. Apparatus and flow manifold

The flow set up for speciation of total selenium, selenite, and selenate was assembled as depicted in Fig. 1. The solid-phase extraction resin column (SPERC) was prepared by packing the anion exchange resin into the PTFE tubing (2 mm i.d. × 5 cm) with the plugs of cotton wool at both ends. Smaller PTFE tubings (0.5 mm i.d.) were tightly inserted into this column to be placed on the valve. SPERCs were pre-washed with 2.0 M nitric acid. ICP-MS, ELAN® DRC II (PerkinElmer-SCIEX^{TM} Instruements, Concord, Ontario, Canada) equipped with a quartz cyclonic spray chamber and concentric nebulizer was used and it was operated in the dynamic reaction cell mode (DRC) and ammonia gas was used as reaction gas for reduction/elimination of plasma based interferences. The instrument conditions are summarized in Table 1. A peristaltic pump (P3) was used to propel an eluent. Two peristaltic pumps (model U4-MIDI, Alitea, Sweden) were used for introduction of conditioning/washing solution and sample (P1), and ammonia solution (P2). A 6-port selection valve (C25-3186EMH) and three 6-port injection valves (C22-3186 EH) were of Valco Instruments Co., Inc. The data acquisition card (DAQCard-DIO-24) and connector block (CB-50LP I/O) were of National Instruments Corps, TX, USA.

Control of valves (V2, V3, and V4) and pumps (P1 and P2) was achieved via a data acquisition card (DAQCard-DIO-24) and connector block (CB-50LP I/O). The communication of valves and pumps was depicted as shown in Fig. 2. LabVIEW^{TM} (National Instrument Corps, TX, USA), a programming language, was employed for developing analytical-devices-controller software.

2.3. Analytical procedures

Tables 1 and 2 describe the operating conditions of DRC^{TM} ICP-MS and operating steps of flow injection solid-phase extraction system, respectively. The speciation system for total selenium, selenite, and selenate determinations consists of eight steps. Briefly, 0.03 M HNO_3 (pH 1.5) is selected (by valve V1) to flow through the system for 45 s and follows by the sample loading step by which V1 is switched for introducing the sample solution (pH 1.5 by adding with HNO_3) for 300 s. Thereafter, the

Table 1
Operating conditions of DRC^{TM} ICP-MS

Parameters	Conditions
ICP-MS	Perkin-Elmer SCIEX, ELAN DRC II
Argon gas flow rate	
Plasma gas	15 L min^{-1}
Auxiliary gas	1.375 L min^{-1}
Nebulizer gas	0.9 L min^{-1}
RF power	1.3 kW
Dynamic reaction cell	
Cell gas/flow rate	NH_3/0.3 mL min^{-1}
RPa/RPq value	0/0.6
Monitored isotope	^{78}Se
Dwell time	980 ms (2 s/data point)

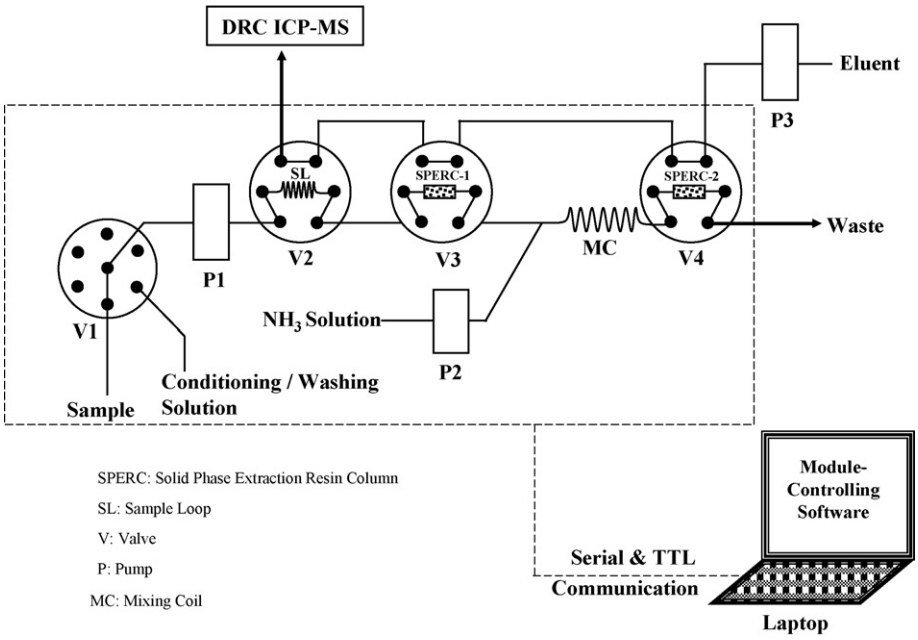

Fig. 1. Flow set up with solid-phase extraction resin columns coupled with DRC™ ICP-MS for speciation of selenium (see text).

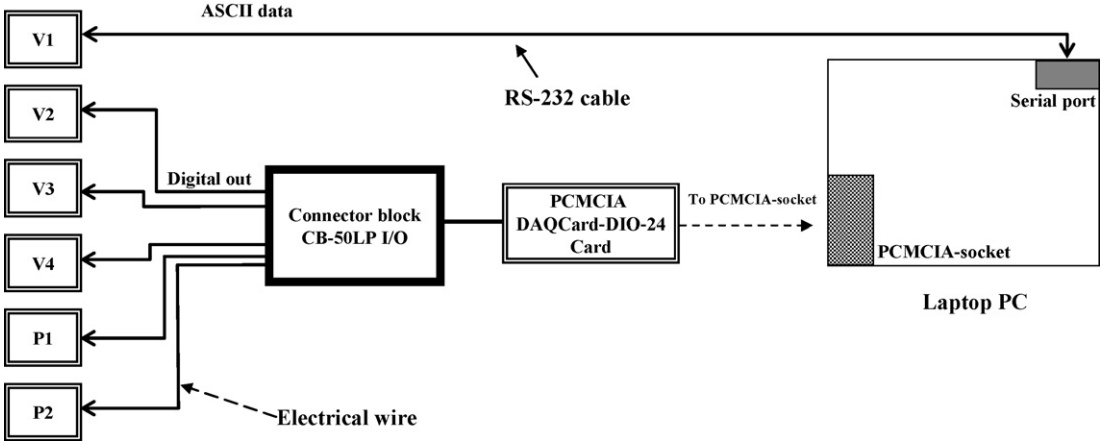

Fig. 2. Buses connection of devices with Laptop PC.

injection/washing steps are performed by switching the position of V1 to position 1 and of V2 to inject position. This switching of V1 is corresponding to the washing of matrix whereas of V2 is corresponding to the injection of sample in the sample loop for total selenium measurement. Selenium species are eluted from both SPERCs effectively by nitric acid. The elution is performed by the switching of V4 to inject position for 120 s, which is resulting in desorption of selenite from the SPERC-2. There-

Table 2
Operating steps of sample pretreatment system

Operating steps	Solution	Position of valves				Function of pumps		Delay time (s)
		V1	V2	V3	V4	P1	P2	
1. Conditioning	Dil. HNO_3, pH 1.5	1	Load	Load	Load	On	On	45
2. Sample loading	Sample, pH 1.5	2	Load	Load	Load	On	On	300
3. Injection and washing	Injection, 1 M HNO_3/2% CH_3OH; Washing, Dil. HNO_3, pH 1.5	1	Inject	Load	Load	On	On	60
4. Elution 1; for selenite	1 M HNO_3/2% CH_3OH	1	Load	Load	Inject	Off	Off	120
5. Elution 2; for selenate	1 M HNO_3/2% CH_3OH	1	Load	Inject	Load	Off	Off	120
6. Line washing 1	New sample, pH 1.5	2	Inject	Inject	Inject	On	On	20
7. Line washing 2	Dil. HNO_3, pH 1.5	1	Load	Load	Load	On	On	90
8. Ready	–	1	Load	Load	Load	Off	Off	2

after, the V3 is switched to inject position for elution of selenate from the SPERC-1. Each eluate is introduced to ICP-MS. We used one port (port 2) for introducing samples and therefore, the steps 6 and 7 are necessary for analysis of next sample.

2.4. Sample preparation

Tap water was taken in our laboratory and the bottled drinking water samples were purchased from a super market. After sampling, concentrated nitric acid was added to the sample for lowering pH to 1.5 (2.5 mL/1000 mL sample). It was filtered through the membrane filter (mixed cellulose ester, 0.45 μm, Advantec, Toyo Roshi Kaisha, Ltd., Japan). All samples were kept in a refrigerator and analyzed as soon as possible.

3. Results and discussion

3.1. Instrumental parameter on reaction gas flow rate

The dynamic reaction cell (DRC) technology is useful for removing/eliminating plasma-based interferences. Therefore, the reduction of interferences was studied for the detection of Se. The plasma-based interferences such as $^{40}Ar^{37}Cl$ for ^{77}Se, $^{40}Ar^{38}Ar$ for ^{78}Se, $^{40}Ar^{40}Ar$ for ^{80}Se and $^{40}Ar_2{}^2H$ for ^{82}Se, affect directly to the accuracy and sensitivity of the ICP-MS measurement. By using a 10.0 $\mu g\,L^{-1}$ standard selenium solution prepared in 0.1 M HCl, the effect of flow rate of ammonia reaction cell gas was studied for elimination of interferences. As shown in Fig. 3, increasing in the flow rate of ammonia gas from 0 to 1.0 mL min^{-1} decreased the background signal of ^{77}Se, ^{78}Se, ^{80}Se, and ^{82}Se drastically, however, decrease in the sample signal was observed as well. At a flow rate of 0.3 mL min^{-1}, the background signal at *m/z* of 77, 78 and 82 were greatest reduced and it gave the high net signal of sample. Effective reduction of the background signal at *m/z* of 80 required a higher ammonia gas flow rate of 0.6 mL min^{-1}, but this led to much reduction in the signal of sample, too. Therefore, a flow rate of 0.3 mL min^{-1} was used to detect selenium at the less abundant isotope ^{78}Se (23.8% abundance).

3.2. Design of automated flow injection system with anion exchange resin columns

LabVIEW™, an established graphical programming language, has been useful to automate an analytical system [24–27]. An in-house developed devices-controller software employing LabVIEW™ was designed for the electric actuation of valves (V1, V2, V3, and V4) and for turning on/off of peristaltic pumps (P1 and P2). Valves (V2, V3, V4) and pumps (P1 and P2) were actuated and activated, respectively. All connections were achieved via the interface (DAQCard-DIO-I/O and connector block) (see Fig. 2).

The software also sent the commands in ASCII format to the valve V1 via an RS-232 for actuation of valve (port changing). Although all the valves in this study can be controlled using serial communication, the USB-to-Serial cables are necessary for adding the addition serial ports to laptop PC. A digital I/O interface (NI DAQCard-DIO-24, National Instrument, USA) was employed.

3.3. Collection of selenite and selenate

The separation and concentration of selenite and selenate are feasible by different acid dissociation constants (pK_a). The pK_{a1} and pK_{a2} values of selenite are 2.62 and 8.32 and of selenate are <1 and 1.7 [28]. Therefore at pH of ca. 1.5, selenate presents

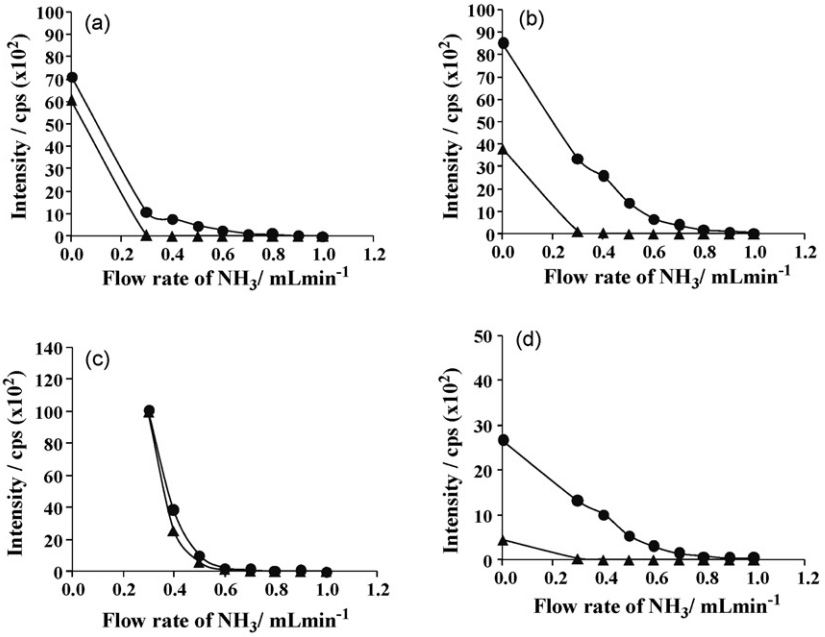

Fig. 3. Effect of cell gas flow rate on intensity of Se. (a) ^{77}Se; (b) ^{78}Se; (c) ^{80}Se; (d) ^{82}Se. The circle and triangle symbols represent for sample and reagent blank, respectively.

mainly as $HSeO_4^{-1}$ while selenite was uncharged, H_2SeO_3. Both species should be able to separate by using ion exchange resin where charged selenate species could be retained. On the other hand, uncharged selenite should not be retained on the anion exchange resin. Employing the manifold in Fig. 1, selenate was collected on SPERC-1 whereas selenite was collected on SPERC-2 after deprotonation by raising pH above its pK_a value. Muromac® 2 × 8, 100–200 mesh was preferable for collection of selenite and selenate.

3.4. Study of flow injection parameters for collection/concentration of selenite and selenate

In order to raise the pH of effluent from SPERC-1, three alkaline solutions were examined for 5.0 μg L^{-1} selenite. By using 0.05 M ammonium acetate at pH 7.0, 9.7 and 0.5% (v/v) ammonia solution, pH of the effluent from SPERC-2 at a flow rate of 0.5 mL min^{-1} was checked. The resulting pH values were 3.8, 5.6 and 9.3. Using 0.5% (v/v) ammonia solution, the signals due to sample loading time of 4 min at flow rate of 1 mL min^{-1} was higher than that of the ammonium acetate solutions. Therefore, 0.5% (v/v) ammonia solution was selected for further use.

The effect of the concentration of ammonia solution on the pH of effluent from SPERC-2 was studied. The pH of effluent from SPERC-2 was found to be 2.0, 2.3, 9.5 and 9.9 when the ammonia solution at a concentration of 0.1, 0.3, 0.5 and 1.0% (v/v) was used. An ammonia solution concentration of 0.5% (v/v) was selected for raising the pH of effluent from SPERC-1 above pK_{a2} of selenite.

The length of mixing coil, MC in Fig. 1, was investigated for mixing ammonia solution and the effluent from SPERC-1, which would affect the retention of selenite at SPERC-2. The length (PTFE tubing, 0.5 mm i.d.) was varied in the range of 2–8 m. A length of 5 m resulted in the highest signal of selenite. With further increase in the length (8 m), peak area remained constant whereas the peak height decreased slightly. Therefore, a 5 m length was selected.

The elution of selenium species from SPERC was performed using nitric acid. Selenium anion species is protonated by acidic solution and therefore it can be eluted from anion exchange resin easily. However, the ionic strength of the acid solution would play an important role for the elution based on ion-exchange mechanism. The concentration of nitric acid was investigated in the range of 0.1–2.0 M for effective elution of the selenium species. The 20 ng (2.0 mL of 10.0 μg L^{-1}) of selenite and selenate were effectively eluted by nitric acid at a concentration above 0.5 M. However, considering the possibly co-existing anionic species in a sample such as sulphate, phosphate, etc., which retain on the anion exchange resin strongly, 1.0 M nitric acid was selected.

The time period for introducing the sample to the system should involve the detection sensitivity. A solution containing 1.0 μg L^{-1} of both selenite and selenate at a flow rate of 1.0 mL min^{-1} was introduced and the effect to the signals, peak area and peak height, was investigated. As a result, the signals for selenite and selenate gradually increased for 2–10 min. For the sensitive detection of selenium at a level below 10.0×10^{-2} μg L^{-1}, the sample introduction time of 10 min was selected.

The organic solvent such as methanol was added to enhance the detection sensitivity of selenium [29,30]. In this work, the effect of methanol concentration in 1.0 M nitric acid was studied in the range of 0.5–3% (v/v). The results showed that the signal of selenium increased with increasing the concentration of methanol while the baseline background signal and noise decreased. The highest signal of selenium was obtained using methanol of 2%, but the signal decreased when a methanol concentration being over 2%. Two percent methanol was therefore selected.

The flow rates of sample and of the washing/conditioning solutions were varied from 0.5 to 2.0 mL min^{-1}. As results, a flow rate of 2.0 mL min^{-1} which provided effective analysis time was selected for sample, washing/condition solution. By injecting the sample via the loop of the valve V2, the total selenium is directly detected by DRC™ ICP-MS. The effect of volume of sample injected into the carrier stream (1.0 M nitric acid/2% methanol, a flow rate of 1.0 mL min^{-1}) was studied. For 10.0×10^{-2} μg L^{-1} selenium, the peak of Se could not be observed when using a loop of 50 μL. By increasing the loop to 100 μL, the peak of Se (total Se) could be detected. However, the peak became broad for a volume over 200 μL. A sample loop of 100 μL was selected.

3.5. Analytical characteristics of the proposed system and application to water samples

Under the selected conditions for the system (Fig. 1), typical flow signals of selenium species correspond to the total selenium, selenite and selenate are illustrated in Fig. 4.

The calibration graphs, using 10 mL of sample, were linear in the range of 2.0×10^{-2} to 1.0 μg L^{-1} for selenite and selenate and 10.0×10^{-2} to 1.0 μg L^{-1} for total Se. The cal-

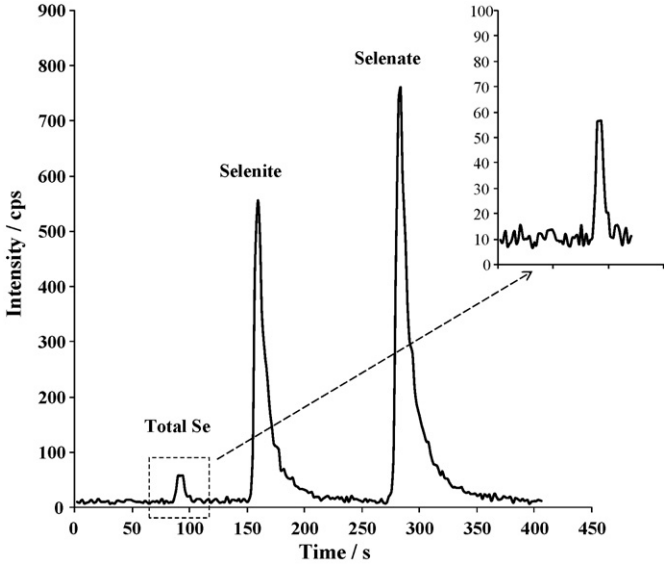

Fig. 4. Flow signals of standard solution of 20.0×10^{-2} μg L^{-1} selenite and selenate (40.0×10^{-2} μg L^{-1} for total Se). The asset shows the enlarge scale of total-Se peak.

Table 3
Determination of selenium species in water samples

Sample	Add ($\times 10^{-2}$ μg L^{-1})			Found ($\times 10^{-2}$ μg L^{-1}) ($n=3$)			Recovery		
	Total Se	Selenite	Selenate	Total Se	Selenite	Selenate	Total Se	Selenite	Selenate
Tap water	–	–	–	<LOD	1.3 ± 0.1	1.8 ± 0.1	–	–	–
	10.0	5.0	5.0	11.2 ± 1.4	6.7 ± 0.1	6.6 ± 0.5	–	108	96
Bottled drinking water A	–	–	–	<LOD	1.3 ± 0.2	5.8 ± 0.2	–	–	–
	10.0	5.0	5.0	16.2 ± 1.0	6.3 ± 0.2	10.0 ± 0.6	–	100	84
Pond water A	–	–	–	9.7 ± 0.8	2.1 ± 0.0	3.6 ± 0.2	–	–	–
	10.0	5.0	5.0	19.3 ± 1.3	7.2 ± 0.2	8.0 ± 0.3	96	102	88
River water	–	–	–	12.3 ± 0.2	3.9 ± 0.1	7.9 ± 0.1	–	–	–
Mt. River water	–	–	–	<LOD	<LOD	6.8 ± 0.1	–	–	–
Pond water B	–	–	–	<LOD	<LOD	2.1 ± 0.2	–	–	–
Well water	–	–	–	16.7 ± 1.6	1.3 ± 0.1	14.8 ± 0.4	–	–	–
Bottled drinking water B	–	–	–	13.8 ± 0.8	<LOD	12.9 ± 0.4	–	–	–
Bottled drinking water C	–	–	–	<LOD	1.2 ± 0.1	3.2 ± 0.2	–	–	–

ibration equation of $Y = 2.86 \times 10^3 X - 0.577$; $r^2 = 0.9999$ for selenite, $Y = 3.76 \times 10^3 X - 10.7$; $r^2 = 0.9999$ for selenate, and $Y = 1.48 \times 10^2 X - 1.89$; $r^2 = 0.9988$ for total selenium, were obtained where Y, X and r^2 are the peak height (count s^{-1}), the concentration in μg L^{-1} and the correlation coefficient, respectively. The limits of detection (LOD) based on the 3-S/N criteria were 0.9×10^{-2}, 0.7×10^{-2}, and 8.0×10^{-2} μg L^{-1} for selenite, selenate, and total selenium. The proposed system was applied to water samples. The results are summarized in Table 3.

4. Conclusion

A flow injection system with solid-phase extraction resin columns coupled with DRC^{TM} ICP-MS was proposed for speciation of inorganic selenium, selenite and selenate. The on-line flow injection pre-concentration column system can improve sensitivity for selenium. The automated analytical system using the in-house writing software has the benefit for the inattention operation with sample throughputs of about 5 h^{-1}. Total selenium, selenite, and selenate can be determined in a single analysis run. Applications have been demonstrated to uncontaminated water samples, such as natural and bottled drinking water.

Acknowledgements

The present work was partly supported by a grant of the Frontier Research Project "Material for the 21st Century-Materials Development for Environment, Energy and Information" (for 2002–2006 fiscal years) from Ministry of Education, Culture, Sports, Science and Technology, Japan. The authors would like to thank Dr. Narong Lenghor and Mr. Lucksagoon Ganranoo for kind help on electronics and programming software.

References

[1] R. Abdulah, K. Miyazaki, M. Nakazawa, H. Koyama, J. Trace Elem. Med. Biol. 19 (2005) 141.
[2] D.W. Nyman, M.S. Stratton, M.J. Kopplin, B.L. Dalkin, R.B. Nagle, A.J. Gandolfi, Cancer Detect. Prev. 28 (2004) 8.
[3] K.T. Suzuki, J. Health Sci. 51 (2005) 107.
[4] World Health Organization (WHO), http://www.who.int/, last accessed March 24, 2007.
[5] The US Environmental Protectin Agency (US EPA), http://www.epa.gov/, last accessed March 24, 2007.
[6] O. Palacios, J.R. Encinar, G. Bertin, R. Lobinski, Anal. Bioanal. Chem. 383 (2005) 516.
[7] V. Gergely, K.M. Kubachka, S. Mounicou, P. Fodor, J.A. Caruso, J. Chromatogr. A 1101 (2006) 94.
[8] I. Lavilla, A. Mosquera, J. Millos, J. Cameselle, C. Bendicho, Anal. Chim. Acta, in press.
[9] E. Dumont, Y. Ogra, K.T. Suzuki, F. Vanhaecke, R. Cornelis, Anal. Chim. Acta 554 (2005) 123.
[10] A.P. Vonderheide, S. Mounicou, J. Meija, H.F. Henry, J.A. Caruso, J.R. Shann, Analyst 131 (2006) 33.
[11] T. Guerin, A. Astruc, M. Astruc, Talanta 50 (1999) 1.
[12] J.L. Capelo, C. Fernandez, B. Pedras, P. Santos, P. Gonzalez, C. Vaz, Talanta 68 (2005) 1447.
[13] B.D. Wake, A.R. Bowie, E.C.V. Butler, P.R. Haddad, Trends Anal. Chem. 23 (2004) 516.
[14] Y. Cai, M. Cabnas, J.L. Fernandez-Turiel, M. Abalos, J.M. Bayona, Anal. Chim. Acta 314 (1995) 183.
[15] M. Bueno, M. Potin-Gautier, J. Chromatogr. A 963 (2002) 185.
[16] J.L. Gomez-Ariza, J.A. Pozas, I. Giraldez, E. Morales, Analyst 124 (1999) 75.
[17] F. Sahin, M. Volkan, A.G. Howard, O.Y. Ataman, Talanta 60 (2003) 1003.
[18] T. Ferri, P. Sangiorgio, Anal. Chim. Acta 321 (1996) 185.
[19] K. Pyrzynska, P. Drzewicz, M. Trojanowicz, Anal. Chim. Acta 363 (1998) 141.
[20] A. Larraya, M.G. Cobo-Fernandez, M.A. Palacios, C. Camara, Fresenius' J. Anal. Chem. 350 (1994) 667.
[21] K. Jitmanee, M. Oshima, S. Motomizu, Talanta 66 (2005) 529.
[22] S. Motomizu, K. Jitmanee, M. Oshima, Anal. Chim. Acta 499 (2003) 149.
[23] K. Jitmanee, M. Oshima, S. Motomizu, J. Flow Injection. Anal. 21 (2004) 49.
[24] A.R. Bowie, E.P. Achterberg, S. Ussher, P.J. Worsfold, J. Autom. Methods Manage. Chem. 2005 (2005) 37.
[25] J. Jakmunee, L. Patimapornlert, S. Suteerapataranon, N. Lenghor, K. Grudpan, Talanta 65 (2005) 789.
[26] C.E. Lenehan, N.W. Barnett, S.W. Lewis, J. Autom. Methods Manage. Chem. 24 (2002) 99.
[27] S.-H. Lee, O.-J. Sohn, Y.-S. Yim, K.-A. Han, G.W. Hyung, S.H. Chough, J.I. Rhee, Talanta 68 (2005) 187.
[28] Handbook of Chemistry and Physics, 84th ed., CRC Press, Boca Raton, 2003–2004.
[29] E.H. Larsen, S. Sturup, J. Anal. Atom. Spectrom. 9 (1994) 1099.
[30] K. Sathrugnan, S. Hirata, Talanta 64 (2004) 237.

Available online at www.sciencedirect.com
ScienceDirect
Talanta 73 (2007) 246–250
Talanta
www.elsevier.com/locate/talanta

Determination of ochratoxin A in maize bread samples by LC with fluorescence detection

C. Juan [b], C.M. Lino [a,*], A. Pena [a], J.C. Moltó [b], J. Mañes [b], I. Silveira [a]

[a] *Group of Bromatology, CEF, Faculty of Pharmacy, University of Coimbra, Rua do Norte s/n, 3000-295 Coimbra, Portugal*
[b] *Laboratory of Food Chemistry and Toxicology, Faculty of Pharmacy, University of Valencia, Av. Vicent Estellés s/n, 46100 Burjassot, Valencia, Spain*

Received 4 January 2007; received in revised form 13 March 2007; accepted 15 March 2007
Available online 24 March 2007

Abstract

Ochratoxin A (OTA) is a secondary fungal metabolite produced by several moulds, mainly by *Aspergillus ochraceus*, *A. carbonarius*, *A. niger* and by *Penicillium verrucosum*. The present work shows the results of comparative studies using different procedures for the analysis of OTA in maize bread samples. The studied analytical methods involved extraction with different volumes of PBS/methanol, different extraction apparatus, and clean-up through immunoaffinity columns. The separation and identification were carried out by high-performance liquid chromatography with fluorescence detection. The optimized method for analysis of OTA in maize bread involved extraction with PBS:methanol (50:50), and clean-up with IAC column. The limit of quantification was 0.033 ng g^{-1}. Recoveries ranged from 87% to 102% for fortifications at 2.000 and 0.500 ng g^{-1}, respectively, within-day R.S.D. of 1.4% and 4.7%. The proposed method was applied to 15 samples and the presence of OTA was found in nine samples at concentrations ranging from nd to 2.650 ng g^{-1}.

Keywords: Ochratoxin A; Maize bread; LC

1. Introduction

OTA is mainly produced by some species of *Aspergillus* and *Penicillium,* particularly *Aspergillus ochraceus*, *A. carbonarius*, *A. niger* and *Penicillium verrucosum*. These moulds can easily contaminate foodstuffs, although the occurrence of OTA in foods may depend on climatic conditions [1].

Toxicity of OTA is well documented in many animal species, including human beings [2]. It is probably related to the Balkan endemic nephropathy (BEN), and the International Agency for Research on Cancer [3] has classified OTA as Group 2B, a possible human carcinogen. Exposure to OTA is worldwide, as known by its detection in human serum or urine of people from many countries [4].

OTA occurs predominantly in cereal grains, cereal products, cocoa, spices, oilseeds, coffee beans and legumes. However, cereal products are the major group of food commodities where the toxin is of greatest impact. The frequency of food contamination with OTA represents an important source of daily OTA intake, with consequences to human health [5]. Consequently, the European Union Scientific Committee for Human Feeding deemed necessary to take prudential measures in order to reduce the degree of exposure to OTA to levels below 5 ng/kg body weight (b.w.)/day [6].

The bread is a product of daily consumption and highly demanded; thus several authors have indicated bread as one of the main sources of daily intake of OTA [7–9]. The presence of OTA in bread results from the contamination of wheat flour, and probably only partly is destroyed during the bread making process [10].

Maize bread is a traditional and special type of bread very appreciated in Portugal, and it is consumed mainly in the North and Central Zone of country. This bread is made with cereals such as maize (*Zea mays*) and wheat (*Triticum aestivum*), where the ochratoxigenic moulds *A. ochraceus* and *P. verrucosum,* respectively, grows.

In Portugal, the agricultural production primarily consists in 1,425,000 tons of cereals such as rice (146,000 tons), maize (780,000 tons), wheat (300,000 tons) and barley (10,000 tons) [11]. According to the FAO, the consumption of cereal in

* Corresponding author. Tel.: +351 239859994; fax: +351 239827126.
E-mail address: cmlino@ci.uc.pt (C.M. Lino).

0039-9140/$ – see front matter © 2007 Elsevier B.V. All rights reserved.
doi:10.1016/j.talanta.2007.03.029

Portugal was 1,335,000 tons in 2002, and according to IACA was 152,7000 tons. The human consumption increased in the following order: barley, maize, rice and wheat [12].

Few analytical methodologies for OTA determination in bread have been reported. González et al. [13] used pressurised liquid extraction with methanol, and liquid chromatography with fluorescence detection (LC–FD) for determination. Frequently for cereals and derivatives, the common extraction methodologies are based on the solubility of OTA in organic solvents. In this way it has been used liquid extraction with different solvents such as chloroform [14,15], methanol [1,16,17] or methanol with aqueous solution bicarbonate [18,19], and acetonitrile/water mixture [20,21]. For the sample preparation and clean-up, immunoaffinity columns (IAC) [19,20], ion exchange columns [21], matrix solid phase dispersion with C_8 and C_{18} (MSPD) [22,23], solid phase microextraction (SPME) [24,25] and molecularly imprinted solid phase extraction (MISPE) [15] have been used. IAC clean-up is widely used, allowing lower limit of detection compared to MSPD clean-up with C_{18} and accurate and reproducible results [23,26]. For detection and quantification of OTA and mycotoxins in general, the methods are based on thin-layer chromatography (TLC), enzyme-linked immunosorbent assay (ELISA) [27], liquid chromatography with electrospray ionization tandem mass spectrometry (LC/ESI/MS/MS) [21] and mainly liquid chromatography with fluorescence detection (LC–FD) [19,20].

As far as we know, bread and maize bread, very much consumed in Portugal, have never been evaluated regarding OTA contamination. Furthermore, even for other countries only few papers reported OTA levels in wheat bread [10,13].

The objective in the present study was to optimize a sensitive and accurate method for determination of OTA in the maize bread samples by LC–FD, and providing data on the occurrence of OTA in 15 maize samples consumed in the central zone of Portugal.

2. Experimental

2.1. Apparatus

A Moulinex blender 700 W (230–240 V, 50–60 Hz) (Barcelona, Spain), a Braun MR 5000 M multiquick/minipimer 500 W (220–230 V, 50–60 Hz, Esplugues del Llobregat, Spain), an Ultra-Turrax homogenizer Ystral Gmbh Drive X10/25 (230 V; 50/60 H, Dottingen, Germany), a vacuum manifold of Macherey–Nagel (USA), a pump of Dinko (mod. D-95, 130 W, 220 V), a centrifuge (Meditroni S-599, Selecta, Barcelona, Spain), a magnetic stirrer (Agimatic-S, Selecta, Barcelona, Spain), a Retsh vortex mixer (Haan, Germany), and a Sonorex RK 100 ultrasonic bath (Berlin, Germany) were used.

The LC apparatus used consisted of a pump (Model 307, Gilson Medical Electronics, Villiers-le-Bel, France), one 50 μL Rheodyne injector (mod. 7125, Cotati, CA, USA), a guard column Hichrom Ltd., HI-173 (30 mm × 4 mm i.d.) (England), and a column Hichrom C_{18} (5 μm, 250 mm × 4.6 mm i.d.). A Perkin-Elmer spectrofluorimeter (Model LS 45, Perkin-Elmer, Beaconsfield, UK), operating at an excitation wavelength of 333 nm and an emission wavelength of 460 nm, was used. The spectral bandwidth was 10 nm for both excitation and emission. The mobile phase (acetonitrile/water/acetic acid 49.5:49.5:1.0, v/v/v) was maintained at a flow rate of 1 mL/min.

The results were recorded on a 3390A integrator (Hewlett-Packard, Philadelphia, PA, USA).

2.2. Chemicals

Filter paper Whatman N° 4 (150 mm Ø, Whatman International Ltd. Maidstone England) was used.

LC grade acetonitrile, methanol and toluene were purchased from Carlo Erba (Milan, Italy). Acetic acid, hydrochloride acid, sodium hydroxide, potassium chloride, potassium dihydrogenphosphate, anhydrous disodium hydrogenphosphate, and sodium chloride analytical grade were obtained from Merck (Darmstadt, Germany). Water was purified by distillation and passage through a Milli-Q system (Millipore, Bedford, MA, USA). OTA was purchased from Sigma Chemical Co. (St. Louis, MO, USA) with purity grade ≥98%. Boron trifluoride–methanol (14% solution) was obtained from Sigma Chemicals Co (St. Louis, USA).

A standard solution of OTA was prepared from the OTA vial purchased from Sigma. The standard stock solution was made in 4 mL toluene:acetic acid (99:1) at 250 μg/mL, and stored at −20 °C. An intermediate standard solution was prepared at 10 μg/mL, by diluting 1 mL of stock standard solution with 25 mL toluene:acetic acid (99:1).

For fortification assays, a standard solution was prepared in toluene:acetic acid (99:1) at 1 μg/mL and two work solutions with mobile phase at 0.025 and 0.1 μg/mL. For the calibration curve, standard solutions were prepared by evaporating 100 μL of intermediate standard solution to dryness and diluting to 10 mL with mobile phase (0.1 μg/mL). After suitable dilutions in water:methanol:acetic acid (49.5:49.5:1), the working standard solution was used to prepare solutions at10 and 5 ng/mL, and 25 μL were injected.

Phosphate buffer solution (PBS) was prepared from potassium chloride (0.2 g), potassium dihydrogen phosphate (0.2 g), anhydrous disodium hydrogen phosphate (1.2 g), and sodium chloride (8 g) added to distilled water (900 mL). After dissolution, the pH was adjusted to 7.4 (with 0.1 M HCl or 0.1 M NaOH as appropriate), and the solution was made to 1 L.

IAC Ochratest columns (Vicam, Watertown, MA, USA) were used for clean-up.

All chromatographic solvents and water were degassed for 15 min in ultrasonic bath. Decontamination of the glassware was performed using a sodium hypochlorite solution. It was then acid-washed by immersing the glassware in a solution of 4 mL/L H_2SO_4, and then washed to neutral pH by rinsing with distilled water.

2.3. Sampling

A total of 15 samples were purchased in commercially available size during September 2005 from bakeries, confectionery's shops and supermarkets located in the city of Coimbra and its

countryside, central zone of Portugal. The samples were transported to the laboratory under ambient conditions. Samples were milled using a blender Moulinex.

All of the information about the samples was obtained from the labels. The milled samples were analysed as quickly as possible after the purchase. When this was not possible, they were stored at −20 °C.

2.4. Recoveries

For recovery studies, 26.5 μL of the OTA work solution prepared in mobile phase at 25 ng/mL, and 50, 100 and 400 μL of the OTA work solution at 100 ng/mL were added to 20 g maize bread, and allowed to stand for 15 min at room temperature before extraction, for three replications. Because no certified reference materials for bread were available, trueness was assessed through recovery of additions of known amounts of OTA. The fortification levels were 0.033, 0.25, 0.50 and 2.00 ng/g, respectively (Tables 1–4).

Table 1
Mean recoveries and R.S.D.s obtained ($n = 3$) with different volumes of PBS/methanol (50:50) as extracting solvent using Minipimer apparatus

PBS:methanol volumes	Fortification level (ng/g)	Recovery (%)	R.S.D. (%)
50:50 (100 mL)	0.5	102.0	4.7
50:50 (75 mL)	0.5	65.0	17.8
50:50 (50 mL)	0.5	51.0	6.0

Table 2
Mean recoveries and R.S.D.s obtained ($n = 3$) with different proportion of PBS/methanol as extracting solvent

PBS:methanol volumes	Fortification level (ng/g)	Recovery (%)	R.S.D. (%)
50:50 (100 mL)	0.5	102.0	4.7
80:20 (100 mL)	0.5	99.6	0.7

Table 3
Mean recoveries and R.S.D.s obtained ($n = 3$) between different agitation techniques using 100 mL PBS:MeOH (50:50) and OTA fortification level at 0.25 ng/g

Agitation (time)	Recovery (%)	R.S.D. (%)
Manual (15 min)	50.0	6.0
Ultra-Turrax (5 min)	53.0	3.2
Centrifugation (15 min)	30.0	5.8
Agitation plate (15 min)	22.0	5.0

Table 4
Accuracy and intra-assay validation results ($n = 3$) and inter-assay ($n = 3$) obtained with the optimized method

Fortification (ng/g)	Recovery (%)	R.S.D. intraday (%)	R.S.D. interday (%)
0.033	80.4	8.8	12.1
0.25	92.3	5.2	10.9
0.5	102.0	4.7	11.4
2.0	87.0	1.4	9.3

2.5. Sample extraction and clean-up

An aliquot of sample (20 g) was extracted with 100 mL PBS/methanol (50:50, v/v) using the Braun Minipimer homogeniser for 5 min; the mixture was filtered through a Whatman filter paper. After 20 mL aliquot of the filtered was diluted with 30 mL of PBS and then this solution was passed through an IAC column for clean-up using a vacuum manifold. The column was washed with 10 mL of water before eluting OTA with 3 mL of methanol. The methanol was dried at ±50 °C under a gentle nitrogen stream, and the residue was reconstituted in 250 μL of mobile phase by mixing, and 50 μL were injected in the LC system.

2.6. Chemical confirmation of OTA by methyl ester formation

For confirmation, OTA was converted into its methyl ester using boron trifluoride methanolic solution 14% (BF_3-CH_3OH 14%) [5,28]. Sample extracts were evaporated to dryness, 150 μL of the BF_3-CH_3OH 14% solution was added, and the mixture was left at 60 °C for 10 min. After evaporation, the residue was dissolved in 250 μL of mobile phase.

3. Results and discussion

The calibration curves were obtained using the linear least squares regression procedure of the peak area versus the concentration. The linearity for OTA, in the working standard solutions at three determinations of five concentration levels, between 1 and 25 ng/mL, was good as shown by the fact that the determination of the correlation coefficients (r^2) are above 0.9990 for six calibration curves, prepared in three different days.

To optimize the extraction of OTA from maize bread, the extraction efficiencies were studied in order to achieve good analytical performance (Fig. 1). Firstly, OTA was extracted using the method of Pena et al. [28], previously used for rice samples. However, some modifications were needed. Three different volumes of PBS:methanol (50:50) were assayed as extracting solvent, using Minipimer apparatus: 50, 75 and 100 mL by using 20 g of maize bread fortified with OTA at 0.5 ng/g. The best recoveries were obtained with 100 mL of PBS:methanol (50:50) (Table 1). The extracting solvent was proved in different proportions and recoveries obtained with PBS:methanol (80:20) were slightly lower, 102% versus 99.6% (Table 2). This phenomenon may be due to the solubility power of methanol [28,29]. Higher percentage of methanol were not studied because OTA was able to could be elute from IAC columns [28], since methanol is one of the most potent desorbents [15].

Due to the characteristics of the sample, a more efficient process to separate the matrix residue from the solvent extract was essential. So, firstly filter paper Whatman N°4 and secondly centrifugation at 3400 × g for 15 min, were evaluated, and it was observed that with the second approach the recovery was 30%.

During the optimization of the method, different extraction procedures were assayed such as manual agitation, Ultra-Turrax,

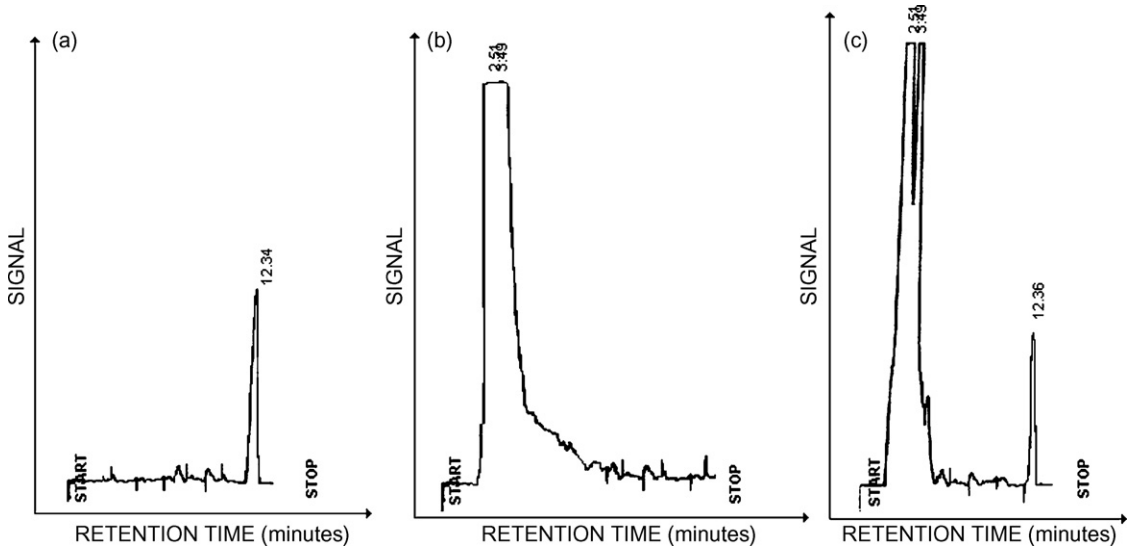

Fig. 1. LC-spectrofluorimeter chromatograms of: (a) solution of OTA standard at 10 ng/mL; (b) a maize bread blank sample; and (c) a maize bread sample fortified with 0.5 ng/g.

centrifugation and agitation plate. With these apparatus the recovery results oscillated between 22% and 53% (Table 3), which were overcome by Minipimer apparatus.

The accuracy for the optimized methodology was determined by calculating the mean recovery values used for each fortification level (Table 4). The recovery values oscillated between 102.0% and 80.4% for fortification levels at 0.5 and 0.033 ng/g, respectively. The precision was calculated through intraday repeatability ($n = 3$) and interday repeatability (3 days). The intraday repeatability was between 8.8% and 1.4% for 0.033 and 2.0 ng/g fortification levels, respectively. The interday repeatability was between 12.1% and 9.3% for the same fortification levels.

The LOQ was determined by the signal-to-noise approach, defined as that level resulting in a signal-to-noise ratio of approximately 10:1. The LOQ of the method was 0.033 ng/g. This value is lower than the obtained by González et al. [13] using pressurized liquid extraction with methanol for the analysis of OTA in bread, 0.06 ng/g.

3.1. Application to real samples

The optimized method of OTA extraction in maize bread followed by LC–FD was applied for the OTA analysis in 15 maize bread samples (Fig. 2). The frequency and incidence obtained are shown in Table 5. The frequency of OTA in analysed samples was

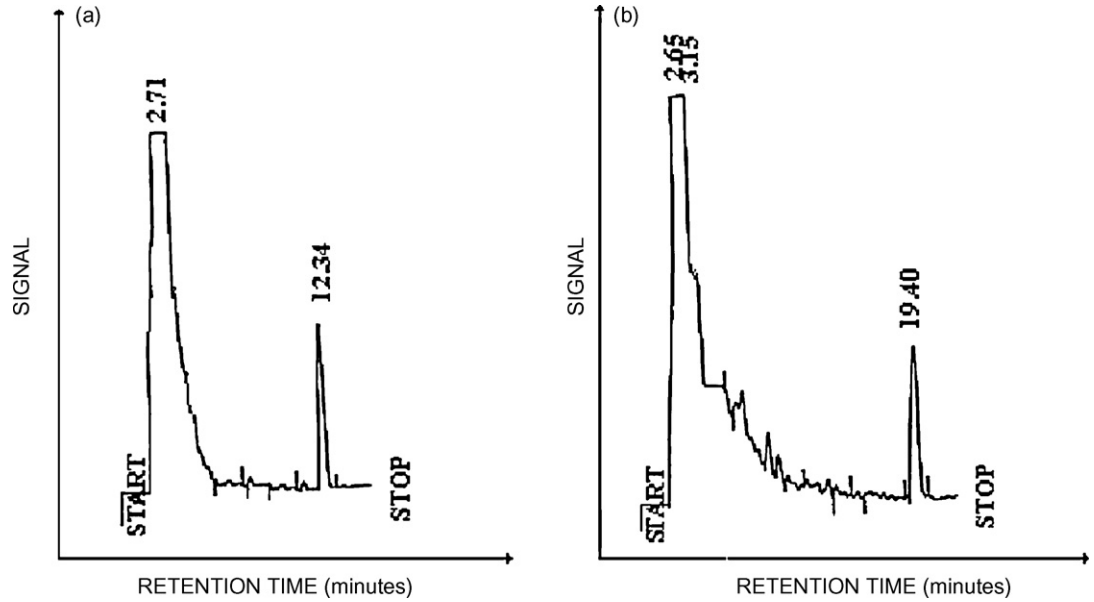

Fig. 2. LC-spectrofluometric chromatograms of: (a) a positive maize bread sample with 0.87 ng/g and (b) OTA methyl ester after boron fluoride–methanol derivatization.

Table 5
Prevalence and levels of OTA in maize bread

No of analysed samples	15
No of positive samples	9
Frequency (%)	60
<LOQ	1
Range (ng/g)	n.d.-2.65
Mean ± S.D. (ng/g)	0.43 ± 0.9
Median (ng/g)	0.08

60% (nine positive samples). The OTA contaminated samples revealed levels ranging from 0.033 and 2.65 ng/g and were being the OTA mean level 0.43 ± 0.9 ng/g and the median 0.08 ng/g. Among the nine positive samples, one presented an OTA level of 2.65 ng/g, which is near the maximum permitted level of OTA in cereal products established by the EU Commission Regulation, 3 ng/g, [30].

Few studies about OTA levels in bread samples are available. González et al. [13] found two contaminated samples in 20 bread samples analysed in Spain with OTA levels of 2.55 and 1.82 ng/g. Legarda and Burdaspal [10], in 255 samples of wheat bread from different countries, found 100% of incidence. The mean OTA levels ranged from 0.08 ng/g Austrian samples to 0.45 ng/g Spanish samples. The highest OTA level was found in one Spanish sample with 7.37 ng/g.

In the contaminated samples, the presence of OTA was confirmed by methyl ester formation with boron trifluoride in methanol (14%), followed by LC analysis. With this derivation the methyl ester was estimated to be 93% [28], therefore this reaction was not used for quantitative purposes.

4. Conclusions

Extraction with PBS/methanol, filtration and dilution with PBS allows the supernatant to be applied onto the IAC column, making it possible to achieve low limits of detection. This optimized analytical methodology provides good results in terms of accuracy, repeatability, intermediate precision and sensitivity, and has shown to be reliable for determination of OTA in maize bread, presenting limits of detection of 33 ng kg^{-1}.

The application of the procedure to 15 samples from the central zone of Portugal has demonstrated that 60% were contaminated, although none of the samples exceeded the recommended limit.

Acknowledgments

This study was supported by the FCT, FEDER/POCTI, and CRUP (Integrated Action programme between Portugal and Spain, E-1/05 and HP04-69). The authors are gratefully acknowledged. C. Juan thanks the Spanish Ministry of Education and Science for the grant BI04-40.

References

[1] M. Arroyo, D. Aldred, N. Magan, Int. J. Food Microbiol. 98 (2005) 223–231.
[2] D. Hohler, Z. Ernahrungswiss 37 (1998) 2–12.
[3] IARC (International Agency for Research on Cancer). In "IARC Monographs on the Evaluation of Carcinogenic Risks to Humans: Some Naturally Occurring Substances; Food Items and Constituents, Heterocyclic Aromatic Amines and Mycotoxins" 56 (1993) 489 IARC (Ed). Geneve.
[4] A. Pena, M. Seirtová, C. Lino, I. Silveira, P. Solich, Food Chem. Toxicol. 44 (2006) 1449–1454.
[5] E. Moreno Guillamont, C.M. Lino, M.L. Baeta, A.S. Pena, I.N. Silveira, J. Mañes Vinuesa, Anal. Bioanal. Chem. 383 (2005) 570–575.
[6] EU (2002) Assessment of dietary intake of ochratoxin A by the population of EU member states (report for SCOOP task 3.2.7.) Available at http://europa.eu.int/comm/food/fs/scoop/index_en.html.
[7] B.C. Cholmakov, J. Wolff, M. Gareis, H. Bresch, P. Majerus, H. Rosner, R. Schneider, Archiv. füer Lebensmitterlhygiene 51 (2000) 111–115.
[8] M. Gareis, T. Scheuer, S. Ehrheardt, Mitteilungsblatt Derbundesanstalt füer Fleischforchung Kulmbach 39 (2000) 707–715.
[9] T.M. Legarda, P.A. Burdaspal, Alimentaria 321 (2001) 89–96.
[10] I. Subirade, Food Addit. Contam. 13 (1996) 25–26.
[11] FAO, Worldwide Regulations for Mycotoxins in Food and Feed in 2003, vol. 81, FAO Food and Nutrition Paper, Rome, 2004.
[12] IACA, Associação Portuguesa dos Industriais de Alimentos Compostos para Animais. 2004. Available in http://www.iaca.pt/index.jsp?page=noticias&id=74.
[13] L. González, J.M. Soriano, J.C. Moltó, J. Mañes, J. Chromatogr. A. 1113 (2006) 32–36.
[14] M.W. Trucksess, A.E. Pohland, Mycotoxin protocols, in: J.M. Walker (Ed.), Methods in Molecular Biology, vol. 157, Humana Press, New Jersey, 2001.
[15] S.N. Zhou, E.P.C. Lai, J.D. Miller, Anal. Bioanal. Chem. 378 (8) (2004) 1903–1906.
[16] S. De Saeger, L. Sibanda, A. Desmet, Int. J. Food Microbiol. 75 (2002) 135–142.
[17] A.H.W. Abdulkadar, A. Al-Ali Abdulla, M. Al-Kildi Afrah, H. Jassim Al-Jedah, Food Control. 15 (2004) 543–548.
[18] J.W. Park, S.Y. Choi, H.J. Hwang, Y.B. Kim, Int. J. Food Microbiol. 103 (2005) 305–314.
[19] C. Araguas, E. Gonzalez-Penas, A.L. de Cerain, Food Chem. 92 (3) (2005) 459–464.
[20] D. Chan, S.J. MacDonald, V. Boughtflower, P. Brereton, J. Chromatogr. A 1059 (2004) 13–16.
[21] B. Delmulle, S. De Saeger, A. Adams, N. De Kimpe, C. Van Peteghem, Rapid Commun. Mass Spectrom. 20 (2006) 771–776.
[22] R. Biffi, M. Munari, L. Dioguardi, C. Ballabio, A. Cattaneo, C.L. Galli, P. Restani, Food Addit. Contam. 21 (6) (2004) 586–591.
[23] J. Blesa, H. Berrada, J.M. Soriano, J.C. Moltó, J. Mañes, J. Chromatogr. A 1046 (2004) 127–131.
[24] L. Monaci, F. Palmisanom, Anal. Bioanal. Chem. 378 (2004) 96–103.
[25] P.M.M. Scott, M.W. Trucksess, J. AOAC. Int. 80 (1997) 941–949.
[26] J. Gilbert, E. Anklam, Trends. Anal. Chem. 21 (2002) 468–471.
[27] T. Baydar, A.B. Egin, G. Girgin, S. Aydin, G. Sahin, Ann. Agric, Environ. Med. 12 (2005) 193–197.
[28] A. Pena, F. Cerejo, C. Lino, I. Silveira, Anal. Bioanal. Chem. 382 (2005) 1288–1293.
[29] K.A. Scudamore, M.T. Hetmanski, S. Nawaz, J. Naylor, Food Addit. Contam. 14 (1997) 175–178.
[30] European Commission 2005. Commission regulation (EC) No 123/2005 of 26 January 2005 amending regulation (EC) No 466/2001 as regards ochratoxin A. Official Journal of the European Union L25:3–5.

Available online at www.sciencedirect.com
ScienceDirect
Talanta 73 (2007) 282–286
Talanta
www.elsevier.com/locate/talanta

Simultaneous determination of sorbic and benzoic acids in commercial juices using the PLS-2 multivariate calibration method and validation by high performance liquid chromatography

Valeria A. Lozano [a], José M. Camiña [a,*], María S. Boeris [a], Eduardo J. Marchevsky [b]

[a] *Departamento de Química, Facultad de Ciencias Exactas y Naturales, Universidad Nacional de La Pampa, Av. Uruguay 151, 6300 Santa Rosa, La Pampa, Argentina*
[b] *Area de Química Analítica, Facultad de Química, Bioquímica y Farmacia, Universidad Nacional de San Luis, Chacabuco y Pedernera, 5700 San Luis, Argentina*

Received 23 November 2006; received in revised form 19 March 2007; accepted 20 March 2007
Available online 25 March 2007

Abstract

A new method to determine a mixture for preserving sorbic and benzoic acids in commercial juices is proposed. The PLS-2 model was obtained preparing 40 standard solutions adding concentration of sorbic and benzoic acid to filtered natural juices of apple, lemon, orange and grapefruit. The concentration of analytes in the commercial samples was evaluated using the obtained model by UV spectral data. The PLS-2 method was validated by high performance liquid chromatography (HPLC), finding a relative error less than 12% between the PLS-2 and HPLC methods in all cases.

Keywords: Preservings; Juices; Benzoic and sorbic acids; PLS-2 method; Multivariate calibration; HPLC

1. Introduction

Due to the fact that the simultaneous determination of diverse analytes concentration with similar spectral characteristics is almost impossible by ordinary absorptiometric methods, computer programs are needed to obtain reliable analytical results in shorter intervals.

The determination of food additives using conventional methods is difficult because of high-cost instruments and time-consuming pretreatment technique separations, such as extraction liquid–liquid, chromatography in column or fine plate [1]. Besides, equipment such as liquid and gas chromatography [1,2] are not available for small laboratories due to their high cost. This is the case for the determination of the benzoic and sorbic acid in food samples, which are employed as antimicrobial species in a wide number of foods, fruit juices, jams, beverages, salads, etc. [3].

On the other hand, there are spectrophotometric methods which require low-cost equipment and they can incorporate powerful chemometric tools of data analysis, such as the partial least square regression (PLS) multivariate calibration method. This low-cost analytical system avoids the time-consuming process during previous separation techniques, which may incorporate contamination.

In recent works, benzoic and sorbic acids in fruit juices were studied by Marsili et al. [4,5], using other multivariate calibration methods such as net analyte signal [4] and second-order spectrophotometric data [5]; yet, the PLS-2 multivariate calibration method has not been used, so far, to evaluate these analytes. For this reason, this paper discusses the simultaneous determination of benzoic and sorbic acids present in commercial samples of fruit juices, by means of the

* Corresponding author. Tel.: +54 2954 425166; fax: +54 2954 432535.
E-mail address: jcaminia@exactas.unlpam.edu.ar (J.M. Camiña).

0039-9140/$ – see front matter © 2007 Elsevier B.V. All rights reserved.
doi:10.1016/j.talanta.2007.03.041

PLS-2 multivariate calibration method validated by the HPLC method.

1.1. The PLS method

Partial least square (PLS) regression is an important multivariate calibration tool based on the use of a large number of variables, which permits to evaluate the concentration of interesting analytes [6,7]. PLS can be used in two ways: PLS-1 calculates the concentration of one analyte per model, while PLS-2 can determine all analytes in a unique model. The PLS method is an important multivariate calibration tool that has been growing in importance for the last years and has been incorporated in new analytical chemistry textbooks [8].

PLS regression [9] is a full-spectrum method based on the resolution of two initial multivariate matrices, R (response matrix) and C (concentration matrix), by projection onto smaller matrices T and U (or R and C score matrices, respectively). They contain the coordinates of the objects on the new axes or PLS components, with orthogonal columns, and relates the information in the response matrix R to the concentration matrix C, through correlation between R and C covariance matrices. In this work, R represents the independent variables (the original absorbance data of the calibration set), while C represents the dependent variables (concentration of benzoic and sorbic acids in the calibration set). The determination of a significant number of model dimensions (number of PLS principal components) was made by cross-validation.

The PLS-2 method was employed using absorbance values every 2 nm, from 210 to 300 nm wavelength. Forty standard solutions were prepared to generate the response matrix R, adding known concentration of benzoic and sorbic acids and constant quantities of natural juices, to simulate the matrix effect during the calibration step.

In this work, five samples of commercial fruit juices were analyzed and the results were validated using high performance liquid chromatography (HPLC) [10,11].

2. Experimental

2.1. Reagents

Water: HPLC-grade water was used to prepare both standard and sample solutions. Sodium benzoate and potassium sorbate stock solutions (10 g L^{-1}), 1.000 g of sodium benzoate and 1.000 g of potassium sorbate ACS grade (Baker, Phillipsburg, NJ, USA) were diluted with HPLC-grade water into a 100 mL volumetric flask. For the PLS-2 method, all standard solutions (calibration and validation sets) were prepared diluting adequate volumes of stock solutions with HCl 5×10^{-4} mol L^{-1} into 100 mL volumetric flasks, to obtain pH values around 3 [4]. For the HPLC method, standards were prepared diluting adequate volumes of stock solutions with mobile phase into 100 mL volumetric flasks. Mobile phase: 20% acetonitrile HPLC grade (Merck, Durmsted, Germany) and 80% sodium acetate–acetic acid buffer solution prepared with HPLC-grade water.

Sample preparation. For the PLS-2 method, five commercial juices were prepared transferring 1 mL of each juice into a 100 mL volumetric flask diluted with HCl 5×10^{-4} mol L^{-1}. For the HPLC method, 1 mL of each filtered juice was transferred into a 100 mL volumetric flask and diluted with the HPLC mobile phase.

2.2. Instrumental

Spectrophotometric measurements were taken using a Metrolab 1700 UV-V spectrophotometer (Buenos Aires, Argentina), Czerny Turner monochromator and a photomultiplier detector. pH measurements were taken with a pH meter HORIBA F42 (Tokio, Japan). The HPLC data were obtained by KONIK KNK-500-A Series (Miami, FL, USA). A 25 cm C-18 column Lichrosorb RP18 (USA) was used with KONIK UV detector (Miami, FL, USA). The HPLC parameters were: flow rate 1 mL min^{-1}; injection 20 μL; wavelength 234 nm and a chromatographic time of 15 min per sample. The PLS-2 data analysis was carried out using the Unscrumbler 6.11 software (CAMO ASA, Trondheim, Norway).

3. Results and discussion

3.1. HPLC data

Six standard solutions and six replicates of each one were prepared for both benzoic and sorbic acids, with concentrations of 2.0, 4.0, 6.0, 10.0, 14.0 and 20.0 ($\times 10^{-3}$ g L^{-1}). HPLC conditions were similar to those stated by Pylypiw and Grether [10], but using a single wavelength at 234 nm. The obtained calibration curve yielded a r^2 regression coefficient of 0.9947 and 0.9972 for benzoic and sorbic acids, respectively.

3.2. The PLS model

The model was obtained using a total of 40 standard solutions of filtered natural apple, orange, lemon and grapefruit juices and adding different levels of sorbic and benzoic acids to each one: 0.0, 2.5, 5.0, 7.5 and 10.0 ($\times 10^{-3}$ g L^{-1}). As shown in a previous study [12] a factorial design was used to build the calibration matrix, with five levels and two variables. Nevertheless, another 15 standard solutions were prepared to obtain 10 standard solutions for each fruit juice. Spectrophotometrical readings were carried out in different days in order to bring more robustness to the PLS-2 model and to produce minor error levels in the prediction step. This is an important aspect due to the use of complete full-spectra data which are affected by the instrumental variations, producing little changes in absorbance values and significant levels of noise. The concentration matrix used in the calibration step is shown in Table 1. All standard solutions were read from 210 to 300 nm every 2 nm. Standard solutions 1–10 were prepared with lemon; 11–20 with orange; 21–30 with grapefruit and 31–40 with apple natural juices to obtain a unique model useful for all samples.

The PLS-2 model was made using the Unscrumbler 6.11 software tools. The calibration step was performed by the

Table 1
Concentration matrix for the PLS-2 model

Std	Benzoic acid[a]	Sorbic acid[a]	Std	Benzoic acid[a]	Sorbic acid[a]
1	0.0000	0.0100	21	0.0000	0.0100
2	0.0025	0.0075	22	0.0025	0.0075
3	0.0050	0.0050	23	0.0050	0.0050
4	0.0075	0.0025	24	0.0075	0.0025
5	0.0100	0.0000	25	0.0100	0.0000
6	0.0025	0.0100	26	0.0025	0.0100
7	0.0050	0.0075	27	0.0050	0.0075
8	0.0075	0.0050	28	0.0075	0.0050
9	0.0100	0.0025	29	0.0100	0.0025
10	0.0100	0.0100	30	0.0100	0.0100
11	0.0000	0.0100	31	0.0000	0.0100
12	0.0025	0.0075	32	0.0025	0.0075
13	0.0050	0.0050	33	0.0050	0.0050
14	0.0075	0.0025	34	0.0075	0.0025
15	0.0100	0.0000	35	0.0100	0.0000
16	0.0025	0.0100	36	0.0025	0.0100
17	0.0050	0.0075	37	0.0050	0.0075
18	0.0075	0.0050	38	0.0075	0.0050
19	0.0100	0.0025	39	0.0100	0.0025
20	0.0100	0.0100	40	0.0100	0.0100

[a] Concentrations expressed in g L^{-1}.

combination of the response matrix (R) 40 × 45: (40 standard solutions × 45 wavelength absorbance values) and the concentration matrix (C): (40 standard solutions × 2 analytes). The built model was obtained using auto scaled data.

Fig. 1 shows the spectral overlapping of benzoic and sorbic acids in a 210–300 nm range.

Table 2 shows the explained variance (cumulative percentage) obtained in the calibration and validation processes with the PLS-2 method. Four PLS components were needed to explain 99.6 and 99.7% of the original information for both, benzoic and sorbic acids in the calibration and validation model sets. The percentage of the explained variance, as well as the root mean square error of calibration (RMSEC) and the root mean square error of prediction (RMSEP) are important diagnostic tools [7]. The percentage of variance represents the amount of

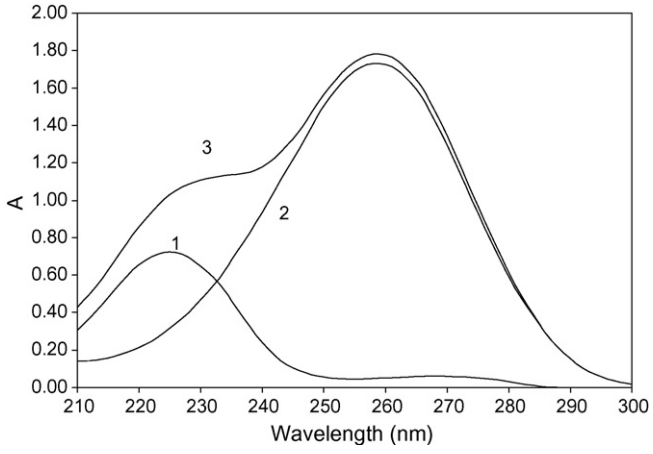

Fig. 1. Spectral curves of benzoic, sorbic and mixture of acids $C_{Benz} = C_{Sorb} = (1/2)C_{Mixt} = 0.01$ g L^{-1}.

Table 2
Percentage of explained variance for benzoic and sorbic acids in the calibration and validation model set

PC	Benzoic acid		Sorbic acid	
	Calibration	Validation	Calibration	Validation
0	0	0	0	0
1	33.2	27.2	95.2	95.2
2	58.2	54.1	97.6	97.5
3	85.4	82.7	97.5	97.2
4	99.6	99.6	99.8	99.7

variance explained by the PLS-2 model with a given number of PLS principal components, relative to the total variance in the R and C matrices in the data set. Another model evaluation tool is shown in Fig. 2, in the observed predicted concentration plot for benzoic (a) and sorbic (b) acids. The obtained r^2 coefficients were 0.9966 and 0.9979, respectively, suggesting a good fit in the model.

In Fig. 3, the loading weight plot, shows the PLS principal components' behavior as function of wavelength, describes the influence of wavelength for each principal component and represents their relative contribution to the model [7].

Frequently the loading plot is similar to the spectra of pure components. The first PLS principal component has a minimum at 262 nm, coinciding with the maximum of sorbic acid

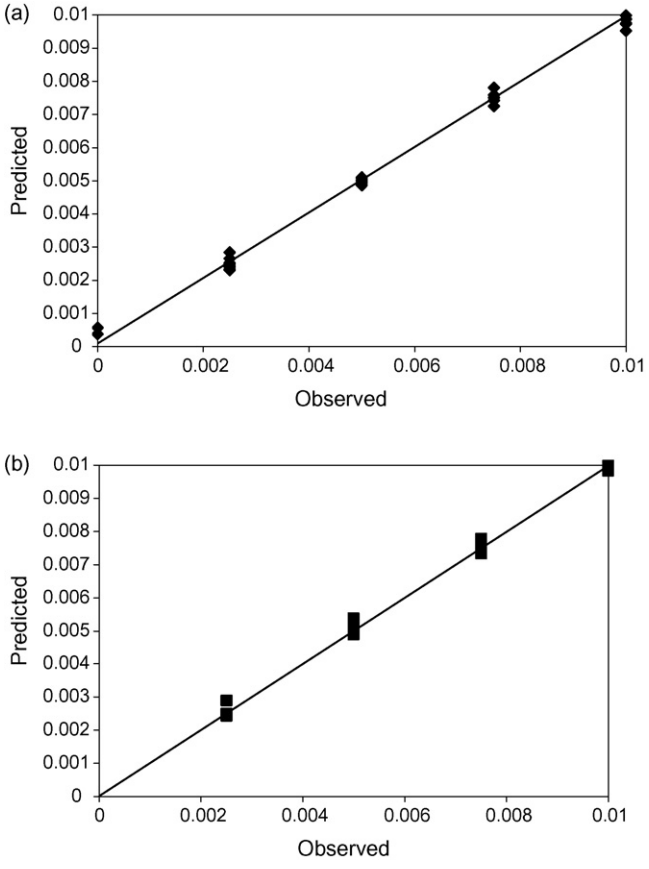

Fig. 2. Observed predicted plot, obtained by the cross-validation model with four principal components: (a) Benzoic (g L^{-1}) and (b) sorbic acids (g L^{-1}).

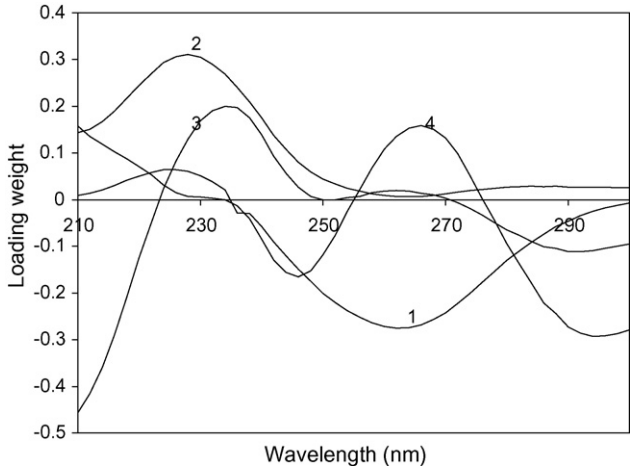

Fig. 3. Loading weights as function wavelength for first (1), second (2), third (3) and fourth (4) PLS principal components.

spectra, and a maximum that is in agreement with the maximum at 225 nm of benzoic acid spectra. The second component describes almost exactly the benzoic acid spectra. The third component shows an influence range from 210 to 250 nm with a maximum at 235 nm, which is the wavelength crossing of both pure spectra. The fourth component presents a minimum at 245 nm that corresponds to the inflection wavelength in the benzoic acid spectra; at 265 nm coincides with maximum of sorbic acid spectra, and at 295 nm agrees with the inflection zone of both benzoic and sorbic acid spectra.

3.3. Model validation

The model was built using, in the first place, internal validation (cross-validation method), where the model leaves out one standard of the calibration set. This standard was used to predict and find the internal error of the model. When all standards were left out once, the calibration and validation model error could be calculated, through root mean square of calibration (RMSEC) and root mean square of prediction (RMSEP) [6,7]. Fig. 4 shows RMSEC and RMSEP of the PLS-2 model for sorbic and benzoic acids.

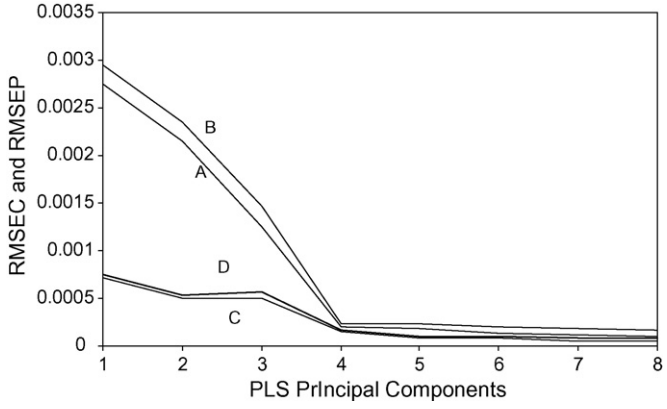

Fig. 4. RMSEC and RMSEP for benzoic and sorbic acids. Benzoic acid: (A) calibration, (B) validation. Sorbic acid: (C) calibration, (D) validation.

Table 3
Results of obtained prediction in the validation set for the PLS-2 model

Sample	Benzoic acid		Sorbic acid	
	Reference[a]	Predicted[a]	Reference[a]	Predicted[a]
Lemon 1	0.0030	0.0029	0.0060	0.0060
Lemon 2	0.0060	0.0062	0.0030	0.0029
Orange 1	0.0030	0.0029	0.0060	0.0063
Orange 2	0.0060	0.0056	0.0030	0.0033
Grapefruit 1	0.0030	0.0029	0.0060	0.0060
Grapefruit 2	0.0060	0.0061	0.0030	0.0029
Apple 1	0.0030	0.0031	0.0060	0.0059
Apple 2	0.0060	0.0061	0.0030	0.0027

[a] Concentrations expressed in $g\,L^{-1}$.

This figure also shows that four PLS principal components were properly chosen, because there were no significant changes in error values after the fourth component.

Then, a second validation was carried out through a validation set, preparing standard solutions of filtered natural juices, with concentration levels different from those used for the PLS-2 model to find the prediction error. The purpose of the validation set was to predict concentrations as unknown samples, to find errors and also the predictive ability of the model. Table 3 shows the results obtained with eight validation samples, which were prepared using lemon, orange, grapefruit and apple natural juices; benzoic and sorbic acids known concentrations were the references while the predicted values were the results. In this case, model relative error of less than 10% was found in all validation sample sets.

3.4. Outlier samples in the prediction step

Outlier detection during prediction in calibration methods is primarily based on *X*-residuals (response matrix residuals) and the prediction leverage. The *Y*-residuals (concentration matrix residuals) do not exist in the prediction step and consequently, measurements based on *f* cannot be used. *F* is the response error matrix obtained in the calibration step, and *f* (if it were possible to calculate it) must be the error matrix of an unknown sample in the prediction step. In the calibration step, detected outliers can be removed to obtain an adequate calibration model. In the prediction step, the leverage h_i summarizes extremeness in all factors applied in the modeling. Like the leverage of the calibration set, the leverage of the prediction set is defined as a truncated Mahalanobis distance. For outlier detection, the prediction leverage can be tested against the average leverage of the *I* object in the calibration set as follows:

$$h_i = \frac{k(A+1)}{I}$$

where *A* is the number of PLS-2 components and *k* is a constant, e.g. 3. In spite of the fact that leverage could never be higher than 1 in the calibration set, in the prediction step this limitation does not apply, and new input spectra can generate large factor scores.

In this work, the obtained leverage values for the real samples analyzed were the following: lemon (Leader Price) 0.092;

Table 4
Predicted concentrations by the PLS-2 model in real samples and validation results by the HPLC method

Sample	Benzoic acid		Sorbic acid	
	PLS-2[a]	HPLC[a]	PLS-2[a]	HPLC[a]
Lemon	1.100 ± 0.102	0.997 ± 0.011	0.340 ± 0.073	0.327 ± 0.008
Orange 1	0.980 ± 0.026	0.902 ± 0.019	0.190 ± 0.019	0.181 ± 0.004
Orange 2	0.900 ± 0.019	0.827 ± 0.019	0.000	0.000
Grapefruit	1.040 ± 0.049	0.971 ± 0.018	0.320 ± 0.035	0.310 ± 0.005
Apple	0.350 ± 0.010	0.335 ± 0.012	0.000	0.000

[a] Concentrations in undiluted bottled juices expressed in $g\,L^{-1}$.

orange 1 (Leader Price) 0.227; orange 2 (Zulueta) 0.178; grapefruit (MiJu) 0.228 and apple (Delifrú) 0.326. The low leverage values obtained show clearly that there are no sample outliers for this analyzed data set. Thus, this fact provides additional support for the very low influence of possible interferences on the analyzed samples [9].

3.5. Real samples prediction and HPLC validation results

Five samples with three replicates of commercial juices were predicted by the PLS-2 model: lemon (Leader Price), orange 1 (Leader Price), orange 2 (Zulueta), grapefruit (MiJu) and apple (Delifrú). Results were validated by the HPLC method.

The results obtained by the PLS-2 and HPLC methods are shown in Table 4. The relative error between the PLS-2 and HPLC methods was less than 12% in all cases.

On the other hand, the chromatogram shows that there are not relevant species that absorb at 234 nm (almost in the center between 210 and 300 nm range) in a large chromatographic time (60 min), which allows us to suppose that interfering absorbance values are not significant with respect to benzoic and sorbic acid values, due to the dilution phenomena, as can be seen through the low relative error and low leverage values for the sample set.

To summarize, the results obtained point out that the spectrophotometric methods combined with the PLS-2 data analysis permit the simultaneous determination of benzoic and sorbic acids in commercial fruit juices. The proposed method can be used without previous chemical separations, which suggests the great potential of the PLS-2 method with non-expensive equipment. Besides, it offers fast and precise results becoming an alternative procedure for laboratories of routine analysis.

Acknowledgements

We would like to thank Prof. Roberto Olsina (Universidad Nacional de San Luis) for providing the UNCRUMBLER 6.11 software. We are also grateful for grants received from Universidad Nacional de La Pampa, Universidad Nacional de San Luis and Consejo Nacional de Investigaciones Científicas y Técnicas (CONICET) that provide financial support for this research.

References

[1] P. Cunniff, Official Methods of Analysis AOAC International, vol. 2, 16th ed., AOAC International, Maryland, 1999, pp. 7–9 (Chapter 47), p. 22 (Chapter 37).
[2] S.A.V. Tfoundi, M.C.F. Toledo, Food Control 13 (2) (2002) 117.
[3] Y. Xie, P. Chen, W. Wei, Microchem. J. 61 (1999) 58.
[4] N.R. Marsili, M.S. Sobrero, H.C. Goicoechea, Anal. Bioanal. Chem. 376 (2003) 126.
[5] N. Marsili, A. Lista, B. Fernandez Band, H. Goicoechea, A. Olivieri, J. Agric Food Chem. 52 (2004) 2479.
[6] D.L. Massart, B.G.M. Vandeginste, L.M.C. Buydens, S. de Jong, P.J. Lewi, J. Smeyers-Verbeke, Handbook of Chemometrics and Qualimetrics, vol. A, Elsevier, Amsterdam, 1997, pp. 366–368.
[7] K.R. Beebe, R.J. Pell, M.B. Seasholtz, Chemometrics A Practical Guide, John Wiley and Sons, New York, 1998, pp. 278–283, 292.
[8] R. Kellner, J.M. Mermet, M. Otto, M. Valcárcel, H.M. Widmer, Analytical Chemistry, Wiley-VCH, Weinheim, 2004, pp. 127–130.
[9] H. Martens, T. Naes, Multivariate Calibration, John Wiley and Sons, New York, 1996, pp. 116, 290, 291.
[10] H.M. Pylypiw, M.T. Grether, J. Chromatogr. A 883 (2000) 299.
[11] O.A. Quattrrocchi, S.I. Abelaira de Andrizzi, R.F. Laba, Introducción a la HPLC, Aplicación y Práctica, Artes Gráficas Farro S.A., Buenos Aires, 1992, pp. 89–134.
[12] A.R. Coscione, J.C. Andrade, R.J. Poppi, C. Mello, B. van Raij, M. Ferreira de Abreu, Anal. Chim. Acta 423 (1) (2000) 31.

Available online at www.sciencedirect.com
ScienceDirect
Talanta 73 (2007) 232–236
Talanta
www.elsevier.com/locate/talanta

A green method for the determination of hypochlorite in bleaching products based on its native absorbance

J.G. March *, B.M. Simonet

Department of Chemistry, Faculty of Sciences, University of Balearic Islands, E-07122 Palma de Mallorca, Spain

Received 11 December 2006; received in revised form 6 March 2007; accepted 15 March 2007
Available online 24 March 2007

Abstract

A new, green method for the determination of hypochloride in bleaching products is here presented. The method, based on a flow injection system and measurement of the native absorbance of hypochlorite at 292 nm, allows the determination of hypochlorite in the range 0.07–0.42 g Cl_2 l^{-1}. In order to achieve high selectivity a mini-column containing cobalt oxide, which effectively catalyses hypochlorite decomposition to chloride and oxygen, was inserted in the flow system. The difference in absorbance of samples no circulated and circulated through the mini-column was selected as analytical signal; thus, the method only requires 20 mg of solid, reusable catalyst, and a NaOH solution of pH 10.4; providing a sample throughput of 12 samples h^{-1} in triplicate injection. Its usefulness for analysis of bleaching products is demonstrated.

Keywords: Hypochlorite determination; Flow analysis; Spectrophotometry; Catalytic decomposition of hypochlorite; Bleach analysis

1. Introduction

Sodium hypochlorite is extensively used as a household cleaning agent and as disinfectant for treatments including drinking water, swimming pool water, treated wastewater for non potable reuse and others. Normally it is handled as concentrated aqueous solutions.

Hypochlorite is an inherently unstable compound that decomposes to chloride and oxygen. So, periodical control of its concentration is needed in order to adjust dosages. In addition, quality control of commercialised formulations is compulsory in a number of countries. These aspects make hypochlorite determination in commercial formulations a routine task.

Chlorine and hypochlorite are related by following chemical equation:

$$Cl_2 + H_2O \leftrightarrow ClO^- + Cl^- + 2H^+$$

The sum of Cl_2, HClO and ClO^- is known in hydrochemistry as free chlorine and its concentration expressed as mass of Cl_2 by litter. This criteria is also followed in this paper.

There is a number of methods available for hypochlorite determination (e.g. the normalised and well known iodometric titration [1], many colorimetric methods based on reaction of hypochlorite with organic reagents as methyl orange [2], *o*-tolidine [3], *N*,*N*′-diethyl-*p*-phenylenediamine [4,5], thionin [6], 3,3′-dimethylnaphtidine [7], and chemiluminiscent methods such as that based on fluorescein test strip [8]). Both some of the reagents and their chloro-derivatives are potential toxic and carcinogenic agents that must be cautiously used. Despite analytical methods based on potentiometric and amperometric measurements have been reported [9,10], spectrophotometry-based methods are preferred both because their proper analytical characteristics and because photometric detectors are common in routine laboratories. Except titration, the methods itemised before have been mainly developed for the determination of free chlorine in water samples, and no for application to commercial formulations; so, high dilution is required for the latter application.

Analytical determinations based on the measurement of native absorbance of the analyte are preferred as they minimise reagents consumption, but these methods must be accurately validated, particularly in terms of selectivity, as any foreign compound that absorbs at the monitoring wavelength will interfere in the measurement. For this reason, interference removal is a recommended, critical step in this kind of methods, as is the case

* Corresponding author. Tel.: +34 971172504; fax: +34 971173426.
E-mail address: joan.march@uib.es (J.G. March).

0039-9140/$ – see front matter © 2007 Elsevier B.V. All rights reserved.
doi:10.1016/j.talanta.2007.03.027

of solid phase spectrophotometry of pharmaceuticals, purified by cation-exchange [11] and the determination of antioxidants in cosmetics with C18 silica as a sorbent phase [12].

An alternative to interference removal is the conversion of the analyte into products that do not absorb at the monitoring wavelength—that of the maximum absorption of the analyte. Additionally, if the reaction is an analyte decomposition catalysed by a solid phase, very low reagent consumption is necessary. But, in turn, it requires a very reproducible catalyst–analyte interaction, and also an easy way to separate the solution from the catalyst. As extensively documented in literature, both requirements can be achieved by using dynamic systems [13–16]. Flow injection analysis (FI) is recognised as an excellent strategy to greener analytical chemistry because its versatility to design manifolds minimising both reagents consumption and waste generation without detriment of analytical features, such as sensitivity, precision and accuracy [17]. In addition, productivity-related characteristics are improved as FI reduces human participation and increase sample throughput.

Hypochlorite decomposition to chloride and oxygen:

$$ClO^- \rightarrow Cl^- + 1/2O_2$$

is efficiently catalysed by several metal oxides as Co_3O_4, NiO, CuO [18], which have been applied to de-chlorination of treated waste water [19,20]. The analytical usefulness of such heterogeneous catalytic decomposition has been explored in this research by selecting cobalt oxide because its higher catalytic activity [18].

2. Experimental

2.1. Chemicals

The solid catalyst, cobalt oxide, was synthesized at our laboratory by slow addition of sodium hypochlorite to cobalt(II) nitrate solution (Scharlab; Barcelona, Spain). The mixture was stirred for 1 h, and the black solid phase was isolated by filtration. After thorough rinsing with water, the crystals thus obtained were dried at room temperature and powdered to particle size 250–500 μm (density = 2.84 g cm^{-3}). The 20 mg was the amount used to pack a mini-column (1.0 cm × 0.1 cm, length × i.d.) provided with cotton end filters.

A 10% sodium hypochlorite standardised by iodometry with sodium thiosulphate was used for daily preparation of diluted working standards. A pH 10.4 aqueous solution prepared with sodium hydroxide (Panreac; Barcelona, Spain) was used as carrier.

2.2. Flow system and apparatus

The manifold used, depicted in Fig. 1, was build with 0.5 mm i.d. PTFE tubing. A six-way switching Rheodyne valve was used for sample injection. The flow was produced with an Ismatec peristaltic pump provided with tygon tubes. A flow through cell (18 μl dead volume and 1 cm of optical path) and a Shimadzu UV-2401 PC spectrophotometer controlled by a personal computer running the UVPC 3.92 application were used for absorbance measurements. Working wavelength was 292 nm. A selection switching Rheodyne valve was used to insert the mini-column in the line to the detector. In this way, the injected solution can be propelled to the detector either directly or through the mini-column by manual switching of the valve (V-4 in Fig. 1).

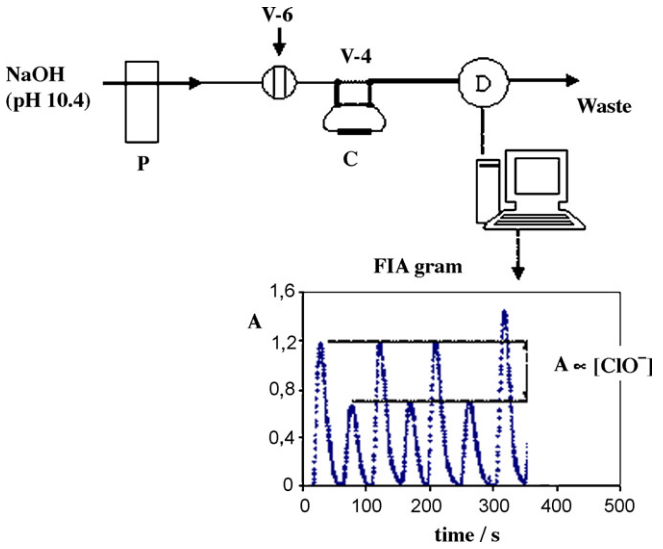

Fig. 1. Flow injection manifold and a typical obtained FIA-gram. P, peristaltic pump; V-6, six-way switch valve for sample injection; V-4, four-way switch valve for selection of the line to the detector; C, mini-column containing 20 mg of cobalt oxide (catalyst); D, detector (absorbance at 292 nm). Experimental conditions corresponding to the graphed FIA-gram: flow rate 1.0 ml min^{-1}, 0.24 g Cl_2 l^{-1}, water was used as carrier.

2.3. Procedure

Standards and samples were diluted to the working range 0.07–0.42 g Cl_2 l^{-1}. To measure the native absorbance of the target analyte, 70 μl of the diluted sample were injected into the FI system working at a flow rate of 1.0 ml min^{-1} and using a NaOH solution at pH 10.4 as a carrier. After obtaining the peak (viz. absorbance lower than 5% of the peak maximum), the selection valve was switched and injection of a second sample passed through the mini-column before reaching the detector, where the native absorbance of the hypochlorite remaining after catalytic decomposition in the mini-column was monitored. The difference between the height of the peaks obtained without and with passage of sample plugs through the mini-column was used as the analytical signal, the data collected being the average of three differences.

3. Results and discussion

Hypochlorite has a well-defined absorption band at the UV region with a maximum at 292 nm. Collection of UV spectra together with the use of chemometric tools allows quantification of the hypochlorite solutions. However, the validation and application of this procedure cannot be extrapolated to the wide variety of commercial hypochlorite formulations because they can also contain potential interferents such as surfactant and/or

organic compounds, added as colorants or perfumes. In order to overcome this selectivity-restriction, another procedure for establishing the analytical signal based on absorbance monitoring, first, of the analyte in the sample and, then, of the remaining analyte after catalytic decomposition was developed. The wavelength at the maximum of the absorbance spectrum of hypochlorite was used in order to achieve optimal sensitivity.

The catalytic decomposition of hypochlorite with the selected catalyst was fast, and, in addition, decomposition products (i.e. chloride and oxygen) do not absorb at the monitoring wavelength. A significant and characteristic absorbance decrease was then measured after a short analyte–catalyst contact time, which was a function of the flow-rate. Preliminary batch experiments showed that: (i) fast decomposition of hypochlorite with absorbance decrease up to 60% by minute was measured, depending on the experimental conditions; (ii) the activity of the solid catalyst was maintained after a large number of samples; (iii) removal of the solid catalyst prior to absorbance monitoring was tedious and time consuming. Based on these findings, it was decided that the option to reach best analytical performance was the development in a continuous mode, thus allowing: (a) automation of sample introduction and measurement of the analyte; (b) high reproducibility for non-equilibrium monitoring; (c) reduction of human participation and decreased experimental error as a result; (d) easy catalyst-sample separation with recovery of the former, thus avoiding the need for filtration steps; (e) the dynamic system also provides a significant improvement of catalytic decomposition rate. After preliminary studies, the manifold depicted in Fig. 1 was selected. Using this approach, water as a carrier and the difference in height-peak provided by sample plugs without and with catalytic degradation of hypochlorite as analytical signal, a hypochlorite concentration–analytical signal relationship was found. Under these working conditions, flow rates, and mini-column dimensions, a sample takes ca. 0.5 s to flow through the mini-column; within this interval absorbance decreases of 40% are obtained, as shown in the FIA-gram in Fig. 1.

Key aspects of the mini-column performance were the particle size of the catalyst and its package in the mini-column. Dispersion of the injected sample into the carrier as a function of the particle size of the catalyst was studied. Despite small particles produced less dispersion, those smaller than 250 μm generated overpressure. So, a particle size between 500 and 250 μm was selected.

The amount of packed catalyst was studied in the range 10–30 mg. Columns containing 20 mg were enough to obtain a representative difference between peaks (see FIA-gram in Fig. 1); so, this amount was selected to develop the method as lower amounts resulted in lower difference between peaks (analytical signal) and higher amounts generated overpressure in the system and a more significant dispersion, probably caused by the intrinsic dead volume, and longer passage through the mini-column. In addition, a higher catalytic degradation of hypochlorite yields a higher amount of oxygen which can result in bubbles formation into the system, thus, distorting photometric measurements. The reduction of peak height when the hypochlorite solution migrates through the mini-column, can be attributed to two effects: (i) catalytic degradation of hypochlorite and (ii) dilution of the sample plug due to dispersion. By using sodium nitrate standard solutions which neither interact nor react with the catalyst and also absorb at 292 nm, it was established that the peak height decrease due to dispersion was in the order of 3%. Then, peak decrease higher than 3% is a consequence of a diminished hypochlorite concentration by catalytic decomposition. The mini-column can be reused for many injections as only after 200 injections a decrease in the signal of about 15% was observed.

3.1. Study of variables

Once the catalyst-packed mini-column was selected, the analytical signal is dependent on few variables. For optimisation of variables affecting the analytical signal (i.e. flow-rate, sample volume and carrier composition) a univariate approach on a maximum sensitivity-precision basis was applied. The results founds are listed in Table 1.

The effect of the flow rate was studied in the range from 0.5 to 1.5 ml min^{-1}. At low flow-rates the analytical signal was higher as more hypochlorite was degraded, but the peak-width increased, thus decreasing precision. Finally, as a compromise between measurement time, precision and sensitivity a flow rate of 1 ml min^{-1} was selected.

Individual peak-height increased with sample volume, but the difference between them that constitutes the analytical signal reached the highest value for a sample loop of 70 μl, which was selected for further experiments. This fact could be attributed to a less catalytic efficiency during the short interaction time

Table 1
Study of variables

	g Cl_2 l^{-1}	Height peak differences	CV (%)
Flow rate[a] (ml min^{-1})			
0.5		0.095	4.3
1.0	0.07	0.062	3.7
1.5		0.046	2.9
0.5		0.203	4.0
1.0	0.14	0.132	2.7
1.5		0.103	2.7
Loop volume[b] (μl)			
50		0.050	3.4
70	0.07	0.078	3.5
100		0.064	3.4
50		0.103	3.5
70	0.14	0.157	2.2
100		0.132	2.6
Carrier[c]			
H_2O		0.160	4.5
NaOH pH 10.4	0.07	0.119	3.5
NaOH pH 10.8		0.116	3.7
H_2O		0.466	4.0
NaOH pH 10.4	0.14	0.346	4.0
NaOH pH 10.8		0.310	3.8

[a] Other conditions: injected volume 100 μl, carrier NaOH pH 10.4.
[b] Other conditions: flow rate 1.0 ml min^{-1}, carrier NaOH pH 10.4.
[c] Other conditions: flow rate 0.5 ml min^{-1}, injected volume 70 μl.

with the catalyst (about 0.5 s) when the amount of hypochlorite increased.

Concerning carrier composition, water and diluted NaOH solutions were tested taking in mind the alkaline nature of samples (bleach can be considered as a solution of chlorine in sodium hydroxide). As diluted real samples typically are in the 10.0–10.9 pH range, that within 8.5–11.0 was studied. A decrease in sensitivity occurred by increasing the pH of the carrier. As analytical signal is the difference between the native absorbance and absorbance after catalytic degradation, the loose of sensitivity was a consequence of a lower catalytic degradation; fact that could be due to loss of hydration molecules which results in the presence of hydroxide groups close to the catalyst surface. The losses are favoured in basic media. Therefore, in alkaline media interaction of hypochlorite (negative charge) with the catalyst are obstructed and slower catalyst–analyte interaction is established. For comparative purposes, the validation of the method has been developed using two different carriers: water and a NaOH solution of pH 10.4, which is in the middle of the pH range of diluted samples.

3.2. Validation of the method

Working as described in recommended procedure, the calibration graphs were obtained for a set of six hypochlorite standards injected in triplicate. Analytical figures of merit are summarised in Table 2, which shows that a lower sensitivity was achieved using NaOH solution of pH 10.4 as carrier. The regression lines obtained with both carriers presented a coefficient of determination close to 1. Under selected working conditions the peak throughput was 72 peaks h^{-1}, which corresponds to 12 samples h^{-1} if three replicates of each peak were run.

3.2.1. Analysis of real samples

In order to test the reliability of the proposed procedure, a set of 11 industrial and commercial samples were analysed. Samples were obtained either from the local marked or supplied by a laboratory devoted to quality control of bleach products for producing factories. The set of samples includes raw solutions obtained by reaction of chlorine gas with sodium hydroxide, hypochlorite for swimming pool water disinfection, household hypochlorite, hypochlorite for drinking water disinfection and perfumed and high-density hypochlorite commercial formulations.

Table 2
Analytical figures of merit

	Carrier	
	H_2O	NaOH pH 10.4
Regression line[a]: $y = a(\pm S_a) + b(\pm S_b)x$	$y = 0.01(\pm 0.01) + 2.05(\pm 0.04)x$	$y = -0.028(\pm 0.006) + 1.52(\pm 0.02)x$
Studied range	0.07–0.42	0.07–0.42
R^2	0.999	0.999
S_{yx}	0.01	0.007
LOD[b]	0.02	0.01
LOQ[c]	0.05	0.04

[a] y = height peak difference; x = g Cl_2 l^{-1}; $n = 6$.
[b] Limit of detection calculated as ($3S_{yx}/b$).
[c] Limit of quantification calculated as ($10S_{yx}/b$).

Table 3
Determination of hypochlorite in industrial and commercial samples

Iodometric method (g Cl_2 l^{-1})	Proposed method (g Cl_2 l^{-1})	
	Carrier NaOH pH 10.4	Carrier H_2O
93.5	93.0	101.8
31.0	32.7	34.9
27.1	28.7	29.9
35.5	36.2	38.1
51.4	54.6	61.7
122.1	128.0	152.8
117.0	113.4	128.9
42.1	42.2	48.5
27.3	24.5	27.9
35.6	35.2	39.8
35.0	31.7	38.7

The concentrations of hypochlorite found were compared with those provided by application of the recommended iodometric method with thiosulphate [1]. The results obtained are summarised in Table 3. The regression lines "concentration found" by the proposed photometric method using both NaOH and water as carrier versus "concentration found" by iodometry were:

Carrier NaOH :

$$[Cl_2]_{proposed} = 0.6(\pm 2) + 1.01(\pm 0.03)[Cl_2]_{iodometry}$$

Carrier H_2O :

$$[Cl_2]_{proposed} = -3(\pm 3) + 1.19(\pm 0.04)[Cl_2]_{iodometry}$$

([Cl_2] expressed as g l^{-1}).

From this it can be stated that the proposed photometric-catalytic method with NaOH pH 10.4 as carrier matches at 95% confidence level with the iodometric method. Nevertheless, under the same working conditions but using water as carrier a proportional error must be expected as a consequence of a slope significantly higher than 1. Such error can be attributed to differences in alkalinity between diluted samples and standards. So, for analysis of real samples pH 10.4 NaOH should be used as carrier, or alternatively, the samples can be diluted with pH 10.4 NaOH and water used as carrier.

It is worth to mentioning that although higher analytical quality can be achieved by already established methods, the method proposed here provides enough information to solve the analytical problem (it is "fit for purpose"). Then, the toxicity of reagents used and the waste generated should be relevant characteristics to be take into account when planning the implementation of an analytical method for the target analyte in routine laboratories.

4. Conclusion

The decrease of the native absorbance of hypochlorite by decomposition catalysed by cobalt oxide provides a new method for hypochlorite determination. Good analytical features have

been achieved by means of a single line flow injection manifold that included a mini-column with the catalytic solid-phase. The method is suitable for the determination of hypochlorite in bleaching products. Noticeable characteristics of the method are a very low consumption of reagents and waste generation, which result in low cost and thus applicable to routine industrial analysis. It constitutes an environmental friendly alternative to already developed methods for hypochlorite determination.

The method proposed in this paper is an example of successful use of recommended strategies for cleaner analytical methodologies, namely: the measurement of intrinsic properties of the analyte, thus avoiding the use of additional reagents to develop the analytical reaction; the use of flow-based techniques that minimise reagents consumption; the use of solid phase reagents which, if properly handled, usually can be reused for multiple determinations.

Acknowledgement

We acknowledge financial support from the University of Balearic Islands and research project CTQ2006-01851 (MEC-DGI, Spain).

References

[1] APHA, AWWA, WPCF, in Metodos Normalizados para el Analisis de Aguas Potables y Residuals, Diaz de Santos, Madrid, 1992, pp. 55–61.
[2] D.J. Leggett, N.H. Chen, D.S. Mahadevappa, Analyst 107 (1982) 433.
[3] J.G. March, M. Gual, B.M. Simonet, Talanta 58 (2002) 995.
[4] L. Moberg, B. Karlberg, Anal. Chim. Acta 407 (2000) 127.
[5] A. Chaurasia, K.K. Verma, Fresenius J. Anal. Chem. 351 (1995) 335.
[6] B. Narayana, M. Mathew, K. Vipin, N.V. Sreekumar, T. Cherian, J. Anal. Chem. 60 (2005) 706.
[7] J. Ballesta-Claver, M.C. Valencia-Miron, L.F. Capitán-Vallvey, Anal. Chim. Acta 522 (2004) 267.
[8] E. Pobozy, K. Pyrzynska, B. Szostek, M. Trojanowicz, Microchem. J. 51 (1995) 379.
[9] A.P. Soldatkin, D.V. Gorchkov, C. Martelet, N. Jaffrezic-Renault, Sensors Actuators, B: Chem. B43 (1997) 99.
[10] A.A. Alwartan, M.A. Abadía, Int. J. Chem. 3 (1992) 105.
[11] M.I. Pascual-Reguera, G.P. Parras, A.M. Diaz, J. Pharm. Biomed. Anal. 35 (2004) 689.
[12] L.F. Capitán-Vallvey, M.C. Valencia, E.A. Nicolas, Anal. Lett. 35 (2002) 65.
[13] R.A. Gil, S. Cerutti, J.A. Gasquez, R.A. Olsina, L.D. Martinez, Talanta 68 (2006) 1065.
[14] L. Nozal, L. Arce, B.M. Simonet, A. Rios, M. Valcárcel, Anal. Chim. Acta 517 (2004) 89.
[15] M.C. Herrera, M.D. Luque de Castro, Anal. Bioanal. Chem. 379 (2004) 1106.
[16] J.A. Rodríguez, E. Barrado, M. Vega, J.L.F.C. Lima, Electroanalysis 17 (2005) 504.
[17] F.R.P. Rocha, J.A. Nobrega, O.F. Filho, Green Chem. 3 (2001) 216.
[18] A. Hamano, Y. Suenaga, Kayaku Gakkaishi 55 (1994) 58.
[19] V.S. Londhe, P.R. Kamath, Water Res. 9 (1975) 1009.
[20] Japan Patent 56108587.

Available online at www.sciencedirect.com
ScienceDirect
Talanta 73 (2007) 340–345
Talanta
www.elsevier.com/locate/talanta

Synthesis and evaluation of new lipomonosaccharide-imprinted polymers as MISPE supports

D. Maury, F. Couderc *, J.-C. Garrigues, V. Poinsot

Laboratoire des Interactions Moléculaires et Réactivité Chimique et Photochimique, Université Paul Sabatier, 118 route de Narbonne, 31062 Toulouse Cedex 9, France

Received 5 February 2007; received in revised form 19 March 2007; accepted 23 March 2007
Available online 31 March 2007

Abstract

Molecular imprinted polymers (MIP) were prepared by the copolymerization of styrene (S) or methyl methacrylate (MMA) and methacrylic acid (MAA) using ethylene glycol dimethacrylate (EGDMA) as the crosslinker with molar ratios of [monomer]/[crosslinker] and [MAA]/[template] of 3:7 (to obtain a rigid structure) and 1:6 (to optimise hydrogen interactions), respectively. The polymerizations occurred in presence of the template molecule (MIP) – GlcNcouma – an amphiphilic monosaccharide. The same materials, non-imprinted polymers (NIP), were also prepared in absence of the template. These MIPs were characterized and used as SPE supports for selective enrichment. The results showed the correlation between retention efficiency and the porogen character of the polymerization solvent.

Keywords: Amphiphilic monosaccharide; Molecular imprinting; MISPE

1. Introduction

In recent years, there has been an increase in interest in the application of highly selective molecularly imprinted polymers (MIPs) in the analysis of drugs [1], biological compounds and sensors. Traditionally, MIPs can be synthesized via a number of approaches including bulk polymerization, "in situ" polymerization, or polymerization in suspension. The functional monomer and the template are mixed in an appropriate solvent and then polymerization is initiated in the presence of a large amount of cross-linking monomer. The template is removed after polymerization, leaving cavities with specific recognition properties that are able to selectively rebind the template and related substances from a complex mixture. Applications of MIPs in analytical chemistry include stationary phases for liquid chromatography (LC) [2], capillary electrochromatography (CEC) [3] and matrices for solid-phase extraction (SPE) [4,5]. SPE is very easy to perform and it is the most widely used technique for sample preparation, however typical SPE sorbents lack selectivity because they are specific to one function or polarity class, not to a complementary both in shape and chemical functionality. This lack of specificity is a problem when a selective extraction has to be performed. Nevertheless, this is not a problem for SPE applications. As MIPs lead to broader peaks and poorer efficiency, this may cause difficulties for their use in HPLC. MIP-based solid-phase extraction (MISPE) has been used for the extraction of a broad range of analytes such as aromatic compounds (4-nitrophenol [6]) and molecules of pharmaceutical (ß-agonists [7], naproxen [8]) and compounds of environmental interest (phenytoine [9], triazine [10]). In addition, MISPE is a highly selective method to determine trace analytes, particularly in complex pharmaceutical and biomedical samples [11–13].

While MISPE is quite useful for pharmaceutical analyses, relatively few applications of MIPs have been described for the analysis of biologically important molecules such as saccharides. In addition, it should be noted that the role of hydrogen bonds, which are at the origin of the saccharide–molecule interaction due to the external function saccharide-OH have not been well explored. However, since saccharides are often water soluble, these weak interactions were inconclusive. Recognition of saccharides by boronic acids and less specifically by ammonium supports is unique in supramolecular chemistry [14]. As an alternative, using monomers with a large number of available functional sites could increase the probability of interaction

* Corresponding author. Tel.: +33 5 61 55 83 33; fax: +33 5 61 55 81 55.
E-mail address: couderc@chimie.ups-tlse.fr (F. Couderc).

0039-9140/$ – see front matter © 2007 Elsevier B.V. All rights reserved.
doi:10.1016/j.talanta.2007.03.051

between the sugar and monomer. The advantage of using hyperbranched co-monomers (leading to star polymers) in creating a responsive and recognitive network is the presence of a large number of functional groups within a small volume [15]. The limitation of such systems would be an extremely high degree of flexibility. Indeed, the use of PEG600DMA leads to a large structure, as the length of the spacer-arm increases from 1 to 14 ethylene glycol subunits. The success of these materials could lead them to be used as a part of modulated drug delivery device. In addition, non-covalent molecular imprinting of sugar compounds in copolymers yielded materials containing highly selective sugar binding sites [16]. In this instance, the resulting polymer imprints had a high degree of both anomeric and epimeric selectivity favouring the original print molecule. For discriminating against epimeric disaccharides, non-covalent interactions were tried using a copper (II) complex as functional monomer [17].

The majority of previous studies report little information on MIP technique and also MISPE with respect to saccharide imprints. In this context, we have been interested in analyzing amphiphilic oligosaccharides, and more particularly their role as of biological signals [18]. Nevertheless, due to structural complexity, imprinting is difficult to set up. For this reason, we chose to simplify the system, initially using a rigid and amphiphilic monosaccharide, called coumarin-glucosamide (GlcNcouma) as a model compound.

In this context, the aim of the present work was to demonstrate the feasibility of using MISPE for the selective retention of lipophilic sugars. To the best of our knowledge this is the first time that a MIP was synthesized using a conventional non-covalent imprinting protocol with an aryl-saccharide as the template molecule. The polymer was used as an SPE sorbent to selectively retain the template molecule GlcNcouma (see Section 2) in the presence of the potential competitors (phenol, glucose) and *N*-palmitoyl glucosamide ($GlcNC_{16}$)).

2. Experimental section

2.1. Reagents and chemicals

Methacrylic acid (MAA), Styrene (S) and ethylene glycol dimethacrylate (EGDMA) were purchased from Sigma. The radical initiator α,α′-Azobisisobutyronitrile (AIBN) was obtained from Fluka and used as such. All other chemicals and solvents were obtained from Normapur, were of highest purity available and were dried over 4 Å molecular sieves. The solvents used for HPLC were filtered using nylon filters (0.45 μm). Both MAA and EGDMA were distilled in vacuum to remove the polymerization inhibitor. S was purified by several water/NaOH (9:1, v:v) washings and finally with water. GlcNcouma (Fig. 1), which was the template molecule was synthesized in the laboratory of "Synthesis of Biomolecules" (Orsay) and used as received. The potential competitors to investigate the imprinted polymer selectivity were phenol (Sigma), glucose (Glc, Sigma) and *N*-palmitoyl glucosamide ($GlcNC_{16}$, synthesized in our laboratory).

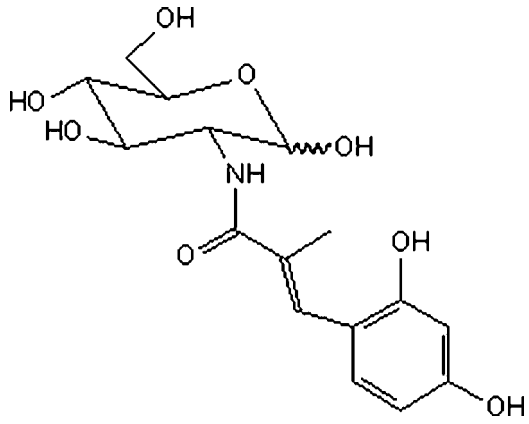

Fig. 1. GlcNcouma molecular structure.

2.2. Chemical compositions of the imprinted polymers

The tested weight percentages of the respective monomers are presented in Table 1. AIBN was used only at 0.1%/mol of monomers. Non-imprinted polymer (NIP) and molecularly imprinted polymer (MIP) are denominations previously explained. All the MIPs used GlcNcouma as template.

2.3. Preparation of the imprinted polymers

Mass polymerization (in flasks) was used for the synthesis of materials 1, 2, 3, 4. The pre-polymerization mixture composed of GlcNcouma (0.1 g, 0.3 mmol), MAA (5%, 0.2 g, 2.3 mmol), S (25%, 1.1 g, 1.8 mmol), the cross-linker EGDMA (70%, 6.0 g, 30.35 mmol) and the initiator AIBN (0.1 g, 0.8 mmol) which was dissolved in 18 mL of the respective solvents (see Table 1) in a 100 mL glass flask. The mixture was sonicated for 5 min

Table 1
All presented materials with weight percentages of respective monomers, solvents of polymerization and designs synthesized according to suspension and mass polymerization, the crosslinker was 70%/mol of the monomers

Materials	AMA (%)	S (%)	MMA (%)	EGDMA (%)	GlcNcouma (%)	Solvent (3:1, v:v)	Type of polymer
1	5	25	0	70	0	Toluene/DMF	NIP(1)
2	5	25	0	70	0.8	Toluene/DMF	MIP(2)
3	5	0	25	70	0	Toluene/DMF	NIP(3)
4	5	25	0	70	0	THF/MeOH	NIP(4)
5	5	25	0	70	0.8	THF/MeOH	MIP(5)
6	5	25	0	70	0.8	Toluene/MeOH	MIP(6)

Solvents were introduced at the ratio of 70%/g of monomer and GlcNcouma was the template for each MIP material.

and bubbled with nitrogen for 5 min to remove dissolved oxygen before the flask was maintained at 70 °C for 24 h. The solid polymer that was formed was crushed, ground, sieved and sedimented to obtain particles in the size range of 36–100 μm. Fine particles were removed by decanting in acetone three times and the particles were dried at 70 °C. The blank polymer (NIP) was prepared and treated identically except that no template was present in the polymer preparation.

2.4. Morphology and porosity observations

The specific surface areas (S_p) were evaluated using the BET method. Nitrogen sorption measurements were performed on a Micrometrics Flowsorb II 2300 automatic adsorption instrument with a measurement precision of 3%. Before measurements, a 150 mg sample was heated at 150 °C under high vacuum for at least 30 min.

An OLYMPUS BX50 optical microscope (magnification 20/1) equipped with a color video camera CCD-IRIS/RGB and a camera adaptor CMA-D2 was used and the scanning electron micrograph (SEM) analyses were performed on a Jeol JSM-6700 F field emission scanning electron microscope.

2.5. SPE conditions used for the recognition properties of the materials

SPE was used to study the affinity of the MIP obtained after mass polymerization. Prior to using the MIPs, they were washed with MeOH (release quantified via HPLC) to ensure that there was no residual template (GlcNcouma) present. For this purpose, 250 mg of the crushed material was stirred in 3 mL methanol. UV absorbance was measured at $\lambda = 360$ nm. Methanol was refreshed until no absorbance could be detected. Cartridges were conditioned with ACN (5 × 2 mL, 1 drop/s). Forty microliters ($C = 10^{-4}$ M) of each sample were deposited on cartridges containing 250 mg of particles. This volume is minor than the dead volume to avoid material loss and the so deposited 10^{-8} mol of compound are also minor than the calculated free recognition sites of the material, deduced from the washing-up experiments. The following sequential percolations were performed: ACN (for the interference elution), ACN 1% AcOH, MeOH (both to compete with hydrogen-bonding) and toluene (to displace π–π interactions), with 2 mL (10 Volumes) of each solvent at a rate of 1 drop/s. The elution efficiencies were evaluated with HPLC, UV spectroscopy and mass spectroscopy.

2.6. Quantification methods

An HPLC (Waters Alliance 2695 HPLC with Model 996 PDA detector and Millenium 4.0 software (Waters Corp. Milford, MA)) was used with a 250 mm × 4.6 mm i.d. X-terra RP 18, 5 μm, analytical column (Waters). The mobile phase was ACN/H_2O (0.1% TFA) (65:35) with a flow rate of 1 mL/min. The injection volume was 10 μL (before injection, all the samples were filtered with a 0.2 μm nylon filter).

UV–vis spectroscopy: An HP 8452 A Diode Array Spectrophotometer (Hewlett Packard, Palo Alto, CA) was used at $\lambda = 292$ nm. Absorbance was measured and quantification is performed via a calibration curve.

Mass spectrometry: MS measurements were performed on a Waters QqTof Ultima Mass Spectrometer equipped with an electrospray ion source operating in the positive mode. The voltages were—capillary: 3 kV; cone: 70 V; Rf lens: 25 V. Samples were introduced by direct infiltration and the intensities of molecular ions ($M + H^+$, $M + Na^+$, $M + K^+$) are summed.

3. Results and discussion

The utility of molecular imprinted polymers has led to the synthesis of a large number of these polymers over the past decade. The use of these materials is based on chemical interactions between the target molecule. The designed polymer material and the functionalized monomer that is selected is made on the basis of forming "strong enough" interactions with functional groups of a template molecule and optimizing their affinity. The second important parameter is that a very high degree of crosslinking is required since the polymer matrix needs a significant degree of rigidity to retain the shape of specific cavities and preserve the imprinted memory after the template is removed. The work presented here focuses on the preparation of new GlcNcouma-imprinted polymer formats to be used as stationary phases in cartridges (SPE). The choice for crosslinker was EGDMA in a ratio of 70%, according to the literature. The nature of interactions expected was hydrogen-bonding implying the carbohydrate hydroxyl groups and the MAA acidic function. For more specificity, π–π interactions between the coumarin rings are enabled by introducing styrene as the interacting monomer. A release study of the template indicated that 45% are definitively encaged in the material after five MeOH washing steps. As these are definitively encaged in the polymer, no competition effect can occur.

3.1. MISPE efficiency

After "in flask" polymerization, the materials were crushed, ground and sieved as can be seen in Fig. 2 (material 2). Isolated particles with dimensions between 40 and 100 μm and the specific surface values are given in Table 2. These particles are suitable for MISPE evaluation [19].

As can be seen in Table 2, the specific surface values are the highest when the solvent is porogeneous (material 1 compared to material 6, for example). It can also be noted that S_p increases when the material is imprinted.

Table 2
BET specific areas (S_p) were calculated from nitrogen adsorption measurements and are relative to materials referred in Table 1

Material	S_p ($m^2\ g^{-1}$)
1	238
4	221
5	226
6	57

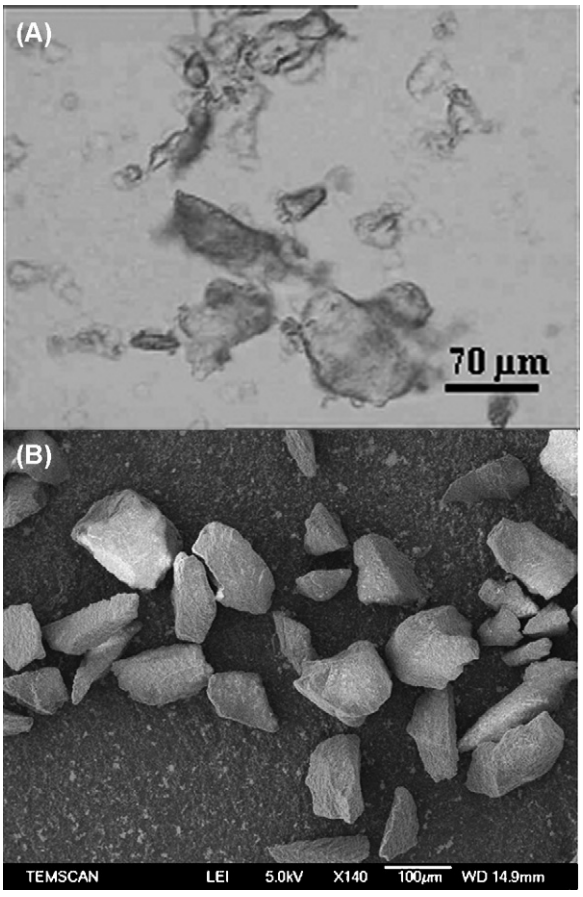

Fig. 2. Crushed and washed particles (material 4) observed via optical microscopy (magnification 20×, A) after polymerization in flasks and by SEM (B).

To investigate the selectivity of the polymers for GlcNcouma, SPE tests were carried out. After making certain that there was no problem of solubilization, several organic solvents were chosen to estimate the imprinting effect of these MISPE cartridges. Sample solutions (GlcNcouma in MeOH) were percolated through the cartridges which had been conditioned with ACN. The conditioning leads to a swelling of the pores even if the polymer is highly reticulated and a minor swelling occurs. Also, the ability of different solvents to disrupt or displace interactions between the deposited template and the host material was investigated. ACN was used for conditioning because it solubilized the template and might eliminate van der Waals interactions, which we want to get rid of in our materials. In this way, the specifically retained compounds are not washed off. GlcNcouma was eluted from the MIP using acetonitrile–1% acetic acid, which was expected to compete with the analyte for the functional group (COOH of MAA) in the binding sites, producing desorption of GlcNcouma from the MIP. Following that, MeOH, a protic and polar solvent was used to suppress strong non-covalent hydrogen-bonding interactions (specific interactions). The last step was the elution with toluene, which was expected to displace π–π stacking between template and aromatic rings present in the polymeric system.

The five elutions corresponding to interaction of (i) van der Waals type, (ii) accessible hydrogen-bonding, (iii) hydrogen-bonding, (iv) π–π stacking and (v) washing samples were analysed with three different analytical methods. These methods were validated doing a calibration ($r^2 = 0.99$):

- UV spectroscopy is a quick method, but absorbtion bands are difficult to quantify when several compounds are present in the elution fraction. Results were reliable when the polymer cartridges were well washed.
- Mass spectrometry allows the measurement of all compounds present in the samples. The quantification was operated with ions intensity but since the response is very dependent on source cleanliness, calibration has to be repeated before every analysis series.
- HPLC is very time consuming but HPLC chromatograms show peaks corresponding to all compounds present (the template as well as also residual monomers). Peak identification is possible by monitoring the retention time and UV spectrum of GlcNcouma.

All these methods were suitable and showed the following results.

The behaviour of the NIP (material 1) under these SPE conditions was evaluated and compared with the corresponding MIP (material 2).

Simultaneous experiments were quite repeatable and errors of less than ±10% were observed. Fig. 3 indicates the same quantity of GlcNcouma is eluted in solvents ACN 1% AcOH and in toluene for both materials. As mentioned above, addition of acetic acid (as polar modifier) to ACN revealed if hydrogen-bonding was accessible. It is possible to note that this effect is higher for MIP than for NIP. Large amounts of GlcNcouma eluted in toluene indicate π–π interactions of surface with the styrene entities even in non-imprinted systems. No significant difference could be demonstrated between MIPs and respective NIPs (see Figs. 3 and 4) except a higher content in the low polar

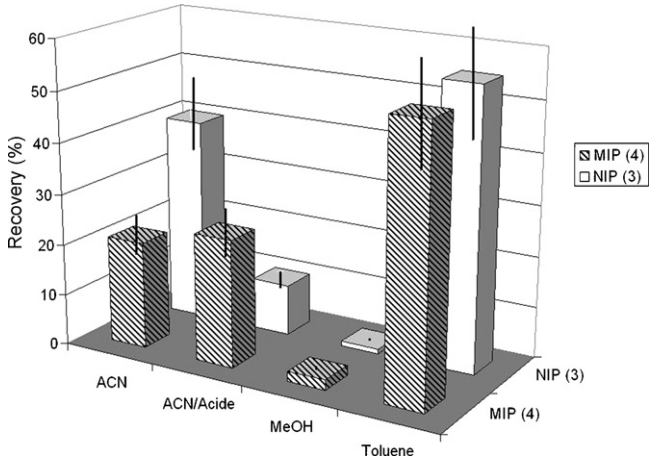

Fig. 3. Comparison of eluted GlcNcouma related to GlcNcouma-MIPs cartridges (material 3 = MIP) and blank (material 4 = NIP) after SPE of standard solution deposited with a mass corresponding to 1/500 phase mass. The repeatability of the measurements was within ±10%.

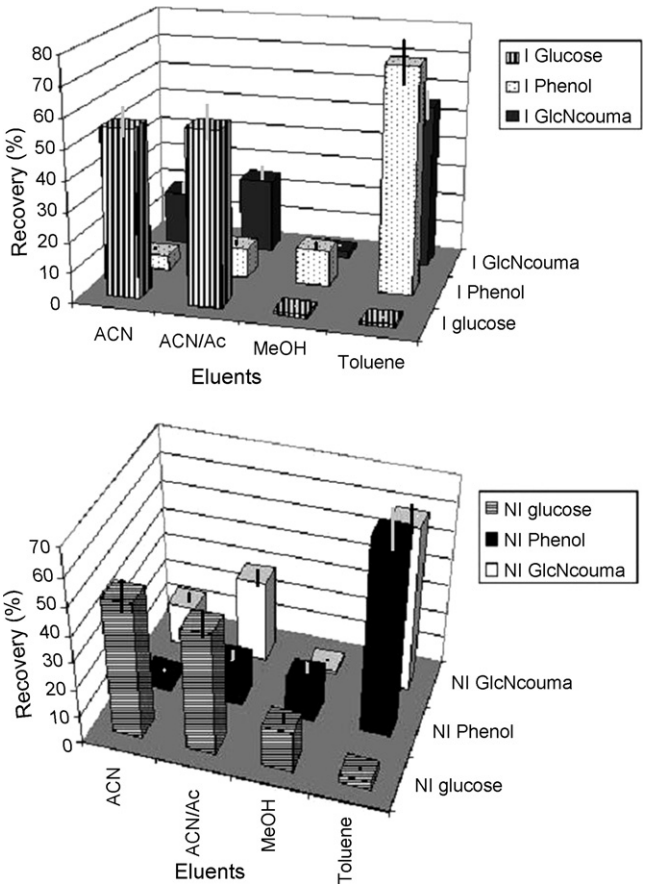

Fig. 4. Comparison of the specificity of GlcNcouma-imprinted (material 2 = MIP and material 1 = NIP) particles for glucose, phenol and GlcNcouma.

ACN 1% AcOH eluent, which might indicate hydrogen-bonding specific to MIP material. It is possible that an imprinting effect occurred, which can also be hypothesized in IRTF where $\nu_{C=O}$ of the template molecule is weakly shifted in the presence of styrene (shift of 6 cm^{-1}).

To ensure the type of interactions present in the system, a study of the interaction between the template and two other compounds, phenol and glucose, have been performed.

GlcNcouma, an amphiphilic monosaccharide which is composed of two parts, was compared with compounds which presented only one of these two groups. The first compound chosen was phenol, which was selected to mime its hydrophobic part, and the second one was glucose because it exhibits hydrophilicity and has the shape of the sugar head. Nevertheless, those two compounds are smaller than GlcNcouma, so this choice is not optimal for cavities to recognize such entities. Fig. 4 shows the profiles of elution of the three compounds after SPE of each one and it is clear that there is a contrast depending on the compound that is considered. With phenol, 75% was eluted in toluene which means that there were interactions between aromatic rings of styrene and phenol. In the case of glucose the results showed a difference of behaviour in the recovery compared to the template. In fact, the total quantity of glucose deposited was eluted in the first step of elution. Significantly, there was no selectivity of the MIP for glucose because it would have been eluted in ACN 1% Ac and MeOH. Since the structure of glucose corresponds to the hydrophilic part of GlcNcouma, the conclusion was that the system did not present specific hydrogen-bonding interactions. Thus, it is possible that the retention of GlcNcouma on the MIP was not due to the hydrophilic part but to the hydrophobic one. Consequently, the imprinting effect that is noted for the MIP is mainly based on the recognition of the hydrophobic part. The question was to be sure that the phenomenon was not due to an increasing of the pore volume. To know if the swelling of the pores before eluting had an influence on the retention of GlcNcouma or recognition of the MIP, the same experiments (for the three compounds mentioned above) were performed on the same phases but previously conditioned with DMF and toluene. The profiles of elution were the same as when ACN was used to condition the cartridges for the three compounds, respectively. These results confirmed that the observed phenomenon implied a π–π stacking effect and was not due to pores swollen. An imprinting effect can be confirmed, in fact, because the specific surface values are not due to "holes" which could have been induced by template aggregates, formed before or during polymerisation. The consequence of such phenomenon should have been an important increasing of S_p from NIP to MIP, but it is not the case (see Table 2). Moreover, synthesis of non-imprinted polymer (material 3) demonstrated (see Section 3.3) that absence of styrene in the polymer did not produce such specific retention.

3.2. Influence of polymerization solvents

Study of porous properties was apprehended by varying the porogen character of different solvents. The solvents used, cited in increasing porogen characteristic order were MeOH, THF/MeOH, Tol/MeOH, Tol/DMF (already described). For all these materials, calculation of the specific area was carried out.

Fig. 5 showed that the higher imprinting effect was exhibited from MIPs which were synthesized in presence of porogeneous solvents such as Tol/MeOH or Tol/DMF. The formation of pores during polymerization was clearly demonstrated to be essential for a better recognition of template molecules. The results are not exactly confirmed by the measuring of specific surfaces because the system Tol/MeOH presents the smallest value (see Table 2).

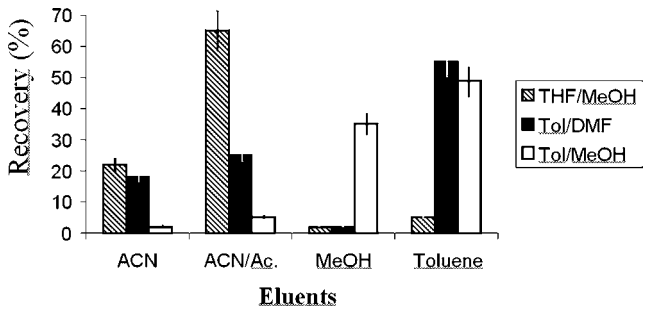

Fig. 5. Comparison of the selectivity of GlcNcouma-imprinted particles for GlcNcouma with three different polymerization solvents. Materials 2 (Tol/DMF); 5 (THF/MeOH); 6 (Tol/MeOH).

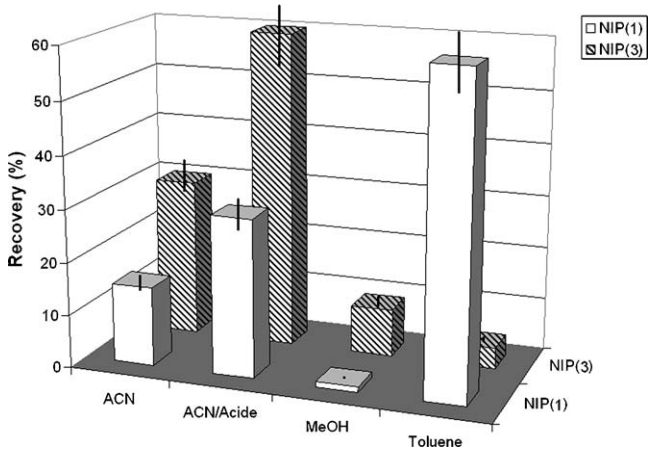

Fig. 6. Influence of the monomer composition studied in the absence of styrene (material).

3.3. Influence of monomer composition

Variation of monomer composition was also performed after the demonstration of π–π stacking between styrene and the aromatic ring of GlcNcouma (NIP1 and MIP2). A new material was tested involving the absence of styrene in the composition by replacing styrene with MMA–NIP3–(methyl methacrylate).

As expected, Fig. 6 showed that there was no GlcNcouma present in the toluene elution, indicating the absence of π–π interactions. All of the GlcNcouma was eluted in the first steps, so the phenomenon of affinity for GlcNcouma was observed only when styrene was used as monomer.

The most likely explanation for such interactions is the presence of pores in the system after polymerization and also the presence of aromatic compounds. To desorb the compound initially deposited on the MIP, the solvent must have an aromatic ring with which to compete with the analyte for the functional groups in the binding sites.

4. Conclusion

The aim of this work was the development of GlcNcouma-MISPE and the evaluation of its efficiency as a stationary phase for solid-phase extraction. Our data clearly indicated that the imprinting effect of MIPs for GlcNcouma was mainly based on π–π interactions and was directly influenced by a number of parameters such as the pore volume, polymerization solvent and monomer composition. The potential advantage of this technique compared to conventional SPE sorbents are immediately evident and include increased reproducibility, a rapid, facile and cost-effective synthesis. Further work involves the optimization of such MISPE as phases of separation techniques.

Acknowledgements

We are grateful to TEMSCAN, the electronic microscopy service of Paul Sabatier University, for the MEB measurements of MIP particles synthesized in this work. We are thankful to Pr. J.M. Beau ICMMO (UMR 8182), Orsay, for the synthesis of GlcNcouma.

References

[1] C. Alvarez-Lorenzo, A. Concheiro, J. Chromatogr. B 804 (2004) 231.
[2] B. Sellergen, J. Chromatogr. A 906 (2001) 227.
[3] L. Schweitz, P. Spégel, S. Nilsson, Electrophoresis 22 (2001) 4053.
[4] N. Masqué, R.M. Marcé, F. Borrull, TrAC 20 (2001) 477.
[5] L.I. Andersson, I. Lars, J. Chromatogr. B 739 (2000) 163.
[6] E. Caro, R.M. Marcé, F. Borrull, J. Chromatogr. A 995 (2003) 233.
[7] C. Widstrand, F. Larsson, M. Fiori, J. Chromatogr. B 804 (2004) 85.
[8] E. Caro, R.M. Marcé, F. Borrull, J. Chromatogr. B 813 (2004) 137.
[9] A. Bereczki, A. Tolokan, G. Horvai, J. Chromatogr. A 930 (2001) 31.
[10] B. Bjarnason, L. Chimuka, O. Ramström, Anal. Chem. 18 (1999) 180.
[11] S.Y. Feng, E.P.C. Lai, E. Dabek-Zlotorzynska, S. Sadeghi, J. Chromatogr. A 1027 (2004) 155.
[12] E. Caro, R.M. Marcé, P.A.G. Cormack, D.C. Sherrington, F. Borrull, J. Chromatogr. A 995 (2003) 233.
[13] M.C. Hennion, J. Chromatogr. A 856 (1999) 3.
[14] X. Gao, Y. Zhang, B. Wang, Tetrahedron 61 (2005) 9111.
[15] E. Oral, N. Peppas, J. Biomed. Res. 68A (2004) 439.
[16] A.G. Mayes, L.I. Andersson, K. Mosbach, Anal. Biochem. 222 (1994) 483.
[17] S. Striegler, Curr. Org. Chem. 7 (2003) 81.
[18] M.O. Rasmussen, B. Hogg, J.J. Bono, Org. Biomol. Chem. 2 (2004) 1908.
[19] F.G. Tama, M.M. Titirici, Anal. Chem. Acta 542 (2005) 38.

Available online at www.sciencedirect.com
ScienceDirect
Talanta 73 (2007) 304–313
Talanta
www.elsevier.com/locate/talanta

A chemometric sensor for determining sulphaguanidine residues in honey samples

A. Muñoz de la Peña *, N. Mora Diez, M.C. Mahedero García, D. Bohoyo Gil, F. Cañada-Cañada

Department of Analytical Chemistry, Faculty of Sciences, University of Extremadura, 06071 Badajoz, Spain

Received 16 November 2006; received in revised form 22 March 2007; accepted 23 March 2007
Available online 30 March 2007

Abstract

The inclusion complex of sulphaguanidine (SGN) in β-cyclodextrin has been investigated. To avoid the problem of the low solubility of β-cyclodextrin in water, solutions of β-cyclodextrin in urea have been used. A 1:1 stoichiometry and an association constant of 450 M^{-1} have been established for the complex. A new spectrofluorimetric method has been developed for the determination of SGN residues in honey samples. This sulphonamide is widely employed for honey treatment. The method for the determination is based on second-order multivariate calibration, applying parallel factor analysis (PARAFAC). No previous separation or samples pre-treatment were required. The calibration solutions were prepared in water, with concentrations in the range from 0.02 to 0.20 μg mL^{-1} for SGN. The use of the second-order calibration method in the standard addition mode, using the excitation–emission matrices (EEMs) as analytical signal, allowed its determination in honey samples, even in the presence of interferences, with satisfactory results. The proposed procedure was validated by comparing the obtained results with a HPLC method, with satisfactory results for the assayed method.

Keywords: Second-order multivariate calibration; Excitation–emission matrices; Sulphaguanidine; Honey; β-Cyclodextrin/urea

1. Introduction

Sulphonamides are a class of antimicrobial drugs that are employed in human and veterinary medicine for therapeutic and prophylactic purposes to fight common bacterial diseases [1].

Residues of sulphonamides have been found in animal products for human consumption, such as honey, milk, eggs, fish or meat [2]; then, different methods of analysis have been reported [3–9]. Such antibiotics are, for example, employed to treat bees infected with bacterial diseases such as the American or European foulbrood [10,11]. However, if bees are treated during the harvest season, residues of these compounds may be found in honey. Most used sulphonamides show a relatively long half-life, generating serious problems in human health, such as allergic or toxic reactions [12]. Currently, no maximum residue level (MRL) exits for this antibiotics/commodity combination in Europe [13], but some countries within the European Union have established action limits or tolerated levels. Belgium and the United Kingdom have action limits of 20 and 50 ng g^{-1}, respectively, referring to the sum of all substances within the sulphonamide-group. France has a limit of 10 ng g^{-1} for sulphathiazole. Switzerland has established a fixed limit of 50 ng g^{-1}, referring to the sum of initial substances (sulphonamides and their metabolites) [14]. For the determination of sulphonamides in honey, HPLC [15–17] methods have been mainly proposed.

Sulphaguanidine (SGN), chemically 4-amino-*n*-(amino-iminomethyl)benzenesulphonamide, is an antimicrobial agent that is used to treat enteric infections. Some methods have been described for its determination in honey, mainly by HPLC [18–20] by using, in some cases, fluorimetric detection after a derivatization [17,21] or MS detection [22,23].

It is known that cyclodextrins (CDs) have the property of forming inclusion complexes, with guest molecules that have suitable characteristics of polarity and dimension [24–26]. The inclusion complex formation in the CD systems is favoured by substitution of the high-enthalpy water molecules located inside the CD cavity, with an appropriate guest molecule of

* Corresponding author. Tel.: +34 924 289375; fax: +34 924 289375.
E-mail address: arsenio@unex.es (A. Muñoz de la Peña).

0039-9140/$ – see front matter © 2007 Elsevier B.V. All rights reserved.
doi:10.1016/j.talanta.2007.03.047

low polarity. There are a few reports dealing with the analytical determination of sulphonamides by using cyclodextrins; and they employ, in general, a capillary electrophoresis technique. In some cases, the inclusion complexes with guest molecules have a higher fluorescence signal than the previous fluorescence signal of the molecule; which is important in order to develop more sensitive analytical methods and, at the same time, it permits working in aqueous media. In the case of SGN, there is a communication following this purpose and it has been proposed a method of determination in urine, by using partial least-squares (PLS) calibration [27].

While the aqueous solubilities of α- and γ-CD at 25 °C are 0.121 and 0.168 M, respectively, that of β-CD is roughly a factor of 10 less, i.e. 0.0163 [28]. Consequently, in many instances, it has been observed that the magnitude of fluorescence enhancement attainable with β-CD is restricted due to its limited water solubility. That is, the fluorescence intensity of many analyte molecules increases with cyclodextrin concentration until the β-CD solubility limit in water is reached. In addition to mixed solvent systems [29], or water-soluble β-CD derivatives [30–32], base media and/or urea [33,34] may be used to increase the water solubility of cyclodextrins, particularly β-CD, and urea has been used in this study.

On the other hand, multivariate calibration is gaining acceptance for the determination of analytes in complex mixtures. Full-spectrum multivariate calibration methods offer the advantage of speed in the determination of the components of interest, avoiding separation steps in the analytical procedure. In this work, multivariate calibration is applied to determine SGN in honey samples. It is known that all first-order calibration methods, including PLS, are sensitive to the presence of uncalibrated interferences. This situation is encountered when dealing with natural samples of complex composition, such as the presently studied honey samples. A good alternative to the problem of unexpected interferences is to move to second-order data [35]. High-order data are particularly suitable for the quantitative analysis of complex multicomponent samples [36]. In recent years, second-order data following the trilinear model, such as excitation–emission fluorescence matrices (EEMs), have been gaining wide-spread analytical acceptance [37]. Data of this kind, when joined for a group of samples, are also known as three-way data. Additionally, the recording of three-way fluorescence information conveys certain advantages: the measurements are carried out on a single instrument, the signals are selective and sensitive, and the obtained models are trilinear.

Example of a usually employed second-order calibration method is parallel factor analysis (PARAFAC) [35]. The PARAFAC algorithm is based on least-squares minimization. The decomposition of the three-way data array built with matrices measured for a number of samples is often unique. This property has been named the second-order advantage [38] and allows spectral profiles and relative concentrations of individual sample components to be extracted directly. EEMs have been used in combination with this chemometric method for quantitative analysis of biological compounds. In this context, quantification of chlorophylls and pheopigments [39], antitumoral [40], anti-inflammatory drugs [5] and antibiotics [41,6] has been proposed. On the other hand, the PARAFAC application to food samples has been scarce [42,7,8].

In the present paper, the interactions of SGN with β-CD in presence of urea were studied, in order to propose a new and more sensitive fluorescence method for its determination in aqueous media. The final purpose is the determination of SGN in honey samples, free of different types of interferences and by using a simple pre-treatment of the sample. For this purpose, the chemometric method PARAFAC, in the standard addition mode, is assayed.

2. Theory: three-way trilinear data

When a sample produces a $J \times K$ data matrix (a second-order tensor), such as an EEM (J = number of emission wavelengths, K = number of excitation wavelengths), the corresponding set obtained by 'stacking' the matrices recorded for each of the I samples included in the calibration set is a three-dimensional or three-way array. Appropriate dimensions of such an array are $I \times J \times K$ (I = number of samples). Since EEMs follow a trilinear model, the array can be written as a sum of tensor product of three vectors for each fluorescent component. If $\mathbf{a}_n$, $\mathbf{b}_n$ and $\mathbf{c}_n$ collect the relative concentration ($I \times 1$), emission ($J \times 1$) and excitation ($K \times 1$) profiles for the component n, respectively, the data array $\underline{\mathbf{F}}$ can be written as

$$\underline{F}_{ijk} = \sum_{i=1}^{N} a_{in} b_{jn} c_{kn} + \underline{E}_{ijk} \quad (1)$$

where $\underline{F}_{ijk}$ is the intensity recorded for the ith sample at j and k channels, N is the total number of responsive components, a_{in} is the relative concentration (or score) of component n in the ith sample, b_{jn} and c_{kn} are the signal intensities at channels j and k in each dimension for component n, and $\underline{E}_{ijk}$ are the elements of the array $\underline{\mathbf{E}}$, which is a residual error array of the same dimensions as $\underline{\mathbf{F}}$. The column vectors $\mathbf{a}_n$, $\mathbf{b}_n$ and $\mathbf{c}_n$ are usually collected into the three loading matrices $\mathbf{A}$, $\mathbf{B}$ and $\mathbf{C}$.

A characteristic property of $\underline{\mathbf{F}}$ is that it can be uniquely decomposed, providing access to spectral profiles ($\mathbf{B}$ and $\mathbf{C}$) and relative concentrations ($\mathbf{A}$) of individual components in the I mixtures, whether they are chemically known or not. This constitutes the basis of the so-called second-order advantage. One popular alternative to decomposing the array $\underline{\mathbf{F}}$ of Eq. (1) is to employ the PARAFAC algorithm. Its underlying theory has been exhaustively described [43]. This method has been implemented in the present study using the standard addition mode [44,45], because this allows to avoiding the internal filter effect caused by the honey components on the fluorescence signal of the analytes.

The PARAFAC components will estimate the signals from the individual fluorophores if the data are approximately low-rank trilinear and the correct number of components is used. The number of components can be estimated using the core consistency diagnostic (CORCONDIA) test [43].

3. Experimental

3.1. Apparatus

Fluorescence spectral measurements were performed on a Fluorescence Spectrophotometer Varian Model Cary Eclipse. The instrument consists of two Czerny-Turner monochromators (excitation and emission), a Xenon light source, a range of fixed width selectable slits, selectable filters, attenuators and two photomultiplier tubes as detectors. The fluorimeter is connected to a PC microcomputer via an IEE serial interface. The Cary Eclipse Version 1.0 software was used for data acquisition, data interpretation and graphical display. All measurements were performed in 10 mm quartz cells at 20 °C, by use of a thermostatic cell holder and a Selecta Model Frigiterm thermostatic bath.

3.2. Reagents

All solvents used were of analytical reagent quality. SGN was purchased from Sigma. Standard solutions of the compound (100 μg mL^{-1}) were prepared by dilution in deionized water. Stock solutions of α-cyclodextrin (α-CD), β-cyclodextrin (β-CD), γ-cyclodextrin (γ-CD), (2-hydroxy)-propyl-β-cyclodextrin (HP-β-CD) and heptakis-(2,6-di-*O*-methyl)-β-cyclodextrin (DIMEB) of concentration 1.5×10^{-2} M in water and β-CD 1×10^{-1} M in 4 M urea, were prepared. A 1 M sodium acetate–acetic acid (pH 5.5) buffer solution was prepared from analytical reagents.

3.3. Software

The calculations were done using MATLAB 5.3 [46]. Appropriate routines for applying PARAFAC, developed by Bro, are available on the internet [47], although a useful MATLAB graphical interface has been used for easy data manipulation and graphics presentation [48]. This interface provides a simple mean of loading the data matrices into the MATLAB environment. It also allows selecting appropriate recording spectral regions, optimizing the number of factors, and plotting emission and excitation spectral profiles and pseudo-univariate calibration graphs.

Ground-state geometry optimization of the proposed structures for the inclusion complexes was performed with the AM1 method contained in the CHEM3D package, version ultra 8.00, on a Pentium PC microcomputer. The molecular mechanics method was used to obtain the initial structures. Afterward, the energy was minimized by the AM1 method.

3.4. Procedure for determining sulphaguanidine in honey samples

A honey dilution factor of 1:20 was optimum, as a compromise between internal filter effects from honey and the linear analytical range. In a 5.00 mL flask, 1 g of honey was spiked with SGN and, after 10 min, completion to the mark was achieved with deionized water. From this latter solution, 0.70 mL were diluted in a 3.00 mL flask with 0.90 mL of 1 M solution of acetic acid/sodium acetate of pH 5.5, then 1.40 mL of 10^{-1} M solution β-cyclodextrin/urea 4 M solution were added and, finally, completing to the mark with deionized water. After that, the flask was vigorously shaken and the final solution was placed in a quartz cell, and the fluorescence EEM was registered in the selected spectral regions for this analyte.

4. Results and discussion

4.1. Fluorimetric study of the inclusion complex of sulphaguanidine with β-CD

SGN shows native fluorescence. The excitation spectrum shows a maximum located at 264 nm and the emission spectrum shows a maximum at 340 nm, spectrum (1) in Fig. 1.

Although α-, β-, γ-, HP-β-CDs and DIMEB were investigated, only β-CD, HP-β-CD and DIMEB produced changes on the fluorescence spectra of SGN. In Fig. 1, the emission spectra of SGN:α-CD (2), SGN:γ-CD (3) and SGN:β-CD (5) are shown. β-CD was selected because produces the higher signal of fluorescence and the smaller blank signal. As may be appreciated, the changes in the fluorescence signals are significant, and the excitation and emission wavelengths of the fluorescence spectra do not change. The fact that the fluorescence enhancement in β-CD is higher than with the other ones CDs is related to a better compatibility of the molecular size of SGN with respect to the β-CD cavity. The α-CD cavity is too small to accommodate the SGN molecule, and no inclusion complex is formed in the presence of this CD. On the contrary, γ-CD is too large to SGN size and the inclusion complex formed is weaker than in β-CD. It was observed that the intensity of fluorescence increases when increasing the concentration of β-CD. A value of β-CD concentration of 9×10^{-3} M was selected as optimum for the experiments, by dissolving β-CD in water.

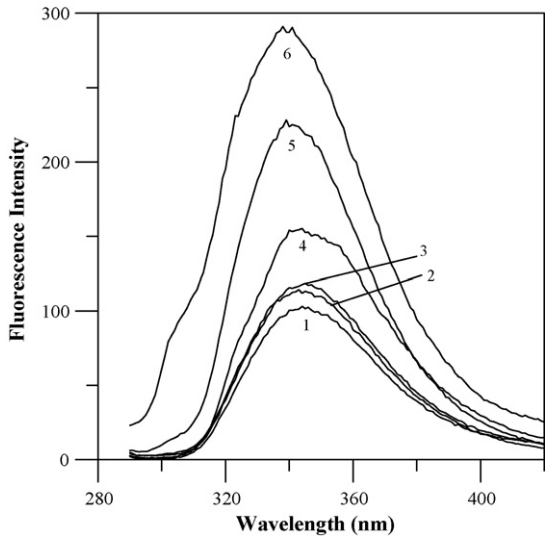

Fig. 1. Emission spectra of (1) SGN in water; (2) SGN:α-CD; (3) SGN:γ-CD; (4) SGN in urea 4 M; (5) SGN:β-CD; (6) SGN: β-CD/urea; λ_{ex}: 264 nm, [SGN] = 1 μg mL^{-1}, [α-, β- and γ-CD] = 9×10^{-3} M, [β-CD]/urea 1×10^{-1} M in urea 4 M.

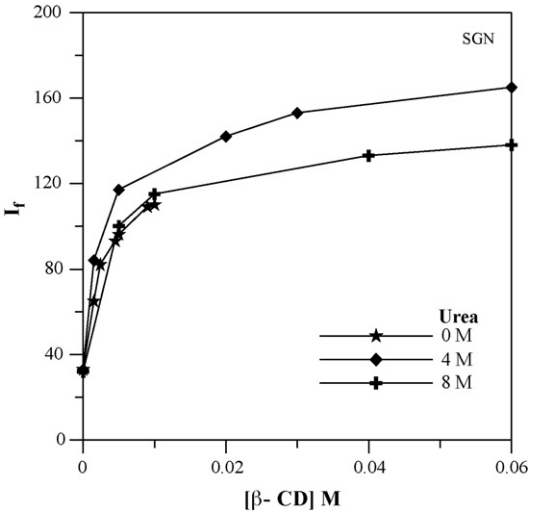

Fig. 2. Effects of urea and β-CD concentration in the fluorescent signal of SGN complex. [SGN] = 1 μg mL^{-1}; λ_{ex} = 264 nm; λ_{em} = 340 nm.

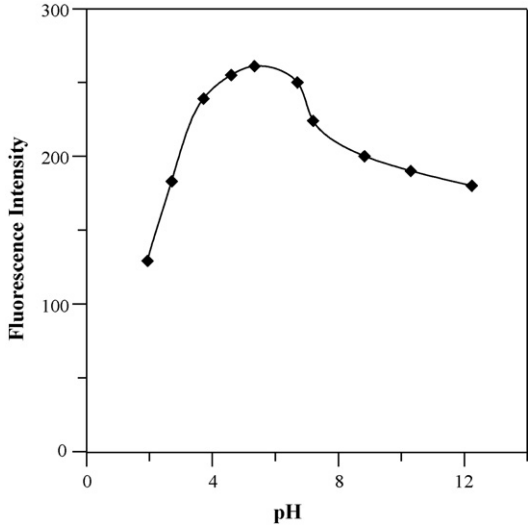

Fig. 3. Influence of pH on the fluorescence intensity of SGN:β-CD/urea complex; λ_{ex} = 264 nm; λ_{em} = 340 nm, [SGN] = 1 μg mL^{-1}, [β-CD]/urea 1×10^{-1} M in urea 4 M.

4.2. Influence of urea concentration

The fluorescence intensity of SGN increases in urea solutions, as is represented in Fig. 1, spectrum (4), but is smaller than in β-CD (5) as can be appreciate in this Fig. 1. We have investigated the SGN:β-CD complex formation, using solutions of β-CD in urea, with the aim of increasing the solubility of β-CD and then the fluorescence enhancement.

A great increase in the solubility of β-CD was observed in presence of urea, and solutions containing 10^{-1} M of β-CD were prepared, 10 times more concentrated than in aqueous solutions. The influence of urea concentration in the fluorescence signal was studied by monitoring the influence of the β-CD concentration in the fluorescent signal in presence of 0, 4, and 8 M of urea, as shown in Fig. 2. A significant increase in the fluorescent signal was observed and a concentration of 4 M was selected as optimum urea concentration, because it provided the highest fluorescence signal enhancement. Emission spectrum of SGN:β-CD/urea 4 M complex is shown in Fig. 1, spectrum (6) and, as can be seen, the fluorescence intensity increases three-fold with regard to SGN solutions in water, spectrum (1).

The presence of urea produces a higher enhancement of the fluorescence of SGN because β-CD is more soluble in urea than in water. This allows the use of more concentrated β-CD solutions, which imply to increase the proportion of analyte molecules that is included in the β-CD cavity. It is important to note that the binding constants reported for some compounds decreased in the β-CD/urea medium and the equilibrium constant values were found to decrease as the urea concentration was increased [49], as it is appreciated in Fig. 2. This is presumably due to the fact that, at high concentrations, the urea competes with the analyte molecule for cavity binding site.

4.3. Study of the influence of pH

A study of the influence of pH in the fluorescence spectra of the SGN:β-CD system has been carried out. The results obtained are presented in Fig. 3. As can be appreciated, the fluorescence is maximum and practically constant for pH values between 4.5 and 6.5. For values of pH higher than this range, the fluorescence decreases. For sulphaguanidine, values of pK_1 of 2.75 [49,50], 2.7 [51], and 3.3 [52] have been reported. The pK values reported in the references are consistent with the results presented in Fig. 3. In a previous work [27], the influence of pH on SGN fluorescence intensity, in the absence and presence of β-CD, was established, showing that the inclusion processes of the SGN in the cyclodextrin cavity is not affecting its acid–base properties. This fact may be explained taking into account that the changes in the spectra with pH are due to the proton exchange between the monocationic nitrogen atom of the *p*-amino benzene group and the neutral molecule, and this part of the molecule is protruding outside of the cavity.

4.4. Influence of the buffer concentration and order of addition of reagents

Several buffer solutions were studied in the optimum pH range, with the aim of proposing a method for the determination of SGN in presence of β-CD. Acetic acid/sodium acetate buffer at pH 5.5 and potassium dihydrogen phosphate buffer adjusted to pH 6.5 with NaOH, were tested. No significant differences were found, Fig. 4, and the acetic acid/sodium acetate buffer (pH 5.5) was selected, and the changes of the fluorescence intensity with the buffer concentration were not appreciable. A 0.3 M concentration was chosen as the optimum. The order of addition of the reagents had no influence on the complexation, and the inclusion process was attained immediately.

4.5. Stoichiometry of the inclusion complex

The stoichiometry of the complex with β-CD/urea 4 M was established by the methods of Benesi–Hildebrand [53] and

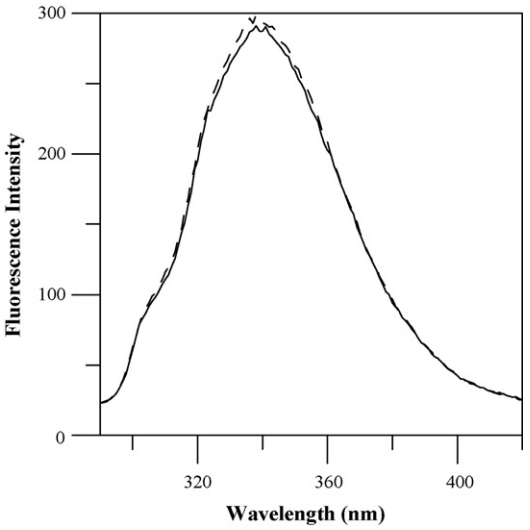

Fig. 4. Influence of the buffer: (- - -) acetic acid/sodium acetate buffer 0.3 M at pH 5.5, (—) potassium dihydrogen phosphate buffer 0.2 M adjusted to pH 6.5 with NaOH. [SGN] = 1 μg mL^{-1}, [β-CD]/urea 1×10^{-1} M in urea 4 M.

Scatchard [54]. The following equilibrium can be considered:

$$\beta\text{-CD} + \text{SGN} \rightleftharpoons \text{SGN} : \beta\text{-CD/urea}$$

In the Benesi–Hildebrand's method, in the case of a 1:1 complex, the following equation is applicable:

$$\frac{1}{F - F_0} = \frac{1}{(F_\infty - F_0)K_1[\beta\text{-CD}]_0} + \frac{1}{F_\infty - F_0} \quad (2)$$

where $[\beta\text{-CD}]_0$ denotes the initial β-CD concentration, F_0 denotes the fluorescence intensity of SGN molecule in the absence of β-CD, F_∞ denotes the fluorescence intensity when SGN is essentially complexed with β-CD, and F is the observed fluorescence at each β-CD concentration tested.

If the stoichiometry is 1:1, the representation of $1/(F - F_0)$ versus $1/[\beta\text{-CD}]_0$ gives a linear plot as in Fig. 5A, which supports the existence of a 1:1 complex.

In the Scatchard's method, in the case of a 1:1 complex, the relationship between the observed fluorescence intensity enhancement $(F - F_0)$ and the β-CD concentration is given by

$$\frac{F - F_0}{[\beta\text{-CD}]_0} = (F_\infty - F_0)K_1 - (F - F_0)K_1 \quad (3)$$

If the stoichiometry is 1:1, the plotting of $(F - F_0)/[\beta\text{-CD}]_0$ versus $(F - F_0)$ gives a straight line as in Fig. 5B, confirming the 1:1 stoichiometry.

4.6. Association constant of the inclusion complex

Once the stoichiometry of the system is known, the association constant can be calculated. A good estimation can be made by using non-linear least-squares regression analysis (NLR) [55]. The value calculated for the constant of formation of the investigated complex by means of the NLR approach is 450 M^{-1}.

4.7. Characterizing the inclusion complex

With the purpose of further characterizing the inclusion complex, semiempirical MO calculations using the AM1 program were performed. This program is commonly used to study geometric and thermodynamic properties of organic molecules, especially when hydrogen bonding occurs [56]. Several initial modes of inclusion were probed and optimized by energy minimization. The complex structure leading to the minimum heat of formation shows the amino ring located inside of the β-CD cavity. This fact is not surprising, since the most probable mode of binding in the CD inclusion complexes involves the insertion of the less polar part of the molecule into the cavity, while the more polar groups are exposed to the bulk solvent outside the opening of the cavity. The optimized structures of β-CD, SGN and the complex, obtained by energy minimization, are displayed in Fig. 6a–d, respectively. It is important to note that urea has not been included in the inclusion complex because is considered to be the solvent due to its high concentration. However, it is necessary to consider that, in accordance with the small size of the urea molecules and its high concentration, several urea molecules may be included in the

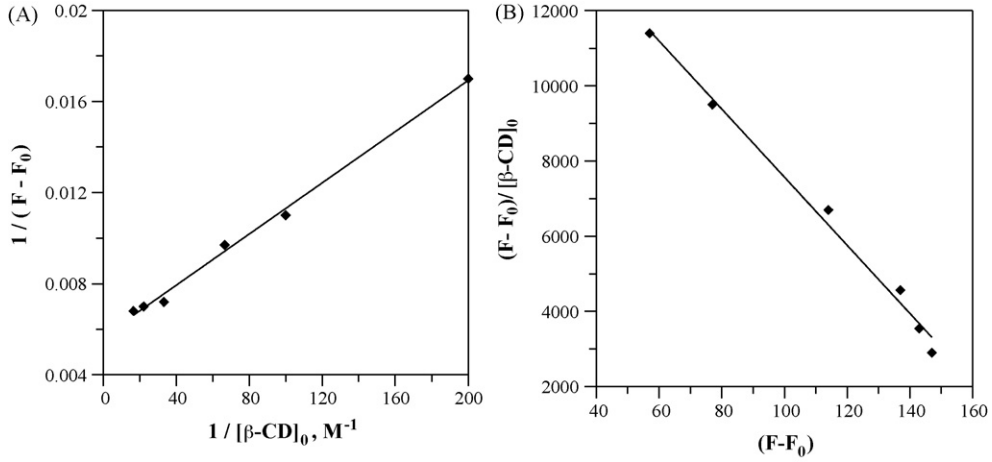

Fig. 5. (A) Benesi–Hildebrand plot for the SGN:β-CD/urea 4 M complex. (B) Scatchard plot for the complex.

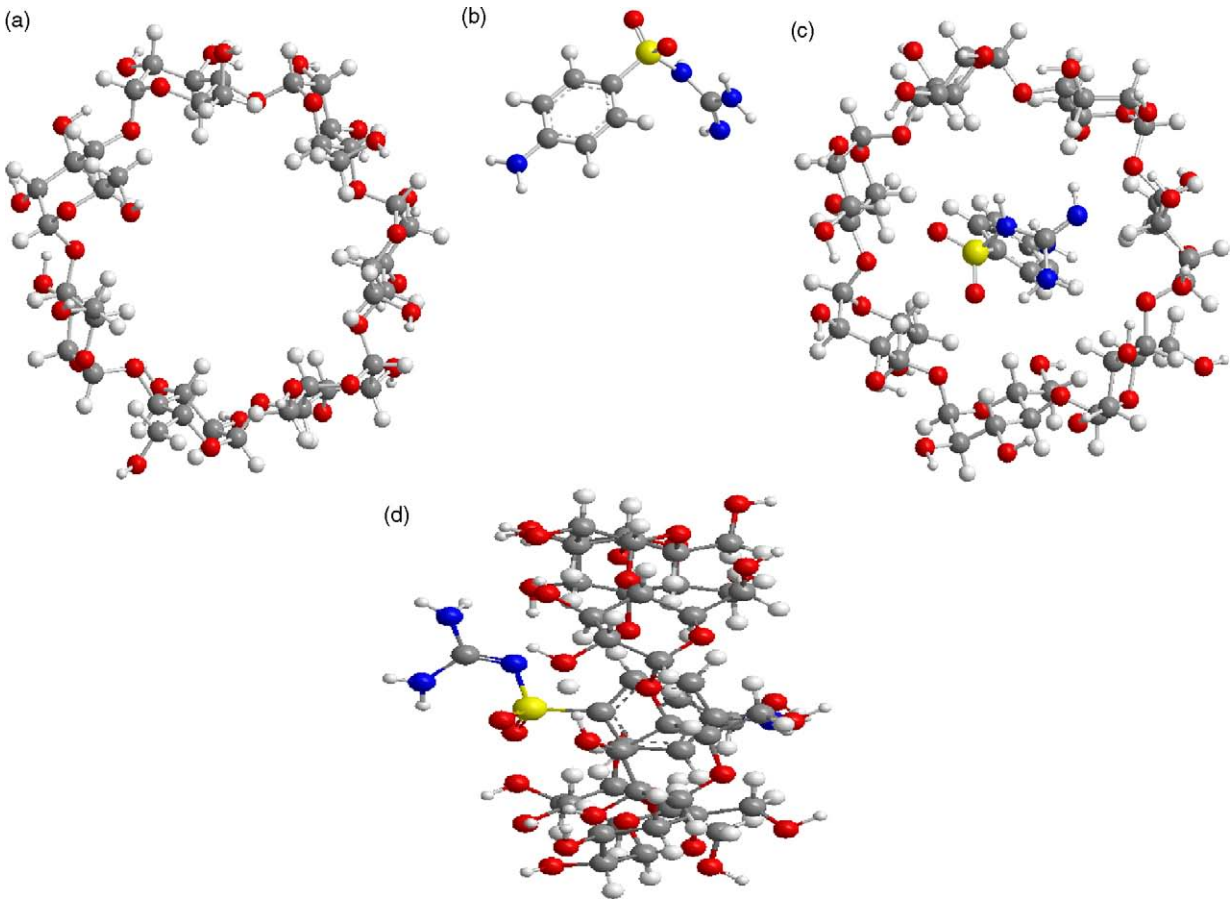

Fig. 6. Optimized structures of (a) β-CD; (b) SGN; (c) SGN:β-CD/urea 4 M complex; (d) size view of the inclusion complex.

empty space of the cyclodextrin. With regard to the driving forces leading to the inclusion complexation of cyclodextrin, these should include the electrostatic interaction, van der Waals interaction, hydrophobic interaction, hydrogen bonding, and charge-transfer interaction. Usually, it is found that van der Waals interaction and hydrophobic interaction constitute the major driving forces for cyclodextrin complexation, whereas electrostatic interaction and hydrogen bonding can significantly affect the conformation of a particular inclusion complex [57].

4.8. Determination of sulphaguanidine in honey samples

4.8.1. Selection of spectral ranges to register excitation–emission matrices

In the above-mentioned chemical conditions: β-CD/urea 6×10^{-2} M/4 M, acetic acid/sodium acetate buffer 0.3 M pH 5.5, maximum information on this drug can be scanned in the region $\lambda_{em} = 310–380$ nm, at 2 nm intervals, exciting in the range 220–290 nm, at 5 nm intervals. In these spectral ranges, with complete EEMs (Fig. 7A), the presence of the first-order Rayleigh is detected. It is well known that these scatterings do not contain any information concerning the fluorescence properties of the analyte. In order to avoid them and to focus on the responsive spectral regions for this analyte, the wavelength ranges have been appropriately reduced (Fig. 7B): emission from 320 to 364 nm and excitation from 235 to 290 nm, for SGN complex analysis.

4.8.2. PARAFAC in the standard addition mode

To apply the standard addition method, a separate calibration scheme is necessary for the analyte. First, to an aliquot of the diluted honey problem sample, four different amounts of SGN were added, keeping the final concentration within the linear range, and the EEM was then registered for each of the resulting solutions. It is to say, the way of working with PARAFAC in the standard addition mode is different than in the external calibration mode. The difference is that the calibration matrix is constructed by directly working with the problem samples, to which different standard additions of the analyte of interest are made. In this mode of calibration, the procedure is slightly more time consuming than in the external calibration mode, as for each sample problem to be analyzed, we have to perform a series of standard additions for our analyte.

The advantage of this chemometric approach is related to the minor time necessary to perform the determination of SGN in honey samples, when is compared with a chromatographic method, because no pre-conditioning are needed in this procedure.

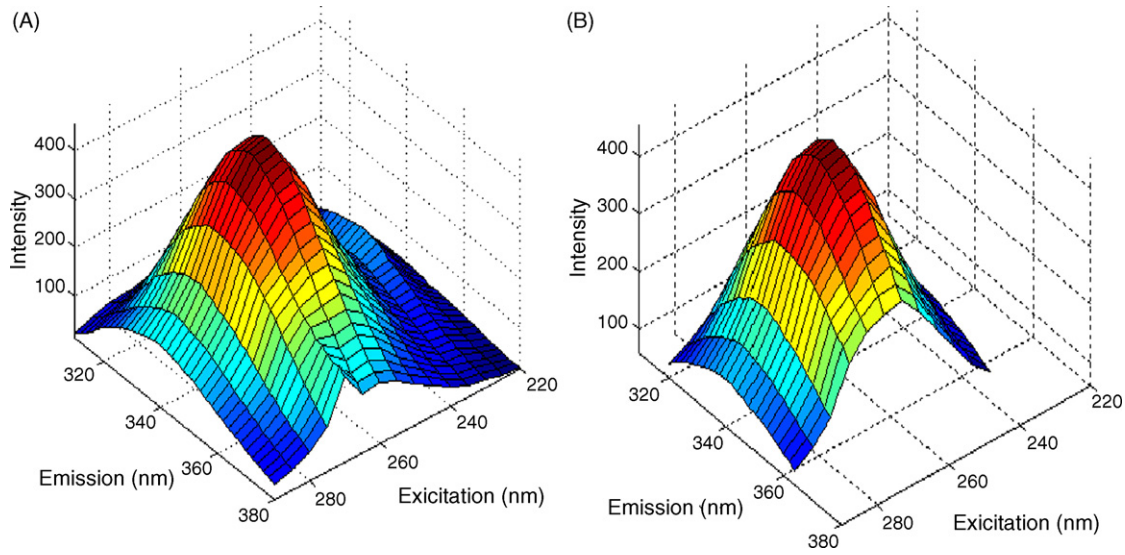

Fig. 7. Three-dimensional excitation–emission matrices (EEMs) of a standard solution of SGN in the complete spectral regions (A) and in the corresponding selected spectral ranges (B). In both cases, the concentration of the analyte is 0.2 μg mL^{-1}.

4.8.3. Selection of the number of components

In order to determine the optimal number of factors for each test honey sample in the case of PARAFAC, the value of the core consistency parameter was analyzed as a function of a trial number of components [43]. For the Canadian honey sample (Table 1), this diagnostic tool indicated that the number of loadings needed to model the data, N, is 2 (Fig. 8). As can be seen, the core consistency drops to a very low value when using three spectral components to model the cube, suggesting that $N = 2$ is a sensible choice. The same number of factors was also found for the remaining honey samples, showing that the presence of honey adds new fluorescent components to the data cube, collectively considered as a single extra component by PARAFAC.

Table 1
Prediction results for SGN in spiked honey samples using PARAFAC in the standard addition mode

Sample	SGN			SMTX
	Spiked[a] (μg L^{-1})	Found[b]	Rec. (%)	Spiked (μg L^{-1})
Switzerland honey	42	44 (2)	105	–
	46	43 (1)	93	–
Canadian honey	51	53 (3)	104	–
	56	54 (3)	96	–
Spain honey	44	47 (4)	107	–
	49	46 (3)	94	–
Belgium honey	42	44 (3)	104	44
	46	45 (2)	98	49
Switzerland honey	51	52 (1)	102	42
	54	53 (2)	98	46
Spain honey	44	46 (2)	104	51
	49	47 (4)	96	54

[a] Concentration in the final solution to measure.
[b] Standard deviation in parentheses.

Once the number of components was estimated, the array formed by joining the EEMs for the test sample and those obtained by standard addition was subjected to decomposition. Employment of this method implies that the array decomposition should be repeated for each newly analyzed sample. The identification of the chemical constituents under investigation is required before quantitation by resorting to the pseudo-univariate calibration graph provided by PARAFAC. This is done with the aid of the spectral profiles extracted by this algorithm, and comparing them with those for a standard solution of the pure analyte of interest (Fig. 9). Absolute analyte concentrations are obtained after proper standard addition calibration, starting from the known amounts of analyte added to the test samples.

These emission and excitation spectral profiles are contained in matrices **B** and **C**, respectively. The components have been

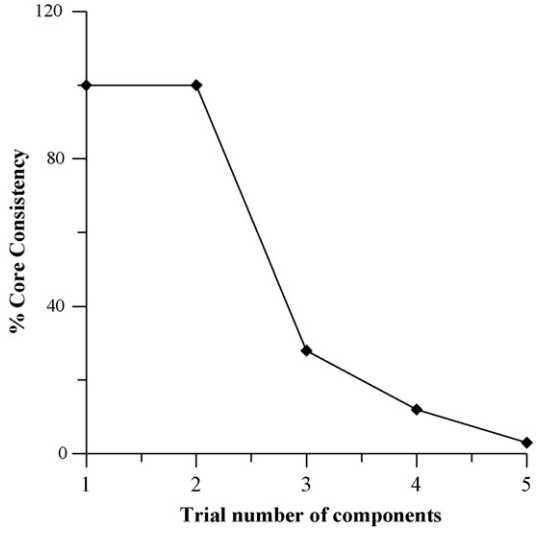

Fig. 8. Plot of the PARAFAC core consistency values as function of the trial number of components.

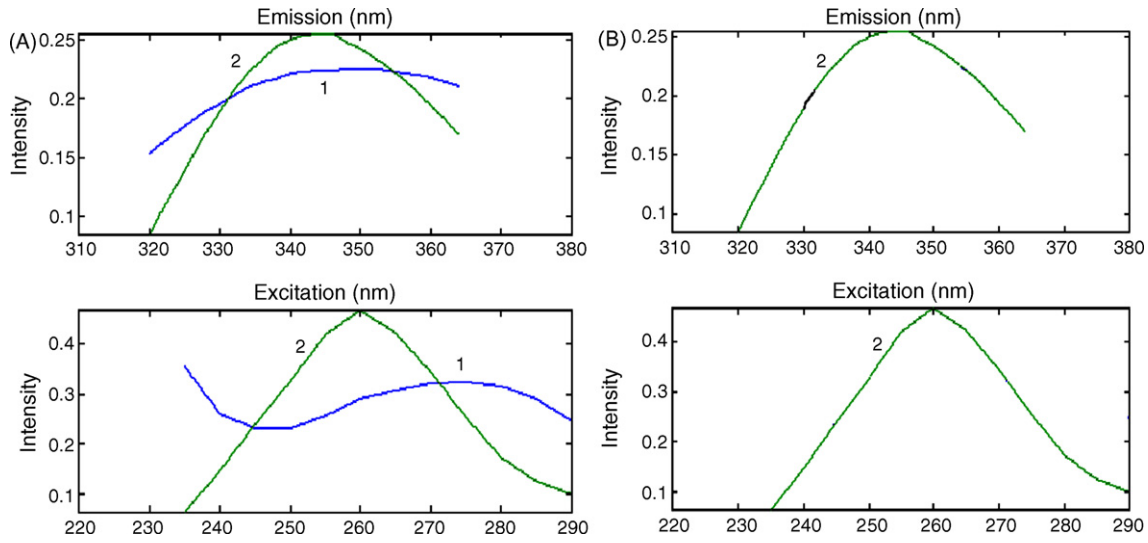

Fig. 9. (A) Emission and excitation profiles provided by a three-component PARAFAC model (**B** and **C** matrices, respectively), obtained after processing the array formed by the EEM for honey sample number 5 and those recorded after standard additions of SGN. The profiles shown as (1) can be matched with the honey components, and those as (2) with spectra of SGN. (B) Normalized experimental emission and excitation spectra for the one studied analyte.

labelled with the order assigned by the model, i.e., they appear in the order of their contribution to the total of the variance. The comparison of the excitation and emission profiles extracted by the PARAFAC model with the experimental ones shows a satisfactory agreement. Similar success was observed on studying the remaining samples of Table 1 with this chemometric model, after the standard addition of the analyte.

4.8.4. Figures of merit

The sensitivity (SEN) for a particular analyte has been estimated as the net analyte signal at unit concentration, whereas the selectivity (SEL) has been computed as the ratio between the sensitivity and the total signal, as suggested by Kalivas and coworkers [58]. The analytical sensitivity, in analogy with univariate calibration, has been computed as the ratio between sensitivity and spectral noise:

$$\gamma = \frac{\mathrm{SEN}}{[V(R)]^{1/2}} \tag{4}$$

The inverse (γ^{-1}) establishes the minimum concentration difference that can be appreciated by the method [59]. The factor $V(R)$ in Eq. (4) is the variance of the instrumental signal, which may be estimated by replicate blank measurements. The limit of detection of the method can be estimated as

$$\mathrm{LOD} = 3.3s(0) \tag{5}$$

where $s(0)$ is the standard deviation in the predicted concentration of the analyte of interest in a blank sample [60].

The analytical figures of merit of the PARAFAC calibration model for SGN calibration are: SEN (fluorescence units) ($\mathrm{L\,mg^{-1}}$) = 1654; SEL = 0.50; γ^{-1} ($\mathrm{mg\,L^{-1}}$) = 0.0022; LOD ($\mathrm{mg\,L^{-1}}$) = 0.010.

4.8.5. Prediction results in honey samples

In Fig. 10, the pseudo-univariate calibration graph obtained by applying PARAFAC in the standard addition mode, for SGN determination in the first sample of Table 1, is plotted. Four different amounts of SGN (40, 80, 120 and 160 $\mu\mathrm{g\,L^{-1}}$) were added, keeping the final concentration within the linear range. Honey samples spiked with SGN in the range between 42 and 56 $\mu\mathrm{g\,L^{-1}}$ were analysed by the above proposed method. The concentrations found for SGN in honey samples are summarized in Table 1. All predictions are seen to be reasonable for samples of the complexity of honey. Comparison of the predicted concentrations and recoveries provided by the algorithm shows a good predictive ability towards the test set of spiked honey samples, and confirms the potentiality of the presently studied second-order methods for the analysis of complex food samples.

4.9. Validation of the proposed method

The proposed fluorimetric method, for the determination of SGN residues in honey samples, was validated by comparison

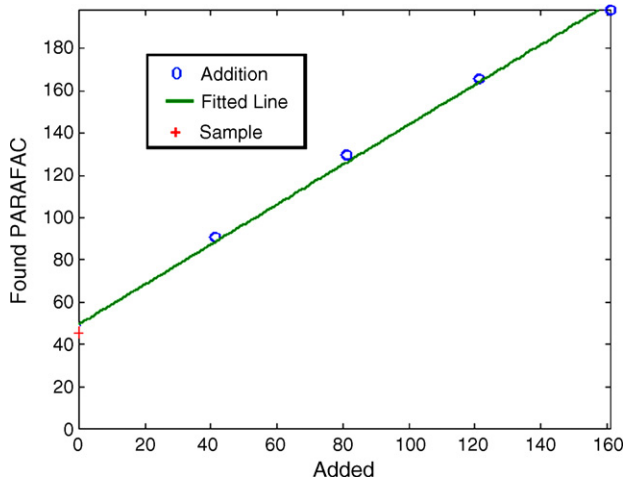

Fig. 10. Pseudo-univariate calibration obtained after standard additions of SGN processing the array formed by the EEM for honey sample number 1.

with a method based on HPLC separation [19], modified by us. We have utilized fluorescent detection, as the sensitivity of the method gets better considerably. An excitation wavelength of 260 nm and an emission wavelength of 340 nm were selected to monitoring SGN. The mobile phase was formed by a mixture of solvent A, being a pH 3.0 aqueous citric–citrate buffer and 0.019 M SDS. The buffer concentration was 10 mmol L^{-1}. Solvent B, acetonitrile. The mobile phase composition was 94% A and 6% of B.

A comparison of the mean recoveries and standard deviations provided by both methods (HPLC: 101.5 ± 6.6 and PARAFAC: 100.1 ± 4.8) was done by applying the "*t*-Student" and "*F*-test", respectively [61]. The comparison of the mean values of two methods can be performed by means of a *t*-test. To apply this test it is necessary to know if the variances of both methods differ or not significantly. These variances are estimated by s_1^2 and s_2^2 (*s* is the standard deviation of the method) and a two-sided *F*-test is used to determine if there is any statistical difference between the variances. The statistic *F* is calculated by $F_{cal} = s_1^2/s_2^2$. The number of degrees of freedom of the numerator and denominator are $n_1 - 1$ and $n_2 - 1$, respectively. The comparison between the $F_{cal} = 1.89$ and *F* tabulated, $F_{11,11} = 3.47$, being the calculated value less than the tabulated one, so there is no significant difference between the two variances at the 5% significance level ($P = 0.05$), therefore, the precision of both methods is similar. As residual variances are equal, the pooled estimated variance is calculated according to the expression: $s^2 = [(n_1 - 1)s_1^2 + (n_2 - 1)s_2^2]/(n_1 + n_2 - 2)$. The *t*-test is then performed by calculating t_{cal}, equation: $t = (\bar{x}_1 - \bar{x}_2)/s[(1/n_1 + 1/n_2)]^{1/2}$, where $\bar{x}$ is the mean value of each method. This t_{cal} (0.54) is compared with the tabulated *t* value ($t_{tab} = 2.09$) having $n_1 + n_2 - 2$ degrees of freedom at the 5% significance level ($P = 0.05$), in this case, t_{cal} (0.54) < t_{tab} (2.09), indicating that the two methods give results that are not statistically different.

4.10. Interferences studies

The possibility of other sulphonamides interference was investigated. For that, the fluorimetric signal of SGN at 0.5 μg mL^{-1}, was compared with the fluorimetric signals in the presence of different concentrations of the others (0.5, 1, 1.5 μg mL^{-1}). The sulphonamides assayed were: sulphamethoxazole, sulphathiazole, sulphadimethoxine, sulphamethazine, sulphamerazine, sulphaquinoxaline, sulphadiazine and sulphacetamine.

There was only interference in the case of sulphamethoxazole above the concentration relation, sulphaguanidine:sulphamethoxazole, 1:3.

4.11. Determination of sulphaguanidine in honey samples in presence of sulphamethoxazole

In order to prove the robustness of the proposed method, and taking into account that sulphamethoxazole (SMTX) is an interference in the determination of sulphaguanidine by the proposed method and, at the same time, it is possible to find residues of SMTX in honey, the determination of SGN in honey in the presence of SMTX was investigated.

The PARAFAC calibration model was established, in the standard addition mode, by treating the honey samples, contaminated with SGN and SMTX, as previously described. In this case, although we have two analytes and the honey background signal, the number of factors is 2 and not 3, because the calibration is realized with respect to SGN, considering the model SMTX and the honey signal as only one interference.

All predictions (Table 1) are good and similar to those obtained in the absence of SMTX interference. Then, the potentiality of the presently studied second-order method in the standard addition mode is proved.

5. Conclusions

The fluorimetric determination of sulphaguanidine in a complex matrix such as honey, using a second-order multivariate calibration technique, is demonstrated to be feasible. The method is developed in β-cyclodextrin/4 M urea medium, enhancing the fluorescence emission of the aqueous solutions of the analyte, which is advantageous in terms of sensitivity. An adequate selection of the EEMs excitation and emission ranges, to avoid first-order Rayleigh and second-order diffraction grating harmonic signals, improved the predictive capacity of the model. The employed PARAFAC second-order calibration method, when applied using the standard addition mode, is able to model the system in the present situation, through the unique decomposition of the three-way data array. This allowed the direct extraction of excitation and emission spectral profiles, as well as the relative concentrations of the analyte. Reasonably good recovery values were obtained in all the analyzed honey samples. Then, the proposed method shows the possibility of a chemometric sensing of sulphaguanidine residues in honey samples free of interference from the matrix components and other possible interferences as sulphamethoxazole, by using a very simple sample pre-treatment.

Acknowledgements

Financial support was provided by DGI-MEC of Spain (Project CTQ 2005-02389) and Junta de Extremadura-Consejería de Educación Ciencia y Tecnología and FEDER (Project 2PR 04A007). Diego Bohoyo Gil is grateful to the Consejería de Educación, Ciencia y Tecnología de la Junta de Extremadura for a fellowship (DOE 21/06/01). The authors are grateful to Diego Airado Rodríguez for his help in the validation of the method by the liquid chromatography method.

References

[1] G.L. Mandell, M.A. Sande, in: A. Goodman, T.W. Gilman, A.S. Rall, P. Nies, Taylor (Eds.), The Pharmacological Basis of Therapeutics, Pergamon Press, New York, 1990, pp. 1047–1064.
[2] A. Adesiyun, N. Offiah, V. Lashley, N. Seepersadsingh, S. Rodrigo, K. Georges, J. Food Prot. 68 (2005) 1501.
[3] W. Horwitz, J. Assoc. Off. Anal. Chem. 64 (1981) 104.
[4] W. Horwitz, J. Assoc. Off. Anal. Chem. 64 (1981) 814.

[5] G. Stoev, A. Michailova, J. Chromatogr. A 871 (2000) 37.
[6] D.H. Kim, J.O. Choi, J. Kim, D.W. Lee, J. Liq. Chromatogr. Relat. Technol. 26 (2003) 1149.
[7] N.J. Lee, C.K. Holtzapple, M.T. Muldoon, S.S. Deshpande, L.H. Stanker, Food Agric. Immunol. 13 (2001) 5.
[8] B. Roudant, M. Garnier, Food Addit. Contam. 19 (2002) 373.
[9] M.C. Mahedero Garcia, N. Mora Diez, D. Bohoyo Gil, F. Salinas Lopez, J. Pharm. Biomed. Anal. 38 (2005) 349.
[10] T.A. Gochnauer, Bee World 35 (1954) 187.
[11] P.S. Milne, Nature 155 (1945) 335.
[12] J.P. Sanderson, D.J. Naisbitt, B.K. Park, AAPS J. 8 (2006) E55.
[13] Commission of the European Communities, Council Regulation EEC 2377/90, Off. J. L 224 (1990) 1.
[14] K.E. Maudens, G.-F. Zhang, W.E. Lambert, J. Chromatogr. A 1047 (2004) 85.
[15] G.F. Pang, Y.Z. Cao, C.L. Fan, J.J. Zhang, X.M. Li, Z.Y. Li, G.O. Jia, Anal. Bioanal. Chem. 376 (2003) 534.
[16] L. Verzegnassi, M.C. Savog-Perround, R.H. Stadler, J. Chromatogr. A 977 (2002) 77.
[17] K.E. Maudens, G.F. Zhang, W.E. Lambert, J. Chromatogr. A 1047 (2004) 85.
[18] R.D. Caballero, J.R. Torres-Lapasio, J.J. Baeza-Baeza, M.C. Garcia-Alvarez-Coque, J. Liq. Chromatogr. Relat. Technol. 24 (2001) 117.
[19] A. Szymanski, Chem. Anal. (Warsaw) 45 (2000) 521.
[20] F. Belliardo, J. Apic. Res. 20 (1981) 44.
[21] I. Schwaiger, R. Schuch, Dtsch. Lebensm. Rundsch. 96 (2000) 93.
[22] A. Kaufmann, S. Roth, B. Ryser, M. Widmer, D. Guggisberg, J. AOAC Int. 85 (2002) 853.
[23] A. Krivohlavek, Z. Smit, M. Bastinac, I. Zuntar, F. Plavsic-Plavsic, J. Sep. Sci. 28 (2005) 1434.
[24] J. Szejtli, Cyclodextrins and their Inclusion Complexes, Akademiai Kiado, Budapest, 1982.
[25] S. Scypinski, L.J.C. Love, Anal. Chem. 56 (1984) 331.
[26] A. Muñoz de la Peña, T.T. Ndou, J.B. Zung, K.L. Greene, D.H. Live, I.M. Warner, J. Am. Chem. Soc. 113 (1991) 1572.
[27] N. Mora Díez, A. Muñoz de la Peña, M.C. Mahedero García, D. Bohoyo Gil, F. Cañada-Cañada, J. Fluoresc. 17 (2007) 309.
[28] N. Wiedenhof, J.N. Lammers, Carbohydr. Res. 143 (1968) 409.
[29] M.J. Jozqiakowski, K.A. Connors, Carbohydr. Res. 143 (1985) 51.
[30] J. Debowski, D. Sybilska, J. Chromatogr. 353 (1986) 409.
[31] T. Cserhati, J. Bojarski, E. Fenyvesi, J. Szejtli, J. Chromatogr. 351 (1986) 356.
[32] M. Tanaka, T. Miki, T. Shono, J. Chromatogr. 330 (1985) 253.
[33] R.P. Frankewich, K.N. Thimmaiah, W.L. Hinze, Anal. Chem. 63 (1991) 2924.
[34] A. Muñoz de la Peña, F. Salinas, I. Durán-Merás, M.D. Moreno, Anal. Lett. 27 (1994) 1893.
[35] R. Bro, Chemom. Intell. Lab. Syst. 38 (1997) 149.
[36] K.S. Booksh, B.R. Kowalski, Anal. Chem. 66 (1994) 782A.
[37] A. Smilde, R. Bro, P. Geladi, Multi-way Analysis, Applications in the Chemical Sciences, Wiley, England, 2004.
[38] C.M. Andersen, R. Bro, J. Chemom. 17 (2003) 200.
[39] L. Moberg, G. Robertsson, B. Karlberg, Talanta 54 (2001) 161.
[40] J.A. Arancibia, G.M. Escandar, Talanta 60 (2003) 1113.
[41] A. Muñoz de la Peña, A. Espinosa Mansilla, D. González Gómez, A.C. Olivieri, H. Goicoechea, Anal. Chem. 75 (2003) 2640.
[42] M.C. Mahedero, N. Mora Díez, A. Muñoz de la Peña, A. Espinosa Mansilla, D. González Gómez, D. Bohoyo Gil, Talanta 65 (2004) 806.
[43] R. Bro, H.A.L. Kiers, J. Chemom. 17 (2003) 274.
[44] M.M. Sena, M.G. Trevisan, R.J. Poppi, Talanta 68 (2006) 1707.
[45] A. Muñoz-de-la-Peña, N. Mora, D. Bohoyo, A.C. Olivieri, G.M. Escandar, Anal. Chim. Acta 569 (2006) 250.
[46] MATLAB 5.3, The Mathworks, Inc., Natick, MA, USA, 1999.
[47] http://www.models.kvl.dk/source/.
[48] A.C. Olivieri, MVC2, Universidad Nacional de Rosario, Argentina, 2003.
[49] C.J. Drayton, Comprehensive Medicinal Chemistry, vol. 6, Pergamon, Oxford, 1990.
[50] R.D. Caballero, J.R. Torres-Lapasió, J.J. Baeza-Baeza, M.C. García-Alvarez-Coque, J. Liq. Chromatogr. Relat. Technol. 24 (2001) 117.
[51] J.W. Bridges, L.A. Gifford, W.P. Hayes, J.N. Miller, D. Thorburn Burns, Anal. Chem. 46 (1974) 1010–1017.
[52] T.A.M. Msagati, M.M. Nindi, Talanta 64 (2004) 87.
[53] H.A. Benesi, J.K. Hildebrand, J. Am. Chem. Soc. 71 (1949) 2703.
[54] G. Scatchard, Ann. NY Acad. Sci. 51 (1949) 660.
[55] K.A. Connors, Binding Constants: The Measurement of Molecular Complex Stability, John Wiley and Sons, New York, 1987.
[56] M.J.S. Dewar, E.G. Zoebisch, E.F. Healy, J.J.P. Stewart, J. Am. Chem. Soc. 107 (1985) 3902.
[57] L. Liu, A.-X. Guo, J. Inclus. Phenom. Macrocycl. Chem. 42 (2002) 1–14.
[58] N.J. Messick, J.H. Kalivas, P.M. Lang, Anal. Chem. 68 (1996) 1572.
[59] L. Cuadros Rodríguez, A.M. García Campaña, C. Jiménez Linares, M. Román Ceba, Anal. Lett. 26 (1993) 1243.
[60] R. Boque, J. Ferré, N.M. Faber, F.X. Rius, Anal. Chim. Acta 451 (2002) 313.
[61] D.L. Massart, B.G.M. Vandeginste, L.M.C. Buydens, S. De Jong, P.J. Lewi, J. Smeyers-Verbeke, Handbook of Chemometrics and Qualimetrics: Part A, Elsevier, 1997.

Available online at www.sciencedirect.com
ScienceDirect
Talanta 73 (2007) 400–403
Talanta
www.elsevier.com/locate/talanta

Short communication

Improvement of sensitivity in flow analysis by exploiting a multi-reversed software-assisted system

José Y. Neira [a,*], Elizabeth González [b], Joaquim A. Nóbrega [c]

[a] *Departamento de Análisis Instrumental, Facultad de Farmacia, Universidad de Concepción, Casilla 237, Concepción, Chile*
[b] *Facultad de Ciencias, Departamento de Química Ambiental, Universidad Católica de la Santísima Concepción, Casilla 297, Concepción, Chile*
[c] *Grupo de Análise Instrumental Aplicada, Departamento de Química, Universidade Federal de São Carlos, P.O. Box 676, 13560-970 São Carlos, SP, Brazil*

Received 24 January 2007; received in revised form 16 March 2007; accepted 17 March 2007
Available online 24 March 2007

Abstract

A multi-reversed flow system software-assisted was developed for improvement of sensitivity in flow analysis. The performance of the flow system proposed was evaluated by using as a model the conventional Griess' colorimetric reaction for determination of nitrite in waters. The manifold incorporated three 3-way solenoid valves, a relay box solenoid actuated, a peristaltic pump, and a photometric detector. A tailored software was designed and written in Visual Basic 6.0 which allows full control of all flow system components and simultaneous acquisition and processing of the data. The sensitivity measured as the slope of the calibration curve was improved 2.5- and 1.4-fold regarding those obtained by continuous- and stopped-flow systems, respectively. Other valuable features such as analytical throughput of 55 determinations per hour, limit of detection of 5 $\mu g\,L^{-1}$ ($3\sigma_{blank}$/slope), relative standard deviation < 2% ($n = 8$), and a linear dynamic range up to 1800 $\mu g\,L^{-1}$ were also achieved.

Keywords: Software-assisted; Multi-reversed flow; Nitrite; Water

1. Introduction

Flow injection analysis (FIA) is well established as an analytical technique for speeding up determinations [1–3]. The management of solutions is easily performed employing FIA and features such as precision, selectivity, and control of contamination are improved [4–6]. However, after more than 30 years of its conception by Ruzicka and Hansen [1], FIA has evolved to more modern strategies as sequential injection analysis [7] (SIA), stopped-flow [8,9], multidetection [10], multicommutation [11], etc. All these offsprings resulted from better understanding of the dispersion process in open tubes and the search for higher degree of automation for the analytical process. Nowadays, there are no doubts that the application of automation is increasing and the path of science is closely related to the development of automated instruments helped by the so-called software-assisted or computer-assisted strategies [12,13].

In this study, it was developed a simple and robust automatic method named multi-reversed flow (MRF) system based on exploitation of SIA concepts which was implemented by dedicated software for the direct determination of nitrite in waters. The proposed method is more sensitive than those based on stopped- and continuous-flow systems.

2. Experimental

2.1. Apparatus

The manifold for multi-reversed flow system software-assisted is shown in Fig. 1 and consist of a peristaltic pump (Ismatec MCP ISM726, equipped with a serial port RS 232, Switzerland), three 3-way solenoid valves (NResearch 161 T031, USA), and conventional photometric detector (spectrophotometer Shimadzu model 120 02, Japan). All solutions are propelled by action of the peristaltic pump and the direction of the flow is moved either forward or backward by changing the rotation of the pump rotor clockwise or counter-clockwise. This strategy was called multi-reversed flow and its implementation relies in the control of the peristaltic pump by a personal computer via RS 232 port in order to activate/deactivate it using written dedicated software. Additionally, flow-rate, flow direc-

* Corresponding author. Tel.: +56 41 2204368; fax: +56 41 2226382.
E-mail address: yneira@udec.cl (J.Y. Neira).

0039-9140/$ – see front matter © 2007 Elsevier B.V. All rights reserved.
doi:10.1016/j.talanta.2007.03.035

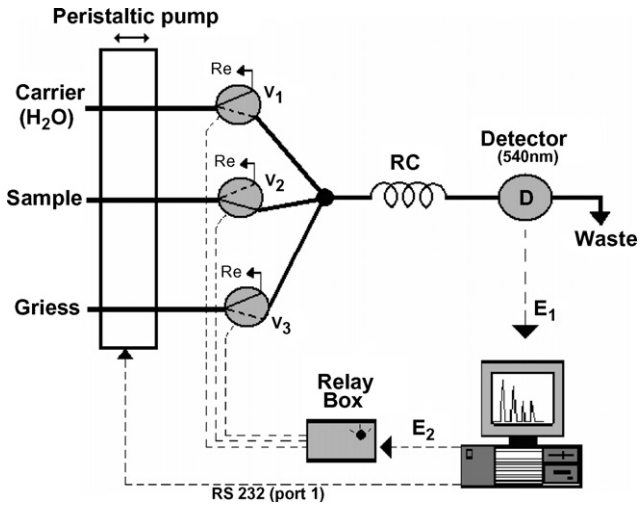

Fig. 1. Diagram of the multi-reversed flow set up for nitrite determination in waters. V_1, V_2 and V_3: three-way solenoid valves; Re: recycle; RC: reaction coil (polyethylene i.d. 0.8 mm and length 110 cm); E1: data acquisition using minilab card; E2: action via LPT1 port. (– – –) electric connection; (—) tube (i.d. = 0.8 mm).

tion, volume and action of the three-way solenoid valves, were controlled by the tailored software. The manifold was built using polyethylene tube with 0.8 mm of internal diameter and the solutions were propelled by peristaltic pump action on Tygon® tubes.

Absorbance measurements were performed at 540 nm using a single-beam Shimadzu spectrophotometer model 120-02 equipped with a Hellma glass flow-cell model 178.710-OS with 10 mm optical path length. The computer communicates with the spectrophotometer through a minilab analogic/digital conversion card (Avantech Measurements, minilab model 1008, Middleboro, MA, USA). The developed software was used with a personal computer Pentium 166 MHz. Further details about requirements to switch relay box actuated, the three-way solenoid valve, control and flow direction of peristaltic pump and data acquisition were previously described [5].

2.2. Reagents and solutions

All solutions were prepared using deionised water from Milli-Q system (Millipore, Bedford, MA, USA). The standards nitrite solutions were prepared from a concentrated stock solutions containing 1 g L^{-1} of the sodium salt (Panreac, 98%, Barcelona, Spain). The chromogenic reagent was prepared by dissolving 10 g of sulfanilamide dihydrochloride (NED) (Panreac, 98%) in 100 mL of phosphoric acid in a final volume of 1000 mL in Milli-Q water.

2.3. Multi-reversed software-assisted system

The software was written in Visual Basic 6.0 and allows the total real time control of the process. The software front panel contained ready-to-use switches, buttons, controls, and graphical displays of detector readings.

The software named MRFA (i.e. multi-reversed flow analysis) is user-friendly and can be used for others applications. The software has three main areas: analytical method development, calibration and measurements. The first series of instructions consists in making a sequence program for three-way valve activation based on specified times, and also, a program sequence to control the peristaltic pump (flow-rate and flow direction). In the second group of instructions, the system performs automatic calibration adopting one of the two possibilities, either a calibration curve using reference solutions with low concentrations of nitrite (0–1600 μg L^{-1}) or a calibration curve using reference solutions with high concentrations of nitrite (0–20 000 μg L^{-1}). Finally, the third part of the software allows the automatic determination of nitrite concentrations in the samples.

2.4. Nitrite determination

The determination of nitrite is based on the Griess' reaction [14,15]. Distilled-deionised water was employed as carrier, and both sample and chromogenic reagent were added adopting binary sampling [11]. The flow diagram is shown in Fig. 1. The sequence control of the three-way valves and of the peristaltic pump is detailed in Table 1. This table includes a sequence program for multi-reversed, stopped- and continuous-flow systems. These two later systems were employed to compare the performance of the multi-reversed flow system proposed. The multi-reversed flow system was applied for determination of nitrite in some coastal sea waters and underground waters that were collected 1 L polyethylene bottles, added drops of chloroform, transported immediately to the laboratory, filtered through 0.45 μm membranes and stored at 4 °C at their natural pH (measured between 5.0 and 5.6) until analysis. Nitrite determinations were performed within 48 h after sample collection.

3. Results and discussions

3.1. Multi-reversed flow system

It is well-known that the formation of colored product in a continuous flow system depends on two principal requisites for a better development of the chemical reaction: the sample plug should be well mixed with the chromogenic reagent and a sufficient time should be provided for reaction development before detection. The residence time can be increased by using either longer reaction coils or a stopped-flow approach. This later strategy is advantageous because the dispersion of the sample zone is greatly avoided when the carrier stream is stopped, once that axial diffusion, which is the most responsible for dispersion, is ceased. However, in both cases the analytical throughput is deteriorated. Regardless the adopted strategy, better sensitivity is attained when the mixture between sample and reagents is improved.

The proposal of a multi-reversed flow system is based on incrementing the mixture conditions by promoting a mechanical shaking of the reaction zone. The mechanical shaking is caused by changing the flow direction of the peristaltic pump controlled by software. In order to study the application of

Table 1
Operation steps for activation of three-way solenoid valves and peristaltic pump[a]

Step	Event	V_1	V_2	V_3	Time (s)	Rotation speed	Flow direction	Volume (μL)
Multi-reversed flow system								
1	Sample transport	Off	On	Off	3	35	Forward	50
2	Reactant transport	Off	Off	On	3	35	Forward	15
3	Sample transport	Off	On	Off	3	35	Forward	50
4	Reactant transport	Off	Off	On	3	35	Forward	15
5	Sample transport	Off	On	Off	3	35	Forward	50
6	Reactant transport	Off	Off	On	3	35	Forward	15
7	Sample transport	Off	On	Off	3	35	Forward	50
8	Reactant transport	Off	Off	On	3	35	Forward	15
9	Sample transport	Off	On	Off	3	35	Forward	50
10	Reactant transport	Off	Off	On	3	35	Forward	15
11	Sample transport	Off	On	Off	3	35	Forward	50
12	Reactant transport	Off	Off	On	3	35	Forward	15
13	Multi-reversed flow	On	Off	Off	1	60	Reverse	0
14	Multi-reversed flow	On	Off	Off	1	60	Forward	0
15	Multi-reversed flow	On	Off	Off	1	60	Reverse	0
16	Multi-reversed flow	On	Off	Off	1	60	Forward	0
17	Multi-reversed flow	On	Off	Off	1	60	Reverse	0
18	Multi-reversed flow	On	Off	Off	1	60	Forward	0
19	Multi-reversed flow	On	Off	Off	1	60	Reverse	0
20	Reaction zone transport	On	Off	Off	25	60	Forward	956
Stopped-flow system, steps 1–12 the same as in multi-reversed flow system								
13	Stopped-flow system	Off	Off	Off	10	Stop	–	–
14	Reaction zone transport	On	Off	Off	25	60	Forward	956
Continuous flow system, steps 1–12 the same as in multi-reversed flow system								
13	Reaction zone transport	On	Off	Off	25	60	Forward	956

[a] For details, see Fig. 1.

the multi-reversed flow system, the reaction between nitrite and chromogenic reagents (Griess' reactants) was chosen as a model.

3.2. Analytical figures of merit

A comparison was made of calibration curves obtained by multi-reversed, stopped and continuous flow as is shown in Fig. 2. All them were implemented with minor changes in the developed software as discussed in Section 2 (see also Table 1). As it can be seen in Table 2, the linear dynamic range of the calibration curve obtained by applying the multi-reversed approach was slightly better than those obtained by stopped- or continuous-flow system. Additionally, a satisfactory correlation was obtained with six experimental points (each one corresponding to the mean value of three measurements). The sensitivity measured as the slope of the calibration curve of the multi-reversed flow was 2.5- and 1.4-fold better than those obtained by continuous- and stopped-flow systems. It may be considered that the best detection limit achieved using the multi-reversed flow system is related to the better repeatability of blank signals, to the decrease of radial dispersion and to the improved homogenization of the colored reaction zone. In the proposed system, the multi-reversed flow allows a better homogenization of the reactants—analyte reaction zone. The reaction reached a completeness of 80% and the analytical throughput was 55 determinations per hour.

3.3. Application and recovery study

The results obtained by using the multi-reversed flow system for determination of nitrite in two underground waters

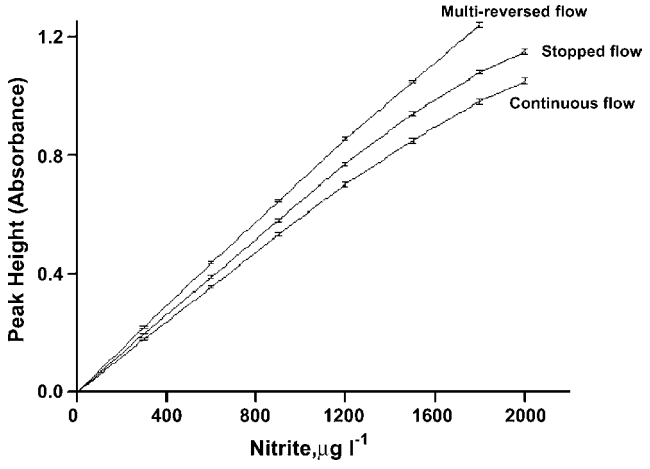

Fig. 2. Calibration curves for multi-reversed flow, stopped- and continuous-flow systems.

Table 2
Comparison of analytical parameters for multi-reversed, stopped- and continuous-flow systems

Parameter	Multi-reverse flow	Stopped-flow	Continues flow
LOD[a] ($\mu g\,L^{-1}$)	5	8	20
LOQ[b] ($\mu g\,L^{-1}$)	16	26	66
R.S.D.[c] (%)	1.1	1.2	1.8
Linear range ($\mu g\,L^{-1}$)	Up to 1800	Up to 1600	Up to 1500
Regression equation	$y = 0.00373x + 7.14 \times 10^{-4}$	$y = 0.00262x + 6.43 \times 10^{4}$	$y = 0.0015x + 5.89 \times 10^{4}$
Correlation coefficient (R^2)	0.99995	0.99999	0.99989
Throughput [d] (h^{-1})	55	55	70

[a] LOD: detection limit ($3\sigma_{blank}$/slope, $n = 14$).
[b] LOQ: quantification limit ($10\sigma_{blank}$/slope, $n = 14$).
[c] R.S.D. (%): relative standard direction, nitrite concentration = 600 $\mu g\,L^{-1}$.
[d] Throughput: estimated for 1 h working session.

Table 3
Determined concentrations and recovery study for nitrite in natural waters by multi-reversed flow system

Sample	Nitrite[a] ($\mu g\,L^{-1}$)	Nitrite ($\mu g\,L^{-1}$)		Recovery[a] %
		Added	Found[a,b]	
Underground water 1	<16[c]	50	48	96
Underground water 2	<16[c]	50	48	96
Coastal sea water 1	60	50	46	92
Coastal sea water 2	65	50	45	90
Coastal sea water 3	70	50	46	92

[a] Mean; $n = 3$.
[b] Calculated after subtraction of the original nitrite concentration.
[c] Quantification limit.

collected in Guarilihue (Chile) and three coastal sea waters collected in Coliumo Bay (Chile) are presented in Table 3. An addition-recovery study performed in these samples spiked with 50 $\mu g\,L^{-1}$ of nitrite led to recoveries of $95 \pm 2\%$ ($n = 3$) in underground water and $91 \pm 2\%$ ($n = 15$) in coastal sea waters which can be considered suitable. It can be supposed that the lower recoveries observed for the three coastal sea waters can be related to matrix effects caused by the elevated concentration of salts but this investigation is beyond the goals of this work.

4. Conclusions

The multi-reversed flow system is a new and simple approach to process solutions in flow analysis, and led to a better homogenization of the reaction zone and improved sensitivity compared to stopped- and continuous-flow systems. The multi-reversed flow system can also be considered as an alternative to different flow systems, such as SIA. It should be mentioned that on-line extraction of solid biological materials can be easily implemented with multi-reversed flow system and investigations on this topic are under progress.

Acknowledgements

J.Y.N. is thankful to Dirección de Investigación, Universidad de Concepción-Chile, by financial support. The authors also expresses their gratitude to MECESUP UCO 0202 project by 1-month leaving license conceded J.Y.N. for working at University Federal of São Carlos (São Carlos, SP, Brazil).

References

[1] J. Ruzicka, E.H. Hansen, Anal. Chim. Acta 78 (1975) 145.
[2] K.K. Stewart, G.R. Beecher, P.E. Hare, Anal. Biochem. 70 (1976) 167.
[3] J. Ruzicka, E.H. Hansen, Flow Injection Analysis, 2nd ed., Wiley, New York, 1989.
[4] M. Valcárcel, M.D. Luque de Castro, Análisis por Inyeccíon en Flujo, Imprenta San Pablo, Córdoba, 1985.
[5] J.Y. Neira, J.A. Nóbrega, Lab. Robot. Autom. 11 (1999) 260.
[6] J.Y. Neira, N. Reyes, J.A. Nóbrega, Lab. Robot. Autom. 12 (1999) 246.
[7] J. Ruzicka, G.D. Marshall, Anal. Chim. Acta 237 (1990) 329.
[8] J. Kurzawa, A. Wiśniewska, K. Janowicz, Anal. Chim. Acta 567 (2006) 286.
[9] D.T. Paraskevas, K.Z. Constantinos, A.T. Georgios, A.K. Eftichios, N.V. Anastasios, Anal. Chim. Acta 547 (2005) 98.
[10] F.R.P. Rocha, P.B. Martelli, B.F. Reis, Anal. Chim. Acta 438 (2001) 11.
[11] F.R.P. Rocha, B.F. Reis, E.A.G. Zagatto, J.L.F.C. Lima, R.A.S. Lapa, J.L.M. Santos, Anal. Chim. Acta 468 (2002) 119.
[12] C.C. Oliveira, R.P. Sartini, B.F. Reis, E.A.G. Zagatto, Anal. Chim. Acta 332 (1996) 173.
[13] D. Filippini, I. Lundström, Anal. Chim. Acta 557 (2006) 393.
[14] A. Cerdà, M.T. Oms, R. Forteza, V. Cerdà, Anal. Chim. Acta 371 (1998) 63.
[15] M.F. Giné, F.H. Bergamin, E.A.G. Zagatto, Anal. Chim. Acta 114 (1980) 191.

Available online at www.sciencedirect.com
ScienceDirect
Talanta 73 (2007) 258–261
Talanta
www.elsevier.com/locate/talanta

Validation of a direct non-destructive quantitative analysis of amiodarone hydrochloride in Angoron® formulations using FT-Raman spectroscopy

M.G. Orkoula [a,b], C.G. Kontoyannis [a,b,*], C.K. Markopoulou [c], J.E. Koundourellis [c]

[a] *Department of Pharmacy, University of Patras, Greece*
[b] *Institute of Chemical Engineering and High Temperature Chemical Processes, FORTH, P.O. Box 1414, GR-26504 Patras, Greece*
[c] *Laboratory of Pharmaceutical Analysis, School of Pharmacy, Aristotelian University of Thessaloniki, 54124 Thessaloniki, Greece*

Received 5 October 2006; received in revised form 5 March 2007; accepted 16 March 2007
Available online 24 March 2007

Abstract

Raman spectroscopy was applied for the direct non-destructive analysis of amiodarone hydrochloride (ADH), the active ingredient of the liquid formulation Angoron®. The FT-Raman spectra were obtained through the un-broken as-received ampoules of Angoron®. Using the most intense vibration of the active pharmaceutical ingredient (API) at 1568 cm^{-1}, a calibration model, based on solutions with known concentrations, was developed. The model was applied to the Raman spectra recorded from three as-purchased commercial formulations of Angoron® having nominal strength of 50 mg ml^{-1} ADH. The average value of the API in these samples was found to be 48.56 ± 0.64 mg ml^{-1} while the detection limit of the proposed technique was found to be 2.11 mg ml^{-1}. The results were compared to those obtained from the application of HPLC using the methodology described in the European Pharmacopoeia and found to be in excellent agreement. The proposed analytical methodology was also validated by evaluating the linearity of the calibration line as well as its accuracy and precision. The main advantage of Raman spectroscopy over HPLC method during routine analysis is that it is considerably faster and no solvent consuming. Furthermore, Raman spectroscopy is non-destructive for the sample. However, the detection limit for Raman spectroscopy is much higher than the corresponding for the HPLC methodology.

Keywords: Raman spectroscopy; Angoron®; Quantitative analysis; Liquid formulations; Amiodarone hydrochloride; HPLC

1. Introduction

Amiodarone hydrochloride (2-butyl-3-benzofuranyl-4-[2 (diethylamino)ethoxy]-3,5-diiodophenyl ketone hydrochloride) is a class III anti-arrhythmic agent and one of the most powerful drugs used in the treatment of ventricular and supraventricular tachycardias. In drug stores, it can be found as tablets or injectable formulations. The official method for determining the active ingredient in the formulation, as described in the European Pharmacopoeia [1], is based on HPLC. Reports on the use of HPLC for amiodarone hydrochloride (ADH) determination are spanned from the 1980s [2,3] to 2004 where a methodology based on the reverse phase HPLC for quality control purposes was developed [4]. A recent article for ADH determination based on capillary electrophoresis can also be found in the literature [5]. A spectrophotometric method has been developed as well, for the determination of amiodarone hydrochloride in pure form and commercial dosage form and is based on the reaction of amiodarone base as *n*-electron donor with *p*-chloranilic acid and 2,3-dichloro-5,6-dicyano-1,4-benzoquinone as pi-acceptors to give highly colored complex species [6]. An amiodarone-selective membrane electrode has been also constructed and tested [7].

Application of the above-mentioned methodologies is rather difficult, time and/or solvent consuming and destructive for the liquid formulation. In the recent past, FT-Raman spectroscopy, a technique that requires minimal sample preparation, has been used for quantitative analysis of liquid mixtures, including biological fluids, but only two reports were found related to the quantitative application of Raman spectroscopy on active pharmaceutical ingredients (API) in commercial formulations. One is involving API in an aqueous suspension [8] and one dissolved API in an elixir [9]. In both publications the formulation was removed from the commercial container (the syringe or the bottle respectively), and in this way the technique was destructive.

* Corresponding author at: Department of Pharmacy, University of Patras, Greece. Tel.: +30 2610969328; fax: +30 2610997658.
E-mail address: cgk@iceht.forth.gr (C.G. Kontoyannis).

0039-9140/$ – see front matter © 2007 Elsevier B.V. All rights reserved.
doi:10.1016/j.talanta.2007.03.033

There is also a report in the recent bibliography [10] on the use of Raman spectroscopy for quantitative determination of powders through chromatographic standard glass vials.

In the present work, Raman spectroscopy was applied for the determination of ADH in Angoron® injectable formulations. The Raman spectra were obtained from intact ampoules and thus the methodology was non-destructive. This is the first time, to our knowledge, that Raman spectroscopy is applied for the development of non-destructive API assay in liquid formulation through sealed ampoules. The results were compared against those obtained from the application of the Pharmacopoeia method on the same samples.

2. Experimental

2.1. Chemicals and reagents

Amiodarone hydrochloride was kindly provided by Sanofi-Aventis. Benzyl Alcohol and Polysorbate 80 were purchased from Sigma–Aldrich.

Angoron® is an injectable solution with 150 mg ADH in 3 ml as the active ingredient. Benzyl alcohol, polysorbate 80 and water are the excipients. Three formulations of Angoron® (A1, A2 and A3) from Sanofi-Synthelabo were bought from a local pharmacy store.

All chemicals and reagents used for HPLC were USP-NF grade. The solvents, methanol, acetonitrile and water were "gradient grade for liquid chromatography" supplied from Merck company. Dilute ammonia solution was prepared by suitable aqueous dilution using deionised water, filtered by a "Millipore-Q plus 185" equipment.

2.2. Spectroscopic conditions

The Raman spectra were recorded using a FRA-106/S FT-Raman (Bruker) with the following characteristics: The laser excitation line used was the 1064 nm of a Nd:YAG laser. A secondary filter was used to remove the Rayleigh line. The scattered light was collected at an angle of 180°. The system was equipped with a liquid N_2 cooled Ge detector (D 418). The power of the incident laser beam was about 370 mW on the sample's surface. Typical spectral line width was 0.5 cm^{-1} while the recorded spectra were the average of 300 scans.

The mirror coated side from a Hellma QS quartz cell with coated backside was cut and placed in direct contact with the ampoules in order to reflect the Raman signal. Three of the ampoules were emptied and used for placing the standards for constructing the calibration lines as described below.

The spectra were obtained on different days and, as it was anticipated, there were changes in the recorded intensities due to laser fluctuations or to slightly different position of the ampoules. In order to be able to compare Raman spectra from different days, six spectra from the same solution were recorded every day. The average absolute intensity of the strong vibration at 1568 cm^{-1}, after the subtraction of the background, was compared with the respective intensity that was recorded on the first day and the ratio between these intensities was calculated. All subsequent spectra recorded in the same day were multiplied by this ratio.

2.3. HPLC instrumentation and chromatographic conditions

A Shimadzu HPLC system, consisting of a LC-6A module pump and a SIL-10ADVP programmable auto sampler (50 μl), was used for the analysis. The method was carried out, according to European Pharmacopoeia [1], on a Hypersil BDS C-18 (150 mm × 4.6 mm, particle size 3 μm) column as a stationary phase. The isocratic mobile phase (flow rate 1 ml/min) was composed of acetic acid/ammonia buffer solution pH 4.9, methanol, acetonitrile (30:30:40 v/v/v). The mobile phase was degassed by filtering through a Millipore HV 0.45 μm pore membrane filter. The LC-75 UV-detector operated at 240 nm was used to detect the analyte. The analysis was carried out at room temperature. A ClassVp software was used to process the chromatograms.

2.4. Sample and standard preparation

2.4.1. For the Raman method

Raman spectroscopy method was based on a simple linear regression model obtained from a series of standard solutions containing 31.00, 40.10, 42.80, 50.40, 54.30, 60.28 mg ml^{-1} ADH, respectively. The standards were prepared using practically the same procedure used for the preparation of the commercial formulations. 100 mg ml^{-1} polysorbate 80 and 20.2 mg ml^{-1} benzyl alcohol were carefully weighed in a 5 ml volumetric flask. The appropriate amount of amiodarone hydrochloride and a quantity of water were added. The mixture was sonicated until dissolution of the powder. Then the flask was filled with water until the mark.

The standards were placed in empty Angoron® ampoules. The ampoules were positioned between the laser source and the mirror, as mentioned in Section 2.2, and their spectra were recorded through the glass walls of the ampoules. Each standard was measured six times.

The standard addition method was evaluated using three spiking ADH solutions 8.70, 16.50 and 25.86 mg ml^{-1} to a diluted Angoron® formulation.

2.4.2. For the HPLC method

The standards used for the development of the HPLC calibration model were the same as those for FT-Raman.

Concretely, 2 ml of each FT-Raman solution was further diluted (1:25) twice, with acetonitrile:water (50:50, v/v) to get the following final concentrations of analyte: 49.60, 64.16, 68.48, 80.64, 86.82, 96.45 μg ml^{-1}.

3. Results and discussion

3.1. Development of the Raman analytical methodology

The intensity of a Raman line depends on a number of factors including the incident laser power, the frequency of the scattered

radiation, the absorptivity of the materials involved in the scattering and the response of the detection system. In addition, the area under a Raman peak is analogous to the concentration of the Raman active species [11].

The Raman spectrum of a 50 mg ml^{-1} ADH dissolved in water, benzyl alcohol and polysorbate 80, can be seen in Fig. 1 along with the spectrum of the as-received Angoron® and the spectrum of powder ADH. It is apparent that the most intense vibration at 1568 cm^{-1} of ADH, marked with an arrow, should be used for the quantitative analysis.

Six Raman spectra were recorded from each standard solution (Fig. 1 inset) and for reason of simplicity the peak intensities, I, after background subtraction, were used, instead of the areas A of the Raman vibration. A plot of I versus the concentration of ADH, C_{ADH}, as expected, yielded a straight line, Eq. (1):

$$I_{ADH}^{1568} = -1.03\ (\pm 2.31) \times 10^{-4} + 1.00\ (\pm 0.05) \times 10^{-4}\, C_{ADH} \quad (1)$$

The error of the slope and the intercept were calculated at 95% confidence level. The correlation coefficient was 0.99939. The limit of detection (LOD) was calculated according to [12] and found to be 2.11 mg ml^{-1}.

The accuracy of the proposed FT-Raman method was checked by spiking a diluted Angoron® formulation with known quantities of ADH. Three solutions were prepared, having 8.70, 16.50 and 25.86 mg ml^{-1} ADH in addition to the concentration of the diluted formulation. Four Raman measurements from each solution were obtained and the plot of the average I versus C_{AADH} was found to yield a straight line, Eq. (2):

$$I_{ADH}^{1568} = 8.88 \times 10^{-4} + 9.60 \times 10^{-5}\, C_{AADH} \quad (2)$$

where C_{AADH} is the concentration of the ADH, in mg ml^{-1}, added in the diluted formulation. The S.D. for the slope was 4.21×10^{-7} and for the intercept 7.75×10^{-6}. The concentration of the ADH in the diluted formulation should be equal to intercept divided by the slope. The concentration of the formulation, taking into account the dilution factor, was found to be 48.25 mg ml^{-1} and the confidence limit at 95% confidence level was 1.63 mg ml^{-1}. The three as-received Angoron® formulations were also analyzed and comparison of the results with those obtained employing the Pharmacopoeia method (HPLC). The mean concentration for each of the three testing samples calculated from six repetitions is quoted in Table 1, together with their confidence limits at 95% confidence level.

In order to test the variation of the FT-Raman signal with time and the validity of the results taken from the proposed method, the ANOVA within-day and between-day variation test was followed. Three standard solutions were chosen: one at approximately the same concentration as the formulation (50.40 mg ml^{-1}) and two around this value (40.10 and 60.28 mg ml^{-1}). Four Raman spectra for each of the standard solutions were obtained in each of three different days. An one-sided F-test [13] was used at 0.05 significant level. Since the calculated values of F ($F_{experimental}$ = 2.360, 3.296, 3.714 for the three samples, respectively) were lower than the critical ($F_{critical}$ = 4.256), it was concluded that the day-means do not differ significantly.

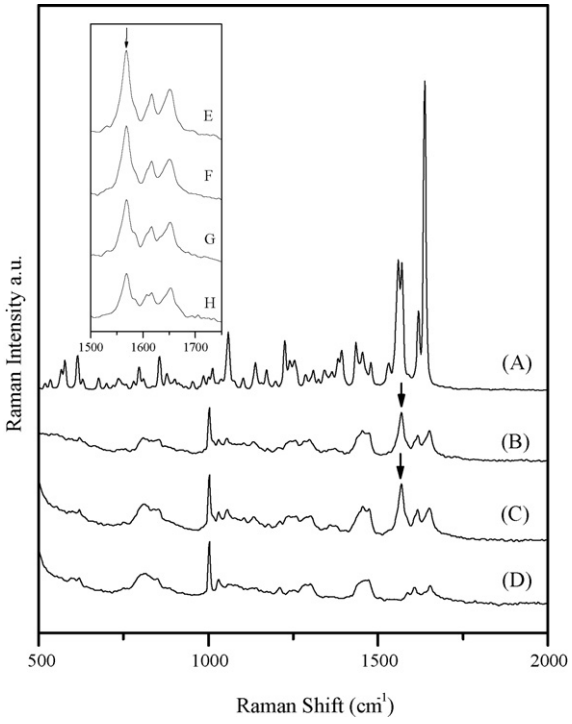

Fig. 1. FT-Raman spectra of (A) amiodarone powder, (B) the as-received Angoron® from the intact ampoule, (C) ADH solution (50 mg ml^{-1}) placed in an emptied Angoron® ampoule and (D) Placebo of Angoron® placed in an emptied Angoron® ampoule. Inset: FT-Raman spectra of ADH solutions in various concentrations: (E) 60.28 mg ml^{-1}, (F) 50.40 mg ml^{-1}, (G) 40.10 mg ml^{-1} and (H) 31.00 mg ml^{-1}. All solutions were placed in emptied Angoron® ampoules.

3.2. Pharmacopeia methodology

In order to be able to compare the results extracted by the FT-Raman method, the Pharmacopeia proposed methodology, based on HPLC, was also developed. The calibration line derived from the standard solutions is described by the following equation:

$$A = 3.68\ (\pm 18.43) \times 10^{-3} + 1.35\ (\pm 0.02) \times 10^{-2}\, C_{ADH} \quad (3)$$

Table 1
FT-Raman and HPLC results obtained from three commercial formulations of Angoron®

Formulation	Mean ± conf. limit (mg/ml)[a]		$F_{experimental}$	$F_{critical}$
	FT-Raman	HPLC		
A1	48 ± 1	48.8 ± 0.8	5.68	7.15
A2	48.9 ± 0.5	47.5 ± 0.4	3.18	7.15
A3	48.4 ± 0.2	48.6 ± 0.6	3.24	7.15
Average	48.6 ± 0.6	48.3 ± 0.6		

Two-tailed F-test for comparing the standard deviations for the results of the two methods (degrees of freedom = $(n_1 - 1, n_2 - 1)$ = (5, 5), confidence level = 95%).
[a] 95% confidence level.

The error of the slope and the intercept were calculated at 95% confidence level. The correlation coefficient was 0.99992. The limit of detection (LOD) was calculated and found to be 1.51 $\mu g\,ml^{-1}$.

The accuracy of the HPLC method was established using the spiked formulations which were prepared for the determination of the accuracy of Raman methodology. The samples were properly diluted and four measurements from each solution were obtained. The equation of the straight line constructed by the absorbances in relation to the concentration of the samples was the following:

$$A = 0.20 + 1.38 \times 10^{-2}\, C_{\mathrm{AADH}} \quad (4)$$

The S.D. for the slope was 4.11×10^{-4} and for the intercept 0.01. The concentration of the formulation, taking into account the dilution, was found to be 48.21 mg ml^{-1} and the 95% confidence limit 0.71 mg ml^{-1}.

The three as-received Angoron® formulations were also analyzed employing the Pharmacopoeia method. The mean concentration for each of the three testing samples calculated from six repetitions is also quoted in Table 1, together with their confidence limits at 95% confidence level.

3.3. Comparison of Raman and HPLC

In order to compare the results and hence detect systematic errors between the two methods, a two-tailed *F*-test [13] was employed to check whether the standard deviations for the same sample differ significantly (Table 1). Since the experimental value of *F* is lower than the critical, it is concluded that the proposed FT-Raman methodology is equally precise to the HPLC.

From the previous analysis it is apparent that both techniques yield equally reliable results for the quantitation of ADH either in laboratory prepared samples or in pharmaceutical dosage forms. However, the detection limit of the HPLC methodology was found to be much lower than the respective yielded by the FT-Raman method.

The main advantage of FT-Raman spectroscopy over the well-established HPLC in liquid formulations is the time and solvent consumption. The application of the FT-Raman method in routine analysis (content uniformity, assay and dissolution tests) can be accomplished directly to intact ampoules and thus the methodology is fast and non-destructive. HPLC method for the same analysis needs sample pretreatment and time or solvent consumption.

References

[1] European Pharmacopoeia, 5th ed., Council of Europe, 2004, pp. 977–978.
[2] M. Pena, C. Moro, J. Pharma. Biomed. 7 (1989) 1909–1913.
[3] J. Cervelli, J. Kerkay, K. Pearson, Anal. Lett. Pt B 14 (1981) 137–153.
[4] N. Thyagarajapuram, K. Alexander, J. Liquid Chromatogr. Rel. Technol. 26 (2003) 1315–1326.
[5] Z. Shihabi, M. Hinsdale, J. Liquid Chromatogr. Rel. Technol. 28 (2005) 2235–2244.
[6] N. Rahman, N. Khan, S. Azmi, Anal. Sci. 20 (2004) 1231–1235.
[7] R.-I. Stefan, H. Aboul-Enein, G.E. Baiulescu, Sens. Actuators B 37 (1996) 141–144.
[8] T.R.M. De Beer, G.J. Vergot, W.R.G. Baeyens, J.P. Remon, C. Vervaet, F. Verpoort, Eur. J. Pharm. Sci. 23 (2004) 355–362.
[9] M.G. Orkoula, C.G. Kontoyannis, C.K. Markopoulou, J.E. Koundourellis, J. Pharm. Biomed. Anal. 41 (2006) 1406–1411.
[10] S. Armenta, S. Garrigues, M. de la Guardia, Anal. Chim. Acta 521 (2004) 149–155.
[11] D. Strommen, K. Nakamoto, Laboratory Raman Spectroscopy, J. Wiley, New York, 1984, p. 71.
[12] The European Agency for the Evaluation of Medical Products, ICH Topic Q2B Note for Guidance on Validation of Analytical Procedures: Methology GPMP/ICH/281/95, 1996.
[13] J.C. Miller, J.N. Miller, Stat. Anal. Chem. (1986) 98 (Chapter 4).

Available online at www.sciencedirect.com
ScienceDirect
Talanta 73 (2007) 202–219
Talanta
www.elsevier.com/locate/talanta

Review

Recent developments in the field of screen-printed electrodes and their related applications

O. Domínguez Renedo, M.A. Alonso-Lomillo, M.J. Arcos Martínez *

Department of Chemistry, Factulty of Sciences, University of Burgos, Plaza Misael Bañuelos s/n, 09001 Burgos, Spain

Received 19 January 2007; received in revised form 14 March 2007; accepted 23 March 2007
Available online 31 March 2007

Abstract

The development of analytical methods that respond to the growing need to perform rapid 'in situ' analyses shows disposable screen-printed electrodes (SPEs) as an alternative to the traditional electrodes. This review presents recent developments in the electrochemical application of disposable screen-printed sensors, according to the types of materials used to modify the working electrode. Therefore, unmodified SPE, film-modified SPE, enzyme-modified SPE and antigen/antibody-modified SPE are described. Applications are included where available.

Keywords: Screen-printed electrodes; Review; Film-modified sensors; Biosensors; Immunosensors; Electrochemistry

Contents

* Corresponding author. Tel.: +34 947 258818; fax: +34 947 258831.
E-mail address: jarcos@ubu.es (M.J.A. Martínez).

0039-9140/$ – see front matter © 2007 Elsevier B.V. All rights reserved.
doi:10.1016/j.talanta.2007.03.050

1. Introduction

One of the main challenges facing the analytical chemist is the development of methods that respond to the growing need to perform rapid 'in situ' analyses. These methods must be sensitive and accurate, and able to determine various substances with different properties in 'real-life' samples. In recent years, many of the methods developed with this end in sight have been based on the use of electrochemical techniques due to their high sensitivity and selectivity, portable field-based size and low-cost.

Electroanalytical methods, particularly stripping analysis, are the most widely used alternative methods that compete with atomic spectroscopy or other techniques, as far as trace analytes determination is concerned. Conventional laboratory-based stripping measurements had hitherto relied on Hg-based electrodes. The substitution of these electrodes for new disposable test strips is an alternative that presents many advantages for these determinations [1]. Such strips rely on planar carbon, gold, etc. working electrodes as well as silver reference electrodes which are printed on an inexpensive plastic or ceramic support. The strip can therefore be considered as a disposable electrochemical cell onto which the sample droplet is placed.

Since the 1990s, screen-printing technology, adapted from the microelectronics industry, has offered high-volume production of extremely inexpensive, and yet highly reproducible and reliable single-use sensors; a technique which holds great promise for on-site monitoring. Therefore, the use of screen-printing technology in the serial production of disposable low-cost electrodes for the electrochemical determination of a wide range of substances is currently undergoing widespread growth [2].

Screen-printed electrodes (SPEs) are devices that are produced by printing different inks on various types of plastic or ceramic substrates. Polyester screens are generally used for printing with patterns designed by the analyst in accordance with the analytical purpose in mind. The composition of the various inks used for printing on the electrodes determines the selectivity and sensitivity required for each analysis. Alternatively, a wide variety of devices of this type are commercially available.

The great versatility presented by the SPEs lies in the wide range of ways in which the electrodes may be modified. The composition of the printing inks may be altered by the addition of very different substances such as metals, enzymes, polymers, complexing agents, etc. On the other hand, the possibility also exists of modifying the manufactured electrodes by means of depositing various substances on the surface of the electrodes such as metal films, polymers, enzymes, etc. [1,3].

This work intends to review the various different applications of SPEs. These are categorized according to the types of materials used to modify the working electrode, which are basically unmodified SPE, film-modified SPE, enzyme-modified SPE and antigen/antibody-modified SPE.

2. SPEs

2.1. Screen-printed carbon-based electrodes (SPCEs)

There are very few works related to the use of unmodified SPCEs in the determination of interesting analytes [4]. Graphite materials are preferred due to their simple technological processing and low-cost.

Different graphite pastes have been compared for hydrogen peroxide detection [5], the best case of which obtained a detection limit of 2.28 μM.

A rapid and simple method for procaine determination was developed by flow injection analysis (FIA) using a SPCE as amperometric detector [6]. Bergamini and Boldrin Zanoni [7] also determine aurothiomalate, widely used for treatment of reumatoid arthiritis, in human urine samples. Also in this kind of 'real-life' samples, it has been carried out the determination of creatinine, which is useful for evaluation of renal, muscular and thyroid dysfunctions [8].

The behaviour of the SPCEs towards cysteine and tyrosine has been investigated using linear sweep and hydrodynamic voltammetries [9] in commercial pharmaceutical samples. These sensors operate at a lower oxidation potential (versus Ag/AgCl) compared with traditional carbon and platinum electrodes.

Methodologies for the determination of vitamin B2 in food matrixes and a premix has been reported [10]. Electrochemical analysis based on differential pulse voltammetry (DPV) coupled to carbon electrodes gave a well-defined reduction peak at −0.42 V versus Ag/AgCl quasi-reference electrode.

Moreover, the derivatization of phloroglucinol by acidified nitrite has been investigated as a means through which the latter can be quantified within freshwater and saline samples. The resulting nitroso derivative is shown to provide a number of options through which an electroanalytical signal can be obtained [11]. Three distinct species can be electrochemically addressed and their respective sensitivities and practical implementations have been evaluated.

Direct cyclic voltammetric determination of chlorophyll *a* (Chl *a*) at a SPCE resulted in a single, irreversible anodic oxi-

dation peak at +400 mV versus Ag/AgCl [12]. Electrochemical investigations revealed that Chl *a* was adsorbing onto the SPCE surface, which contribute to the development of a method for Chl *a* determination, based on medium exchange followed by adsorptive stripping voltammetry (AdSV). The method was applied to the determination of Chl *a* in faeces from dairy cows.

Another field of application for these types of electrodes is found in the determination of metals. Honeychurch et al. [13] performed the determination of Pb by differential pulse anodic stripping voltammetry (DPASV). A detection limit of 2.5 ng mL^{-1} was obtained and the coefficient of variation, determined on one single electrode, was at 2.4% ($n = 5$). The method was used in the determination of Pb in water samples. Similarly, trace levels of Cu(II) were determined using this procedure in samples of water and bovine serum, which established a detection limit of 8.2 ng mL^{-1} [14]. Ag(I) determination in photographic solutions was also performed using square wave anodic stripping voltammetry (SWASV) for low concentrations of the metal, and chronoamperometry for high concentrations. Both methods were based on the measurement of silver ammonium thiocyanate complexes, which are adsorbed onto the electrode surface [15].

2.2. Metal-based SPEs

Although most SPEs are fabricated with graphite inks, other materials such as gold and silver-based inks are also used in their construction for the analysis and determination of various elements. Thus, Mascini and co-workers performed the determination of Pb and other environmentally hazardous metals such as Cu, Hg and Cd on gold-based SPEs using SWASV, which resulted in detection limits of 0.5, 2.0, 0.9 and 1.4 μg L^{-1} and RSDs of 7, 12, 4 and 14%, respectively [16]. This method has also been applied to the determination of Pb in wastewater and soil extracts by Noh et al. [17].

Equally, SWASV determination of Pb(II) has recently been performed on an Ag-SPE, without chemical modification, which could also be exploited as a disposable Pb(II) sensor with a detection limit of 0.46 ppb (46 pg mL^{-1}) [18].

3. Film-coated SPCEs

3.1. Hg film-modified SPCEs

In most cases, the working electrode consists of thin mercury film plating applied to the graphite surface of the electrode, which enables electrochemical preconcentration of heavy metals.

Wang pioneered the use of these electrodes by demonstrating the viability of determining Pb at ppb levels using stripping voltammetry and potentiometric measurements in urine and water samples [19]. Subsequently, he went on to perform a joint determination of various metals such as Cd, Pb and Cu at ppb levels on mercury-coated carbon strip electrodes [2] demonstrating results that were as satisfactory as those obtained on glassy carbon electrodes, and on hanging mercury drop electrodes (HMDEs).

Since the research conducted by Wang, other authors have fine-tuned various methods for the determination of metals such as Pb(II), Cu(II), Zn(II) and Cd(II) among others, which are based on the easy accumulation on mercury films. Likewise, mercury-coated SPCEs form the subject of a number studies by Ashley et al. [20–22], and Desmond et al. [23,24] obtained detection limits of 55, 71, 64 and 123 ng mL^{-1} for Zn^{2+}, Cd^{2+}, Pb^{2+} and Cu^{2+}, respectively, using DPASV and a deposition time of 300 s. Palchetti et al. [25] applied SWASV and potentiometric stripping analysis (PSA) in order to determine Cu, Pb and Cd on mercury-coated SPCEs. The detection limits they obtained were 0.4 ppb for Pb(II), 1 ppb for Cd(II), and 8 ppb for copper by using SWASV, and 0.6 ppb for Pb(II), 0.4 ppb for Cd(II) and 0.8 ppb for Cu(II) by using PSA.

The mercury-coated screen-printed sensors can be prepared beforehand in the lab for immediate on-site use. In this way, handling, transport and disposal of toxic mercury(II) solutions during decentralized measurements is avoided, as the coating is pre-deposited on the electrode surface [26]. This method combined with SWASV analysis has been successfully applied in the determination of various metals and detection limits of 0.3, 1 and 0.5 μg L^{-1} were found for Pb(II), Cd(II) and Cu(II), respectively.

Macca et al. [27] have also investigated the use of dry-preservable chemicals in batch measurements with mercury-coated SPCEs.

Modification of Hg-coated SPCEs with crown-ether based membranes also seems to be a convenient and inexpensive technique for trace metal detection. Analytical results showed that these electrodes were simultaneously able to detect μg L^{-1} levels of Pb^{2+} and Cd^{2+} with good sensitivity and reproducibility, at different pH values by using linear scan anodic stripping voltammetry (LSASV) [28].

In the work conducted by Choi et al. [29], the working electrode was screen-printed with phenol resin-based carbon ink containing fine particles of mercury oxide as a built-in mercury precursor. The mercuric oxide particles exposed on the surface were reduced to fine mercury droplets by in situ or pre-cathodic conditioning so that they behaved as heavy metal collectors in the anodic stripping analysis. This sensor was evaluated using Pb and Cd as probe metals.

In order to make additional improvements, Wang designed a system of screen-printed carbon-microdisc arrays [30]. Screen-printed microelectrode arrays have successfully been used for low-level lead exposure and blood lead level analyzes as part of a programme to develop a low-cost, portable device for childhood lead poisoning screening programmes [31]. Liu et al. [32] have determined blood lead levels using SWASV by means of a single 10 μm diameter carbon microdisk electrode as well as a 287-element carbon microelectrode array, with indium as the internal standard. The ratio of the anodic stripping peak currents for Pb and In has a linear relationship with the concentration of Pb in blood samples that ranges between 1.2 and 30.0 μg dL^{-1}.

As Hg is toxic, its incorporation in sensors poses environmental problems, especially bearing in mind that these SPEs are

disposable and, as a consequence, other metal films and even unmodified SPEs are under investigation.

3.2. Other film-modified SPCEs

Other metal films on SPCEs such as Au, Ag, Ni and Bi have been used in the determination of various analytes.

3.2.1. Bi-coated SPCEs

For some years, bismuth film SPCEs have offered an attractive alternative to mercury-coated electrodes. The favourable stripping behaviour of bismuth electrodes reflects the ability of bismuth to form fused alloys with heavy metals [33]. The use of pre-plated Bi-SPCEs have been studied in the determination of Pb(II) in the presence of interferents such as Cu [34], achieving detection limits of 0.3 ng mL^{-1} [35,36].

Pb(II) and Cd(II) were simultaneously detected using stripping chronopotentiometry at the bismuth film electrode. Detection limits of 8 and 10 ppb were obtained for Cd(II) and Pb(II), respectively, for a deposition time of 120 s. The proposed method was applied to their determination in soil extracts and wastewaters taken from contaminated sites [37].

Co and Cd in soil extracts were also determined by using a bismuth film electrode operated in the anodic stripping (ASV) and the cathodic adsorptive stripping voltammetry (CAdSV) mode. Two types of Bi-coated SCPEs were used: the 'in situ' prepared Bi-SCPE applied to ASV determination of Cd, and the 'ex situ' prepared Bi-SCPE that was used in CAdSV of Co with dimethylgyoxime (DMG) as the complexing agent.

3.2.2. Gold-coated SPCEs

Gold has also been used to modify SPCEs thereby eliminating the use of toxic elements such as Hg. One such example is the work carried out in 1993 by Wang, which demonstrates the possibility of analysing Pb [38] and Hg [39] on gold-coated SPCEs to obtain highly reproducible responses for both elements.

Pb has also been evaluated in spiked drinking and tap water samples [40]. The recoveries of Pb^{2+} were 103% (R.S.D.: 2.8%) and 97.9% (R.S.D.: 7.1%), $n = 5$, respectively. Measurements in the presence of typical interferences such as copper, cadmium, zinc, iron, chromium and mercury were reported.

SPCE, coated with a thin gold film, are used for highly sensitive potentiometric stripping measurements of trace levels of mercury [39]. Applicability to trace measurements of alkyl mercury and selenium is also demonstrated. Such adaptation of screen-printing technology for the development of reliable sensors for trace mercury should benefit numerous field applications.

3.2.3. Ni-coated SPCEs

Other elements such as Nickel have also been successfully used in the determination of organic materials. Slater and Dilleen [41] carried out a comparative study of the determination of 2-furaldehyde at nickel-modified SPCEs and mercury-coated silver-modified SPCEs. This study shows the advantages of using the mercury-modified SPCEs rather than the nickel-modified SPCEs in the analysis of fural derivatives.

3.3. Metallic nanoparticle-modified SPEs

The design of new nanoscale materials has acquired ever-greater importance in recent years due to their wide-ranging applications in various fields. Among these materials, metallic nanoparticles are of great interest due to their important properties and multiple applications. The bibliography lists numerous methods describing the synthesis of metallic nanoparticles in solution as well as by deposition on solid surfaces. They include chemical synthesis by means of reduction with different reagents [42], UV light or electron-beam irradiation [43] and electrochemical methods [44–50]. The latter provides an easy and rapid alternative for the preparation of metallic nanoparticle electrodes within a short period of time. The combination of electrodeposition and the screen-printing process is beginning to allow mass production of electrochemical sensors that possess various catalyst activities. The sensor strips fabricated by this process are promising tools with more sensitive detection rates that are now starting to come on stream.

Direct construction of Au and Pt nanoparticles by electrodeposition processes on the SPCE strips has been performed by Chikae et al. [50] and applied to the determination of H_2O_2.

Poly(L-lactide) stabilized gold nanoparticles were also used to modify a disposable SPCE for the detection of As(III) by DPASV. The sensitivity was good enough to detect As(III) at ppb levels and provides a direct and selective detection method for As(III) in natural waters [51].

Similarly, an indirect electrochemical approach in the determination of sulphide achieved a detection limit of 0.04 μM by measuring the inhibited oxidation current of As(III) using a poly(L-lactide) stabilized gold nanoparticle-modified SPCE.

Dominguez and Arcos [52] have fine-tuned a novel, user-friendly and rapid method of incorporating Ag nanoparticles onto the surface of SPCEs. This method is based on the direct electrodeposition of these nanoparticles. The modification of SPCEs with silver nanoparticles increases the already well-known performance of these kinds of disposable electrodes. In order to demonstrate their practical applications, they were used to analyze Sb(III), a significant pollutant of priority interest. The silver nanoparticle-modified SPCE developed in our work presents an environmentally friendly method for the analysis of antimony. It brings with it important advantages that include a high degree of sensitivity and selectivity in antimony determination. Moreover, the electrochemical response is not influenced by common interferents in ASV antimony determination, such as bismuth.

3.4. Other modified SPEs

Metal–chelate adsorptive stripping schemes have also been coupled with SPEs and applied in the determination of a uranium–cupferron complex [53].

In the on-going search for more friendly alternatives to Hg, strip-type preconcentrating/voltammetric sensors, prepared by incorporating a cation exchange resin within screen-printed carbons inks, have been described by Wang and applied to the determination of Cu(II) [54]. The device presents good repro-

ducibility (a relative standard deviation of 2%) and a detection limit of 0.5 μM with a 10-min accumulation time.

Besides metals, other molecules have been determined using modified SPCE. In this way, hydrazines can be analyzed by incorporating cobalt phthalocyanine (CoPC) within the carbon inks or by covering the printed electrode surface with a mixed valent ruthenium cyanide coating [55]. Ascorbic acid and hydrogen peroxide have been analyzed as well using an electrochemically modified SPCE by electropositing nickel hexacyanoferrate onto the carbon electrode surface [56]. Hydrogen peroxide has also been amperometrically determine using a carbon tick film electrode modified with a MnO_2-film in flow injection analysis (FIA) [57].

An interesting application of disposable SPCE is the selective detection of sulphide in cigarette smoke by modification of the working electrode with a cinder/tetracyano nickelate hybrid [58].

4. Enzyme-modified SPEs

In the construction of biosensors, enzymes are the most commonly used biological elements, despite their high extraction, isolation and purification costs, as they rapidly and cleanly form selective bonds with the substrate.

Enzymes are proteins (polypeptide structures) which catalyze specific chemical reactions in vivo. They accelerate the reaction rate of specific chemical reactions. Enzymes were the first biocatalysts used in biosensors and remain by far the most commonly employed. Clark and Lyons [59] were the pioneers who showed that an enzyme could be integrated into an electrode, thus making a biosensor for the determination of glucose. Since then, enzymes have been extensively used in biosensor construction [60].

Enzyme specificity is a key property which can be exploited in biosensor technology. Compared with chemical catalysts, enzymes demonstrate a significantly greater level of substrate specificity, primarily because of the constraints placed on the substrate molecule by the active site environment. This fact involves factors such as molecular size, stereochemistry, polarity, functional groups and relative bond energies.

Disposable biosensors based on enzyme immobilization on SPEs have been widely used for the analysis of several analytes. In this paper, we compile an exhaustive review of the various disposable enzymatic SPE applications, covering a broad spectrum of different interests and activities.

4.1. Applications in environmental analysis

Disposable biosensors offer a wide-range of applications for analysis in the environmental field. The detection limits that these systems obtain are suitable for the determination of contaminants such as pesticides and heavy metals, amongst others.

4.1.1. Analysis of pesticides and herbicides

Enzymatic sensors constructed with SPEs present a great number of applications in the analysis of pollutants such as pesticides. The determination of carbamate and organophosphorous pesticides with these kinds of sensors is often based on enzymatic inhibition processes.

Among the most commonly used enzymatic disposable biosensors in pesticide determination are those based on enzymatic inhibition of acetylcholinesterase (AChE). When AChE is immobilized on the working electrode surface, its interaction with the substrate (for example, with acetylthiocholine) produces an electroactive species (thiocoline) and its corresponding carboxylic acid [61]:

$$\text{Acetylthiocholine} + H_2O + \text{AChE} \rightarrow \text{thiocholine (TCh)} + \text{acetic acid}$$

The subsequent electrodic oxidation of the thiocholine gives rise to a current intensity that constitutes a quantative measurement of the enzymatic activity:

$$2\text{TCh (red)} \rightarrow \text{TCh (ox)} + 2H^+ + 2e^-$$

The presence of pesticides in the analytical sample inhibits enzymatic activity that leads to a drop in the current intensity, which is then measured. The sensitivity of these types of biosensors depends considerably on the chosen method of enzyme immobilization.

Although in practically all of the methods described for the construction of AChE–SPEs the working electrode surface is modified with different mediators, Shi et al. [62] have recently developed a mediator-free screen-printed biosensor for the screening of organophosphorus pesticides with a FIA system. The AChE enzyme was immobilized in an Al_2O_3 sol–gel matrix. This matrix not only provided a friendly microenvironment for the immobilization of AChE that retained its activity for a long time, but also effectively promoted the electron transfer process between the thiocholine and the electrode. This promoting effect greatly decreased the overpotential in the detection of the thiocholine and minimized interference from other co-existing impurities.

Electrode modification with mediators reduces the working potential, avoids electrochemical interferences and increases the reversibility of electrode reactions [61,63]. One of the simplest methods is described by Bonnet et al. [64] for the determination of chlorpyrifos ethyl oxon. It is based on the immobilization of AChE through simple adsorption on the surface of the working electrode using 7,7,8,8-tetracyanoquinonedimethane (TCNQ) as a mediator on the graphite paste, which enables electrochemical oxidation of the thiocholine at 100 mV.

Immobilization of the enzymes on a graphite surface is difficult, as the number of active groups on the surface is insufficient for direct immobilization. Vakurov et al. [65,66] propose two methods of immobilization that use electrochemical reduction of 4-aminobenzene in derivatized SPEs. AChE was immobilized either covalently onto dialdehyde-modified electrodes or non-covalently onto polyethyleneimine (PEI) modified electrodes.

Another of the most widely employed methods in the construction of AChE–SPCEs is based on cross-linking using bovine serum albumin (BSA) and glutaraldehyde (GA). Suprun et al. [63] employed this method of immobilization to deter-

mine aldicarb and paraoxon using Prussian Blue (PB) as the electrochemical mediator. This same method of enzymatic immobilization was employed by Solna et al. [67] in the construction of a multienzyme electrochemical array sensor based on the cross-linking immobilization of AChE, tyrosinase (TYR), peroxidase and butyrylcholinesterase on a screen-printed platinum working electrode. This multi-enzymatic sensor allows determination of a great number of phenolic compounds such as *p*-cresol, cathecol and phenol, and pesticides such as carbaryl, heptenophos and fenitrothion. A multienzyme biosensor array was also constructed by cross-linking immobilization of a wild-type AChE and three engineered variants of Nippostrongylus brailiensis acetylcholinesterase (NbAChE) [68] in order to determine neurotoxic insecticides. The use of engineered variants of the AChE is also reported by other authors [69] who employed a genetically modified AChE from *Drosophila malanogaster* in the determination of methamidophos pesticides. The biosensor was constructed using a screen-printed TCNQ-modified working electrode. The enzyme was immobilized in a polymer using photocross-linkable poly(vinyl alcohol) bearing styrylpyridinium groups (PVA-SbQ). Generally, the use of AChE mutants contributes to the construction of more sensitive biosensors.

Sol–gel immobilization of AChE has also been performed [70,71]. Sotiropoulu and Chaniotakis [70] employed this method of immobilization in the determination of the pesticide dichlororvos using an amperometric biosensor constructed with a graphite working electrode using cobalt phtalocyanine as the mediator. Sol–gel immobilization of AChE and cytochrome P450 MB-3 on a SPCE allowed Waibel et al. [71] to elaborate a bienzymatic sensor for sensitive determination of parathion and paraoxon.

More novel methods to perform the immobilization of AChE have been developed in recent years. A new immobilization technique consists of creating different bioaffinity bonds between an activated support and a specific group present on the enzyme surface [72]. The support can contain functional amino groups that can be activated through cross-linking with GA. Once the support is activated, the regulation of Concanavalin A (Con A) commences on the activated support. The enzyme is finally immobilized thanks to the strong affinity links formed between Con A and the mannose residues of the enzyme.

Dondoi et al. [73] recently proposed a method of analysing organophosphorus insecticides using AChE sensors with a previous preconcentration on a solid-phase column. The combination of solid-phase extraction with enzymatic biosensors offers a solution to two principle issues of environmental monitoring: insufficient sensitivity, and susceptibility to multiple sources of interference for paraoxon and dichlorvos pesticides.

The work of Bucur et al. [74] describes the use of three modified AChEs from *D. melanogaster* enzymes used in the construction of biosensors for fast and ultra-sensitive detection of carbamate insecticides. The authors found that AChEs obtained from different sources presented different sensitivities towards insecticides. The introduction of various mutations in the enzyme structure improved the sensitivity of the biorecognition molecules and consequently of the biosensors.

4.1.2. Analysis of heavy metals

Heavy metals are highly toxic and dangerous pollutants, second only to pesticides in terms of environmental impact. Monitoring of heavy metals at trace levels is therefore an increasingly important issue [75].

It is a well-known fact that some metallic ions, especially heavy metals, can inhibit the activity of various enzymes. Disposable biosensors based on the principle of inhibition have to date been applied for a wide range of significant analytes, amongst which heavy metals [75–79].

The most widely employed enzyme in the inhibitive detection of heavy metals ions using SPE is urease. The urease enzyme catalyzes the hydrolysis of urea and the reaction produces ammonium:

$$\text{Urea} + H_2O + \text{urease} \rightarrow CO_2 + 2NH_3$$

As a consequence of the ammonium liberation, a variation in the pH value takes place. This change might cause a decrease in the potential of an internal pH-subsensor. Thus, for example, the presence of ruthenium dioxide in the biosensing film causes pH-dependent potentiometric sensitivity [77,79]. The presence of Ag(I) and Cu(II) causes the heavy metals to inhibit the enzyme which leads to a decrease in enzymatic activity and, as a result, a lower quantity of ammonium is liberated that is recorded as an analytical signal by the sensor [77].

The analysis of Cu(II), Hg(II) and Cd (II) can be carried out employing a disposable screen-printed biosensor [75,78]. Amperometric measurements of urease activity are possible after coupling this enzyme to glutamate dehydrogenase (GLDH), which catalyzes the synthesis of L-glutamate from α-ketoglutarate. Both dihydronicotinamide adenine dinucleotide (NADH) and NH_4^+ are required in equimolecular amounts for this reaction to take place:

$$\text{Urea} + H_2O + \text{urease} \rightarrow CO_2 + 2NH_3$$

$$NH_3 + \alpha\text{-ketoglutarate} + \text{NADH} + H^+ + \text{GLDH} \rightarrow \text{l-glutamate} + NAD^+$$

NADH consumption is monitored by measuring the decrease in its amperometric signal. The urease enzyme is inhibited by the presence of heavy metal ions resulting in decreased ammonia production. This leads to a reduction in the oxidation rate obtained for NADH. The presence of metal ions can be determined by comparing the latter with the NADH oxidation rate in an uninhibited reaction.

4.2. Cholesterol analysis

The analysis of cholesterol using enzymatic biosensors is frequently based on the determination of hydrogen peroxide, using cholesterol oxidase (ChOX) [80] as the enzyme inmobilized on a SPCE surface. The enzymatic reaction scheme is as follows:

$$\text{Cholesterol} + O_2 + H_2O + \text{ChOX} \rightarrow \text{cholest-4-en-3-one} + H_2O_2$$

Oxidation of H_2O_2 on conventional working electrodes requires the use of high potentials which causes a considerable degree of selectivity to be lost. The use of mediators such as cobalt phthalocyanine (CoPC) [80] avoids this problem.

A second method of performing the determination of cholesterol using SPCEs consists of using peroxidase (POD) as the second enzyme, as well as ChOX, with potassium ferrocyanide ($K_4Fe(CN)_6$) [81,82] as the electrochemical mediator. In this type of sensor, cholesterol analysis is based on oxidation, catalyzed by the enzyme POD, of potassium ferrocyanide by hydrogen peroxide produced as a result of the ChOX enzymatic reaction:

$$H_2O_2 + H^+ + 2K_4Fe(CN)_6 + POD \rightarrow 2K_3Fe(CN)_6 + 2K^+ + 2H_2O$$

The resulting potassium ferricyanide is reduced at the electrode and the current obtained is proportional to the amount of cholesterol originally present in the sample:

$$2K^+ + 2K_3Fe(CN)_6 + 2e^- \rightarrow 2K_4Fe(CN)_6$$

The sensitivity of these types of sensors can be improved using carbon nanotubes modified biosensors [81]. The modification of the carbon nanotubes promotes electron transfer and thereby improves the sensitivity of the cholesterol sensor and provides a rapid, economic and reproducible method of manufacturing sensor electrodes for the analysis of cholesterol levels in blood.

Shumyantseva et al. [83] opted for a different enzyme, cytochrome-P450scc, due to the specificities of its interaction with cholesterol. This enzyme is a mono-oxygenase that catalyzes the cholesterol side chain cleavage reaction. These authors constructed a sensor based on the immobilization of the latter enzyme through GA cross-linking or by entrapment in a matrix of agarose hydrogel on a rhodium–graphite SPE. The analytical signal measured, which allows analysis of the cholesterol, is the intensity of the reduction of cytochrome-P450 heme iron. In order to construct these types of sensors it is necessary to use an electrochemical mediator such as riboflavin that can promote this reduction reaction. Modification of these types of sensors with gold nanoparticles integrated with cytochrome-P450scc yields a more highly sensitive amperometric biosensor for cholesterol measurements [84].

4.3. Glucose analysis

Rapid and accurate analysis of glucose is of great interest in the diagnosis and treatment of diabetes. For this reason, numerous biosensors have been developed with this objective in mind. In fact, today's biosensor market is dominated by glucose biosensors [85].

Most of these biosensors are constructed using SPCEs modified with the enzyme glucose oxidase (GOx). Glucose is oxidized by the enzyme and the electrons involved in the redox reaction may sometimes be relayed to the electrode through a mediator, resulting in electric currents that are proportional to the level of glucose in sample solutions [86]. One of the first enzymatic carbon screen-printed biosensors was developed by Newman et al. [87]. GOx was immobilized by cross-linking with GA and tetrathiafulvalene (TTF) was used as a mediator. The reactions at the electrode are as follows:

$$\text{Glucose} + 2TTF^+ \rightarrow \text{gluconic acid} + 2TTF + 2H^+$$

$$2TTF \rightarrow 2TTF^+ + 2e^-$$

The last oxidation reaction takes place on the electrode.

A great number of the disposable biosensors used in the analysis of glucose are based on electrochemical determination of enzymatic-generated hydrogen peroxide brought about in the following reaction:

$$\text{Glucose} + O_2 + GOx \rightarrow \text{gluconic acid} + H_2O_2$$

Oxidation or reduction of H_2O_2 generally requires high potentials at bare electrodes, which implies a very poor sensitivity. For this reason, most of the glucose sensors use mediators that enable the reduction of hydrogen peroxide at low potentials, thereby avoiding any kind of electrochemical interferent. There are many methods for the immobilization of GOx on SPCEs using different mediators, which may be found in the bibliography.

Cui et al. [88] have reported that the use of SPCEs on nitrocellulose (NC) with two separate reagent zones effectively eliminates interference from both easily oxidable species and hematocrit in the glucose determination. To exploit the advantages of NC strip-based electrochemical sensors, they developed a new disposable-type of glucose sensor using hexamineruthenium(III) chloride ($[Ru(NH_3)_6]^{3+}$) as a mediator. The authors found that the use of this mediator eliminates the interference from other oxidizable species providing improved analytical results in the determination of glucose in blood [86].

Another mediator used in the construction of screen-printed biosensors for the analysis of glucose is pyocyanin [89]. The enyme GOx and the mediator are mixed which forms a solution that is deposited on the SPCE as a thin layer after drying at 60 °C for 20 min. The constructed biosensor was successfully applied to the analysis of glucose in soft drinks.

Mersal et al. [90] have developed screen-printed glucose electrodes for repetitive use in an automated FIA system. The biosensors were constructed by entrapment of the enzyme GOx on a screen printable paste polymerized by irradiation with UV-light. The resultant biosensor was used in the analysis of glucose in juice samples. A FIA system has also been used for the analysis of glucose using chemically modified ferric hexacyanoferrate (Prussian Blue) SPCEs. Following the chemical modification of the electrodes, the enzyme was immobilized using a cross-linking method that employs GA and Nafion [91]. PB is a very common mediator used in the production of enzymatic biosensors for the analysis of glucose. Lupu et al. [92] have developed a biosensor using PB as a mediator which has the property of catalyzing the hydrogen peroxide reduction. The following reactions took place at the electrode:

$$\text{Glucose} + O_2 + GOx \rightarrow \text{gluconic acid} + H_2O_2$$

$$H_2O_2 + PB_{red} \rightarrow OH^- + PB_{ox}$$

$$PB_{ox} + e^- \rightarrow PB_{red}$$

The biosensor developed by Mattos et al. [93] is based in the same sequence of reactions. In their case, crystallized GOx was used instead of ordinary commercial GOx. The immobilization of cross-linked GOx crystals in Nafion on PB-modified gold and platinum screen-printed electrodes gives greater stability to the biosensor when compared with the electrodes prepared with ordinary GOx. Pravda et al. [94] have also employed PB as a mediator in the preparation of screen-printed biosensors by mixing the mediator with GOx and carbon ink microparticles in different ratios.

Ferrocene and its derivatives are also frequently used as mediators in the production of screen-printed enzymatic biosensors. Nagata et al. [95] constructed a glucose sensor employing ferrocene-bound GOx imbobilized on screen-printed gold electrodes. In this case, ferrocenecarboxylic acid was used as the electron mediator. 1,1′-Ferrocenedimethanol [96,97] is one of the ferrocene derivatives used in the elaboration of disposable sensitive glucose sensors. Forrow and Walters [98] demonstrated that only one of the cyclopentadienyl rings of ferrocenium can interact with the enzyme co-factor, for this reason these authors developed disposable biosensors using chromium and manganese half-sandwich complexes as electronic mediators. These complexes have just one cyclopentadienyl ring and their oxidized forms show great stability in an aqueous medium. Their small molecular size is a further advantage, which facilitates GOx penetration at the active site.

Another method for glucose determination at low potentials using GOx–SPCEs employs copper [99,100] to modify the carbon electrode. Kumar and Zen [99] have developed a screen-printed copper-plated glucose-biosensor using a SPCE. The electrode was immersed in a Cu^{2+} solution and copper was deposited on the SPCE surface by applying a potential of −0.7 V. This Cu-SPCE facilitated an extremely sensitive analysis of glucose. Good results were also obtained by Luque et al. [100] using a biosensor made by modifying its carbon ink with CuO and GOx. CuO promotes excellent electrocatalytic activity towards the oxidation and reduction of hydrogen peroxide, which leads to a significant decrease in oxidation and reduction overpotentials, and a significant enhancement of the corresponding currents. Other metallic oxides used as mediators are MnO_2 [101], RuO_2 [102] and RhO_2 [103]. The analysis of glucose in beer samples was carried out using a FIA system constructed using a screen-printed amperometric biosensor. The sensor consisted of carbon ink electrodes double bulk-modified with MnO_2 as a mediator and GOx as the biocomponent [101]. SPCEs modified with ruthenium dioxide and GOx were constructed for the amperometic determination of glucose using FIA. In these cases, the enzyme was immobilized with Nafion films [102]. Ruthenium has also been employed in the modification of SPCEs for the development of glucose biosensors. Ruthenium-dispersed carbon surfaces offer a strong and preferential catalytic action towards the oxidation of enzymatically-liberated hydrogen peroxide [104]. Miscoria et al. [105] have also constructed a very sensitive glucose biosensor using rhodium as a catalyst. In this case, an ‘in situ’ electrogenerated polytyramine was used as an anti-interferent barrier, which also made the electrode highly selective.

Osmium complex mediators have also been used in the development of GOx–SPCEs. Zhang et al. [106] developed a novel disposable capillary-fill device using an Os-Tris(4,7-dmphen) complex as a mediator. A different Os-complex used in an FIA system to determine glucose is Os-4,7-dimethyl-1,10-phenanline, which was used as the electron transfer mediator [107]. Gao et al. [108] have constructed a glucose biosensor through the electrodeposition of GOx and a redox polymer, formed by poly(vinylimidazole) and complexed with osmium(4,4′-dimethyl-2,2′-bipyridine) chloride, on a SPCE surface.

More recently, three works have been published on the construction of glucose sensors using hexacyanoferrate as an electron transfer mediator. Sato and Okuma [109] have used this mediator in the construction of a sensor for the simultaneous determination of glucose and lactate in lactic fermenting beverages. Lee et al. [110] have described a glucose sensor based on SPCEs modified with a mixture of ferrycianide and chitosan oligomers. An enhanced response was observed thereby demonstrating that the presence of chitosan could increase the interfacial concentration of the mediator. Finally, bienzymatic screen-printed biosensors have been fabricated for glucose analysis in grape fruit. HRP and GOx have been immobilized by crosslinking with BSA and GA on the carbon working electrode surface showing good values of reproducibility and repeatability [111].

In order to improve the properties of the disposable glucose biosensor base for GOx immobilization, new materials and construction techniques have been developed over the last few years. Crouch et al. [112,113] demonstrated the possibility of fabricating a disposable amperometric glucose sensor using a water-based carbon ink. This kind of ink presents a great advantage: it avoids problems of enzyme denaturalization as it is not necessary to employ organic solvents, and the curing stage is therefore not required, which avoids problems with high temperatures. In these works, cobalt phthalocyanine was successfully used as a mediator towards the oxidation of hydrogen peroxide. The developed disposable biosensor was applied to the determination of glucose in serum.

Gao et al. [114] describe the construction of a screen-printed glucose biosensor based on the formation of a nanoparticulate membrane on SPCEs. The nanoparticulate membrane not only fulfilled biosensing, but also analyte-regulating functions. Nanotechnology has also been employed by Guan et al. [115] in the construction of a glucose biosensor using multi-wall carbon nanotubes. This biosensor showed greater sensitivity and a wider linear response range than a typical glucose electrochemical biosensor. Other nanomaterials used in the construction of glucose disposable biosensors are magnetic Fe_3O_4 nanoparticles. Lu and Chen [116] have developed a glucose biosensor based on drop-coating GOx on SPCEs modified with a ferrinano-Fe_3O_4 mixture. The sensor constructed had a fast response with high sensitivity and good reproducibility.

The properties of enzymes such as GOx can be improved through genetic engineering. Chen et al. [117] developed an improved glucose biosensor using genetically modified GOx immobilized on a SPCE. The modification of the enzyme was performed through the addition of a poly-lysine chain at the C-terminal with a peptide linker inserted between the enzyme and the poly-lysine chain. The use of this modified enzyme improved the signal level, the response range and the lifetime of the glucose sensor.

GOx is an oxygen-dependent enzyme which complicates the analysis of certain samples, for this reason other enzymes, such as glucose dehydrogenase (GDH), have also been used in the construction of disposable glucose sensors. GDH biosensors need to be used with mediators which facilitate NAD^+ coenzyme regeneration. Razumiene et al. [118] describe a biosensor for glucose analysis using GDH as the biocomponent and a ferrocene derivative (4-ferrocenylphenol) as an electron transfer mediator. Ferrocene derivatives are widely used as mediators with GDH glucose biosensors. 2-Ferrocenyl-4-nitrophenol (FNP) and *N*-(4-hydroxybenzylidene)-4-ferrocenylaniline (HBFA) are both frequently used as mediators in GDH disposable sensors. SPCEs modified with these bioorganometallic ferrocene derivatives enable highly sensitive determination of glucose, the most sensitive of which were the HBFA-modified electrodes [119]. 4-(4-Ferrocenephenyliminomethyl)phenol (FP1) has also been used to modify SPCEs. These modified electrodes may be used in FIA systems to analyze glucose in beverages [120]. Silber et al. [121] have also employed GDH for the elaboration of a biosensor using the phenothiazine derivative Methylene Blue (MB) as a mediator. This mediator was deposited on the thick-film gold electrode surface by means of electropolymerization from a solution of the monomer. The enzyme was subsequently immobilized by two different techniques: electropolymerization of MB in the presence of GDH and entrapment in a polymer matrix made of poly(vinylacetate)–poly(ethylene).

A recent work describes the direct determination of glucose using two types of PQQ dependent glucose dehydrogenases: the soluble *s*-PQQ-GDH and the membrane-bound enzyme *m*-PQQ-GDH. It was shown, that both enzymes are able to donate electrons to the carbon paste [122].

4.4. Analysis of superoxide and hydrogen peroxide

The determination of hydrogen peroxide may be performed by using SPEs with different immobilized enzymes, among which horse-radish peroxidase (HRP). There are various methods of immobilizing the enzyme on SPEs. Gao et al. [123] propose an immobilization method involving prior modification of SPCEs with amino groups carried out by the electrochemical oxidation of thionine in a neutral phosphate buffer. The H_2O_2 biosensor is then constructed by covalently binding multilatilayer HRP enzymes on the modified electrodes. Amperometric analysis of hydrogen peroxide is subsequently performed.

This same enzyme is used by authors such as Ledru et al. [124] in the construction of amperometric screen-printed biosensors for the analysis of hydrogen peroxide in flow injection mode. In this case, the biosensor was constructed by modification of the graphite-binder ink with HRP.

A novel method for the immobilization of HRP on SPCEs is described by Morrin et al. [125] using polyaniline nanoparticles. The best method of incorporating the HRP enzyme was by simultaneously drop-coating the conductive polyaniline nanoparticles and the enzyme onto disposable SPCEs. Polyaniline can act as an effective non-diffusional mediating species coupling electrons from the enzyme redox site directly to the electrode. This allows for very effective direct electrical communication between the biomolecule and the electrode surface.

Cytochrome *c* is another enzyme used in the preparation of biosensors that are sensitive to hydrogen peroxide concentrations. Krylov et al. [126] used a superoxide sensor based on thick-film gold electrodes for the quantification of superoxide radicals and hydrogen peroxide concentrations. The sensor was constructed through a self-assembly approach by immobilizing cytochrome *c* using mixed monolayers of mercaptoundecanoic acid and mercaptoundecanol. It is based on the reduction of cytochrome *c* by hydrogen peroxide or superoxide radicals, after which, the application of a suitable potential allows the electrode to re-oxidize the enzyme, resulting in a current that is proportional to the H_2O_2 or radical concentration.

4.5. Ethanol analysis

Highly selective, accurate and sensitive detection and quantification of alcohols is required in many different areas. Many analytical methods have been developed for the analysis of ethanol, methanol and other aliphatic alcohols, among which are found the enzymatic biosensors [127]. Two enzymes, alcohol oxidase (AOX) and alcohol dehydrogenase (ADH) have been extensively used in the construction of these biosensors.

AOX catalyzes the oxidization of low molecular weight alcohols into their corresponding aldehydes by using the molecular structure O_2 as an electronic acceptor as in the following reaction:

$$RCH_2OH + O_2 + AOX \rightarrow RCHO + H_2O_2$$

The analysis is generally performed through the electrochemical response of the hydrogen peroxide generated.

This enzyme has been used in the preparation of screen-printed biosensors by authors such as Boujtita et al. [128], who have developed a biosensor for the determination of ethanol in beer based on SPCEs modified with CoPC that acts as an electrocatalyst in the oxidation of hydrogen peroxide. This same enzyme has also been chosen for the construction of low-cost screen-printed sensors consisting of platinum working electrodes. A mixture of AOX with poly(carbamoyl)sulphonate (PCS) hydrogel was used for enzyme immobilization onto the platinum electrodes. The sensor was successfully applied to the analysis of ethanol in wine samples [129].

ADH catalyzes the reversible oxidation of primary aliphatic and aromatic alcohols other than methanol according to the following reaction [127]:

$$RCH_2OH + NAD^+ + ADH \rightarrow ADHRCHO + NADH + H^+$$

Practically, all of the disposable biosensors constructed for the analysis of ethanol are modified with some type of mediator. A disposable reagentless screen-printed biosensor has been elaborated by Sprules et al. [130] that consisted of a Meldola's Blue modified SPCE coated with a mixture containing ADH and NAD^+. Analysis of the ethanol concentration is performed by tracking the amperometric oxidization reaction of Meldola's Blue on the electrode surface.

Ferrocene derivatives are the other mediators used in the preparation of disposable ethanol sensors based on the ADH enzyme. Razumiene et al. [118,120] have developed disposable ethanol biosensors by modifying SPCEs with 4-ferrocenylphenol (FP). The use of FP as an electron transfer mediator decreases the oxidation/reduction potential of hydrogen peroxide. Certain bioorganometallic ferrocene derivatives have proven to be good electron transfer mediators in the construction of ethanol biosensors, amongst which are found FNP and HBFA [119].

Other disposable biosensors constructed for ethanol analysis use dispersed ruthenium particles which offer an efficient electrocatalytic action towards the detection of enzymatically-liberated NADH [104]. These ADH enzyme biosensors were obtained by covering the ruthenium-containing SPCEs with a mixture solution of ADH and NAD^+.

Screen-printed ethanol biosensors were also constructed with quinohemoprotein alcohol dehydrogenase immobilized by cross-linking to an Os-complex-modified poly(vinylimidazole) redox polymer. The resulting biosensor was successfully applied to the determination of ethanol in wine samples [131].

4.6. Phenolic compounds

Phenolic compounds represent a large and environmentally widespread group of organic pollutants as a result of their industrial applications. Certain phenolic compounds are highly toxic or carcinogenic which is the main reason for their determination in the environment [132].

The most widely used enzymatic biosensors in the SPE analysis of phenolic compounds are based on the immobilization of the enzyme TYR. The determination is carried out through amperometric detection according to the following sequence [133]:

$$\text{Phenol} + O_2 + \text{TYR} \rightarrow \text{catechol}$$

$$\text{Catechol} + O_2 + \text{TYR} \rightarrow o\text{-quinone} + H_2O$$

$$o\text{-Quinone} + 2H^+ + 2e^- \rightarrow \text{catechol}$$

One of the first works in the bibliography on these types of disposable biosensors describes a methylphenazonium-zeolite-modified TYR sensor. The enzyme was immobilized using a novel polyurethane hydrogel [134]. TYR immobilization using hydrogels has been used by other authors in the preparation of a sensor highly sensitive to concentrations of catechol. In this case, TYR was immobilized on the surface of two types of Au-screen-printed four-channel electrode arrays (graphite-coated-Au- and Carbopack C-coated-Au) by entrapment in a redox hydrogel composition [135]. Different methods of immobilizing this enzyme have been successfully tested for the construction of sensors, among which the immobilization of TYR in a thin layer of Eastman AQ polymer on the surface of the SPCE has been carried out [136]. Cummings et al. [137] also performed TYR immobilization on SPCEs using a polymer, in this case, an amphiphilic substituted pyrrole.

A simple method of constructing a TYR-based biosensor consists of enclosing the enzyme in the graphite ink by simple mixing, then printing the ink on the active area of the electrodes to supply the sensitive layer of the biosensors [133].

A comparison between a TYR-based and HRP-based disposable biosensor has been carried out by Busch et al. [138]. Both sensors were tested for rapid measurements of polar phenolics of olive oil. The two biosensors showed different specifities towards different groups of phenolic.

Another enzyme used in the preparation of sensors for the analysis of phenolic compounds is the cellobiose dehydrogenase (CDH) enzyme. In this case, the phenols are first anodically oxidized to quinonomes:

$$\text{Catechol} \rightarrow o\text{-quinone} + 2H^+ + 2e^-$$

The *o*-quinone is then reduced to catechol by CDH in the presence of cellobiose:

$$\text{Cellobiose} + \text{CDH} \rightarrow \text{cellobionolactone} + 2e^- + 2H^+$$

$$o\text{-Quinone} + 2H^+ \rightarrow 2e^- \text{catechol}$$

and finally the following oxidation reaction takes place on the electrode:

$$\text{Catechol} \rightarrow o\text{-quinone} + 2H + + 2e^-$$

The analytical response obtained is more sensitive in the presence of CDH than in its absence [139,140].

There are many authors who have used multienzymatic systems in the construction of biosensors for the determination of phenolic compounds using SPEs. In all of them, the immobilized TYR enzyme is present alongside other enzymes. Chang et al. [141] developed a phenol sensor using HRP-modified SPCEs coupled with immobilized TYR prepared using poly(carbamoylsulphonate) hydrogels or a poly(vinyl alcohol) bearing styrylpyridinium groups. Other bi-enzymatic biosensors based on the combination of HRP and TYR are described by Sapelnikova et al. [142]. In this work, the authors analyze the compatibility of the latter biosensor with a bi-enzymatic one that combines TYR and cholinesterase in FIA of different phenolic compounds.

Some multi-enzymatic biosensors manage to combine up to three different enzymes. One such biosensor described by Solná et al. [132] is constructed by the immobilization of TYR, HRP and laccase on gold SPEs modified with self-assembled monolayers. The idea of combining different enzymes on electrode arrays increases the recognition power of a detection system.

5. Immunosensors

Bioanalytical assays such as immunoassays (IAs), which use specific antigen antibody complexation, are very important in many fields, e.g. biological and medical research, diagnostic medicine, genetics, forensics, drug and pesticide testing. IAs with electrochemical detection can offer enhanced sensitivities and reduced instrumentation costs compared to their optical counterparts, and an increasing effort was made during the last decade lo link the specificity of bioaffinity assays with the sensitivity and low detection limits afforded by modern electrochemical techniques [143].

Warsinke et al. [144] already showed electrochemical IAs as promising alternatives to existing immunochemical tests for the development of hand-held devices which can be used for point of care measurements. In this way, SPE contribute to develop miniaturized, easy to handle, reliable and inexpensive IAs devices, which produce results within a few minutes [145–149].

Electrochemical immunosensing requires labelling of either antigen or antibody, since their binding is accompanied by only small physico-chemical changes [144,150]. The use of labels began in 1956 when Yalow and Berson [151] developed the first radioimmunoassay with a radioactive compound as label. Peroxidases, phosphatases, ureases and glucose oxidases proofed to be best-suited enzyme labels [150,152]. In the same way, fluorophors, redox compounds, co-factors, fluorescence quenchers, chemiluminescence metals, latex particles and liposomes have been applied in IAs [144].

Here, we recount the recent publications in IAs based on SPEs, focusing on their final analytical application.

5.1. Indirect electrochemical immunoassays

5.1.1. Hormones

IAs based on SPEs are commonly used in the case of the analysis of hormones. The ability to determine estradiol levels, naturally occurring steroid hormone, in biological fluids such as serum and saliva is of value for various applications, including gynecological endocrinological investigations of infertility status, post-menopausal status and estradiol status after fertility treatment. Investigations into the development of a prototype electrochemical immunosensor for estradiol have been described [153]. Antibodies (rabbit anti-mouse IgG and monoclonal mouse anti-estradiol) were immobilized by passive adsorption onto the surface of SPCEs. A competitive IA was then performed using an alkaline-phosphatase (ALP)-labelled estradiol conjugate. Electrochemical measurements were then performed using differential DPV following the production of 1-naphthol from 1-naphthyl phosphate. The immunosensor, with a detection limit of 50 pg mL^{-1}, was applied only to one spiked serum sample after an extraction step with diethyl ether. Analogously, Volpe et al. [154] develop a cost-effective, single-use, electrochemical immunosensor for a simple and fast measurement of picogram amounts of 17 β-estradiol in non-extracted bovine serum using estradiol–ALP and portable instrumentation.

Butler and Guilbault [155] describe an amperometric immunosensor, based on disposable SPCE, for the determination of 17-β estradiol in water, since rivers and lakes are the ultimate sink for steroid hormones. Both monoclonal and polyclonal antibodies were assessed and the use of monoclonal antibodies resulted in a more sensitive assay. Detection was facilitated by labelling the antibody with ALP and amperometric measurements were performed at +300 mV versus Ag/AgCl using *p*-aminophenyl phosphate as substrate.

Bagel et al. [156] developed a disposable electrochemical sensor based on an ion-exchange film-coated SPE adapted to the bottom of a polystyrene microwell for human chorionic gonadotropin hormone determination. In this case, the ALP label was used to hydrolyze the monoester phosphate salt of [(4-hydroxyphenyl)aminocarbonyl]-cobaltocenium. This anionic substrate is transformed into a cationic electroactive product, which is then accumulated by ion-exchange at the electrode surface to give an amplified electrochemical response.

In cattle breeding industry, where artificial insemination techniques are employed, the successful prediction of oestrus onset leads to considerably cost saving in herd management. One way to detect the oestrus onset is to monitor progesterone levels in milk [157]. Therefore, several progesterone immunosensors have been developed. SPCEs coated with antibodies were employed in competitive assays involving progesterone labelled with ALP [157–160].

The use of natural and synthetic hormones for growth promoting purposes in animals is banned in the European Union. Boldenone and methylboldenone are anabolic steroids often illegally used to boost animal growth during the breeding of animals for human consumption, thereby causing potential health risks to consumers. Lu et al. [161] fabricated immunosensors by immobilizing boldenone–BSA conjugate on the surface of SPCEs, and followed by the competition between the free analyte and coating conjugate with corresponding antibodies. The use of anti-species IgG–HRP conjugate determined the degree of competition. The electrochemical technique chosen in this case was chronoamperometry. This technique was also employed for the determination of testosterone in bovine urine [162].

In recent years, feminization of male fish has been detected as a consequence of their exposure to female hormones and chemicals that mimic estrogens that are present in an aquatic environment. Vitellogenin (Vtg) is an egg yolk precursor protein that has been proposed as a biomarker for xenobiotics estrogen, causing endocrine disruption. A disposable amperometric immunosensor was studied for the rapid detection of carp (*Carassius auratus*) Vtg [163]. The sensor was fabricated based on SPC arrays containing eight-carbon working and an integrated carbon counter electrode. A conducting polymer (poly-terthiophene carboxylic acid) was electropolymerized on the surface of working electrodes. HRP and a monoclonal antibody (anti-Vtg) specific to carp Vtg were covalently attached. In order to detect the amount of Vtg, GOx-labelled Vtg bound to the sensor surface under competition with the Vtg analyte was quantified amperometrically using glucose as substrate.

5.1.2. Genetic testing

The detection of specific base sequences in human, viral and bacterial nucleic acids is becoming increasingly important in several areas, with applications ranging from the detection of disease-causing and food-contaminating organisms to the forensic and environmental research. Mutations responsible for numerous inherited human disorders are now known and pathogens responsible for disease states, bacteria and viruses, are also detectable via their unique nucleic acid sequence; accordingly, the interest in their detection continues to grow [164].

An electrochemical genosensor for the detection of specific sequences of DNA has been reported, using disposable screen-printed gold electrodes [164]. An enzyme-amplified detection scheme, based on the coupling of a streptavidin-ALP conjugate and biotinylated target sequences was applied. The enzyme catalyzed the hydrolysis of alpha-naphthyl phosphate to alpha-naphthol, which is electroactive and can be detected by means of DPV. The results showed that the genosensor enabled sensitive and specific detection of GMO-related sequences, thus providing a useful tool for the screening analysis of bioengineered food samples.

5.1.3. Clinical analysis

5.1.3.1. Infections. The diagnosis of infections in human beings or animals is based on the detection of either the infectious agent itself, i.e. the microorganism or virus, through classical microbiological methods, specific proteins, or DNA sequences, or the specific antibodies produced by the host's immune system [149]. In order to improve the diagnostic yield for patients, antigen detection assays have been developed.

The above-mentioned immunosensor described by Bagel et al. [156] was used for a DNA enzyme hybridization assay of an oligonucleotide sequence related to the human cytomegalovirus. Rapid, specific and sensitive determinations of infections are required because it is an important cause of morbidity and mortality in immunocompromized individuals, like transplant recipients, AIDS patients and newborns.

Immunosensors for pneumococcal pneumonia [165,166] and mycobacerium tuberculosis antigens [167] have been described. The enzyme ALP was used in combination with the substrate 3-indoxyl phosphate [168,169]. The single-use immunosensors were fabricated by deposition of biotinylated monoclonal antibodies onto SPCEs.

The detection of antibodies to Salmonella [170] in the serum of patients deserves special attention. An indirect enzyme-linked immunosorbant assay (ELISA) was used for detection of antibodies to *S. typhi*. These electrodes were tested for their ability to detect 1-naphthol, which is the product formed due to the hydrolysis of the substrate 1-naphthyl phosphate by the enzyme ALP. These electrodes were coated with recombinant flagellin fusion protein made by recombinant DNA technology and blocked with BSA. Further they were incubated with patient serum and goat anti-human ALP conjugate. The immunosensing was performed by using an amperometric method.

The analysis of theophylline, used to prevent and treat lung diseases, has also attracted attention [171]. The immunosensor, based on the principles of liposome signal amplification, is composed of two major parts including a SPCE and an immunochromatographic nitrocellulose membrane strip. On the membrane, anti-theophylline antibody is immobilized in an antibody competition zone and hexacyanoferrate(II)-loaded liposomes are immobilized in a signal generation zone. When a theophylline sample solution is applied to the immunosensor pre-loaded with theophylline-melittin conjugate in sample loading zone, the theophylline and theophylline-melittin conjugate migrate through the antitheophylline antibody zone, where competitive binding occurs. Unbound theophylline-melittin conjugate further migrates into the signal generation zone, where it disrupts the liposomes to release the electroactive hexacyanoferrate(II) which can be then detected amperometrically. The current produced is directly proportional to the concentration of hexacyanoferrate(II) which, in turn, can be related to the concentration of free analyte in the sample.

Granulocyte-macrophage colony-stimulating factor (GM-CSF) [172] is a cytokine which regulates the proliferation and differentiation of granulocytes, monocytemacrophages and certain related haematopoietic cells. Its medical applications include restoration of haematopoietic dysfunction by raising cell counts and augmentation of host defence against infection. Thus, it helps cancer patients to resist secondary infections. It is also administered to patients with suppressed bone marrow function or those undergoing bone marrow transplantation after intense chemotherapy. An amperometric immunosensor for GM-CSF has been reported [172]. It was based on a competitive assay, using SPCEs and ALP labelled GM-CSF, which converted *p*-aminophenyl phosphate to *p*-aminophenol.

Similar immunosensor was developed by Kreuzer et al. [173] for the determination of allergy antibody (IgE) in blood samples. IgE levels are often raised in allergic diseases and grossly elevated in parasitic infestations. Therefore, a raised level of IgE aids the diagnosis of allergic diseases, e.g. asthma, eczema and hay fever.

Food contaminated with the bacterium *Listeria monocytogenes* can cause serious infections. The manifestations of listeriosis include septicemia, meningitis (or meningoencephalitis), encephalitis and intrauterine or cervical infections in pregnant women, which may result in spontaneous abortion (2nd/3rd trimester) or stillbirth. The onset of the aforementioned disorders is usually preceded by influenza-like symptoms including persistent fever. It was reported that gastrointestinal symptoms such as nausea, vomiting and diarrhoea may precede more serious forms of listeriosis or may be the only symptoms expressed.

An immunosensor for the detection of this bacteria in milk has been described [174]. A direct sandwich assay was employed and the affinities of two polyclonal (goat and rabbit) and one monoclonal (mouse) anti-*L. monocytogenes* antibodies were compared. Owing to low sensitivity being obtained, biotin–avidin amplification was employed. SPCEs and amperometric method were used.

A disposable amperometric immunosensor has been described for the rapid detection of *Vibrio cholerae* (*V. cholerae*), the causative agent of cholera, employing an indirect sandwich ELISA principle [175]. SPCEs were employed for capturing

antibodies and antigen. Whole cell lysate (WCL) of *V. cholerae* was used to raise antibodies in rabbits and mice. The antibodies raised against WCL of *V. cholerae* were found to be specific, and no cross-reactivity was observed with other enteric bacteria. 1-Naphthyl phosphate was used as a substrate with the amperometric detection of its enzymatic hydrolysis product 1-naphthol. A comparison between the amperometric detection technique and the standard ELISA was made in terms of the total assay time, the amount of biological materials used and the sensitivity of detection.

The development of an amperometric immunosensor for the diagnosis of Chagas' disease using a specific glycoprotein of the trypomastigote surface, which belongs to the Tc85-11 protein family of *Trypanosoma cruzi* (*T. cruzi*), has been reported [176]. An atomically flat gold surface on a silicon substrate and gold SPEs were functionalized with cystamine and later activated with GA, which was used to form covalent bonds with the purified recombinant antigen (Tc85-11). The antigen reacts with the antibody from the serum, and the affinity reaction was monitored directly using atomic force microscopy or amperometry through a secondary antibody tagged to HRP. In the amperometric immunosensor, peroxidase catalyzes the L2 formation in the presence of hydrogen peroxide and potassium iodide, and the reduction current intensity was measured at a given potential with SPEs. The immunosensor was applied to sera of chagasic patients and patients having different systemic diseases.

5.1.3.2. Seafood toxins. A large variety of poisoning arises in seafood as with terrestrial based foods, after ingestion of certain low molecular weight marine toxins [177]. Examples of such poisoning include diarrheic shellfish poisoning (DSP) resulting from okadaic acid ingestion [177,178], brevetoxin produced neurotoxic shellfish poisoning (NSP) [177], amnesic shellfish poisoning (ASP) due to domoic acid [177,179] and pufferfish poisoning (tetrodotoxin) which is of bacterial origin. Kreuzer et al. [177] have attempted to develop a generic immunosensor, which can rapidly assess, with high accuracy, trace levels of these marine toxins. A disposable SPCE coupled with amperometric detection of *p*-aminophenol produced by the label, ALP, was used for signal measurement. In the case of domoic acid [179], the construction of an electrochemical immunosensor coupled to DPV involves the use of SPCEs, based on a 'competitive indirect test'. Domoic acid conjugated to BSA (BSA-DA) was coated onto the working electrode of the SPCE, followed by incubation with sample (or standard toxin) and anti-DA antibody. An anti-goat IgG-alkaline hosphatase (AP) conjugate was used for signal generation.

5.1.3.3. Carcinogens: mycotoxins. The presence of mycotoxins, which are produced by fungi in a high amount of food, in levels higher than the accepted ones represent a threat for the food harmlessness, as well as an important risk in alimentary health.

Milk is usually contaminated with small amounts of aflatoxin M1 (AFM1) as a consequence of the metabolism by the cow of aflatoxin B1 (AFB1), a mycotoxin that is commonly produced by the fungal strains *Aspergillus flavus* and *Aspergillus parasiticus* and found in certain animal foodstuff. Toxicological concern about AFM1 arises principally from its close structural similarity to AFB1, the latter having been shown to be one of the most potent known carcinogens. European Community limits the concentration of AFB1 in foodstuffs for dairy cows. This limit was chosen taking into account the quantities of feed consumed and the fact that 1–4% of the ingested AFB1 appears as AFM1 in the milk.

Micheli et al. [180] describe electrochemical immunosensors based on the direct immobilization of antibodies on the surface of SPCEs, where the competition between free AFMI and that conjugated with HRP is allowed to occur.

It has also been shown the development of a disposable electrochemical immunosensor based on the indirect competitive ELISA, for simple and fast measurement of AFB1 in barley using DPV and SPCEs [181,182]. The detection of the selected analyte is carried out through competition between BSA–AFB1 immobilized on the support and free antigen (standard or sample) for the binding sites of the antibody. After the competition step, the amount of antibody that reacted with the immobilized BSA–AFB1, was evaluated using a secondary antibody labelled with ALP.

SPCEs bearing a surface-adsorbed antibody against AFB1 were also used in a competitive immunoassay, based on competition of free analyte with a biotinayleted AFB1 conjugate [183]. Subsequent adition of streptavidin-ALP conjugate, followed by a 1-naphtyl phosphate substrate resulted in the production of the electrochemically active product, 1-naphtol; this was oxidized using linear sweep voltammetry (LSV) and constituted the measurement step. These immunosensors were fabricated in an array configuration, which represent the initial studies towards the development of an automated instrument for multi-analyte determinations.

Alarcon et al. [184,185] describe a direct, competitive ELISA for the quantitative determination of another mycotoxin, ochratoxin A (OTA), using polyclonal antibodies and SPCEs. The immunosensor appears to be suitable for OTA contamination screening in food samples.

5.1.3.4. Tumor markers. The determination of serum tumor markers plays an important role in clinical diagnoses for the patients with certain tumor-associated disease. Thus, many small, semi-automated and portable immunosensors have been developed [186]. Yu et al. [187] developed a SPCE system as the basis of an immunosensor for fast clinical diagnosis of α-1-fetoprotein (AFP). The serum AFP concentration rises greatly in patients with liver cancer. Thus, it is necessary to measure AFP for the clinical diagnosis and even early detection of original liver carcinoma. The immunosensor was prepared by entrapping a HRP-labeled AFP antibody in chitosan membrane. The active site of the enzyme labelled to the antibody was shielded and the access of substrate molecules to the enzyme was either partially or completely blocked after the immobilized HRP-AFP antibody reacted with AFP to form immunocomplex during the incubation. The decreased percentage of peak current of the product from the enzymatic reaction was proportional to AFP concentration. In the same way, Guan et al. [188] a rapid method

to measure AFP in human serum by use of one-step sandwich ELISA-based immunobiosensor with disposable SPCE technology. PB was deposited using cyclic voltammetry (CV) on the surface of electrode to catalyze H_2O_2 from the reaction of GOx.

A simple IA method for carcinoembryonic antigen (CEA) detection using a disposable immunosensor coupled with a flow injection system was developed as well [189]. The immunosensor was prepared by coating CEA/colloid Au/chitosan membrane at a SPCE. Using a competitive IA format, the immunosensor inserted in the flow system with an injection of sample and HRP-labelled CEA antibody was used to trap the labelled antibody at room temperature for 35 min. The current response obtained from the labelled HRP to thionine–H_2O_2 system decreased proportionally to the CEA concentration. The immunoassay system could automatically control the incubation, washing and current measurement steps with good stability and acceptable accuracy.

5.1.3.5. Myocardial biomarkers. Clinical diagnoses, especially that of heart infarction, require and reliable test systems. Amperometric immunosensors for the rapid estimation of the heart-type fatty acid-binding protein (FABP) in human plasma samples, which can serve as marker for the early diagnosis of heart injury in man, have been reported [190,191]. The electrochemical immunosensors was based on anti-FABP antibodies covalently immobilized on preactivated nylon membranes mounted onto a modified Clark-type SPCE [190]. Upon formation of the sandwich with analyte FABP and second antibodies labelled with GOx the signal was generated after addition of glucose. The resulting oxygen consumption allows the estimation of analyte concentrations of clinical relevance without dilution of the sample. O'Regan et al. [191] developed a one-step direct sandwich assay in which analyte and ALP labelled antibody were simultaneously added to the immobilized primary antibody, using two distinct monoclonal mouse anti-human H-FABP antibodies. *p*-Aminophenyl phosphate was converted to *p*-aminophenol by ALP and the current generated by its subsequent oxidation was measured.

Another myocardial biomarker studied by O'Reagan et al. [192] was myoglobin. A one-step indirect sandwich assay was employed using a polyclonal goat anti-human cardiac myoglobin antibody with monoclonal mouse anti-myoglobin and goat anti-mouse IgG conjugated to ALP, as the detecting antibodies.

5.1.4. Drug testing

Amphetamine and its analogues are popular recreational drugs of abuse due to the fact that they are potent stimulants of the central nervous system. Butler et al. [193] and Luangaram et al. [194] describe amperometric immunosensors for their determination in urine and saliva, based on SPCEs and amperometic techniques. The first one includes a competitive assay in which free analyte and HRP labelled species were simultaneously added to an immobilized polyclonal antibody. The second one is characterized by the use of a monoclonal anti-methamphetamine antibody as the biorecognition element, as well as ALP as enzyme label.

5.1.5. Environmental pollutants

The increasing use of pesticides, mineral fertilizers, pharmaceuticals, surfactants, and many other biologically active substances results in serious environmental problems. Immunochemical methods of analysis, which are based on the binding of an antigen (pesticide) molecule to specific antibodies, are finding increasing use for determining pesticides in various samples, such as water, soil, food products and biological fluids [195].

Therefore, several immunosensors have been reported for the detection of the herbicide chlorsulphuron [196], polychlorinated biphenyls (PCB) in soil samples [197–199] and food samples [200], polycyclic aromatic hydrocarbons (PAHs) [201], 2,4,6-trichloroanisole (TCA) [202] and acetochlor [203].

Moreover, a dipstick-type electrochemical immunosensor for the detection of the organophosphorus insecticide fenthion [204] has been described. The assay of the biosensor involved competition between the pesticide in the sample and pesticide–GOx conjugate for binding to the antibody immobilized on the membrane. This was followed by measurement of the activity of the bound enzyme, which was inversely proportional to the concentration of pesticide.

Atrazine is detected following the method developed by Keay and McNeil [205] and Grennan et al. [206]. The first one involves a competitive ELISA incorporating disposable screen-printed HRP-modified electrodes as the detector element in conjunction with single-use atrazine immune-membranes. Grennan uses recombinant single-chain antibody fragments and a conductive polymer, which enables direct mediatorless coupling to take place between the redox centres of antigen-labelled HRP and the electrode surface.

An electrochemical immunosensor combining three monoclonal antibodies on the same measuring element produced by screen-printing was constructed for the semiquantitative group-specific detection of herbicides belonging to phenoxyalkanoic acids [207]. The combination of different monoclonal antibodies covalently immobilized on three working electrodes and one additional electrode containing immobilized albumin provided a more reliable detection of phenoxyalkanoic acids. Peroxidase-2,4-dichlorophenoxyacetic acid conjugate was used as a tracer suitable for all the antibodies employed in a competitive immunoassay. Several herbicides were used to characterize this immunosensor, which was tested on samples of surface water spiked with different herbicides and binary mixtures of herbicides.

The herbicide 2,4-dichlorophenoxyacetic acid (2,4-D) has been widely analyzed in different samples by amperometry [208–212] and electrochemical impedance spectroscopy (EIS) [213]. Specific antibody against 2,4-D has been immobilized onto different gold and graphite electrodes by means of several methods of antibody immobilization.

Alkylphenol ethoxylates and essentially nonylphenol (NP) derivatives are widely used as non-ionic surfactants in the formulations of detergents, textiles, paints, petroleum additives, etc. They are present as plasticizers in polycarbonate and epoxy resins, PVC and can contaminate food when released from packaging. In the environment, ethoxylated NP isomers biodegrade via shortening the oxyethylene chain and form more lipophilic

and hence more toxic compounds. The final product of degradation, i.e. NP, is considered as most dangerous because of its enhanced resistance in the environment and its toxicity. The NP used in industry contains about 90% of the 4-NP and other isomers with straight and branched side chain. Symptoms of the NP exposure include eye and skin irritation, headaches, nausea and vomiting. Besides, the estrogen disruption effect of the NP has been highlighted in the past decade. It mimics natural estrogens and causes reproductive abnormalities in natural populations. Although NP undergoes microbial and enzymatic degradation, the efficiency of these processes in conventional water treatment is insufficient. As a result, the NP residues were found in the sediments formed in water. For these reasons, it is necessary to develop fast and cost-effective methods for NP monitoring. A novel immunosensor for NP determination has been developed by immobilization of specific antibodies together with HRP on the surface of SPCEs [214]. The signal of the immunosensor is generated by the involvement of NP accumulated in the peroxidase oxidation of mediator (Methylene Blue, hydroquinone or iodide). This results in the increase of the signal recorded by LSV.

5.2. Direct electrochemical immunoassays

As it can be seen above, the bulk of literature detailing electrochemical immunosensor development reports systems based on the use of enzyme labels, requiring modification of antigen/antibody activity. Reports regarding labeless detection have started to be published as well.

In the case of food pathogens, due to their large size, the use of labels can be eliminated [215]. This immunosensor is based on the measurement of the diffusion of a redox probe. Thus, following antibody immobilization, diffusion of a potassium hexacyanoferrate redox probe was measured and the diffusion co-efficient (D) calculated, pre- and post-addition of analyte. The formation of the bacteria-antibody immunocomplex introduces a barrier for interfacial electron transfer and the change in diffusion co-efficient of the redox probe was measured using chronocoulometry. A linear relationship between D and the concentration of analyte introduced was observed.

The fabrication of another label-free and reagentless immunosensor has also been reported [216]. It is based on the direct incorporation of antibodies into conducting polymer films along with a subsequent ac impedimetric electrochemical interrogation. Model sensors of this type have been prepared by electrochemically polymerizing conducting polypyrrole films containing anti-BSA at the surface of SPCEs. Films containing chloride or anti-human IgG as counter-ions have been used as controls. An ac measurement protocol has been used to determine the impedance of the electrodes when immersed in water or analyte solutions. A selective and reversible binding of analyte to the electrode could be monitored electrochemically and studies were reported in detail relating analyte concentrations to bulk impedimetric measurements, the real component, the imaginary component and the phase angle of the responses. The results of this study have showed detectable and reversible antibody–antigen interactions could be measured and mainly affected the Faradaic behaviour of the electrode. BSA could be detected with a linear response from 0 to 75 ppm.

6. Conclusions and future trends

In the recent years, a great development in screen-printed sensors for several analytical applications has been observed, taking into account the huge amount of references reported. This kind of sensors fits for the growing need to perform rapid and accurate ‘in situ’ analyses as well as in the development of compact and portable devices.

This review provides information about the application of screen-printed technology in fields of especial interest such as

Table 1
Most important applications of SPEs

Analyte	Working SPE	References
Metals	SPCE	[4,13–15]
	Metal-based SPEs	[16,18]
	Hg-film-modified SPCE	[2,19-26,28,29,217]
	Bi-coated SPCE	[33–37]
	Au-coated SPCE	[38–40]
	Ni-coated SPCE	[41]
	Metallic nanoparticle-modified SPE	[51,52]
	Enzyme-modified SPE	[75–79]
H_2O_2	SPCE	[5,56,57]
	Metallic nanoparticle-modified SPE	[50]
	Enzyme-modified SPE	[123–126]
Procaine	SPCE	[6]
Aurothiomalate	SPCE	[7]
Creatinine	SPCE	[8]
Cysteine and tyrosine	SPCE	[9]
Vitamin B2	SPCE	[10]
Phloroglucinol derivatives	SPCE	[11]
Chlorophyll	SPCE	[12]
Dopamine and uric acid	SPCE	[218]
Pesticides and herbicides	Enzyme-modified SPE	[61–74]
	SPE immunosensor	[195–214]
Cholesterol	Enzyme-modified SPE	[80–84]
Glucose	Enzyme-modified SPE	[87–115,117–122]
Ethanol	Enzyme-modified SPE	[104,118,120,127–131]
Phenolic compounds	Enzyme-modified SPE	[132–137,139–142]
Hormones	SPE immunosensor	[153–163]
DNA	SPE immunosensor	[164]
Human cytomegalovirus	SPE immunosensor	[156]
Pneumococcal pneumonia	SPE immunosensor	[165,166]
Mycobacerium tuberculosis	SPE immunosensor	[167]
Salmonella	SPE immunosensor	[170]
Allergy antibody (IgE)	SPE immunosensor	[173]
Listeria monocytogenes	SPE immunosensor	[174]
Vibrio cholerae	SPE immunosensor	[175]
Seefood toxins	SPE immunosensor	[177–179]
Mycotoxins	SPE immunosensor	[180–185]
Tumor markers	SPE immunosensor	[187–189]
Myocardial biomarkers	SPE immunosensor	[190–192]
Amphetamine	SPE immunosensor	[193,194]
Food pathogens	SPE immunosensor	[215,216]

environmental science, food industry, pharmaceutical and clinical assays. Table 1 summarizes the great scope applications reported in this work.

The versatility and low-cost of this technology is responsible for its continuous development. Their significative improvements are mainly expected from two different ways. First, the incorporation of new printed materials, as well as new support surfaces, will lead to enhance the reproducibility and sensitivity of the screen-printed based sensors. With this aim, new attempts for the modification of the working electrode are also in continuous growth, focusing on new ligands, polymers and nanostructure materials.

Acknowledgements

The authors would like to acknowledge funding via the Junta de Castilla y León (Burgos, 08/04) and the Spanish Ministry of Education and Science (MAT2005-01767). M. Asunción Alonso-Lomillo is funded by a Ramón y Cajal fellowship from the Spanish Ministry of Education and Science.

References

[1] J.P. Hart, A. Crew, E. Crouch, K.C. Honeychurch, R.M. Pemberton, Anal. Lett. 37 (2004) 789.
[2] J. Wang, Analyst 119 (1994) 763.
[3] B.R. Eggings, Chemical Sensors and Biosensors, John Wiley and Sons, Chichester, 2002.
[4] K.C. Honeychurch, J.P. Hart, Trac-Trends Anal. Chem. 22 (2003) 456.
[5] J. Krejci, J. Prasek, L. Fujcik, S. Khatib, E. Hejatkova, L. Jakubka, L. Giannoudi, Microelectron. Int. 21 (2004) 20.
[6] M.F. Bergamini, A.L. Santos, N.R. Stradiotto, M.V.B. Zanoni, J. Pharm. Biomed. Anal. 43 (2007) 315.
[7] M.F. Bergamini, M.V. Boldrin Zanoni, Electroanalysis 18 (2006) 1457.
[8] J.C. Chen, A.S. Kumar, H.H. Chung, S.H. Chien, M.C. Kuo, J.M. Zen, Sens. Actuators, B 115 (2006) 473.
[9] M. Vasjari, A. Merkoci, J.P. Hart, S. Alegret, Microchim. Acta 150 (2005) 233.
[10] R.O. Kadara, B.G.D. Haggett, B.J. Birch, J. Agric. Food Chem. 54 (2006) 4921.
[11] N. Karousos, L.C. Chong, C. Ewen, C. Livingstone, J. Davis, Electrochim. Acta 50 (2005) 1879.
[12] R.M. Pemberton, A. Amine, J.P. Hart, Anal. Lett. 37 (2004) 1625.
[13] K.C. Honeychurch, J.P. Hart, D.C. Cowell, Electroanalysis 12 (2000) 171.
[14] K.C. Honeychurch, D.M. Hawkins, J.P. Hart, D.C. Cowell, Talanta 57 (2002) 565.
[15] J.W. Dilleen, S.D. Sprules, B.J. Birch, B.G.D. Haggett, Analyst 123 (1998) 2905.
[16] S. Laschi, I. Palchetti, M. Mascini, Sens. Actuators, B 114 (2006) 460.
[17] M.F.M. Noh, I.E. Tothill, Anal. Bioanal. Chem. 386 (2006) 2095.
[18] J.M. Zen, C.C. Yang, A.S. Kumar, Anal. Chim. Acta 464 (2002) 229.
[19] J. Wang, B.M. Tian, Anal. Chem. 64 (1992) 1706.
[20] K. Ashley, Electroanalysis 6 (1994) 805.
[21] K. Ashley, Electroanalysis 7 (1995) 1189.
[22] K. Ashley, T.J. Wise, W. Mercado, D.B. Parry, J. Hazard. Mater. 83 (2001) 41.
[23] D. Desmond, B. Lane, J. Alderman, G. Hall, M. AlvarezIcaza, A. Garde, J. Ryan, L. Barry, G. Svehla, D.W.M. Arrigan, L. Schniffner, Sens. Actuators, B 34 (1996) 466.
[24] D. Desmond, B. Lane, J. Alderman, M. Hill, D.W.M. Arrigan, J.D. Glennon, Sens. Actuators, B 48 (1998) 409.
[25] I. Palchetti, A. Cagnini, M. Mascini, A.P.F. Turner, Mikrochim. Acta 131 (1999) 65.
[26] I. Palchetti, S. Laschi, M. Mascini, Anal. Chim. Acta 530 (2005) 61.
[27] C. Macca, L. Solda, R. Voltan, I. Calliari, Electroanalysis 16 (2004) 1311.
[28] C. Parat, S. Betelu, L. Authier, M. Potin-Gautier, Anal. Chim. Acta 573–574 (2006) 14.
[29] J.-Y. Choi, K. Seo, S.-R. Cho, J.-R. Oh, S.-H. Kahng, J. Park, Anal. Chim. Acta 443 (2001) 241.
[30] J. Wang, J.M. Lu, C. Yarnitzky, Anal. Chim. Acta 280 (1993) 61.
[31] B.J. Feldman, J.D. Osterloh, B.H. Hata, A. Dalessandro, Anal. Chem. 66 (1994) 1983.
[32] T.Z. Liu, D. Lai, J.D. Osterloh, Anal. Chem. 69 (1997) 3539.
[33] J. Wang, Electroanalysis 17 (2005) 1133.
[34] J. Wang, U.A. Kirgoz, J.M. Lu, Electrochem. Commun. 3 (2001) 703.
[35] J. Wang, J.M. Lu, S.B. Hocevar, B. Ogorevc, Electroanalysis 13 (2001) 13.
[36] R.O. Kadara, L.E. Tothill, Talanta 66 (2005) 1089.
[37] R.O. Kadara, I.E. Tothill, Anal. Bioanal. Chem. 378 (2004) 770.
[38] J. Wang, B. Tian, Anal. Chem. 65 (1993) 1529.
[39] J. Wang, B. Tian, Anal. Chim. Acta 274 (1993) 1.
[40] P. Masawat, S. Liawruangrath, J.M. Slater, Sens. Actuators, B 91 (2003) 52.
[41] J.M. Slater, J.W. Dilleen, Electroanalysis 9 (1997) 1353.
[42] L. Sun, Z.J. Zhang, H.X. Dang, Mater. Lett. 57 (2003) 3874.
[43] M. Fukushima, H. Yanagi, S. Hayashi, N. Suganuma, Y. Taniguchi, Thin Solid Films 438 (2003) 39.
[44] E. Majid, S. Hrapovic, Y.L. Liu, K.B. Male, J.H.T. Luong, Anal. Chem. 78 (2006) 762.
[45] X. Dai, O. Nekrassova, M.E. Hyde, R.G. Compton, Anal. Chem. 76 (2004) 5924.
[46] M.S. El-Deab, T. Okajima, T. Ohsaka, J. Electrochem. Soc. 150 (2003) A851.
[47] C.M. Welch, C.E. Banks, A.O. Simm, R.G. Compton, Anal. Bioanal. Chem. 382 (2005) 12.
[48] B.S. Yin, H.Y. Ma, S.Y. Wang, S.H. Chen, J. Phys. Chem. 107 (2003) 8898.
[49] Z.Y. Tang, S.Q. Liu, S.J. Dong, E.K. Wang, J. Electronanal. Chem. 502 (2001) 146.
[50] M. Chikae, K. Idegami, K. Kerman, N. Nagatani, M. Ishikawa, Y. Takamura, E. Tamiya, Electrochem. Commun. 8 (2006) 1375.
[51] Y.S. Song, G. Muthuraman, Y.Z. Chen, C.C. Lin, J.M. Zen, Electroanalysis 18 (2006) 1763.
[52] O. Dominguez, J. Arcos, Electrochem. Comm. 9 (2007) 820.
[53] J. Wang, T. Baomin, R. Setiadji, Electroanalysis 6 (1994) 317.
[54] C.G. Neuhold, J. Wang, V.B. doNascimento, K. Kalcher, Talanta 42 (1995) 1791.
[55] J. Wang, P.V.A. Pamidi, Talanta 42 (1995) 463.
[56] J. Lin, D.M. Zhou, S.B. Hocevar, E.T. McAdams, B. Ogorevc, X.J. Zhang, Front Biosci. 10 (2005) 483.
[57] K. Schachl, H. Alemu, K. Kalcher, H. Moderegger, I. Svancara, K. Vytras, Fresenius J. Anal. Chem. 362 (1998) 194.
[58] J.M. Zen, J.L. Chang, P.Y. Chen, R. Ohara, K.C. Pan, Electroanalysis 17 (2005) 739.
[59] L.C. Clark, C. Lyons, Ann. N.Y. Acad. Sci. 102 (1962) 29.
[60] J.M. Kauffmann, G.G. Guilbault, Methods Biochem. Anal. 36 (1992) 63.
[61] G.S. Nunes, G. Jeanty, J.L. Marty, Anal. Chim. Acta 523 (2004) 107.
[62] M.H. Shi, J.J. Xu, S. Zhang, B.H. Liu, J.L. Kong, Talanta 68 (2006) 1089.
[63] E. Suprun, G. Evtugyn, H. Budnikov, F. Ricci, D. Moscone, G. Palleschi, Anal. Bioanal. Chem. 383 (2005) 597.
[64] C. Bonnet, S. Andreescu, J.L. Marty, Anal. Chim. Acta 481 (2003) 209–211.
[65] A. Vakurov, C.E. Simpson, C.L. Daly, T.D. Gibson, P.A. Millner, Biosens. Bioelectron. 20 (2005) 2324.
[66] A. Vakurov, C.E. Simpson, C.L. Daly, T.D. Gibson, P.A. Millner, Biosens. Bioelectron. 20 (2004) 1118.
[67] R. Solna, S. Sapelnikova, P. Skladal, M. Winther-Nielsen, C. Carlsson, J. Emneus, T. Ruzgas, Talanta 65 (2005) 349.
[68] Y.D. Zhang, S.B. Muench, H. Schulze, R. Perz, B.L. Yang, R.D. Schmid, T.T. Bachmann, J. Agric. Food Chem. 53 (2005) 5110.

[69] P.R.B. de Oliveira Marques, G.S. Nunes, T.C.R. dos Santos, S. Andreescu, J.-L. Marty, Biosens. Bioelectron. 20 (2004) 825.
[70] S. Sotiropoulou, N.A. Chaniotakis, Biomaterials 26 (2005) 6771.
[71] M. Waibel, H. Schulze, N. Huber, T.T. Bachmann, Biosens. Bioelectron. 21 (2006) 1132.
[72] B. Bucur, A.F. Danet, J.L. Marty, Biosens. Bioelectron. 20 (2004) 217.
[73] M.P. Dondoi, B. Bucur, A.F. Danet, C.N. Toader, L. Barthelmebs, J.L. Marty, Anal. Chim. Acta 578 (2006) 162.
[74] B. Bucur, D. Fournier, A. Danet, J.L. Marty, Anal. Chim. Acta 562 (2006) 115.
[75] B.B. Rodriguez, J.A. Bolbot, I.E. Tothill, Anal. Bioanal. Chem. 380 (2004) 284.
[76] A. Amine, H. Mohammadi, I. Bourais, G. Palleschi, Biosens. Bioelectron. 21 (2006) 1405.
[77] D. Ogonczyk, L. Tymecki, I. Wyzkiewicz, R. Koncki, S. Glab, Sens. Actuators, B 106 (2005) 450.
[78] B.B. Rodriguez, J.A. Bolbot, I.E. Tothill, Biosens. Bioelectron. 19 (2004) 1157.
[79] L. Tymecki, E. Zwierkowska, R. Koncki, Anal. Chim. Acta 538 (2005) 251.
[80] M.A.T. Gilmartin, J.P. Hart, Analyst 119 (1994) 2331.
[81] R. Foster, J. Cassidy, E. O'Donoghue, Electroanalysis 12 (2000) 716.
[82] G. Li, J.M. Liao, G.Q. Hu, N.Z. Ma, P.J. Wu, Biosens. Bioelectron. 20 (2005) 2140.
[83] V. Shumyantseva, G. Deluca, T. Bulko, S. Carrara, C. Nicolini, S.A. Usanov, A. Archakov, Biosens. Bioelectron. 19 (2004) 971.
[84] V.V. Shumyantseva, S. Carrara, V. Bavastrello, D.J. Riley, T.V. Bulko, K.G. Skryabin, A.I. Archakov, C. Nicolini, Biosens. Bioelectron. 21 (2005) 217.
[85] J.D. Newman, S.J. Setford, Mol. Biotechnol. 32 (2006) 249.
[86] G. Cui, J.H. Yoo, B.W. Woo, S.S. Kim, G.S. Cha, H. Nam, Talanta 54 (2001) 1105.
[87] J.D. Newman, A.P.F. Turner, G. Marrazza, Anal. Chim. Acta 262 (1992) 13.
[88] G. Cui, S.J. Kim, S.H. Choi, H. Nam, G.S. Cha, K.J. Paeng, Anal. Chem. 72 (2000) 1925.
[89] K. Ohfuji, N. Sato, N. Hamada-Sato, T. Kobayashi, C. Imada, H. Okuma, E. Watanabe, Biosens. Bioelectron. 19 (2004) 1237.
[90] G.A.M. Mersal, M. Khodari, U. Bilitewski, Biosens. Bioelectron. 20 (2004) 305.
[91] F. Ricci, D. Moscone, C.S. Tuta, G. Palleschi, A. Amine, A. Poscia, F. Valgimigli, D. Messeri, Biosens. Bioelectron. 20 (2005) 1993.
[92] A. Lupu, D. Compagnone, G. Palleschi, Anal. Chim. Acta 513 (2004) 67.
[93] I.L. de Mattos, L. Gorton, T. Ruzgas, Biosens. Bioelectron. 18 (2003) 193.
[94] M. Pravda, M.P. O'Halloran, M.P. Kreuzer, G.G. Guilbault, Anal. Lett. 35 (2002) 959.
[95] R. Nagata, K. Yokoyama, H. Durliat, M. Comtat, S.A. Clark, I. Karube, Electroanalysis 7 (1995) 1027.
[96] F. Ge, X.-E. Zhang, Z.-P. Zhang, Z. Xiao-Mei, Biosens. Bioelectron. 13 (1998) 333.
[97] T. Hu, X.E. Zhang, Z.P. Zhang, L.Q. Chen, Electroanalysis 12 (2000) 868.
[98] N.J. Forrow, S.J. Walters, Biosens. Bioelectron. 19 (2004) 763.
[99] A.S. Kumar, J.M. Zen, Electroanalysis 14 (2002) 671.
[100] G.L. Luque, M.C. Rodriguez, G.A. Rivas, Talanta 66 (2005) 467.
[101] E. Turkusic, J. Kalcher, E. Kahrovic, N.W. Beyene, H. Moderegger, E. Sofic, S. Begic, K. Kalcher, Talanta 65 (2005) 559.
[102] P. Kotzian, P. Brazdilova, K. Kalcher, K. Vytras, Anal. Lett. 38 (2005) 1099.
[103] P. Kotzian, P. Brazdilova, S. Rezkova, K. Kalcher, K. Vytras, Electroanalysis 18 (2006) 1499.
[104] J. Wang, Q.A. Chen, M. Pedrero, J.M. Pingarron, Anal. Chim. Acta 300 (1995) 111.
[105] S.A. Miscoria, G.D. Barrera, G.A. Rivas, Sens. Actuators, B 115 (2006) 205.
[106] C.X. Zhang, T. Haruyama, E. Kobatake, M. Aizawa, Anal. Chim. Acta 442 (2001) 257.
[107] C.X. Zhang, Q. Gao, M. Aizawa, Anal. Chim. Acta 426 (2001) 33.
[108] Q. Gao, M.R. Yang, Chem. Commun. (2004) 30.
[109] N. Sato, H. Okuma, Anal. Chim. Acta 565 (2006) 250.
[110] S.-H. Lee, H.-Y. Fang, W.-C. Chen, Sens. Actuators, B 117 (2006) 236.
[111] J. Gonzalo-Ruiz, M. Asuncion Alonso-Lomillo, F. Javier Munoz, Biosens. Bioelectron. 22 (2007) 1517.
[112] E. Crouch, D.C. Cowell, S. Hoskins, R.W. Pittson, J.P. Hart, Biosens. Bioelectron. 21 (2005) 712.
[113] E. Crouch, D.C. Cowell, S. Hoskins, R.W. Pittson, J.P. Hart, Anal. Biochem. 347 (2005) 17.
[114] Z.Q. Gao, F. Xie, M. Shariff, M. Arshad, J.Y. Ying, Sens. Actuators, B 111 (2005) 339.
[115] W.-J. Guan, Y. Li, Y.-Q. Chen, X.-B. Zhang, G.-Q. Hu, Biosens. Bioelectron. 21 (2005) 508.
[116] B.-W. Lu, W.-C. Chen, J. Magn. Magn. Mater. 304 (2006) e400.
[117] L.-Q. Chen, X.-E. Zhang, W.-H. Xie, Y.-F. Zhou, Z.-P. Zhang, A.E.G. Cass, Biosens. Bioelectron. 17 (2002) 851.
[118] J. Razumiene, V. Gureviciene, A. Vilkanauskyte, L. Marcinkeviciene, I. Bachmatova, R. Meskys, V. Laurinavicius, Sens. Actuators, B 95 (2003) 378.
[119] J. Razumiene, A. Vilkanauskyte, V. Gureviciene, V. Laurinavicius, N.V. Roznyatovskaya, Y.V. Ageeva, M.D. Reshetova, A.D. Ryabov, J. Organomet. Chem. 668 (2003) 83.
[120] J. Razumiene, V. Gureviciene, V. Laurinavicius, J.V. Grazulevicius, Sens. Actuators, B 78 (2001) 243.
[121] A. Silber, N. Hampp, W. Schuhmann, Biosens. Bioelectron. 11 (1996) 215.
[122] J. Razumiene, A. Vilkanauskyte, V. Gureviciene, J. Barkauskas, R. Meskys, V. Laurinavicius, Electrochim. Acta 51 (2006) 5150.
[123] Q.A. Gao, F. Yang, Y. Ma, X.R. Yang, Electroanalysis 16 (2004) 730.
[124] S. Ledru, N. Ruille, M. Boujtita, Biosens. Bioelectron. 21 (2006) 1591.
[125] A. Morrin, F. Wilbeer, O. Ngamna, S.E. Moulton, A.J. Killard, G.G. Wallace, M.R. Smyth, Electrochem. Commun. 7 (2005) 317.
[126] A.V. Krylov, M. Beissenhirtz, H. Adamzig, F.W. Scheller, F. Lisdat, Anal. Bioanal. Chem. 378 (2004) 1327.
[127] A.M. Azevedo, D.M.F. Prazeres, J.M.S. Cabral, L.P. Fonseca, Biosens. Bioelectron. 21 (2005) 235.
[128] M. Boujtita, J.P. Hart, R. Pittson, Biosens. Bioelectron. 15 (2000) 257.
[129] N.G. Patel, S. Meier, K. Cammann, G.C. Chemnitius, Sens. Actuators, B 75 (2001) 101.
[130] S.D. Sprules, I.C. Hartley, R. Wedge, J.P. Hart, R. Pittson, Anal. Chim. Acta 329 (1996) 215.
[131] M. Niculescu, T. Erichsen, V. Sukharev, Z. Kerenyi, E. Csoregi, W. Schuhmann, Anal. Chim. Acta 463 (2002) 39.
[132] R. Solna, P. Skladal, Electroanalysis 17 (2005) 2137.
[133] A. Avramescu, S. Andreescu, T. Noguer, C. Bala, D. Andreescu, J.L. Marty, Anal. Bioanal. Chem. 374 (2002) 25.
[134] H. Kotte, B. Grundig, K.D. Vorlop, B. Strehlitz, U. Stottmeister, Anal. Chem. 67 (1995) 65.
[135] S. Sapelnikova, E. Dock, T. Ruzgas, J. Emneus, Talanta 61 (2003) 473.
[136] J.C. Schmidt, Field Anal. Chem. Technol. 2 (1998) 351.
[137] E.A. Cummings, S. Linquette-Mailley, P. Mailley, S. Cosnier, B.R. Eggins, E.T. McAdams, Talanta 55 (2001) 1015.
[138] J.L.H.C. Busch, K. Hrncirik, E. Bulukin, C. Boucon, M. Mascini, J. Agric. Food Chem. 54 (2006) 4371.
[139] E. Dock, T. Ruzgas, Electroanalysis 15 (2003) 492.
[140] R. Solna, E. Dock, A. Christenson, M. Winther-Nielsen, C. Carlsson, J. Emneus, T. Ruzgas, P. Skladal, Anal. Chim. Acta 528 (2005) 9.
[141] S.C. Chang, K. Rawson, C.J. McNeil, Biosens. Bioelectron. 17 (2002) 1015.
[142] S. Sapelnikova, E. Dock, R. Solna, P. Skladal, T. Ruzgas, J. Emneus, Anal. Bioanal. Chem. 376 (2003) 1098.
[143] P. Skladal, Electroanalysis 9 (1997) 737.
[144] A. Warsinke, A. Benkert, F.W. Scheller, Fresenius J. Anal. Chem. 366 (2000) 622.
[145] M. Diaz-Gonzalez, M.B. Gonzalez-Garcia, A. Costa-Garcia, Electroanalysis 17 (2005) 1901.

[146] J.M.F. Romero, M. Stiene, R. Kast, M.D.L. de Castro, U. Bilitewski, Biosens. Bioelectron. 13 (1998) 1107.
[147] A.J. Killard, S.Q. Zhang, H.J. Zhao, R. John, E.I. Iwuoha, M.R. Smyth, Anal. Chim. Acta 400 (1999) 109.
[148] K. Grennan, A.J. Killard, M.R. Smyth, Electroanalysis 13 (2001) 745.
[149] M. Stiene, U. Bilitewski, Anal. Bioanal. Chem. 372 (2002) 240.
[150] F. Darain, S.U. Park, Y.B. Shim, Biosens. Bioelectron. 18 (2003) 773.
[151] R.S. Yalow, S.A. Berson, Nature 184 (1959) 1648.
[152] E.J. Moore, M. Pravda, M.P. Kreuzer, G.G. Guilbault, Anal. Lett. 36 (2003) 303.
[153] R.M. Pemberton, T.T. Mottram, J.P. Hart, J. Biochem. Biophys. Methods 63 (2005) 201.
[154] G. Volpe, G. Fares, F.D. Quadri, R. Draisci, G. Ferretti, C. Marchiafava, D. Moscone, G. Palleschi, Anal. Chim. Acta 572 (2006) 11.
[155] D. Butler, G.G. Guilbault, Actuators Sens. B 113 (2006) 692.
[156] O. Bagel, C. Degrand, B. Limoges, M. Joannes, F. Azek, P. Brossier, Electroanalysis 12 (2000) 1447.
[157] R.M. Pemberton, J.P. Hart, J.A. Foulkes, Electrochim. Acta 43 (1998) 3567.
[158] M.P. Kreuzer, R. McCarthy, M. Pravda, G.G. Guilbault, Anal. Lett. 37 (2004) 943.
[159] R.M. Pemberton, J.P. Hart, P. Stoddard, J.A. Foulkes, Biosens. Bioelectron. 14 (1999) 495.
[160] R.M. Pemberton, J.P. Hart, T.T. Mottram, Biosens. Bioelectron. 16 (2001) 715.
[161] H.H. Lu, G. Conneely, M. Pravda, G.G. Guilbault, Steroids 71 (2006) 760.
[162] G. Conneely, M. Aherne, H.H. Lu, G.G. Guilbault, Anal. Chim. Acta 583 (2007) 153.
[163] F. Darain, D.S. Park, J.S. Park, S.C. Chang, Y.B. Shim, Biosens. Bioelectron. 20 (2005) 1780.
[164] G. Carpini, F. Lucarelli, G. Marrazza, M. Mascini, Biosens. Bioelectron. 20 (2004) 167.
[165] M. Diaz-Gonzalez, M.B. Gonzalez-Garcia, A. Costa-Garcia, Sens. Actuators, B 113 (2006) 1005.
[166] M. Alvarez, M. Abedul, A. Garcia, Anal. Chim. Acta 462 (2002) 31.
[167] M. Diaz-Gonzalez, M.B. Gonzalez-Garcia, A. Costa-Garcia, Biosens. Bioelectron. 20 (2005) 2035.
[168] M. Diaz-Gonzalez, D. Hernandez-Santos, M.B. Gonzalez-Garcia, A. Costa-Garcia, Talanta 65 (2005) 565.
[169] P. Fanjul-Bolado, M.B. Gonzalez-Garcia, A. Costa-Garcia, Talanta 64 (2004) 452.
[170] V.K. Rao, G.P. Rai, G.S. Agarwal, S. Suresh, Anal. Chim. Acta 531 (2005) 173.
[171] K.S. Lee, T.H. Kim, M.C. Shin, W.Y. Lee, J.K. Park, Anal. Chim. Acta 380 (1999) 17.
[172] E. Crowley, C. O'Sullivan, G.G. Guilbault, Anal. Chim. Acta 389 (1999) 171.
[173] M.P. Kreuzer, C.K. O'Sullivan, M. Pravda, G.G. Guilbault, Anal. Chim. Acta 442 (2001) 45.
[174] E.L. Crowley, C.K. O'Sullivan, G.G. Guilbault, Analyst 124 (1999) 295.
[175] V.K. Rao, M.K. Sharma, A.K. Goel, L. Singh, K. Sekhar, Anal. Sci. 22 (2006) 1207.
[176] A.A.P. Ferreira, W. Colli, M.J.M. Alves, D.R. Oliveira, P.I. Costa, A.G. Guell, F. Sanz, A.V. Benedetti, H. Yamanaka, Electrochim. Acta 51 (2006) 5046.
[177] M.P. Kreuzer, M. Pravda, C.K. O'Sullivan, G.G. Guilbault, Toxicon 40 (2002) 1267.
[178] A. Tang, M. Kreuzer, M. Lehane, M. Pravda, G.G. Guilbault, Int. J. Environ. Anal. Chem. 83 (2003) 663.
[179] L. Micheli, A. Radoi, R. Guarrina, R. Massaud, C. Bala, D. Moscone, G. Palleschi, Biosens. Bioelectron. 20 (2004) 190.
[180] L. Micheli, R. Grecco, M. Badea, D. Moscone, G. Palleschi, Biosens. Bioelectron. 21 (2005) 588.
[181] N.H.S. Ammida, L. Micheli, G. Palleschi, Anal. Chim. Acta 520 (2004) 159.
[182] N.H.S. Ammida, L. Micheli, S. Piermarini, D. Moscone, G. Palleschi, Anal. Lett. 39 (2006) 1559.
[183] R.M. Pemberton, R. Pittson, N. Biddle, G.A. Drago, J.P. Hart, Anal. Lett. 39 (2006) 1573.
[184] S.H. Alarcon, L. Micheli, G. Palleschi, D. Compagnone, Anal. Lett. 37 (2004) 1545.
[185] S.H. Alarcon, G. Palleschi, D. Compagnone, M. Pascale, A. Visconti, I. Barna-Vetro, Talanta 69 (2006) 1031.
[186] J.H. Lin, H.X. Ju, Biosens. Bioelectron. 20 (2005) 1461.
[187] H. Yu, F. Yan, Z. Dai, H.X. Ju, Anal. Biochem. 331 (2004) 98.
[188] J. Guan, Y. Miao, J. Chen, Biosens. Bioelectron. 19 (2004) 789.
[189] J. Wu, J.H. Tang, Z. Dai, F. Yan, H.X. Ju, N. El Murr, Biosens. Bioelectron. 22 (2006) 102.
[190] A. Schreiber, R. Feldbrugge, G. Key, J.F.C. Glatz, F. Spener, Biosens. Bioelectron. 12 (1997) 1131.
[191] T.M. O'Regan, M. Pravda, C.K. O'Sullivan, G.G. Guilbault, Talanta 57 (2002) 501.
[192] T.M. O'Regan, L.J. O'Riordan, M. Pravda, C.K. O'Sullivan, G.G. Guilbault, Anal. Chim. Acta 460 (2002) 141.
[193] D. Butler, M. Pravda, G.G. Guilbault, Anal. Chim. Acta 556 (2006) 333.
[194] K. Luangaram, D. Boonsua, S. Soontornchai, C. Promptmas, Biocatal. Biotransform. 20 (2002) 397.
[195] V.S. Morozova, A.I. Levashova, S.A. Eremin, J. Anal. Chem. 60 (2005) 202.
[196] B.B. Dzantiev, E.V. Yazynina, A.V. Zherdev, Y.V. Plekhanova, A.N. Reshetilov, S.C. Chang, C.J. McNeil, Sens. Actuators, B 98 (2004) 254.
[197] W. Del Carlo, M. Mascini, Field Anal. Chem. Technol. 3 (1999) 179.
[198] S. Laschi, M. Franek, M. Mascini, Electroanalysis 12 (2000) 1293.
[199] S. Laschi, M. Mascini, Ann. Chim. 92 (2002) 425.
[200] S. Laschi, M. Mascini, G. Scortichini, M. Franek, M. Mascini, J. Agric. Food Chem. 51 (2003) 1816.
[201] K.A. Fahnrich, M. Pravda, G.G. Guilbault, Biosens. Bioelectron. 18 (2003) 73.
[202] E. Moore, M. Pravda, G.G. Guilbault, Anal. Chim. Acta 484 (2003) 15.
[203] R. Solna, P. Skladal, S.A. Eremin, Int. J. Environ. Anal. Chem. 83 (2003) 609.
[204] Y.A. Cho, G.S. Cha, Y.T. Lee, H.S. Lee, Food Sci. Biotechnol. 14 (2005) 743.
[205] R.W. Keay, C.J. McNeil, Biosens. Bioelectron. 13 (1998) 963.
[206] K. Grennan, G. Strachan, A.J. Porter, A.J. Killard, M.R. Smyth, Anal. Chim. Acta 500 (2003) 287.
[207] A. Kasna, P. Skladal, Int. J. Environ. Anal. Chem. 83 (2003) 101.
[208] T. Kalab, P. Skladal, Anal. Chim. Acta 304 (1995) 361.
[209] T. Kalab, P. Skladal, Electroanalysis 9 (1997) 293.
[210] S. Kroger, S.J. Setford, A.P.F. Turner, Anal. Chem. 70 (1998) 5047.
[211] J. Zeravik, P. Skladal, Electroanalysis 11 (1999) 851.
[212] M. Gerdes, F. Spener, M. Meusel, Quim. Anal. 19 (2000) 8.
[213] I. Navratilova, P. Skladal, Bioelectrochemistry 62 (2004) 11.
[214] G.A. Evtugyn, S.A. Eremin, R.P. Shaljamova, A.R. Ismagilova, H.C. Budnikov, Biosens. Bioelectron. 22 (2006) 56.
[215] S. Susmel, G.G. Guilbault, C.K. O'Sullivan, Biosens. Bioelectron. 18 (2003) 881.
[216] S. Grant, F. Davis, K.A. Law, A.C. Barton, S.D. Collyer, S.P.J. Higson, T.D. Gibson, Anal. Chim. Acta 537 (2005) 163.
[217] M.C. Weston, E.C. Anderson, P.U. Arumugam, P.Y. Narasimhan, I. Fritsch, Analyst 131 (2006) 1322.
[218] J.M. Zen, C.T. Hsu, Y.L. Hsu, J.W. Sue, E.D. Conte, Anal. Chem. 76 (2004) 4251.

Available online at www.sciencedirect.com
ScienceDirect
Talanta 73 (2007) 296–303
Talanta
www.elsevier.com/locate/talanta

Effects of the receptors bearing phenol group and copper(II) on the anion recognition and their analytical application

Xue-Fang Shang [a], Hai Lin [b], Zun-Sheng Cai [a], Hua-Kuan Lin [a,*]

[a] *Department of Chemistry, Nankai University, Tianjin 300071, People's Republic of China*
[b] *Key Laboratory of Functional Polymer Materials of Ministry of Education, Nankai University, Tianjin 300071, People's Republic of China*

Received 4 February 2007; received in revised form 17 March 2007; accepted 22 March 2007
Available online 27 March 2007

Abstract

Two novel artificial receptors based on diamide and bearing phenol group and copper(II) have been synthesized. Their anion-binding properties are evaluated for F^-, Cl^-, Br^-, I^-, AcO^-, $H_2PO_4^-$ and OH^- by UV–vis and ^1H NMR titration experiments to further elucidate the impact of phenol group and copper(II) on the chemistry of anion-recognition. Results indicate that the interacted model of fluoride anion with receptor **1** is different from other anions and the ^1H NMR signals of receptor **2** occur changes after the addition of fluoride anion. This may be related with the small radius and strong electronegative property of fluoride. The receptors should have many chemical and analytical applications and the sensing principle should be widely applicable to the sensing of other receptors.

Keywords: Phenol group; Copper(II); Anion recognition; Analytical application

1. Introduction

Anion recognition by artificial receptors has attracted considerable attention in the field of host–guest chemistry because of the important roles of anions in biomedicinal and chemical processes [1–10]. The recognition of anionic guests by artificial hosts is an area of ever increasing research activity [11]. Artificial anion receptor has presented unique application prospects in the synthesis of anion sensors [12,13], membrane transmit carriers [14,15] and mimic enzyme catalysts, etc. [16,17]. The synthetic nitrogen-based receptors designed for the selective binding of anions usually consist of either positively charged ammonium salts, i.e., protonated polyamines and/or quaternized amines, or neutral species such as amides, sulfonamides, pyrroles, ureas, and thioureas [18,19]. Davis and co-workers [20,21] have reported that rigid steroid-based anion receptors bearing hydroxyl groups can bind anionic species in organic solvents, such as $CDCl_3$ and hydrocarbons. Albert and Hamilton [22] have reported that receptors having both urethane N-Hs and hydroxyl groups will exhibit considerably large affinity constants for binding acetate anion in acetonitrile. Zhang et al. [23] also reported that there are hydrogen bonds formed between amide, phenol group and anions. In general, the roles of phenol group on anion-recognition have been less studied correspondingly. Also, the effect of copper(II) on anion recognition has not yet been reported to our knowledge. According to this information, we synthesized two receptors **1** and **2** (Scheme 1) to examine the roles of the phenol group and copper(II) for F^-, Cl^-, Br^-, I^-, AcO^-, $H_2PO_4^-$ and OH^- on anion recognition.

2. Experimental

Most of the starting materials were obtained commercially and all reagents, and solvents employed were of analytical grade. All anions, in the form of tetrabutylammonium salts, were purchased from Sigma–Aldrich Chemical Co., stored in a desiccator under vacuum containing self-indicating silica, and used without any further purification. Dimethyl sulfoxide (DMSO) was distilled in vacuo after dried with CaH_2. Tetra-*n*-butylammonium salts (such as $(n\text{-}C_4H_9)_4NF$, $(n\text{-}C_4H_9)_4NCl$, $(n\text{-}C_4H_9)_4NBr$, $(n\text{-}C_4H_9)_4NI$, $(n\text{-}C_4H_9)_4NAcO$, $(n\text{-}C_4H_9)_4NH_2PO_4$ and $(n\text{-}C_4H_9)_4NOH$) were dried for 24 h in vacuum with P_2O_5 at 333 K before use. C, H, N elemental analysis was made on Vanio-EL. ^1H NMR spectrum was recorded on a Varian UNITY

* Corresponding author.
E-mail address: hklin@nankai.edu.cn (H.-K. Lin).

0039-9140/$ – see front matter © 2007 Elsevier B.V. All rights reserved.
doi:10.1016/j.talanta.2007.03.042

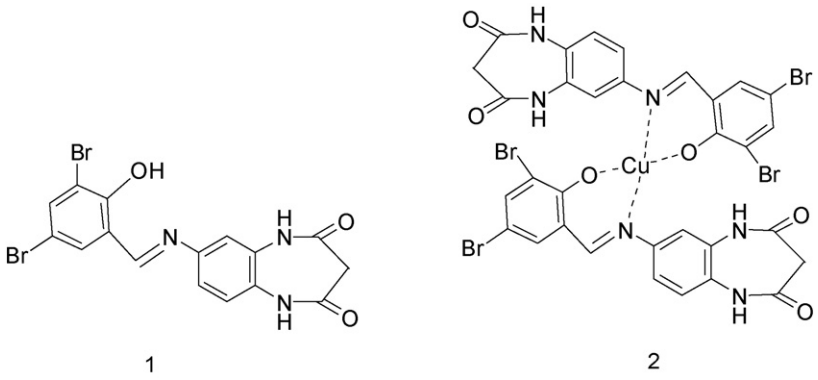

Scheme 1. Chemical structure of receptors **1** and **2**.

Plus-400 MHz Spectrometer. FAB-MS was made on VG ZAB-HS. UV–vis spectroscopy titrations were made on a Shimadzu UV2450 Spectrophotometer at 298 K. The affinity constants K_s were obtained by the non-linear least square calculation method through data fitting. Receptor **1** was synthesized according to the route shown in Scheme 2.

*2.1. Benzo-1,4-diazacycloheptane[2,3-d]-5,7-dione (**3**) [24]*

1,2-Phenylenediamine (10.8 g, 0.1 mol), diethyl malonate (16 ml, 0.1 mol) and pyridine (200 ml) were put in a 250 ml three-neck flask. The mixture was refluxed with N_2 for 72 h. After cooling, the mixture was filtrated and the colorless solid obtained. The solid was washed with ethanol and ether sequentially, and dried in vacuum. Yield: 72%. ^{1}H NMR(400 MHz, DMSO-d_6, 298 K) $\delta = 10.38$ (s, 2H), 7.11–7.18 (m, 4H), 3.17 (s, 2H). Elemental analysis: Calc. for $C_9H_8N_2O_2$: C, 61.36; H, 4.58; N, 15.90; Found: C, 61.69; H 4.59; N, 15.96. FAB-MS (*m*/*z*): 177 $(M+H)^+$.

*2.2. (4′-Nitrobenzo)[1′,2′-d]-1,4-diazacycloheptane[2,3-d] -5,7-dione (**4**)*

Benzo-1,4-diazacycloheptane[2,3-d]-5,7-dione (10 mmol, 1.7 g) was dissolved in concentrated H_2SO_4 (43 ml). Fuming HNO_3 (1.1 ml) was added dropwise with stirring at 273 K. After the addition was completed, the mixture was stirred for 2 h and then poured into ca. 200 ml ice-water. The solution was filtered to give a yellow solid, which was washed with distilled water, recrystallized from methanol and dried in vacuum. Yield: 85%. ^{1}H NMR(400 MHz, DMSO-d_6, 298 K) $\delta = 10.96$ (s, 1H), 10.74 (s, 1H), 8.04, 7.3 (3H), 3.3 (s, 2H), Elemental analysis: Calc. for $C_9H_7N_3O_4$: C, 48.88; H, 3.19; N, 19.00; Found: C, 48.76; H 3.58; N, 18.61.

*2.3. (4′-Aminobenzo)[1′,2′-d]-1,4-diazacycloheptane [2,3-d]-5,7-dione (**5**)*

A slurry of compound (4′-nitrobenzo)[1′,2′-d]-1,4-diazacycloheptane[2,3-d]-5,7-dione (221 mg) and Pd/C (10%, 70 mg) in dry ethanol (200 ml) was maintained under hydrogen with stirring for 12 h. The mixture was filtered through a bed of Celite and then washed twice with ethanol (2× 20 ml). The solvents were removed under reduced pressure and the yellowish solid dried in vacuum. Yield: 92%. ^{1}H NMR (400 MHz, DMSO-d_6, 298 K) $\delta = 10.15$ (s, 1H), 9.91 (s, 1H), 6.76 (d, 1H), 6.38 (m, 1H), 6.27 (d, 2H), 5.16 (s, 2H) 3.08 (s, 2H). Elemental analysis: Calc. for $C_9H_9N_3O_2$: C, 56.54; H, 4.74; N, 21.98; Found: C, 56.41; H 4.96; N, 21.87.

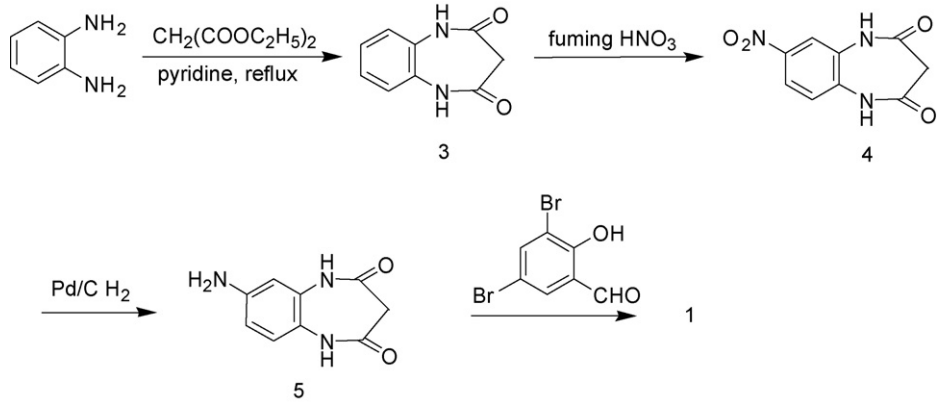

Scheme 2. Synthesis route for **1**.

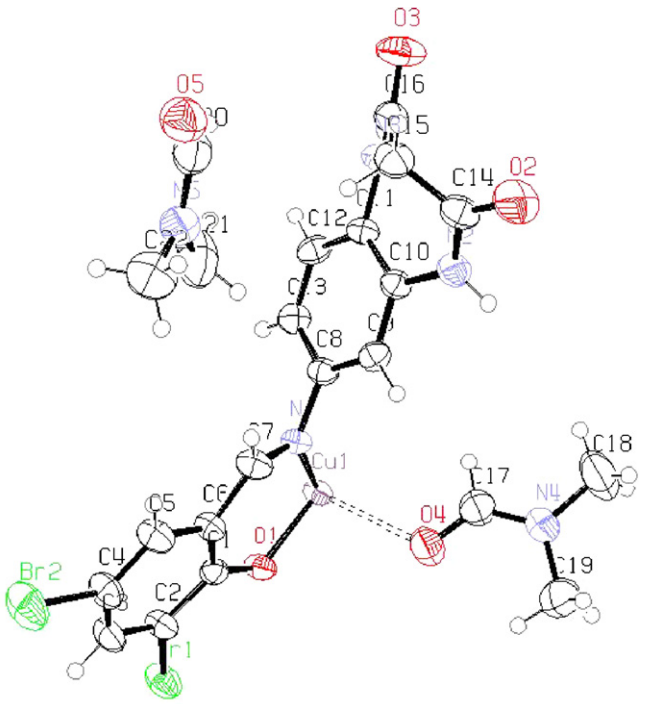

Fig. 1. The crystal structure of **2** and the hydrogen atoms are shown as small circles with arbitrary radii (ellipsoids at 50% probability).

Table 1
Crystallographic data of **2**

Compound	**2**
Empirical formula	$C_{44}H_{48}Br_4CuN_{10}O_{10}$
Formula weight	1260.10
Temperature (K)	294(2)
System, space group	Monoclinic, *P*2(1)/*n*
a (Å)	12.035(2)
b (Å)	8.9193(14)
c (Å)	23.017(4)
α (°)	90
β (°)	94.422(5)
γ (°)	90
V (Å^3)	2463.4(7)
Z	2
Crystal size (mm^3)	0.20 × 0.14 × 0.06
D_{calcd} (mg m^{-3})	1.699
F (000)	1262
2θ range (°)	1.77–27.46
Reflections collected	20636
R(int)	0.0619
GOF on F^2	1.020
Data/restraints/parameters	5613/0/326
Final R_1 and wR_2 [$I > 2\sigma(I)$]	0.0522, 0.1067
R_1 and wR_2 [all data]	0.0856, 0.1220
Largest diff. Peak hole (e Å^{-3})	0.607 and −0.657
Extinction coefficient	0.0022(4)

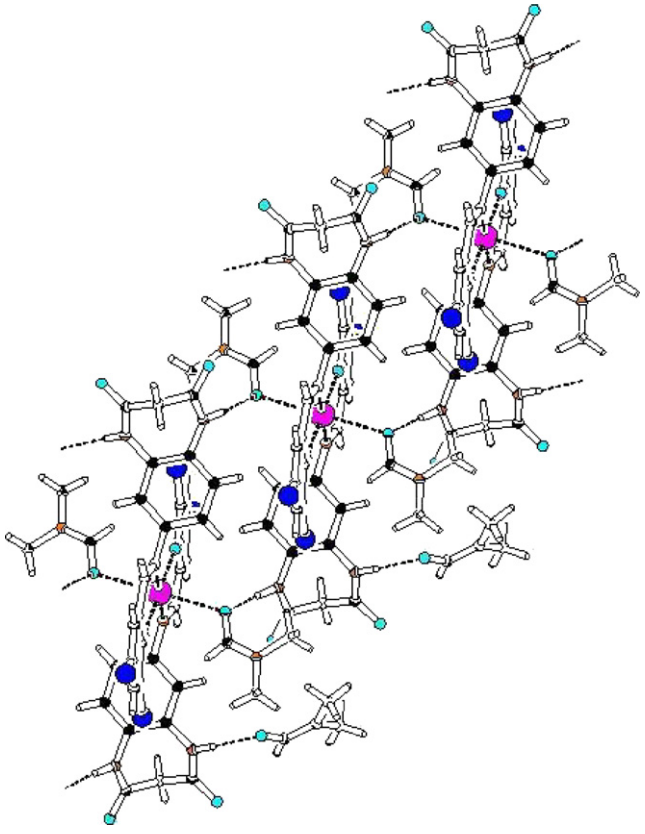

Fig. 2. View of **2** with hydrogen bonds and coordinated bonds shown as dotted lines.

*2.4. N-(2″-Hydroxyl-3″,5″-dibromophenyl-methylene-yl)-4′-imino-benzo[1′,2′-d]-1,4-diazacycloheptane[2,3-d]-5,7-dione [HODBrphC = NphDNHexDO] (**1**)*

(4′-Aminobenzo)[1′,2′-d]-1,4-diazacycloheptane[2,3-d]-5,7-dione (1 mmol, 191 mg) and 3,5-dibromo-salicylaldehyde (1 mmol, 278 mg) were suspended in dry ethanol (100 ml). The mixture was heated under reflux for 8 h and the orange-yellow precipitate was separated by filtration. The solid was washed with diethyl ether and dried under vacuum. Yield: 89%. ^{1}H NMR (400 MHz, DMSO-d_6, 298 K) δ = 14.41 (s, 1H), 10.54 (s, 2H), 8.97 (s, 1H), 7.9 (d, 2H), 7.3 (d, 2H), 7.2 (m, 1H) 3.24 (s, 2H). Elemental analysis: Calc. for $C_{16}H_{11}N_3OBr_2{\cdot}2H_2O$: C, 42.04; H, 3.31; N, 9.19; Found: C, 42.35; H 2.88; N, 9.45.

*2.5. Cu(II)[HODBrphC = NphDNHexDO]$_2$ (**2**)*

1 (0.1 mmol) and $Cu(NO_3)_2$ (0.05 mmol) were stirred for 1 h in DMF (20 ml), then stood at room temperature. After a month, the green crystal appeared. Elemental analysis: Calc. for $C_{32}H_{22}N_6O_2Br_4Cu{\cdot}5H_2O$: C, 39.33; H, 3.68; N, 9.17; Found: C, 39.22; H 3.55; N, 8.91.

2.6. X-ray crystallography

A green crystal of **2** with dimensions of 0.20 mm × 0.14 mm × 0.06 mm was mounted on a glass fiber. X-ray single-crystal diffraction data were collected on a Rigaku Saturn CCD area detector at 294(2) K with Mo-Ka radiation (λ = 0.71073 Å). The structure was solved by direct methods and refined on F^2 by

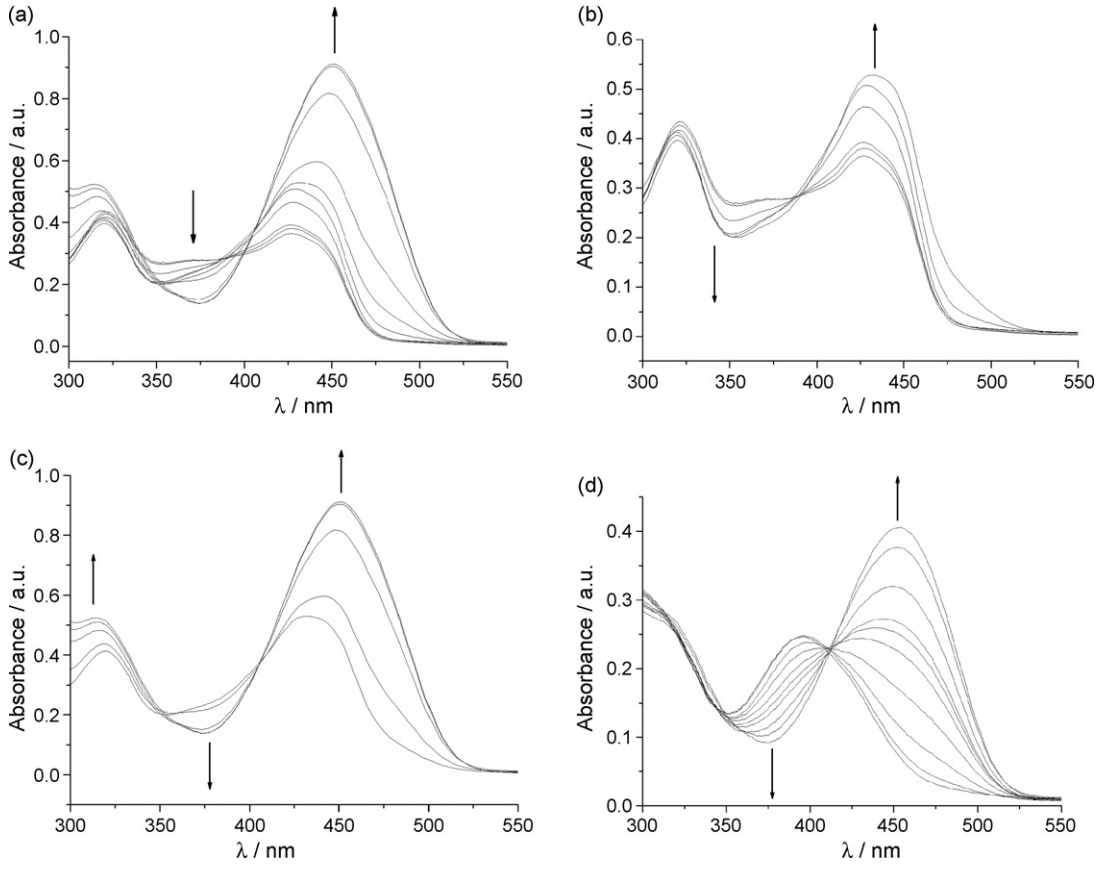

Fig. 3. UV–vis spectral changes of receptor **1** and **2** upon the addition of TBAF; [**1**] = [**2**] = 6.0×10^{-5} M: (a) **1**, [TBAF] = 0–160×10^{-5} M; (b) **1**, [TBAF] = 0–80×10^{-5} M; (c) **1**, [TBAF] = 80–160×10^{-5} M; (d) **2**, [TBAF] = 0–160×10^{-5} M. Arrows indicate the direction of increasing anion concentration.

full-matrix least squares methods with SHELXL-97 [25]. More details of the crystallographic determination are given in Table 1.

3. Results and discussion

Receptor **1** was synthesized according to the route shown in Scheme 2. Receptor **2** was obtained by the reaction of **1** and $Cu(NO_3)_2$ in *N*,*N*-dimethylformamide (DMF). The crystal of receptor **2** suitable for X-ray crystal analysis has been obtained and the structure has been confirmed (Fig. 1). The overall coordination environment of the Cu(II) atom involves two receptor **1** and two DMF molecules (Fig. 2). The bonds of Cu1–O1, Cu1–O1A, Cu1–N1, and Cu1–N1A are relatively longer (bond lengths 1.913 Å, 1.914 Å, 2.033 Å and 2.033 Å), and they constitute a plane quadrangular geometry around the Cu(II) atom (O1–Cu1–O1A, 180°, O1–Cu1–N1, 90.7°, O1–Cu1–N1A, 89.3°, O1A–Cu1–N1, 89.3°, O1A–Cu1–N1A, 90.7°, N1–Cu1–N1A, 180°); while the other two contacts of Cu–O4, and Cu–O4A are significantly shorter (bond lengths 1.653 Å and 1.653 Å), completing a distorted octahedron as the overall complexation geometry around the Cu(II) atom. The NH of amide forms hydrogen bonds with oxygen atoms of DMF molecules that are derived from two resources: one is the coordinated DMF; the other is the uncoordinated DMF. The overall crystal structure features a chain type with DMF molecules joining in through the hydrogen bonds along the *b* axis.

Fig. 3 shows the changes in the absorption spectra of receptor **1** and **2** observed upon the addition of F^- (in the form of tetrabutyl ammonium, TBAF). Fig. 3a is the whole titration spectrum of receptor **1** and shows that there are two processes shown in the titration with TBAF. The UV–vis spectrum of receptor **1** exhibit a strong absorption band at about 323 nm and a broad band at about 426 nm, which are assigned to the 3,5-dibromo-salicylaldehyde centered charge transfer (CT) and the charge transfer of the benzo-1,4-diazacycloheptane[2,3-d]-5,7-dione moiety, respectively [26]. The main absorption decreases at 323 nm and increases at 426 nm, when the fluoride salt concentration increases from 0 to 80×10^{-5} M (Fig. 3b). The presence of one distinct isosbestic point at 385 nm is clear, and the molar ratio analysis based on this concentration indicates that the spectral change in this concentration range can be ascribed to the formation of 1:1 complexation of **1** with fluoride anion (for a discussion of the complexation equilibrium, see below in Table 2). Significantly, the further addition of a large excess of TBAF causes subsequent spectral changes with red-shift (∼25 nm). And two new isosbestic points appear at 355 and 410 nm (Fig. 3c) that indicate a stable complex with certain stoichiometric ratio forms between the receptor **1** and anion. The additions of TBAAcO, $TBAH_2PO_4$ and TBAOH induce similar spectral changes. On the other hand, as exposure to TBACl, TBABr and TBAI, only minor binding to receptor **1** happens.

Table 2
Affinity constants of receptor **1** and **2** with various anions

Anion	K_s (**1**)	K_s (**2**) (M^{-1})
F^-	$(5.13 \pm 0.68) \times 10^4$	$(9.58 \pm 0.07) \times 10^3$
AcO^-	$(2.25 \pm 0.87) \times 10^5$	$(1.46 \pm 0.11) \times 10^4$
$H_2PO_4^-$	$(2.73 \pm 0.28) \times 10^4$	$(1.15 \pm 0.09) \times 10^4$
OH^-	$(1.30 \pm 0.12) \times 10^4$	$(5.27 \pm 0.24) \times 10^3$
Cl^-	<10	<10
Br^-	<10	<10
I^-	<10	<10

As shown in Fig. 3d, the spectrum of receptor **2** changes upon the addition of TBAF. Notably, the characteristic strong absorption band of receptor **2** at 385 nm decreases and a new absorption band at 452 nm, which is the charge transfer (CT) band [27], develops. In addition, the presence of a well-defined isosbestic point at 412 nm indicates that a stable complex with certain stoichiometric ratio forms between the receptor **2** and the fluoride anion. The additions of TBAAcO, $TBAH_2PO_4$ and TBAOH lead to similar spectral changes, but the additions of TBACl, TBABr and TBAI basically lead to no spectral changes.

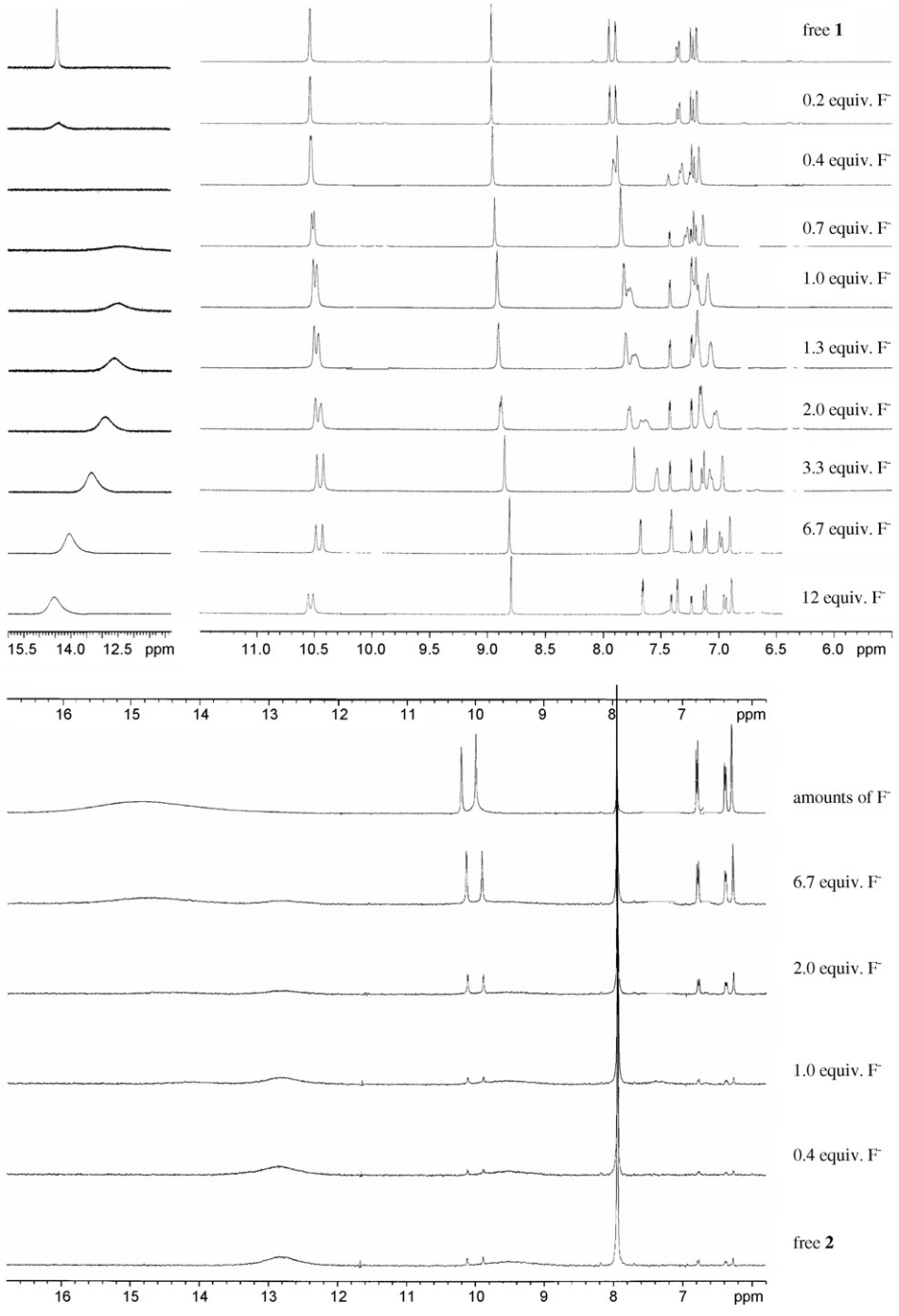

Fig. 4. Plots of ^{1}H NMR spectrum of receptor **1** and **2** in DMSO-d_6 upon the addition of various quantities of anionic tetrabutyl ammonium salt (from 0 to amounts).

Very recently, a number of fluorogenic and/or chromogenic anion sensors comprising recognition moieties such as urea, thiourea, or amide have been reported that they are to undergo an anion-induced deprotonation [28–30]. According to these reports, one new triplet resonance signal should appear at about 16.1 ppm, the characteristic resonance of bifluoride (F-H-F), and the chemical shifts of the proton signals of the non-interacted sites will occur up-field in ^{1}H NMR spectrum. Therefore, to look into the anion-binding properties of receptor **1** and **2** for various anions and the roles of phenol group and copper(II) on anion recognition, ^{1}H NMR titration experiments in DMSO-d_6 were performed (Fig. 4). From Fig. 4, the phenol group signal (14.5 ppm) of receptor **1** becomes broadened after the addition of only small quantities of TBAF and completely disappears after the addition of 0.4 equiv. F^-. Then a new signal at 12.4 ppm appears, enhances and moves to the downfield till 14.5 ppm. This may be explained as follows: Firstly the signal of phenol proton of receptor **1** (14.5 ppm), before addition of F^-, is due to the formation of intramolecular H-bonding with the imine nitrogen. And the added fluoride salt breaks up the intramolecular H-bonding while forms the $(HNCO)_2LOH\cdots F^-$ with receptor **1** ($(HNCO)_2LOH$) by intermolecular H-bonding, which changes the conformation of receptor **1** (Scheme 3). After the addition of 12 equiv. of fluoride salt, the double peak signal

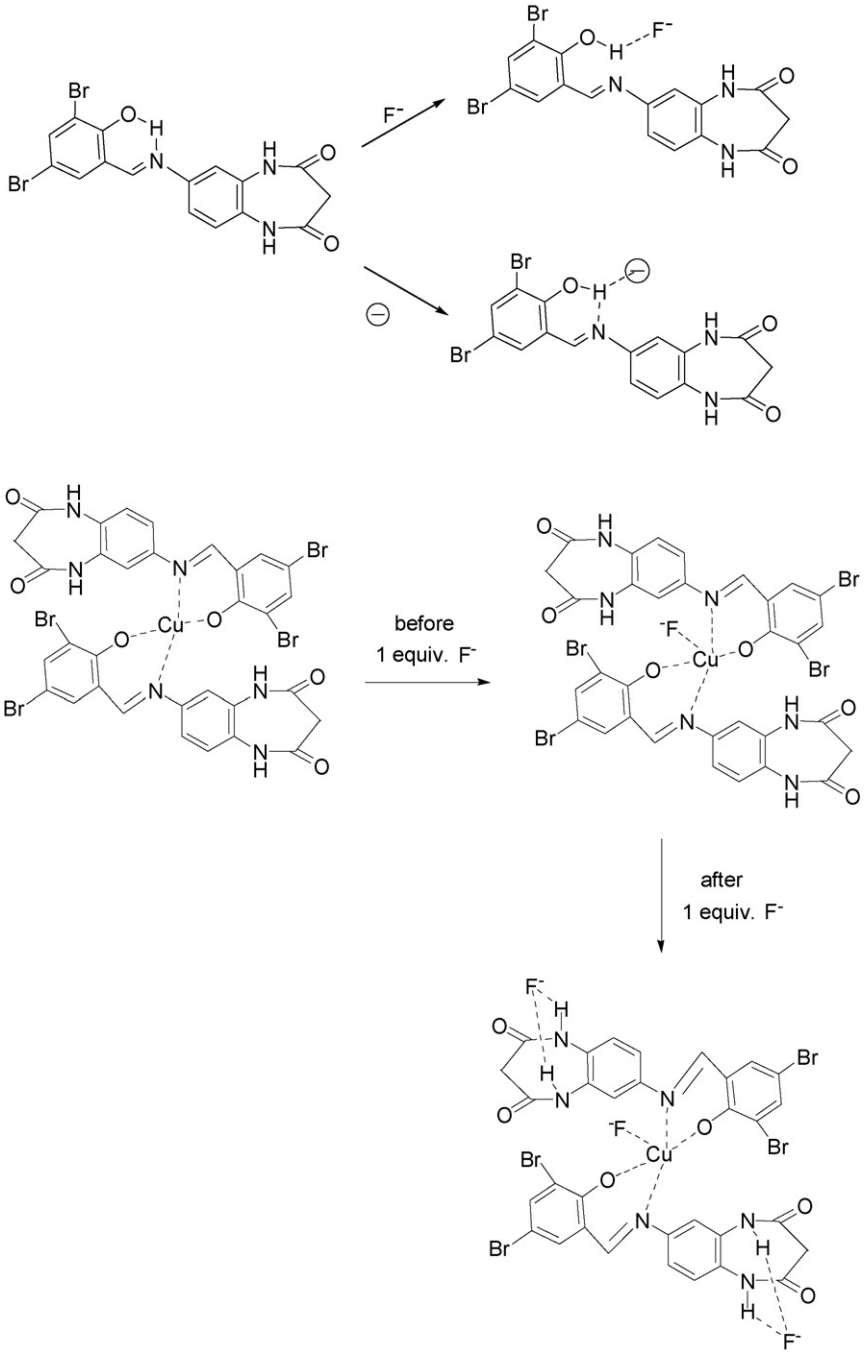

Scheme 3. Proposed model of anion-binding of **1** and **2** (⊖ represents AcO^-, $H_2PO_4^-$ and OH^-).

of amides moves to the downfield direction due to the hydrogen bond formation between the added fluoride and the two amides of receptor **1**. Why the UV–vis spectrum titration exists two processes (Fig. 3)? One way to rationalize it may be the above results. After various amounts of acetate anion salt is added (the ^{1}H NMR titrations spectrum of AcO^-, $H_2PO_4^-$, OH^-, Cl^-, Br^- and I^- are in the supporting information), the phenol signal of receptor **1** (14.5 ppm) broadens gradually and even disappears completely, but no new peak appears at about 12.4 ppm. This probably indicates that the added acetate salt does not either break up the intramolecular H-bonding or form the intermolecular H-bonding at the same time (Scheme 3). The similar phenomena of ^{1}H NMR titration exist in the addition of $TBAH_2PO_4$ and TBAOH. However, after the additions of TBACl, TBABr and TBAI, the chemical shifts in ^{1}H NMR spectrum have no changes. This suggests that Cl^-, Br^- and I^- have no binding abilities with receptor **1**.

The chemical shift of the amides (12.8 ppm) of receptor **2** (Fig. 4) keeps the same even adding up to 1 equiv. of the fluoride salt, because at the initial stage of titration the added F^- interacts with Cu(II) only through replacing the coordinated DMF. Indeed, from the crystal structure of receptor **2** (Fig. 2), DMF molecules take part in the coordination with Cu(II). Therefore, anions may interact with Cu by replacing DMF molecules in DMSO solution, since the coordination between Cu(II) and oxygen atom (electron-enriched) of DMF is weaker than that of Cu(II) with the anion (with one negative charge) in DMSO solution. After the addition of 1 equiv. fluoride salt: (1) the chemical shift of the amides shifts to the downfield direction gradually from 12.8 ppm to 14.9 ppm, and this may ascribe to the hydrogen bond formation between the NH of amides and F^-; (2) the phenyl signal enhances gradually. The reasons may involve the coordination of the paramagnetic copper centre with F^- and the concentration effect of the fluoride anion around Cu(II). Further studies on this line are worthy of conducting. The probable interacted model of receptor **2** with fluoride is shown in Scheme 3. Why does only 1 equiv. F^- interact with Cu(II)? This needs to be researched further.

4. Analytical application

In order to examine the potential application of the proposed receptors for analytical chemistry, the receptors are applied in the monitoring of binding ability with various anions (F^-, Cl^-, Br^-, I^-, AcO^-, $H_2PO_4^-$ and OH^-) which exist widely in living system, e.g., fluoride anion is being explored extensively as a treatment for osteoporosis, a type of fluoride toxicity that generally manifests itself clinically in terms of increasing bone density; naturally occurring phosphate-binding protein selectively and strongly bind hydrogen phosphate. Thus the development of sensitive detection systems for their bindingability is very important.

The binding ability of **1** and **2** with a variety of anions are investigated through UV–vis spectral titrations in DMSO by taking 6.0×10^{-5} M **1** and **2** solution. Additions of various anions (F^-, Cl^-, Br^-, I^-, AcO^-, $H_2PO_4^-$ and OH^-, in the form of tetrabutyl ammonium) cause the formation of anion-**1** or anion-**2** complex. The analyses are performed by UV–vis titration using the method of non-linear least square fitting and the results are summarized in Table 2 [31,32]. Obviously, the anion affinity constants of receptor **1** are in the order: $AcO^- > F^- > H_2PO_4^- > OH^- \gg Cl^- \sim Br^- \sim I^-$. While, that of receptor **2** are in the order: $AcO^- > H_2PO_4^- > F^- > OH^- \gg Cl^- \sim Br^- \sim I^-$. Therefore, the binding ability is related with the electronegative property of anions and the configuration match of the receptor with the anions. The above results may provide experimental analysis method for the monitoring of AcO^-, F^-, $H_2PO_4^-$ or OH^- and receptor **1** and **2** are useful for the detection of the above anions. This approach is expected to be applicable to the detection of other anions. Especially, if the interaction between receptor and anion accompanies the color change, it will be convenient and quick application in the practical detection of anion. This direction has wide application aspect.

5. Conclusions

In summary, we have demonstrated that a new diamide receptor bearing phenol group (**1**) shows anion-binding ability in DMSO. After the additions of TBAF, the phenol group of receptor **1** acts as H-bonding donors, which forms the intermolecular H-bonding while breaks up the intramolecular H-bonding during the anion recognition process, while, the additions of TBAAcO, $TBAH_2PO_4$ and TBAOH do not accompany with the breaking up of the intramolecular H-bonding. The interacted model of fluoride anion with receptor **1** is different from other anions and this may be related with the small radius and strong electronegative property of fluoride. When over amount of anions are added, the interaction with amides of **1** by H-bonding appears. In the crystal structure of receptor **2**, DMF molecules take part in the coordination with copper atom; anions may first displace DMF and then form H-bonding with amides. The electron-withdrawing effect of copper(II) may increase the affinities of amide with anions.

Receptors **1** and **2** could become the anion sensor in many biological and analytical applications. The same sensing principle should also be widely applicable to the sensing of other receptors.

Acknowledgements

This work was supported by the National Natural Science Foundation of China (20371028, 20671052) and the Natural Science Foundation of Tianjin (023605811).

Appendix A. Supplementary data

Supplementary data associated with this article can be found, in the online version, at doi:10.1016/j.talanta.2007.03.042.

References

[1] S.V. Sjevcjuk, V.M. Lynch, J.L. Sessler, Tetrahedron 60 (2004) 11283.
[2] F.P. Schmidtchen, M. Berger, Chem. Rev. 97 (1997) 1609.
[3] T.S. Snowden, E.V. Anslyn, Curr. Opin. Chem. Biol. 3 (1999) 740.

[4] P.A. Gale, Coord. Chem. Rev. 199 (2000) 181.
[5] P.D. Beer, P.A. Gale, Angew. Chem. Int. Ed. 40 (2001) 486.
[6] P.A. Gale, Coord. Chem. Rev. 213 (2001) 79.
[7] J.L. Sessler, J.M. Davis, Acc. Chem. Rev. 34 (2001) 989.
[8] F. Sancenon, R. Martinez-Manez, M.A. Miranda, M.J. Segui, J. Soto, J. Angew. Chem., Int. Ed. 42 (2003) 647.
[9] C.R. Bondy, S.J. Loeb, Coord. Chem. Rev. 240 (2003) 77.
[10] P.A. Gale, Coord. Chem. Rev. 240 (2003) 191.
[11] K. Shin-ichi, Tetrahedron Lett. 43 (2002) 7059.
[12] P. Buhlmann, E. Pretsch, E. Bakker, Chem. Rev. 98 (1998) 1593.
[13] S.S.M. Hassan, A.M.Y. Attawiya, Talanta 70 (2006) 883.
[14] V. Kral, J.L. Sessier, Tetrahedron 51 (1995) 539.
[15] M.J. Seguí, J. Lizondo-Sabater, A. Benito, R. Martínez-Máñez, T. Pardo, F. Sancenón, J. Soto, Talanta 71 (2007) 333.
[16] K. Kavauierators, R.H. Carbtree, Chem. Commun. 20 (1999) 2109.
[17] J.C. Vidal, S. Esteban, J. Gil, R. Castillo, Talanta 68 (2006) 791.
[18] S. Yamaguchi, S. Akiyama, K. Tamao, J. Am. Chem. Soc. 123 (2001) 11372.
[19] D.A. Jose, D.K. Kumar, B. Ganguly, A. Das, Org. Lett. 6 (2004) 3445.
[20] A.P. Davis, J.F. Gilmer, J.J. Perry, Angew. Chem. Int. Ed. Engl. 35 (1996) 1312.
[21] A.P. Davis, J.J. Perry, R.S. Wareham, Tetrahedron Lett. 39 (1998) 4569.
[22] J.S. Albert, A.D. Hamilton, Tetrahedron Lett. 34 (1993) 6363.
[23] X. Zhang, L. Guo, F.Y. Wu, Y.B. Jiang, Org. Lett. 5 (2003) 2667.
[24] W.B. Lu, Guangzhou Chem. 27 (2002) 26.
[25] G.M. Sheldrick, SHELX97 (1997).
[26] Y. Zhao, Z. Lin, S. Ou, C. Duan, H. Liao, Z. Bai, Inorg. Chem. Commun. 9 (2006) 802.
[27] X. Peng, Y. Wu, J. Fan, M. Tian, K. Han, J. Org. Chem. 70 (2005) 10524.
[28] C.Y. Wu, M.S. Chen, C.A. Lin, S.C. Lin, S.S. Sun, Chem. Eur. J. 12 (2006) 2263.
[29] B.G. Zhang, J. Xu, Y.G. Zhao, C.Y. Duan, X. Cao, Q.J. Meng, Dalton Trans. (2006) 1271.
[30] D. Esteban-Gomez, L. Fabbrizzi, M. Licchellic, J. Org. Chem. 70 (2005) 5717.
[31] P. Gans, A. Sabatini, Talanta 43 (1996) 1793.
[32] Y. Liu, B.H. Han, H.Y. Zhang, Curr. Org. Chem. 8 (2004) 35.

Available online at www.sciencedirect.com
ScienceDirect
Talanta 73 (2007) 404–406
Talanta
www.elsevier.com/locate/talanta

Short communication

Detection of aniline at boron-doped diamond electrodes with cathodic stripping voltammetry

Tanţa Spătaru [a,*], Nicolae Spătaru [a], Akira Fujishima [b]

[a] *Institute of Physical Chemistry of the Romanian Academy, 202 Spl. Independentei, 060021 Bucharest, Romania*
[b] *Kanagawa Academy of Science and Technology, KSP Building, West 614, 3-2-1 Sakado, Takatsu-ku, Kawasaki-shi, Kanagawa 213-0012, Japan*

Received 15 December 2006; received in revised form 15 March 2007; accepted 23 March 2007
Available online 6 April 2007

Abstract

Boron-doped diamond (BDD) electrodes were used to investigate the possibility of detecting aniline by linear-sweep cathodic stripping voltammetry. It was found that the dimeric species (*p*-aminodiphenylamine and benzidine) formed by anodic oxidation of aniline during the accumulation period are involved in electrochemically reversible redox processes and, in acidic media, the shape of the stripping voltammetric response is suitable for aniline detection in the micromolar concentration range. The low background current of conductive diamond is an advantage compared to other electrode materials and allows a detection limit of 1 μM. Weak adsorption properties and the extreme electrochemical stability are additional advantages of BDD and it was found that, even after long-time measurements, the electrode surface can regain its initial activity by an anodic polarization in the potential region of water decomposition.

Keywords: Boron-doped diamond; Aniline detection; Cathodic stripping voltammetry

1. Introduction

Aniline and some of its derivatives are used on a large scale as raw materials for various industrial applications, including the production of urethanes, the manufacture of intermediates for herbicides and other pesticides, the manufacture of dyes and pigments, and the production of accelerators and antioxidants for the rubber industry. The toxic effects resulting from exposure to aniline seem to arise from the formation of methemoglobin and could result in anoxia, erythrocyte damage and spleen effects [1]. For these reasons there have been numerous studies aiming to develop reliable methods for the determination of aniline, and several analytical procedures have been proposed, including spectrophotometry [2,3], NIR spectrometry [4], gas chromatography [5], capillary electrophoresis [6], and HPLC [7]. The use of electrochemical methods for aniline determination is rendered difficult by the fact that the surface of glassy carbon and noble metals electrodes is deactivated as a result of irreversible adsorption of polymeric reaction products. Nevertheless, modified carbon-paste electrodes have been successfully used with both voltammetric [8] and amperometric methods [9] and promising results have been also obtained for the electrochemical detection with prior derivatization [10,11].

The outstanding electrochemical features of boron-doped diamond (BDD), such as low background current, long-term stability of the response, and inertness to adsorption [12] prompted us to investigate the possibility of using it as electrode material for electrochemical determination of aniline.

2. Experimental

The boron-doped polycrystalline diamond coatings were deposited on Si (1 1 1) wafers by means of microwave plasma-assisted chemical vapor deposition, in accordance with a previously described procedure [13]. Electrochemical measurements were performed in a conventional three-electrode glass cell, at room temperature. BDD electrodes with 1 cm^2 surface area were used as working electrodes in all the experiments. A platinum wire and a saturated calomel electrode (SCE) were used as the counter electrode and the reference electrode, respectively.

* Corresponding author. Tel.: +40 212248895; fax: +40 213121147.
E-mail address: tspataru@chimfiz.icf.ro (T. Spătaru).

0039-9140/$ – see front matter © 2007 Elsevier B.V. All rights reserved.
doi:10.1016/j.talanta.2007.03.056

Aniline (Special Grade from Wako) was used as received. All the other substances were analytical-reagent grade, and all the solutions were prepared using bidistilled water. Standard 0.04 M Britton–Robinson buffer solution (boric acid + phosphoric acid + acetic acid) containing 0.1 M $LiClO_4$ was used as the supporting electrolyte. Typical cathodic stripping voltammetry (CSV) experiments were performed using linear-sweep technique (within the potential range 0.95–0.00 V) in quiescent solutions, under the following conditions: accumulation potential 0.95 V, accumulation time 15 s, and scan rate 300 mV s^{-1}.

3. Results and discussion

The electrochemical behavior of aniline at the BDD electrode was investigated within the potential range 0.0–1.0 V (SCE) and Fig. 1 shows characteristic voltammetric patterns recorded at a sweep rate of 50 mV s^{-1} in a Britton–Robinson buffer solution (pH 1.8). It was observed that during the first anodic run (curve 1 in Fig. 1) the voltammogram exhibits a single peak (labeled III) located at ca. 0.95 V. After the anodic limit is reached for the first time, two well-defined peaks are evidenced on the cathodic branch of the cyclic voltammetric curve, with peak potentials of ca. 0.55 and 0.35 V. Further cycling of the electrode potential within the same range (curve 2 in Fig. 1) will result in the occurrence of two redox couples evidenced by the presence of two pairs of reversible peaks, labeled I and II. As Fig. 1 shows the shape of the voltammograms is essentially identical with that reported by Bacon and Adams for aniline oxidation at the carbon-paste electrode [14]. Therefore, there are reasons to assume that, at the BDD electrodes, the overall oxidation reaction takes place by the same widely accepted mechanism involving the formation of nitrene cations of aniline within the range of peak III. By rapid fallow-up reactions, nitrene cations give rise to the dimeric products *p*-aminodiphenylamine and benzidine which are responsible for the occurrence of reversible redox peaks I and II, respectively [15–17].

Cyclic voltammograms recorded at several aniline concentrations have shown that the variation of the height of peak III as a function of aniline content is not well-suited for analytical applications. A reasonable explanation for this behavior is provided by the observation that, within the range of this peak, the overall anodic current is due not only to aniline oxidation, but also to the oxidation of the dimeric species formed by head-to-tail and tail-to-tail coupling of nitrene cations (i.e. *p*-aminodiphenylamine and benzidine, respectively) [15]. It is noteworthy that, unlike aniline oxidation, the anodic oxidation of both *p*-aminodiphenylamine and benzidine are electrochemically reversible processes, as illustrated by the shape of the voltammograms in Fig. 1. These findings are important because they suggest the possibility of using the height of the cathodic peaks as the basis for aniline determination by CSV.

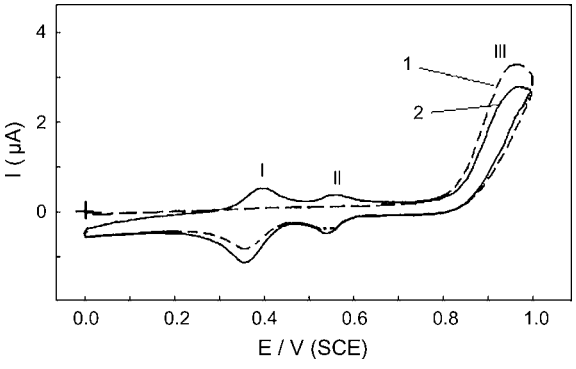

Fig. 1. Cyclic voltammograms recorded at the BDD electrode in pH 1.8 buffer solution containing 20 μM aniline: initial potential, 0.0 V (SCE); scan rate, 50 mV s^{-1}. (1) First run and (2) second run.

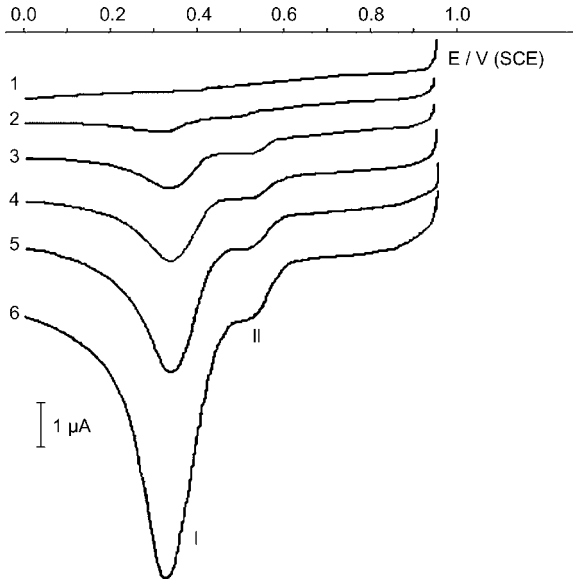

Fig. 2. Effect of aniline concentration on the cathodic linear-sweep voltammograms in pH 1.8 buffer solution. Aniline concentration (μM): (1) 0.0, (2) 1.0, (3) 2.9, (4) 4.8, (5) 12.4, (6) 27.5. Stripping conditions: accumulation potential 0.95 V, accumulation time 15 s, scan rate 300 mV s^{-1}.

Fig. 2 shows linear-sweep voltammograms (scan rate 300 mV s^{-1}) obtained at the BDD electrode in Britton–Robinson buffer solution (pH 1.8) for several aniline concentrations. The voltammograms were recorded after performing an accumulation at 0.95 V for 15 s. It can be observed that, in the presence of aniline, the voltammetric curves exhibit a well-defined stripping peak (labeled I) at ca. 0.33 V and a wave-shaped one (labeled II) at ca. 0.50 V that can be ascribed to the presence of *p*-aminodiphenylamine and benzidine, respectively. It was found, however, that at concentrations higher than ca. 100 μM peak II becomes less evidenced and vanishes completely for aniline contents higher than ca. 450 μM. This behavior is in line with the observation that, during anodic oxidation of aniline, benzidine yields are maximized by operating at low parent concentrations [16].

The effect of the pH on the cathodic stripping voltammetric response of aniline was also investigated. It was found that, for analytical applications, acidic media (pH values lower than ca. 2.2) are most suitable because they allow obtaining more reproducible stripping peaks. This was not surprising because it was previously shown that, at the BDD electrodes, the stability of the adsorbed blocking species (that could result from further

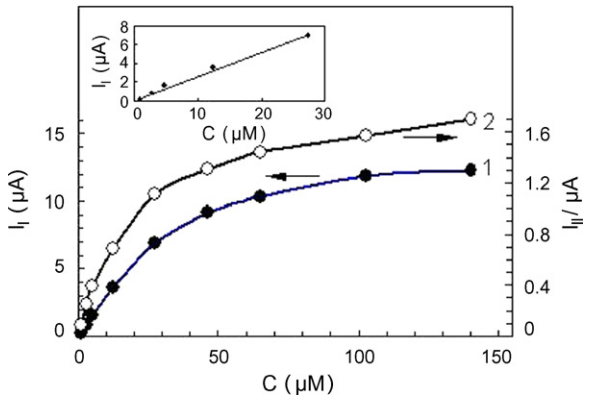

Fig. 3. The variation of the average peak current for the stripping peaks I (curve 1) and II (curve 2) as a function of aniline concentration. Stripping conditions, same as in Fig. 2. Inset: effect of aniline in the lower concentration range on the peak I current.

polymerization of the dimeric species) is lower at low pH values [18].

As shown in Fig. 3 the average peak currents (seven measurements at each concentration) for the stripping peaks I and II are nonlinear functions of the aniline concentration within the range 1–140 μM. From the standpoint of aniline determination, the most important concentration range lies below 30 μM. Thus, under typical conditions (pH 1.8, accumulation potential 0.95 V, accumulation time 15 s, scan rate 300 mV s^{-1}), the height of the stripping peak I is linearly proportional to the aniline concentration (see the inset in Fig. 3). The least-squares analysis yielded for the calibration graph ($I = aC$) a sensitivity (a) of 0.260 μA μM^{-1}, with $R^2 = 0.9898$. The sensitivity of the method can be adjusted to some extent by changing the deposition time. In order to illustrate this behavior, Fig. 4 shows the variation of the height of peak I as a function of aniline concentration for an accumulation time of 30 s. Within the same concentration range (below 30 μM) the sensitivity was found to be higher (0.310 μA μM^{-1}), although with lower correlation factor

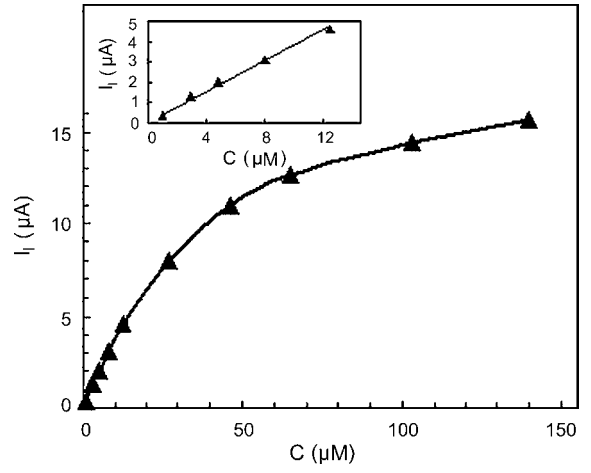

Fig. 4. The variation of the average peak current for the stripping peak I as a function of aniline concentration. Stripping conditions: accumulation potential 0.95 V, accumulation time 30 s, scan rate 300 mV s^{-1}. Inset: effect of aniline at concentrations below 15 μM.

($R^2 = 0.9550$). Nevertheless, as the inset in Fig. 4 suggests, excellent parameters of the calibration curves ($a = 0.380$ μA μM^{-1}, $R^2 = 0.9902$) are still available within a less wide concentration range (below ca. 15 μM). The fact that, for aniline concentrations lower than ca. 30 μM, the accumulation time can be increased up to ca. 30 s without significant fouling of the electrodes is in line with the observation that at the conductive diamond electrode the formation of polymeric films by anodic oxidation of aniline is a slow process [18]. The relative standard deviations (R.S.D.) for seven runs at 3 and 46 μM were of 13.0% and 3.6%, respectively.

Under the same experimental conditions, the height of the stripping peak II is also linearly proportional ($I = aC$) to the aniline concentration, within the range 1–5 μM. Although the sensitivity (0.08 μA μM^{-1}) is lower than that available by using peak I, the use of peak II as the basis for aniline detection at concentrations below 5 μM allows a better reproducibility of the results. For example, in this case a R.S.D. of 4.4% was found for seven runs at 3 μM.

The long-term stability of the response was found to be satisfactory. Rather small changes (<10%) in the voltammetric response were observed for a given electrode over a period of at least 1 week. It is worthy to note that, due to the excellent stability of the conductive diamond, the activity of the electrode can be completely restored by applying high anodic potential (3.0 V) for a few minutes, in the supporting electrolyte solution. Additional advantages of using BDD electrodes are extremely low background current and the extreme robustness of the material.

References

[1] N.I. Sax, Dangerous Properties of Industrial Materials, Van Nostrand Reinhold Company, New York, 1979, p. 379.
[2] G. Norwitz, P.N. Keliher, Anal. Chem. 53 (1981) 1238.
[3] S.A. Rahin, N.D. Ismail, W.A. Bashir, Microchim. Acta 90 (1986) 417.
[4] J. McDonald, A. McIntyre, M.L. Hitchman, D. Littlejohn, Appl. Spectroscopy 52 (1998) 908.
[5] S. Komiura, Y. Tajima, T. Nakahara, Environ. Chem. 7 (1997) 477.
[6] A. Asthana, D. Bose, A. Durgbanshi, S.K. Sanghi, W.T. Kok, J. Chromatogr. A 895 (2000) 197.
[7] M.I. Evgenev, I.I. Evgeneva, S.Y. Garmonov, R.N. Ismailova, J. Anal. Chem. 58 (2003) 542.
[8] L. Hernandez, P. Hernandez, Z.S. Ferrera, Fresen. J. Anal. Chem. 329 (1988) 756.
[9] P. Dominguez-Sanchez, C.K. O'Sullivan, A.J. Miranda-Ordieres, P. Tunon-Blanco, M.R. Smyth, Anal. Chim. Acta 291 (1994) 349.
[10] J.A. Rodrigues, A.A. Barros, Talanta 42 (1995) 915.
[11] E.H. Seymour, N.S. Lawrence, E.L. Beckett, J. Davis, R.G. Compton, Talanta 57 (2002) 233.
[12] N. Spataru, D.A. Tryk, A. Fujishima, in: A. Fujishima, Y. Einaga, T.N. Rao, D.A. Tryk (Eds.), Diamond Electrochemistry, Elsevier, Amsterdam, 2005, p. 287.
[13] T. Yano, D.A. Tryk, K. Hashimoto, A. Fujishima, J. Electrochem. Soc. 145 (1998) 1870.
[14] J. Bacon, R.N. Adams, J. Am. Chem. Soc. 90 (1968) 6569.
[15] R.N. Adams, Electrochemistry at Solid Electrodes, Marcel Dekker, New York, 1969, p. 331.
[16] R.L. Hand, R.F. Nelson, J. Am. Chem. Soc. 96 (1974) 850.
[17] F. Cases, F. Huerta, P. Garces, E. Morallon, J.L. Vazquez, J. Electroanal. Chem. 501 (2001) 186.
[18] M. Mitadera, N. Spataru, A. Fujishima, J. Appl. Electrochem. 34 (2004) 249.

Available online at www.sciencedirect.com
ScienceDirect
Talanta 73 (2007) 251–257
Talanta
www.elsevier.com/locate/talanta

Evaluation of extraction methods for the simultaneous analysis of simple and macrocyclic trichothecenes

Günther Stecher [a,*], Kanokwan Jarukamjorn [b], Pola Zaborski [a], Rania Bakry [a], Christian W. Huck [a], Günther K. Bonn [a]

[a] *Institute of Analytical Chemistry and Radiochemistry, Leopold-Franzens University of Innsbruck, Innrain 52a, 6020 Innsbruck, Austria*
[b] *Department of Pharmaceutical Chemistry, Faculty of Pharmaceutical Sciences, Khon Kaen University, 40002 Khon Kaen, Thailand*

Received 16 January 2007; received in revised form 13 March 2007; accepted 15 March 2007
Available online 24 March 2007

Abstract

The article is concerned with the simultaneous determination of simple and macrocyclic trichothecenes using high-performance liquid chromatography (LC) coupled to UV and mass spectrometric (MS) detection. Emphasis is put on the liquid–liquid extraction (LLE) and solid phase extraction (SPE) procedure from plant material such as wheat, comparing SPE cartridges packed with different stationary phases based on silica and polymer sorbents. In this coherence a polymeric material on the basis of poly(glycidyl methacrylate-divinylbenzene) (GMA-DVB) is developed with special regard on synthesis procedures to enhance the extraction recovery of trichothecenes in a broad polarity range. Evaluation of extraction techniques showed that the introduced material is competitive with commercially available high quality SPE materials. Percentage recovery is 82% for polar compounds, 89% for medium polar compounds and 98% for lipophilic compounds.

Keywords: Trichothecenes; Solid phase extraction; LC–UV; Poly(glycidyl methacrylate-divinylbenzene)

1. Introduction

Trichothecene mycotoxins are secondary metabolites produced by certain types of fungi including *Fusarium*, *Mycothecium*, *Stachybotrys*, and *Trichothecium*, which grow on plants of agricultural importance during cultivation, harvest, transport and storage [1–6]. Trichothecenes are a family closely related to sesquiterpenoids with a common 12,13-epoxide-trichothec-9-ene ring system [6–11]. They are classified into two major groups, simple and macrocyclic, based on their chemical structures (Fig. 1). The simple trichothecenes are divided as type A or B depending on the occurrence (type B) or the absence (type A) of a carbonyl group at position C-8. Macrocyclic trichothecenes are the di- or triesters of simple trichothecenes, having large thermally labile, exocyclic ester bridges at position 15 and 4. The diversity of trichothecenes leads to a wide range of toxic effects in animals and humans such as skin irritation, feeding refusal, nausea, vomiting, diarrhea, anemia, hemorrhage, immunosuppression, protein synthesis inhibition, and bone marrow depletion [8,12–14]. Since they are generally considered to be toxic compounds, their occurrence in food has been recognized as potential human health hazard either caused by direct or by "carry over" of mycotoxins in animal tissues. They are of special concern and consequently require monitoring in plant material destined for human consumption or as animal feed. Due to their frequent occurrence and their severe toxic properties, guidelines and recommendations of these compounds have been set for feeding stuff and foods in several countries [1,7,13,15]. Accurate and reliable methods for the determination of the most common trichothecenes, suitable for determination of trichothecenes naturally contaminated samples, are therefore required.

Since all trichothecenes vary extremely in polarity, compromise has to be made for the optimal clean-up procedure for all groups of trichothecenes. Solid-phase extraction (SPE), especially combined polar and non-polar materials, becomes a preferred technique as a selective and time-saving sample

Abbreviations: ACN, acetonitrile; DON, deoxynivalenol; DAS, diacetoxyscirpenol; F-X, fusarenone-X; H_2O, water; MeOH, methanol; NIV, nivalenol; Ro-a, roridin-A; T-2, T-2 toxin; Ve-a, verrucarin-A; VOL, verrucarol; GMA-DVB, poly(glycidyl methacrylate-divinylbenzene)

* Corresponding author. Tel.: +43 512 5075176; fax: +43 512 5072767.
E-mail address: Guenther.Stecher@uibk.ac.at (G. Stecher).

0039-9140/$ – see front matter © 2007 Elsevier B.V. All rights reserved.
doi:10.1016/j.talanta.2007.03.028

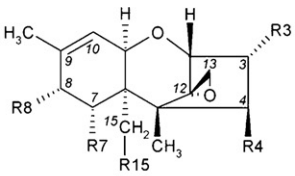

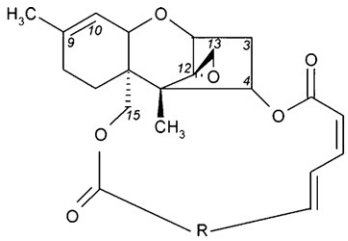

Simple trichothecenes ***Macrocyclic trichothecenes***

Type		MW	R3	R4	R7	R8	R15
A	**VOL**	266	H	OH	H	H	OH
A	**DAS**	366	OH	OAc	H	H	OAc
A	**T-2**	466	OH	OAc	H	*i*-Val	OAc
B	**NIV**	312	OH	OH	OH	=O	OH
B	**DON**	296	OH	H	OH	=O	OH
B	**F-X**	354	OH	OAc	OH	=O	OH

MW, molecular weight; OAc, acetyl; *i*-Val, iso-valeryl; =O, carbonyl

	MW	R
Ve-A	502	-CHOHCHCH$_3$CH$_2$CH$_2$OC=O
Ro-A	532	-CHOHCHCH$_3$CH$_2$CH$_2$OCHCHOHCH$_3$

Fig. 1. Structures of investigated trichothecenes; VOL = verrucarol, DAS = diacetoxyscirpenol, T-2 = T-2 toxin, NIV = nivalenol, DON = deoxynivalenol, F-X = fusarenone-X, Ve-A = verrucarin-A, Ro-A = roridin-A.

clean-up technique enabling almost complete removal of possibly interfering matrices [1–3,7–14,16–24]. Alternatively, liquid–liquid partitioning, immunoaffinity chromatography, and gel permeation chromatography were employed [4,6,15,25–31]. A variety of chromatographic methods for determination of trichothecenes have been published using thin-layer chromatography (TLC) [32–34], high-resolution gas chromatography (HRGC) with electron capture (ECD) [2,3,6,7,11,19,21,26,31] or mass spectrometric (MS) detection [7,13,14,21,22,35,36] and high-performance liquid chromatography (LC) with UV [7,15,17,20,26,29,30], fluorescence (FLD) [2,3,7,18,23,25,31], MS or tandem mass spectrometric (MS/MS) [7–9,13,15,21,22,27,28,37–42] detection. New techniques such as supercritical fluid chromatography–mass spectrometry (SFC–MS) and enzyme-linked immunosorbent assay (ELISA) were also used [4,43–45]. For several TLC and GC based methods, derivatization is required either for separation or identification. Particularly, due to the lack of a UV chromophore of type A-trichothecenes, derivatization can enable their determination by LC–FLD. On the naturally co-occurrence of trichothecenes, the employment of MS brings advantages on characterization and identification of trichothecenes and omitting the pre-derivatization step, consequently enhancing sensitivity of the analytical method. Besides the efficient method for simultaneous determination of all naturally occurring trichothecenes at trace level by LC–MS, the routine method for quantification of simple type B and macrocyclic trichothecens by LC–UV is noteworthy for epidemiological surveys, health and economic ramification.

The paper describes the comparison of various sample clean-up approaches, presenting also the application of a newly synthesized polymeric material on the basis poly(glycidyl methacrylate-divinylbenzene) (GMA-DVB) for the extraction of trichothecenes in a broad range of polarity. Nivalenol, deoxynivalenol, fusarenone-X, verrucarol, diacetoxyscirpenol, T-2 toxin, verrucarin-A, and roridin-A are considered within this investigation.

2. Experimental

2.1. Materials

Trichothecene standards, including nivalenol (NIV), deoxynivalenol (DON), fusarenone-X (F-X), verrucarol (VOL), diacetoxyscripenol (DAS), T-2 toxin (T-2), verrucarin-A (Ve-A), and roridin-A (Ro-A) were purchased from Sigma (Vienna, Austria).

Acetonitrile (gradient grade), methanol (gradient grade), ethyl acetate (analytical reagent), diethyl ether (analytical reagent), phosphoric acid (analytical reagent), acetic acid (analytical reagent), sodium hydroxide (p.a.) and divinylbenzene (65%) were from Merck (Darmstadt, Germany). α, α′-azobisisobutyronitril (98%), divinylbenzene (80.4%) and sodium sulphate were delivered from Fluka (Buchs, Switzerland). Glycidyl methacrylate (GMA) was from Sigma Aldrich. Water was purified by an Infinity NanoPure Unit (Barmstead, Boston, USA).

2.2. Preparation of poly(glycidyl methacrylate-divinylbenzene) (GMA-DVB) particles

For preparation of GMA-DVB particles the monomeric units divinylbenzene and glycidyl methacrylate were purified: DVB

was washed with 10% NaOH and H_2O, dried over Na_2SO_4 and distilled under vacuum ($p = 10$ Torr) at 100 °C. GMA was purified by distillation under reduced pressure ($p = 10$ Torr) at 120 °C. Both monomers were finally stored at −20 °C in dark bottles. Polymerization was performed basically according to Zhang et al. [46] and Aprilita et al. [47], but with several optimization and evaluation steps: Synthesis was performed within a four-neck 250 mL round-bottom flask epuipped with a mechanical stirrer, a condenser, a nitrogen inlet and a thermometer for temperature control. Depending on the molar ratio between the two monomers different amounts of DVB and AIBN were placed together with 120 mL ACN in the round-bottom flask. The mixture was first purged with nitrogen for 10 min under stirring. After heating the solution at 60 °C and stirring for 4 h, GMA was added and the temperature raised to 70 °C. After 20 h, temperature was lowered to room temperature (20 °C) and reaction product was filtered and washed with 60 mL ACN and 60 mL MeOH, respectively. Finally the polymeric particles were dried for 4–8 h under reduced pressure ($p = 10$ Torr) in a desiccator.

2.3. Preparation of standards and reference materials

Standards were individually dissolved in ACN at a concentration of 1 mg/ml as stock solutions and stored at −20 °C until use. Standard working solutions were prepared by diluting each stock solution with the mobile phase consisting of H_2O–MeOH (90:10 v/v).

For LC–UV six-point calibration curves were performed in concentration range from 0.5 to 30 μg/mL. For LC–MS four-point calibrations in the range of 0.5–15 μg/mL were established. The resulting response data were fit using linear regression analysis. Inter-day and intra-day precisions within the indicated calibration range and lower limit of detection were evaluated. Quantification of analytes content was performed using the formula from the standard calibration curve of trichothecene peak area versus trichothecene standard concentration.

2.4. Sample extraction

Several solid-phase extraction cartridges with different polarities were used in the trials: Supelclean LC-18 (Supelco, Bellefonte, PA, USA), Isolute C8 (International Sorbent Technology, Mid Glamorgan, UK), Mycosep 227 (Romer Labs, Inc., Washington, MO, USA), OASIS™ HLB (Waters, Milford, MA, USA) and GMA-DVB.

For recovery determination, 10 g of homogeneous wheat from a retail market were spiked with a mixture of trichothecenes (NIV, DON, F-X, Ro-A, Ve-A) in ACN (2 mg/kg) and left to dry for 30 min at ambient temperature (20 °C). The spiked samples were extracted with 40 mL of ACN–H_2O (84:16, v/v) for 1 h as proposed for Mycosep 227 clean-up. For SPE and LLE the spiked samples were extracted for 30 min with MeOH–H_2O (20:80, v/v). Extracts were filtered and stored at 4 °C for further steps (maximum 2 weeks).

2.4.1. Solid phase extraction (SPE)

Before loading cartridges with 2 mL of standard or sample solution they were activated with 1 mL MeOH and conditioned with 1 mL H_2O or 10% MeOH, depending on the nature of the SPE material itself. Polymeric materials like Oasis® HLB or the produced GMA-DVB were conditioned with H_2O. In contrast, for conditioning reversed phase silica stationary phases 10% MeOH was used, to guarantee optimal availability of carbon chains.

After loading the cartridges with 2 mL of sample the system was washed with 1 mL H_2O and finally dried for 5 min with nitrogen (1.5 bar). Elution of analytes was performed by applying 1 mL of MeOH. Then the eluate was evaporated under nitrogen stream at 40 °C. The residue was reconstituted in 400 μL of the mobile phase (H_2O–MeOH, 90:10, v/v), filtered through a membrane filter and an 20 μL aliquot was consequently applied to the chromatographic system.

2.4.2. Mycosep 227 clean up

The Mycosep 227 clean-up column consists of various adsorbents, such as charcoal, Celite®, ion-exchange resins and others, which are housed in a plastic tube between filter discs with a rubber flange on the lower end containing a porous frit and one-way valve. When the column is inserted into the culture tube the flange seals tight, thus forcing the extract through the packing material of the column. The pure extract appears on the top of the plastic tube.

For clean up of analytes 10 mL aliquot of the filtrate was transferred into a culture tube of a Mycosep 227 column. The purification was executed by rapid pushing the flange end of the column into the culture tube. 4 mL of the clean-up extract were evaporated under nitrogen stream at 40 °C. Then the residue was reconstituted in 400 μL of the mobile phase (H_2O–MeOH, 90:10, v/v), filtered through a membrane filter and finally an 20 μL aliquot was consequently applied to the chromatographic system.

2.4.3. Liquid–liquid extraction (LLE)

For liquid–liquid extraction a 4 mL aliquot of standard or sample solution was extracted with an equal volume of ethyl acetate or diethyl ether. The extraction was repeated for three times. The organic layers were collected and evaporated under nitrogen stream at 40 °C. The residue was reconstituted in 200 μL of the mobile phase (H_2O–MeOH, 90:10 v/v), filtered through a membrane filter and an 20 μL-aliquot was consequently applied to the chromatographic system. The percentage of recovery was evaluated from peak area of spiked sample with indicated concentrations of each trichothecenes before and after the clean-up procedure.

2.5. High performance liquid chromatography–UV-detection (LC–UV)

Chromatographic separation and detection was performed on a LC Module 1+ (Waters, Milford, MA, USA). The system consisted of a low-pressure gradient pump (model 616, Waters), an autosampler (model 717, Waters) and a UV–Vis

detector (model 486, Waters) with a 8 μL flow cell, a helium degassing system, and a column heater (ICI, Welshpool, AUS). Data were recorded on a PC, by use of the manufacturer's software package (Millennium^{32}, Version 3.05.01, Waters). Reversed phase (RP) LC was performed with a Nucleosil 120-3 C18 analytical column (125 mm × 2 mm i.d., 3 μm, 120 Å, Macherey-Nagel AG, Oensingen, Switzerland) connected to a Nucleosil 120-3 C18 guard column (8 mm length, 3 mm i.d., 3 μm, 120 Å, Macherey-Nagel). All separations were performed at 50 °C.

The LC–UV system operated with a linear binary gradient mobile phase consisting of H_2O (solvent A) and MeOH (solvent B) pumped at a constant flow rate of 400 μL/min. Zero time conditions were 90% A, changing from 4 to 5 min to 42% A. At 18 min mobile phase composition changed back to 90% A in 1 min till the end of the run at 35 min.

For determination of trichothecenes detection was performed at 220 and 260 nm, switching from 220 to 260 nm at 15 min and back to 220 nm at 30 min.

2.6. High performance liquid chromatography coupled to atmospheric pressure chemical ionisation mass spectrometric detection (LC–APCI–MS)

For hyphenating the established RP–LC system to a triple quadrupole Finnigan-MAT TSQ 7000 tandem mass spectrometer (Thermo Finnigan, San Jose, CA, USA) the same stationary phase as described in the previous chapter was used. The chromatographic separation system consisted of a low-pressure gradient micro pump (Rheos 4000, Flux Instruments, Basel, Switzerland), an in-line degasser (Brauer, Berlin, Germany) and a Rheodyne 7125 injector (Rheodyne, CA, USA) equipped with a 20 μL injection loop. The LC system operated with a linear binary gradient mobile phase consisting of H_2O (A) and MeOH (B), pumped at a constant flow rate of 400 μL/min without splitting. The gradient system was changed as follows to guarantee baseline separation of analytes: zero time conditions were 90% A for 10.5 min, increase to 44% A within 0.5 min and held for 16.5 min, followed by an 0.5 min-return to 90% A till the end of the run at 35 min.

The MS was performed in the positive ion mode employing atmospheric pressure chemical ionization (APCI+). Mass spectra were carried out in full-scan mode (mass range 100–600 u). Nitrogen was used as sheath gas. The capillary and APCI vaporizing temperature were maintained at 200 and 450 °C, respectively. The MS was calibrated with a myoglobin MRFA mixture as suggested by the supplier and tuned with quercetin ($[m+H]^+/z = 303$).

3. Results and discussion

3.1. Analysis of trichothecenes by high performance liquid chromatography–UV-detection

For evaluation of different extraction and purification methods for trichothecenes an LC–UV method was established in accordance to analytes chosen. Owing to the lack of UV chromophores of type A trichothecenes, B-type and macrocyclic forms were of main interest. Analytes were selected according to their polarity, i.e. very polar forms (DON), analytes of medium polarity (F-X) and lipophilic targets like Ve-A and Ro-A.

Initial LC separations were performed on a silica C18 stationary phase (Nucleosil 120-3 C18, 125 mm × 2 mm i.d., 3 μm, 120 Å) by applying a gradient elution of H_2O in organic solvent (ACN or MeOH). The mixture ACN–H_2O was firstly used as a mobile phase due to being the solvent of choice for trichothecenes [1], nevertheless no separation was achieved. Phosphoric acid or acetic acid were added to the mobile phase to lower peak tailing and therefore improving chromatographic performance, but neither this resulted in improvement. Therefore the mobile phase composition was changed to MeOH–H_2O, what finally provided baseline separation with high resolution ($R > 1.5$). Column temperature was set at 50 °C, which enabled elution with minimum peak tailing. The order of elution was starting with the highly polar NIV with four hydroxyl groups, followed by DON with three hydroxyl groups, F-X with three hydroxyl groups and an acetyl group and finally the two macrocyclic trichothecenes Ve-A and Ro-A with no free hydroxyl group, but a further ring of hydrocarbons. Due to these differences in polarity the gradient of the mobile phase had to be optimized, starting with high amount of H_2O (90% A) to guarantee baseline separation of NIV and DON and decreasing sharply to 42% A after the elution of B-trichothecenes to enable the elution of the macrocyclic ones. Especially the separation of macrocyclic targets was challenging and conditioned the long separation time for fully baseline separated peaks, a fundamental criteria for evaluating extraction systems by LC–UV.

Since B-trichothecenes were very sensitive to the volumetric ratio of MeOH, re-equilibrating of the column was strongly required to achieve reproducible separation. With the developed LC system the targeted five trichothecenes were separated within 22 min.

In order to assure robustness and reproducibility of the established method these parameters were achieved: Reproducibility was evaluated regarding to retention times. Twenty four replicate injections of the standard mixture gave highly consistent retention times for which coefficients of variation (CV) were not more than 1.2% for each mycotoxin (Table 1). The six-point calibration curves of each toxin were obtained by the linear regression analysis and revealed linearity with correlation coefficients $r^2 \geq 0.9802$. The detection limits, established as signal-to-noise (S/N) of 3 with CV less than 6.3% of three replicates, were between 1.41 and 3.47 pmol (Table 1). Precision assessments were generally carried out with concentrations being in the linearity range of calibration curve (6 and 24 μg/ml). Intra-day precision was determined by analysis of triplicate injections of indicated concentrations for each trichothecene. The intra-day CV was less than 3% for all tested trichothecenes. The inter-day precision was assessed by measuring the analytes at indicated concentrations for three different days, and the inter-day CV were less than 5% for all tested B-trichothecenes (Table 2).

Table 1
Reproducibility of retention times, calibration parameters, and detection limits of type B and macrocyclic trichothecenes by LC–UV, chromatographic conditions (see Section 2.1)

Trichothecenes		Retention time [min][a]		Calibration parameters[b]			Detection limit[c]	
Types		Mean value	CV [%]	a ($\times 10^4$)	b ($\times 10^4$)	Correlation coefficient	Amount [pmol]	CV [%]
B	Nivalenol	2.35	0.85	3.98	−6.18	0.9802	2,75	0.00
B	Deoxynivalenol	3.99	1.06	4.56	−2.30	0.9993	3.47	0.00
B	Fusarenone-X	8.88	1.13	4.76	−2.45	0.9990	3.39	0.00
Macrocyclic	Verrucarin-A	20.99	0.14	12.36	−9.54	0.9980	1.49	6.25
Macrocyclic	Roridin-A	21.61	0.14	11.25	−8.72	0.9982	1.41	6.25

[a] Retention time of 24 replicate injections, concentration range 0.5–30 μg/mL.
[b] Linear regression equation: $Y = aX + b$; Y, signal area; X, mycotoxins concentration [μg/mL]; a, slope; b, intercept on Y-axis.
[c] Detection limits, as signal-to-noise (S/N) of 3/1.

3.2. Extraction of trichothecences – solid phase extraction (SPE) using commercially available materials and liquid liquid extraction (LLE)

The clean-up procedure is a fundamental step prior analysis to remove co-eluting matrix components from the solution as completely as possible, particularly regarding different types of trichothecenes which attribute wide-ranging polarity. Among the trichothecenes determined in the present study the polarity was declined from type B and macrocyclic trichothecenes, respectively (Fig. 1). Standard mixtures in ACN–H_2O and in MeOH–H_2O were investigated for facilitating further purification approaches and subsequently reaching highest extraction efficiency. Six different purification procedures including (a) Mycosep 227 clean-up columns, (b) SPE on C-8 cartridges, (c) SPE on C-18 cartridges, (d) SPE on OASIS® HLB cartridges, (e) LLE using ethyl acetate and (f) LLE using diethyl ether were evaluated for B and macrocyclic trichothecenes by analyzing the purified extracts on the LC–UV system. ACN–H_2O (84:16, v/v) is normally recommended for further purification by Mycosep 227 columns as the crude extract can be concurrently followed on the Mycosep without modification. Concerning percentage of recovery, this sample clean-up method conferred a satisfactory efficiency for determination of type B (approximately 94%), but less for macrocyclic trichothecenes (Table 3).

Concerning SPE and LLE different volumetric ratios of MeOH–H_2O were evaluated concerning the extraction efficiency of trichothecenes providing optimal conditions with a MeOH–H_2O ratio of 20:80 (v/v). The effectiveness of the SPE cartridges was high for macrocyclic trichothecenes with all SPE cartridges, while only OASIS® HLB provided superior recovery for B-trichothecenes (Table 3). As the recovery for B-trichothecenes was enhanced from C-18 to C-8, the purification by C-4 cartridge, which is less hydrophobic than C-8 and C-18 cartridges, was additionally examined. However, the recovery was inferior for both B and macrocyclic trichothecenes (data not shown). Both of liquid–liquid partition approaches using ethyl acetate or diethyl ether provided varying recoveries either for B or macrocyclic trichothecenes with high CV values for three replicates (data not shown).

Obtained results were proved by extracting next to B type and macrocyclic trichothecenes also A type forms. For this the LC–UV method was slightly modified in order to analyse targets via LC–MS. Mycosep 227 clean-up columns and SPE using OASIS® HLB were evaluated for simultaneous determination of 8 trichothecenes (NIV, DON, F-X, VOL, DAS, T-2, Ve-A, Ro-A). The same result as already observed with B type and macrocyclic trichothecenes was obtained (Table 4). By the Mycosep clean-up method, the effectiveness for type A and B trichothecenes was high with recoveries ranged from 71.95 to

Table 2
Reproducibility of the LC–UV method for type B and macrocyclic trichothecenes, chromatographic conditions see (Section 2.1)

Trichothecenes		Concentration [μg/ml]	Coefficient of variation [%]	
Types			Intra-day precision	Inter-day precision
B	Nivalenol	6	2.16	3.91
		24	1.24	0.94
B	Deoxynivalenol	6	2.87	3.24
		24	1.45	3.23
B	Fusarenone-X	6	2.93	3.51
		24	1.61	4.63
Macrocyclic	Verrucarin-A	6	2.84	4.55
		24	1.43	4.52
Macrocyclic	Roridin-A	6	2.15	4.04
		24	1.95	3.75

Table 3
Effectiveness of the standard and new developed clean-up procedures and SPE materials for wheat sample spiked with 2 ppm of type B and macrocyclic trichothecenes by HPLC–UV, chromatographic conditions (see Section 2.1)

Trichothecenes		Percentage of recovery[a]					
Types		Solid-phase extraction (SPE)				SPE with DVB-GMA	
		Mycosep 227	Supelclean LC-18	Isolute C-8	OASIS™ HLB	60% DVB	80% DVB
B	Deoxynivalenol	93.84	ND	46.45	85.81	51.49	82.38
B	Fusarenone-X	94.52	ND	64.53	81.90	73.71	89.27
Macrocyclic	Verrucarin-A	1.24	87.95	89.97	97.35	85.67	81.77
Macrocyclic	Roridin-A	8.77	90.36	88.56	97.76	89.94	103.63

[a] Results are expressed as mean [%] ($n = 3$).

97.76%, whereas those for macrocyclic trichothecenes was very low. On the other hand, the effectiveness of OASIS® HLB was relatively better with recoveries ranging from 79.43 to 102.47%, except the extremely polar trichothecene, NIV, with recovery of 17.93%.

3.3. Preparation of poly(glycidyl methacrylate-divinylbenzene) (GMA-DVB) particles for the selective SPE of trichothecenes

The combination of a polar monomer with a rather lipophilic cross linker within the stationary phase is covering a wide range of polarity. Therefore GMA-DVB particles were produced under different conditions in order to evaluate their effectiveness for purification of trichothecenes. Special regard was placed on quality of educts, molar ratio of educts and stirring velocity. First of all the influence of DVB quality (60 and 80%) on the extraction performance of produced particles starting with a molar ratio of 2 to 1 (DVB:GMA) was investigated. Stirring velocity was set to maximum. Resulting particles were irregular in shape, owing to the stirring during the production process. Particles produced with 60% DVB resulted in absolute extraction recoveries of 51–90%. In relation to Oasis® HLB, this corresponds to 60% for the polar analyte DON and approximately 90% for the more lipophilic analytes F-X, Ve-A and Ro-A. In contrary, particles produced with 80% DVB resulted with equivalent extraction performance as Oasis® HLB (Table 3).

Studying the influence of the monomeric ratio on the extraction quality of GMA-DVB particles showed clear tendencies (Fig. 2). Changing the actual composition to a higher content of GMA (1:1 and 1:2; DVB:GMA) resulted in significant worse extraction efficiencies. On the other hand increasing the DVB content did not further improve the extraction efficiency.

In a further approach the influence of stirring on the particle size and on the extraction performance was evaluated. Synthesis of the material without stirring during the polymerization process resulted in homogenous spherical particles [46]. Extraction efficiency of these homogenous particles was significantly lower in comparison to the irregular shaped ones synthezised, especially for macrocylic trichothecenes. Comparing the surface area of materials produced under different conditions resulted in 1.82 m^2/g for homogeneous spherical particles [46] and 7.92 m^2/g for irregular particles.

Summing up all optimization processes, best results could be obtained using a DVB:GMA ratio of 2:1, using DVB with a purity grade of 80% and producing irregular particles by stirring.

The obtained results proved the performance of the newly synthesized material delivering same and partially higher extraction efficiencies as commercially available material such as Oasis® HLB (Table 3). The high performance of the GMA-DVB in a wide range of polarity is in well agreement with already published results from Mohamed et al. [48], where NSAIDS were investigated and 10% higher extraction efficiencies in comparison to Oasis® HLB were obtained.

Table 4
Effectiveness of the clean-up procedures for wheat sample spiked with 2 ppm of simple and macrocyclic trichothecenes by LC–APCI–MS, chromatographic conditions (see Section 2.1)

Trichothecenes		Percentage of recovery[a]	
Types		Mycosep 227	OASIS® HLB
B	Nivalenol	71.95	17.93
B	Deoxynivalenol	78.01	79.43
B	Fusarenone-X	95.76	97.73
A	Verrucarol	85.90	93.45
A	Diacetoxyscri penol	97.76	99.99
A	T-2 toxin	94.04	83.97
Macrocyclic	Verrucarin-A	2.25	83.39
Macrocyclic	Roridin-A	39.90	102.47

[a] Results are expressed as mean [%] ($n = 2$).

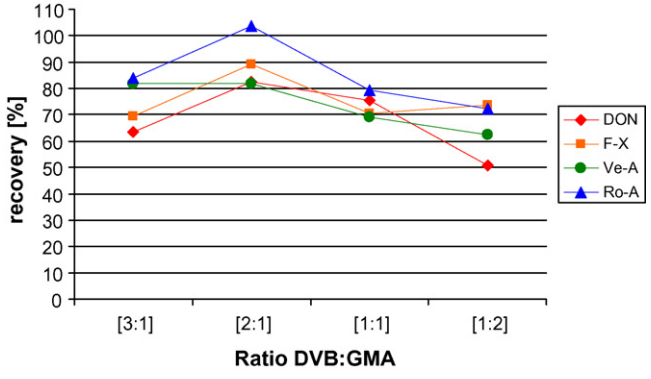

Fig. 2. Influence of the monomeric ratio of DVB and GMA on the extraction performance of investigated compounds.

4. Conclusion

Aim of the presented study was the evaluation of extraction techniques for trichothecenes on the basis of a chromatographic determination system. For this purpose an LC–UV and LC–MS method was established. Afterwards different extraction systems on the basis of LLE and SPE (silica C18, silica C8, silica C4; Oasis® HLB; Mycosep 227) were evaluated and in this coherence compared to a newly produced irregular material (poly(glycidyl methacrylate-divinylbenezene)). Results showed clearly that Oasis® HLB and the synthesized GMA-DVB delivered highest extraction efficiencies for investigated trichothecenes in comparison to other SPE materials.

Acknowledgements

G. Stecher and C.W. Huck would like to thank University of Innsbruck (Nachwuchsförderung 2004) and the Technology Grant Southeast Asia (Project No.1202/1/EZA/2001, Austria) for support of present work.

References

[1] R. Krska, S. Baumgartner, R. Josephs, Fresenius J. Anal. Chem. 371 (2001) 285.
[2] T. Yoshisawa, in: J.E. Smith, R.S. Henderson (Eds.), Mycotoxins and Animal Foods, CRC Press, Boca Raton, FL, 1991, p. 423.
[3] J.D. Miller, in: J.D. Miller, H.L. Trenholm (Eds.), Mycotoxins in Grains, Compounds Other than Aflatoxins, Eagan Press, St. Paul, MN, 1994, p. 19.
[4] J.J. Park, F.S. Chu, JAOAC Int. 79 (1996) 465.
[5] Y. Ueno, Trichothecenes: Chemical, Biological and Toxicological Aspects, Developments in Food Science, Vol. 4, Elsevier, Amsterdam, 1983, p. 1 and 135.
[6] F. Kotal, K. Holadová, J. Hajslová, J. Poustka, Z. Radová, J. Chromatogr. A 830 (1999) 219.
[7] W. Langseth, T. Rundberget, J. Chromatogr. A 815 (1998) 103.
[8] U. Berger, M. Oehme, F. Kuhn, J. Agric. Food Chem. 47 (1999) 4240.
[9] T. Tuomi, L. Saarinen, K. Reijula, Analyst 123 (1998) 1835.
[10] H. Kurata, Y. Ueno, Toxicogenic Fungi. Their Toxinx and Health Hazards, Developments in Food Science, Vol. 7, Elsevier, Amsterdam, 1984, p. 118.
[11] Z. Radová, K. Holadová, J. Hajslová, J. Chromatogr. A 82 (1998) 259.
[12] D.B. Prelusky, B.A. Rotter, R.G. Rotter, in: J.D. Miller, H.L. Trenholm (Eds.), Mycotoxins in Grains, Compounds Other than Aflatoxins, Eagan Press, St. Paul, MN, 1994, p. 359.
[13] G.A. Lombaert, Adv. Exp. Med. Biol. 504 (2002) 141.
[14] C.J. Mirocha, E. Kolaczkowski, W. Xie, H. Yu, H. Jelen, J. Agric. Food Chem. 46 (1998) 1414.
[15] A. Visconti, A. Bottalico, Chromatographia 17 (1983) 97.
[16] R. Schmidt, K. Dose, J. Anal. Toxicol. 8 (1984) 43.
[17] D.R. Lauren, R. Greenhalgh, JAOAC Int. 70 (1987) 479.
[18] A. Sano, S. Matsutani, M. Suzuki, S. Takitani, J. Chromatogr. 410 (1987) 427.
[19] J. Weingaertner, R. Krska, W. Praznik, M. Grasserbauer, H. Lew, Fresenius J. Anal. Chem. 357 (1997) 1206.
[20] R.D. Josephs, R. Krska, M. Grasserbauer, J.A.C. Broekaert, J. Chromatogr. A 795 (1998) 297.
[21] M. Schollenberger, U. Lauber, H. Terry Jara, S. Suchy, W. Drochner, H.M. Müller, J. Chromatogr. A 815 (1998) 123.
[22] T. Tanaka, A. Yoneda, S. Inoue, Y. Sugiura, Y. Ueno, J. Chromatogr. A 882 (2000) 23.
[23] M. Jiménez, J.J. Mateo, R. Mateo, J. Chromatogr. A 870 (2000) 473.
[24] Y. Sugita-Konsihi, T. Tanaka, S. Tabata, M. Nakajima, M. Nouno, Y. Nakaie, T. Chonan, M. Aoyagi, N. Kibune, K. Mizuno, E. Ishikuro, N. Kanamaru, M. Minamisawa, N. Aita, M. Kushiro, K. Tanaka, K. Takatori, Mycopathologia 161 (2006) 239.
[25] H. Cohen, B. Boutin-Muma, J. Chromatogr. 595 (1992) 143.
[26] A. Visconti, J. Chelkowski, A. Bottalico, Mycotoxin Res. 2 (1986) 59.
[27] T. Krishnamurthy, D.J. Beck, R.K. Isensee, J. Chromatogr. 469 (1989) 209.
[28] E. Rajakylä, K. Laasasenaho, P.J.D. Sakkers, J. Chromatogr. 384 (1987) 391.
[29] L.M. Cahill, S.C. Kruger, B.T. McAlice, C.S. Ramsey, R. Prioli, B. Kohn, J. Chromatogr. A 859 (1999) 23.
[30] R.P. Huopalahti, J. Ebel Jr., J.D. Henion, J. Liq. Chrom. Rel. Technol. 20 (1997) 537.
[31] R. Krska, J. Chromatogr. A 815 (1998) 49.
[32] L. Czerwiecki, H. Giryn, Pol. J. Food Nutr. Sci. 44 (1994) 111.
[33] C. Fernandez, M.E. Stack, S.M. Musser, JAOAC Int. 77 (1994) 253.
[34] M.W. Trucksess, M.T. Flood, M.M. Mossobu, S.W. Page, J. Agric. Food Chem. 35 (1987) 445.
[35] K.F. Neilsen, U. Thrane, J. Chromatogr. A 929 (2001) 75.
[36] M. Jestoi, A. Ritieni, A. Rizzo, J. Agric. Food Chem. 52 (2004) 1464.
[37] C. Dall'Asta, S. Sforza, G. Galaverna, A. Dossena, R. Marchelli, J. Chromatogr. A 1054 (2004) 389.
[38] F. Berthiller, R. Schuhmacher, G. Buttinger, R. Krska, J. Chromatogr. A 1062 (2005) 209.
[39] M. Klotzel, B. Gutsche, U. Lauber, H.U. Humpf, J. Agric. Food Chem. 16 (2005) 8904.
[40] M. Klotzel, U. Lauber, H.U. Humpf, Mol. Nutr. Food Res. 50 (2006) 261.
[41] M. Sulyok, F. Berthiller, R. Krska, R. Schuhmacher, Rapid Commun. Mass Spectrom. 20 (2006) 2649.
[42] B. Delmulle, S. De Saeger, A. Adams, N. De Kimpe, C. Van Peteghem, Rapid Commun. Mass Spectrom. 20 (2006) 771.
[43] R.D. Smith, H.R. Udseth, B.W. Wright, J. Chromatogr. Sci. 23 (1985) 192.
[44] E. Usleber, E. Märtlbauer, R. Dietrich, G. Terplan, J. Agric. Food Chem. 39 (1991) 2091.
[45] E. Schneider, R. Dietrich, E. Märtlbauer, E. Usleber, G. Terplan, Food Agric. Immunol. 3 (1991) 185.
[46] S. Zhang, X. Huang, N. Yao, Cs. Horváth, J. Chromatogr. A 948 (2002) 193.
[47] N.H. Aprilita, C.W. Huck, R. Bakry, I. Feuerstein, G. Stecher, S. Morandell, H.-L. Huang, T. Stasyk, L.A. Huber, G.K. Bonn, J. Proteome Res. 4 (2005) 2312.
[48] S. Mohamed, G. Stecher, W.M. Stöggl, R. Bakry, P. Zaborski, C.W. Huck, N.M. El Kousy, G.K. Bonn, Curr. Med. Chem. 12 (2005) 763.

Available online at www.sciencedirect.com
ScienceDirect
Talanta 73 (2007) 387–393
Talanta
www.elsevier.com/locate/talanta

Selective extraction and transport of copper(II) with new alkylated pyridinecarboxylic acid derivatives

Tsutomu Tasaki, Tatsuya Oshima, Yoshinari Baba *

Department of Applied Chemistry, Faculty of Engineering, University of Miyazaki, 1-1Gakuen-Kibanadai Nishi, Miyazaki 889-2192, Japan

Received 30 January 2007; received in revised form 3 April 2007; accepted 3 April 2007
Available online 7 April 2007

Abstract

Two kinds of *N*-(6-alkylamido)-2-pyridine carboxylic acid with a pyridine moiety and a carboxylic acid as chelating ligands were newly synthesized for the selective extraction and the transport of copper(II) from aqueous solution. Liquid–liquid extraction was carried out to examine the extraction ability of extractants with metal ions. The selectivity for the metal ions with *N*-6-(2-ethylhexylamido)-2-pyridine carboxylic acid (EHPA) was in the following order: Cu(II)≫Zn(II) ≈ Pb(II) ≈ Ni(II) ≈ Co(II) > Cd(II) > Mn(II). All metals tested in this study were selectively extracted at a lower pH by 2–3 units compared with commercial available alkyl carboxylic acids such as naphthenic acid and Versatic 10. The extraction equilibria of copper(II) were measured by a batchwise method at 303 K with EHPA and *N*-6-(*t*-dodecylamido)-2-pyridinecarboxylic acid (*t*-DAPA). Copper(II) was extracted as a 1:2 complex according to the following reaction: $Cu^{2+} + 2(\overline{HR})_2 = \overline{CuR_2 2HR} + 2H^+$. The extraction equilibrium constant, K_{ex} was evaluated and the values were found to be 1.13 and 0.31 for EHPA and *t*-DAPA, respectively. It was demonstrated that *t*-DAPA was very stable to be incorporated into a polymer inclusion membrane (PIM) consisting of cellulose triacetate (CTA) as a base polymer and 2-nitrophenyl octylether (NPOE) as a plasticizer. This novel PIM containing *t*-DAPA as a carrier exhibited an excellent copper(II) transport characteristic and a high selectivity for copper(II) over cadmium(II) from aqueous solution.

Keywords: Polymer inclusion membrane; Alkylated pyridinecarboxylic acid derivatives; Active transport of copper(II); Liquid–liquid extraction

1. Introduction

Solvent extraction using chelating reagents has been widely applied in the fields of analytical and separation technology [1]. A large number of commercial chelating extractants are available and used in solution in organic diluents such as kerosene. The large-scales of solvent extraction are successfully utilized, but the use of high volume of volatile organic diluents poses considerable environmental and health risks for industrial use. An alternative approach for metal separation and concentration, which offers significant advantages over conventional solvent extraction methods and alleviates the problems mentioned above, is based on the use of liquid membrane (LM). The type of LM that has been used successfully so far is supported liquid membrane (SLM) [2,3]. In the SLMs the organic phase containing extractant and diluent is impregnated within the pores of a solid, inert supported phase and retained there by capillary forces. In previous studies, it was demonstrated that a SLM pilot plant could be applied for recovery of copper [4,5]. However, SLMs show an inherent lack of stability caused by the loss of extractant and solvent from the pore of liquid membrane into the aqueous phase [6,7]. The instability of SLMs has become the major obstacle for industrialization of the process.

In recent years, a novel type of liquid membrane, commonly called polymer inclusion membrane (PIM) has been developed to improve membrane stability [8–11]. The PIMs are formed by casting a polymer matrix such as cellulose triacetate (CTA) and poly vinyl chloride (PVC) containing an extractant and a plasticizer to form a thin and stable film. The resulting self-supporting homogenous membranes containing extractants, which complex preferentially with the metal ions of interest and act as mobile carriers, can pump these metal ions from more dilute to more concentrated solutions. It has been shown recently that PIMs consisting of liquid extractants such as hydroxyaryloximes (LIX® reagents) and di(2-ethylhexyl) phosphoric acid (D2EHPA) immobilized in the CTA polymer matrix can be used successfully for extraction of copper(II) from acetic acid solutions [12,13]. These types of membrane are characterized by

* Corresponding author. Tel.: +81 985 58 7307; fax: +81 985 58 7323.
E-mail address: t0g202u@cc.miyazaki-u.ac.jp (Y. Baba).

0039-9140/$ – see front matter © 2007 Elsevier B.V. All rights reserved.
doi:10.1016/j.talanta.2007.04.001

sufficient mechanical strength to make them self-supporting and a lower rate of leaching of the liquid extractant from the membrane into the aqueous solution. Since the efficiency of PIMs depends mainly on the extraction capability of the carrier, the use of an appropriate extractant as a carrier is very important factor to fabricate a PIM system. Several kinds of commercial extractants such as 2-hydroxy-5-nonlylacetophenone oxime (LIX® 84-I), quinolines (Kelex 100) and D2EHPA have been used in PIMs to date [14–16]. However, LIX® reagents with copper(II), generally, have a slow reaction rate while Kelex 100 and D2EHPA have a low copper(II) selectivity over the other divalent metal ions. From the above reasons, we are interested in the design and synthesis of a novel extraction reagent that have high potential applications in the fields of hydrometallurgy and analytical chemistry [17,18].

The aim of this present work is to develop a novel PIM for the highly selective extraction and rapid transport of copper(II) using new alkylated pyridinecarboxylic acid derivatives as a carrier. The synthesis of *N*-(6-alkylamido)-2-pyridine carboxylic acid derivatives and evaluation of their extraction ability and transport characteristic for the separation of copper(II) over cadmium(II) from aqueous solution were reported in this paper.

2. Experimental

2.1. Materials and analysis

Analytical-grade copper(II), zinc(II), nickel(II), cobalt(II), lead(II), cadmium(II), manganese(II) and iron(III) nitrates (Wako Pure Chemical Ind. Ltd.) were used to prepare the test solution of the respective metals. The Primene 81-R® (Rohm and Haas Co. Ltd.) was used as one of the raw material for the synthesis of the extractant. Cellulose triacetate (CTA, acetyl content 43.6 wt.%, Mw = 72–74 kDa, Aldrich) was used as the polymer support for the preparation of membranes. 2-Nitrophenyl octylether (NPOE, >99.0% purity, Dojindo Laboratory) was used as plasticizer. Analytical TLC was performed using Merck prepared plates (silica gel 60 F254 on aluminium). Flash chromatography separations were performed on Merck Silica Gel 60 (70–230 Mesh). Nuclear magnetic resonance spectra were recorded on a Bruker AC250P for ^{1}H NMR (250 MHz) and for ^{13}C NMR (62.8 MHz) in $CDC1_3$ with TMS as internal standard for the identification of products.

2.2. Synthesis of N-6-(2-ethylhexylamido)-2-pyridinecarboxylic acid ester (EHPE)

A mixture of 2,6-pyridinecarboxylic acid di methyl ester (9.50 g, 0.048 mol), 2-ethylhexyl amine (6.5 g, 0.05 mol) and triethylamine (4.0 g, 0.05 mol) in chloroform (200 ml) was refluxed for 48 h at 342 K in Scheme 1. The reaction mixture was then added to chloroform and neutralized with aqueous sodium bicarbonate solution, followed by washing with 1.0 M HC1 for the removal of unreacted amine. The organic phase was washed with water several times and then dried over anhydrous $MgSO_4$. After decantation, the chloroform was evaporated in vacuo. The crude product was purified by chromatography on silica gel with *n*-hexane/ethyl acetate (5:1) as eluent to afford a white liquid with 59% yield. ^{1}H NMR (250 MHz, $CDC1_3$) δ 8.41 (dd, J = 7.7, 1.2 Hz, 1H), 8.23 (dd, J = 7.7, 1.2 Hz, 1H), 8.18 (t, 1H, NH), 8.03 (t, J = 7.7 Hz, 1H), 4.01 (s, 3H, OMe), 3.49 (t, 2H), 1.89 (m, H), 1.61 (m, 8H), 0.97 (m, 6H). ^{13}C NMR (62.8 MHz, $CDC1_3$) δ 165.0, 163.4, 150.3, 146.4, 138.4, 127.0, 125.3, 52.8, 42.5, 39.5, 31.0, 28.8, 24.3, 22.9, 14.0, 10.8.

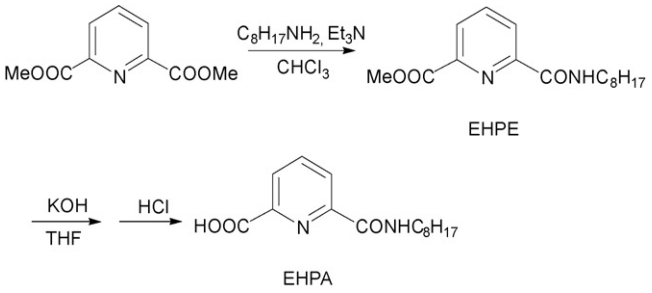

Scheme 1. Synthesis route for *N*-6-(2-ethylhexylamido)-2-pyridinecarboxylic acid (EHPA).

2.3. Synthesis of N-6-(2-ethylhexylamido)-2-pyridinecarboxylic acid (EHPA)

A mixture of EHPE (7.8 g, 0.024 mol) and 0.5 M KOH (50 ml) was refluxed in THF (150 ml) for 3 h at 332 K in Scheme 1. The reaction mixture was filtered and the solvent was evaporated in vacuo. The residue was dissolved in chloroform, washed with distilled water several times and then dried over anhydrous $MgSO_4$. After decantation, the chloroform was evaporated in vacuo to produce a white solid. The resulting solid was recrystallized from *n*-hexane to afford a white crystal with 98% yield.^{1}H NMR (250 MHz, $CDC1_3$) δ 8.59 (t, 1H, NH), 8.49 (dd, J = 7.8, 1.2 Hz, 1H), 8.38 (dd, J = 7.8, 1.2 Hz, 1H), 8.13 (t, J = 7.8 Hz, 1H), 7.27 (br, 1H, OH), 3.43 (t, 2H), 1.60 (m, 1H), 1.43 (m, 8H), 0.89 (m, 6H). ^{13}C NMR (62.8 MHz, $CDC1_3$) δ 165.3, 163.6, 149.6, 145.0, 139.9, 126.9, 126.3, 43.0, 39.4, 30.9, 28.7, 24.1, 22.9, 24.1, 22.9, 13.9, 10.7.

2.4. Synthesis of N-6-(t-dodecylamido)-2-pyridinecarboxylic acid (t-DAPA)

In the first step, a mixture of 2,6-pyridinecarboxylic acid ester (4.0 g, 0.02 mol), Primene 81-R® (4.0 g 0.02 mol) and sodium methoxide (1.0 g, 0.02 mol) in toluene (200 ml) was refluxed for 12 h at 342 K in Scheme 2. The reaction mixture was filtered and then added to chloroform. The solution was neutralized with aqueous sodium bicarbonate solution, followed by washing with 1.0 M HCl. The crude product was purified by chromatography on silica gel with *n*-hexane/ethyl acetate (6:1) as an eluent to afford a yellow liquid. In the second step, a mixture of *N*-6-(*t*-dodecylamido)-2-pyridinecarboxylic acid ester (3.8 g, 0.024 mol) and 0.5 M KOH (50 ml) was refluxed in THF (150 ml) for 3 h at 332 K. The crude product was treated by the same method as for EHPA. The fine product was washed with cold *n*-hexane and dried in vacuo to provide viscous yellow oil with 70% yield.^{1}H NMR (250 MHz, $CDC1_3$) δ 8.37 (dd,

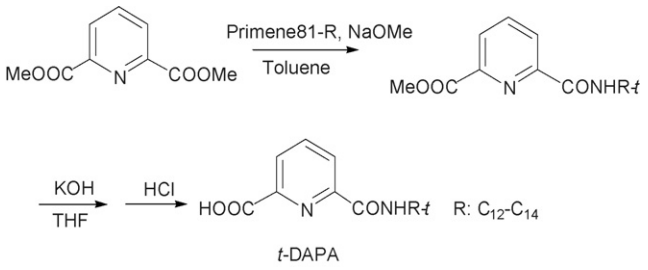

Scheme 2. Synthesis route for *N*-6-(*t*-dodecylamido)-2-pyridinecarboxylic acid (*t*-DAPA).

J = 7.8, 1.2 Hz, 1H), 8.21 (d, *J* = 7.7 Hz, 1H), 8.18-8.00 (br, 1H, NH), 8.01 (t, *J* = 7.7 Hz, 1H), 7.25 (br, 1H, OH), 2.04 (m, 2H), 1.51 (m, 11H), 0.94 (m, 12H). ^{13}C NMR (62.8 MHz, $CDC1_3$) δ 165.0, 162.2, 150.9, 146.2, 139.4, 126.6, 124.7, 52.7, 29.3, 26.4, 24.1-22.5, 14.2, 8.1.

2.5. Liquid–liquid extraction

To evaluate extraction ability of synthesized extractants, liquid–liquid extraction was carried out with various metal ions. A 1.0 mM aqueous metal ions solution in 1.0 M ammonium nitrate solution with pH adjusted with concentrated HNO_3 or NH_3 was prepared. In a 30 ml L-form tube, equal volume (10 ml) of the aqueous metal solution and extractant (0.01, 0.05 and 0.1 M) in toluene were shaken mechanically for 24 h at 303 ± 0.1 K. After phase separation, the pH of the aqueous solution was measured with pH meter (HM-30S, DKK-TOA Co. Ltd., Japan). The metal ion concentration in the aqueous solution was determined by atomic absorption spectrophotometry (AAS, Perkin-Elmer Annalyst 100, Japan). The metal ion concentration in organic phase was calculated from the mass balance between aqueous and organic phases. A percentage extraction (% extraction) and metal distribution ratio (*D*) were calculated according to Eqs. (1) and (2), respectively.

$$\%\text{extraction} = \frac{[M]_{\text{org}}}{[M]_{\text{aq,init}}} \times 100 \quad (1)$$

$$D = \frac{[M]_{\text{org}}}{[M]_{\text{aq}}} \quad (2)$$

where $[M]_{\text{aq,init}}$ represents the initial concentration of metal ion in the aqueous phase. $[M]_{\text{aq}}$ and $[M]_{\text{org}}$ are the total concentrations of metal ion in the aqueous and organic phases after equilibrium, respectively.

2.6. Membrane preparation

The polymer inclusion membrane (PIM) was prepared according to the reported procedure [19]. Solution of cellulose triacetate was prepared by dissolving CTA (0.08 g) in chloroform (10 ml). Another solution in chloroform (10 ml) containing NPOE (0.15 g) and *t*-DAPA (0.08 g) was prepared. A casting solution was prepared by mixing the two solutions, and then homogenizing for 30 min, and casting onto a leveled 8-cm diameter Petri dish. Chloroform was allowed to evaporate slowly over 24 h as to obtain a polymer membrane with a smooth surface. After the evaporation of chloroform, the obtained membrane was carefully peeled off the dish. The resulting membrane was completely transparent and exhibited a good mechanical strength. The identification of NPOE and *t*-DAPA contained in the membrane was preformed by FT-IR (Perkin-Elmer FT-IR 300, Japan) and TG-DTA (SSC-5200, Seiko Instruments Inc., Japan) analysis. Measurement on the membrane containing NPOE and *t*-DAPA shows additional peaks at 1608, 1671 and 2902 cm^{-1} corresponding to NO_2, C=O and CH_2 bonds, respectively. The average membrane thickness measured by optical microscope (LH50A, Olympus, Japan) with calibrated lens (Carton Optical Ind. Ltd., Japan) was 60.2×10^{-6} m.

2.7. Copper(II) transport study with PIM containing t-DAPA

Membrane transport studies were conducted in a two compartment cell that was thermostated at 303 ± 0.1 K in a water bath. Each compartment had a volume capacity of 100 ml. The effective membrane surface area was 1.25×10^{-3} m^2. The membrane was sandwiched between the two compartment cells. The stirring rates in both the feed and receiving solutions were measured with digital tachometer (HT-4100, Ono Sokki Co., Ltd., Japan) and each solution was stirred at a constant rate throughout each experiment. The initial conditions used were a feed solution of 0.3 mM copper(II) in 0.1 M 2-[4-(2-hydroxyethyl)-l-piperazinyl]ethanesulfonic acid (HEPES) buffer solution adjusted to pH 3.20 with concentrated HNO_3 solution and a receiving solution of 1.0 M HC1. The extraction of copper(II) was monitored by taking 1.0 ml aliquots from each compartment at preselected time intervals and determining the metal concentration by AAS.

2.8. Separation of copper-(II) from cadmium(II) with PIM containing t-DAPA

Transport experiment involving the separation of copper(II) from cadmium(II) was conducted to examine the separation characteristics of PIM containing *t*-DAPA as a carrier. This experiment was carried out similarly to the copper(II) transport experiment outlined above. The feed solution of 0.3 mM copper(II) and 1.0 mM cadmium(II) in 0.1 M HEPES buffer solution adjusted to pH 3.20 with concentrated HNO_3 and a receiving solution of 1.0 M HCl were used in this study. The concentration of each metal ion in the feed and the receiving solution was determined by AAS.

3. Results and discussion

3.1. Liquid–liquid extraction of copper-(II) with EHPE and EHPA

In order to evaluate the extraction ability of the extractants, liquid–liquid extraction of copper(II) was carried out with both intermediate product *N*-6-(2-ethylhexylamido)-2-pyridinecarboxylic acid ester and final product *N*-6-(2-

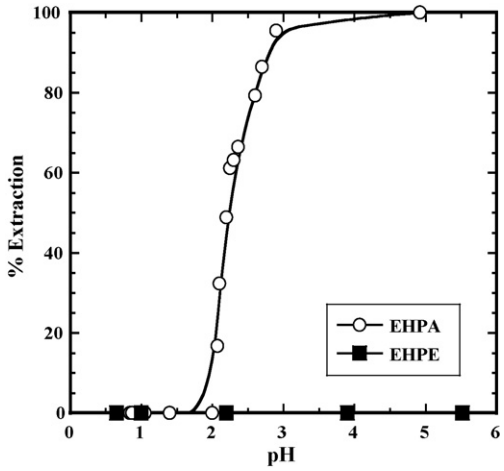

Fig. 1. Effect of pH on the percentage extraction of Cu(II) with EHPA and EHPE.

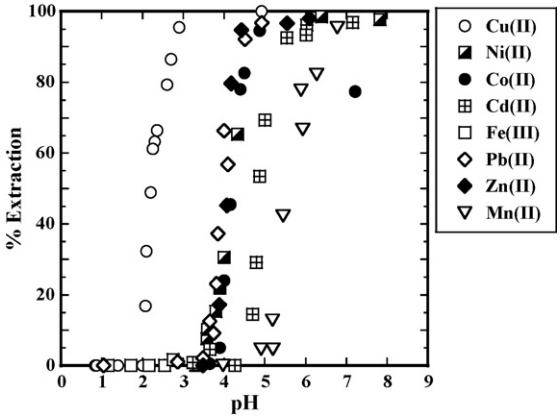

Fig. 2. Effect of pH on the percentage extraction of metal ions with EHPA. $[M] = 1$ mM, $[\overline{HR}] = 0.01$ M.

ethylhexylamido)-2-pyridinecarboxylic acid. Fig. 1 shows the effect of pH on the percentage extraction of copper(II) with EHPA and EHPE. It can be seen that copper(II) was extracted with EHPA from pH 2.0 in 1.0 M ammonium nitrate solution. However, copper(II) was not extracted with EHPE in all pH regions tested in this study. These results suggest that EHPA with pyridine moiety and carboxylic acid as chelating ligands plays an important role in complex formation with copper(II). Based on the experimental results, it is likely that the alkylamide group of EHPA has no direct participation for the complex formation with copper(II). This observation agrees with those reported on the *N*-alkyl-pyridinecarboxamides in the solvent extraction studies, i.e., copper(II) in chloride media was not extracted with *N*-octyl-3-pyridinecarboxamide [20,21]. From the experimental result obtained in Fig. 1, it is assumed that EHPA complexes with copper(II) so as to form five-membered ring with pyridine moiety and carboxylic acid of EHPA.

3.2. Liquid–liquid extraction of various metal ions with EHPA

Based on the result of Fig. 1, EHPA was further investigated for the extraction with various divalent metal ions and iron(III). Fig. 2 shows the effect of pH on the percentage extraction of various metal ions with EHPA. A 10 vol.% 2-ethyl-l-hexanol was added to the organic phase as a modifier to avoid a formation of the third phase between aqueous and organic phase. As seen in Fig. 2, copper(II) was extracted with EHPA at lower pH by 2–4 units compared with other divalent metal ions such as nickel(II), zinc(II), lead(II), cadmium(II) and manganese(II). There was 95.5% extraction of copper(II) with EHPA at equilibrium pH 2.90 while there was no extraction of other divalent metal ions and Fe(III) with EHPA. These results suggest that the separation of copper(II) over other metal ions could be established at a low pH in acidic leach solution. Furthermore, it was found that all metals tested in this study were selectively extracted with EHPA at a lower pH by 2–3 units compared with commercial available alkyl carboxylic acids such as naphthenic acid and Versatic 10 [22–24]. The finding of this result appears to reflect the electron-withdrawing effect of pyridine, causing lower the pK_a of carboxylic acid on EHPA. It was observed that iron(III) was not extracted by EHPA at all pH region tested in this study. This is very promising result from the viewpoint of copper hydrometallurgical application. Extraction order for divalent metal ions with EHPA was $Cu(II) \gg Zn(II) \approx Pb(II) \approx Ni(II) \approx Co(II) > Cd(II) > Mn(II)$. This selectivity can be attributed to the high affinity of carboxylic group and pyridine nitrogen atom with divalent metal ions such as copper(II), zinc(II) and nickel(II) as evidence from Pearson's HSAB (hard, soft, acid, base) concept [25,26]. Moreover, the high selectivity of EHPA toward copper(II) over other divalent metal ions can be explained by the formation of a neutral complex in the organic phase where copper(II) should be present in tetra-coordinate geometry. It is known that copper(II) can form these complexes, where other metal ions, such as zinc(II), cobalt(II) and manganese(II) preferably form octahedral-coordinate complexes [27,28].

3.3. Extraction equilibrium of copper(II) with EHPA

The extraction data of copper(II) presented in Fig. 2 was further analyzed as a function of equilibrium pH variations at fixed concentration of EHPA (0.01, 0.05, 0.1 M in toluene) to examine an extraction equilibrium of copper(II) with EHPA. Fig. 3 shows the effect of pH on the distribution ratio of copper(II) with EHPA. The plots of log D versus pH were liner with slope of 2.0, indicating that the release of 2 mol of hydrogen ions from the extractant into the aqueous phase during the Cu(II)-EHPA complex formation and metal transfer to the organic phase. Similarly, the extraction data as a function of extractant variation at fixed pH was analyzed to draw the plots of log D versus log $[\overline{HR}]$. Fig. 4 shows the effect of dimmer concentration of extractant on the distribution ratio of copper(II) with EHPA (HR). It can be seen that that 2 mol of extractant were involved in metal complex formation with copper(II). Based on the above results and taking into consideration that EHPA exists in dimeric form in toluene, the extraction equilibrium of copper(II) with EHPA can

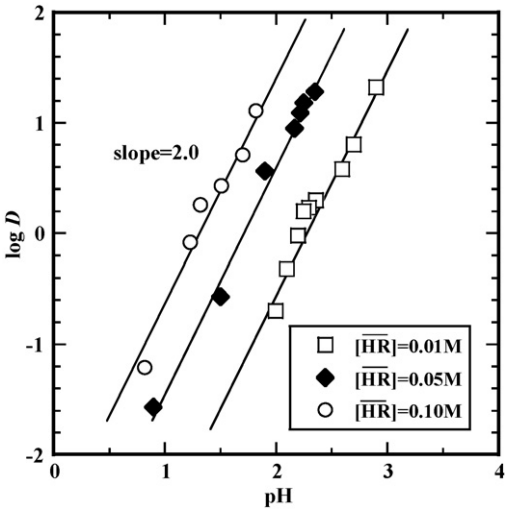

Fig. 3. Effect of pH on the distribution ratio of Cu(II) with EHPA.

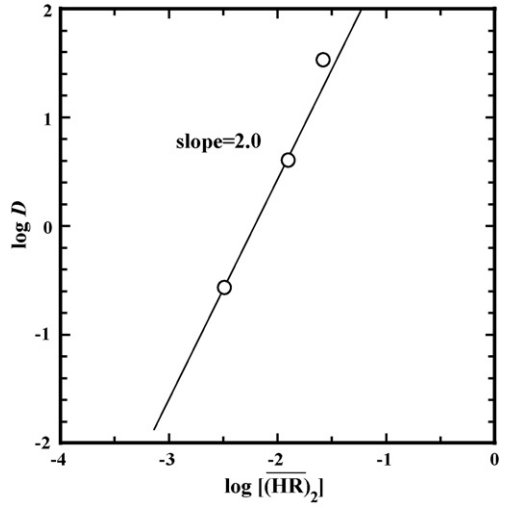

Fig. 4. Effect of dimmer concentration of extractant on the distribution ratio of Cu(II) with EHPA at pH = 2.0.

be expressed as follows:

$$Cu^{2+} + 2(\overline{HR})_2 \rightleftarrows \overline{CuR_2 2HR} + 2H^+ \quad (3)$$

where the bar denotes species in organic phase.
The extraction equilibrium constant K_{ex} is given by Eq. (4):

$$K_{ex} = \frac{[\overline{CuR_2 2HR}][H^+]^2}{[(\overline{HR})_2]^2[Cu^{2+}]} \quad (4)$$

The mass balance equation for $(\overline{HR})_2$ is given by following expression:

$$[(\overline{HR})_2]_T = [(\overline{HR})_2] + 2[\overline{CuR_2 2HR}] \quad (5)$$

Also, distribution ratio of copper(II) between organic and aqueous phase is defined according to

$$D = \frac{[\overline{CuR_2 2HR}]}{[Cu]_{total}} \quad (6)$$

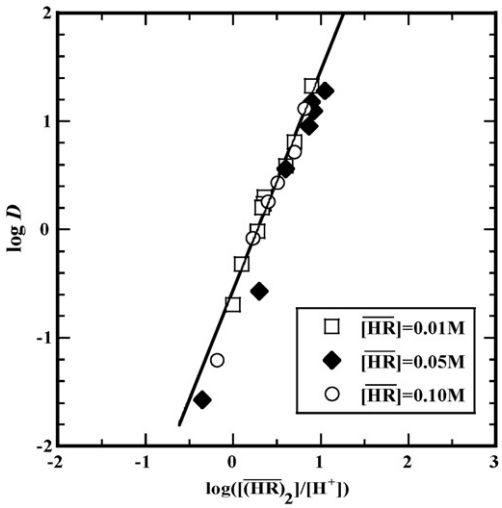

Fig. 5. $\log([(\overline{HR})_2])/[H^+])$ vs. distribution ratio of Cu(II) with EHPA.

Hence, by combining Eqs. (4) and (6), we obtained the following equation in its logarithmic form:

$$\log D = 2 \log[(\overline{HR})_2] + 2\,pH + \log K_{ex} \quad (7)$$

To determine K_{ex}, the experimental results are plotted in Fig. 5 according to Eq. (7). The K_{ex} was obtained from the intercept of the straight line with the ordinate in Fig. 5. The extraction equilibrium constant was determined to be $K_{ex} = 1.13$. The solid line in Fig. 5 is the theoretical line based on Eq. (7). The theoretical line is good agreement with the experimental results.

3.4. Synthesis of t-DAPA from Primene 81-R® for the preparation of PIM

N-6-(*t*-dodecylamido)-2-pyridinecarboxylic acid (*t*-DAPA) was synthesized from commercially available Primene 81-R® to increase the hydrophobicity of the extractant for a PIM system. The Primene 81-R® is a primary aliphatic amine with highly branched alkyl chains and consists of mixtures of isomeric amines in the $C_{12–14}$ range. We expected that solubility of the extractant into organic solvents was enhanced by introducing highly branched alkyl chains on the amide group of the extractant. Liquid–liquid extraction of copper(II) was carried out with *t*-DAPA using only toluene as a diluent to compare the extraction ability with EHPA which has 2-ethylhexyl as a branched alkyl chain. Fig. 6 shows the effect of pH on the percentage extraction of copper(II) with EHPA and *t*-DAPA. As seen in Fig. 6, copper(II) extraction with *t*-DAPA was very similar to that with EHPA even though no modifier was added to *t*-DAPA. The values of log $P_{cta/w}$ for extractants which indicate *n*-octanol/water partition coefficients were calculated from CS ChemDraw Ultra® to determine solubility characteristics [29]. The values of log $P_{cta/w}$ were found to be 4.46 and 3.14 for *t*-DAPA and EHPA, respectively. The value of log $P_{cta/w}$ for *t*-DAPA was higher than that for EHPA, suggesting that the introducing highly branched alkyl chains on amide group improved the solubility of extractant into the organic solvent. This finding agrees with the experimental results showing improved solubility of *t*-DAPA into plasticizers

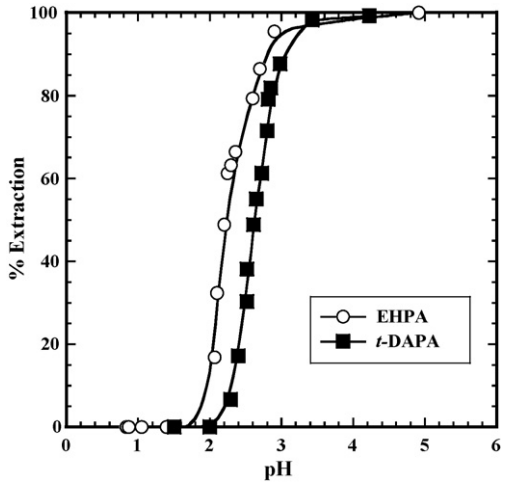

Fig. 6. Effect of pH on the percentage extraction of Cu(II) with EHPA and *t*-DAPA.

Table 1
Properties of EHPA and *t*-DAPA

Type of extractants	Diluent	Extraction stoichiometry	log $P_{oct/w}$	K_{ex}	Solubility test into NPOE
EHPA	Toluene[a]	$CuR_2 2HR_2$	3.14	1.13	Insoluble
t-DAPA	Toluene	$CuR_2 2HR_2$	4.46	0.31	Soluble

[a] 10 vol.% 2-ethyl-l-hexanol was added as modifier.

such as 2-nitrophenyl octylether (NPOE). Table 1 summarizes the extraction stoichiometry, extraction equilibrium constants and solubility test into plasticizer for extractants. Taking account of these results, *t*-DAPA was used as a carrier to be incorporated into CTA membrane for making a PIM for the transport and separate copper(II) over cadmium(II).

3.5. Copper(II) transport with PIM containing t-DAPA

In the transport experiment, the system was constructed that the membrane extraction of the species of interest was accompanied by its simultaneous stripping from the other side of the membrane into a receiving phase [30,31]. The transport of copper(II) through PIM containing *t*-DAPA as carrier from feed solution of [Cu(II)] = 0.3 mM to receiving solution of 1.0 M HCl was carried out. Fig. 7 shows the transport result for copper(II) with PIM containing 25 wt.% *t*-DAPA and 50 wt.% NPOE. As evident from Fig. 7, the concentration of copper(II) in the feed solution was started to decrease continuously and reach a concentration lower than the detection limit after 24 h. On the other hand, the concentration of copper(II) in the receiving solution was increased with transport time. Therefore, the present investigation shows that there is active transport of copper(II) through PIM in the membrane extraction system. The rapid transport of copper(II) was a promising result from the standpoint of its industrial application. It should be the case that the driving force for the fast transport is the pH gradient between the feed and receiving solutions as expected from Eq. (3).

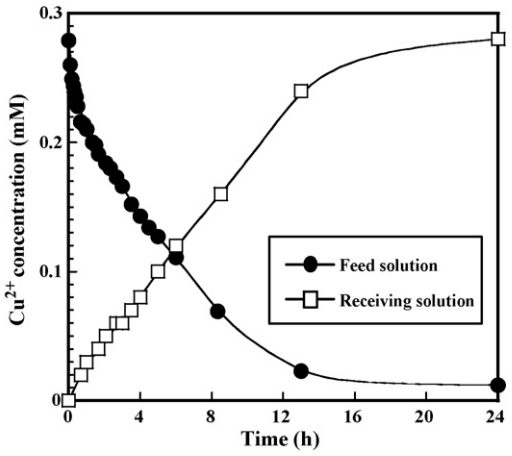

Fig. 7. Results of Cu(II) transport across PIM. Feed solution: [Cu(II)] = 0.3 mM in 0.1 M HEPES buffer at pH 3.20. Receiving solution: 1.0 M HC1. PIM containing 25 wt.% *t*-DAPA and 50 wt.% NPOE.

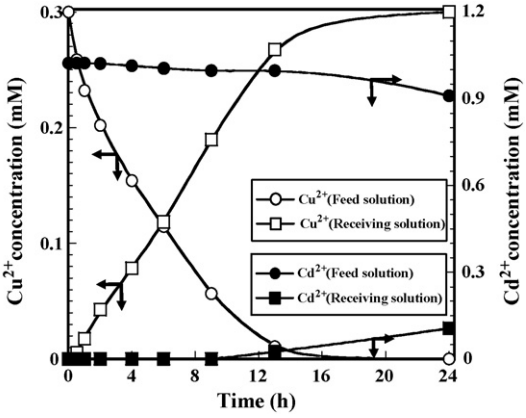

Fig. 8. Competitive transport of Cu(II) and Cd(II) across PIM. Feed: [Cu(II)] = 0.3 mM, [Cd(II)] = 1.0 mM in 0.1 M HEPES buffer at pH 3.20. Receiving solution: 1.0 M HCl. PIM containing 25 wt.% *t*-DAPA and 50 wt.% NPOE.

3.6. Selective transport study between copper(II) and cadmium(II) with PIM containing t-DAPA

Based on the results of liquid–liquid extraction experiments, the selective transport of copper(II) over cadmium(II) was carried out with PIM containing 25 wt.% *t*-DAPA and 50 wt.% NPOE. The selective transport study was conducted in feed solution of [Cu(II)] = 0.3 mM, [Cd(II)] = 1.0 mM in 0.1 M HEPES buffer at pH 3.20 and receiving solution of 1.0 M HCl. Fig. 8 shows the competitive transport of copper(II) and cadmium(II) through PIM. It was established that copper(II) was selectively transported from the feed to the receiving solution and the transport of copper(II) was achieved almost completely after 12 h experiment. On the other hand, the transport of cadmium(II) appears to be only just beginning when the transport of copper(II) has almost reached completion. These findings suggest that copper(II) was selectively transported through the PIM due to the excellent extraction ability of carrier toward copper(II) over cadmium(II). Under the experimental condition, it is possible after 12 h to obtain a separation factor (SF) of 933, calculated from Eq. (8) [32]. The high value of separation factor obtained

in this study demonstrates that the novel PIM is very effective to transport and separate copper(II) over cadmium(II) from the feed solution to the receiving solution.

$$SF = \frac{[Cu^{2+}]_r[Cd^{2+}]_f}{[Cu^{2+}]_f[Cd^{2+}]_r} \quad (8)$$

4. Conclusion

It was noted that new alkylated pyridinecarboxylic acid derivatives extracts copper(II) over other divalent metal ions and iron(III) at low pH in 1.0 M ammonium nitrate solution. The finding of this study suggests that the pyridine moiety and carboxylic acid of EHPA plays an important role in selectively extracting copper(II) over other metal ions. It was demonstrated that alkylated pyridinecarboxylic acid derivatives as a novel extraction reagent offer attractive possibilities in the fields of not only the separation chemistry but the hydrometallurgy as well. The transport of copper(II) from the feed solution to the receiving solution through PIM consisted of CTA as a base polymer, NPOE as a plasticizer and *t*-DAPA as a carrier was found to be rapid and quantitative. It was found that PIM developed in this study is very effective to transport and separate copper(II) from a high concentration of cadmium(II) solution. On the basis of results obtained from this study, it can be concluded that PIM containing *t*-DAPA as novel carrier provides an attractive alternative to conventional solvent extraction methods for the separation of copper(II) over cadmium(II) from aqueous solution.

References

[1] Y. Nagaosa, Y. Binghua, Talanta 44 (1997) 327.
[2] J.D. Gyves, E.R.D.S. Miguel, Ind. Eng. Chem. Res. 38 (1999) 2182.
[3] A. Kumar, A.M. Sastre, Ind. Eng. Chem. Res. 39 (2000) 146.
[4] J.V. Linden, R.F.D. Ketelaere, J. Membr. Sci. 42 (1998) 125.
[5] J.A. Riddick, W.B. Bunger, T.K. Sakano, Organic Solvents: Physical Properties and Methods of Purifications, II, fouth ed., John Wiley & Sons, New York, 1986.
[6] T.M. Dreher, G.W. Steven, Sep. Sci. Technol. 33 (1998) 835.
[7] X.J. Yang, A.G. Fane, K. Soldenhoff, Ind. Eng. Chem. Res. 42 (2003) 392.
[8] M. Sugiura, M. Kikkawa, S. Urita, J. Membr. Sci. 42 (1989) 47.
[9] J.D. Lamb, A.Y. Nazarenko, J.C. Uenshi, H. Tsukube, Anal. Chim. Acta. 373 (1998) 167.
[10] S.D. Kolev, L. Wang, R. Paimin, R.W. Cattrall, W. Shen, J. Membr. Sci. 176 (2000) 105.
[11] A.H. Blitz-Raith, R. Paimin, R.W. Cattrall, S.D. Kolev, Talanta 71 (2007) 419.
[12] G. Salazar-Alvarez, A.N. Bautisata-Flores, E.R.D.S. Miguel, M. Muhammed, J.D. Gyves, J. Membr. Sci. 250 (2005) 247.
[13] J.D. Gyves, A.M. Hernandez-Andaluz, E.R.D.S. Miguel, J. Membr. Sci. 268 (2006) 142.
[14] E.R.D.S. Miguel, A.M. Hernandez-Andaluz, J.G. Banuelos, J.M. Saniger, J.C. Aguilar, J.D. Gyves, Mater. Sci. Eng. A. 434 (2006) 30.
[15] J.C. Aguilar, M. Sanchez-Castellanos, E.R.D.S. Miguel, J.D. Gyves, J. Membr. Sci. 190 (2001) 107.
[16] A. Gherrou, H. Kerdjoudj, R. Molinari, P. Seta, E. Drioli, J. Membr. Sci. 228 (2004) 149.
[17] Y. Baba, M. Iwakuma, H. Nagami, Ind. Eng. Chem. Res. 41 (2002) 5835.
[18] Y. Baba, T. Oshima, T. Tasaki, Proceedings of the 37th annual Australasian Chemical Engineering Conference, Aukland, New Zealand, 2006 (Conference Media CD).
[19] T. Hayashita, M. Kumazawa, J.C. Lee, R.A. Bartsch, Chem. Lett. (1995) 711.
[20] A. Borowiak-Resterna, Solv. Extr. Ion. Exch. 12 (3) (1994) 557.
[21] M. Regel-Rosocka, M. Winiewski, A. Borowiak-Resterna, A. Cieszynska, A. Sastre, Sep. Purif Technol. 53 (2007) 337.
[22] C.Y. Cheng, Hydrometallurgy 84 (2006) 109.
[23] J.S. Preston, A.C. Preez, Hydrometallurgy 58 (2000) 239.
[24] J.S. Preston, Hydrometallurgy 14 (1985) 171.
[25] D. Min, S.S. Yoon, D.Y. Jung, C.Y. Lee, Y. Kim, W.S. Han, S.W. Lee, Inorg. Chim. Acta. 324 (2001) 293.
[26] R.C. Pearson, J. Amer. Chem. Soc. 85 (1963) 3533.
[27] J. Pons, R. March, J. Rius, J. Roa, Inorg. Chim. Acta 357 (2004) 3789.
[28] R. March, W. Clegg, R.A. Coxall, L. Cucurull-Sanchez, Inorg. Chim. Acta 353 (2003) 129.
[29] I. Szczepanska, A. Borowiak-Resterna, M. Wisniewiski, Hydrometallurgy 68 (2003) 159.
[30] G. Argiropoulos, R.W. Cattrall, I.C. Hamilton, S.D. Kolev, R. Paimin, J. Membr. Sci. 138 (1998) 279.
[31] Y. Baba, K. Hoaki, J.M. Perera, G.W. Stevens, T.J. Cardwell, R.W. Catrall, S.D. Kolev, Proceedings of the 6th World Congress of Chemical Engineering, Melbourne, Australia, 2001 (Conference Media CD).
[32] M.E. Nunez, E.R.D.S. Miguel, F. Mercader-Trejo, J.C. Aguilar, J.D. Gyves, Sep. Purif. Technol. 51 (2006) 57.

Available online at www.sciencedirect.com
ScienceDirect
Talanta 73 (2007) 237–245
Talanta
www.elsevier.com/locate/talanta

Experimental design approach for the solid-phase extraction of residual aluminium coagulants in treated waters

P. Vanloot [a], J.-L. Boudenne [a,*], Laurent Vassalo [a], M. Sergent [b], B. Coulomb [a]

[a] *Université de Provence – CNRS, Laboratoire de Chimie et Environnement, FRE2704, 3 Place Victor Hugo, Case 29, 13331 Marseille Cedex 3, France*
[b] *Université Paul Cézanne – CNRS, Laboratoire de Méthodologie de la Recherche Expérimentale, UMR6171, Avenue Escadrille Normandie Niémen, 13397 Marseille Cedex 20, France*

Received 13 December 2006; received in revised form 3 March 2007; accepted 15 March 2007
Available online 24 March 2007

Abstract

Solid-phase extraction (SPE) of trace elements before their analysis has become a conventional pretreatment step of analytes because of their frequent low concentrations in numerous samples. Additionally, interfering compounds often accompagny analytes of interest, thus requiring a clean-up step. The preconcentration step and/or matrix removal can be efficiently improved by chemometric approaches allowing obtention of reliable results. Single variable approach is often used but is time and cost consuming, and may be the source of mistakes; multivariable approach allows to overcome these problems and increases the probability of global optimum finding.

In order to obtain a set of experimental conditions for the selective extraction of Al(III) in water samples, onto a modified organic support (salicylic acid grafted on XAD-4), a multicriteria approach (response surface methodology) has been applied. The extraction method was optimized by the aid of a factorial design and a uniform shell Doehlert design for six variables: sample percolation flow rate, trace metal amount, sample volume, concentration and volume of HCl used for elution of aluminium. Results demonstrate the synergic effects of four factors and allow us to define working ranges for each parameter tested. The designed SPE procedure was then sucessfully applied to synthetic and real samples, issued from a potable water treatment unit.

Keywords: Aluminium; Solid phase extraction; Functionalized resin; Response surface methodology; Desirability indice

1. Introduction

Aluminium determination at low level is of particular interest in potable water units because this metallic ion is commonly used as reactant for coagulation–floculation in the treatment of raw waters to remove colloidal or suspended particles or to eliminate organic matter. At the outlet of these units, maximum tolerable level of this cation has been fixed to 200 $\mu g\,l^{-1}$ by European Legislation [1]. This cation is associated with various health problems in numerous studies, from gastrointestinal damage and phosphate deficiency to dialysis encephalopathy, renal oestrodistrophy and Alzheimer's disease [2,3]. In order to optimise coagulation process in drinking water plants and to minimise aluminium levels in finished water, monitoring of this metal contents during and after raw water treatment is therefore needed. Up to now, the coagulant quantities are generally determined by the empiric Jar-test technique [4], that induces problems of excess (or insufficient) reagent, particularly during period of fast variation in water quality [5]. Moreover, an European Directive has recently introduced the principle of self-monitoring, i.e. that producers must constantly ensure that the water distributed to consumers meets the minimum requirements set out. In response to any failure to meet a standard for drinking water quality, the water company must establish the cause and the nature of the failure [6]. These more and more stringent regulations have induced during last years many advances in the automation of analytical procedures, and in the development of coupled methods associating solid-phase extraction (SPE) or solid-phase microextraction (SPME) – to reach required low levels of metallic trace elements – with, in most cases, spectrophotometric methods [7–10].

These last ones are actually the easiest detection methods suitable for automation and miniaturization, and have thus direct application for on site and/or on-line micropollutant determina-

* Corresponding author. Tel.: +33 4 91106140; fax: +33 4 91106378.
E-mail address: jean-luc.boudenne@univ-provence.fr (J.-L. Boudenne).

0039-9140/$ – see front matter © 2007 Elsevier B.V. All rights reserved.
doi:10.1016/j.talanta.2007.03.030

tion [11–13]. Commonly used SPE sorbents consist of specific functional groups immobilized on a solid support, improving the efficiency of metal extraction by providing better contact area with the samples [14]. Sorbents may be in the form of extraction disks [15–17] or in the form of resins [18,19]. Recently, our research group has developped a new sorbent intended for the selective determination of aluminum in water samples. This support is a modified commercial resin (Amberlite® XAD-4) onto which we have chemically bond a chelating function (salicylic acid). Its synthesis scheme has already been published in a previous paper [20].

In this paper, our purpose is to determine factors affecting the extraction–elution steps of aluminum onto this support, in order to spectrophotometrically detect this cation in future studies. Levels of aluminum at the outlet of potable water treatment unit are relatively low and lay down this extraction–preconcentration step. Factors influencing accuracy of the spectrophotometric method will be directly linked to the step of elution, and this last one will be strongly correlated to the factors linked to the sequestration step onto the support. This paper will at first determine the relative influence of three factors affecting the elution yield (elution rate, concentration and volume of hydrochloric acid) thanks to a new experimental design approach and to the use of a desirability function (95% of aluminum recovery during the elution step. Next, a desirability function will be applied to the global procedure (extraction + elution) and will allow us to determine optimal conditions to reach a minimum of 95% yield.

2. Experimental

2.1. Reagents

All solutions were prepared with ultra-high quality deionised water (Millipore, resistivity >18 MΩ cm).

Amberlite XAD-4 resin was obtained from Acros Organics (Noisy-le-Grand, France). It was suspended under agitation in methanol for 24 h after which the washed resin was filtered off, rinsed with methanol and dried at 60 °C for 48 h before use.

All chemicals used in this work were of analytical grade and purchased from Acros Oragnics and used without further purification, except for thionyl chloride, which was purified before use by distillation under argon at atmospheric pressure (76 °C fraction) and was used immediately.

A commercial stock solutions of 1 g l^{-1} of Al^{3+} was purchased from Merck (Darmstadt, Germany). Further dilutions were prepared daily as required. Synthetic multielement samples were prepared as required from dilution of a stock solution used for ICP–AES calibration. This PlasmaTEST® solution, purchased from SCP Sciences (Canada) was constituted of 18 elements (As, Be, Ca, Cd, Co, Cr, Cu, Fe, Mg, Mo, Ni, Pb, Sb, Se, Ti, Tl, V, Zn) at 10 mg l^{-1} (±0.08 mg l^{-1}). Before each extraction, samples were acidified to pH 2.5 with nitric acid. For on-line detection of Al(III) ions, a chromazurol-S (CAS) solution was used at a concentration of 1.5×10^{-4} mol l^{-1}, with cetyltrimethylammonium bromide at 4.5×10^{-4} mol l^{-1}. *o*-Phenanthroline (4×10^{-4} mol l^{-1}) and hydroxylammonium hydrochloride (1×10^{-3} mol l^{-1}) were added to mask interfering species (Fe^{3+} and Cu^{2+}). Acetate buffer was used to adjust colorimetric reagent solution pH at 5.1

2.2. Synthesis of SA-XAD resin

The sorbent SA-XAD was prepared by a procedure already described in a previous paper [20] and described briefly herein. Amberlite XAD-4 resin (5 g) was treated with 2.7 ml acetyl chloride and 5.62 g anhydrous aluminium chloride in 1,2-dichloroethane. The system was refluxed for 16 h at 40 °C. The solid was washed with hydrochloric acid, water and methanol before repeated treatments with $KMnO_4$ (2.5 g) and sodium hydroxide (5.75 g). The carboxylated resin was refluxed with thionyl chloride (30 ml) at 70 °C for 2.5 h and then stirred with 2-methylanisole (15 ml) and anhydrous aluminium chloride (3.6 g) during 12 h at 60 °C. Methyl groups were then oxidized into carboxylic groups by a mixture of sodium hydroxide (0.16 g) and $KMnO_4$ (3.76 g) in water at 60 °C. Finally, methoxy groups were converted into hydroxy groups by mixing previous resin with anhydrous aluminum chloride (5.76 g) and toluene (30 ml) at 60 °C for 8 h. The final resin (SA-XAD) was collected by filtration, washed with water and methanol, and dried under vacuum.

2.3. MSFIA aluminium determination: apparatus and procedure

The manifold used for aluminium extraction and determination is depicted Fig. 1. It is mainly composed of three modules: the new resin (40 mg) packaged into a methyl polymetacry-

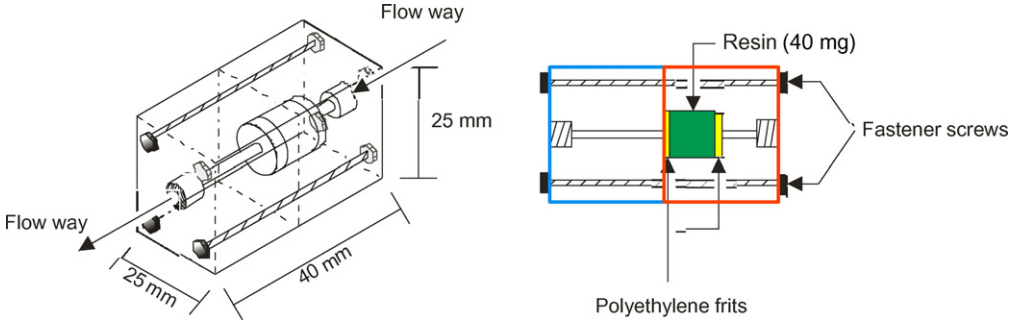

Fig. 1. Design of the microcolumn used for Al(III) solid-phase extraction.

late micro-column of 6 mm i.d. and 10 mm length, affording thus flow-through percolation of samples, an automatic multiburette CRISON Microbur BU4S (Crison Instruments, Alella, Spain) equipped with three 5 ml syringes (Hamilton, Interchim, France), each of them being connected to a three-way selection valve CRISON 2045. The fourth selection valve of multiburette was only used for sampling. Tubings, 0.8 mm i.d., are made of Teflon. A Secomam S1000 UV–vis spectrophotometer (Secomam, Alès, France) was used to perform absorbance measurements. SPE system was adapted to a flow-through quartz suprasil cell (2 cm optical pathlength) of the UV–vis spectrophotometer.

The whole modules of the MSFIA system (automatic burettes, valves, spectrophotometer) were connected to a computer via a RS-232C interface and controlled by the Autoanalysis Station 3.0 software (SCIware, Palma, Spain) [21].

The operation of the on-line aluminium extraction and determination was as follows: during extraction step, sample was aspired in an holding coil, whereas the three other syringes were filled with water used as carrier, with hydrochloric acid (HCl) and with the reagent (R). Then the four modules pushed each of their liquids upwards: sample and water were percolated through the microcolumn that retained the metal, while HCl and reagent came back to their own tanks. Thus, Al(III) ions were retained on the SA-XAD sorbent and the remaining solution was discharged.

During the elution step, HCl and the spectrophotometric reagent are pushed together, the first one to the inlet of column to elute Al^{3+}, the second one to the outlet of the column to be mixed with eluate in a mixing loop. Complexes thus formed were then determined by spectrophotometry at $\lambda = 546$ nm.

2.4. Metal analysis and resin characterization

Graphite furnace–atomic absorption spectrometry (GF–AAS) was used to determine recovery rates after the aluminium extraction–elution procedure. GF–AAS measurements are carried out on a Perkin-Elmer 1100B spectrometer equipped with an HGA700 graphite furnace. A Perkin-Elmer aluminium hollow-cathode lamp was operated at 25 mA. Argon flow was 300 ml min^{-1} except during atomisation. Pyrolytically-coated graphite furnace tubes were used.

Furnace settings were: drying at 160 °C, ramp for 20 s, hold for 35 s; cracking at 1200 °C for Al; no ramp; hold for 5 s; atomising at 2400 °C, no ramp and 2 s hold; and cleaning at 2800 °C, no ramp and 2 s hold.

Inductively coupled plasma–atomic emission spectrometry (ICP–AES) measurements were carried out with a Jobin YVON JY2000 Ultratrace spectrometer, equipped with a CMA spray chamber and a Meinhard TR50-C1 glass nebuliser, when considering interfering cations. Determinations were performed with the following parameters: power 1000 W, pump speed 20 ml min^{-1}, plasma flow rate 12 l min^{-1}, coating gas flow rate 0.2 l min^{-1}, nebuliser flow rate 0.83 l min^{-1} and nebuliser pressure 3.1 bar.

Infrared (IR) spectra were recorded on a Nicolet Impact 410 Spectrometer (Montigny-le-Bretonneux, France). Samples were pressed into KBr pellets.

2.5. Experimental design

2.5.1. Experimental factors

Preliminary studies have shown that six parameters – noted as factors X afterwards – have to be considered during SPE optimization in order to obtain three experimental responses – noted as factors Y later on – that are extraction (Y_1), elution (Y_2) and aluminium recovery (Y_3) rates: flow-through sample volume (X_1), sample percolation rate (X_2), sample metal concentration (X_3), (all three directly linked to extraction step), eluent volume (X_4), elution flow-rate (X_5) and concentration of eluent (X_6), (all three directly linked to elution step). The domains of variation for each factor was determined based on knowledges of the system (mainly volume of syringes and piston speed available with CRISON Instruments) and acquired from initial experimental trials:

- X_1: 0.5–5 ml
- X_2: 0.5–9 ml min^{-1}
- X_3: 20–200 μg l^{-1}
- X_4: 0.2–5 ml
- X_5: 0.5–9 ml min^{-1}
- X_6: 0.1–0.5 mol l^{-1}

For calculation, the factors were transformed in coded factors, varying from −1 to + 1, and the experimental domain of the coded factors (X_i) is represented by a six-dimensional hypersphere (radius 1).

2.5.2. Experimental design methodology

The aim of this study was to determine the best conditions for extraction and elution, and for that, the value of extraction yields over the whole experimental domain is desired. To get this information, an empirical mathematical model was used, which establishes the relationship between the variation of the responses, η, and the variation of the factors X. This model is a quadratic model of the form:

$$\eta = \beta_0 + \beta_1 X_1 + \beta_2 X_2 + \cdots + \beta_k X_k + \beta_{11} X_1^2 + \beta_{22} X_2^2 + \cdots + \beta_{kk} X_k^2 + \beta_{12} X_1 X_2 + \cdots + \beta_{k-1,k} X_{k-1} X_k$$

where η represents the variation of the responses; k is the number of factors; β_0 is the constant factor; β_i, β_{ii} and β_{ij} are coefficients of the linear, quadratic and cross-product terms, respectively.

To estimate the coefficients of this model, we need a set of experiments well spread in the domain, that is a design of experiments optimal for a second order polynomial model. Indeed, the quality of the coefficient estimation and the quality of the prevision only depend on the choice of the experimental points. Among the set of designs, we chose a uniform shell Doehlert design, which is an optimal design for the spherical domain defined by the factors [22]. For a studied response (η), the estimates (β_i, β_{ii}, β_{ij}) were calculated using a multilinear regression. Some experiments were replicated in order to estimate the variance of the experimental results. Then, to minimize the effect of systemic errors, experiments were carried out in a random fashion. The calculations have been performed with the Nemrod-W

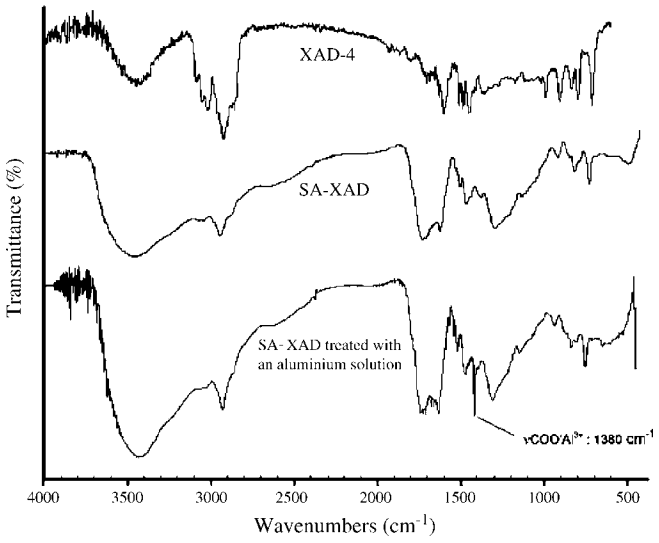

Fig. 2. FTIR spectra of Amberlite XAD-4, modified resin (SA-XAD) and treated with an aluminium solution.

software (LPRAI, Marseille, France), which was developed for building and processing designs of experiments [23].

The isoresponse curves and the desirability function [24] were used to determine the best compromise in the experimental domain.

Table 2 shows ANOVA results for aluminium recovery rate (Y_3). The F-ratio shown is used to determine the statistical significance of the extraction–elution process. The F-value is a ratio of two independent estimates of experimental error. Associated with this ratio is a P-value wich quantifies the probability of making an error by associating an effect with a given factor. The P-value also provides the exact level of significance of a hypothesis test. The R-square values indicate the percentage of variation of the response that is explained by the deliberate variation of the factors in the case of experiment [25].

3. Results and discussion

3.1. Resin characterization

Each step of the grafting procedure was characterized by FTIR (Fig. 2). FTIR spectra of original Amberlite XAD-4 revealed the presence of pendant ethylbenzene groups; 2955 and 2871 cm^{-1} valence vibrations of CH_3 were observed. The groups originate from the presence of ethylvinylbenzene in the commercial divinylbenzene used for preparation of the resin. Presence of pendant vinylbenzene groups was assessed as well by the valence vibration of the C–H bonds at 3083 cm^{-1} (vinylic CH_2) and 3017 cm^{-1} (vinylic CH) and of C=C vinylic bond at 1628 cm^{-1}. After the first acylation, those three vibration bands disappeared which showed that pendant vinylbenzene groups reacted with aluminum chloride and acetyl chloride. Addition of acetyl groups on the phenyl rings of poly(styrene-*co*-divinylbenzene) was evidenced by bands at 1266 and 1196 cm^{-1} (aryl ketones), 1359 cm^{-1} (deformation vibration of CO–CH_3) and 1685 cm^{-1} (vibration band of C=O fixed on a aromatic ring). Oxidation of these acetyl groups by $KMnO_4$ in basic medium leads to a small modification of the C=O vibration band (1668 cm^{-1}) and an emergence of an O–H band at 2624 cm^{-1}. Grafting of 2-methylanisole was assessed by the FTIR bands: 1262 cm^{-1}, aryl ether and aryl ketone; 1122 cm^{-1}, C–O vibration band of ethoxy group; and 1025 cm^{-1}, deformation band of trisubstituted phenyl. Oxidation induced the presence of a valence vibration of the C=O bond of the carboxy group at 1720 cm^{-1} and of the C–O bond of this group at 1231 cm^{-1}. Deprotection of the methoxy group caused the disappearance of the aryl ether band at 1122 cm^{-1}.

The comparison of FTIR spectra for grafted complexed and uncomplexed resin shows a modification of intensity of the band previously assigned to carboxylic group. A band of medium intensity, in the region near 1380 cm^{-1} appeared. This band could be attributed to the formation of a carboxylate moiety resulting from complexation with aluminium. This phenomenon has been reported for several metallic complexes of salicylic acid [26].

3.2. Doehlert design

Two factors have been prefixed according to previous batch experiments [27].

Mass of sorbent used during extraction–elution optimization has been fixed to 40 mg which is a large excess when considering extraction capacity of the modified resin (4.4 ± 0.3 mg g^{-1} for Al^{3+}). pH aluminium extraction has been fixed to 2.5 according to chelating properties of modified resin towards Al^{3+}.

The six other factors affecting solid-phase extraction of aluminium have been optimized by use of a Doehlert design. This one was devoted to the extraction step optimization as a experimental design within six factors: flow-through sample volume (X_1), sample percolation rate (X_2), sample metal concentration (X_3), HCl volume (X_4), elution flow-rate (X_5) and concentration of eluent (X_6).

This design consists of a set of 43 distinct experiments and the central point of the experimental domain – represented by experiment #43 – was repeated three times to evaluate the repeatability of the measurements (Experiments 43, 44 and 45). Experiments required for this design are described in Table 1. This design includes the possibility of adding additional factors without any adverse effects on the quality of the design.

From these results, coefficients estimation were calculated using multilinear regression from NEMROD-W [24] for aluminium extraction yield Y_1 (Eq. (1)) – which depends only on factors X_1, X_2 and X_3 – for aluminium elution Y_2 (Eq. (2)) and aluminium recovery rates Y_3 (Eq. (3)):

$$Y_1 = 85.93 - 0.48X_1 - 8.55X_2 + 0.39X_3 + 2.82X_1^2 + 3.15X_2^2 + 0.43X_3^2 - 1.96X_1X_2 - 3.23X_1X_3 - 1.23X_2X_3 \quad (1)$$

$$Y_2 = 90.967 - 2.771X_1 + 0.544X_2 - 0.980X_3 + 4.391X_4 - 13.410X_5 - 2.411X_6 - 1.167X_1^2 - 0.333X_2^2 - 1.425X_3^2 - 2.802X_4^2 - 6.540X_5^2 - 1.148X_6^2$$

Table 1
Doehlert design and experimental results

Experiment	X_1 (ml)	X_2 (ml min^{-1})	X_3 (μg l^{-1})	X_4 (ml)	X_5 (ml min^{-1})	X_6 (mol l^{-1})	Y_1 (%)	Y_2 (%)	Y_3 (%)
1	5.00	4.75	110.00	2.60	4.75	0.30	88.20	86.60	76.40
2	0.50	4.75	110.00	2.60	4.75	0.30	89.30	93.00	83.00
3	3.88	8.45	110.00	2.60	4.75	0.30	79.80	87.60	69.90
4	1.63	1.05	110.00	2.60	4.75	0.30	96.50	91.50	88.30
5	3.88	1.05	110.00	2.60	4.75	0.30	96.00	89.20	85.60
6	1.63	8.45	110.00	2.60	4.75	0.30	83.70	93.40	78.10
7	3.88	6.00	185.00	2.60	4.75	0.30	83.70	89.10	74.60
8	1.63	3.50	35.00	2.60	4.75	0.30	86.90	87.50	76.10
9	3.88	3.50	35.00	2.60	4.75	0.30	91.50	89.50	81.90
10	2.75	7.20	35.00	2.60	4.75	0.30	82.30	92.50	76.10
11	1.63	6.00	185.00	2.60	4.75	0.30	85.50	91.50	78.20
12	2.75	2.30	185.00	2.60	4.75	0.30	93.40	88.50	82.70
13	3.88	6.0	128.75	4.50	4.75	0.30	85.90	90.50	77.70
14	1.63	3.50	91.25	0.70	4.75	0.30	87.90	86.40	75.90
15	3.88	3.50	91.25	0.70	4.75	0.30	88.40	83.70	74.00
16	2.75	7.20	91.25	0.70	4.75	0.30	81.70	85.90	70.20
17	2.75	4.75	166.25	0.70	4.75	0.30	87.60	84.90	74.30
18	1.63	6.00	128.75	4.50	4.75	0.30	86.50	93.80	81.20
19	2.75	2.30	128.75	4.50	4.75	0.30	92.20	92.80	85.60
20	2.75	4.75	53.75	4.50	4.75	0.30	88.20	92.80	81.80
21	3.88	6.00	128.75	2.98	8.10	0.30	86.70	74.50	64.60
22	1.63	3.50	91.25	2.22	1.40	0.30	86.50	97.40	84.30
23	3.88	3.50	91.25	2.22	1.40	0.30	88.40	94.90	83.80
24	2.75	7.20	91.25	2.22	1.40	0.30	81.70	96.10	78.50
25	2.75	4.75	166.25	2.22	1.40	0.30	87.60	94.80	83.00
26	2.75	4.75	110.00	4.12	1.40	0.30	86.30	97.40	84.00
27	1.63	6.00	128.75	2.98	8.10	0.30	86.50	78.00	67.50
28	2.75	2.30	128.75	2.98	8.10	0.30	93.00	76.00	70.70
29	2.75	4.75	53.75	2.98	8.10	0.30	86.20	78.30	67.50
30	2.75	4.75	110.00	1.08	8.10	0.30	86.30	77.30	66.70
31	3.88	6.00	128.75	2.98	5.3	0.45	86.70	85.20	73.90
32	1.63	3.50	91.25	2.22	4.2	0.15	87.90	95.90	84.30
33	3.88	3.50	91.25	2.22	4.2	0.15	88.40	93.20	82.40
34	2.75	7.20	91.25	2.22	4.2	0.15	82.90	94.70	78.50
35	2.75	4.75	166.25	2.22	4.2	0.15	86.10	92.10	79.40
36	2.75	4.75	110.00	4.12	4.2	0.15	85.20	95.00	81.00
37	2.75	4.75	110.00	2.60	7.55	0.15	86.30	75.80	65.40
38	1.63	6.00	128.75	2.98	5.3	0.45	85.60	88.00	75.40
39	2.75	2.30	128.75	2.98	5.3	0.45	92.20	86.80	80.00
40	2.75	4.75	53.75	2.98	5.3	0.45	86.20	90.50	78.00
41	2.75	4.75	110.00	1.08	5.3	0.45	86.30	77.30	66.70
42	2.75	4.75	110.00	2.60	1.95	0.45	85.20	96.80	82.50
43	2.75	4.75	110.00	2.60	4.75	0.30	86.30	91.00	78.50
44	2.75	4.75	110.00	2.60	4.75	0.30	86.30	91.00	78.50
45	2.75	4.75	110.00	2.60	4.75	0.30	85.20	90.90	77.50

X_1: flow-through sample volume; X_2 = Sample percolation rate; X_3 = Sample metal concentration; X_4 = Volume of HCl; X_5 = HCl flow-rate; X_6 = [HCl]; Y_1 = Al^{3+} extraction rate; Y_2 = Al^{3+} elution rate; Y_3 = Al^{3+} recovery rates.

$$\begin{aligned} &-2.021X_1X_2-1.980X_1X_3-1.261X_2X_3+0.870X_1X_4\\ &-0.466X_2X_4-0.349X_3X_4+0.452X_1X_5+0.961X_2X_5\\ &-0.917X_3X_5-2.915X_4X_5+0.971X_1X_6+0.321X_2X_6\\ &-1.203X_3X_6+7.0559X_4X_6+2.581X_5X_6 \end{aligned} \quad (2)$$

$$\begin{aligned} Y_3 = {} & 78.167-2.436X_1-6.545X_2-0.044X_3+4.728X_4\\ &-10.636X_5-1.582X_6+1.533X_1^2+2.567X_2^2-0.875X_3^2\\ &-1.572X_4^2-5.453X_5^2-0.957X_6^2-3.175X_1X_2\\ &-4.634X_1X_3-2.039X_2X_3+1.344X_1X_4-0.119X_2X_4\\ &-2.466X_3X_4+0.581X_1X_5+1.617X_2X_5-1.592X_3X_5\\ &-2.213X_4X_5+2.324X_1X_6+0.309X_2X_6\\ &-0.169X_3X_6+7.239X_4X_6+2.812X_5X_6 \end{aligned} \quad (3)$$

The experimental results and the predicted values could be compared – from three last columns in Table 1 – and they match properly (S.D. = 3.454 for Y_1, 2.316 for Y_2, 2.070 for Y_3).

The statistical significance of the ratio of mean square variation due to regression and mean square residual error was tested using analysis of variance. ANOVA is a statistical technique which subdivides the total variation in a set of data into component parts associated with specific sources of variation for the

Table 2
ANOVA of the regression for aluminium recovery rates (Y_3)

Source	Sum of square	Degrees of freedom	Mean square	F-ratio	P-value (significance)
Regression	1523.87	27	56.4398	13.1700	<0.01
Residual	72.8531	17	4.28548		
Lack of fit	72.1864	15	4.81243	14.4373	6.7
Pure error	0.6666	2	0.3333		
Total	1596.73	44			

purpose of testing hypotheses on the parameters of the model. Only results obtained for aluminium recovery rates (Y_3) are presented herein for clarity of purpose. According to the ANOVA (Table 2), the regression mean squares (56.4398) and the residual mean square (4.81243) allowed the calculation of the Fisher ratios (F-value) for assessing the statistical significance. The model F-value of 56.44 implies that most of the variation in the response can be explained by the regression equation. The associated P-value is used to judge whether F-ratio is large enough to indicate statistical significance. A P-value lesser than 0.01 (i.e. $\alpha = 0.01$ or 99% confidence) indicates that the model is considered to be statistically significant. The P-value for the regression obtained ($r^2 = 0.954$) was less than 0.01 and means consequently that at least one of the term in the regression equation has a significant correlation with the response variable. The ANOVA table also shows a term for residual error, which measures the amount of variation in the response data left unexplained by the model. The form of the model chosen to explain the relationship between the factors and the response is correct.

3.3. Response surface regression analysis

After validation, these equations were used to represent the responses in the whole domain and to determine, in a first time, what step of solid-phase extraction is most influencial on aluminium recovery rates.

In Fig. 3, Y_3 has been plotted versus aluminium extraction rate Y_1 and versus aluminium elution rate Y_2. This representation allows one to see at the first glance that the elution step is preponderant upon the extraction step.

In order to determine what parameters are significant during aluminium elution step, response surfaces have been represented graphically. Aluminium recovery rates (Y_3) were plotted versus levels of X_4, X_5 and X_6 (respectively, HCl volume, elution flow-rate and HCl concentration) with the three factors linked to the elution step fixed. Flow-through sample volume (X_1) was fixed at 2.75 ml, sample percolation rate (X_2) was fixed at 4.75 ml min^{-1} and sample metal concentration (X_3) was fixed at 110 $\mu g\,l^{-1}$.

In the first contour plot (Fig. 4a), we see that for a Y_3 superior to 95%, HCl volume has to be at least equal to 1.77 ml with elution flow-rate below 3.9 ml min^{-1}; the second one (Fig. 4b) confirms this 95% yield is obtained when working with elution flow-rate below 3.9 ml min^{-1} and with HCl at a concentration below 0.40 mol l^{-1}.

These primary results show a preponderant effect of elution flow-rate upon aluminium recovery rate. In order to confirm preponderance of elution step and to assess the suitability of the micro-column used for Al^{3+} extraction in the range 0–200 $\mu g\,l^{-1}$, supplementary contour plots have been drawn (Fig. 5).

Y_3 has been plotted versus levels of elution flow-rate (X_5) and (i) flow-through sample volume (Fig. 5a), (ii) sample percolation rate (Fig. 5b) and (iii) sample metal concentration (Fig. 5c). These contour plots confirm when working below 3.9 ml min^{-1}, a 95% aluminium recovery rate may be reached whatever sample percolation rate (X_2) – in the range 0.45–9.05 ml min^{-1} – and whatever sample metal concentration (X_3) – in the range 20–200 $\mu g\,l^{-1}$.

3.4. Desirability function

The maximization of each response was not obtained at the same conditions. One way to overcome this difficulty was to define an acceptable range for response Y_3. The satisfactory zone was that part of domain for which the value of the response was acceptable. To determine this acceptable zone, we use a multicriteria optimization procedure based on desirability function. This varied from 0 to 1, according to the closeness of the response to its target value. For Y_3, we have chosen to reach a target value of 95% and the desirability D at this point was equal to 1. An

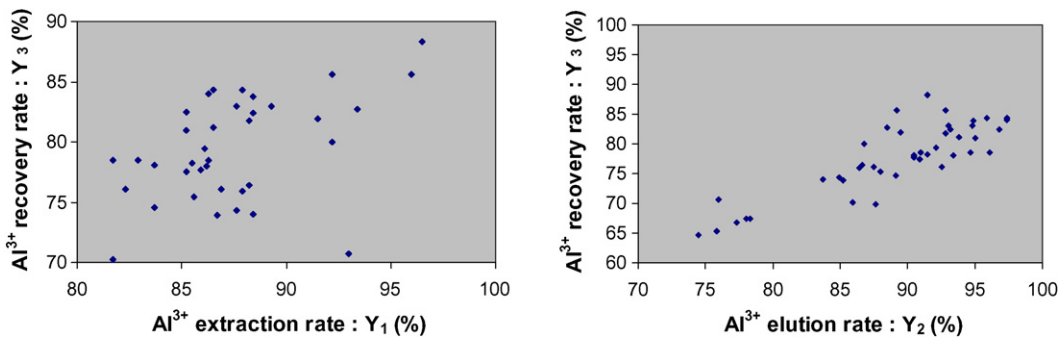

Fig. 3. Correlation between aluminium extraction rate Y_1, aluminium elution rate Y_2 and aluminium recovery rate Y_3.

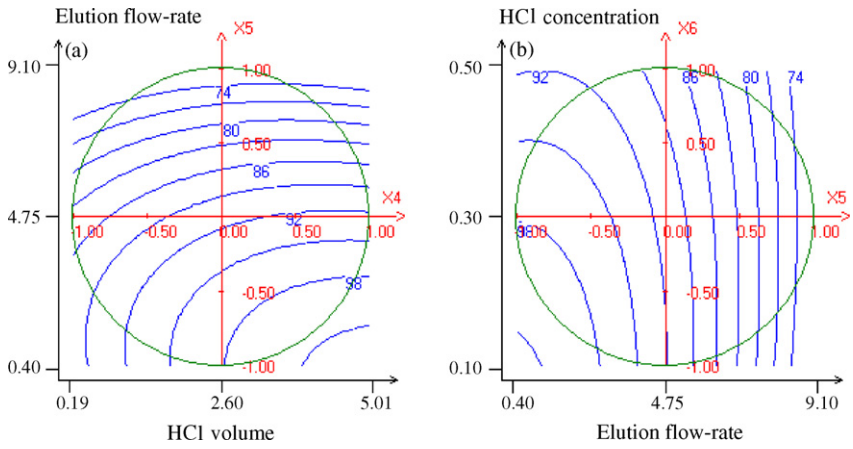

Fig. 4. Study of elution parameters (a) variation of the response-Y_3 in the plane: X_4 (HCl volume), X_5 (elution flow-rate) and fixed factors, flow-through sample volume = 2.75 ml, sample percolation rate = 4.75 ml min^{-1}, sample metal concentration = 110 $\mu g\,l^{-1}$ and HCl concentration = 0.30 mol l^{-1}. (b) Variation of the response-Y_3 in the plane: X_5 (elution flow-rate), X_6 (HCl concentration) and fixed factors, flow-through sample volume = 2.75 ml, sample percolation rate = 4.75 ml min^{-1}, sample metal concentration = 110 $\mu g\,l^{-1}$ and HCl volume = 2.60 ml.

aluminium recovery rate between 90 and 95% was acceptable, but the desirability was equal to 0 if Y_3 was lower than 90%. This function was physically mapped over the domain for X_1, X_2, X_3, X_4, X_5 and X_6 (Fig. 6), giving a reliable general picture of the acceptable region. From these desirability functions and by combining each response, it has been possible to establish an application domain of each factor for at least 95% aluminium recovery rate.

In order to determine analytical features and study application of the optimized extraction procedure, factors were then fixed with following values: a flow-through sample volume of 1.5 ml, a sample percolation (or extraction) flow-rate of 2 ml min^{-1}, a HCl volume of 2 ml, an elution flow-rate of 3 ml min^{-1} and a HCl concentration of 0.10 mol l^{-1}.

3.5. Analytical features

The calibration graph under the conditions previously quoted is given as $A = 3.38 \times 10^{-1} + 4.6 \times 10^{-3}\,C$ in the range of 2.2–200 $\mu g\,l^{-1}$ (A is aborbance of complex, C is aluminium concentration in solution, $\mu g\,l^{-1}$). The precision of the procedure, determined as the relative standard deviation in sample solutions containing between 10 and 150 $\mu g\,l^{-1}$ of aluminium is in the range of 9.3–2.8%, respectively, calculated by 10 measurements. The limit of detection (LOD), defined as the aluminium concentration that gives a response equivalent to three times the standard deviation (s) of the blank ($n = 11$) was found to be 1.1 $\mu g\,l^{-1}$ in 1.5 ml of sample solution.

3.6. Effect of foreign ions

The effect of potential interfering species in the determination of 100 $\mu g\,l^{-1}$ Al(III) was studied. Amounts of each species were considered tolerable, when the signal in the presence of the species resulted in a deviation of the absorbance less than 5%, compared with the signal for aluminium alone. Cations Fe^{3+} (3 mg l^{-1}) and Fe^{2+} (5 mg l^{-1}) are potential interfering ions, but these concentrations are not allowed in finished waters, according European legislation for waters intended for human consumption [1]. It is the same for all the other cations (Mn^{2+},

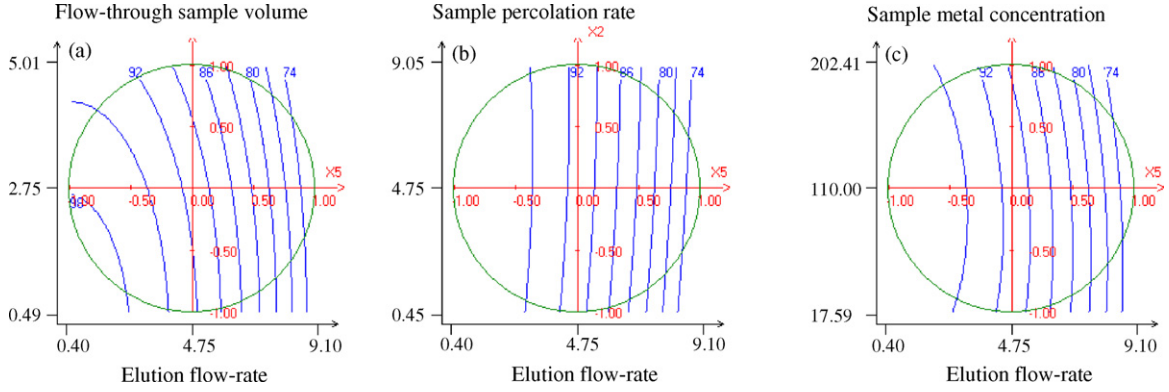

Fig. 5. Study of extraction parameters (a) variation of the response-Y_3 in the plane: X_1 (flow-through sample volume), X_5 (elution flow-rate) and fixed factors, sample percolation rate = 4.75 ml min^{-1}, sample metal concentration = 110 $\mu g\,l^{-1}$, HCl volume = 2.60 ml and HCl concentration = 0.30 mol l^{-1}. (b) Variation of the response-Y_3 in the plane: X_2 (sample percolation rate), X_5 (elution flow-rate) and fixed factors, flow-through sample volume = 2.75 ml, sample metal concentration = 110 $\mu g\,l^{-1}$, HCl volume = 2.60 ml and HCl concentration = 0.30 mol l^{-1}. (c) Variation of the response-Y_3 in the plane: X_3 (sample metal concentration), X_5 (elution flow-rate) and fixed factors, flow-through sample volume = 2.75 ml, sample percolation rate = 4.75 ml min^{-1}, HCl volume = 2.60 ml and HCl concentration = 0.30 mol l^{-1}.

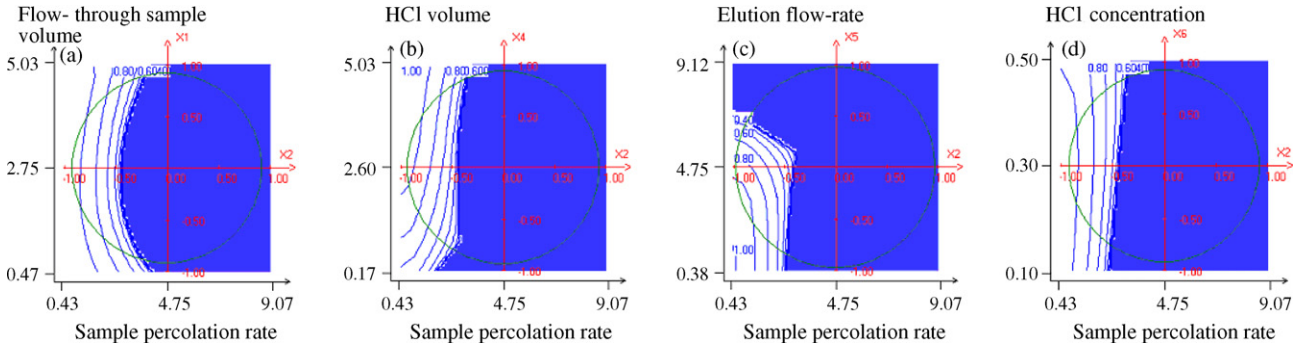

Fig. 6. Study of the desirability (a) variation of the desirability in the plane X_1, X_2 (sample volume, sample percolation rate) with fixed factors: X_3 (sample metal concentration) = 121.05 μg l^{-1}; X_4 (HCl volume) = 3.05 ml; X_5 (elution flow-rate) = 3.32 ml min^{-1}; X_6 (HCl concentration) = 0.30 mol l^{-1}. (b) Variation of the desirability in the plane X_4, X_2 (HCl volume, sample percolation rate) with fixed factors: X_1 = 2.94 ml; X_3 = 121.05 μg l^{-1}; X_5 = 3.32 ml min^{-1}; X_6 = 0.30 mol l^{-1}. (c) Variation of the desirability in the plane X_5, X_2 (elution flow-rate, sample percolation rate) with fixed factors: X_1 = 2.94 ml; X_3 = 121.05 μg l^{-1}; X_4 = 3.05 ml; X_6 = 0.30 mol l^{-1}. (d) Variation of the desirability in the plane X_6, X_2 (HCl concentration, sample percolation rate) with fixed factors: X_1 = 2.94 ml; X_3 = 121.05 μg l^{-1}; X_4 = 3.05 ml; X_5 = 3.32 ml min^{-1}.

Cu^{2+}, Ni^{2+}, Zn^{2+}, K^+, Na^+) tested during these experiments. Method is nevertheless sensitive to waters containing Mg^{2+} above 100 mg l^{-1} and Ca^{2+} above 250 mg l^{-1}. Method is not sensitive to the presence of PO_4^{3-} but presence of fluoride ions may have an impact by the formation of Al–F complexes [28]. The whole results of system selectivity are given Table 3.

3.7. Application

In order to evaluate the accuracy of the developed procedure, aluminium was determined at the outlet of a potable water treatment unit operating with aluminium polychloride as a flocculating reagent (Vallon Dol Water Treatement Unit, Société des Eaux de Marseille, Marseille, France – 170 000 m^3 raw water treated each day).

During these procedures, aluminium amounts were determined successively determined by our developped procedure – flowing through microcolumn, acid desorption and spectrophotometric determination – and by GF–AAS. Aluminium amounts found by both procedures varied between 41 and 68 μg l^{-1} (Table 4).

The results from GF–AAS and the proposed method are in good agreement, and the statistical comparison applied showed no significant difference between the two methods (r^2 = 0.9979). These results proved that the procedure could be applied satisfactorily for aluminium determination in finished waters.

Table 3
Maximum tolerable amounts of foreign ions in on-line system using SA-XAD microcolumn (aluminium concentration = 100 μg l^{-1})

Substance	Maximum tolerable amount (mg l^{-1})
Fe^{3+}	0.5
Mn^{2+}, F^-, Fe^{2+}	1
Cu^{2+}, PO_4^{3-}	5
Ni^{2+}, Zn^{2+}	10
Mg^{2+}	100
Ca^{2+}, SO_4^{2-}, Cl^-	250
K^+, Na^+	1000

Table 4
Results obtained for aluminium determination at the outlet of a potable water treatment unit

Sample	Reference method (μg l^{-1})	Proposed method (μg l^{-1})	Recovery (%)
1	44.1 ± 0.3	44.8 ± 0.2	−1.59
2	43.3 ± 0.1	44.6 ± 0.1	−3.00
3	48.1 ± 0.2	48.7 ± 0.4	−1.25
4	41.2 ± 0.1	41.9 ± 0.3	−1.70
5	47.5 ± 0.1	48.6 ± 0.1	−2.32
6	64.6 ± 0.1	64.8 ± 0.1	−3,19
7	67.5 ± 0.2	67.7 ± 0.1	−0.31
8	65.7 ± 0.3	65.1 ± 0.2	0.91
9	68.2 ± 0.3	68.4 ± 0.3	−0.30
10	67.4 ± 0.1	67.9 ± 0.1	−0.74

Confidence interval: 95%.

4. Conclusion

The use of an experimental design to determine global optimum to retain at least 95% of initial amount of aluminium has allowed us to obtain this result in only 43 experiments, while being sure not to privilege one parameter against another one. On-site validations have allowed us to assess the relevance of factors tested during the exprimental design approach: flow-through sample volume, sample percolation rate, sample metal concentration, eluent volume, elution flow-rate and concentration of eluent. However, results obtained from this study show that the elution step is largely predominant upon the extraction step. Moreover, it has been proved that it is HCl concentration and/or HCl volume which is the most influential parameter when operating with this modified chelating resin.

The fact that extraction yield value as a function of metal amount in the range 20–200 μg l^{-1} is quasi-independent is an important result, and shows that the modified resin is well suited for the extraction of aluminium at the outlet of potable water treatment units.

This work has also demonstrated the potentialities of functionalized SA-XAD resin combined with spectrophotometry and

a flow injection system for aluminium determination in aqueous samples such as effluents from potable water treatment unit. Further experiments are needed to enlarge potentialities of such a device.

Acknowledgements

The authors wish to thanks Société des Eaux de Marseille for their technical and financial support, and especially Mr. Gérard Lieutaud. This study has although been supported by OSEO-ANVAR and European FSE Programme.

References

[1] Directive 98/83/EC on the quality of water intended for human consumption, 1990.
[2] K. Derend, G. Van der Voet, W.H. Boer, Kidney Int. 59 (2001) 746.
[3] T.P. Flaten, Brain Res. Bull. 55 (2001) 187.
[4] X. Lu, Z. Chen, X. Yang, Water Res. 33 (1999) 3271.
[5] C. Gagnon, B.P.A. Grandjean, J. Thibault, Artif. Intell. Eng. 11 (1997) 401.
[6] Directive 2000/60/CE of the European Parliament and the Council of 23 October 2000 establishing a framework for Community action in the field of water policy, Official J. L327 (2000) 1.
[7] N.C. Dias, M.D. Porter, J.S. Fritz, Anal. Chim. Acta 558 (2006) 230.
[8] Z. Legnerova, D. Satinsky, P. Solich, Anal. Chim. Acta 497 (2003) 165.
[9] M. Luo, S. Bi, J. Inorg. Biochem. 97 (2003) 173.
[10] G. Yang, Z. Huang, Q. Hu, J. Yin, Talanta 58 (2002) 511.
[11] A. Economou, TrAC Trend. Anal. Chem. 24 (2005) 416.
[12] C. Pons, R. Forteza, V. Cerdà, Anal. Chim. Acta 550 (2005) 33.
[13] C. Pons, R. Forteza, V. Cerdà, Talanta 66 (2005) 210.
[14] B.S. Garg, R.K. Sharma, N. Bhojak, S. Mittal, Microchem. J. 61 (1999) 94.
[15] B.R. Ree, L.A. Errede, G.B. Jefson, B.A. Langager, U.S. Patent 4, 153,661 (1979).
[16] E.M. Thurman, K. Snavely, Trend Anal. Chem. 19 (2000) 18.
[17] S. Boussetta, C. Branger, A. Margaillan, J.-L. Boudenne, B. Coulomb, Sep. Sci. Technol. 41 (2006) 1619.
[18] M.E. Léon-Gonzalez, L.V. Perez-Arribas, J. Chromatogr. A 902 (2000) 3.
[19] P.K. Tewari, A.K. Singh, Talanta 53 (2001) 823.
[20] J.-L. Boudenne, S. Boussetta, C. Brach-Papa, C. Branger, A. Margaillan, F. Théraulaz, Polym. Int. 51 (2002) 1050.
[21] E. Becerra, A. Cladera, V. Cerda, Lab. Robot. Automation 11 (1999) 131.
[22] D.H. Doehlert, Appl. Stat. 19 (1970) 231.
[23] D. Mathieu, J. Nony, R. Phan-Tan-Luu, NEMROD-W, LPRAI, Marseille, 1998.
[24] G.C. Derringer, KGK-Kaut. Gummi Kunst. 33 (1980) 619.
[25] D.C. Montgomery, Design and Analysis of Experiments, fifth ed., Wiley, 2001.
[26] M.C. Alavarez-Ros, S. Sanchez-Cortez, J.V. Garcia-Ramos, Spectrochim. Acta A 56 (2000) 2471.
[27] C. Brach-Papa, B. Coulomb, C. Branger, A. Margaillan, F. Théraulaz, P. Vanloot, J.-L. Boudenne, Anal. Bioanal. Chem. 378 (2004) 1652.
[28] V. Manoharan, P. Loganathan, R.W. Tillman, R.L. Parfitt, Environ. Pol. 145 (2007) 778.

Available online at www.sciencedirect.com
ScienceDirect
Talanta 73 (2007) 262–268
Talanta
www.elsevier.com/locate/talanta

Application of activated glassy carbon electrode for the detection of nuciferine in lotus leaves

Qin Xu, Ren-Xia Guo, Chen-Yin Wang, Xiao-Ya Hu *

College of Chemistry and Chemical Engineering, Yang Zhou University, Yang Zhou 225002, China

Received 16 January 2007; received in revised form 16 March 2007; accepted 18 March 2007
Available online 30 March 2007

Abstract

The electrochemical behavior of nuciferine has been studied for the first time. Nuciferine is irreversibly oxidized at high potentials, resulting in the formation of orthoquinone. The amount of the obtained orthoquinone is pH-dependent, and it demonstrates quasi-reversible electrochemical behavior at less positive potential. The concentration of nuciferine was successfully determined by using the redox character of the electrochemically obtained orthoquinone. A linear range between 8.7×10^{-9} and 5.6×10^{-7} mol/L and a detection limit of 5.0×10^{-9} mol/L were obtained. The method has also been used to quantify nuciferine concentration in lotus leaves that obtained from the Slim West Lake, and the average result was 0.29% (w/w).

Keywords: Aromatic ether; Nuciferine; Activated glassy carbon electrode

1. Introduction

The fundamental electron-transfer properties of quinones have been extensively examined in both aqueous and non-aqueous environments [1,2]. They represent one of the oldest and most basic redox processes [3], and they have stimulated widespread effort related to their electrochemical analysis, particularly for monitoring neurotransmitters in vivo [4,5]. In view of the widespread study of the quinone entity in naturally occurring systems, we were somewhat surprised that few work reported the electrochemistry of quinone that obtained by electrochemical oxidation, though it has been reported that the electrochemical oxidation of aromatic ethers can result two types of generally useful quinones [6].

Nuciferine, an aromatic ether containing compound (Scheme 1), is the constituent of lotus leaves. It has been known to relax smooth muscle tissue and to have vasodilating, hypotensive, and anti-arrhythmic properties, to possess an inhibitory action toward acetylcholine in rat Renshaw cells [7], to lower hyperlipemia [8], to level off cholesterol [9], to resist karyokinesis and to exhibit antimicrobial activity [10]. Recently, it is newly reported to show anti-HIV activity [11]. Detecting nuciferine's concentration is very important. Gas chromatography [12], high-performance liquid chromatography–mass spectrometry (HPLC–MS) [13,14] and thin-layer chromatography (TLC) [15] methods have been used, however none of them was based on the electrochemical character of nuciferine.

In this article, we tried to oxidize nuciferine into orthoquinone containing compound by electrochemical method firstly, and then determine its concentration by using the redox character of the obtained orthoquinone. To realize this purpose, an active and reproducible electrode surface is very important. Glassy carbon electrodes (GC electrodes) have gained great interest owing to their physical and chemical properties. However the electrodes that had been freshly polished by alumina showed relatively poor activity toward the oxidations of several electroactive species. In most cases, the electrode behavior degrades with time due to the adsorption of impurities from the solution or chemical changes to the electrode surface, and the solid electrode becomes unsuitable for quantitative measurements. Therefore the GC electrode should be activated and renewed quickly and reproducibly. Different methods have been applied to obtain the purpose, including electrochemical pretreatments [16], laser irradiation [17], vacuum heat treatment [18], and exposure to UV-generated ozone [19]. Though these methods

* Corresponding author. Tel.: +86 514 7971690; fax: +86 514 7975587.
E-mail address: xyhu@yzu.edu.cn (X.-Y. Hu).

0039-9140/$ – see front matter © 2007 Published by Elsevier B.V.
doi:10.1016/j.talanta.2007.03.044

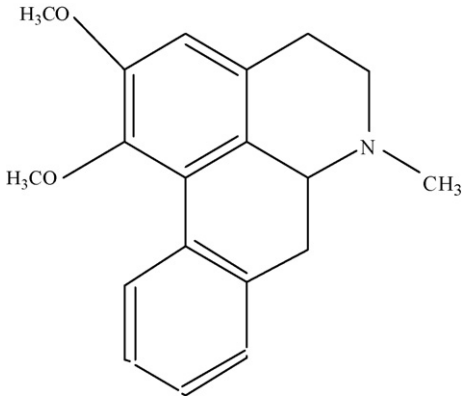

Scheme 1. The structure of nuciferine.

have large beneficial effects on electrode performance, none of them mentioned so far can be carried out quickly.

Here we reported an easy and facile way to activate the GC electrode by dipping it in chromatic acid for a few minutes. Cyclic voltammetry and atomic forced microscopy (AFM) were used to study the surface properties of the activated electrode. The activated electrode was used to determine the concentration of nuciferine. The performances of the electrode, i.e. linear range, sensitivity, selectivity, stability and reproducibility were described. The nuciferine concentrations in lotus leaves that obtained from the Slim West Lake have been quantified successfully, and the result obtained was in good accordance with that obtained by high-performance liquid chromatography (HPLC).

2. Experimental

2.1. Instruments and reagents

All the electrochemical experiments were performed with CHI 660A electrochemical workstation (Shanghai Chenhua, China). A three-electrode system was selected, with a GC electrode (diameter 3 mm, Shanghai Chenghua, China) (GC electrode) as the working electrode, a saturated calomel electrode (SCE) as the reference electrode and a platinum spiral used as the counter electrode. Atomic force microscopy (AFM) images were obtained using a Nanoscope IIIa controller operates in tapping mode (VEECO, USA).

Ultra-pure water was obtained with a Milli-Q plus water purification system (Millipore Co. Ltd., USA) (18 MΩ). Nuciferine standard solution (obtained from National Institute for the control of Pharmaceutical and Biological Products, China) was prepared by dissolving it in 0.01 mol/L HCl solution. Chromic acid was prepared according to Ref. [19]. One hundred milliliters pH 3 B–R (Britton–Robinson) buffer solution was prepared by dissolving 0.46 mL acetic acid, 0.54 mL phosphoric acid and 0.5 g boric acid in 100 mL pure water, and then adjusted pH by 1 mol/L NaOH. Before experiments, all the glassware were cleaned with H_2O_2–nitric acid (1:1, v/v) solution and rinsed with deionized water.

2.2. Preparing of nuciferine sample solution

The lotus leaves were picked from the Slim West Lake (Yang Zhou, Jiangsu, China), and then pulverized after drying. 0.1 g sample of the pulverized leaves was extracted with methanol–1.0% hydrochloric acid aqueous solutions (50:50, v/v; 20 mL) by sonicating for 15 min, and then centrifuging for 5 min. Extraction was repeated once. The supernatant was placed in a 50 mL volumetric flask, diluted to volume [12]. The solution was filtered through a 0.45 μm filter before use, and 0.1 mL of it was added to 10 mL pH 3 B–R buffer solution for determination.

2.3. Procedures

The GC electrode was polished by 0.3 μm alumina aqueous slurry, and then thoroughly washed with purified water. The procedure for the activation of the electrode was as follows. Firstly, it was activated in chromatic acid for some minutes. After thoroughly washed with purified water, it was immersed in the supporting electrolyte and then cycled from −0.2 to 1.2 V at the scan rate of 100 mV/s until the cyclic voltammograms became stable. After adding nuciferine, the solution was stirred for about 5 s to ensure thorough mixing of nuciferine within the solution. For repeated use, the electrodes were renewed in chromatic acid and cycled from −0.2 to 1.2 V in the supporting electrolyte to ensure that no product remained on the electrode.

3. Results and discussion

3.1. Characterization of the slurry polished and activated GC electrode

Fig. 1 compares the cyclic voltammograms of a alumina slurry freshly polished GC electrode and an activated GC electrode in 1.0×10^{-3} mol/L $K_3Fe(CN)_6$. The ΔE_p of the alumina slurry freshly polished GC electrode is about 75 mV. After activation, this value decreases to 65 mV. On the other hand, the current of the activated GC electrode increases. These indicate

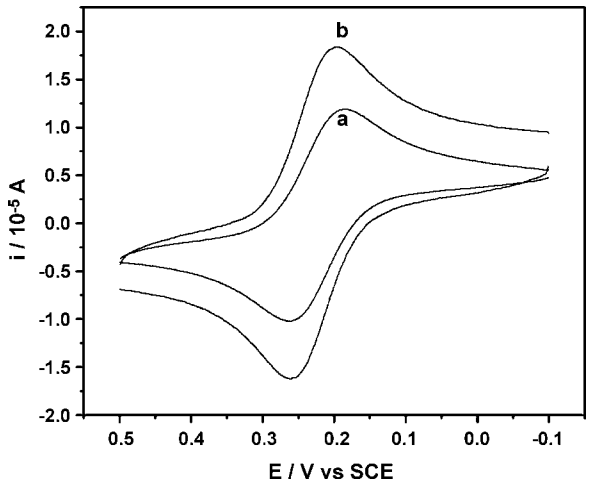

Fig. 1. Cyclic voltammetry of 1.0×10^{-3} mol/L $K_3Fe(CN)_6$ on the alumina slurry polished GC (a) and the activated GC (b) with a scan rate of 100 mV/s.

the quick charge transfer kinetics of the electrons on the activated electrode, which are in agreement with the previously studies [21].

The enhancement of the current and the decrease of ΔE_p of the activated electrode may be caused by the following reasons: (1) surface cleanliness or lack of impurities to adsorb on the surface blocking active sites; (2) surface roughness causing the effective area for electron transfer than the geometric area; (3) the presence of surface functional groups that mediate electron transfer. To prove those assumptions, atomic forced microscopy (AFM) and electrochemical method were applied.

It is well known that chromatic acid can be used to clean the experiment apparatus. In our experiment, it was used not only for the activation of the electrode but also for the cleaning of the electrode. By AFM, we could observe that there were many impurities in the alumina slurry polished GC electrode, while few were observed in the activated GC electrode. It implied that the activation process removed impurities from the polished GC electrode surface. AFM images also revealed that the activation process increased the roughness of the electrode. Fig. 2 shows the morphology of the GC electrode before and after activation. Fig. 2A is an ordinary polished surface, showing the small dots

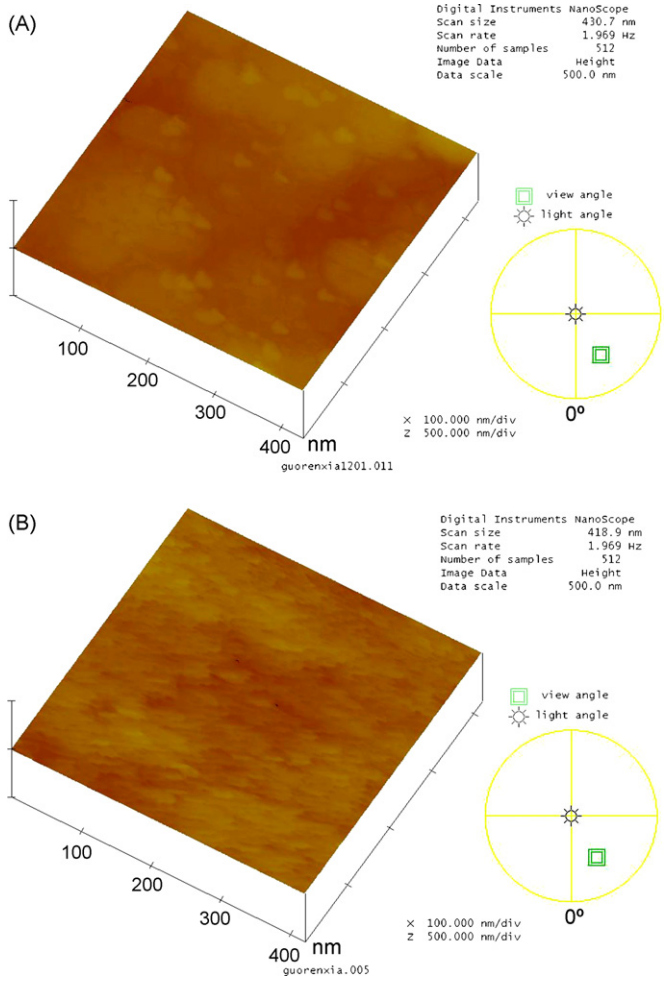

Fig. 2. AFM images of the alumina slurry polished GC electrode (A) and the activated GC electrode (B).

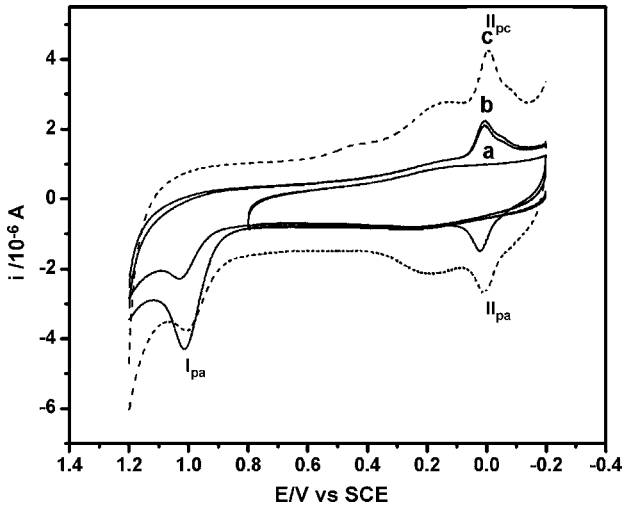

Fig. 3. Electrochemical behavior of 8.7×10^{-6} mol/L nuciferine in pH 3 B–R buffer solution on the alumina slurry polished GC electrode at the scan range of −0.2 to 0.8 V (a); at the scan range of −0.2 to 1.2 V (b); and on the activated GC electrode at the scan range of −0.2 to 1.2 V (c). Scan rate 100 mV/s.

common to glassy carbon. After activation, the surface became rougher (Fig. 2B). The roughness of the electrode surface could provide more sites for the accumulation of nuciferine, and could improve the sensitivity of the electrode.

After dipping in chromatic acid for different time, the activated GC electrode cycled in bare pH 3 B–R buffer solution would show a couple of redox peaks at ca. 200 mV, and the background charging current would increase too. The redox peaks was due to the formation of functional groups, such as quinine and surface oxide [21]. The presence of these functional groups could mediate electron transfer and increase the sensitivity of the electrode. With the increase of the dipping time, the charge current increased, and became stable after 5 min.

3.2. Electrochemical behavior of nuciferine

Fig. 3 shows the cyclic voltammograms of 8.7×10^{-6} mol/L nuciferine at the alumina slurry polished GC (Fig. 3a and b) and the activate GC electrode (Fig. 3c) in pH 3 B–R solutions. As it can be observed, an anodic oxidation peak is obtained at about 1000 mV versus SCE on the positive scan at the first cycle both on the alumina slurry polished GC electrode and the activated electrode (Fig. 3a and c). It decreases in size at the second scan. The return scan of the first cycle shows a wave at 0 mV. The second voltammetric cycle shows an oxidation at a lower potential (20 mV) and again a reduction at 0 mV on the return scan. Therefore nuciferine at the GC electrode undergoes an ECE process, as defined by Kissinger and Heineman [22]. This mechanism involves the electrochemical generation of a product at high positive potentials with a chemical follow up reaction occurring, give rise to a product which exhibit a quasi-reversible couple at lower positive potentials. It was proven by scanning (with a new slurry polished electrode) to a potential lower than the oxidation potential (Fig. 3a). The absence of the reduction waves on the reverse scan and the subsequent reoxidation waves on the forward scan indicates that the quasi-reversible couple is

due to a product formed at higher potentials. It has been reported that anodic oxidation of appropriate aromatic ethers serves as a reasonably general method for the preparation of benzoquinone and naphthoquinone bisketals [23,24], and a catechol orthoformate group can undergoes an irreversible two-electron oxidation to produce the orthoquinone, with simultaneous release of the orthoformate substituent [25]. Until now, several observations have support these interpretations [26]. Compared with the electrochemical response of nuciferine at the polished electrode, the activation process made the electrode sensitive to the presence of nuficerine (Fig. 3c). On the other hand, the apparent capacitance of the activated GC electrode increased. It could be caused by the increase in microscopic surface area or by an increase in the capacitance per unit of microscopic area or both [27], and AFM image has verified it.

Oxidations of nuciferine at the activated electrode were studied in detail by using cyclic voltammetry in the solution containing 8.7×10^{-6} mol/L nuciferine. With respect to the first circle, $E_{I_{pa}}$ at ca. 1000 mV shifted negatively with the increase of the logarithm of the scan rate according to the equation: $E_p(I_{pa}) = 1.09 + 0.08 \log v (R = 0.998)$. On the other hand, the current of peak I increased linearly with the square root of scan rate. It indicated that nuciferine was irreversibly oxidized at high potential [28]. However, the potentials of peaks II at about 0 mV remain constant for a scan rate from 10 to 300 mV/s. On the other hand, the separation of the redox peaks II (ΔE_p) remains constant at 10 mV. It is well known that ΔE_p can be used as a measure of the apparent electrochemical rate constant. The small peak separation is close to the theoretical value for an immobilized redox couple in equilibrium with the electrode potential [29], which has been studied in detail [30]. The peak currents of II_{pa} and II_{pc} have linear relationships with the scan rated from 10 to 300 mV/s, as expected for the thin-layer electrochemical behavior.

By comparing the potentials of the peaks at different pH values, some information on the mechanism of nuciferine oxidation was provided. The peak potential of the first anodic peak shifted towards more negative potentials as the pH increased. When pH was over 6, peak I_{pa} changed into two peaks, and disappeared gradually. It is the reason that nuciferine cannot dissolve in neutral or alkaline solution and it even can change into other substances. For peaks II, their potential shifted negatively with the increase of pH according to the following equation: $E_p(II_{pa}) = 0.17–0.058\text{pH} (R = 0.999)$ and $E_p(II_{pc}) = 0.18–0.056\text{pH} (R = 0.999)$. The values are reasonably close to the theoretical value of −58 mV/pH for equal electron and proton transportation. On the other hand, the width at half-peak height of peak II is about 55 mV at different scan rate and different pH, which is close to the theoretical value 90/*n* for a two electron, two proton electrochemical reaction involving an adsorbed species [31,33]. When pH was above 6, the reduction peak of II_{pc} disappeared too. The same was found during the oxidation of luteolin [33]. From this, it was concluded that the reaction at higher pH follows a different pathway from that at lower pH and the quinones generated at high pH are unstable.

According to the evidences mentioned above, the mechanism of nuciferine at the GC electrode may be expressed as follows:

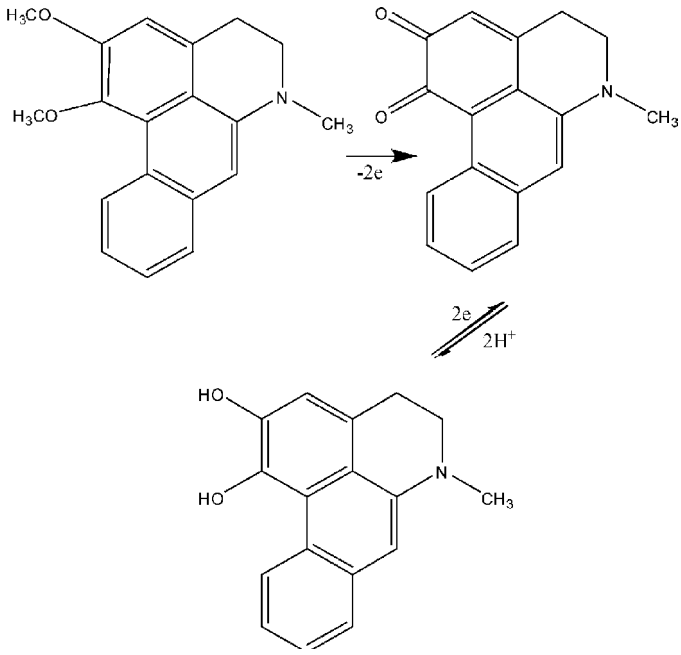

During the anodic oxidation process, quinone was formed (II). The quinone was particularly useful for the appearance of the redox peaks at about 0 mV. The redox activity of the quinone was an advantage because it permits the use of cyclic voltammetry (CV) or differential pulse voltammetry (DPV) to characterize the products and to quantify nuciferine. More experiments would be performed to verify the mechanism in the forthcoming study.

3.3. Detect nuciferine by the activated GCE

After some preliminary experiments, the activated GC electrode was applied for the detection of nuciferine, and the influences were studied.

3.3.1. Influence of pH

The effects of pH on the current of peak I_{pa} and II of nuciferine were investigated in the range of pH values from 2.0 to 7.0. The result was shown in Fig. 4. It was found that the peak currents reached the maximum when the pH was 3. Further increasing the solution pH yielded a gradual decrease in the nuciferine peak currents. As a result, solutions of pH 3 was used in the following experiments.

3.3.2. Influence of the accumulation potential and accumulation time

It has been observed that the adsorption of quinone on the electrode is essential for the rapid electron transfer to the ortho hydroquinone/quinone redox center for quinone, DA and several other catechols [30,31]. Therefore we studied the accumulation potential and time for the sensitivity of nuciferine detection.

The effect of the accumulation potential on the peak II_a current was examined in the range of 0.2–0.6 V. The slurry polished GC electrode showed no accumulation of the peak II_a of nuciferine. For the activated electrode, however, the peak II_a current increased when the applied potential shifted negatively from 0.2 V. The functional groups on the activated electrode would

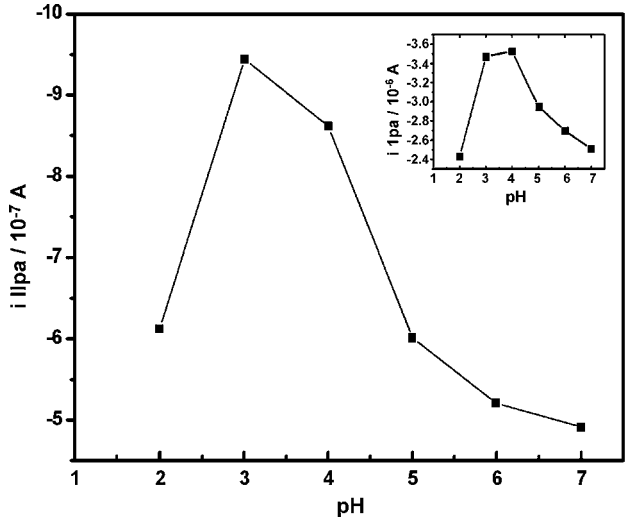

Fig. 4. Effects of pH on the currents of peak II and I_{pa} (insert of the figure) in the presence of 8.7×10^{-6} mol/L nuciferine.

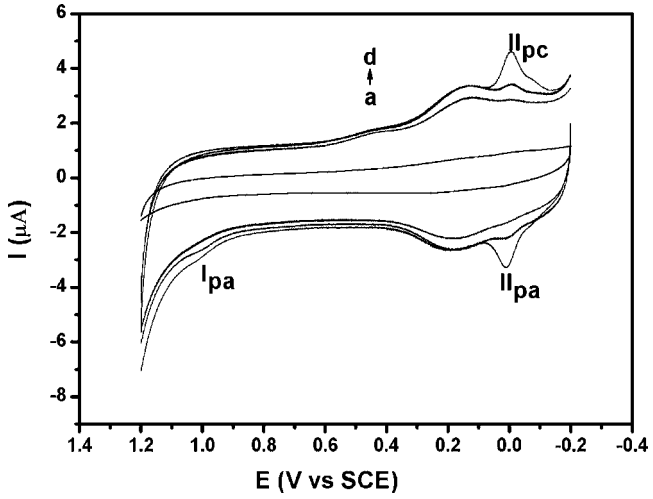

Fig. 5. Electrochemical behavior of 5.0×10^{-7} mol/L nuciferine on the alumina slurry polished GC electrode (a) after accumulation at 0 V for 100 s and the activated GC electrode after accumulation at 0 V for 0 s (b), 5 s (c) and 100 s (d) in pH 3 B–R buffer.

contribute to the adsorption of nuciferine on the electrode. On the other hand, nuciferine was positively charged in pH 3 solution, so it would be preconcentrated on the activated electrode at 0 mV or negative potentials. However, the background current increased too at negative potentials, which would decrease the sensitivity of the electrode. So, we chose 0 mV as the accumulation potential.

Another important parameter influencing the sensitivity of the detection is the accumulation time of nuciferine. The peak II currents increased with the increase of the accumulation time, which indicated an enhancement of nuciferine at the modified electrode. Before adsorptive equilibrium reached, the longer the accumulation time, the more the nuciferine adsorbed was and thus the larger the peak currents became. For higher nuciferine concentration such as 4.0×10^{-7} mol/L, the peak currents tended to level off even after accumulating 70 s, illustrating that adsorptive equilibrium was achieved. To increase the sensitivity for lower concentrations, the accumulation time was set at 100 s. Fig. 5 shows the cyclic voltammograms of 5.0×10^{-7} mol/L nuciferine at the alumina slurry polished GC electrode (a) and the activated (b–d) in pH 3 B–R solutions. Such low concentration nuciferine did not yield any signal at the conventional polished GC electrode even after accumulating at 0 mV for about 100 s (Fig. 5a). However, on the activated electrode, the peak currents increased with the increase of the accumulation time due to the high surface and the accumulation process (Fig. 5a–c). It was 15 times higher than that obtained without pre-concentrating procedure, which indicated that the accumulation process would increase the sensitivity of the detection.

3.3.3. Linear range and detection limits

To verify the linear relationship between peak currents and nuciferine concentrations, six calibration graphs were constructed under optimum conditions and after 100 s accumulation time (Fig. 6). The results of this study indicated that in all cases the current–concentration relationships were linear in the concentration range of 8.7×10^{-9} to 5.6×10^{-7} mol/L with the correlation coefficients $0.998(i_{II_{pc}})(10^{-6}\ A) = 0.016 + 0.97C(10^{-7}\ mol/L)$ ($R = 0.998$).

According to the IUPAC definition [34], the detection limit (DL) is related to the smallest response that can be detected with reasonable certainty. For a given analytical method, the detection limit is given as follows:

$$DL = \frac{kS_B}{b}$$

where S_B is the standard deviation of the blank measurement, b the sensitivity of the method (determined as the slope of the calibration curve), and k is a statistical constant (a value of $k = 3$ is strongly recommended by IUPAC, based on the confidence interval). Using a least-squares regression program (for a linear fit, and not forcing zero), the slopes for the data of nuciferine from differential pulsed voltammetric analysis (Fig. 6) were

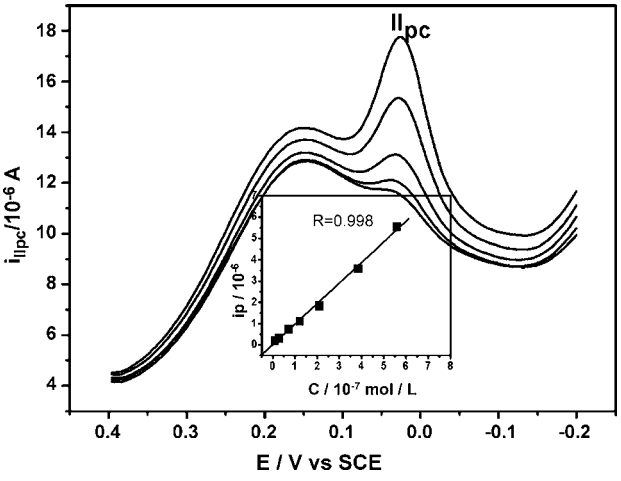

Fig. 6. DPV of nuciferine on the activated GCE at different concentrations (bottom to up): 8.7×10^{-9}, 2.6×10^{-8}, 1.2×10^{-7}, 3.8×10^{-7}, 5.6×10^{-7} mol/L (insert fig.: calibration plot between nuciferine concentration and the current of peak II_{pc}).

Table 1
Influence of the interferents on the peak current of 5.0×10^{-8} mol/L nuciferine under optimal conditions

Interferents	Concentration (mol/L)	Error (%)
Na^+, K^+, Ca^{2+}, Cl^-, SO_4^{2-}, CH_3COO^-	0.005	<5
Citric acid, glucose, tartaric acid, vitamin B_2, vitamin C	5.0×10^{-5}	<5

determined as 0.97. Thus, the detection limit of nuciferine is 5.0×10^{-9} mol/L. At high concentrations, deviation from linearity occurred due to the saturation of the electrode surface.

3.3.4. Interference

The influence of other ions in the analyte solution on the current response was investigated, as shown in Table 1. So all of them have negligible effect on the determination of nuciferine.

3.3.5. Repeatability of the activated electrode

In further study, it was found that nuciferine could adsorb on the slurry polished GC electrode strongly. Even after 50 scan in blank buffer solution, the peak II of nuciferine was still observed. Such strong adsorption would influence the results of the next detection, so the electrode should be renewed each time. Some methods have been used to remove the adsorbed substances, such as polishing, ultrasonic washing and nitric acid oxidation. However, each of them has disadvantages. Polishing would change the surface circumstance of electrode, while ultrasonic and nitric acid could not remove the substances completely. In conclusion, the slurry polished GC electrode cannot be directly used to detect nuciferine, not only because nuciferine and its oxidation product can adsorb on the electrode strongly, but also because the sensitivity of the bare electrode is not good enough.

The activated electrode can be renewed without of polishing, and it can obtain good reproducibility and stability. The response of 5.0×10^{-7} mol/L nuciferine at the activated electrode was examined after re-modify the electrode. Ten successive measurements yield a R.S.D. of 3.0%. In fact, only if the electrode surfaces were properly cleaned, they could exhibit good electrocatalytic behavior and reproducibility. In our experiment the simply activation process circumvents the problem of slow electrode deactivation by adsorbed solution species. The excellent performance of activation process was obtained repeatedly if desired. Such process is renewability and reproducibility.

3.3.6. Determination of nuciferine in standard samples and lotus leaves

In order to verify the reliability of the activated electrode, it was applied to determine nuciferine in standard samples and lotus leaves obtained from the Slim West Lake with different locations. The values were determined with the activated GC electrode using the standard addition method and direct interpolation in the linear regression. After the current responses were determined in 10.0 mL of pH 3 solutions containing different concentration samples of nuciferine, different concentration of nuciferine samples were successively added to the system for standard addition determination. All the concentrations of nuciferine in detection solutions were in the linear response range (Table 2). The nuciferine samples obtained from the lotus leaves of the Slim West Lake were analyzed by the same method. A previous extraction procedure of the lotus leaves was carried out, as described in Section 2.2. Table 3 shows that the results were satisfactory. The precision of the two sets of the experiments was compared by *F*-test. The quantity *F* is defined as the ratio of the variances of the two measurements. In our experiment, *F* is 2.02, which is less than 6.39 [35]. So the results obtained by our method were in good agreement with the values obtained by HPLC method at the 95% probability level. They were in good agreement with the values obtained by HPLC method.

Table 2
Result of recovery test

Added (mol/L)	Measured (mol/L)	Recovery (%)	R.S.D. (%)	Average recovery (%)
8.70×10^{-8}	9.60×10^{-8}	110.3	2.7	102.4
1.74×10^{-7}	1.77×10^{-7}	101.7	3.8	
2.61×10^{-7}	2.61×10^{-7}	100.0	2.9	
3.48×10^{-7}	3.54×10^{-7}	101.7	4.0	
5.22×10^{-7}	5.12×10^{-7}	98.1	3.5	

Table 3
Quantity analysis of nuciferine in lotus leaves obtained from the Slim West Lakes

Real sample	Electrochemical method (g/g) $n = 3$	HPLC (g/g)	R.S.D. (%)
A	0.271	0.276	2.7
B	0.260	0.286	
C	0.330	0.326	
D	0.300	0.310	
E	0.29	0.293	
Average	0.2902	0.298	
Standard deviation (s)	0.027	0.019	

4. Conclusions

In this paper, the electroanalytical chemistry of nuciferine was studied in detail. The mechanism of the electrochemical process was assumed. The electrode activated by chromatic acid was successfully fabricated and used for the detection of nuciferine. It increased the sensitivity of the electrode, and the detection limit was down to 5.0×10^{-9} mol/L. The improved stability, sensitivity and reproducibility of the activated electrode should benefit routine measurements of nuciferine in connection to HPLC or FIA analyses. Additional studies would be performed for gaining further insights into the mechanism of the nuciferine oxidation reaction at the activated electrodes.

Acknowledgements

This work was supported by the National Natural Science Foundation of China (Nos. 20375034, 20675071) and the Novel Foundation of Jiangsu Provincial Education Department for Doctors (2005).

References

[1] G.E. Cabaniss, A.A. Diamantis, W.R. Murphy, R.W. Linton, T.J. Meyer, J. Am. Chem. Soc. 107 (1985) 1845.
[2] T.G. Strein, A.G. Ewing, Anal. Chem. 66 (1994) 3864.
[3] E.J. Laviron, J. Electroanal. Chem. 146 (1983) 15.
[4] K.T. Kawagoe, R.M. Wightman, Talanta 41 (1994) 865.
[5] M.F.S. Teixerira, M.F. Bergamini, C.M.P. Marques, N. Bocchi, Talanta 63 (2004) 1083.
[6] J.S. Swenton, Acc. Chem. Res. 16 (1983) 74.
[7] A.W. Duggan, D. Lodge, T.J. Bixcoe, P.M. Headley, Arch. Int. Parmacodyn. Ther. 204 (1973) 147.
[8] C.C. Tu, X.Y. Li, J.P. Yang, L. Zhou, J. Jianxi, College Tradit. Chin. Med. 13 (2001) 120.
[9] L.J. Du, H. Sun, M. Li, W. Jin, L.Z. Xu, Zhongcaoyao 31 (2000) 526.
[10] L.P. Ji, Shipin Kexue 20 (1999) 64.
[11] A. Aoshima, Y. Ikeshiro, Y.-P. Chen, H. Furukawa, M. Itoigawa, T. Fujioka, K. Mihashi, M. Cosentino, S.L. Morris-Natschke, K.H. Lee, Bioorgan. Med. Chem. 13 (2005) 443.
[12] J. Kunitomo, Y. Yoshikawa, S. Tanaka, Y. Imori, K. Isoi, Y. Masada, K. Hashimoto, T. Inoue, Phytochemistry 3 (1973) 699.
[13] X.B. Luo, B. Chen, J.J. Liu, S.Z. Yao, Anal. Chim. Acta 538 (2005) 129.
[14] L.X. Xu, A. Liu, Chinese J. Pharm. Anal. 6 (1991) 349.
[15] X.O. Wu, Y. Xiong, China Pharma 7 (2004) 262.
[16] A. Dekanskia, J. Stevanović, R. Stevanović, B. Nikolić, V.M. Jovanović, Carbon 39 (2001) 1195.
[17] R.J. Rice, R.L. McCreery, Anal. Chem. 61 (1989) 1637.
[18] K.J. Stutts, P.M. Kovach, W.G. Kurh, R.M. Wightman, Anal. Chem. 55 (1983) 1632.
[19] J. Zhoul, D.O. Wipf, J. Electroanal. Chem. 499 (2000) 121.
[21] D.T. Fagan, I.-F. Hu, T. Kuwana, Anal. Chem. 57 (1985) 2759.
[22] P.T. Kissinger, W.R. Heineman, Laboratory Techniques in Electroanalytical Chemistry, 2nd ed., Marcel Dekker, New York and Basel, 1996, p. 39.
[23] D.K. Jackson, J.S. Swenton, Synth. Commun. 7 (1977) 333.
[24] M.G. Dolson, D.K. Jackson, J.S. Swenton, J. Chem. Soc., Chem. Commun. 7 (1979) 327.
[25] S.K. Lunsford, H. Choi, J. Stinson, A. Yeary, D.D. Dionysiou, Talanta, in press.
[26] B. Nasr, G. Abdellatif, P. Canizares, C. Sáez, J. Lobato, M.A. Rodrigo, Environ. Sci. Technol. 39 (2005) 7234.
[27] S.H. DuVall, R.L. McCreery, Anal. Chem. 71 (1999) 4594.
[28] J. Wang, Analytical Electrochemistry, 2nd ed., Wiley–VCH, 2000, p. 32 (chapter 2).
[29] E.J. Laviron, J. Electroanal. Chem. 52 (1974) 395.
[30] S.H. DuVall, R.L. McCreery, J. Am. Chem. Soc. 122 (2000) 6759.
[31] M. Poon, R.L. McCreery, Anal. Chem. 58 (1986) 2745.
[33] M. Filipiak, Anal. Sci. 17 (Suppl. i) (2001) 1667.
[34] G.L. Long, E.G. Voigtman, M.A. Kosinski, J.D. Winefordner, Anal. Chem. 55 (1983) 1432–1434.
[35] D.A. Skoog, D.M. West, F.J. Holler, Fundamentals of Analytical Chemistry, 7th ed., Thompson Brooks/COLE, p. 56 (chapter 4).

Available online at www.sciencedirect.com
ScienceDirect
Talanta 73 (2007) 269–273
Talanta
www.elsevier.com/locate/talanta

Fast simultaneous determination of 14 nucleosides and nucleobases in cultured *Cordyceps* using ultra-performance liquid chromatography

F.Q. Yang, J. Guan, S.P. Li *

Institute of Chinese Medical Sciences, University of Macau, Taipa, Macao SAR, PR China

Received 22 February 2007; received in revised form 18 March 2007; accepted 18 March 2007
Available online 24 March 2007

Abstract

Determination of nucleosides and their metabolic compounds is important for physiological and pharmacological studies. Herein, a rapid ultra-performance liquid chromatography (UPLC) method was developed for the simultaneous determination of 14 nucleosides and nucleobases, namely adenine, adenosine, cytosine, cytidine, uracil, uridine, guanine, guanosine, hypoxanthin, inosine, thymine, thymidine, 2′-deoxyuridine and cordycepin. The separation was performed on Waters Acquity UPLC system with Acquity UPLC BEH C_{18} column and gradient elution of 0.5 mM acetic acid and acetonitrile in 5 min. The correlation coefficients of 14 analytes were high ($R^2 > 0.9995$) within the test ranges. The LOD and LOQ were lower to 11.9 and 47.0 ng/ml with 1 μl of injection volume, respectively. The overall R.S.D. for intra- and inter-day of 14 analytes were less than 1.8%. The developed method was applied for the analysis of nucleosides and nucleobases in cultured *Cordyceps*, which also could be used for the fast determination of the analytes in pharmaceutical products and biological fluids.

Keywords: Ultra-performance liquid chromatography (UPLC); Nucleosides; Nucleobases; Pressurized liquid extraction; *Cordyceps*

1. Introduction

Nucleosides and their metabolic compounds play the important roles in biochemical processes which relate to several diseases and metabolic disorders. The levels of nucleosides and their metabolic compounds have been proposed as markers for diagnosis of cancers, AIDS, myocardial cellular energy status, diseases progress and therapy responses [1–4]. Therefore, determination of nucleosides and their metabolic compounds is important for physiological and pharmacological studies.

To date, a series of methods, including thin layer chromatography (TLC) [5,6], gas chromatography (GC) [7,8], high performance liquid chromatography (HPLC) [9–11], ion-pair reverse-phase chromatography (IP-RPC) [12,13], liquid chromatography–mass spectrometry (LC–MS) [14,15], capillary zone electrophoresis (CZE) [16,17], micellar electrokinetic chromatography (MEKC) [18,19], capillary electrophoresis–mass spectrometry (CE–MS) [20], capillary electrochromatography (CEC) [21] and immunoassays [22,23], have been developed for the simultaneous determination of nucleosides in biological fluids and herbal materials. Unfortunately, these methods mentioned above have disadvantages such as limit of analytes [5–9,14,16–18,20,21], long analysis time [10,12,13,15,19], low sensitivity [5,6,22,23] and/or environmental unfriendly solvents [9,10,12–15,20] or expensive instrumentation [14,15,20]. Ultra-performance liquid chromatography (UPLC) makes it possible to perform very high-resolution separations in short periods of time with little organic solvent consumption [24], which has attracted wide attention of pharmaceutical and biochemical analysts [25,26].

In this paper, an UPLC method for fast simultaneous determination of 14 nucleosides and nucleobases, namely adenine, adenosine, cytosine, cytidine, uracil, uridine, guanine, guanosine, hypoxanthin, inosine, thymine, thymidine, 2′-deoxyuridine and cordycepin was developed. The validated method was also applied for the determination of the analytes in cultured *Cordyceps*.

2. Experimental

2.1. Materials and chemicals

Adenine, adenosine, cytosine, cytidine, uracil, uridine, guanine, guanosine, hypoxanthin, inosine, thymine, thymidine,

* Corresponding author. Tel.: +853 397 4692; fax: +853 2884 1358.
E-mail address: lishaoping@hotmail.com (S.P. Li).

0039-9140/$ – see front matter © 2007 Elsevier B.V. All rights reserved.
doi:10.1016/j.talanta.2007.03.034

2′-deoxyuridine and cordycepin were purchased from Sigma (St. Louis, MO, USA). Ammonium acetate was from Fluka (Buchs, France). Acetic acid, triethylamine (TEA) and acetonitrile were purchased from Merck (Darmstadt, Germany). Deionized water was prepared using a Millipore Milli-Q Plus system (Millipore, Bedford, MA, USA). Reagents not mentioned here were from standard sources. The materials of cultured *C. sinensis* mycelia were obtained from Hebei, HongKong (HK), Anhui, Jiangxi, Huadong and Wanfeng. Cultured *C. militaris*, one of the substitutes of *C. sinensis*, was obtained from Guobao, HK, Quanxin, Aoli and Xiankang. The species of the cultured *Cordyceps* were certified by State Food and Drug Administration of China or the corresponding author. The voucher specimens of *Cordyceps* are deposited at the Institute of Chinese Medical Sciences, University of Macau, Macao, China.

2.2. UPLC analysis

All analysis were performed on a Waters Acquity UPLC system (Waters, MA, USA), including binary solvent manager, sampler manager, column compartment and PDA detector, connected to a Waters Empower 2 software. An Acquity UPLC BEH C18 column (50 mm × 2.1 mm i.d. particle size, 1.7 μm) also from Waters was used. The column temperature was maintained at 25 °C. The standards and samples were separated using a gradient mobile phase consisting of 0.5 mM acetic acid (A) and acetonitrile (B). The gradient condition is: 0–3 min, 0–3% B; 3–10 min, 3–20% B; and finally, reconditioning the column with 100% A isocratic for 3 min after washing column with 50% B for 3 min. The flow rate was set at 0.25 ml/min and the injection volume was 1 μl. The sample manager temperature was set at 10 °C. The peaks were detected at 254 nm.

2.3. Sample preparation

Sample preparation was performed on a Dionex ASE 200 system (Dionex Corp., Sunnyvale, CA, USA) under the optimized conditions reported before [10]. In brief, the powder of *Cordyceps* (0.2 g) was mixed with diatomaceous earth in a proportion (1:1) and placed into an 11 ml stainless steel extraction cell, and extracted with methanol under optimum conditions: temperature, 160 °C; static extraction time, 5 min; pressure, 1.034×10^4 kPa and one static cycle and one for the number of extraction. The methanol PLE extract was dried at 40 °C using a rotary evaporator (BÜCHI, Switzerland), and the residue was vortaxed with 10 ml deionized water, then filtered through a 0.22 μm MILLEX GV syringe filter (Millipore, MA, USA) prior to inject into the UPLC system.

3. Results and discussion

3.1. Optimization of UPLC conditions

Acetonitrile and water with different modifiers, including ACN–water, ACN–1 mM TEA, ACN–1 mM ammonium acetate and ACN–1 mM acetic acid, were used as mobile phase for optimization of the separation. The results show that mobile phase contains acetic acid is beneficial for the separation (Fig. 1). Furthermore, it was found that lower concentration of acetic acid (1–0.25 mM) could improve the resolution of compounds **2** and **3** but decrease that of compounds **6** and **7**. Especially, the separation of adenine (**6**) and uridine (**7**) could not be achieved when 0.25 mM acetic acid was used. Finally, gradient elution of ACN and 0.5 mM acetic acid aqueous solution was chosen for the separation.

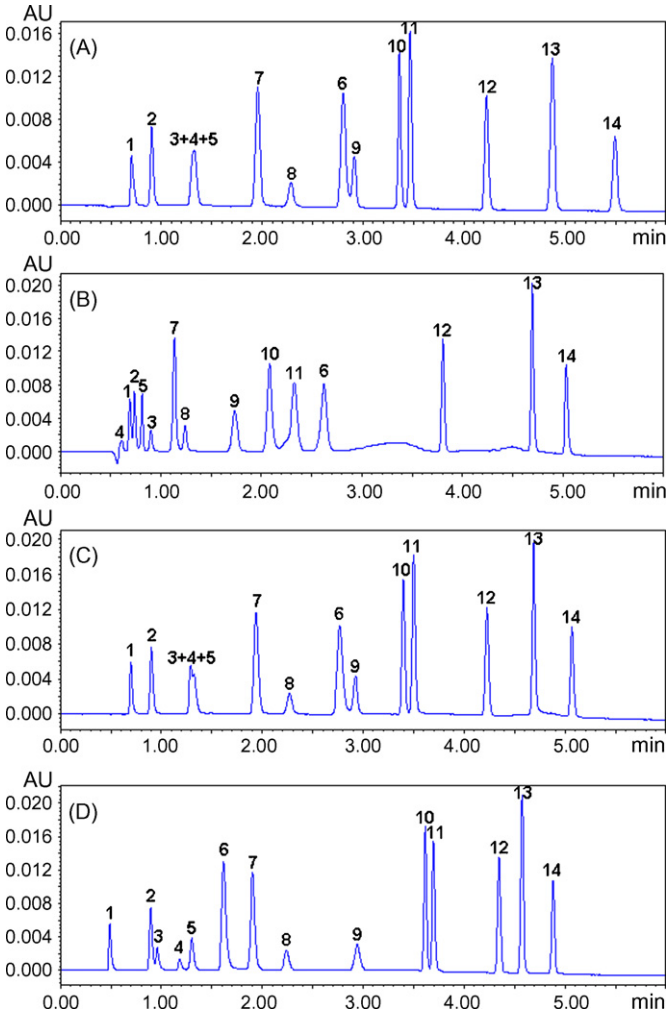

Fig. 1. UPLC chromatograms of mixed standards eluted by different mobile phases. (A) ACN–water; (B) ACN–1 mM TEA; (C) ACN–1 mM ammonium acetate; (D) ACN–1 mM acetic acid. **1**: cytosine; **2**: uracil; **3**: cytidine; **4**: guanine; **5**: hypoxanthin; **6**: adenine; **7**: uridine; **8**: thymine; **9**: 2′-deoxyuridine; **10**: inosine; **11**: guanosine; **12**: thymidine; **13**: adenosine; **14**: cordycepin.

3.2. Stability test

For high throughput analysis, samples usually have to be stayed in auto-sampler for a long time, which should be considered carefully for the unstable analytes. Actually, nucleosides easily degrade [27]. In this study, the stabilities of 14 analytes were tested by inject standard solution at 0, 1, 2, 4, 8, 12 and 18 h under 10 and 25 °C of auto-sampler temperature, respectively.

Table 1
Linear regression data, LOD and LOQ of the investigated compounds

Analytes	Resolution[a]	Linear regression data			LOD (ng/ml)	LOQ (ng/ml)
		Regressive equation[b]	Test range (μg/ml)	r^2		
Cytosine	–	$y = (9891.3 \pm 9.8)x + (18.2 \pm 5.5)$	0.17–4.19	0.9999	11.9	47.0
Cytidine	5.3	$y = (5169.7 \pm 15.7)x - (756.9 \pm 8.3)$	0.56–17.94	0.9999	71.8	239.3
Uracil	1.4	$y = (17664.3 \pm 25.5)x + (573.6 \pm 62.7)$	0.24–61.50	1.0000	40.0	135.9
Uridine	2.4	$y = (8843.9 \pm 22.2)x - (877.1 \pm 112.8)$	0.75–144.00	0.9998	39.5	135.0
Hypoxanthine	1.6	$y = (18188 \pm 4.6)x - (264.8 \pm 13.0)$	0.23–7.22	1.0000	16.9	56.4
2′-Deoxyuridine	4.5	$y = (9699.1 \pm 15.4)x - (73.8 \pm 15.8)$	0.24–5.66	1.0000	50.2	190.8
Inosine	2.9	$y = (9215.7 \pm 21.1)x - (12.3 \pm 9.9)$	0.16–10.36	1.0000	32.0	106.7
Guanine	3.9	$y = (26679.3 \pm 24.8)x - (2550.6 \pm 127.1)$	0.40–12.75	0.9999	25.3	85.4
Guanosine	6.9	$y = (9202.6 \pm 24.9)x - (455.7 \pm 116.0)$	0.35–89.82	0.9998	30.3	98.1
Thymine	10.6	$y = (12623.7 \pm 34.0)x - (242.6 \pm 30.8)$	0.26–4.09	1.0000	32.2	119.9
Thymidine	2.2	$y = (7363.3 \pm 11.5)x + (3.4 \pm 29.7)$	0.19–11.86	1.0000	35.7	125.1
Adenine	12.5	$y = (19744.3 \pm 21.5)x + (735.3 \pm 123.4)$	0.37–47.82	0.9995	18.3	60.5
Adenosine	6.0	$y = (12760.7 \pm 15.5)x - (781.3 \pm 42.8)$	0.32–120.82	0.9995	20.4	78.7
Cordycepin	7.1	$y = (12248.0 \pm 2.0)x + (82.6 \pm 237.4)$	5.52–486.00	0.9997	20.9	72.5

[a] Resolutions of the peaks in HPLC profile of reference compounds were calculated using Waters Empower 2 software.
[b] The regressive equations were determined triplicates, and the data were presented as $y = (\text{mean} \pm \text{S.D.})x \pm (\text{mean} \pm \text{S.D.})$.

The results show that the analytes are stable at both conditions during the test time period except guanine significantly degrades at 25 °C (Table 2). Thus, the sample manager was controlled at 10 °C of temperature and the quantification of investigated compounds was preformed in 18 h.

3.3. Calibration curves

Water stock solutions containing 14 reference compounds were prepared and diluted to appropriate concentrations for the construction of calibration curves. At least six concentrations of the solution were analyzed in triplicate, and then the calibration curves were constructed by plotting the peak areas versus the concentration of each analyte. The results were shown in Table 1.

3.4. Limits of detection and quantification

The water stock solution containing 14 reference compounds was diluted to a series of appropriate concentrations with the same solvent, and an aliquot of the diluted solutions was injected into UPLC-PDA for analysis. The limits of detection (LOD) and quantification (LOQ) under the present chromatographic conditions were determined at a signal-to-noise ratio (S/N) of about 3 and 10, respectively. Table 1 showed the data of LOD and LOQ for each investigated compounds.

3.5. Precision and accuracy

Intra- and inter-day variations were chosen to determine the precision of the developed method. For intra-day variability test,

Table 2
Stability, intra- and inter-day precision of the investigated compounds

Analytes	Stability (R.S.D., %)		Intra-day ($n = 6$)		Inter-day ($n = 6$)	
	10 °C	25 °C	Accuracy (%)[a]	R.S.D. (%)[b]	Accuracy (%)	R.S.D. (%)
Cytosine	1.0	0.6	99.6[c]	1.7	99.7	1.6
Cytidine	0.7	1.9	101.3	0.8	100.9	1.8
Uracil	0.8	0.9	99.6	0.7	100.1	1.0
Uridine	0.8	0.6	96.0	0.6	95.9	0.5
Hypoxanthine	0.8	1.8	100.1	0.4	100.2	0.5
2′-Deoxyuridine	1.2	0.8	99.4	1.5	98.6	1.2
Inosine	0.8	0.7	97.6	0.2	97.8	0.3
Guanine	1.9	7.3	103.3	0.6	104.2	1.3
Guanosine	1.8	3.1	100.0	0.1	99.7	0.2
Thymine	0.7	1.7	96.7	1.2	96.7	0.9
Thymidine	0.7	1.1	97.7	0.3	97.8	0.2
Adenine	0.9	0.8	99.0	0.2	99.0	0.3
Adenosine	0.9	1.1	96.5	1.0	96.3	0.9
Cordycepin	0.8	0.8	98.0	0.3	98.0	0.3

[a] Accuracy (%) = 100 × (mean of measured concentration/nominal concentration).
[b] Mean and relative standard deviation (R.S.D.s).
[c] Mean value for three different concentrations.

Table 3
Recoveries for the assay of 14 compounds in *Cordyceps*

Analyte	Original (μg)	Spiked (μg)	Found[a] (μg)	Recovery[b] (%)	R.S.D.[c] (%)
Cytosine	38.1	34.9	72.9	99.7	0.2
Uracil	349.8	384.4	733.6	99.9	0.2
Cytidine	299.1	224.2	523.8	100.2	1.2
Guanine	69.3	79.7	145.3	95.4	0.8
Hypoxanthin	37.4	45.1	81. 9	98.7	0.1
Adenine	144.1	149.4	294.1	100.4	0.4
Uridine	898.0	900.0	1812.7	101.6	0.3
Thymine	10.3	12.8	22.9	98.4	1.6
2′-Deoxyuridine	42.0	47.2	88.4	98.4	3.2
Inosine	164.9	129.5	293.9	99.7	0.2
Guanosine	1227.7	1122.7	2375.1	102.2	0.4
Thymidine	+[d]	37.1	37.5	101.1	0.8
Adenosine	1320.6	1006.8	2331.8	100.4	0.2
Cordycepin	+	276.1	273.7	99.1	0.1

[a] The data were present as average of three determinations.
[b] Recovery (%) = 100 × ((amount found − original amount)/amount spiked).
[c] R.S.D. (%) = 100 × (S.D./mean).
[d] Under the limit of quantitation.

the mixed standards solution was analyzed for six replicates within 1 day, while for inter-day variability test, the solution was examined in duplicates for consecutive 3 days. Variations were expressed by the relative standard deviations (R.S.D.) for intra- and inter-day, which were less than 1.7 and 1.8%, respectively. For every calibration curve, the calibration concentrations were back-calculated from the peak area of the analytes. The deviation from the nominal concentration defined as accuracy (Table 2).

The recovery was preformed by adding a known amount of individual standards into a certain amount (0.10 g) of *Cordyceps* material (cultured *C. sinensis* from Hebei). Three replicates were performed for the test. The mixture was extracted and analyzed using the method mentioned above. Table 3 shows the recoveries of 14 investigated compounds.

3.6. Application for analysis of real sample—cultured *Cordyceps*

Cordyceps sinensis (Berk.) Sacc., also called as Winter worm Summer grass, is one of the well-known traditional Chinese medicines, which has multiple pharmacological activities [28,29]. Natural *Cordyceps* (wild *C. sinensis*) is rare and expensive. Therefore, cultured *C. sinensis* and other species such as *C. militaris* of *Cordyceps* genus have been developed and used as medicine and/or health food supplements in China and Asia [30]. In addition, nucleosides are believed to be the active components in *Cordyceps*, and more than 10 nucleosides and its related compounds have been isolated from it [30]. Herein, the validated UPLC method was applied for the determination of the nucleoside and nucleobases in cultured *Cordyceps*.

Typical chromatograms of the PLE extract from cultured *C. sinensis* and *C. militaris* were shown in Fig. 2. The identification of investigated compounds was carried out by comparison of their retention time and their UV spectra with those obtained injecting standards in the same conditions, as well as by spiking *Cordyceps* samples with stock standard solutions.

By using the calibration curves of the analytes, cultured *C. sinensis* and *C. militaris* were analyzed. Table 4 shows the summary results. Uridine, guanosine and adenosine, which are main compounds in cultured *Cordyceps*, are much higher than those in cultured *C. militaris*. However, cordycepin, which is abundant in cultured *C. militaris*, is only found in a few samples of cultured *C. sinensis* (Hebei and HKUST). Therefore, it is possible to identify cultured *C. sinensis* and *C. militaris* based on their UPLC chromatograms in a short time.

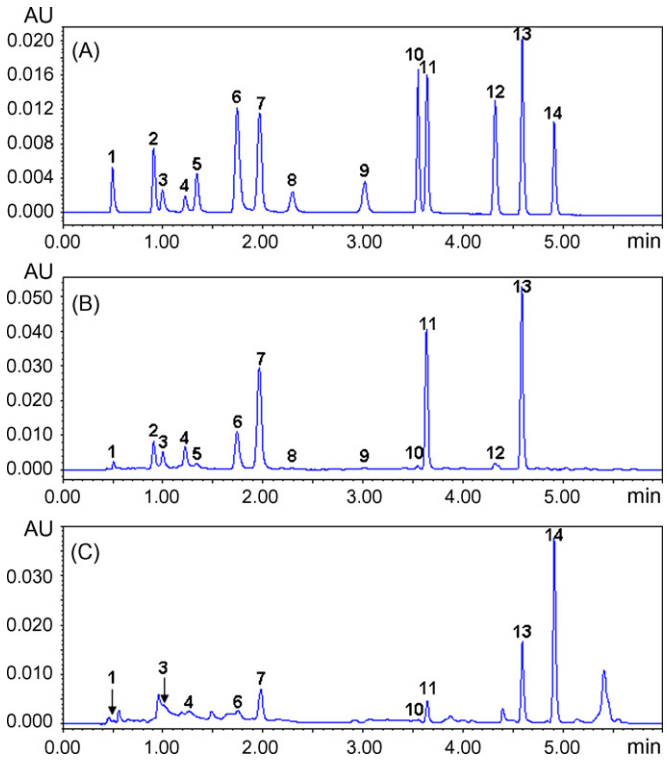

Fig. 2. Typical UPLC chromatograms of (A) mixed standards, (B) cultured *C. sinensis* and (C) cultured *C. militaris*. Labels **1**–**14** are the same as Fig. 1.

Table 4
Contents (μg/g) of investigated compounds in cultured *Cordyceps*

Analyte	Cultured *C. militaris*					Cultured *C. sinensis*					
	Guobao	Aoli	Quanxin	Xiankang	HKUST	Hebei	Huadong	Wanfeng	Jiangxi	Anhui	HKUST
Cytosine	–[a]	–	±[b]	±	–	76.1[c]	53.3	+[d]	98.9	+	+
Uracil	+	–	–	–	+	699.5	±	±	301.3	1999.8	±
Cytidine	+	±	±	±	±	598.1	±	±	832.8	+	±
Guanine	+	+	34.2	61.3	34.7	138.5	81.6	316.4	237.0	427.5	+
Hypoxanthin	–	–	+	+	–	74.8	–	+	63.2	236.0	+
Adenine	472.4	237.3	62.2	95.0	461.6	288.1	229.7	353.7	566.2	1228.1	+
Uridine	654.5	280.7	591.1	1468.0	848.6	1798.3	1285.9	7519.8	3214.4	1265.4	545.3
Thymine	–	61.8	–	+	–	20.6	–	+	31.2	148.2	15.8
2′-Deoxyuridine	28.9	–	–	+	69.8	83.9	15.5	157.0	92.2	86.9	+
Inosine	29.3	–	33.9	70.0	+	329.7	16.3	28.2	62.5	68.2	+
Guanosine	211.4	93.8	286.4	370.3	175.2	2455.4	1710.3	4223.8	2939.1	1761.8	211.8
Thymidine	–	–	–	–	–	+	+	143.9	118.1	83.7	+
Adenosine	602.8	562.4	918.4	1527.3	667.3	2641.2	1781.5	5108.1	2747.1	956.5	258.5
Cordycepin	22964.5	4709.2	1984.0	2256.0	22673.9	+	–	–	–	–	+

[a] Undetectable.
[b] Resolution and content were not available for quantitation.
[c] Average of triplicates.
[d] Under the limits of quantitation.

4. Conclusion

This work first developed an UPLC method for fast simultaneous determination of 14 nucleosides and nucleobases, which may be applied for fast determination of the analytes in herbal materials, pharmaceutical products and biological fluids.

Acknowledgements

We are grateful to Leon Lai from our institute for his expert technical assistances. The research was supported grants from Macao Science and Technology Development Fund (077/2005/A and 028/2006/A2), University of Macau (RG086/04-05S) to S.P. Li.

References

[1] T. Rasmuson, G.R. Bjork, Acta Oncol. 34 (1995) 61.
[2] K. Koshida, J. Harmenberg, U. Stendahl, B. Wahren, E. Borgstrom, L. Helstrom, Urol. Res. 13 (1985) 213.
[3] R.W. Trewyn, R. Glaser, D.R. Kelly, D.G. Jackson, W.P. Graham, C.E. Speicher, Cancer 49 (1982) 2513.
[4] C.C. Marvel, J. Del Rowe, E.G. Bremer, J.R. Moskal, Mol. Chem. Neuropathol. 21 (1994) 353.
[5] M.L. Hao, Drug Stand. Chin. 4 (2003) 340.
[6] L.L. Mi, S.W. Zhang, J.J. Sun, Z.H. Wang, X.K. Hong, Chin. Trad. Pat. Med. 25 (2003) 402.
[7] W.G. Stillwell, H.X. Xu, J.A. Adkins, J.S. Wishnok, S.R. Tannenbaum, Chem. Res. Toxicol. 2 (1989) 94.
[8] A.J.R. Teixeira, J.H. Gommers-Ampt, G.V. de Werken, J.G. Westra, J.F.C. Stavenuiter, A.P.J.M. de Jong, Anal. Biochem. 214 (1993) 474.
[9] S.K. Yan, G.A. Luo, Y.M. Wang, Y.Y. Cheng, J. Pharm. Biomed. Anal. 40 (2006) 889.
[10] S.P. Li, P. Li, C.M. Lai, Y.X. Gong, K.K.W. Kan, T.T.X. Dong, K.W.K. Tsim, Y.T. Wang, J. Chromatogr. A 1036 (2004) 239.
[11] L.S. Li, M. Liu, S.L. Da, Y.Q. Feng, Talanta 63 (2004) 433.
[12] W. Fürst, S. Hallström, J. Chromatogr. 578 (1992) 39.
[13] K.F. Childs, X.H. Ning, S.F. Bolling, J. Chromatogr. B 678 (1996) 181.
[14] A. Brink, U. Lutz, W. Völkel, W.K. Lutz, J. Chromatogr. B 830 (2006) 255.
[15] H. Fan, S.P. Li, J.J. Xiang, C.M. Lai, F.Q. Yang, J.L. Gao, Y.T. Wang, Anal. Chim. Acta 567 (2006) 218.
[16] S.P. Li, P. Li, T.T.X. Dong, K.W.K. Tsim, Electrophoresis 22 (2001) 144.
[17] Y.X. Gong, S.P. Li, P. Li, J.J. Liu, Y.T. Wang, J. Chromatogr. A 1055 (2004) 215.
[18] H.Y. Cheung, C.W. Ng, D.J. Hood, J. Chromatogr. A 911 (2001) 119.
[19] H.M. Liebich, R. Lehmann, G. Xu, H.G. Wahl, H.U. Haring, J. Chromatogr. B 745 (2000) 189.
[20] X. Cahours, H. Dessans, P. Morin, M. Dreux, L. Agrofoglio, J. Chromatogr. A 895 (2000) 101.
[21] T. Helboe, S.H. Hansen, J. Chromatogr. A 836 (1999) 315.
[22] K. Itoh, S. Aida, S. Ishiwata, S. Sasaki, N. Ishida, M. Mizugaki, Clin. Chim. Acta 217 (1993) 221.
[23] K. Itoh, T. Konno, T. Sasaki, S. Ishiwata, N. Ishida, M. Misugaki, Clin. Chim. Acta 206 (1992) 181.
[24] M.E. Swartz, J. Liq. Chromatogr. 28 (2005) 1253.
[25] L. Novakova, L. Matysova, P. Solich, Talanta 68 (2006) 908.
[26] X.X. Ying, X.M. Lu, X.H. Sun, X.Q. Li, F.M. Li, Talanta, in press.
[27] K. Kawamura, Biochim. Biophys. Acta 1620 (2003) 199.
[28] J.S. Zhu, G.M. Halpern, K. Johns, J. Alt. Comp. Med. 4 (1998) 289.
[29] J.S. Zhu, G.M. Halpern, K. Johns, J. Alt. Comp. Med. 4 (1998) 429.
[30] S.P. Li, F.Q. Yang, K.W.K. Tsim, J. Pharm. Biomed. Anal. 41 (2006) 1571.

Available online at www.sciencedirect.com
ScienceDirect
Talanta 73 (2007) 372–379
Talanta
www.elsevier.com/locate/talanta

MPTS-silica coated capillary microextraction on line hyphenated with inductively coupled plasma atomic emission spectrometry for the determination of Cu, Hg and Pb in biological samples

Fei Zheng, Bin Hu *

Department of Chemistry, Wuhan University, Wuhan 430072, PR China

Received 20 November 2006; received in revised form 28 March 2007; accepted 29 March 2007
Available online 8 April 2007

Abstract

A novel sol–gel 3-mercaptopropyltrimethoxysilane (MPTS) modified silica coating was developed for capillary microextraction (CME) of trace Cu, Hg and Pb prior to their on line determination by inductively coupled plasma–atomic emission spectrometry (ICP–AES). This organic–inorganic hybrid coating was in situ created on the inner walls of fused silica capillary using a sol solution containing TMOS (tetramethoxysilane) as a precursor, MPTS as a co-precursor, ethanol as the solvent and hydrochloric acid as a catalyst. The structure of the capillary coating was characterized by FT-IR spectroscopy, Raman spectroscopy, SEM and TEM. The factors affecting on the capillary microextraction of analytes such as pH, sample flow rate and volume, elution solution and interfering ions had been investigated, and the optimized experimental parameters were obtained. Under the optimized conditions, the absorption capacity of MPTS-silica coated capillary was found to be 1.17, 1.96 and 1.19 $\mu g\,m^{-1}$ for Cu, Hg and Pb, and the limits of detection were as low as 0.17 0.22 and 0.52 $ng\,mL^{-1}$, respectively. With a sampling frequency of $12\,h^{-1}$, the relative standard deviations (R.S.D.s) were 4.2, 2.6 and 3.8% (C=4 $ng\,mL^{-1}$, $n=7$, sample volume = 1 mL) for Cu, Hg and Pb, respectively. The proposed method had been successfully applied to the determination of Cu, Hg and Pb in human urine, human serum and preserved egg. To validate the proposed method, certified reference materials of BCR151 milk powder, GBW07601 (GSH-1) human hair, GSBZ 50016-90 and GSB 07-1183-2000 water samples were analyzed and the determined values were in a good agreement with the certified values.

Keywords: MPTS-silica coating; Capillary microextraction; ICP–AES; Cu; Hg and Pb; Biological samples

1. Introduction

Copper is a kind of essential trace elements, which are required to implement multiple functions in the organism but can be harmful when at high concentration. Both mercury and lead are extremely toxic elements. When exposed to mercury for a long time, people may easily get hydrargyrism, which is a common kind of occupational diseases. Lead has been used at least since biblical times in a variety of products in inorganic form, its impact as a major environmental pollutant was recognized until the last century. Children are the main victim of lead because the damnification is an irreversible process and moderately increased lead accumulated in human body may cause chronic poisoning. Therefore, the determination of Cu, Hg and Pb in various biological samples, in particular human serum and urine, is recommended as a mean of estimating the degree of metal contamination at the workplace and in the environment.

Though inductively coupled plasma mass spectrometry (ICP-MS) is suitable for trace heavy metal determination due to its excellent ability of detection and multi-elements, the cost of such instrumentation may be prohibitive to many laboratories. Meanwhile, inductively coupled plasma–atomic emission spectrometry (ICP–AES) is an ideal one at present, which has better tolerance to salt and organic solvent compared to ICP–MS. ICP–AES had been applied to directly analyze trace metals in biological and environmental samples, such as Pb [1,2], Cu and Pb in pumpkin seed oil and pumpkin seeds [3], Cu in beer [4] and Hg in soil and plant [5], in which the best detection limit of Cu, Hg and Pb were 1.1, 10 and 20 $ng\,mL^{-1}$, respectively. The results were much higher than the content of analytes (usually Hg < 10 $ng\,mL^{-1}$) in many biological and environmental samples. Though the low-powered microwave thermospray

* Corresponding author. Tel.: +86 27 87218764; fax: +86 27 68754067.
E-mail address: binhu@whu.edu.cn (B. Hu).

0039-9140/$ – see front matter © 2007 Elsevier B.V. All rights reserved.
doi:10.1016/j.talanta.2007.03.060

nebulizer [6] could improve the detection limit of the method, the precision would be decreased at the same time and the cost is too much. So it is necessary to develop a fast, miniaturized and highly selective preconcentration and separation technique prior to analysis to improve the sensitivity and decrease the matrix interference.

Compared to other separation and preconcentration technologies such as coprecipitation [7], liquid–liquid extraction [8], liquid chromatography [9], solid phase extraction [10], capillary electrophoresis [11], and solid phase microextraction [12], capillary microextraction (CME) is one of the most suitable preconcentration and separation techniques due to its advantages of low cost, simple operation, fast speed, high selectivity, low consumption of sample and solvent and easy automation. Up to now, CME has been widely used for analysis of trace organic analytes by on-line coupling with different detection instrumentations such as GC [13], HPLC [14], CE [15] and ES–MS [16].

Sol–gel capillary microextraction (sol–gel CME) was first introduced by Bigham [17] as a viable solvent free extraction technique for the preconcentration of trace analytes, in which the coating technology used to prepare the capillaries involved a single-step procedure and allowed for the in situ creation of chemically bonded coatings that are characterized by high thermal and solvent stabilities. Sol–gel coated capillaries were employed for the extraction and preconcentration of a wide variety of polar and nonpolar analytes. The coating material plays a fundamentally important role in CME which determines its selectivity; however, the capillaries used at present are mainly commercial GC capillary columns [18]. So it is essential for CME to develop highly selective, stable and efficient coating material. Besides the PDMS and PEG coatings [19] lots of new capillary coatings have been developed. Kim [20] described sol–gel titania–poly (dimethylsiloxane) (TiO_2–PDMS) coating for CME to perform on-line preconcentration of trace polycyclic aromatic hydrocarbons, ketones and alkylbenzenes in aqueous samples. Sol–gel polytetrahydrofuran (poly THF) [13] coated capillaries were found to be effective in carrying out simultaneous extraction of both polar and nonpolar analytes. In-tube SPME with PPY-coated capillary was coupled with LC–ESI–MS for organoarsenic compounds studies [21]. Besides, monolithic capillary column [14] had also extended the applications of CME.

Among various coatings, silica gel [22] especially modified by various organic compounds with metal chelating ability has received great attention due to its rapid sorption, low-swelling, high mass-exchange and good selectivity. 3-mercaptopropytrimethoxysilane (MPTS) is a kind of silylating and coupling reagent that has often been used to modify the surface of inorganic materials [23], owing to the good affinity of its terminal –SH group for heavy metal ions. However, to our knowledge, there is no report on the use of sol–gel MPTS-silica coated capillary up to now.

In this work, a novel coating of sol–gel MPTS-silica with a functional group of –SH was prepared, and was applied to capillary microextraction (CME) for on line preconcentration/separation of trace Cu, Hg and Pb in biological and food samples followed by ICP–AES detection. Different experimental parameters affecting the capillary microextraction were studied in detail and the optimized conditions were established. With a sampling frequency of 12 h^{-1}, the limits of detection were 0.17, 0.22 and 0.52 ng mL^{-1}, and the relative standard deviations (R.S.D.s) were 4.2, 2.6 and 3.8% (C = 4 ng mL^{-1}, $n = 7$, sample volume = 1 mL) for Cu, Hg and Pb, respectively. The accuracy of the method was validated by the analysis of four certified reference materials of BCR151 milk powder, GBW07601 (GSH-1) human hair, GSBZ 50016-90 and GSB 07-1183-2000 environmental water, and the determined values are found to be in good agreement with the certified values. The MPTS-silica coated capillary was easy to regenerate and could be used for more than 40 times under the optimized conditions without decreasing absorption efficiency. The developed method is simple, rapid, selective, sensitive and little solvent and sample required, and it is especially suitable for analysis of various biological samples with limited volume (≤1 mL) and complicated matrix.

2. Experimental

2.1. Apparatus

Intrepid XSP Rasial ICP-OES (Thermo, USA) with a concentric model nebulizer and a cinnabar model spray chamber was used for the determination, and the optimum operation conditions were summarized in Table 1. The pH values were controlled with a Mettler Toledo 320-S pH meter (Mettler Toledo Instruments Co. Ltd., Shanghai, China) supplied with a combined electrode. A WX-3000 microwave accelerated digestion system (EU Chemical Instruments Co. Ltd., Shanghai, China) was used for sample digesting. An IFIS-C flow injection system (Ruimai Tech. Co. Ltd., Xi'an, China) was used for online coupled CME with ICP–AES. A minimum length of PTFE tubing (i.d. 0.5 mm) was used for on-line connection. Fused silica capillary (320 μm i.d. × 450 μm o.d.) was obtained from Hebei Yongnian Optical Fiber Factory, China. The structure of MPTS-silica was characterized by 170SX FI-IR (NICOL ET, USA). The scanning electron micrograph and the transmission electron micrograph of the coating was obtained using an X-650 scanning electron microscope (Hitachi, Tokyo, Japan) at an acceleration voltage of 25 kV and a JEOL EM2010 electron microscope (Tokyo, Japan).

2.2. Standard solutions and reagents

The stock standard solutions (1 g L^{-1}) of metal ions (Cu, Hg and Pb) were obtained by dissolving appropriate amounts

Table 1
Operation parameters of Intrepid XSP Rasial ICP–AES

RF generator power (W)	1200
Frequency of RF generator (MHz)	27.12
Carrier gas flow rate (L min^{-1})	0.6
Coolant gas flow rate (L min^{-1})	14
Auxiliary gas flow rate (L min^{-1})	0.5
Max integration times (s)	30
Analytical wavelength (nm)	Cu 224.700, Hg 184.950, Pb 220.353

of $CuSO_4 \cdot 5H_2O$, $HgCl_2$ and Pb $(NO_3)_2$ (A.R. The First Reagent Factory, Shanghai, China) in high purity deionized water, respectively. The standard stock solutions ($1\,g\,L^{-1}$) of other elements were prepared from their salts by a conventional method. TMOS (tetramethoxysilane) and MPTS (3-mercaptopropyltrimethoxysilane) were of analytical reagent grade and were purchased from Organic Silicon Material Company of Wuhan University. HCl was of a highly pure grade and all the other reagents used were of analytical reagent grade. High purity deionized water was used throughout this work.

All stock standard solutions were stored in polyethylene bottles in a refrigerator held at 4 °C. All glassware was kept in 10% nitric acid for at least 24 h and washed three times with high purity de-ionized water before use.

2.3. Preparation of MPTS-silica sol

2 mL TMOS was dissolved in 5 mL mixture of ethanol–HCl ($C = 0.01\,mol\,L^{-1}$) (4:1, v/v), the solution was stirred at ambient temperature for 30 min, allowing for the complete hydrolysis of TMOS. After adding 0.5 mL MPTS (dissolved in 1 mL ethanol) dropwise, the solution was stirred for another 30 min, leading to the formation of MPTS-silica sol. The sol was stored to age for 1 day at ambient temperature before use.

2.4. Preparation of MPTS-silica coated capillary

The fused-silica capillary was activated at ambient temperature by rinsing sequentially with $1\,mol\,L^{-1}$ sodium hydroxide for 2 h, water for 30 min, $1\,mol\,L^{-1}$ hydrochloric acid for 2 h and water for 30 min, the capillary was then dried at 433 K while purged with nitrogen for 5 h. This left the capillary surface saturated with silanol groups to allow a reproducible conjunction with silane reagents.

The MPTS-silica coated capillary was prepared by first passing the prepared sol through the fused-silica capillary for 1 h, then the residual sol was removed by passing nitrogen through the capillary under 1 bar for 10 min and then under 0.2 bar for 20 min. This process was repeated for three times. Afterwards, the capillary was heated at 393 K for 8 h in a muffle furnace, leading to the formation of mercapto coating.

2.5. General procedure

A 10 mL portion of aqueous sample solution containing Hg^{2+}, Cu^{2+} and Pb^{2+} was prepared, and the pH value was adjusted to 6.0 with $0.01\,mol\,L^{-1}$ NaAc and $0.1\,mol\,L^{-1}$ HCl. The solution was passed through MPTS-silica coated capillary at a flow rate of $0.25\,mL\,min^{-1}$ by using a peristaltic pump. Afterwards, the analytes retained on the capillary were on line eluted with 0.2 mL $0.1\,mol\,L^{-1}$ HCl–4% thiourea for the determination of ICP–AES. The blank solution and the series of standard solution were prepared with the same procedure of CME–ICP–AES.

2.6. Sample preparation

Portions (0.1000 g) of BCR151 milk powder and GBW07601 (GSH-1) human hair were weighed into PTFE vessel, and 1.5 mL of concentrated HNO_3 was added, respectively. The microwave digestion was performed according to the following heating programs: 3 atm for 1 min, 8 atm for 2 min and then 10 atm for 3 min. After digestion, clear solution could be observed. Then heated it to very small volume by a plate heater to remove the superfluous acid, the residue was dissolved with high purity deionized water. After adjustment of the pH to 6.0, the solution was made up with high purity deionized water to 10 mL. The blank sample with the same amount of acid was prepared with the same procedure except for adding no analytes.

1 mL of GSB 07-1183-2000 and 6 mL of GSBZ 50016-90 certified water samples were transferred into two clean plastic tubes and diluted to 10 mL with high purity deionized water after adjustment of the pH to 6.0, respectively.

1 mL of human serum (devoted by hospital patients), 4 mL of human urine (devoted by Hg-exposed researchers) and 0.1000 g of preserved egg (purchased from local supermarket) were transferred into different PTFE vessels and 1.5, 0.5 and 2.5 mL concentrated HNO_3 were added, respectively. The three samples were digested and prepared according to the procedure as above. After adjustment of the pH to 6.0, the solution was made up with water to 10 mL. Still, the blank sample with the same amount of acid was prepared with the same procedure except for adding no analytes.

3. Results and discussions

3.1. Characterization of MPTS-silica coating

The sol–gel MPTS-silica coating was characterized by IR spectroscopy, Raman spectroscopy, SEM and TEM. Fig. 1 gives clear evidence of modification as shown by absorption bands at $2565.7\,cm^{-1}$ and in the region $2900–2850\,cm^{-1}$, which were attributed to the S–H stretching vibration of MPTS and the aliphatic C–H stretching of the attached propyl groups, respectively. No characteristic peak of –S–S– could be observed in Raman spectra of the coating as shown in Fig. 2, indicating no oxidization of –SH at the temperature of 393 K in the muffle furnace.

For preparation of the coating for SEM and TEM measurements, a certain MPTS-silica coated capillary was crushed into lots of small pieces, one piece of which was gilt for the scanning electron micrograph; the MPTS-silica coating scraped off the inner surface of the pieces of capillary was dispersed in 25 mL ethanol (A.R.) for transmission electron micrograph.

The SEM results shown in Fig. 3 indicated that sol–gel MPTS-silica coating was a layer of well-proportioned and compact particles. The micro-structure of the coating was further demonstrated by the TEM result in Fig. 4, a cluster of ordered and spherical particles with a pore size of about 100 nm was observed. As a nanometer-sized and porous material, the coating should possess a high chemical activity and high absorption capacity consequently.

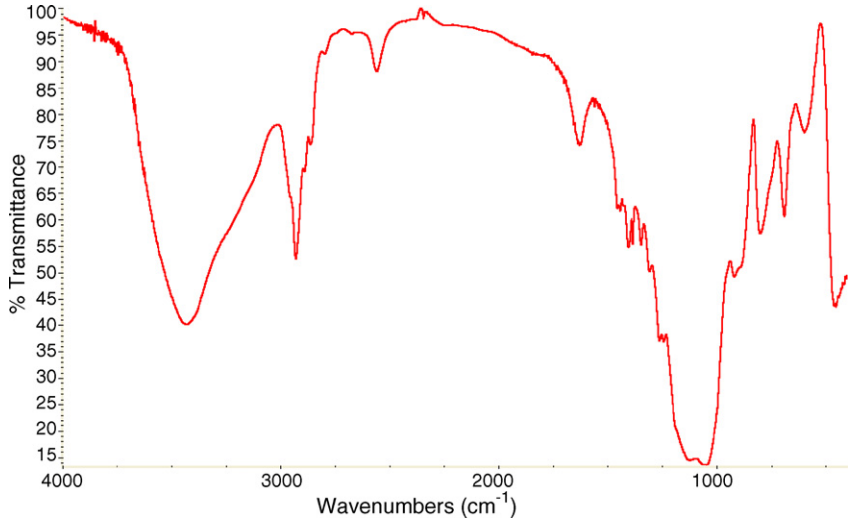

Fig. 1. Infrared spectra of MPTS-silica.

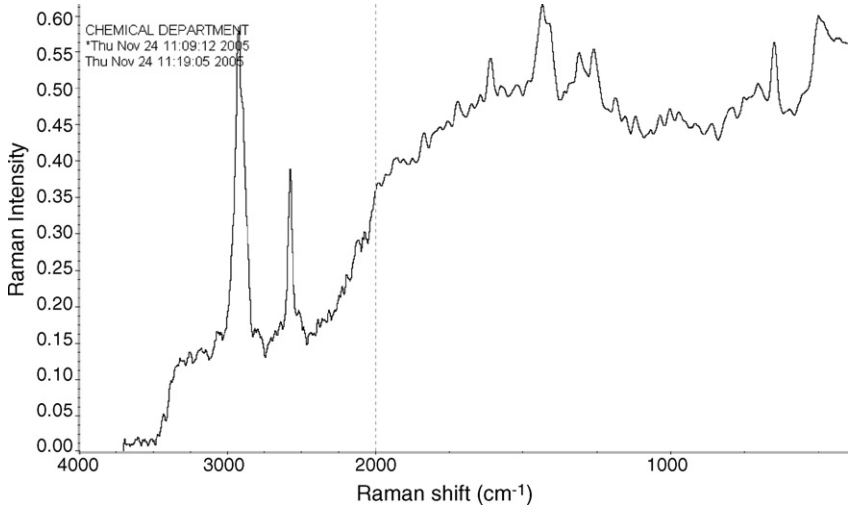

Fig. 2. Raman spectra of MPTS-silica.

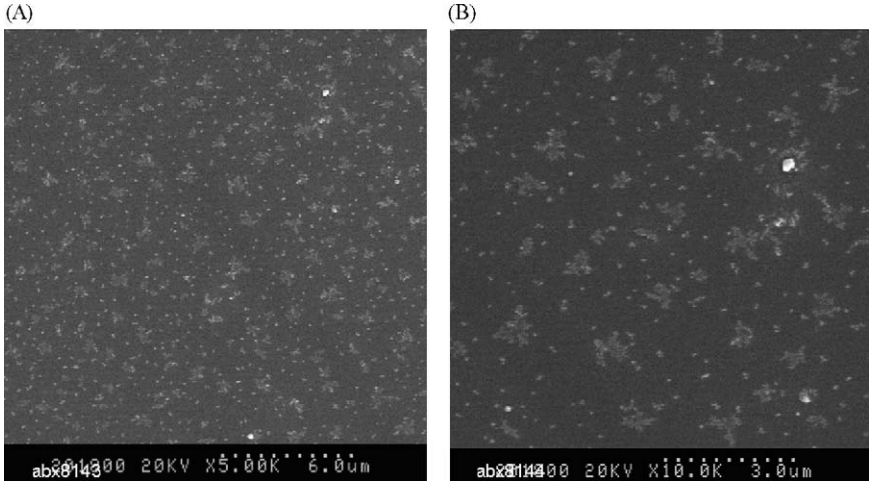

Fig. 3. (A) SEM of MPTS-silica coating × 5000; (B) SEM of MPTS-silica coating × 10000.

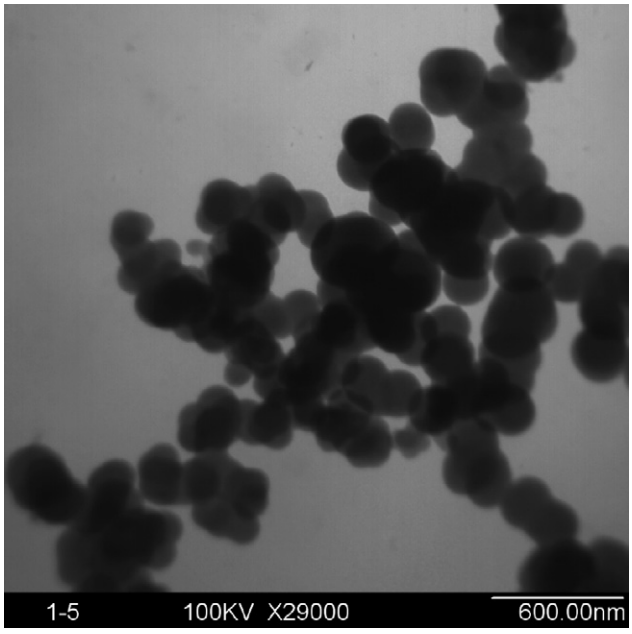

Fig. 4. TEM of MPTS-silica coating.

3.2. Effect of pH

The pH value plays an important role with respect to the absorption of different ions on MPTS-silica coated capillary. The absorption behaviors of a number of metal ions, such as Hg^{2+}, Cu^{2+}, Pb^{2+} Cd^{2+}, Co^{2+} and Ni^{2+} on sol–gel MPTS-silica coated capillary were studied, and the results were showed in Fig. 5. It can be seen that the absorption percentage was increased with the increase of pH from 1.0 to 6.0 for $Cu^{2+}$and Pb^{2+}, a quantitative absorption (>90%) for Hg^{2+}, Cu^{2+} and Pb^{2+} could be obtained in the pH range of 6.0–8.0. For some other analytes, such as Cd^{2+}, Co^{2+} and Ni^{2+}, the quantitative absorption just occurred at pH higher than 8. Obviously, the MPTS-coated capillary exhibited excellent absorption selectivity toward metal ions Hg^{2+}, Cu^{2+} and Pb^{2+} in the pH range of 6.0–8.0. A pH of 6.0 was selected for the preconcentration of Hg^{2+}, Cu^{2+} and Pb^{2+} in the further experiments.

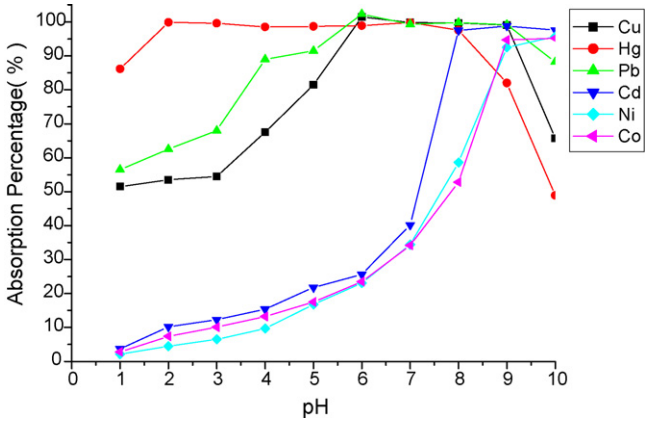

Fig. 5. Effect of pH on the absorption percentage (%) of metal ions Sample volume: 1 mL, Hg^{2+}, Cu^{2+}, Pb^{2+}, Cd^{2+}, Co^{2+} and Ni^{2+}: 20 ng mL^{-1}.

The mechanism of the reaction between the ions and the coating could be represented by the formula of $-SH + M^{2+} \rightarrow -SM + 2H^{+}$. As shown in Fig. 5, the coatings displayed a high selectivity towards Hg^{2+}, Cu^{2+} and Pb^{2+} in the pH range of 6.0–8.0, and the quantitative absorption for some other analytes, such as Cd^{2+}, Co^{2+} and Ni^{2+}, just occurred at pH higher than 8. This could be attributed to the pK_{sp} of sulfides in the sequence of HgS > CuS > PbS > CdS > NiS > CoS. The pK_{sp} of HgS was much larger than those of other sulfides, thus Hg^{2+} could be completely adsorbed at pH values ranging from 2 to 8. This result confirmed the preference of the functional group –SH (soft base) of the MPTS-silica coating to heavy metal ions (soft acids), supporting the view of Pearson's concept of hard and soft acids and bases. For the further experimental, the pH of 6.0 was selected.

Besides the three mechanisms [23] discussed before for the absorption of the metal ions on MPTS: the affinity of –SH, the hydrolyzation of metal ions and the electrostatic charge, here we can propose another explanation – the equilibrium of dissolution and precipitation of the sulfides –SM. This mechanism could be expressed by the model formula:

$$-SH + M^{2+} \rightarrow -SM + 2H^{+}$$

$$\lg K = -\Delta G/2.303RT$$

The K of this reversible reaction should be $K = [-SM][H^{+}]^2/[-SH][M^{2+}]/=[S^{2-}][H^{+}]^2/K_{sp}$ $[-SH]$ and the value of $[S^{2-}]$ and $[-SH]$ were assumed to be constant. In the acidic medium, the value of $[H^{+}]$ was large while the K_{sp} of Hg^{2+}, Cu^{2+} and Pb^{2+} was very small, resulting in a positive value of K, so the ΔG was a negative one which meant the reaction could occur rightwards and Hg^{2+}, Cu^{2+} and Pb^{2+} were adsorbed, however, the ΔG was a positive one for Cd^{2+}, Co^{2+} and Ni^{2+} due to their relative large value of K_{sp}, so the reaction could not occur rightwards and Cd^{2+}, Co^{2+} and Ni^{2+} were not adsorbed. In the basic medium, the H^{+} were neutralized by mass amount of OH^{-}, therefore, the above reaction could occurred rightwards and Cd^{2+}, Co^{2+} and Ni^{2+} were absorbed.

3.3. Effect of sample flow rate

The sample flow rate will influence on the retention of metal ions on the capillary. To study the effect of sample flow rate, 1 mL of sample solution was passed through the capillary with the flow rates varying from 0.1 to 0.5 mL min^{-1}. The experimental results indicated that quantitative recoveries (>90%) could be obtained for the studied metal ions at the sample flow rates less than 0.25 mL min^{-1}. When the sample floe rate was beyond 0.25 mL min^{-1}, the recoveries for these target metal ions will decrease with further increasing of the flow rate, due to a decrease in the absorption kinetics at a high flow rate. Thus, a flow rate of 0.25 mL min^{-1} was employed in this work.

3.4. Concentration of eluent

3.4.1. Concentration of HCl

The absorption of the metal ions was strong enough even at low pH (<3), thus it was difficult to elute the metal ions quantita-

Table 2
The recoveries (%) of metal ions adsorbed in different segments of capillary column under optimized condition; A, B and C represent three capillaries (40 cm × 320 μm i.d.) prepared in one batch (300 cm × 320 μm i.d.)

Cu	Hg	Pb
A 99.0	98.3	102.3
B 96.8	95.3	99.6
C 98.0	97.4	101.2

tively by using high concentration of acid alone. Thus, in order to rapidly recover the analytes retained on the capillary quantitatively, a mixed solution of HCl and thiourea was used. By keeping the thiourea concentration of 4% (m/v) unchanged, the effect of HCl concentration on the recovery of target analytes was studied. It was found that the acidity had little impact on the elution of the metal ions while keeping the thiourea concentration at 4%, all the analytes of Cu, Hg and Pb can be completely eluted by 0.1 mol L^{-1} HCl.

3.4.2. Concentration of thiourea

The effect of thiourea concentration on the recovery of the studied ions was also investigated while fixing the HCl concentration at 0.1 mol L^{-1}, and the experimental results indicated that the recovery of the studied metal ions increased with the increase in concentration of thiourea first and then kept unchanged. When the concentration of thiourea was above 4%, all the analytes could be eluted quantitatively. Finally, the eluent of 0.1 mol L^{-1} HCl−4% thiourea (m/v) was employed for further experiments.

3.5. Eluent volume and flow rate

In addition, the effects of eluent volume and eluent flow rate on the recovery of analytes were examined, respectively. For study the effect of the elution volume, 0.30 mL 0.1 mol L^{-1} HCl–4% thiourea was used as eluent to continuously elute the analytes adsorbed on the capillary, and the analytes in the six effluents (each 0.05 mL) were determinated by ICP–AES. The experimental results indicated that 0.2 mL eluent was sufficient to elute quantitatively (>90%) all the analytes when the elution flow rate was less than 0.2 mL min^{-1}. Finally, 0.2 mL 0.1 mol L^{-1} HCl–4% thiourea with a flow rate of 0.2 mL min^{-1} was employed as the optimized elution conditions.

3.6. Sample volume

The sensitivity of the procedure when determining very low concentration of analytes was investigated. For this purpose, various sample volume of 1–10 mL containing 20 ng the studied metal ions were passed through the capillary, and the adsorbed metal ions were eluted with 0.2 mL mixture of 0.1 mol L^{-1} HCl–4% thiourea elution. It was found that quantitative recoveries were obtained for the studied metal ions with sample volumes ranging from 1 to 10 mL. Thus, the enrichment factor of 50 could be achieved with 10 mL sample solution. However, larger amount of the sample solution required more time in the procedure. To trade off the enrichment factor and analytical speed, 1 mL sample and 0.2 mL 0.1 mol L^{-1} HCl–4% thiourea were used for real sample analysis; therefore, an enrichment factor of 5 was obtained with a sampling frequency of 12 h^{-1}.

Table 3
The recoveries (%) of metal ions adsorbed in different batches of capillary column under optimized condition; I, II and III represent three capillaries (40 cm × 320 μm i.d.) prepared in three batches (300 cm × 320 μm i.d.)

Cu	Hg	Pb
I 98.0	99.6	97.6
II 99.5	99.8	99.0
III 96.2	97.3	97.1

Table 4
Analytical performance of the target analytes (sample volume = 1 mL) under optimized conditions

	Ions		
	Cu	Hg	Pb
R.S.D. (C = 4 ng mL^{-1}, n = 8)	4.2%	2.6%	3.8%
D.L. (ng mL^{-1})	0.17	0.22	0.52
Sampling frequency (h^{-1})		12	
Enrichment factor		5	

3.7. Absorption capacity

The absorption capacity is one of the key factors in evaluating the performance of the absorption material. To study the absorption capacity, 20 mL sample solution containing 200 ng mL^{-1} analytes was passed through the capillary (1 m), and the analytes in the effluent were determined by ICP–AES directly. The breakthrough point, defined as the 5% leakage of analytes, was 6, 10 and 6 mL for Cu, Hg and Pb, respectively, and the adsorption capacity evaluated from the breakthrough curve is 1.17 μg (Cu), 1.96 μg (Hg) and 1.19 μg (Pb) for 1 m capillary, respectively.

3.8. Regeneration of the MPTS-silica coated capillary

The regeneration is another important factor in evaluating the absorption material. The MPTS-silica coated capillary can be re-used more than 40 times under the optimized conditions

Table 5
Analytical results for real samples (average ± S.D., n = 3)

Sample	Element	Measured (ng mL^{-1})
Human urine	Cu	28.3 ± 0.6
	Hg	12.8 ± 0.2
	Pb	22.8 ± 0.5
Human serum	Cu	581.2 ± 9.8
	Hg	8.1 ± 0.3
	Pb	31.8 ± 0.8
Preserved egg	Cu	1.25 ± 0.04[a]
	Hg	0.036 ± 0.001[a]
	Pb	0.141 ± 0.005[a]

[a] μg g^{-1}.

Table 6
Analytical results of Cu, Hg and Pb in certified materials of BCR151 milk powder, GBW07601 (GSH-1) human hair, GSBZ 50016-90 and GSB 07-1183-2000 water samples (average ± S.D., $n = 3$)

Sample	Element	Certified ($\mu g\,g^{-1}$)	Determined ($\mu g\,g^{-1}$)	t-test[c]
BCR 151	Cu	5.23 ± 0.08	5.20 ± 0.10	0.33
Milk powder	Hg	0.101 ± 0.001	0.096 ± 0.003	1.45
	Pb	2.002 ± 0.026	2.01 ± 0.023	2.38
GBW07601(GSH-1)	Cu	10.6 ± 0.7	10.4 ± 0.5	0.40
Human hair	Hg	0.36 ± 0.05	0.35 ± 0.05	1.36
	Pb	8.8 ± 0.9	9.0 ± 0.5	2.89
GSBZ 50016-90	[a]Hg	3.82 ± 0.33	3.65 ± 0.09	3.27
Environmental water GSB 07-1183-2000 Environmental water	[b]Pb	0.303 ± 0.014	0.300 ± 0.014	0.37

[a] $ng\,mL^{-1}$.
[b] $\mu g\,mL^{-1}$.
[c] $t_{0.05,2} = 4.30$.

while the recovery was kept above 90%. However, when HCl concentration in the eluent was high than $2\,mol\,L^{-1}$, the capillary could not be used any more. This may be attributed to the breakage of chemical bonding between MPTS and silica gel or the oxidation of –SH in high acidity.

3.9. Reproducibility of the preparation of the capillary

The extraction efficiencies of three capillaries prepared at one batch were tested under the optimized conditions, and no obvious difference was observed for these three coated capillaries as shown in Table 2. In order to evaluate the reproducibility of batch-to-batch, three capillaries from three batches were used. No distinct difference in recoveries was observed from three capillaries prepared in different batch as shown in Table 3.

3.10. Effects of co-existing ions

For the study of interference by coexisting ions, such as K^+, Na^+, Ca^{2+}, Mg^{2+}, Co^{2+}, Ni^{2+}, Cd^{2+}, Fe^{3+}, Cr^{3+} and Zn^{2+}, solutions of 1 mL of $20\,ng\,mL^{-1}$ of Cu, Hg and Pb, containing the 100–20,000 folds of interfering ions were operated according to the proposed procedure. The results show that in the presence of 20,000 fold K^+ and Na^+, 8000-fold Mg^{2+} and Ca^{2+}, 2000-fold Co^{2+} and Ni^{2+}, 1000-fold Cd^{2+}, 800-fold Fe^{3+} and 500-fold Cr^{3+}, the recoveries of the analytes were still above 90%. From the experimental results obtained, it can be concluded that the MPTS-silica coating has an excellent selectivity for the absorption of Cu, Hg and Pb under selected conditions.

3.11. Detection limits and precision

According to the IUPAC definition, the instrumental detection limits (3σ) were 0.85, 1.1 and $2.6\,ng\,mL^{-1}$ for Cu, Hg and Pb, respectively. Therefore, the detection limits of the method were 0.17, 0.22 and $0.52\,ng\,mL^{-1}$ for Cu, Hg and Pb, respectively, with an enrichment factor of 5. The analytical performance of the method was presented in Table 4.

Compared with the detection limits of 0.17–$1.27\,ng\,mL^{-1}$ for Cu, 0.12–$5\,ng\,mL^{-1}$ for Hg and 0.2–$1.79\,ng\,mL^{-1}$ for Pb which were obtained by ICP–AES after separation/preconcentration with different adsorption materials in literatures [24–28], it was obvious that this method is more sensitive.

3.12. Sample analysis

The proposed method was applied to the determination of Cu, Hg and Pb in human serum (devoted by hospital patients), human urine (devoted by Hg-exposed researchers) and preserved egg (purchased from local supermarket) and the results were given in Table 5.

In order to establish the validity of the proposed procedure, the method has been applied to the determination of the content of Cu, Hg and Pb in certified reference materials (BCR151 milk powder, GBW07601 (GSH-1) human hair, GSBZ 50016-90 and GSB 07-1183-2000 water samples), and the results are listed in Table 6. As can be seen, a good agreement between determined values and the certified values could be obtained.

4. Conclusion

In this paper, sol–gel MPTS-silica coating has been prepared and a new method of sol–gel MPTS-silica coated capillary microextraction on line hyphenated with ICP–AES was developed for determination of trace Cu, Hg and Pb in biological samples. To the best of our knowledge, this is the first work dealing with coupling of MPTS-silica coated capillary microextraction to ICP–AES for trace element analysis. The simplicity, excellent selectivity, little solvent and sample consumption and high sensitivity make it especially suitable for trace analysis of Cu, Hg and Pb in various biological samples with complicated matrix.

Acknowledgement

Financial supports from the Science Fund for Creative Research Groups of NSFC (no. 20621502), National Nature Science Foundation of China (grant no. 20575048), and NCET-04-0658, MOE of China are gratefully acknowledged.

References

[1] E.D. Salin, J.M. Ren, J. Anal. At. Spectrom. 18 (2003) 953.

[2] B. Hu, T.Y. Peng, Y.C. Qin, Talanta 49 (1999) 357.
[3] I. Juranovic, P. Breinhoelder, I. Steffan, J. Anal. At. Spectrom. 18 (2002) 54.
[4] A. Asfaw, G. Wibetoe, Microchim. Acta 152 (2005) 61.
[5] F.X.X. Han, W.D. Patterson, Y.J. Xia, B.B.M. Sridhar, Y. Su, Water Air Soil Pollut. 170 (2006) 161.
[6] L. Ding, F. Liang, Y.F. Huan, Y.B. Cao, H.Q. Zhang, Q.H. Jin, J. Anal. At. Spectrom. 15 (2000) 293.
[7] K. Ide, Y. Nakamura, Mater. Trans. 43 (2002) 1409.
[8] H. Heitzman, B.A. Young, D.J. Rausch, P. Rickert, D.C. Stepinski, M.L. Dietz, Talanta 69 (2006) 527.
[9] V. Oliveira, A.M. Sarmiento, J.L. Gómez-Ariza, J.M. Nieto, D. Sánchez-Rodas, Talanta 69 (2006) 1182.
[10] K. Prasad, P. Gopikrishna, R. Kala, T. Prasada Rao, G.R.K. Naidu, Talanta 69 (2006) 938.
[11] Y. Huang, X.Y. Jiang, W. Wang, J.P. Duan, G.N. Chen, Talanta 70 (2006) 1157.
[12] A.K. Malik, V. Kaur, N. Verma, Talanta 68 (2006) 842.
[13] A. Kabir, C. HamLet, A. Malik, J. Chromatogr. A 1047 (2004) 1.
[14] Y. Fan, Y.Q. Feng, S.L. Da, Z.G. Shi, Anal. Chim. Acta 523 (2004) 251.
[15] J.J. Chen, Y.C. Lee, H.C. Lin, R.L.C. Chen, J. Food. Drug Anal. 12 (2004) 332.
[16] Z. Mester, J. Pawliszyn, Rapid Commun. Mass Spectrom. 13 (1999) 1999.
[17] S. Bigham, J. Medlar, A. Kabir, C. Shende, A. Alli, A. Malik, Anal. Chem. 74 (2002) 752.
[18] H. Kataoka, S. Narimatsu, H.L. Lord, J. Pawliszyn, Anal. Chem. 71 (1999) 4237.
[19] D.X. Wang, S.L. Chong, A. Malik, Anal. Chem. 69 (1997) 4566.
[20] T.Y. Kim, K. Alhooshani, A. Kabir, D.P. Fries, A. Malik, J. Chromatogr. A 1047 (2004) 165.
[21] J.C. Wu, Z. Mester, J. Pawliszyn, Anal. Chim. Acta 424 (2000) 211.
[22] A. Suzuki, L.W. Lim, T. Hiroi, T. Takeuchi, Talanta 70 (2006) 190.
[23] X.L. Pu, Z.C. Jiang, B. Hu, H.B. Wang, J. Anal. At. Spectrom. 19 (2004) 984.
[24] Y.M. Cui, X.J. Chang, Y.H. Zhai, X.B. Zhu, H. Zheng, N. Lian, Microchem. J. 83 (2006) 35.
[25] H. Zheng, X.J. Chang, N. Lian, S. Wang, Y.M. Cui, Y.H. Zhai, Int. J. Environ. Anal. Chem. 86 (2006) 431.
[26] S. Arpadjan, L. Vuchkova, E. Kostadinova, Analyst 122 (1997) 243.
[27] P.C. Rudner, J.M.C. Pavón, F.S. Rojas, A.G. Torres, J. Anal. At. Spectrom. 13 (1998) 1167.
[28] J.A. Salonia, R.G. Wuilloud, J.A. Ga'squez, R.A. Olsina, L.D. Martinez, J. Anal. At. Spectrom. 14 (1999) 1239.